# THE GEOCHEMICAL PALÆO-OCEANOGRAPHY AND MINERALOGY OF MARINE SEDIMENTS FROM THE PERUVIAN CONTINENTAL MARGIN

**Gavin William McNeill**

**Doctor of Philosophy**
**University of Edinburgh**
**1993**

## DECLARATION

I, Gavin William McNeill, hereby declare that, except where otherwise stated, the work presented in this thesis for the degree of Doctor of Philosophy was carried out by myself.

# ABSTRACT

A comprehensive study of marine sediments collected during the *R.R.S. Charles Darwin* Leg 38 cruise from the Peruvian continental margin, has been carried out using a wide range of geochemical analysis techniques. The prime objective of the study has been to determine the strength and down-core variation of many oceanographic processes during the glacial/interglacial stages of the Late Quaternary by means of geochemical palæo-environmental indicators.

Coastal upwelling is a physical movement of cold, nutrient-rich water to replace surface water which has been blown off-shore by Ekman transport, as a result of along-shore winds. This results in high marine productivity levels within the Peruvian coastal upwelling zone, and is recorded by enrichments of organic carbon and other biogenic-remains in the sediments accumulating below. Particular metals, which have a capacity to be scavenged from sea-water as organic matter falls through it, are also enriched in the sedimentary record.

Organic matter and fish-remains supply a continuous source of phosphorus to the surface sediment. Upon bacterial decomposition of this biogenic debris, phosphate can become enriched in the pore-waters until precipitation of carbonate fluorapatite occurs to form the diagenetic mineral known as phosphorite. Within the Peru margin cores, the presence of disseminated phosphorite pellets and zones of nodular hardgrounds has been determined using pore-water modelling and geochemical partitioning equations. Many trace elements can be incorporated into the phosphorite mineral structure. Quantitative analysis of the uranium, strontium and yttrium concentrations within phosphorite zones has allowed for the partitioning of these elements into the organic, carbonate and terrigenous phases respectively. U-series radiochemical age dating of a phosphorite nodule yielded a "maximum" age of about 114,000 years for the phosphatic material. This age corresponds to an initial pellet growth on the continental margin during an interglacial period and supports the hypothesis of nodule diagenesis during the last glacial period as a result of heavy mineral concentration by bottom-water currents during a eustatic drop in sea-level.

The use of statistical and mathematical methods to interpret the large geochemical dataset from the Peru margin sediments has been examined. Both regression analysis and principal component analysis have been used to highlight the existence of strong element-element and element-phase relationships. Multi-component analysis was used to show that the proximity of the South

American continental landmass and the high "coastal upwelling" productivity have produced sediments which are dominated by terrigenous and biogenic phases.

Iodine and bromine, and their ratios to organic carbon, have been used to distinguish between anoxic sediments accumulating within the oxygen minimum zone on the upper shelf and oxic sediments from deeper water sites along the continental margin. The barium profile from a core on the Nazca Ridge displayed remarkable similarity to the foraminifera oxygen isotope record and the flux of biogenic-barium has been used as a proxy for palæo-productivity calculations. The same core showed a strong correlation between strontium and calcium carbonate concentrations, and the Sr/Ca ratio has been examined as an indicator of the dominance of foraminifera in the marine biomass. The ratio of molybdenum to uranium has previously been used as a proxy of palæo-redox conditions at the sediment/water interface. However, in the Peru margin sediments the measured Mo/U ratios contradict the established theory, due to the complex post-depositional behaviour of these two heavy metals.

Many natural processes, including continental erosion, sediment transport patterns, carbonate and silicate dissolution and volcanic activity, and their variation over the Late Quaternary glacial/interglacial stages have been investigated using the concentrations and fluxes of geochemical components contained within the terrigenous and biogenic sedimentary material. Inter-core comparisons are also made in order to interpret these palæo-environmental processes at sites of varying water depth and environment of deposition along the Peruvian continental margin.

# ACKNOWLEDGEMENTS

Firstly, I would like to thank both Dr Graham Shimmield and Dr Brian Price for their expert supervision throughout the duration of this study. It has been a privilege to be introduced to the world of marine sediment geochemistry by two men who share a great knowledge of the subject and whose research interests are at the forefront of this scientific field.

Thanks should also go to Dr Roger Banks and Dr Hilary Kennedy (UCNW) who, as my secondary supervisors, were not often needed but were always willing to help when required.

This Ph.D. study has been funded by the Natural Environment Research Council (NERC) under grant number GT4/89/GS/40. I would like to take this opportunity to acknowledge their financial support.

All the staff, secretaries and technicians at the Department of Geology and Geophysics have been most helpful during the last three years. The following people deserve special thanks for the patience they showed in answering my many questions and demonstrating/fixing analytical equipment; Geoff Angel, Godfrey Fitton, Dodie James, Dick Kroon, Frances Lindsay, Ann Mennim, Jim Smith, Mike Saunders and Sandy Tudehope.

Whilst working alongside Ian Alexander, Nicky Allison, Tim Brand, Debbie Carr, Colin Chilcott, Shirley Derrick, Jerry Lloyd, Al Matthewson, Steve Mowbray, Bryne Ngwenya, Andy Patience, George Ritchie, Christian Robinson and Stuart Young, I have learnt many analysis and computing techniques. I hope that I have managed to give to the Marine Geosciences Unit as much as I have taken.

I have also enjoyed being a part of the large postgraduate community in the department. Many thanks go to all who have helped both academically and sociably with chats over coffee, drinks in the KB bar, games of football, basketball etc.

The officers, crew and scientific personnel of the R.R.S. Charles Darwin Leg 38 cruise must be thanked because without their excellently–recovered sediment cores, there would have been no samples and therefore no thesis to write.

At the Scottish Universities Research and Reactor Centre (SURRC), East Kilbride, the instruction and help received from Tony Fallick and Terry Donnelly on the operation of the stable isotope mass spectrometer was invaluable.

Over the past few years there have been many occupants of Terry Scoffin's flat at 42 Marchmont Road, including myself. Living in such an easy-going atmosphere was great fun and special thanks must go to Andy Powley for teaching us all how to play bridge!

All my family have supported me throughout the many years of my education. I wish to especially thank Mum and Dad for both the endless encouragement and financial support that they have given.

Finally, I must thank the one person "without whom love would remain a mystery". Victoria is my best friend, constant companion and professional proof-reader all rolled into one; what more could anybody ask for.

# LIST OF CONTENTS

Page No.

## LIST OF FIGURES

## LIST OF TABLES

# CHAPTER 1

# INTRODUCTION

## 1.1. MARINE SEDIMENT GEOCHEMISTRY

"By the light by which geology now throws, and will continue to throw, on former changes of climate and of the level of the land, we shall surely be enabled to trace in an admirable manner the former migrations of the inhabitants of the whole world."

Charles Darwin (1859)
*The Origin of Species*

It is less than one hundred and fifty years since Darwin wrote the above comment about the importance of geological studies in the interpretation of climatic and sea-level changes and in the examination of variations in the biomass of the Earth. This thesis is one small addition to the vast amount of scientific research which has followed since the times of Darwin and other pioneers of the science of our natural environment. The marine sediment samples analysed and interpreted in this study were collected from an area of the world's oceans through which Darwin sailed on his historic travels onboard *H.M.S. Beagle*, namely the Peruvian continental margin, and were collected during scientific cruise Leg 38 of the research ship which bears his name, *R.R.S. Charles Darwin*.

The Earth's surface is approximately 70% water and 30% land and therefore marine sediments are quantitatively the most important geological samples available for scientific analysis. However, due to the immense technological difficulty and expense of collecting marine sediments (compared with collecting rock samples from exposed land outcrops) the first collection and study of such sediments began only just over 100 years ago, during the *Challenger* Expedition (1872-1876). With the introduction of improved sample collection and analysis techniques (e.g. mass spectrometry and X-ray fluorescence) marine sediment geochemistry has developed rapidly in the last 20-30 years.

Increased awareness in the importance of the natural environment (and mankind's effect on it) has led to a need for greater understanding of the complex interplay between the atmosphere, hydrosphere and lithosphere (oceanic and continental). Deep-sea sediments are potentially one of the best sources of natural environmental records for two reasons. Firstly, they can contain continuous records of low frequency (in the order of $10^3$ years) cycles and events. Fresh sediment is continuously deposited on top of older sediments, thus preserving the environmental

signals on a vertical depth scale, which corresponds to the age of the sediment. Secondly, the sediments are multi-component mixtures which can include terrigenous (land-derived), biogenic, hydrothermal and authigenic (diagenetic) phases; each of which can be used to answer certain environmental questions about the climatic, geological, chemical and biological conditions that existed in the past.

The time scale for such studies depends on both the depth of sediment core collected and the resolution of the sub-sampling of the core. For example, in this study, piston cores (of up to 9m length) were sub-sampled every 10cm resulting in a high resolution record (< 4000 years between samples) of the Late Quaternary. On the other hand, the Ocean Drilling Program regularly collects cores which are over 500m in length and which contain sediment of Eocene age, but usually sub-samples are taken about every 50cm resulting in a lower-resolution record.

It is important in any study of marine sediments that, if possible, the depth component of the core is converted into an accurate age component. This can be attempted either by direct age determination (e.g. $^{14}C$-dating or radiochemistry) or more usually by comparison of a particular signal (either geophysical or geochemical) with a previously-dated reference core(s). The most common method of age-dating marine sediments uses stable isotope mass spectrometric analysis of the carbonate microfossils of foraminifera and comparison of their oxygen isotope record with the stacked SPECMAP reference curve (Imbrie *et al.*, 1984). This is the method which is used for age modelling of the piston cores in this study.

For climatic and environmental interpretations, age modelling is important so that geochemical signals can be represented in terms of the glacial/interglacial stages of the Late Quaternary. Global climatic changes are caused by fluctuations in the atmospheric insolation of the Earth, as a result of variations in the Earth's orbit around the Sun. The pioneering work of the Scottish scientist James Croll (1821-1890) linked the timing of past ice ages with a 100,000 year cycle, relating to the eccentricity of the Earth's elliptical orbit, and a 19,000-22,000 year cycle, relating to the precession of the seasonal equinoxes (Croll, 1867A and B). His work was later extended by a Yugoslavian engineer Milutin Milankovitch (1879-1958), whose theory added a 41,000 year cycle to Croll's eccentricity and precession cycles. This third orbital frequency is caused by variation in the tilt of the Earth's axis relative to the Sun (Milankovitch, 1941). Together, the three orbital parameters of the Earth are known as the Milankovitch orbital frequencies (Berger, 1978; Imbrie and Imbrie, 1979).

The Earth's glacial/interglacial periodicity influences many environmental parameters including atmospheric wind strength, ice-volume, sea-level, continental aridity and, perhaps, oceanic biological productivity (Sarnthein *et al.*, 1988; Shimmield, 1992). All of the above parameters can affect the composition of the sediment input to a particular area of the ocean and their variation over time will be contained in the geochemical signature of the down-core sediment record.

Age modelling can also benefit marine sediment geochemical records by allowing for the concentration of a particular component or element, which is analytically measured as a weight percent (wt.%) or part per million (ppm) of the total, to be expressed as a mass accumulation rate (MAR) flux (g $cm^{-2}$ $kyr^{-1}$). This means that the variation of input to the sediment of an individual component or element over time can be calculated. The MAR flux is independent of the variation of all the other components, i.e. dilution effects on the geochemical signal are removed, allowing for the true reasons of input fluctuations (productivity, preservation, diagenesis, weathering/erosion etc.) to be examined.

Although this study is concerned with the geochemical analysis of marine sediments, its interpretations are by no means limited to just geological or chemical processes. As the diagram in Fig. 1.1 indicates, marine sediment geochemistry is an inter-disciplinary science which relies on an understanding of four basic sciences (chemistry, physics, biology and geology) and their influence on oceanography, climatology and mineralogy. Each of the following chapters in this thesis concentrates on a particular environmental aspect (involving one or more of the natural processes shown in Fig. 1.1) which can affect the geochemical signature of the ocean sediments from the Peruvian continental margin.

## 1.2. PERU CONTINENTAL MARGIN

The following chapters each contain their own introductory explanations about the various environmental features of interest along the Peru continental margin and their particular geochemical signature. Included in these sections are references to relevant studies by previous authors who have used a wide range of analytical methods to study the sediments of the Peru continental margin (and other similar areas of the world's oceans) in order to further our understanding of the geology, oceanography and climatology of the area. There are two particular textbooks from which many references have been taken and two research cruises

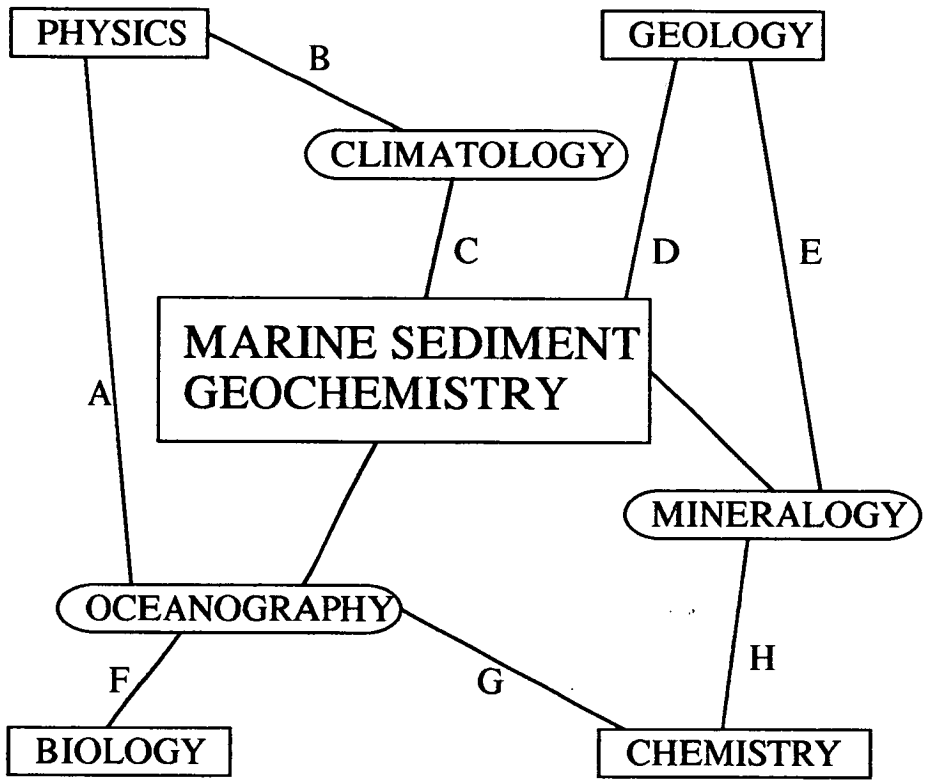


Figure 1.1. Marine sediment geochemistry; an inter-disciplinary science.

Process:

- A Global wind and water mass circulation,
- B Milankovitch orbital frequencies,
- C Glacial/interglacial periodicity,
- D Ocean tectonics,
- E Continental erosion and sediment supply,
- F Marine biomass productivity,
- G Water chemistry,
- H Chemical redox reactions.

during which cores were obtained from the Peruvian margin, which deserve to be mentioned here. The books (*Coastal Upwelling*, Volumes A and B, Suess and Thiede, 1983; Thiede and Suess, 1983; *Upwelling Systems*, Summerhayes *et al.*, 1992) contain papers which analyse and interpret all aspects of coastal upwelling (the main oceanographic feature affecting this area; Chapter 3). The cruises were the Ocean Drilling Program (ODP) Leg 112 (Suess *et al.*, 1988) and the *R.V. Robert D.Conrad* cruise 23–06 (Burnett and Froelich, 1988).

The tectonic history and the oceanic setting of the Peru margin are now briefly introduced in order to highlight the global significance of this area in terms of the environmental records that are contained within the marine sediments accumulating on the sea–floor.

### 1.2.1. Tectonic history

The Andean continental margin , which runs the length of the west coast of South America, is a major boundary in both the global framework of plate tectonics and the global pattern of oceanic circulation. Running parallel to the coastline of Peru, the Peru–Chile Trench (at about 6000m water depth) has been formed by the subduction of the oceanic Nazca plate as it slowly moves south–east (due to sea–floor spreading at the East Pacific Rise) and collides with the continental South American plate. The rate and direction of subduction has been estimated as 7.1cm per year at 102° (Hey *et al.*, 1977). This geological process has produced a complex continental margin, which lacks pervasive compressional deformation and an extensive accretionary complex as seen at other convergent plate margins (Scholl *et al.*, 1970; Rutland, 1971).

The Nazca Plate Project (Kulm *et al.*, 1981) investigated the tectonic history of the margin and observed that the continental crust extended to at least the edge of the shelf and that sediments had accreted along the lower slope. On the continental shelf and upper slope off Peru, a series of elongated, tectonic depressions produced a pattern of off–shore, forearc basins which lie roughly parallel to the coastline, land–ward of the Peru–Chile Trench, and within which marine sediments have slowly accumulated (Thornburg and Kulm, 1981; Suess *et al.*, 1988).

At approximately 15°S, the depth of the Peru–Chile Trench decreases to about 4800m, where it is intersected on the sea–ward side by the Nazca Ridge. The ridge is an aseismic, submarine topographical feature which runs from north east to south west on the Nazca plate and rises over 1200m above the surrounding deep–sea

floor (Couch and Whitsett, 1981; Schweller *et al.*, 1981). The Nazca Ridge has a strong influence on both the water mass circulation and the sedimentation pattern of the Peruvian margin.

### 1.2.2. Oceanic setting

Although it is the tectonic history of the region that controls the physiographic location of the marine sediments, it is the particular oceanographic setting of the Peruvian continental margin which dominantly influences their geochemical composition. During the Eocene/Miocene period, the initiation of the Eastern Pacific Boundary Current circulation pattern, and its associated wind system, established a coastal upwelling regime along the Peru margin. Coastal upwelling is a physical feature which moves surface-water off-shore, as a result of along-shore wind stress, and therefore deeper-water has to be upwelled to replace it (3.1.1).* Coastal upwelling has dominated the oceanography of the area since the Eocene (Reimers and Suess, 1983A; Suess *et al.*, 1988) and sustained an intense marine biological productivity zone (3.1.2) along the coast.

The level of this productivity has been estimated as being an order of magnitude greater than that of normal ocean surface-waters. In the centre of the Peru upwelling cells, between 1 and 6 g of carbon are fixed by photosynthetic organisms (phytoplankton) every day in an area of just one square metre (Chavez and Barber, 1987). This extreme biological production is the main reason why the Peru margin is an important area for study of the palæo-climate and also for future climate prediction models.

Today, this coastal zone (and other areas such as off south west Africa and California) provides a major sink for organic carbon in the oceans and depletes other carbon reservoirs such as the atmospheric $CO_2$ levels (Broecker, 1982, 1984). It may be that some of the increase in the $CO_2$ concentration in the atmosphere over the last 100 years, which has been caused by the anthropogenic burning of fossil fuels, will be compensated for by increased biological production in the oceans, especially at coastal upwelling zones. This may decrease the effects of the global warming scenario as predicted by many climate models.

---

*Numbers in brackets appear throughout this thesis and are used to refer to another section of the thesis. If the number is not prefixed by Figure, Table or Appendix, then it simply refers to another section or sub-section of the text.

Not only has the high biological production an important role to play in the natural carbon cycle, but it also strongly affects the ocean chemistry and sediment geochemistry. Most of the organic matter produced in the surface-water is decomposed and recycled as it falls through the water column upon death of marine organisms. The high flux of organic matter below a coastal upwelling zone results in extreme levels of microbacterial activity at water depths of between 100 and 500m (Veeh *et al.*, 1973). This decomposition/respiration process uses nearly all of the available dissolved oxygen and creates an oxygen minimum zone (OMZ) between the above depths. The organic matter that avoids decomposition reaches the sea-floor and is incorporated into the sediment column. Under a coastal upwelling zone, organic carbon is found at much higher concentrations than in marine sediments from the deep ocean (Reimers and Suess, 1983A). The degradation of organic matter within the sediment column plays an important role both in the redox environment (oxic, suboxic or anoxic conditions) and in the types of diagenetic processes that occur within the sediment. These two parameters can strongly affect the sediment geochemical composition and any *in situ*, authigenic mineral growth.

## 1.3. STATION SITES AND CORE DESCRIPTIONS

As previously mentioned, all the sediment cores which were sampled and analysed to provide the geochemical records presented in this thesis, were collected during the scientific cruise Leg 38 of the *R.R.S. Charles Darwin* (core numbers have the prefix CD38). This was an inter-university research cruise which recovered marine sediments using box and piston cores, and also sea-water and pore-water samples, from the Peru margin and the eastern equatorial Pacific during April and May 1989. The cruise report (Price *et al.*, 1989) presents full details of the cores and water samples, and the information contained in Table 1.1 and Fig. 1.2 is taken directly from it. For the cores used in this study, Table 1.1 lists the station site number, its latitudinal and longitudinal position, and the core water-depth, type and length. Figure 1.2 is a simplified map of the Peruvian continental margin and, as well as illustrating the location of each station site, the important topographical features and water circulation patterns of the region are shown.

The cores can be divided into a northerly group and a southerly group (Table 1.1) as follows. The northerly group forms a transect at about 11°S of increasing water depth and includes two shallow-water cores, CD38-09 and CD38-10, located on the continental shelf directly under the coastal upwelling zone, and one deep-water core, CD38-11, located on the continental slope (Fig. 1.2). These three

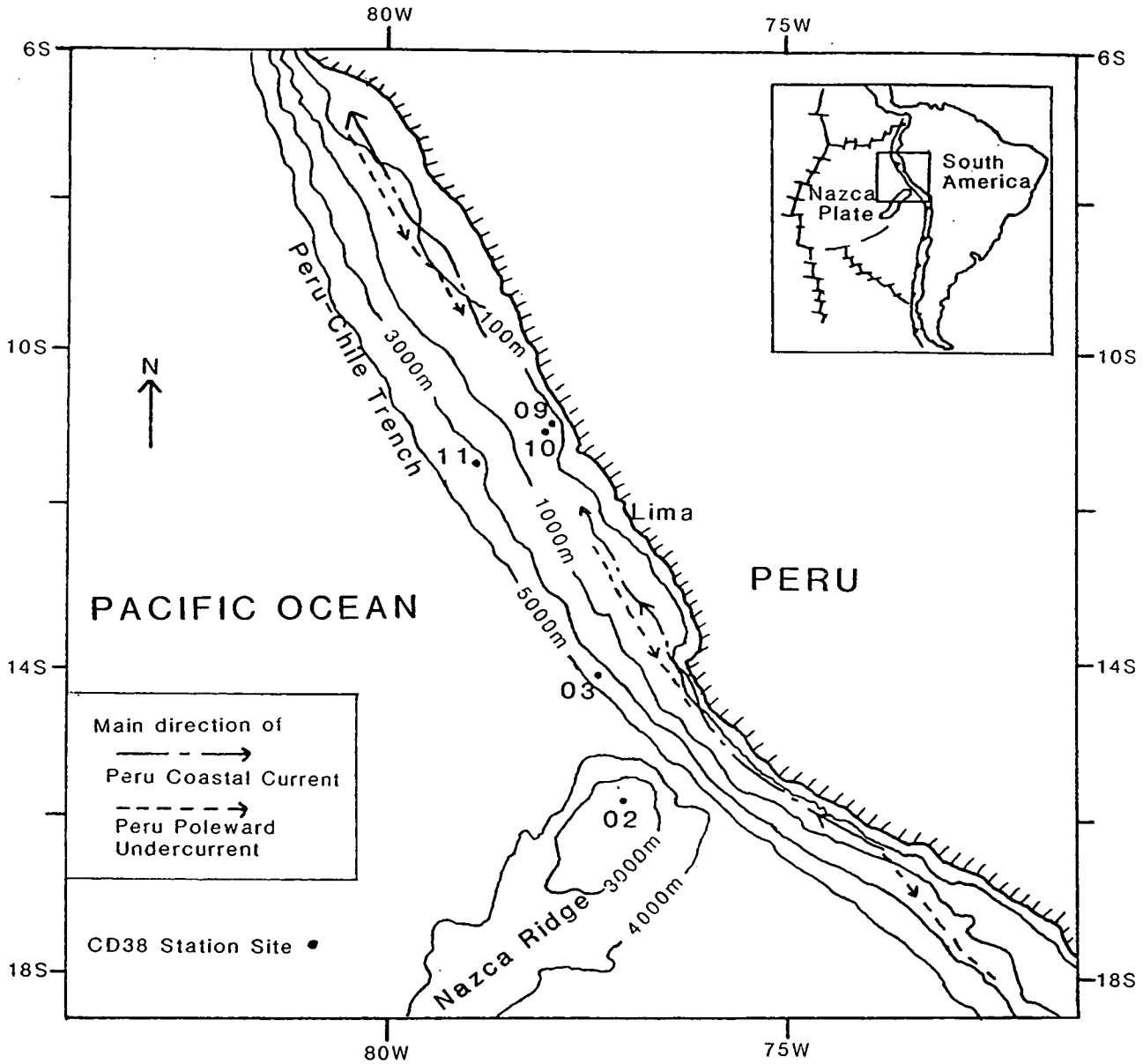


Figure 1.2. Simplified map of the Peru continental margin, indicating the location of the CD38 core sites studied in this thesis, as well as the main topographic and oceanographic features of the area.

cores were drilled at locations close to the ODP Leg 112 sites 681, 680 and 688 respectively to allow for the possibility of inter-core comparisons.

| Station | CD38-09 | CD38-10 | CD38-02 | CD38-02 | CD38-11 | CD38-03 |
|---|---|---|---|---|---|---|
| Location | S.Salaverry Basin | S.Salaverry Basin | Nazca Ridge | Nazca Ridge | Lima Basin | Peru Basin |
| Lat. (S) | 10°58' | 11°04' | 15°56' | 15°57' | 11°32' | 14°36' |
| Long. (S) | 77°57' | 78°04' | 77°04' | 77°04' | 78°56' | 77°45' |
| Core Type | Piston | Piston | Piston | Box | Piston | Box |
| Core Length | 895cm | 822cm | 800cm | 57cm | 594cm | 57cm |
| Water Depth | 148m | 257m | 2525m | 2530m | 3835m | 4289m |

Table 1.1. Core locations

The southerly group (between 14 and 16°S) contains a deep-water box core, CD38-03, from close to the Peru-Chile Trench and intermediate-water box and piston cores, CD38-02, located on the upper slopes of the Nazca Ridge (Fig. 1.2). All the above cores provide a range of water-depth and oceanographic environments from which the geochemical signatures of the marine sediments should contain many contrasting records of the palæo-oceanography of the Late Quaternary along the Peru margin.

In order to illustrate some of the contrasting ocean water conditions at the core sites, Fig. 1.3 displays the dissolved oxygen, temperature and salinity levels measured at three of the above sites (CD38-03, CD38-10 and CD38-09) during the *R.R.S. Charles Darwin* Leg 38 cruise (Price *et al.*, 1989). The profiles are plotted against water depth and display differences in water chemistry between an area of strong coastal upwelling (CD38-09 and CD38-10) and one which lies at the periphery of such an oceanic phenomena (CD38-03).

It should firstly be noticed that the vertical scales of the profiles in Fig. 1.3 correspond to the station site water depths and therefore vary considerably between the shallow- and deep-water sites. The main points of interest about the water chemistry of the Peru margin that are displayed in Fig. 1.3 are as follows.

1) Although the temperature profile of CD38-03 shows a smooth, exponential decrease with increasing water depth, the salinity and dissolved oxygen profiles both contain a minimum zone at 500-1500m and 200-1000m respectively, which indicates the presence of more than one water mass circulating in this region. The surface-waters, with temperatures above 20°C and salinities close to 35.0‰, are

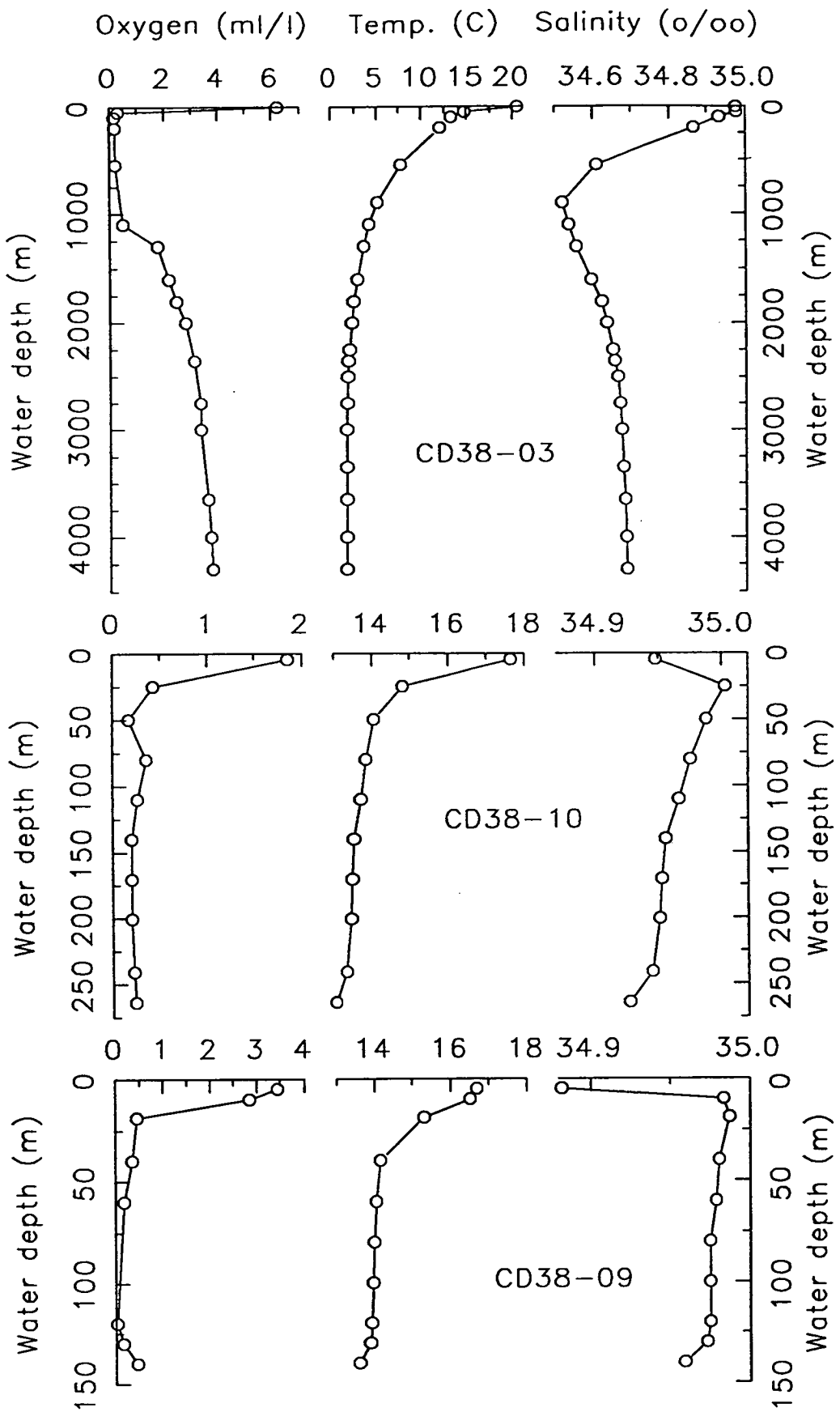


Figure 1.3. Water column profiles of dissolved oxygen content (ml $l^{-1}$), temperature (°C) and salinity (‰) for station sites CD38–03, CD38–10 and CD38–09.

part of the Peru Coastal Current (PCC), underneath which is the Peru Poleward Undercurrent (PPU) between 100 and 500m (Smith, 1983; Huyer *et al.*, 1991; 3.1.1). Below this, lies the Antarctic Intermediate water (AIW); a water mass which flows from the Antarctic Circumpolar Current between 500 and 1000m and is characterised by low salinity and oxygen depletion, resulting respectively from ice melting and high productivity in the polar waters (Lonsdale, 1976). Both the salinity and the dissolved oxygen profiles of CD38–03 increase steadily below 1000m due to the mixing of the AIW with the Pacific Deep Water (PDW). This latter water mass flows southward along the bottom of the continental slope and is more oxygenated with a higher salinity and lower temperature than the AIW due to its relatively older age (Pickard and Emery, 1982).

2) The two shallow–water stations (CD38–09 and CD38–10) display surface–water temperatures which are 2–3°C less than that of the deeper–water site. This is a direct result of the stronger coastal upwelling at the near–shore sites, where colder water (at about 14°C) is upwelled from depths of about 100m (Zuta *et al.*, 1978) to replace the warmer surface–water, which has been moved off–shore by Ekman transport (3.1.1).

3) Stations CD38–09 and CD38–10 show water–depth profiles of dissolved oxygen which drop dramatically in the upper 50m and remain constantly below 0.5ml $l^{-1}$ down to the sediment/water interface. This graphic representation of the oxygen minimum zone (resulting from the microbacterial utilisation of oxygen for the decomposition of the high organic matter flux) implies that the bottom–water oxygen levels at these two core sites are virtually zero and that the sediment may be accumulating under a suboxic/anoxic environment.

## 1.4. OBJECTIVES OF GEOCHEMICAL ANALYSES

The prime objective of this study was to obtain as much information as possible about the concentration and variation over time of the principal components of the Peruvian marine sediments, using a wide range of geochemical analyses. The geochemical data from the CD38 cores will provide high–resolution records of the history of sedimentation along the Peru margin and, as well as adding to the geochemical database from previous work on the region's sediments (e.g. Suess *et al.*, 1988), this study will form an integral part of the multi–disciplinary research that is being carried out on these newly–collected cores (1.5). The results and

interpretations presented in the following chapters answer some of the many questions about the oceanographic history of this important area, but lead to many more unanswered ones. By undertaking this geochemical study, both basic, background data and interesting, novel results have been obtained. Implications and suggestions for further research work are discussed in Chapter 8.

Before any geochemical results are discussed, some of the important physical properties of the sediments must be examined. Pore-water dissolved salts are incorporated into the bulk sediment during drying of sub-samples (Appendix A.6) and it is necessary to subtract, from all analytical geochemical concentrations, the effect of the presence of these salts. By measuring the water content of each sample (calculated from the weight lost upon drying) and by assuming a constant salinity of 35‰ in the pore-waters, the salt content is calculated (2.2.1) and thereafter all geochemical data are presented on a salt-free basis. A rough indication of the average grain-size is achieved by measuring the relative weight of the sediment remaining after sieving through a 63 $\mu$m mesh (2.2.2). It is then possible to compare this physical measurement with particular element ratios which are thought to act as geochemical indicators of grain-size.

For the interpretation of down-core geochemical signals with respect to glacial/interglacial climate changes, it is useful to be able to convert the depth component of a core into an accurate age component. The oxygen isotopic ratios of benthic foraminifera are presented for each of the four piston cores for comparison with the standard reference SPECMAP curve (Imbrie *et al.*, 1984). The two near-shore cores, CD38-09 and CD38-10, contain non-continuous isotopic records due to either a lack of carbonate microfossils and/or the presence of sediment winnowing and erosion in certain horizons (2.3.2). Therefore, only cores CD38-02 and CD38-11 are used for age modelling and the calculation of sediment accumulation rates, which are seen to vary dramatically over the glacial/interglacial stages of the Late Quaternary (2.4.2 and 2.4.3).

Sediments rich in organic matter and other biogenic-remains, and collected from a continental shelf or slope, provide a good indication of accumulation under a coastal upwelling zone (Diester-Haass, 1978; Calvert, 1987). Cores CD38-09 and CD38-10 are chosen to examine in detail the concentrations of organic carbon, biogenic silica, calcium carbonate and fish-remains found in the sediments accumulating under the Peruvian coastal upwelling zone. These two cores are from relatively shallow water, within the depths at which the OMZ impinges on the

continental shelf (Veeh *et al.*, 1973). Mean organic carbon contents (of 4–5 wt.%) an order of magnitude greater than those of deep–sea sediments give evidence of the importance of coastal upwelling zones in the global carbon cycle as sites for the removal of carbon from the atmosphere and its storage in the sediments below (3.3.1).

Redox–sensitive and/or particle–reactive metals can be scavenged out of sea–water by organic matter as it falls through the water column (Bruland *et al.*, 1974; Francois, 1988) and incorporated into marine sediments. Under a coastal upwelling zone, the high organic matter flux can produce a sediment anomalously enriched in organo–metallic elements, such as Mo, U, Ni, Cr, V and Cu (Calvert and Price, 1970; Shimmield and Pedersen, 1990). Cores CD38–09 and CD38–10 contain enrichments of the above metals which correlate strongly with the levels of organic carbon (3.3.3) and whose mean organo–metallic ratios are representative of accumulation under natural, non–anthropogenic conditions on a continental margin. The metal/organic carbon ratios could possibly be useful in future studies of a polluted, coastal environment as the natural, baseline flux for comparison with any extra, anthropogenic input (3.3.4).

Geochemical analysis of marine sediments can illustrate mineralogical variation contained within a core, especially the presence of any diagenetic minerals. The Peru margin is known to be a site for the authigenic mineral growth of dolomites, cherts and phosphorites (Suess *et al.*, 1988; Burnett and Froelich, 1988). In this study, phosphorites are examined by geochemical partitioning of the total phosphorus content into terrigenous, organic and phosphorite phases in the bulk sediments of the three piston cores at 11°S (4.3.3). Compositional characterisation of nodular hardgrounds found in CD38–09 and CD38–10 (4.3.1) and comparison of the surface–sediment pore–water phosphate profiles of the above cores with those of the *R.V. Robert Conrad* research cruise 23–06 (Froelich *et al.*, 1988; 4.3.2) are also carried out.

The incorporation of certain trace elements into phosphatic minerals is displayed by their down–core enrichment coinciding with zones of phosphorite concentration in the two shallow–water cores. Quantification of the trace element/phosphorite ratios allows for the calculation of the fractions of uranium, strontium and yttrium which are respectively associated with organic matter, calcium carbonate and terrigenous phases (4.3.4).

Diagenetic formation of phosphorite hardgrounds is considered to be linked to eustatic changes of sea–level during the Late Quaternary, as a result of ice–sheet

volume variations during glacial/interglacial periodicity (Baturin, 1982). Evidence for this theory is obtained from U/Th radiochemical age dating of a large phosphorite nodule from core CD38–09, which gives an age representative of initial pelletal growth during an interglacial period (4.3.5). The diagenetic history that the nodule's age, shape and appearance suggests is one of phosphorite pellet growth in an organic–rich sediment, followed by a concentration of these pellets into a hardground caused by a dramatic drop in sea–level during the last glacial event. This eustatic variation brought strong bottom–water currents to this shallow–water site, which winnowed fine–grained clays down–slope to leave behind a concentrated phosphorite deposit along with other coarse–grained, heavy minerals (4.3.6).

Three statistical/mathematical methods of dataset analysis are attempted in order to simplify the large geochemical dataset from the Peru margin piston cores, so that interpretations of element correlations and inter–core/down–core component variations can be presented.

Correlation analysis indicates the presence of many element–element and element–phase relationships (5.2.2) but interpretations are limited if there is a particular phase whose variation of concentration dominates the variation of all the other sediment phases or if a particular element is associated with more than one phase.

Principal component analysis (PCA) avoids the above problems by graphically representing the variation of each element or phase as a factor in relation to the total variation of the dataset. From the PCA diagrams of the piston cores (5.3.2) it is possible to examine which geochemical elements are associated with one (or more than one) of the following; organic matter, biogenic silica, calcium carbonate, phosphorite and/or terrigenous phases.

Heath and Dymond (1977, 1981) and Dymond (1981) proposed multi–component analysis (MCA) models which could define marine sediments in terms of the relative abundance of five components representative of the source of the sedimentary material, i.e. terrigenous, biogenic, authigenic, hydrothermal and residual. Adaption of the algorithms and component geochemical compositions in the MCA models of the above authors allows for the conversion of seven geochemical variables from the Peru margin dataset into the above sediment components. In all the cores, the most abundant component is of terrigenous origin, followed by that from a biogenic source (5.4.2). This is as expected from marine sediments accumulating on a continental margin under the influence of strong coastal upwelling.

The concentration of dissolved oxygen in bottom- and pore-waters and the level of marine productivity in surface-waters are two oceanographic parameters which are of prime importance in controlling many processes within the sediment column. Trace elements are used to act as geochemical proxies of the above parameters, and their down-core profiles as indicators of the palæo-redox and/or palæo-productivity environment of the Peru margin during the Late Quaternary.

The close, but differing, association of the halogens (iodine and bromine) with organic carbon is examined in detail. Due to their diagenetic mobility during organic matter degradation upon burial, the halogens are unreliable palæo-productivity indicators (6.2.3). However, the iodine/organic carbon ratio can be used to distinguish between anoxic (at sites CD38-09 and CD38-10) and oxic (at all other sites) environments of sediment deposition (Price and Calvert, 1977; Shimmield and Pedersen, 1990).

Barium is a trace element which shows a strong relationship to the marine biogeochemical cycle (Church, 1979; Dehairs *et al.*, 1980) and therefore may be useful as a proxy for palæo-productivity (Dymond *et al.*, 1992; Von Breymann *et al.*, 1992). In the anoxic cores of CD38-09 and CD38-10, the barium signal is lost upon burial during barite diagenetic mobilisation (6.3.2). However, in the oxic environment of cores CD38-02 and CD38-11, the barium-productivity signal is preserved as a down-core Ba/Al or biogenic-Ba profile; both of which vary sympathetically with the foraminifera oxygen isotope signal across the glacial/interglacial stages (6.3.3). The model and equations of Dymond *et al.* (1992) for the relationship between the flux of biogenic-Ba to the sediment and the production levels in the surface-waters are critically reviewed, and tested using the barium results from core CD38-02 (6.3.4).

Foraminifera and coccoliths are two important groups of marine plankton, which form carbonate shells and remove strontium from sea-water, as a trace element substitute for calcium (Church, 1970). Core CD38-02 is chosen to observe the close relationship between strontium and calcium carbonate, because of its lack of phosphorite diagenesis, which can also enrich the Sr concentration (6.4.2). The temporal variation of the biogenic-Sr/Ca ratio shows glacial/interglacial fluctuations which possibly relate to changes in the degree of dominance of foraminifera over coccoliths in the marine biomass of the Peru margin (6.4.3).

Molybdenum and uranium are redox-sensitive, trace metals whose ratio has been used as a proxy for palæo-redox conditions at the sediment/water interface (Bertine and Turekian, 1973). The Mo/U ratios measured in the anoxic (CD38-09

and CD38–10) and oxic (CD38–02 and CD38–11) piston cores of the Peru margin contradict the hypothesis of the above authors (6.5.2). The relationship between these two heavy metals is highly complex and depends on their uptake by organic matter in the water column, post–depositional mobility and diagenetic incorporation into ferromanganese and phosphorite minerals (Shimmield and Pedersen, 1990). This renders the Mo/U ratio an unreliable indicator of palæo–redox environment of deposition in continental margin sediments (McNeill and Shimmield, 1991).

There are numerous processes which occur in the natural environment whose relative strengths control the exact sedimentological and therefore geochemical, composition of marine sediments. On the Peru continental margin, it is the proximity to the South American landmass and the presence of persistent coastal upwelling which exert the strongest influences on the process of sediment deposition. The terrigenous (land–derived) and biogenic inputs to the sediment cores, therefore, need to be examined in detail (7.2.1 and 7.3.1).

Questions regarding the composition, source supply and mode of transport of material eroded from the Andes and the Peru coastal plain and deposited on the continental margin, are answered using down–core and inter–core trends of terrigenous geochemical data, e.g. the flux of aluminium and silicon, and Ti/Al, Si/Al, K/Al and Zr/Rb element ratios (7.2.3). By examining the geochemical signature of the terrigenous component over time, environmental factors such as continental volcanic activity and fluctuations in the wind strength and sea–level along the margin are also interpreted (Boyle, 1983).

The concentrations of organic carbon, biogenic silica and calcium carbonate within all the cores, and the fluxes of these biogenic inputs to sites CD38–02 and CD38–11, are presented as indicative of variation in the level of biological productivity and/or preservation in the ocean along the Peru margin (7.3.2).

Decomposition of organic matter, both prior to and after burial in the sediment column, significantly diminishes and distorts the original signal of production (Reimers and Suess, 1983A). This means that accurate interpretations from the organic carbon record are difficult to make. However, the palæo–productivity equation of Müller and Suess (1979) is used (7.3.3) in order to contrast the calculated surface–water biological levels between a site on the Nazca Ridge (CD38–02) and one closer to the main coastal upwelling zone (CD38–11). This also allows for comparison with the productivity calculations from the biogenic–barium flux for core CD38–02 (6.3.4).

Both the biogenic silica and the calcium carbonate shells of marine organisms suffer from dissolution within the water column, thereby distorting the initial productivity signal into a preservation–controlled record within the sediment column (Berger, 1976; Volat *et al.*, 1980). The extent of dissolution varies according to the environment of deposition and fluctuates over time, due to the movement of water masses along the Peru margin (7.3.3). The mechanisms for the dissolution of both silicate and carbonate microfossils are discussed with regards to the water depth and ocean chemistry of each core site.

The above objectives for the analysis and interpretation of the geochemistry of the Peru margin sediments has followed the layout of the chapters which make up the bulk of this thesis. These chapters are presented in such a manner that, although only one particular environmental parameter or process is discussed at a time, each chapter relies on observations and interpretations made in previous chapters. The overall palæo–oceanographic history of the Peru continental margin is brought together in the concluding chapter.

## 1.5. CO–WORKERS

The sampling of the Peru margin cores was carried out in conjunction with two postgraduate research students from the Department of Oceanography, University of Southampton (who were both under the supervision of Dr A.E.S. Kemp). They are examining various other records and signals contained within the Peruvian marine sediments, as follows.

1) S. King – micropalæontological studies, foraminifera abundance, isotopic signatures and pollen analysis (palynology).
2) I. Brodie – sedimentological studies, general sediment logging of cores and detailed examination of microscopic laminations.

Two other co–workers involved in analysing some of the sub–samples taken from the cores are Dr T. Clayton (clay mineralogy; Southampton University) and Dr H. Schrader (diatom abundance variations; University of Bergen, Norway).

# CHAPTER 2

# SEDIMENT PHYSICAL PROPERTIES

## 2.1. INTRODUCTION

"Time and tide wait for no man, saith the old adage. But all men have to wait for time and tide."

Charles Dickens (1843)

*Martin Chuzzlewit*

Although the main work in this thesis is based on geochemical analyses, it is necessary to measure some important physical properties of the marine sediments (especially the water content of each sample) before the geochemical data can be correctly interpreted.

The above quote mentions both the physical component of time and the oceanographic parameter which constantly changes with time, the tide. In this palæo-oceanographic study, consideration of the length and period of time over which the marine sediments have accumulated is of prime importance. Taking cores of marine sediments is an ideal method of extracting an historical record of past ocean conditions, in terms of marine biology, chemistry and/or geology. However, no matter what signal is being measured, its down-core interpretation will have much more meaning if the depth component can be converted from a simple measurement in centimetres (cm) to an accurate age in thousands of years before the present (ka). Marine sediments do not accumulate at a constant rate, especially those on a continental margin, because the supply of both the terrigenous and the biogenic components to the sediment can be highly variable with time. Therefore, an accurate age model for each core needs to be constructed so that sediment accumulation rates (SAR, in cm $kyr^{-1}$) and mass accumulation rates (MAR, in g $cm^{-2}$ $kyr^{-1}$) can be calculated and down-core geochemical profiles can be plotted against age (ka) instead of depth (cm).

This chapter will firstly examine the following physical properties of each core; water content, salt content, porosity, dry bulk density and % grain-size > 63μm. Then, for the four piston cores, age model construction will be attempted by the measurement of the oxygen (and carbon) isotopic composition of foraminifera shells and the comparison of each isotope record with an internationally-used and dated record (SPECMAP, Imbrie *et al.*, 1984).

## 2.2. PHYSICAL PROPERTIES OF PERU MARGIN SEDIMENTS

### 2.2.1. Calculations from the measured water content

The bulk-sediment samples from the six cores used in this study (Table 1.1) were all weighed, both before and after drying at 50°C (Appendix A.1) and this allowed for the calculation of the water content (%) of each sample (Eqn 2.1). This is a measurement of the amount of water, relative to the weight (wt.) of sediment in each sample, which is held as pore-water around each grain of sediment.

Equation 2.1. Water content calculation

$$\text{Water content (\%)} = [(\text{Wet wt.} - \text{Dry wt.}) / \text{Wet wt.}] \times 100$$

Figures 2.1 through to 2.6 illustrate depth profiles of the various physical properties which are discussed in this section for cores CD38-09, CD38-10, CD38-02 (Box), CD38-02, CD38-11 and CD38-03 (Box) respectively and the complete data are tabulated in Appendix C.1.

It may be expected that the water content of any marine sediment core would decrease with (increasing) depth because sediment close to the sediment/water interface will contain more pore-water which will be slowly squeezed out as the sediment is buried and compacted under the pressure of accumulating material. This ideal scenario can, in fact, be seen in both the box cores (Figs 2.3 and 2.6) which show maximum water contents (72% and 82% respectively for CD38-02 and CD38-03) at the sediment/water interface, which exponentially decrease down to relatively constant levels (55% and 62% respectively) within the 55cm sampling depth.

It can be seen from the box cores that within the upper 50cm some pore-water has been squeezed out upon compaction of the sediment but that the buried sediment still contains a high water content (on a wt.% basis) held within its pore spaces. With this knowledge, the water content profiles of the four piston cores can be examined. These longer cores do not display a simple steady-state exponential decrease with depth but show more complex and erratic profiles, related to lithological/sedimentological changes.

The shallow-water cores CD38-09 and CD38-10 (Figs 2.1 and 2.2) have water contents that are generally above 60%. Similar high water contents were measured by Busch and Keller (1981) along the Peruvian continental margin and were attributed to

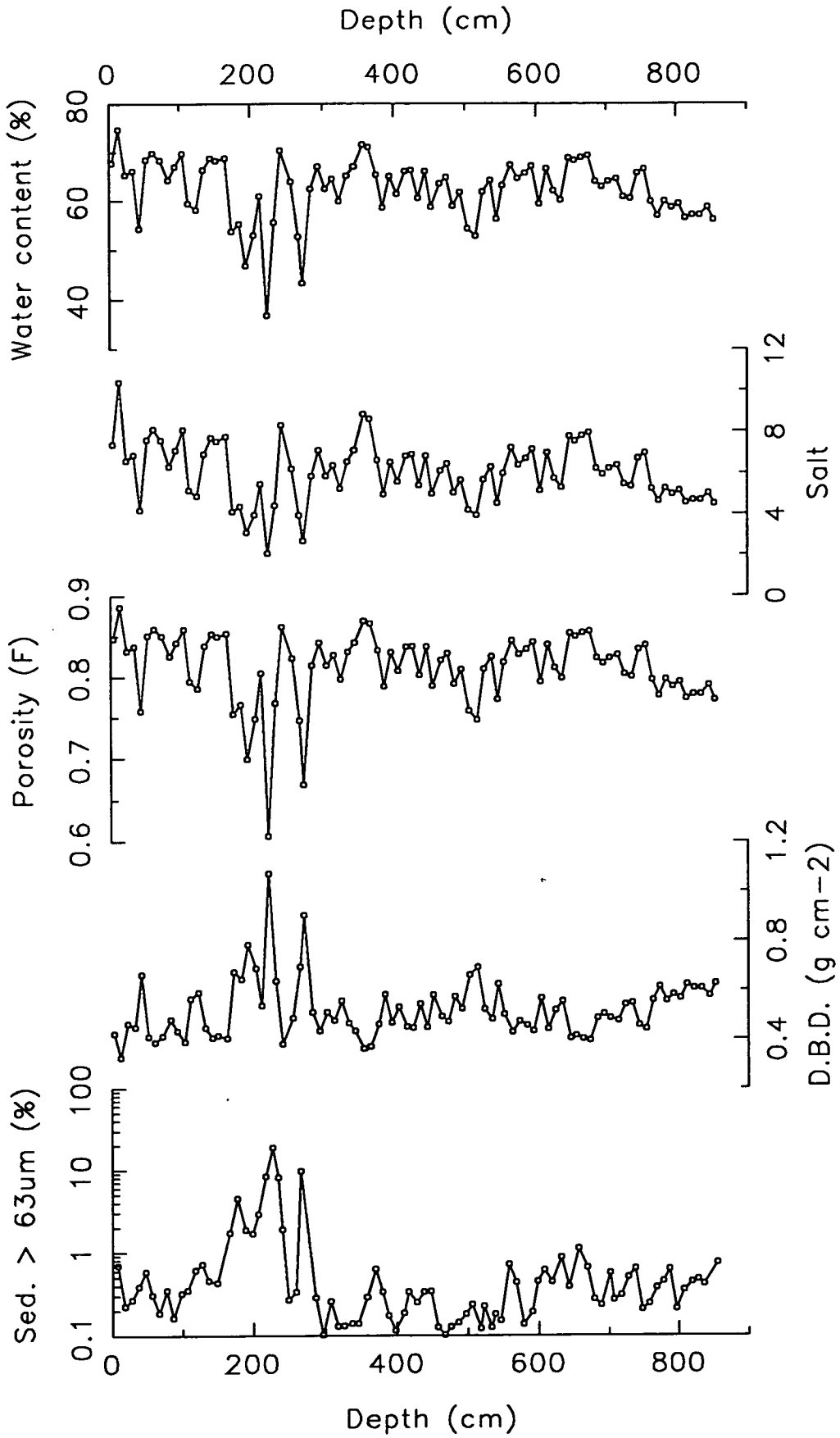


Figure 2.1. Down-core profiles of water content (%), salt content, porosity (F), dry bulk density (g $cm^{-2}$) and sediment > 63μm (%) against depth (cm) for core CD38-09 (148m).

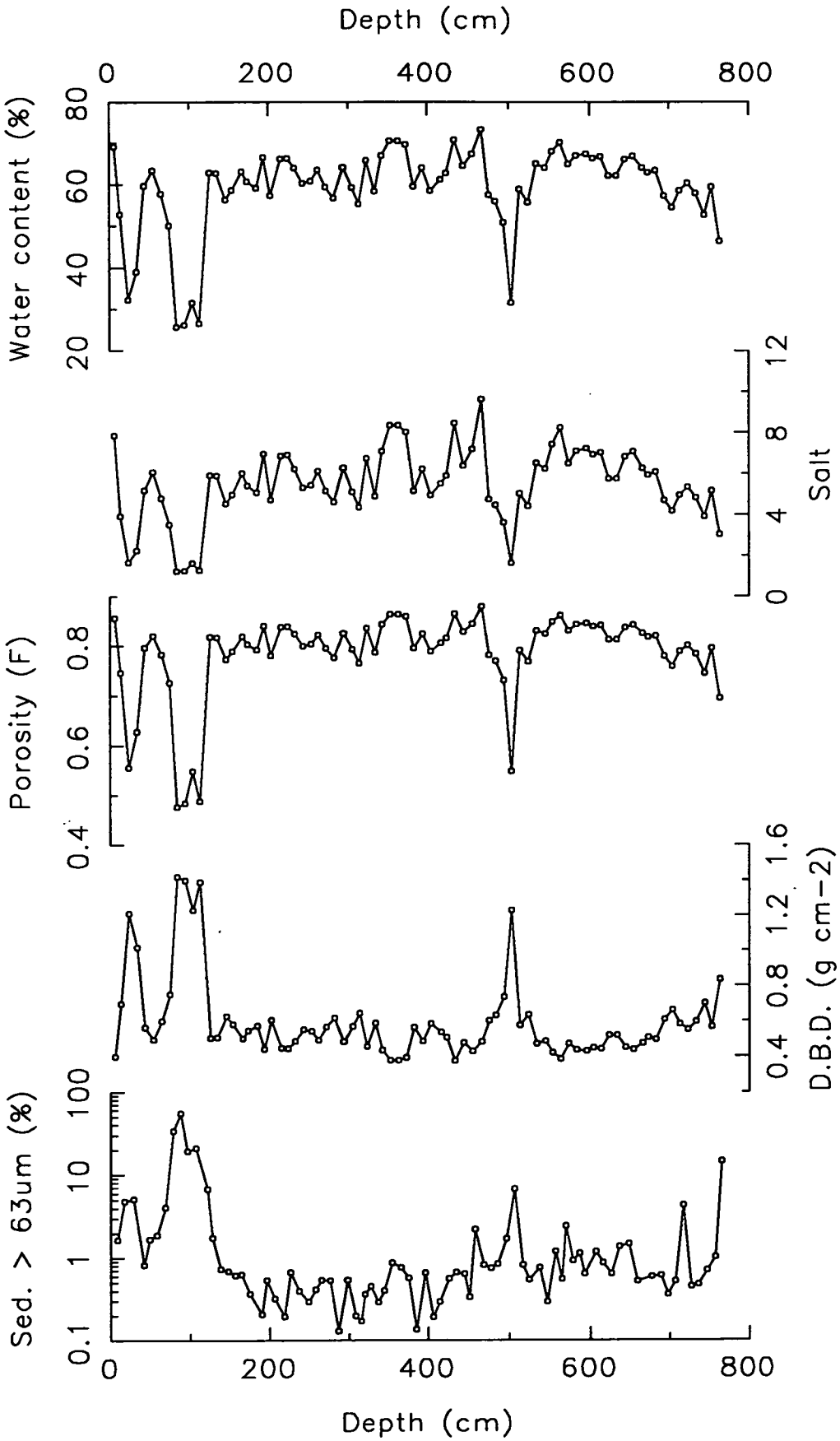


Figure 2.2. Down-core profiles of water content (%), salt content, porosity (F), dry bulk density (g $cm^{-2}$) and sediment > 63μm (%) against depth (cm) for core CD38-10 (257m).

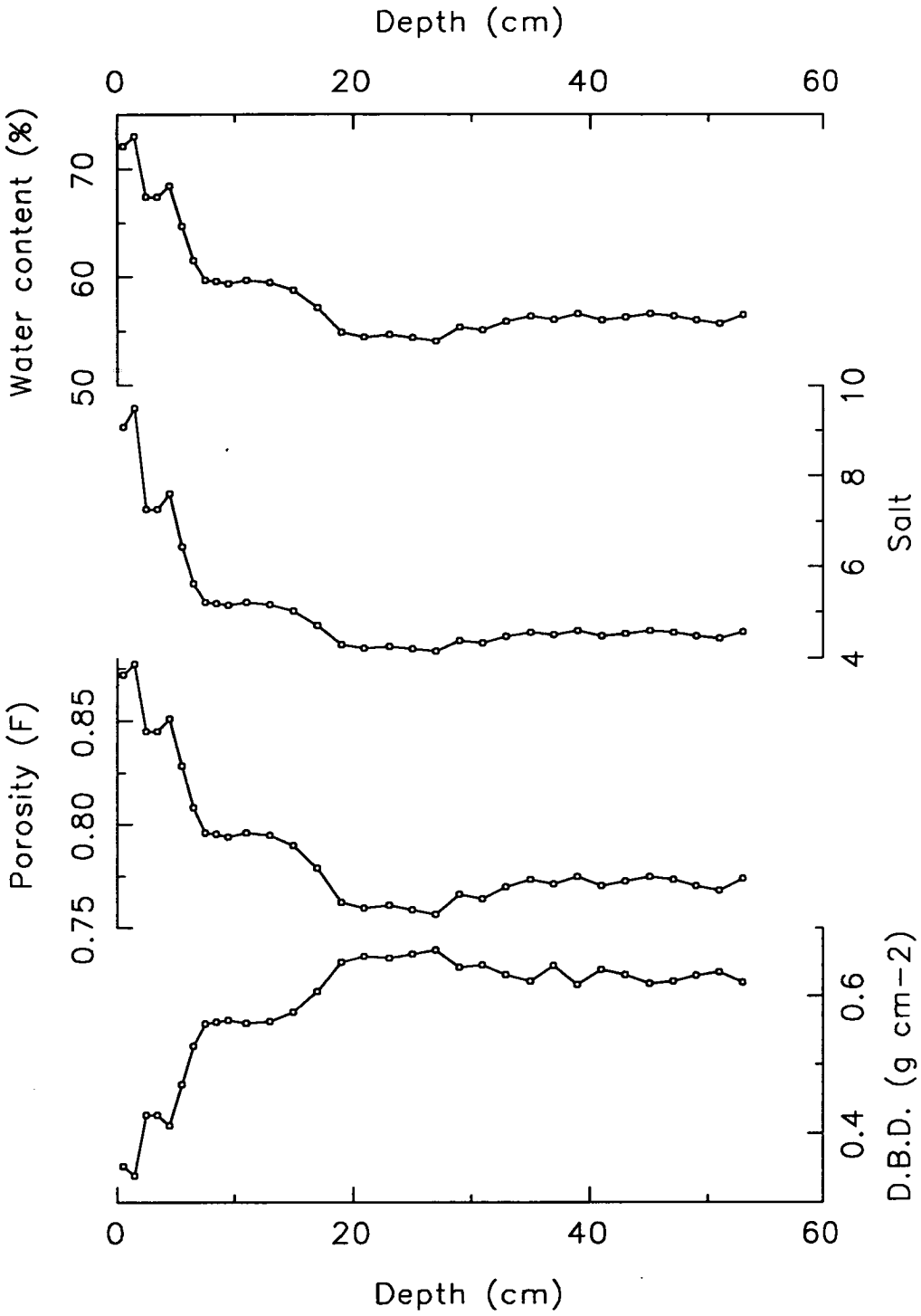


Figure 2.3. Down-core profiles of water content (%), salt content, porosity (F) and dry bulk density (g $cm^{-2}$) against depth (cm) for box core CD38-02 (2530m).

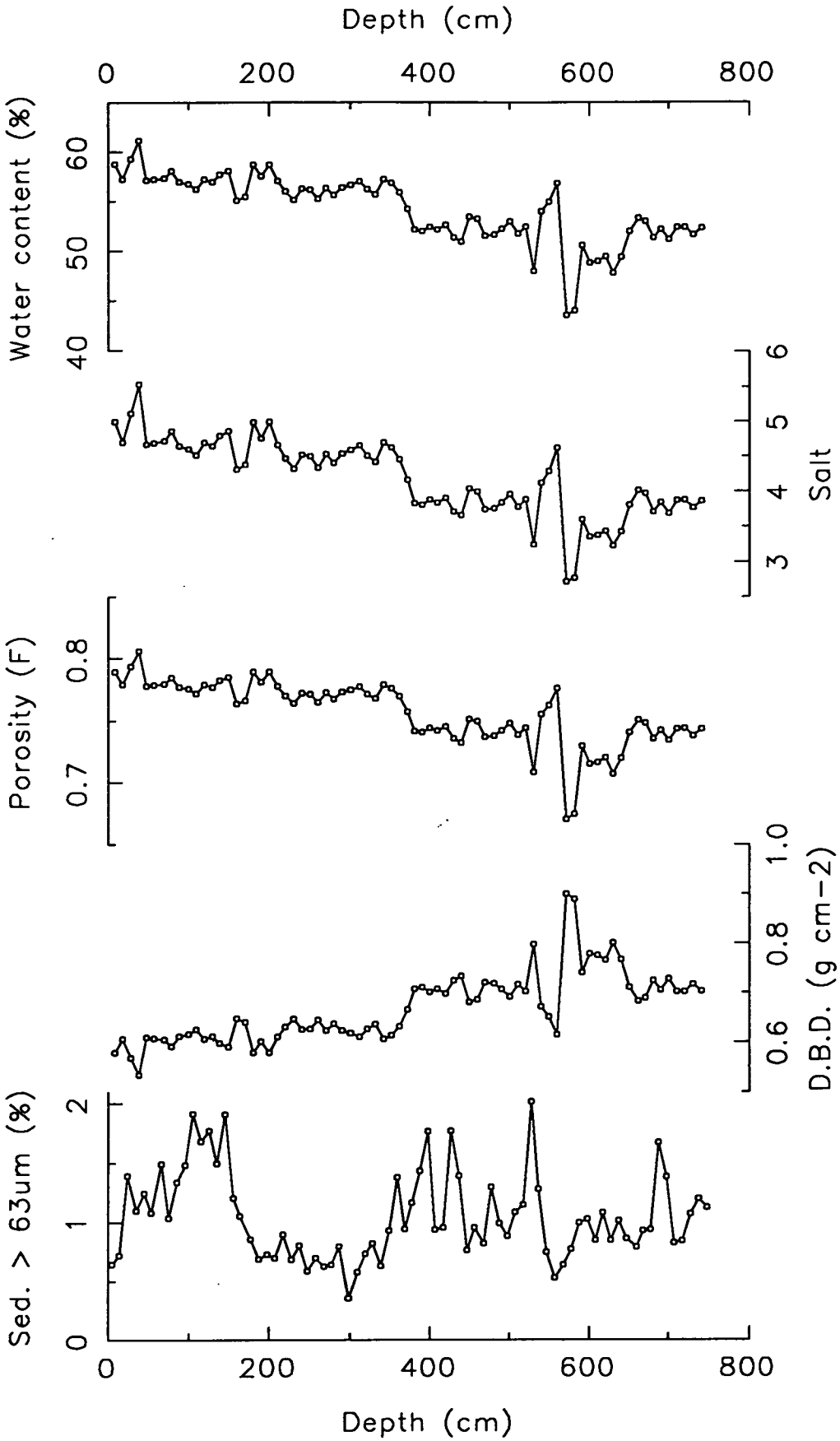


Figure 2.4. Down-core profiles of water content (%), salt content, porosity (F), dry bulk density (g $cm^{-2}$) and sediment > 63μm (%) against depth (cm) for piston core CD38-02 (2525m).

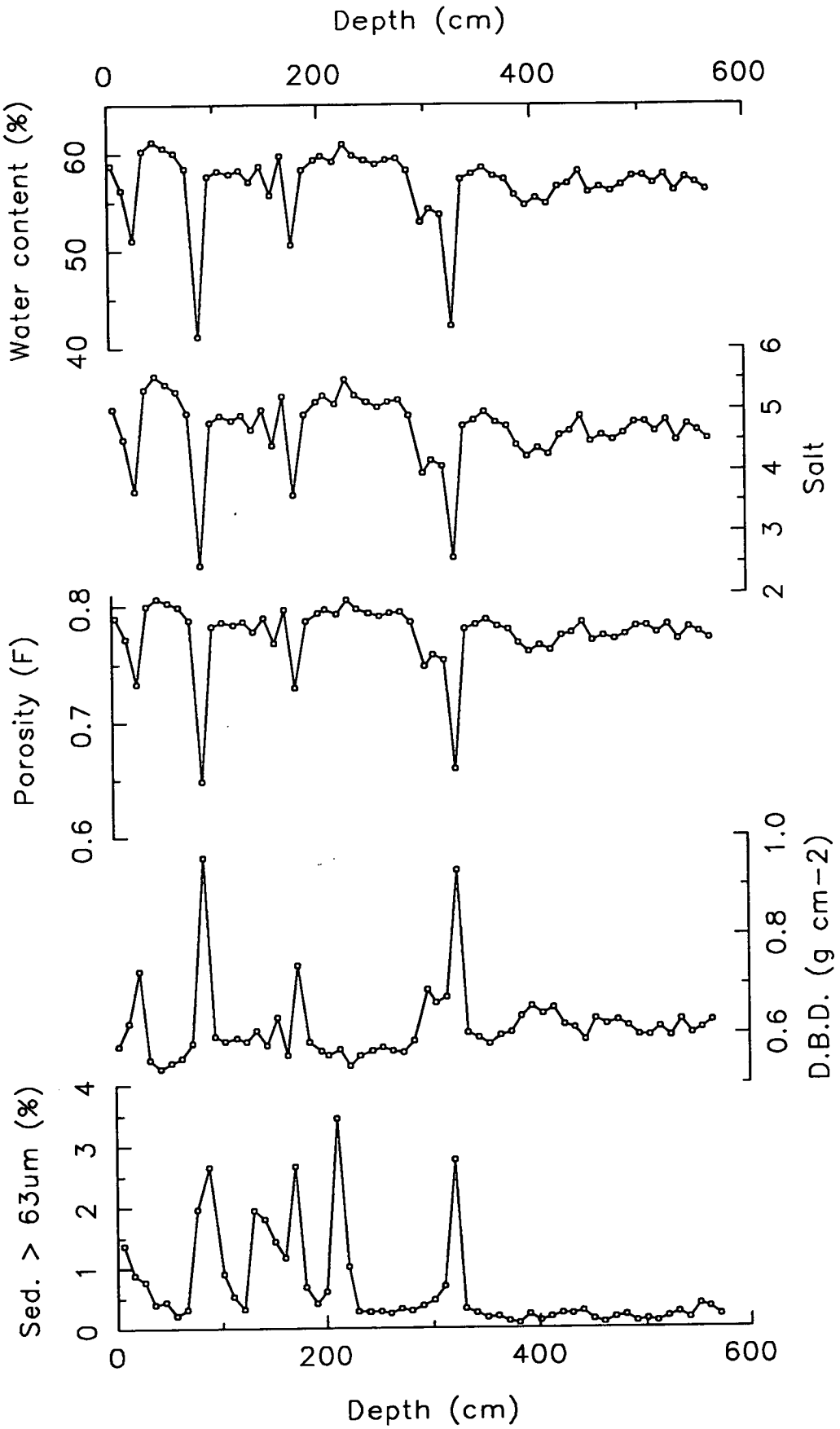


Figure 2.5. Down-core profiles of water content (%), salt content, porosity (F), dry bulk density (g $cm^{-2}$) and sediment > 63μm (%) against depth (cm) for core CD38-11 (3835m).

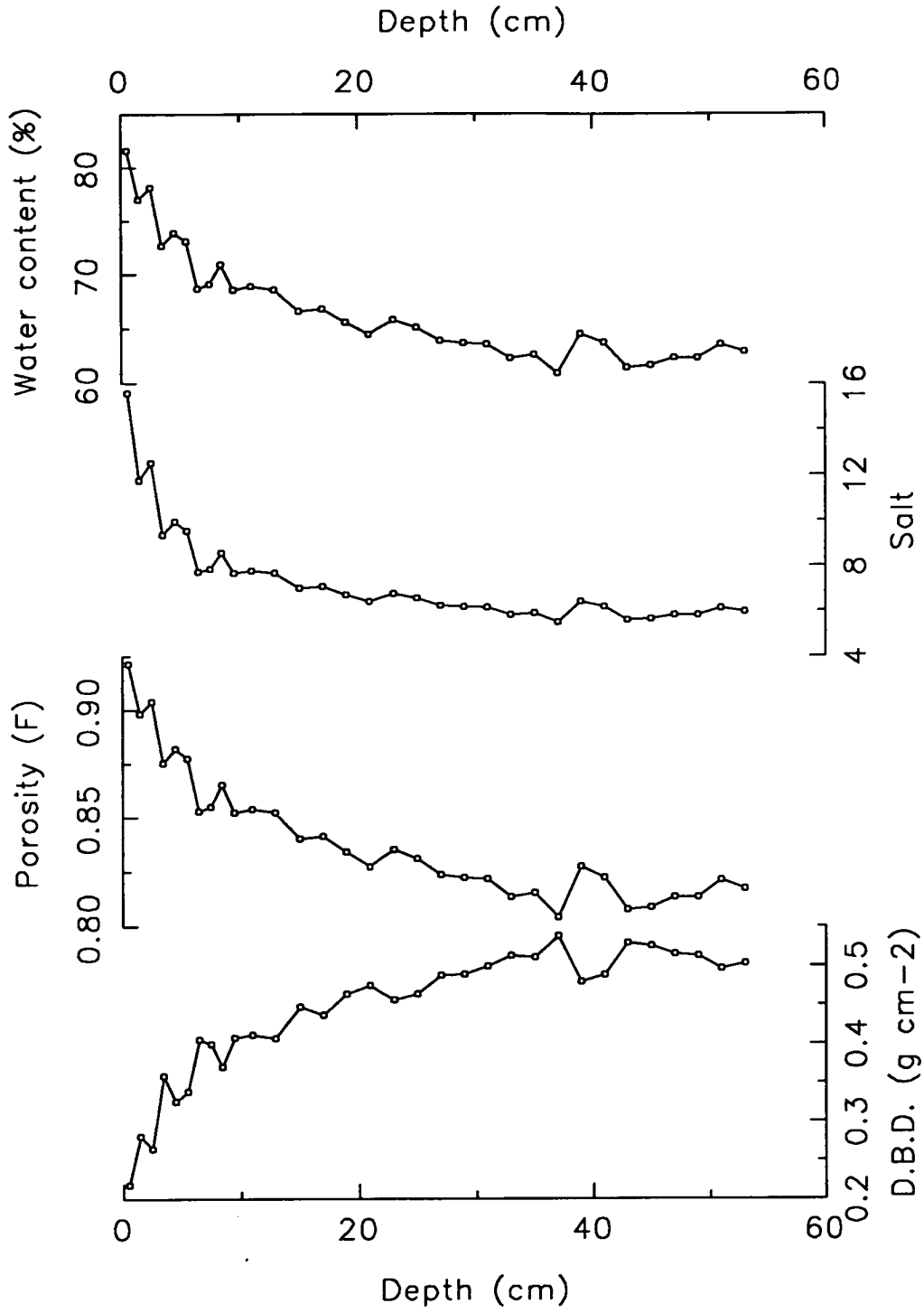


Figure 2.6. Down-core profiles of water content (%), salt content, porosity (F) and dry bulk density (g $cm^{-2}$) against depth (cm) for box core CD38-03 (4289m).

very fine-grained sediments with high organic carbon contents. The profiles of CD38-09 and CD38-10 both show a few anomalous zones of low (< 40%) water content which can be interpreted as horizons, either where the sediment has been compacted more than usual, or where the sediment is coarser-grained and therefore contains less pore space. It will be seen later (Chapter 4) that these zones are of great interest in terms of authigenic mineral growth.

Cores CD38-02 and CD38-11 (Figs 2.4 and 2.5) which are from greater water depths, have water contents which are less than 60%. This possibly indicates that these cores have a lower organic carbon content and/or have a slower sediment accumulation rate compared with cores CD38-09 and CD38-10. The profile of core CD38-02 does, in fact, display a pattern of decreasing water content with depth but it is distorted by regions of steady-state decrease (e.g. 200-240cm and 340-380cm) followed by regions of fairly stable water content (e.g. 240-340cm and 380-510cm). There is also an anomalous increase then sharp decrease of water content in the 540-580cm region. Such a profile may be the result of either variation in concentration of a particular sediment component (e.g. carbonate or clays) which controls the porosity of the sediment, or variation in the sediment accumulation rate. Core CD38-11 has a relatively flat and stable water content profile but, like CD38-09 and CD38-10, it has a number of anomalously low water content regions.

From a geochemical and analytical point of view, the importance of water content measurements is that, by assuming a constant salinity of the pore-waters and using Eqn 2.2, the salt content of each dried bulk-sediment sample can be calculated. The salt content is required for the correction of all geochemical data to allow the true "salt-corrected" concentrations to be calculated (Appendix A.6).

Equation 2.2. Salt content calculation

$$Salt = (3.513 \times W) / (100 - W)$$

where, W = water content (% Wet wt.).

Figures 2.1 through to 2.6 display the salt content for each core but since this is, in effect, just a recalculation of the water content data, the salt down-core profiles have exactly the same trend as the water content profiles and therefore are not discussed in detail.

Another physical property which can be calculated (Eqn 2.3) directly from the wet and dry weight data is the porosity of the sediment. This is a measure of the total sediment volume that is pore space and its pattern of down-core variation on the Peru margin is again very similar to the water content depth profiles (Figs. 2.1 to 2.6). The values of porosity given in this study are expressed as a fraction of the total sediment volume and the average porosity calculated (0.8-0.9) corresponds well to the % porosity (79-86%) measured by Busch and Keller (1981) for marine sediments from the upper slope mud lens and Peru slope.

Equation 2.3. Calculation of porosity

$$\text{Porosity (F)} = (\text{Water wt.} / 1.025) / [(\text{Dry wt.} / 2.7) + (\text{Water wt.} / 1.025)]$$

where, 2.7 = mean solid-phase sediment density,
1.025 = mean sea-water density.

In order to express the down-core variation of any particular geochemical component as a flux to the sediment (g $cm^{-2}$ $kyr^{-1}$) instead of a simple concentration in the sediment (wt.%) it is necessary to know the dry bulk density (D.B.D.) of each sample. This can be calculated from knowledge of the wet and dry weights of each sample using Eqn 2.4.

Equation 2.4. Dry bulk density calculation

$$\text{D.B.D. (g cm}^{-2}) = \text{Dry wt.} / [(\text{Dry wt.} / 2.7) + (\text{Water wt.} / 1.025)]$$

where, 2.7 = mean solid-phase sediment density,
1.025 = mean sea-water density.

Figures 2.1 through to 2.6 illustrate the fact that the dry bulk density and the water content of each core are inversely related. The zones in cores CD38-09, CD38-10 and CD38-11 (Figs. 2.1, 2.2 and 2.5) where the water contents dropped below 40% have dry bulk densities greater than 1.0g $cm^{-2}$ which implies that these are regions where the fine-grained, organic-rich sediment (D.B.D. = 0.5-0.6g $cm^{-2}$) has been replaced by coarser-grained sediment of a denser nature. The box cores CD38-02 and CD38-03 (Figs. 2.3 and 2.6) show steady-state exponential increases in D.B.D. with depth, as the buried sediment becomes compacted.

### 2.2.2. Grain-size measurement

The final physical property, whose profiles for the four piston cores are displayed in Figs 2.1, 2.2, 2.4 and 2.5, is a grain-size measurement of the percentage of sediment > 63μm. This was measured by sieving during the preparation of the sieved-sediment samples which were used for foraminifera picking (Appendix A.2). The sample depths for the > 63μm fraction measurement are slightly different from the other physical measurements in section 2.2.1, but it is immediately apparent from the down-core profiles that the % sediment > 63μm and the D.B.D. are correlated.* The zones of anomalously high D.B.D. correspond to the peaks (> 3%) in the amount of sediment > 63μm, especially in cores CD38-09 and CD38-10. This confirms the hypothesis that these are coarse-grained horizons within the cores (and not errors in the measurement of the water content).

Apart from these anomalous zones, the average amount of sediment > 63μm is only about 1% of the total (wet) weight and this indicates that the sediment accumulating on the Peruvian continental margin is very fine-grained and probably consists mainly of terrigenous, detrital clay particles (Busch and Keller, 1981; Reimers and Suess, 1983).

Core CD38-02 does not contain any large peaks in grain-size (Fig. 2.4) but has a down-core profile which is consistently below 2% sediment > 63μm. This core displays a pattern of regions where the amount of sediment > 63μm is either above 1% (e.g. 30-150cm and 350-540cm) or below 1% (e.g. 180-330cm and 550-680cm). This pattern illustrates that the Nazca ridge site has been affected by variation of a particular sediment component which, when present in higher than normal concentrations, can increase the grain-size of the overall sediment above that of fine-grained clays. It will be shown in Chapter 7 that the component whose concentration varies significantly with time, and thereby controls the grain-size pattern of core CD38-02, is the calcium carbonate shell-remains of marine zooplankton (7.3.3).

*It is important to note that in Figs. 2.1 and 2.2 the % sediment > 63μm is displayed as a log scale compared with a normal scale in Figs. 2.4 and 2.5.

## 2.3. AGE MODELS USING OXYGEN ISOTOPE STRATIGRAPHY

### 2.3.1. Introduction

Defining an age model for the sediments contained within the four piston cores in this study is of utmost importance, so that the historical record of various geochemical signals can be interpreted. One commonly used method of stratigraphy in the field of marine palæo-studies is foraminifera oxygen isotope stratigraphy. The following is a short explanation of the theory behind its use as a dating tool and more thorough evaluations of its accuracy and reliability can be found in the references cited below, particularly in Patience and Kroon (1991).

The fundamental processes involved in oxygen isotopic fractionation in the oceans are the evaporation and precipitation of water in the natural hydrological cycle. Of the two oxygen isotopes that are of interest, the lighter one, $^{16}O$, is preferentially evaporated at low latitudes compared with the heavier one, $^{18}O$. During precipitation and atmospheric movement of water towards the high latitudes, $^{18}O$ is preferentially precipitated first leaving behind a concentration of $^{16}O$. This $^{16}O$-enriched water is then precipitated at high latitudes and incorporated into ice-sheets. This means that during the glacial periods of the Quaternary, when ice-sheets were much larger than at present, the oceans became enriched in $^{18}O$ compared with the present ocean $^{18}O/^{16}O$ ratio.

The $CaCO_3$ which is precipitated from sea-water to form the calcareous shells of marine organisms, especially the zooplankton group of foraminifera, records these changes in the oxygen isotope ratio of the oceans during glacial/interglacial periodicity, because it is in approximate isotopic equilibrium with the surrounding sea-water at the time of formation. Other factors, such as water temperature and species vital effects, can distort the oxygen isotopic signal and these are summarised in Patience and Kroon (1991).

Upon death of the living organism, the carbonate shell of a foraminifera will fall to the sea-floor and, if it survives dissolution (7.3.3), will be buried in the accumulating sediment to provide an historical record of the ocean isotope signal, giving an indication of the global glacial/interglacial conditions at the time of its precipitation. It is because of the global synchroneity of the oxygen isotopic changes in foraminifera shells that this method of stratigraphy allows for a high resolution, correlative chronology in marine sediment cores from throughout the world's oceans (Imbrie *et al.*, 1984).

Using the above rationale, a stratigraphy of the Pleistocene was developed by Emiliani (1955), who subdivided the foraminifera oxygen isotope record into "stages" to establish a standard nomenclature. The $^{18}O/^{16}O$ ratio of a sample was expressed relative to the $^{18}O/^{16}O$ of a fixed standard ($\delta^{18}O$, Eqn A.2.2) and the negative isotopic excursions (i.e. lighter - less $^{18}O$ compared with $^{16}O$) of the interglacial stages were designated odd numbers (starting with 1 to represent the present interglacial stage) and the positive isotopic excursions (i.e. heavier - more $^{18}O$ compared with $^{16}O$) of the glacial stages were given even numbers (Emiliani, 1955). More recently, a direct link between the climatic effects on isotopic variations and the Earth's orbital changes, explained by the Milankovitch theory, has been suggested (Emiliani and Shackleton, 1974).

Measurement of the foraminifera oxygen isotope record in cores from many sites in the world's oceans has resulted in the correlation and stacking of such records and the construction of the SPECMAP age model (Imbrie *et al.*, 1984). By comparison of the $\delta^{18}O$ curve for the piston cores in this study with the SPECMAP reference $\delta^{18}O$ curve and using the stage boundary ages of Martinson *et al.* (1987), it may be possible to create age models for cores CD38-09, CD38-10, CD38-02 and CD38-11 which designate particular sediment depth horizons in each core to particular glacial or interglacial periods.

### 2.3.2. Methods and results of foraminifera stable isotope analysis

Foraminifera samples were picked from sieved-sediment samples (> 63μm) for cores CD38-09, CD38-10, CD38-02 and CD38-11. The oxygen ($\delta^{18}O$) and carbon ($\delta^{13}C$) isotopic composition of the carbonate shells was then analysed using mass spectrometry at the Scottish Universities Research and Reactor Centre (Appendix A.2). Benthic foraminifera were used because these were found to be consistently more abundant than the planktonic foraminifera, especially in the two shallow-water cores.

For cores CD38-09 and CD38-10 the species *Bolivina seminuda* was analysed but because of the low carbonate content of these cores, it was impossible in some regions of the core to pick enough of these very light (approx. 3μg, Heinze and Wefer, 1992) foraminifera and so there are gaps in the oxygen and carbon isotope records. For cores CD38-02 and CD38-11 specimens of the genus *Uvigerina* were picked and analysed. The results of all the isotopic determinations can be found in Appendix C.2.

Figures 2.7 and 2.8 display the $\delta^{18}O$ and $\delta^{13}C$ isotopic records respectively for the four piston cores. These profiles highlight the isotopic differences between the two infaunal groups of foraminifera, *Uvigerina* and *B. seminuda*, which are the result of species-vital effects (Corliss and Chen, 1988; McCorkle *et al.*, 1990). The down-core profiles show that for core CD38-09 the isotope record is incomplete and the signal is very erratic. This is due to the fact that large areas of the core contained very low concentrations of foraminifera shells and even in the samples from which *B. seminuda* were picked and analysed there were not enough specimens to run duplicate samples where necessary. It is therefore impossible to make any sensible interpretations of the oxygen isotope stratigraphy of core CD38-09.

Although the oxygen isotope record of core CD38-10 (Fig. 2.7) looks fairly continuous, there is a problem in interpreting the $\delta^{18}O$ signal in terms of designating specific glacial or interglacial periods. As will be discussed in full in Chapter 4, there is a large zone between 80 and 110cm which represents a period of sediment erosion (and possibly another zone lies at about 500cm). This means that the sedimentation history at this shallow-water site has been non-continuous and it is impossible to accurately state how much of the sediment column has been lost by erosion. It may be interpreted, for example, that the region in core CD38-10 from 500 to 550cm represents an interglacial period (more negative $\delta^{18}O$) and that below 600cm to the base of the core represents a glacial stage (more positive $\delta^{18}O$). However, because it is unknown how much sediment has been lost in the upper metres of the core, it is impossible to decide whether the above regions represent stages 5 and 6 respectively or stages 7 and 8 or are perhaps even older in age. For this reason core CD38-10 cannot be used for oxygen isotope age modelling.

Throughout the rest of this thesis, cores CD38-09 and CD38-10 will always have their down-core profiles plotted against depth (cm) instead of age (ka). It should be mentioned at this point that the ODP hole 680B, which is situated very close to core CD38-10 (Chapter 1), has been dated by Heinze and Wefer (1992) using only the oxygen isotope stratigraphy of the *B. seminuda* record by comparison with the SPECMAP $\delta^{18}O$ curve of Imbrie *et al.* (1984). However, Heinze and Wefer (1992) failed to take into account the many erosion horizons (shown as phosphate zones in their Fig. 6b) which are bound to distort their simple age model. It is for this reason that the $\delta^{18}O$ curve of core CD38-10 (Fig. 2.7) has not been compared with that of ODP hole 680B.

The down-core profiles of the oxygen isotope ratio ($\delta^{18}O$) shown in Fig. 2.7 for cores CD38-02 and CD38-11 do show a continuous and varying pattern associated with the Late Quaternary glacial/interglacial changes of the $\delta^{18}O$ ratio in sea-water

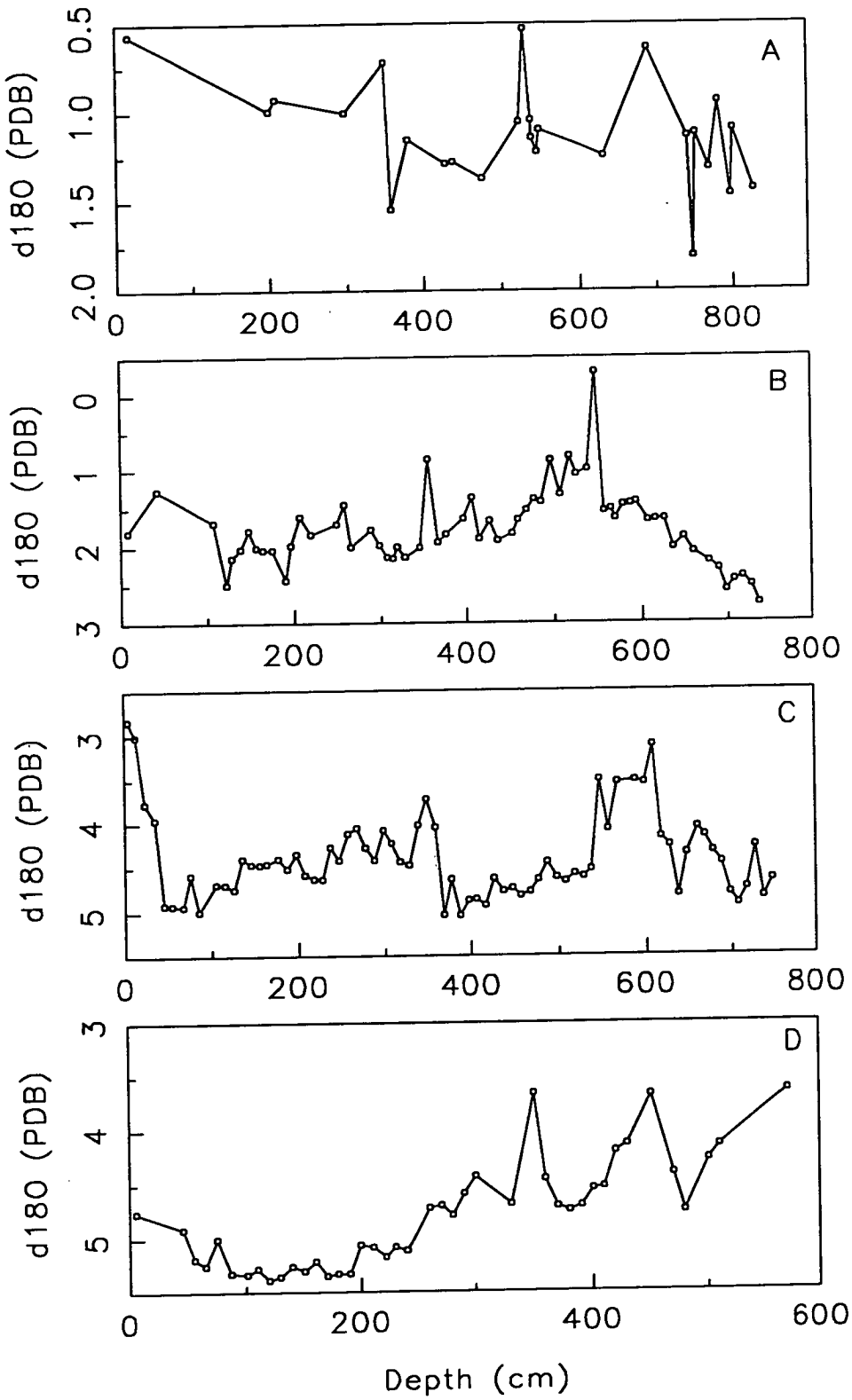


Figure 2.7. Oxygen isotopic composition of foraminifera (expressed as $\delta^{18}O$ ‰ relative to PDB standard) against depth (cm); A) CD38-09 and B) CD38-10 using *Bolivina seminuda*, C) CD38-02 and D) CD38-11 using *Uvigerina*.

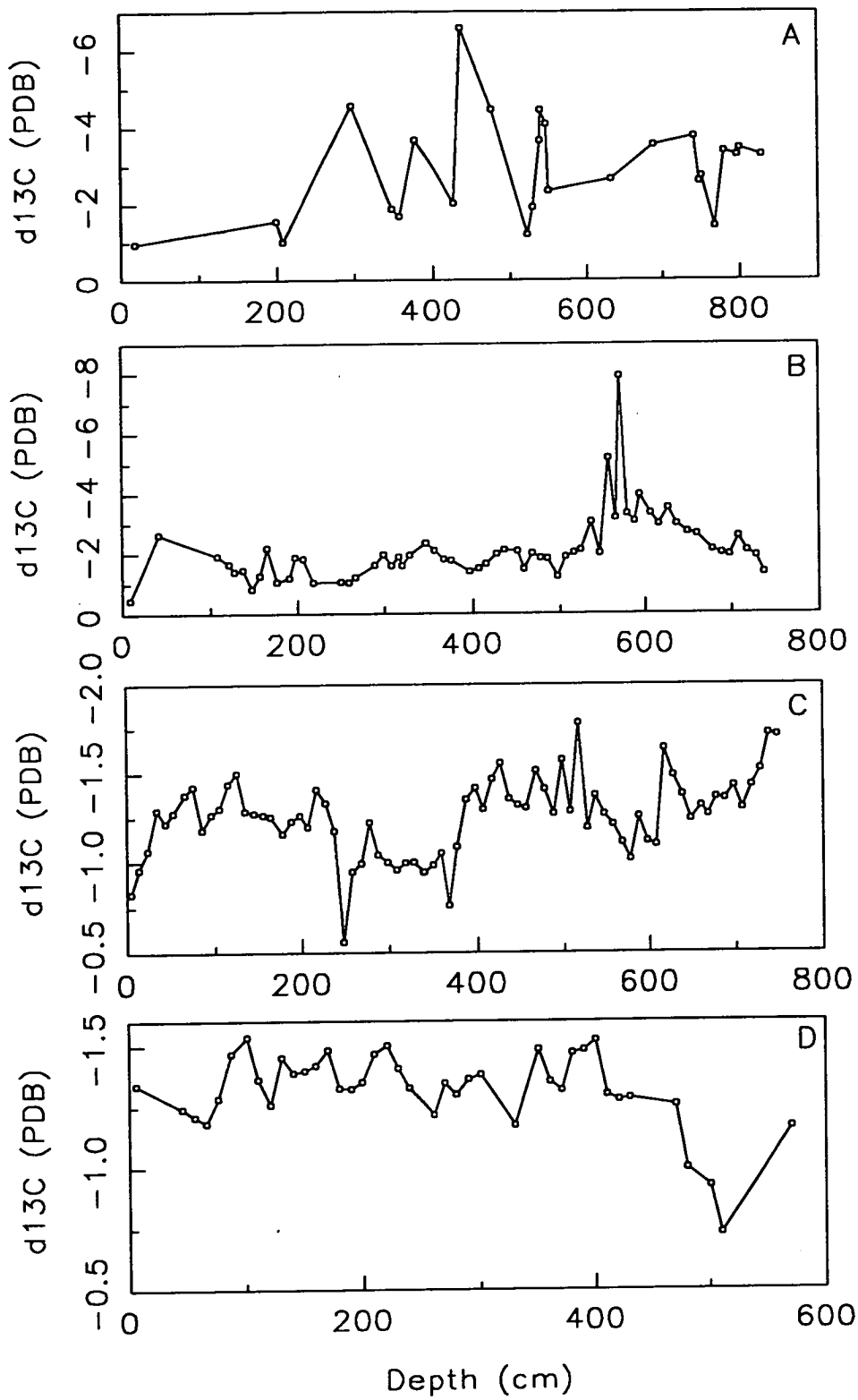


Figure 2.8. Carbon isotopic composition of foraminifera (expressed as $\delta^{13}C$ ‰ relative to PDB standard) against depth (cm); A) CD38-09 and B) CD38-10 using *Bolivina seminuda*, C) CD38-02 and D) CD38-11 using *Uvigerina*.

(Imbrie *et al.*, 1984). The only region where there is a significant gap is in core CD38-11 between 4 and 24cm, which is thought to be a turbidite deposit (6.2.2) and contains few foraminifera shells.

It is important to note that the profiles in Fig. 2.7 are plotted with the $\delta^{18}O$ axis reading from isotopically heavier $\delta^{18}O$ values at the bottom up to isotopically lighter $\delta^{18}O$ values at the top. This is to allow for easy comparison with the stacked SPECMAP $\delta^{18}O$ curve as shown in Fig. 8 of Imbrie *et al.* (1984) and with the plots of Ba/Al for the Peruvian piston cores (6.3.2, Fig. 6.8).

Along with the oxygen isotopic measurements made by mass spectrometry of foraminifera, the two isotopes of carbon, $^{12}C$ and $^{13}C$, are also measured (Appendix A.2) and from these results a carbon isotopic signal, $\delta^{13}C$, can be plotted for each core (Fig. 2.8). As with oxygen isotopes, foraminifera microfossils can record the $\delta^{13}C$ ratio of the surrounding water (bottom-water, in the case of benthic foraminifera) in their carbonate shells. According to Berger and Vincent (1986), long-period signals reflect global fractionation of carbon isotopes (which changes with respect to the changes in the carbon reservoir in the oceans) whereas short-term variations are due to regional and internal factors (water-mass circulation, organism-specific vital effects and/or ocean temperature gradients). Carbon isotopes are difficult to use for stratigraphic interpretations and will not be discussed in detail in this thesis. More detailed work on foraminifera carbon isotopes in these cores is being carried out by S. King at the University of Southampton (1.5). The only interesting feature of the $\delta^{13}C$ profiles (Fig. 2.8) is that in cores CD38-02 and CD38-11 variation tends to mirror the $\delta^{18}O$ signal (Fig. 2.7). However, this inverse relationship between $\delta^{13}C$ and $\delta^{18}O$, as was seen by Dunbar and Wefer (1984) in Peru margin core tops, is not apparent in core CD38-10 where the $\delta^{13}C$ and $\delta^{18}O$ curves seem to run parallel.

The contrast in the dynamic range of down-core $\delta^{13}C$ values between cores CD38-09 and CD38-10 (about 8 ‰) and cores CD38-02 and CD38-11 (only 1.5 ‰) can be explained either by species vital-effect differences between *B. seminuda* and *Uvigerina* respectively (McCorkle *et al.*, 1990) or by the fact that the down-core variation in the former cores is a result of diagenetic overprinting. Whereas in the latter cores it is a result of fluctuations in the chemical composition of the bottom-water masses which varies due to changes in the pattern of water mass circulation during glacial/interglacial periodicity.

### 2.3.3. Comparison of the $\delta^{18}O$ curves for cores CD38-02 and CD38-11 with the SPECMAP record

The method employed for generating an age model for cores CD38-02 and CD38-11 simply involves direct comparison of the peaks and troughs in the $\delta^{18}O$ curve (Fig. 2.7) with those of the SPECMAP record (Imbrie *et al.*, 1984). There is a noticeable scale difference in the $\delta^{18}O$ signal between the two Peruvian cores and the SPECMAP record which is caused by the compositional differences between benthic foraminifera in the former cores and planktonic foraminifera in the latter. Control points were designated in both cores which corresponded to the calculated ages of the SPECMAP $\delta^{18}O$ curve and these are summarised in Table 2.1.

| SPECMAP age (ka) | Stage | CD38-02 (cm) | CD38-11 (cm) | SPECMAP age (ka) | Stage | CD38-02 (cm) |
|---|---|---|---|---|---|---|
| 12.0 | 1 | 35 | 66 | 152.0 | 6 | 388 |
| 18.0 | 2 | 67 | 88 | 170.0 | 6 | 488 |
| 24.5 | 3 | 86 | 121 | 195.0 | 7a | 547 |
| 54.0 | 3 | 198 | 261 | 216.0 | 7c | 608 |
| 64.0 | 4 | 228 | 331 | 238.0 | 7e | 660 |
| 80.0 | 5a | 268 | 351 | 250.0 | 8 | 708 |
| 86.0 | 5b | 288 | 381 | 258.0 | 8 | 728 |
| 100.0 | 5c | 299 | 451 | 266.0 | 8 | 748* |
| 110.0 | 5d | 329 | 481 | | | |
| 122.0 | 5e | 349 | 571* | | | |

Table 2.1. SPECMAP control ages (Imbrie *et al.*, 1984) and corresponding depths in core CD38-02 and CD38-11. The base of each core is indicated by *.

Between each control point, it is assumed that the sediment has accumulated at a constant sediment accumulation rate (SAR) and therefore each of the sieved-sediment subsamples can be assigned an age. Figure 2.9 displays the $\delta^{18}O$ record for cores CD38-02 and CD38-11 plotted against age (ka) along with the SPECMAP profile for comparison.

Finally, the stage boundary ages of Martinson *et al.* (1987) were used to define the depths in both cores at which the sediment changes from accumulation during a glacial period to accumulation during an interglacial period, or vice versa (Table 2.1).

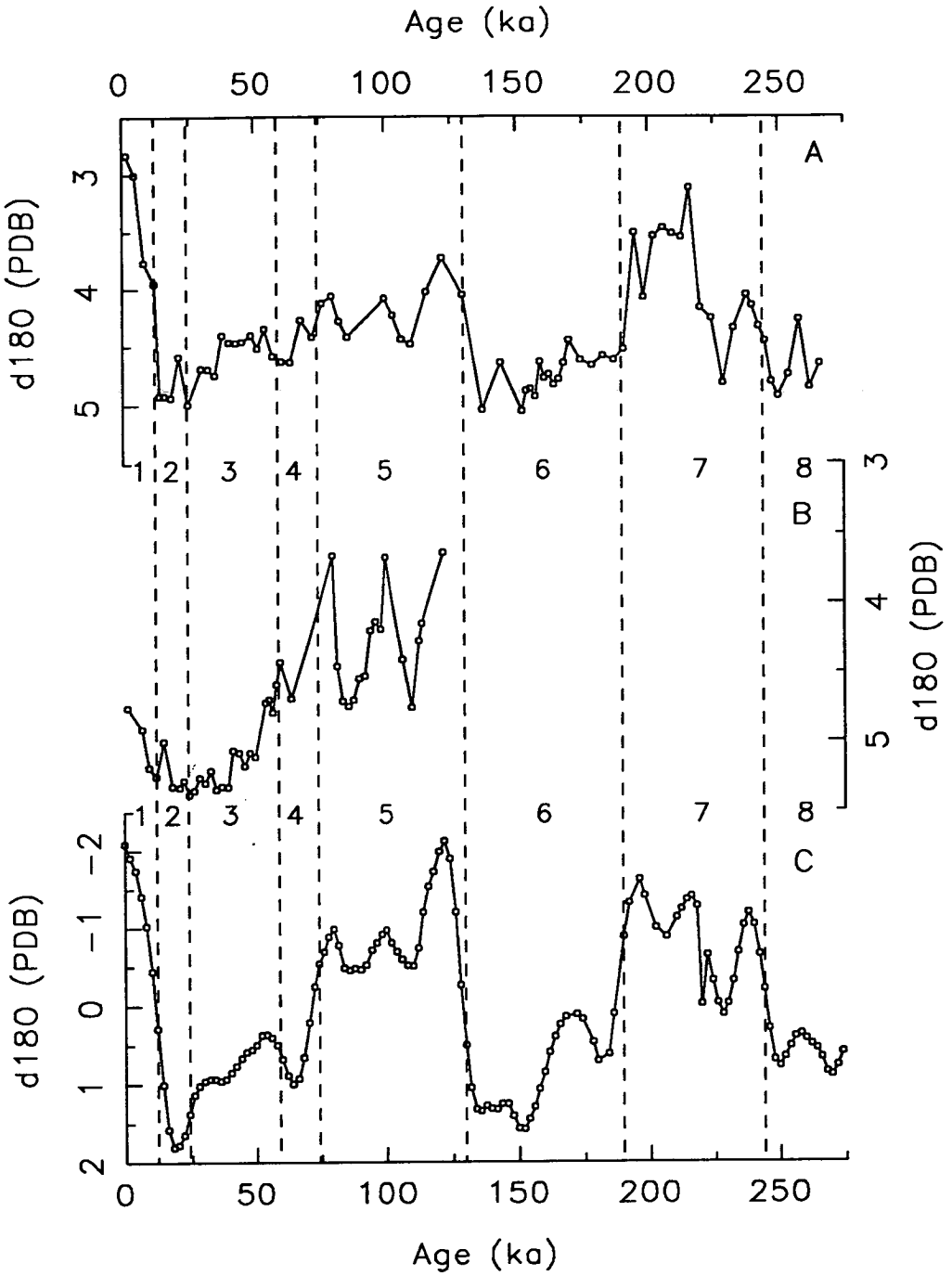


Figure 2.9. Oxygen isotopic composition of foraminifera (expressed as $\delta^{18}O$ ‰ relative to PDB standard) against age (ka); A) CD38-02 and B) CD38-11 using *Uvigerina* and C) SPECMAP planktonic reference curve (Imbrie *et al.*, 1984). Stage boundary ages from Martinson *et al.* (1987).

From this the age models, shown in Table 2.2, were constructed for cores CD38-02 and CD38-11.

| Stage | Boundary Age (ka) | **CD38-02** Depth (cm) | (2525m) SAR (cm $kyr^{-1}$) | **CD38-11** Depth (cm) | (3835m) SAR (cm $kyr^{-1}$) |
|---|---|---|---|---|---|
| 1 | | | 2.90 | | 3.73 |
| | 12.05 | 35 | | 65 | |
| 2 | | | 4.15 | | 4.56 |
| | 24.11 | 85 | | 120 | |
| 3 | | | 3.59 | | 5.02 |
| | 58.96 | 210 | | 295 | |
| 4 | | | 3.01 | | 3.01 |
| | 73.91 | 255 | | 340 | |
| 5 | | | 1.88 | | 4.80 |
| | 129.8 | 360 | | | |
| 6 | | | 2.93 | | |
| | 189.6 | 535 | | | |
| 7 | | | 2.66 | | |
| | 244.1 | 680 | | | |
| 8 | | | 3.12 | | |

Table 2.2. Age models for cores CD38-02 and CD38-11. Stage boundary ages are from Martinson *et al.* (1987). Core CD38-11 contains a 20cm turbidite zone within stage 1 and therefore the SAR = 45cm/12.05 kyr.

## 2.4. SEDIMENT ACCUMULATION RATES AND MASS ACCUMULATION RATES

### 2.4.1. Introduction

One problem that arises from carrying out a geochemical, marine sediment study using bulk-sediment samples is that the sieved-sediment samples (from which the $\delta^{18}O$ foraminifera record was obtained) and the bulk-sediment samples (from which all geochemical data are obtained) are taken from different depths down each core. The age models for cores CD38-02 and CD38-11 (Table 2.2) therefore need to be used to calculate the age of each bulk-sediment sample before the mass accumulation rate can be calculated. Sediment accumulation rate (SAR) and mass

accumulation rate (MAR) are used throughout this thesis and can be defined as follows. SAR is the depth rate at which the total sediment is accumulating (measured in cm $kyr^{-1}$) and MAR is the weight of sediment accumulating in a specific area over time (measured in g $cm^{-2}$ $kyr^{-1}$).

### 2.4.2. Description and use of age model for core CD38-02

The proposed age model for core CD38-02, which is located at a water depth of 2525m on the Nazca ridge, is summarised in Table 2.2. The core is 750cm long and corresponds to continuous sedimentation (but not at a constant SAR) from the present Holocene (stage 1) at the top of the core, back down to glacial stage 8 at the base (270ka).

The sediment accumulation rates for each stage were calculated by simply taking the depth (cm) for a particular stage (e.g. stage 5 = 360cm to 255cm = 105cm depth) and dividing by the corresponding time interval (e.g. stage 5 = 129.8ka to 73.9ka = 55.9kyr);this assumes a constant rate of sediment accumulation for each individual stage. The SARs for core CD38-02 (Table 2.2) display a pattern whereby the glacial stage (even number) SAR is greater than the interglacial stage (odd number) SAR on either side of it. The only exception to this is that stage 3 has a greater SAR than stage 4. The above SAR pattern is to be expected in a core situated on or near a continental margin because the glacial stages are periods when more arid climatic conditions affected the continent, allowing for greater weathering and erosion of the land and, in turn, increasing the terrigenous input to marine sediments (Boyle, 1983; Sarnthein *et al.*, 1988; Patience, 1992). The highest SAR in core CD38-02 is seen during stage 2 (4.15 cm $kyr^{-1}$) during which time the Last Glacial Maximum occurred. The lowest SAR occurs in stage 5 (1.88 cm $kyr^{-1}$) which is the interglacial stage when climate conditions were most similar to the present day.

Using the proposed age model for core CD38-02 the age of each bulk-sediment sample was calculated (Appendix C.3) and it is these ages that the geochemical data presented for CD38-02 are plotted against throughout the rest of this thesis (e.g. Fig. 6.4).

There is one final physical property for core CD38-02 that can be calculated and that is the mass accumulation rate (MAR). This requires knowledge of the SARs, from the proposed age model (Table 2.2), and the dry bulk density, from the measured water content (Eqn 2.4), and uses the relationship shown in Eqn 2.5.

Equation 2.5. Calculation of mass accumulation rate (MAR)

$$MAR\ (g\ cm^{-2}\ kyr^{-1}) = SAR\ (cm\ kyr^{-1}) \times D.B.D.\ (g\ cm^{-2})$$

Figure 2.10 displays both the SAR and MAR for core CD38-02 plotted against age and from the down-core profiles, the glacial/interglacial cyclicity pattern of sedimentation can be easily seen. The MAR will be used later in this thesis to examine terrigenous and biogenic fluxes to the sediment (Chapter 7).

### 2.4.3. Description and use of age model for core CD38-11

The proposed age model for core CD38-11, located at a water depth of 3835m on the lower slope of the Peruvian continental margin (Table 2.2) corresponds to continuous sedimentation (including the 20cm turbidite zone contained within stage 1) from the present Holocene back to interglacial stage 5 at the base of the core (575cm). It should be noted that the amplitude of the isotopically-light, surficial sample (i.e. most recent in age) does not match that of the samples in stage 5 (as seen in core CD38-02, Fig. 2.9) which may imply that some of the true surface sediment of core CD38-11 has been lost during the coring process (Imbrie *et al.*, 1984).

The sediment accumulation rates for each stage in this core were calculated in exactly the same manner as for core CD38-02 in the above subsection and are listed within Table 2.2. The SAR pattern for CD38-11 (Fig. 2.10) contrasts to that of CD38-02 in that the highest SAR is seen in interglacial stage 3 (5.02 cm $kyr^{-1}$) and stage 5 has a much higher SAR than stage 4 (4.80 cm $kyr^{-1}$ compared with 3.01 cm $kyr^{-1}$). The differences between the SARs of cores CD38-02 and CD38-11 are represented graphically in Fig. 2.11. From this simple plot of depth (cm) against age (ka) for both cores it can be seen that within the last few glacial/interglacial periods of the Late Quaternary, CD38-11 has continuously been a site of faster rates of sediment accumulation than the site of core CD38-02. This is due to the fact that the continental slope at site CD38-11 receives a higher input of both terrigenous material from the nearby South American landmass (7.2.3) and biogenic material from the coastal upwelling zone (7.3.3) compared with the Nazca ridge at site CD38-02.

The SAR pattern of core CD38-11 does not conform to the hypothesis (used for CD38-02) that more arid continental conditions during glacial periods will increase the terrigenous input to continental margin marine sediments. This suggests that for core CD38-11 either the stage boundary depths have been incorrectly

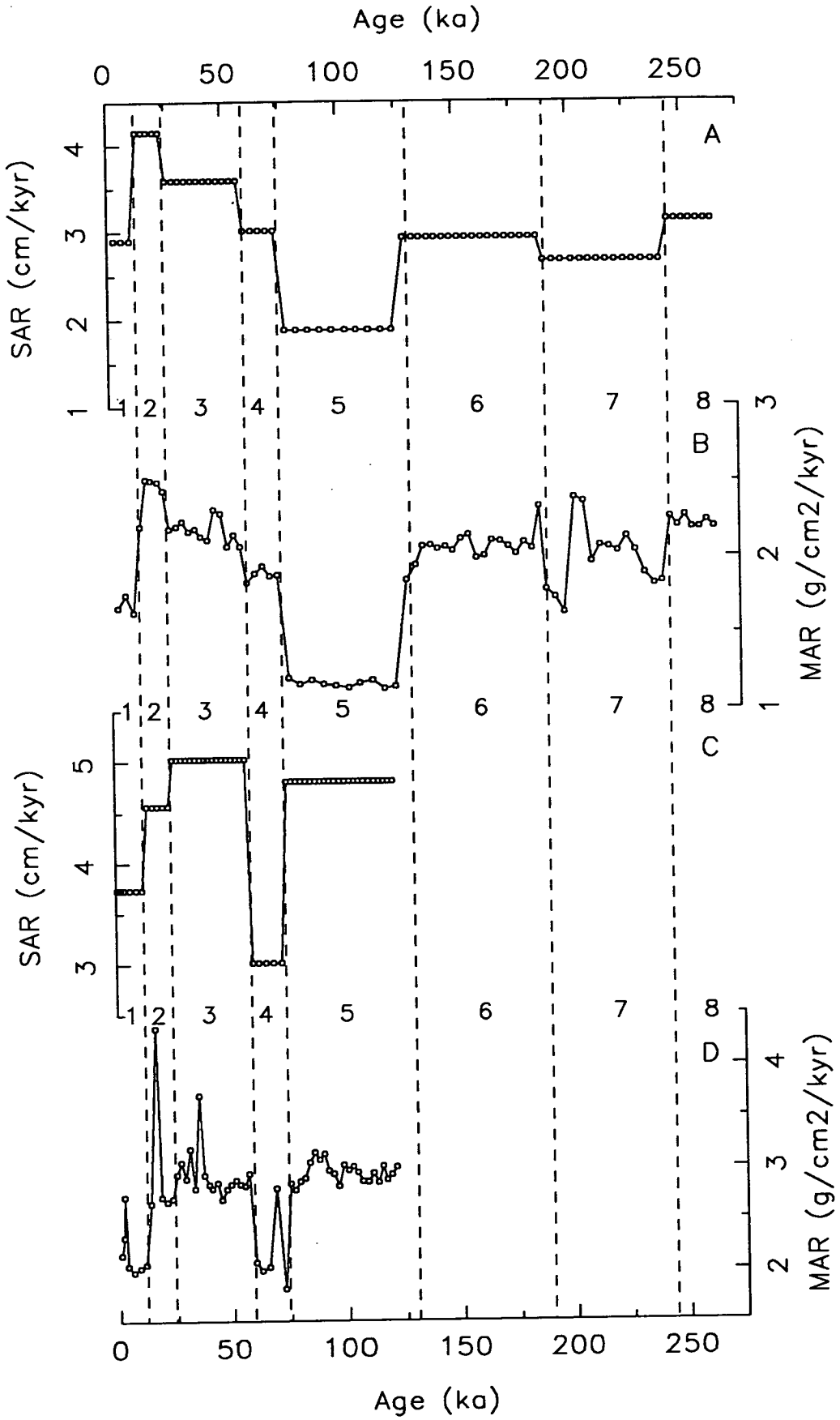


Figure 2.10. Sediment accumulation rate (cm $kyr^{-1}$) and mass accumulation rate (g $cm^{-2}$ $kyr^{-1}$) profiles against age (ka) for cores CD38-02 (A and B) and CD38-11 (C and D).

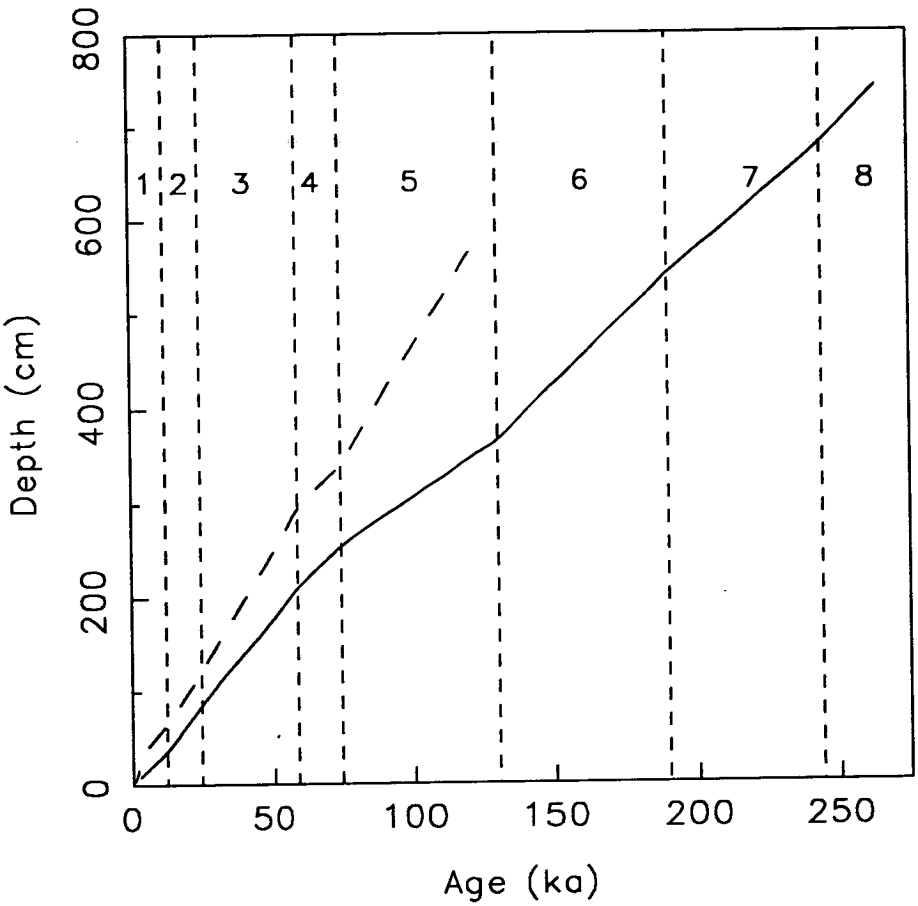


Figure 2.11. Depth (cm) against age (ka) graphic representation of the contrasting sediment accumulation rates for cores CD38-02 (full line) and CD38-11 (dotted line).

designated or, more likely, that higher interglacial biogenic input at this site (6.3.3 and 6.3.4) is controlling the SAR pattern.

The proposed age model for core CD38-11 was then used to convert the depths of each geochemical, bulk-sediment sample from depth (cm) to age (ka) and it is these ages (Appendix C.3) that the geochemical data for this core are plotted against throughout the rest of this thesis.

Finally, as for core CD38-02 above (2.4.2) the mass accumulation rate of each bulk-sediment sample in core CD38-11 was calculated using Eqn 2.5. The down-core profile of MAR for CD38-11 is displayed in Fig. 2.10 and ranges from 2 to 4.5 g $cm^{-2}$ $kyr^{-1}$. These values can then be used in the calculation of fluxes of various geochemical components.

## 2.5. CONCLUSIONS

This chapter has involved a brief study of some of the physical and geochronological properties of the marine sediments from the Peruvian continental margin. It has yielded vital information contained within the box and piston cores under study; which is needed to allow for the correct and full interpretation of the geochemical data presented in the chapters which follow.

Of most importance has been the calculation of the salt content of each sample, which is used to correct the raw geochemical data*, and the age modelling from the oxygen isotopic composition of foraminifera microfossils. It is unfortunate that the shallow water cores, CD38-09 and CD38-10, were not suitable for precise age modelling because geochemical data plotted on a time scale rather than a depth scale are generally much more meaningful in terms of the interpretation of glacial/interglacial climatic and environmental changes. However, it must be stressed again that throughout this thesis the graphic representations of all geochemical data will be plotted against age (ka) for piston cores CD38-02 and CD38-11 only, and that the other piston cores, CD38-09 and CD38-10, and the two box cores, CD38-02 and CD38-03, will be plotted against depth (cm).

---

*All geochemical data presented in the following chapters have been corrected to salt-free concentrations (Appendix A.6).

# CHAPTER 3

# THE SEDIMENT RECORD OF COASTAL UPWELLING

## 3.1. INTRODUCTION

"No waters in the ocean so teem with life as those
on the west coast of South America."

Buchanan (1886)

### 3.1.1. Physical oceanography

The physical hydrography of the Pacific Ocean off the coast of Peru is the dominant influence in determining the chemistry and biology of the near-shore waters and hence the geochemistry of the sediments accumulating below.

Surface winds controlled by the Earth's weather system, move around high pressure cells over the oceans (clockwise in the northern hemisphere and anti-clockwise in the southern) and therefore the western coastlines of the continental land masses experience prevailing winds which sweep along-shore and toward the equator (Fig. 3.1).

The Coriolis force of these winds deflects the oceanic surface waters (upper 20-30m, Brink *et al.*, 1983; Smith, 1983) off-shore, in a direction determined by the Earth's rotation and the forces of internal fluid friction; a physical process named after the Swedish oceanographer, Vagn Ekman. The angle of deflection, which is about 45° at the surface, increases with depth but the force of the current decreases (Ekman, 1905). This Ekman transport forces colder water from depth (between 70 and 133m, Gunther, 1936; Zuta *et al.*, 1978) to move upward and replace the warmer surface waters (Fig. 3.2). It is this process which is known as **coastal upwelling**.

There are five important oceanic sites where coastal upwelling has been reported to be occurring at present (Diester-Haass, 1978; Hartline, 1980; Thiede and Suess, 1983). These are off Peru-Chile and Oregon-California in the Pacific, off north-west Africa and south-west Africa (Namibia) in the Atlantic and off Somalia-Oman in the Indian Ocean (Fig. 3.1). The latter is at an eastern continental margin rather than the more usual western margin, where upwelling is induced by the southwest monsoon.

Upwelling also occurs along the equatorial and southern divergence zones and, although these too are important areas in the world's oceans, they will not be discussed further in this thesis.

The simple two dimensional model described above is useful to explain the basic concept of coastal upwelling but the actual process is vastly complicated by

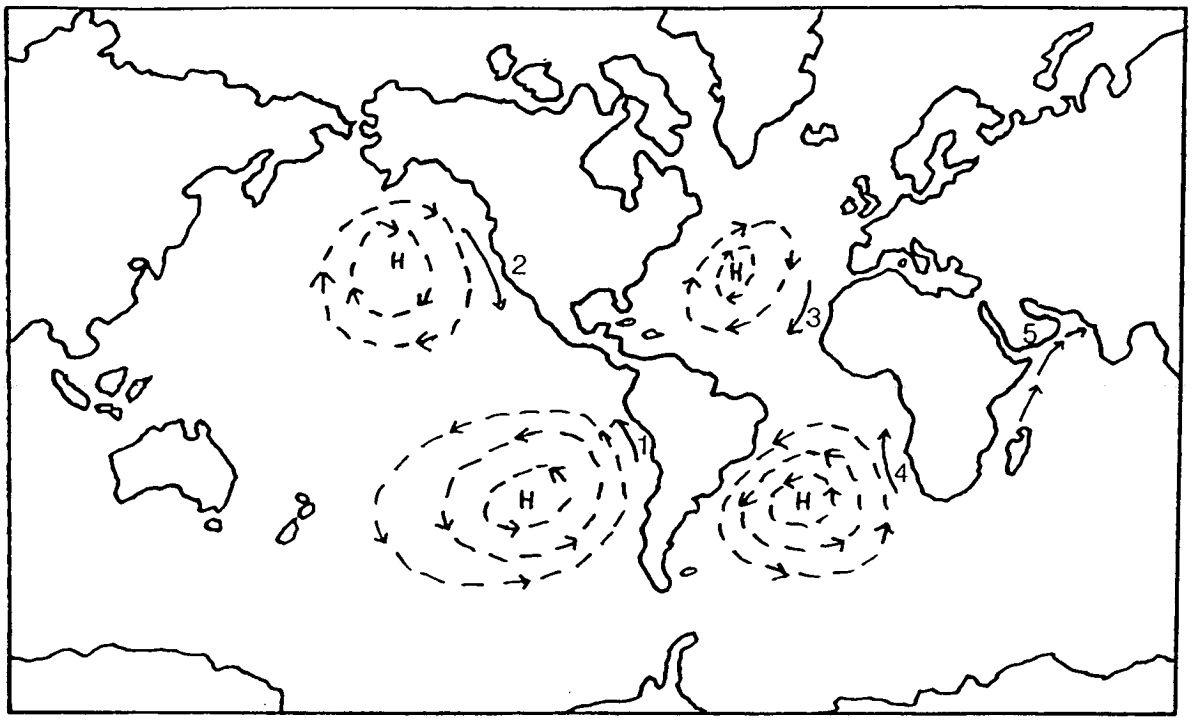


Figure 3.1. World map showing the major zones of coastal upwelling and the wind systems which drive them (adapted from Hartline, 1980).

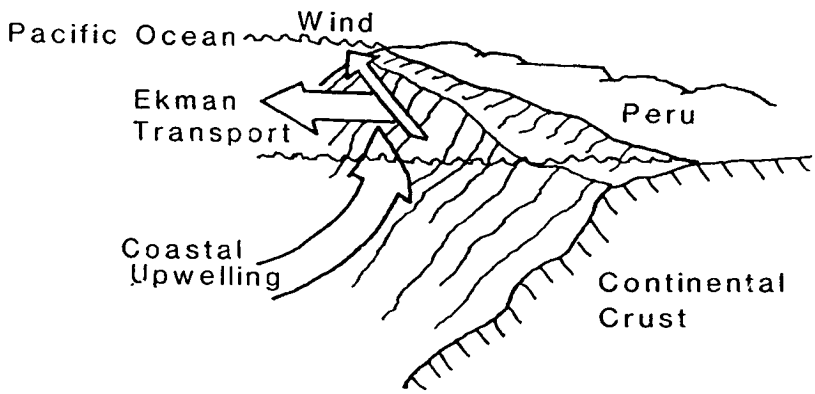


Figure 3.2. Diagram of the processes involved in coastal upwelling . Along-shore wind stress forces off-shore Ekman transport of the surface water, which is replaced by upwelling of deeper water.

three dimensional sea-floor topography and coastal geometry (Hurlburt, 1974) and by ocean currents and wind fields which can vary both temporally and spatially.

Coastal upwelling off the Peru-Chile continental margin is intense and persistent, and has operated since at least the late Miocene (Schrader, 1992). However, large seasonal and latitudinal variations in the strength of modern-day upwelling have been measured (Zuta *et al.*, 1978). The prevailing wind is the southeasterly trade wind which was measured at 15°S as having a mean direction of 163±16° and speed of 4.6ms$^{-1}$ (Burt *et al.*, 1973). Sea surface temperature mapping in the area highlights the upwelling of colder water near-shore (approx. 17°C compared with 20-23°C off-shore) and cold patches indicate zones of intense upwelling within the large-scale area of coastal upwelling (between 5 and 20°S). Measurement of seasonal variation shows that these temperatures reduce to a minimum from June to October (the southern hemisphere's winter and spring) which coincides with the strongest winds and most intense upwelling period (Zuta *et al.*, 1978).

The actual size of the coastal upwelling zone at the Peru-Chile margin and the volume of upwelled water can vary depending on the parameters used to measure these quantities. Busch and Keller (1983) quote a distance of 50km off-shore within which coastal upwelling occurs off Peru north of 20°S. Barber and Smith (1981) limited the off-shore dimension of upwelling to the Rossby radius of deformation, a function of the Coriolis force, which varies latitudinally from 270km at 4°S down to 60km at 18°S. This distance can then be used to calculate an upwelling area of 1.82 x $10^{11}$ m$^2$ (Chavez and Barber, 1987). However, Smith (1983) gives a Rossby radius of only 20km which would substantially reduce the calculated area of the Peruvian upwelling zone. Estimations of the upward flow of water across the 100m water depth level are about $10^4$ m$^3$ year$^{-1}$ (Wyrtki, 1963) for any point along the coastal region from 6 to 24°S.

Coastal upwelling is not the only water movement that occurs in this area of the Pacific Ocean. The main current on the continental margin, which flows opposite in direction to the surface waters, is the Peru poleward undercurrent (Smith, 1983; Huyer *et al.*, 1991). Brockmann *et al.* (1980) measured this current along the Peru coast from 5 to 15°S at various water depths and concluded that the maximum poleward flow was at about 100m and that it was stronger and more persistent to the north. A study of undercurrent variability by Huyer *et al.* (1991) at 10°S found a well-defined core at 150m, where the (100 day) mean speed was 0.1ms$^{-1}$ with a maximum of 0.25ms$^{-1}$. It is this undercurrent which supplies the water for upwelling along the

continental margin (Fig. 3.3.).

### 3.1.2. Nutrients, biomass and organic matter flux

Sea-water contains many dissolved chemical components, some of which are required by marine phytoplankton (microscopic plants) for their growth within the euphotic zone (the surface waters which receive enough sunlight for photosynthesis to occur). These nutrients, principally the silicate, nitrate and phosphate anions, soon get depleted and unless the supplies are replenished, the phytoplankton community will die off. It is because the cold, upwelled water brings with it a fresh supply of nutrients, to replace the nutrient-depleted water pushed off-shore, that coastal upwelling zones are important sites for high and sustainable levels of primary productivity. It should be noted that the relationships between upwelling intensity, euphotic zone nutrient concentrations and biological primary productivity are non-linear (Codispoti, 1983).

Measurements of primary productivity have been published from many studies off Peru and the range of 1.24-6.26 g C $m^{-2}$ $day^{-1}$ (Ryther, 1969; Chavez and Barber, 1987) is over an order of magnitude greater than normal ocean surface waters (0.1-0.2 g C $m^{-2}$ $day^{-1}$; Henrichs and Farrington, 1984). Figure 3.4 illustrates this feature as a high productivity belt along the Peru margin. Conversion of mean primary productivity estimations to a total carbon weight utilised in photosynthesis over the entire coastal zone, gives a value of 1.52 x $10^{14}$ g C $year^{-1}$ (Chavez and Barber, 1987). Brink *et al.* (1983) measured the mixed layer depth off Peru as less than 20m, shallower than the photic zone, and concluded that productivity was not light-limited; this implies nutrient-limitation.

Diatoms are dominant in the phytoplankton community off Peru (De Mendiola, 1981) with a maximum number measured in shallow water stations at 9°S of 195 million cells $m^{-3}$ (Semina, 1971). This is at least 10,000 times greater than the average for ocean surface waters.

The marine phytoplankton are eaten by zooplankton, which in turn are eaten by fish and other marine animals. This results in a greatly enhanced food chain and the coastal waters therefore "teem with life". In fact, the fish stock of the southern anchovy (*Engraulis ringens*) along the Peruvian coast is so high that the anchovy fishery is one of the world's largest (Ryther, 1969; Walsh, 1975 and 1981; Hartline, 1980). The proportion of fish that are not caught and consumed by humans, die along with the rest of the marine biomass, and sink through the water column. Most of this

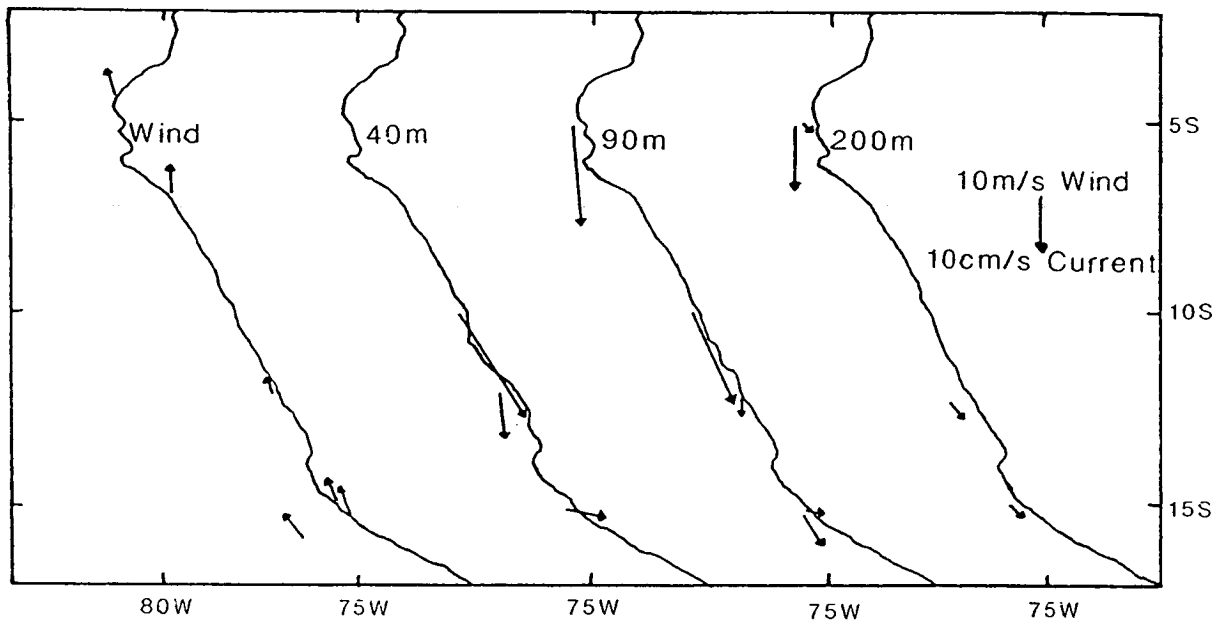


Figure 3.3. Wind and current vectors, at 40, 90 and 200m, along the Peru coast (adapted from Brockmann *et al.*, 1980) illustrating the equatorward wind direction and the poleward undercurrent.

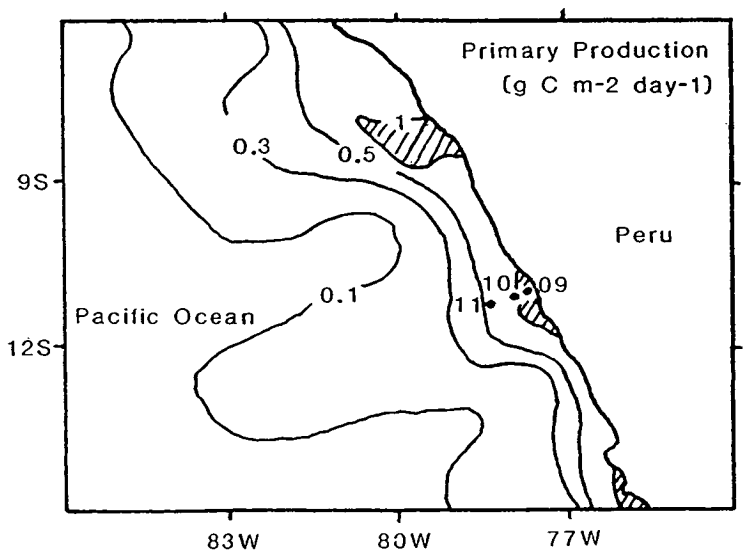


Figure 3.4. Primary productivity (g C $m^{-2}$ $day^{-1}$) map of the Peru coastal upwelling zone. Note the position of core sites CD38–09, CD38–10 and CD38–11 (adapted from Suess *et al.*, 1988).

organic matter is either eaten by other marine organisms or undergoes bacterial decomposition (Baturin, 1982; Henrichs and Farrington, 1984) and there is therefore a recycling of the important nutrients, which are released and dissolved back into the water.

The overall coastal water circulation pattern actually helps to recycle both the nutrients and any phytoplankton communities in a conveyor-belt-like system. Movement off-shore and equatorward by Ekman transport is followed by sinking out of the surface layer. Then the poleward undercurrent acts as the lower part of the conveyor-belt and moves the water back to the zone where upwelling occurs (Brink *et al.*, 1983). This recycling is important in maintaining intense biological productivity in certain centres throughout the Peruvian upwelling margin.

Baturin (1982) stated that only about 0.5% of organic matter does not decompose before deposition in the accumulating sediment but more recent work using sediment traps by Martin *et al.* (1987) as part of the VERTEX experiment, measured the organic carbon flux as it decreases with depth and calculated the increasing percentage regeneration of organic matter down the water column. More than 50% of the original organic matter will still be present at water depths < 300m but by the time the organic matter has sunk to the deep ocean (3000-5000m) less than 5% will remain (Martin *et al.*, 1987). Therefore, the flux of organic matter to the sediment under a zone of coastal upwelling will be much greater than in the open ocean because (a) the surface productivity is greatly enhanced and (b) the water depth to the continental shelf and slope is comparatively shallow.

The data set used by Martin *et al.* (1987) uses the 100m sediment trap as the starting flux, indicative of "new production" sinking down below the euphotic zone. Henrichs and Farrington (1984) however, used sediment traps off Peru at 50m water depth and measured the average downward particulate organic carbon flux as 250mg C $m^{-2}$ $day^{-1}$, which was only 6% of the surface primary productivity. The enhanced marine biomass in coastal upwelling areas is, as expected, utilising most of the organic matter whilst it is still in the euphotic zone. Therefore, the new production of organic carbon [which Martin *et al.* (1987) based their cumulative regeneration calculations on] is at least 1/20th of the total primary productivity in an upwelling zone such as off Peru.

### 3.1.3. Sediment characteristics

The proportion of organic matter which escapes decomposition and recycling

within the water column, will reach the sea-floor and be incorporated in the accumulating sediments (Baturin, 1982). Organic carbon ($C_{org}$) rich sediments found on a continental shelf or slope are, therefore, a good indication of accumulation under an upwelling zone (Diester-Haass, 1978; Calvert, 1987). Calvert and Price (1970) measured concentrations up to 26 wt.% $C_{org}$ in muddy sediments off Walvis Bay, S.W.Africa, and a study of the spatial patterns of accumulation of organic matter on the Peru margin (Reimers and Suess, 1983A) showed two maxima areas with levels >10 wt.% $C_{org}$ located within the upper slope muds between 11 and 14°S. Busch and Keller (1981) concluded that it was the high organic matter content on the Peru slope that strongly affected the physical properties of the sediment. The mud lens sediments, with up to 20 wt.% $C_{org}$, were anomalously fine-grained with high water content and plasticity and low grain specific gravity.

An oxygen-minimum zone (OMZ) is an area within the water column where the dissolved oxygen levels are reduced below 0.2 ml $l^{-1}$ by the respiration of bottom water zooplankton and bacteria as they decompose the rain of organic matter falling through the water column. Under the Peruvian upwelling system, an OMZ lies between 100 and 500m and where this meets the continental slope the sediments accumulate under suboxic to anoxic conditions (Veeh et al., 1973; Burnett *et al.*, 1980). This impingement of the OMZ was originally thought to enhance the preservation of organic matter within the sediments (Müller and Suess, 1979; Demaison et al., 1984). However, this view is not taken by Calvert (1987) and Pedersen et al. (1992) who saw no relationship between the strong OMZ off Oman and well-preserved organic matter in the sediments below. Calvert and Pedersen (1992) have suggested that it is the settling flux of organic matter, dependant on the surface productivity, that controls the accumulation of organic-rich marine sediments. The preservation versus productivity question will be dealt with in more detail in Chapter 7.

Organic matter is not the only biological product of coastal upwelling which can be incorporated into the sediment record. There are the hard skeletons and shells of marine dwellers and also their waste products.

The frustules of diatoms and radiolarians (marine plankton) are composed of silica (biogenic $SiO_2$), and their burial in the sediment removes the important silicate nutrient from ocean waters. DeMaster (1981) reports that the highest biogenic silica accumulation rates in the marine environment are under coastal upwelling zones (69 g $SiO_2$ $cm^{-2}$ $ky^{-1}$). Calvert and Price (1970) measured up to 85 wt.% biogenic silica in

S.W.African sediments and diatom assemblages have been used as coastal upwelling indicators off Portugal (Abrantes, 1988) and Peru (Schrader and Sorknes, 1991).

The calcium carbonate shells of foraminifera and coccoliths are another main biological component of marine sediments. The foraminifera tests have been used in a great number of studies (e.g. Thiede, 1975; Ganssen and Sarnthein, 1983; Wefer *et al.*, 1983; Dunbar and Wefer, 1984; Hermelin and Shimmield, 1990; McCorkle *et al.*, 1990) using both planktonic/benthic species variations and stable isotope chemistry to understand the coastal upwelling environment, both spatially and temporally.*

Fish debris and faecal pellets are also commonly found in continental margin sediments (Busch and Keller, 1981). Fish bones and scales have been observed in shallow-water sediments from the Peru upwelling region (Frankenberg and Menzies, 1968; Ssaidova, 1971; DeVries and Pearcy, 1982). Faecal pellets are important for the rapid transport of fine-grained clay particles (Scheidegger and Krissek, 1982), diatoms (Schrader, 1971) and trace metals and radionuclides (Osterberg *et al.*, 1963) onto the continental slope.

Geochemical study of the sediments accumulating on the continental margin off Peru should indicate the presence of the above biological components and illustrate any variations in the strength of coastal upwelling in the area through time.

## 3.2 ANALYSES AND RESULTS

### 3.2.1. Analytical procedures

The analytical methods used in determining the geochemical parameters described below are detailed in Appendix A. Organic carbon ($C_{org}$) was measured by combustion after acid digestion of carbonate carbon (Appendix A.3), biogenic silica analysis used colorimetric spectrophotometry of silica and alumina in solution after sodium carbonate leaching (Appendix A.4) and the trace elements were measured by X-ray fluorescence of pressed pellets (Appendix A.5). All analyses were carried out on the dried bulk sediment samples (Appendix A.1). The method of calculation of calcium carbonate ($CaCO_3$) levels is detailed in Appendix B.1.

---

*The influence of dissolution within the water column for both diatoms and forams is discussed in 7.3.3.

### 3.2.2. Results

The complete salt-corrected data sets for $C_{org}$, biogenic silica, $CaCO_3$ and the metals Mo, U, Ni, Cr, V and Cu are listed in Appendices C.10 and C.12. Table 3.1 summarises the data set, giving the range, mean and standard deviation of values for the two shallow water cores, CD38-09 and CD38-10, and gives deep-sea clay values (representative of more normal marine sediments; Turekian and Wedepohl, 1961) for comparison. There is a marked enrichment of the above biogenic indicators for both the near-shore core stations from those found in normal marine sediments, caused by the influence of coastal upwelling and increased biological productivity. The $C_{org}$ mean concentration of 4-5 wt.% for the two near-shore cores is an order of magnitude higher than normal ocean sediments. It should be noted that large, dynamic ranges in metal concentrations are possible under these natural, non-anthropogenic conditions.

| | **CD38-09** | | | | **CD38-10** | | | | **Clay** |
|---|---|---|---|---|---|---|---|---|---|
| | Min. | Max. | Mean | S.D. | Min. | Max | Mean | S.D. | Mean |
| Corg | 1.6 | 8.3 | 4.4 | 1.45 | 0.8 | 11.9 | 5.4 | 2.02 | |
| Bio.Sil | 3.1 | 25.8 | 15.4 | 4.58 | 0.5 | 28.6 | 13.4 | 6.11 | |
| CaCO3 | 0 | 6.6 | 3.4 | 1.71 | 0 | 26.4 | 8.9 | 6.03 | |
| Mo | 13 | 99 | 52 | 18.4 | 11 | 129 | 57 | 25.6 | 27 |
| U | 4 | 148 | 9 | 16.3 | 206 | 27 | 13 | 4.0 | 1.3 |
| Ni | 28 | 85 | 51 | 15.1 | 20 | 165 | 69 | 22.4 | 225 |
| Cr | 57 | 150 | 111 | 19.3 | 46 | 182 | 105 | 22.4 | 90 |
| V | 63 | 156 | 119 | 15.5 | 46 | 363 | 147 | 60.2 | 120 |
| Cu | 9 | 51 | 27 | 6.6 | 7 | 49 | 28 | 7.8 | 250 |

Table 3.1. Biogenic component and organo-metallic element concentrations. Values for $C_{org}$, Bio.Sil and $CaCO_3$ are in wt.%, all others are in ppm. Deep-sea clay values from Turekian and Wedepohl (1961).

Depth profiles of the three biogenic components are shown in Figs 3.5 and 3.6 and illustrate the time-varying input to the sediment possibly associated with natural fluctuations in the biological system in the water column above.

In core CD38-09, the $C_{org}$ concentration between 300 and 500cm averages about 6 wt.%, but drops to about 3wt.% below 550cm (Fig. 3.5). The three biogenic components in core CD38-10 seem to increase from a minimum at the base of the core up to about 550cm, before dropping to another minimum at 510cm (Fig. 3.6).

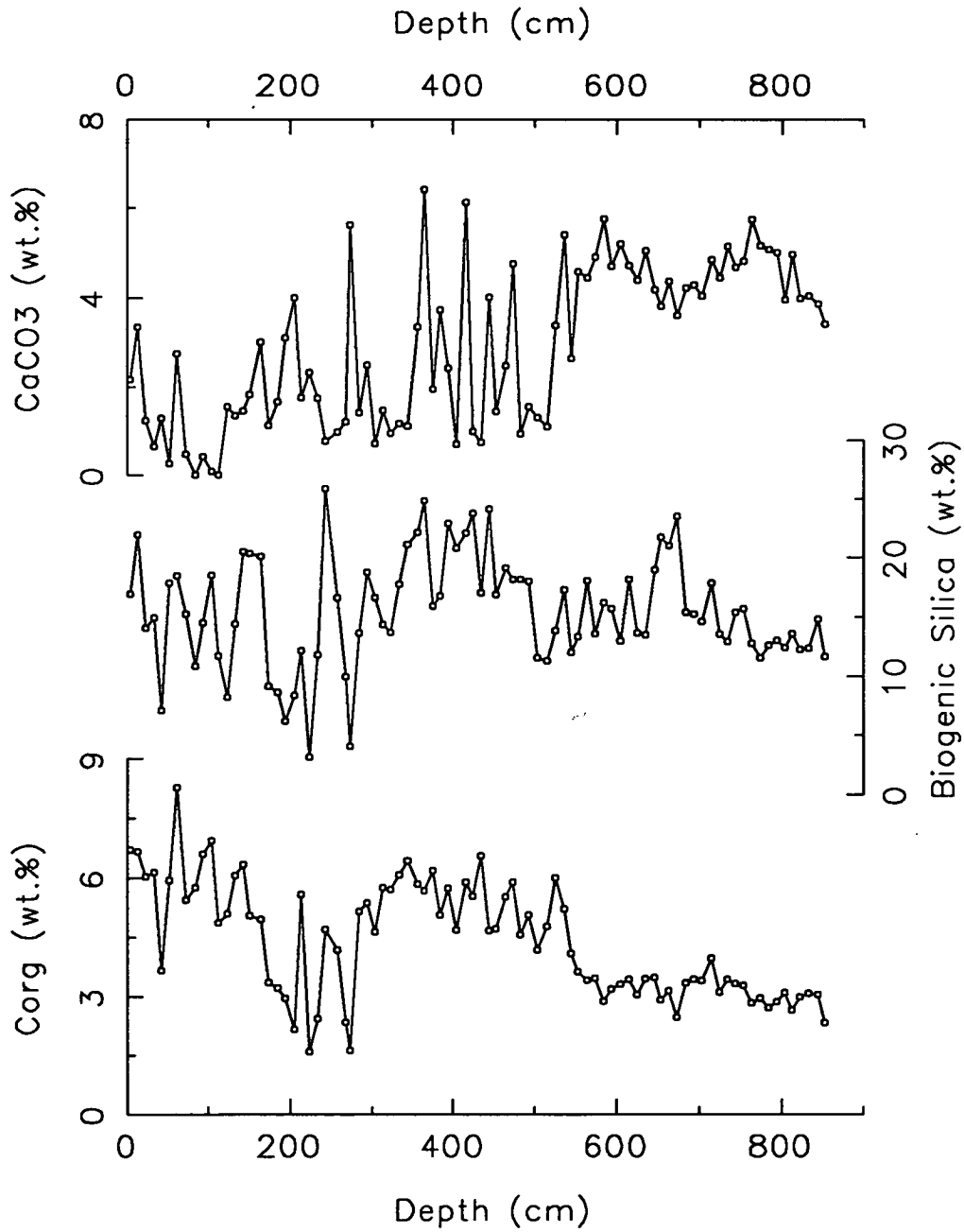


Figure 3.5. Biogenic components ($C_{org}$, biogenic silica and $CaCO_3$) against depth for core CD38-09 (148m).

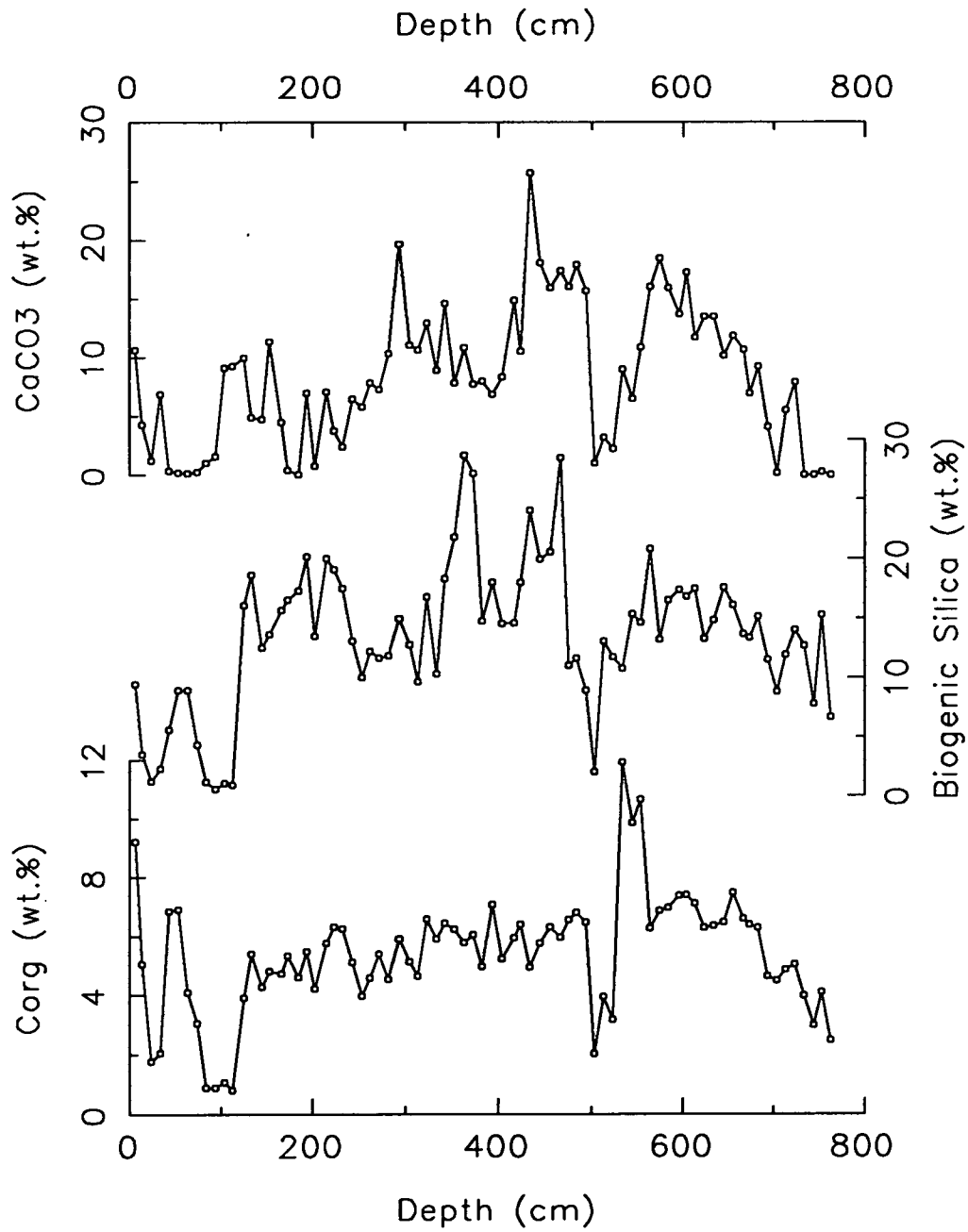


Figure 3.6. Biogenic components ($C_{org}$, biogenic silica and $CaCO_3$) against depth for core CD38-10 (257m).

The $C_{org}$ profile is fairly stable between 125 and 490cm in CD38-10 with an average of about 5wt.%.

Table 3.2 lists the statistical information of the above trace metals expressed as enrichment factors ($E.F._{metal}$ - Equation 3.1 and Appendix B.2). Enrichment factors are calculated in order to highlight any proportion of each metal which is not associated with the fraction of the sediment whose input has been from a terrigenous source. They express the enrichment (or depletion) of a metal as a number in order to allow for inter-comparison between each metal and also with other published metal data sets (Balistreiri and Murray, 1986; Shimmield and Pedersen, 1990). An $E.F._{metal}$ above 1.0 implies an extra, non-terrigenous source for the metal.

Equation 3.1. Metal enrichment factors

$$E.F._{metal} = [Metal_{sample}/Al_{sample}] / [Metal_{clay}/Al_{clay}]$$

where, clay values are for deep-sea clay (Turekian and Wedepohl, 1961).

| | CD38-09 | | | | CD38-10 | | | |
|---|---|---|---|---|---|---|---|---|
| | Min. | Max. | Mean | S.D. | Min. | Max. | Mean | S.D. |
| $E.F._{Mo}$ | 0.70 | 6.87 | 2.92 | 1.27 | 0.62 | 9.46 | 3.82 | 2.25 |
| $E.F._{U}$ | 4.21 | 369.4 | 12.6 | 42.1 | 6.83 | 37.5 | 17.4 | 6.23 |
| $E.F._{Ni}$ | 0.17 | 0.64 | 0.34 | 0.12 | 0.14 | 1.37 | 0.54 | 0.24 |
| $E.F._{Cr}$ | 0.86 | 4.42 | 1.83 | 0.44 | 0.76 | 3.79 | 2.01 | 0.57 |
| $E.F._{V}$ | 0.74 | 2.34 | 1.47 | 0.27 | 0.57 | 5.67 | 2.17 | 1.12 |
| $E.F._{Cu}$ | 0.05 | 0.21 | 0.15 | 0.03 | 0.04 | 0.37 | 0.19 | 0.06 |

Table 3.2. $E.F._{metal}$ : for method of calculation see Eqn 3.1 and Appendix B.2.

Figures 3.7 and 3.8 are depth profiles of these enrichment factors for cores CD38-09 and CD38-10, with the $C_{org}$ profiles also displayed for comparison. In core CD38-09, the drop in $C_{org}$ concentration between 500 and 550cm is seen also in the Ni, Cr, Mo and U enrichment factors (Fig. 3.7). In core CD38-10, the profiles look very similar (Fig. 3.8) especially at the zones with low $C_{org}$ at 25-35cm, 80-115cm and 500-525cm which correspond to low enrichment factors for all the metals except uranium, and all the E.F. depth profiles peak at 534cm where the highest concentration of $C_{org}$ is found.

The similarities between the $C_{org}$ and $E.F._{metal}$ depth profiles indicate the possibility of strong organo-metallic relationships within the sediment. These are

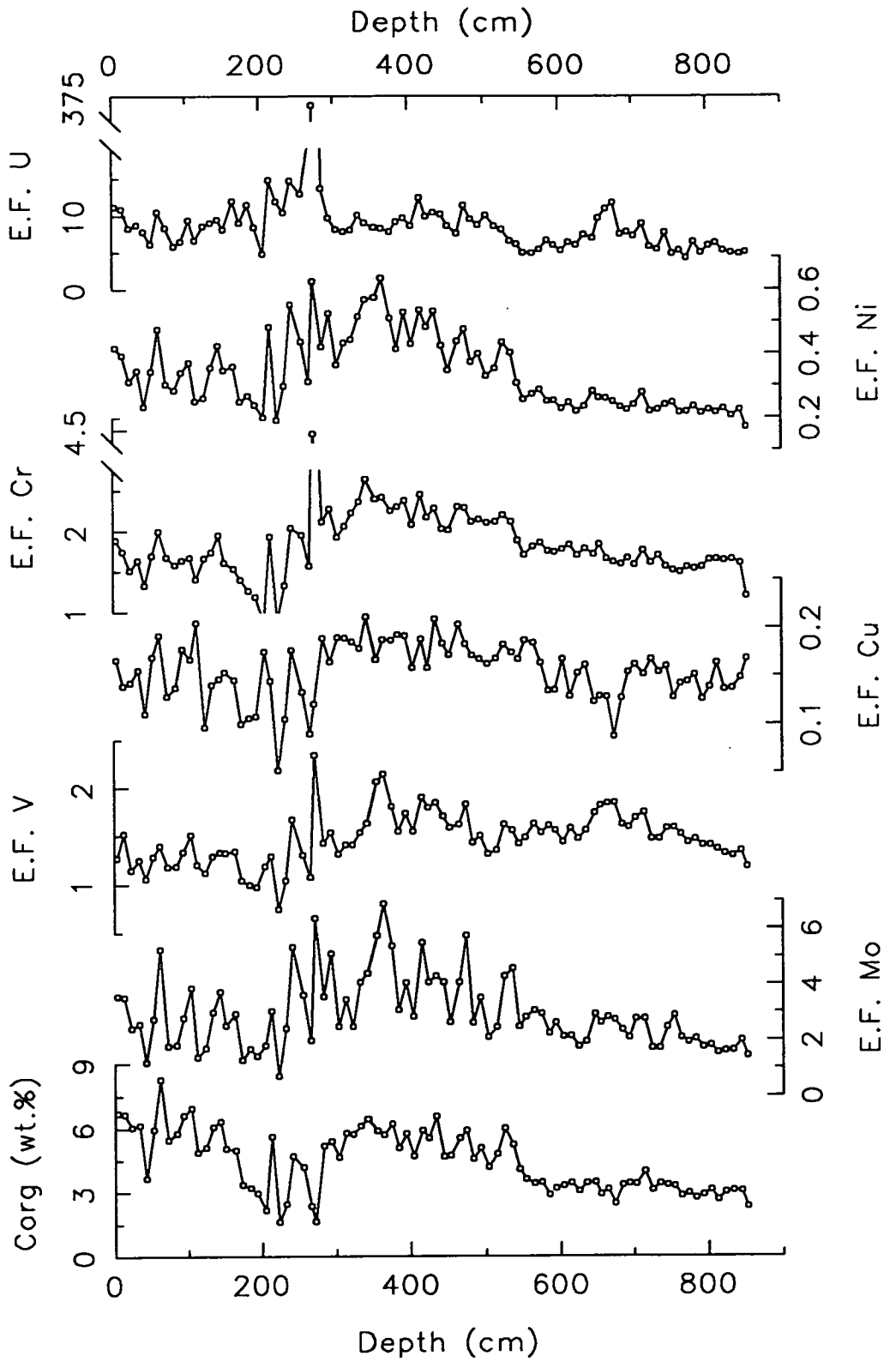


Figure 3.7. Trace metal enrichment factors ($E.F._{metal}$: Mo, V, Cu, Cr, Ni and U) and $C_{org}$ against depth for core CD38-09 (148m).

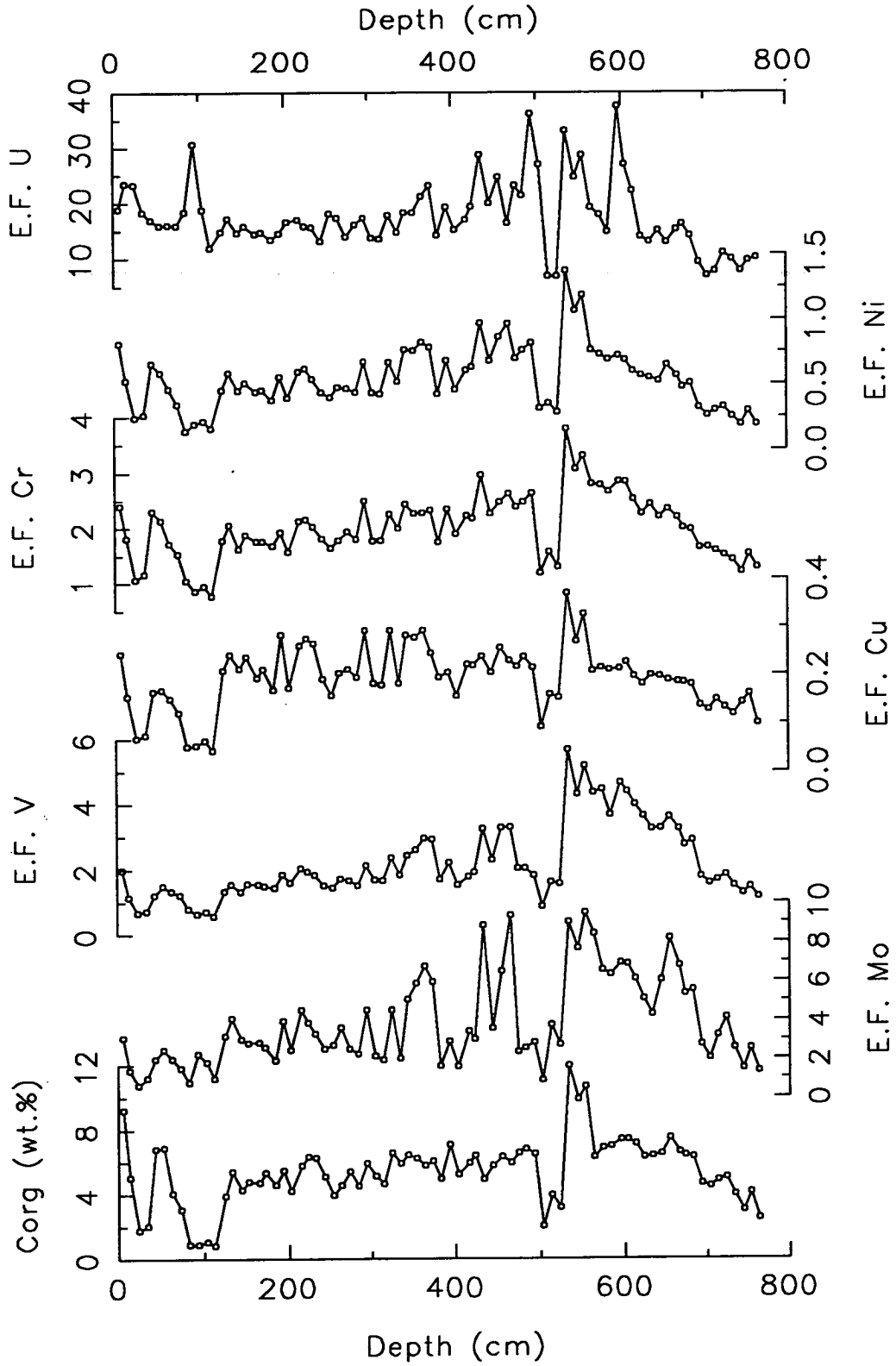


Figure 3.8. Trace metal enrichment factors ($E.F._{metal}$: Mo, V, Cu, Cr, Ni and U) and $C_{org}$ against depth for core CD38-10 (257m).

highlighted by the correlation plots in Figs 3.9 and 3.10 and in the correlation coefficient matrices in Table 3.3.

| CD38-09 (148m) | | | | | | |
|---|---|---|---|---|---|---|
| E.F.Mo | 0.561 | | | | | |
| E.F.U | -0.188 | 0.317 | | | | |
| E.F.Ni | 0.681 | 0.893 | 0.300 | | | |
| E.F.Cr | 0.346 | 0.758 | 0.647 | 0.789 | | |
| E.F.V | 0.123 | 0.709 | 0.355 | 0.504 | 0.694 | |
| E.F.Cu | 0.565 | 0.488 | -0.132 | 0.494 | 0.418 | 0.382 |
| | $C_{org}$ | E.F.Mo | E.F.U | E.F.Ni | E.F.Cr | E.F.V |

| CD38-10 (257m) | | | | | | |
|---|---|---|---|---|---|---|
| E.F.Mo | 0.685 | | | | | |
| E.F.U | 0.338 | 0.363 | | | | |
| E.F.Ni | 0.864 | 0.777 | 0.585 | | | |
| E.F.Cr | 0.916 | 0.798 | 0.503 | 0.944 | | |
| E.F.V | 0.791 | 0.910 | 0.412 | 0.778 | 0.868 | |
| E.F.Cu | 0.808 | 0.642 | 0.303 | 0.838 | 0.817 | 0.624 |
| | $C_{org}$ | E.F.Mo | E.F.U | E.F.Ni | E.F.Cr | E.F.V |

Table 3.3. $E.F._{metal}$ and $C_{org}$ correlation coefficients

Strong $C_{org}$ correlations are present in core CD38-09 for Mo, Ni and Cu, and in core CD38-10, Cr shows a very strong correlation, with Mo, Ni, V and Cu having strong correlations*. Although the V concentration in core CD38-09 has a poor correlation with $C_{org}$, it does correlate strongly with Mo, Cr and Ni. All these correlations are positive which suggests the presence of organo-metallic associations. The possibility that strong correlations are caused by dilution from another component is not suspected because variation in the main dilutant in these continental margin sediments, i.e. terrigenous debris, has already been accounted for by the calculation of enrichment factors for the metals. The poor uranium-$C_{org}$ relationship is interpreted further in 4.3.4.

*Correlation coefficients above 0.9 (or below -0.9) are statistically regarded as being very strongly significant and between 0.5 and 0.9 (or -0.5 and -0.9) as being strongly significant (5.2.1).

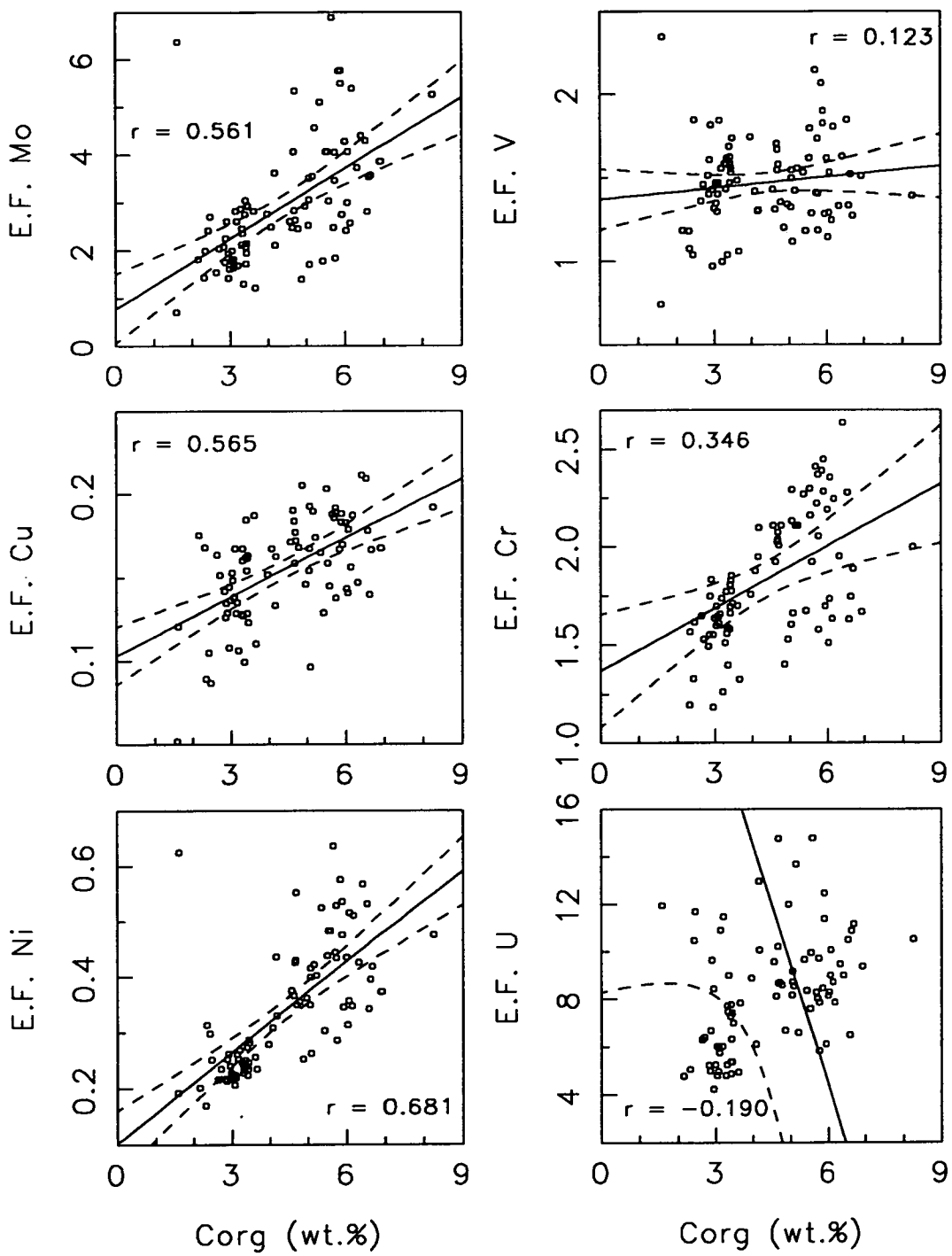


Figure 3.9. Correlation plots of trace metal enrichment factors ($E.F._{metal}$: Mo, V, Cu, Cr, Ni and U) against $C_{org}$ for core CD38-09 (148m). All with a best fit line, showing 95% confidence limits, and correlation coefficient (r).

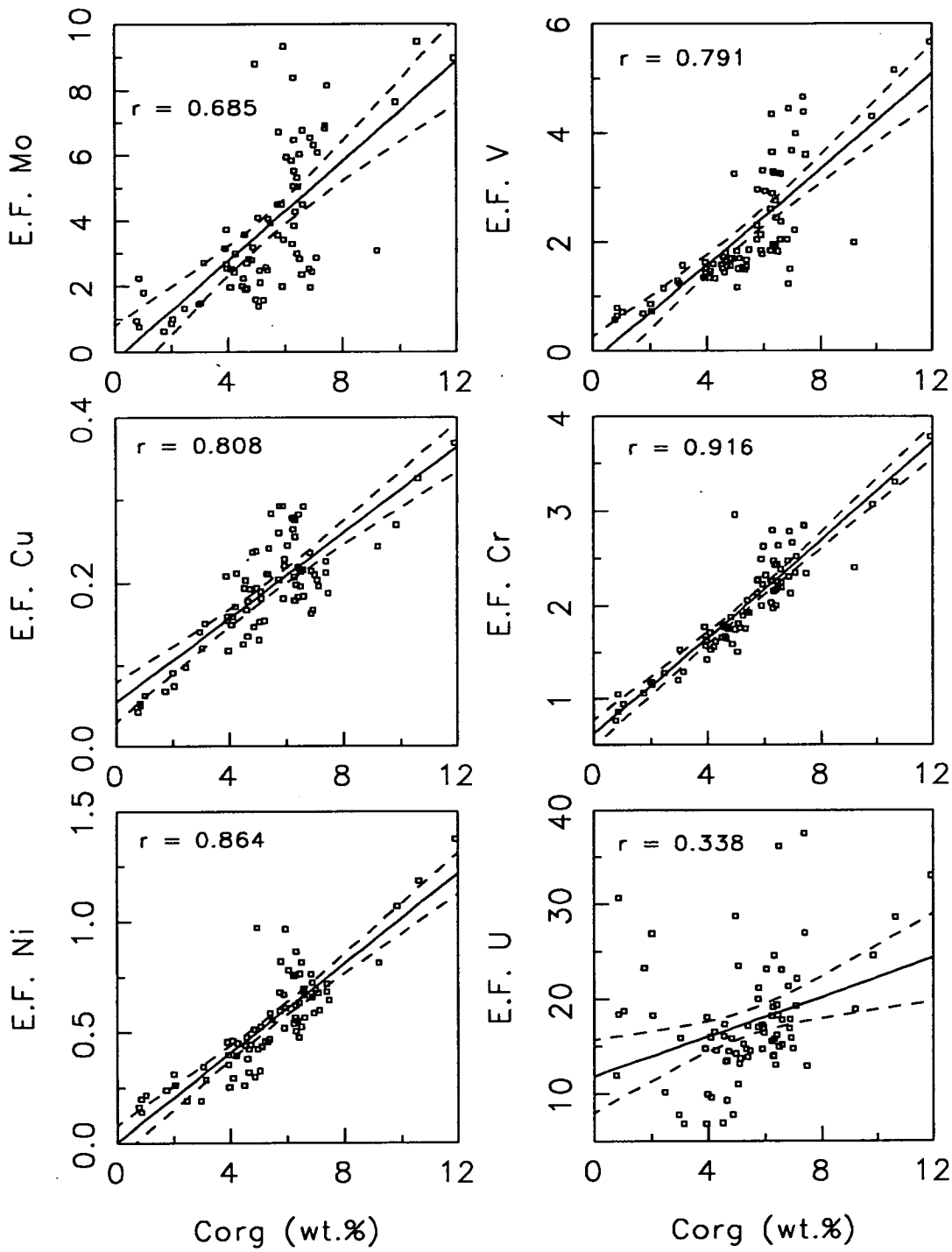


Figure 3.10. Correlation plots of trace metal enrichment factors ($E.F._{metal}$: Mo, V, Cu, Cr, Ni and U) against $C_{org}$ for core CD38-10 (257m). All with a best fit line, showing 95% confidence limits, and correlation coefficient (r).

## 3.3. DISCUSSION

### 3.3.1. Ocean carbon sink

The global carbon cycle contains the two most important processes necessary to sustain life. It is the fine equilibrium between plant photosynthesis ($CO_2$ consuming) and animal respiration ($CO_2$ producing) which keeps the carbon dioxide concentration of the atmosphere at a relatively stable level. As can be seen from Fig. 3.11, the carbon cycle is a very complex series of interactions and one of the major ones is the diffusion of $CO_2$ from the atmosphere to the hydrosphere and the utilisation of that $CO_2$ in the photic zone by marine phytoplankton (process C in Fig. 3.11, Holland, 1978).

The carbon remains in the marine biosphere food chain until it is mostly recycled back as dissolved $CO_2$ in the ocean upon decomposition of the organisms (>99%, Baturin, 1982; up to 96% regeneration in the deep-sea, Martin *et al.*, 1987) or it is buried as organic matter in marine sediments; the latter taking it out of the cycle. Although this carbon sink accounts for only a very small fraction of the carbon moving around the global cycle (process L accounts for only 0.4% of process F, Fig. 3.11), variations in the levels of $C_{org}$ found in marine sediments may be linked to natural fluctuations (or present day anthropogenic increases) in the concentration of atmospheric $CO_2$. This assumes that the level of $C_{org}$ accumulation in the sediment column reflects the magnitude of organic matter flux from the euphotic zone to the sea-floor (Müller and Suess, 1979; Müller *et al.*, 1983; Sarnthein *et al.*, 1988).

The vastly increased level of productivity in the surface waters along the Peru continental margin, and other coastal upwelling zones, means that although these areas only cover 0.1% of the ocean surface, they account for about 0.5% of the total ocean productivity (Ryther, 1969). This 5-fold enrichment compared with normal ocean waters is reflected in the elevated concentrations of $C_{org}$ found in sediments accumulating under upwelling areas. This is illustrated by the high mean $C_{org}$ (wt.%) of cores CD38-09 and CD38-10 in this study.

The $C_{org}$ flux data of Martin *et al.* (1987) suggest that site CD38-09 at 147m water depth will receive 70% of the new production sinking out of the euphotic zone, whereas site CD38-10 at 250m will receive only about 50%. The higher mean $C_{org}$ content measured in CD38-10 (5.4 wt.%) compared with core CD38-09 (4.4 wt.%) seems to be a contradiction of the above statement. The reason for this is that the organic matter signal in core CD38-09 is being diluted by more terrigenous clays than

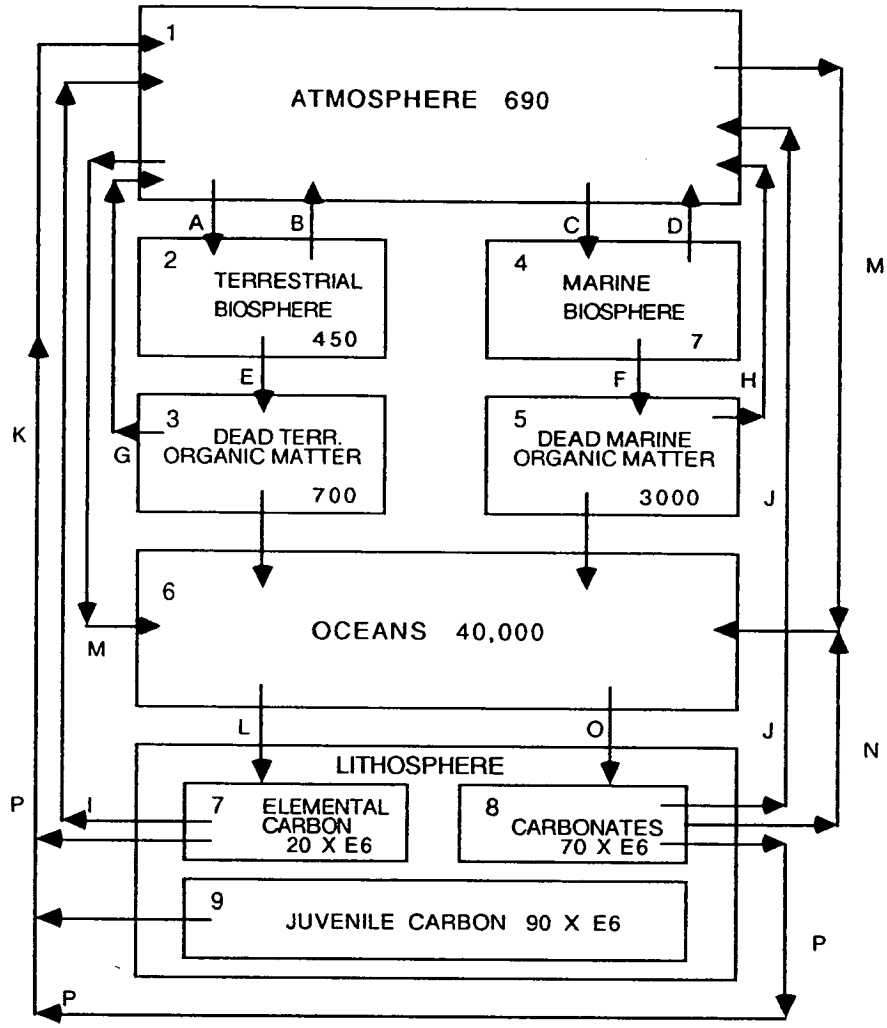


| Process | From | To | Description | Rate |
|---|---|---|---|---|
| A | 1 | 2 | Photosynthesis on land | 48 |
| B | 2 | 1 | Decay of terrestrial organic matter | 23 |
| C | 1 | 4 | Photosynthesis at sea | 35 |
| D | 4 | 1 | Decay of marine organic matter | 5 |
| E | 2 | 3 | Accumulation of dead terr. org. matter | 25 |
| F | 4 | 5 | Accumulation of dead marine org. matter | 30 |
| G | 3 | 1 | Decay of dead terr. org. matter | 25 |
| H | 5 | 1 | Decay of dead marine organic matter | 30 |
| I | 7 | 1 | Fossil fuel burning | 4.2 |
| J | 8 | 1 | Cement manufacture | 0.7 |
| K | 7 | 1 | Oxidation of elemental carbon | 0.09 |
| L | 6 | 7 | Deposition of elemental carbon | 0.12 |
| M | 1 | 6 | Flux to carbonates | 0.06 |
| N | 8 | 6 | Weathering of carbonates | 0.16 |
| O | 6 | 8 | Deposition of carbonates | 0.22 |
| P | 7,8,9 | 1 | Degassing (metamorphic and igneous) | 0.09 |

Figure 3.11. The global carbon cycle (adapted from Holland, 1978). All rates are x $10^{15}$ g $yr^{-1}$ and amounts of carbon in reservoirs are x $10^{15}$ g.

in core CD38-10 because CD38-09 is situated closer to the source of the terrigenous input, i.e. the continental land mass. Once sedimentation rates are taken into account, organic matter fluxes should be higher at CD38-09.

A similar difference in mean $C_{org}$ is seen in the ODP sites 680B (6 wt.%) and 686 (2 wt.%), the latter of which is situated 200m deeper and 2° further south on the continental margin of Peru (Suess *et al.*, 1988). Schrader (1992) attributes the difference to a combination of (a) a reduced $C_{org}$ flux from the euphotic zone, (b) a weaker OMZ allowing for more organic matter oxidation and/or (c) more recycling of organic carbon because of longer sinking times for organic matter, at site 686.

### 3.3.2. Glacial/interglacial climate changes

Variations in the concentrations of $C_{org}$ and the other two biogenic components (biogenic silica and calcium carbonate) should reflect changes in the ocean surface productivity, which in turn is controlled by the climatic environment of the area. Under a zone of coastal upwelling, if climatic change alters the strength and persistency of the physical upwelling of water through time (Suess and Thiede, 1983; Bakun, 1990) then the contents of these three biogenic indicators should vary sympathetically (assuming an equal dilution-effect from the terrigenous component input).

In the Late Quaternary, global phases of glacial and interglacial periods have had a great influence on both physical (sea-level and circulation patterns) and biological oceanography (Lyle, 1988; Pedersen, 1983). The extent to which these extreme climatic variations have affected the strength of coastal upwelling has been widely studied (Labracherie *et al.*, 1983; Müller *et al.*, 1983; Reimers and Suess, 1983; Wefer *et al.*, 1983; Schrader and Sorkness, 1991; Schrader, 1992).

Any down-core fluctuations in $C_{org}$, biogenic silica and $CaCO_3$ concentrations, such as seen in cores CD38-09 and CD38-10 in Figs 2.5 and 2.6, may be attributed to glacial/interglacial cycles by the simple theory that stronger winds during a glacial period produce more upwelling and hence ocean productivity increases (Sarnthein *et al.*, 1988) which is recorded in the sediment column. However, the picture is complicated by other highly variable factors. Dilution from terrigenous debris from the continental land mass (Andean erosion, 7.2.3), preservation of the original biomass (7.3.3) and erosion of the sediment column by stronger bottom water currents during low sea-level stands (4.3.6) are just three of the many influences which affect the accumulation of biogenic components in the continental margin sediments off Peru.

Before an accurate interpretation of the biogenic component concentrations in cores CD38-09 and CD38-10 can be made, sections of the sediment have to be allotted to either a glacial or an interglacial period and this can only be done after accurate age models of the cores have been determined. As described in Chapter 2, age modelling for cores CD38-09 and CD38-10 was not possible due to the unknown amount of erosion of the sediment column that these cores have suffered.

### 3.3.3. Organo-metallics

As organic matter falls out of the surface waters upon death of the marine organism, it scavenges many redox-sensitive metals (e.g. Mo, U, Ni, Cr, V and Cu) out of their dissolved phase and concentrates them in the solid phase (Goldberg, 1954; Bruland *et al.*, 1974; Craig, 1974; Francois, 1988; Shimmield and Pedersen, 1990). Balistieri *et al.* (1981) concluded that the surface metal chemistry of sinking particles was mainly controlled by the organic matter phase.

Organic matter which reaches the sea-floor before decomposition therefore has a high level of these metals incorporated within it and so the concentrations measured in the sediment should reflect the amount of organic matter in the water column (Shaw *et al.*, 1990).

Under a coastal upwelling zone, such as off Peru, the high organic matter flux produces an anomalous enrichment of the metals in the sediment (Calvert and Price, 1970; Bertine and Turekian, 1973; Calvert *et al.*, 1985; Shimmield and Pedersen, 1990). This enrichment can be calculated as an $E.F._{metal}$ value and this is a measure of the concentration above (or below) that expected if no organic matter was present in the sediment and the only metal source was from a terrigenous association.

The order of organo-metallic enrichment, taken from the mean $E.F._{metal}$ values (Table 3.3), for the two near-shore cores is as follows:

CD38-09 U > Mo > Cr > V > Ni > Cu
CD38-10 U > Mo > V > Cr > Ni >Cu.

It should be noted that Cu and Ni have mean enrichment factors less than one (i.e. depleted). However, the enrichment factors and hence their order is very dependant on the Turekian and Wedepohl (1963) deep-sea clay values being accurate for every metal and so it may not accurately quantify the organic-associated enrichments.

The following is an order of the correlation coefficients of the metal enrichment factors with organic carbon (r from Table 3.2, Figs 3.9 and 3.10) for the two cores:

CD38-09 : Ni > Cu > Mo > Cr > V > U

CD38-10 : Cr > Ni > Cu > Mo > V > U.

This latter order is an indication of the relative strength of any organo-metallic association. However, it is strongly affected by any post-depositional processes operating during the decomposition of organic matter (especially for uranium - 4.3.4).

Differences in the two orders illustrate, for instance, that although the enrichment factors of Cu and Ni are generally less than one, which implies that their concentration can wholly be accounted for by a terrigenous source, the strong $C_{org}$-Ni and $C_{org}$-Cu correlations imply that these metals are associated with organic matter as it is buried within the sediment. Ni and Cu maintain strong associations with the $C_{org}$ indicating incorporation into the more refractory fractions of the organic matter. Sclater *et al.* (1976) saw no evidence for direct scavenging of Ni from the water column, but concluded that Ni was involved in the biogeochemical cycle by incorporation into both the hard and soft parts of marine organisms.

Mo and V, on the other hand, are highly enriched within the continental margin sediments off Peru indicating that organic debris can easily scavenge these metals from the water column. However, Mo (in CD38-10) and V (in CD38-09) are low down the order of $C_{org}$-correlation and this implies that these two metals may be connected to the more labile organic phase and thus are more affected by post-depositional remobilisation. Brusmack and Gieskes (1983) observed movement of Mo and V in reducing sediments from the Gulf of California and attributed this to the complexation of these metals with soluble organic material. Mo has been found to be removed from solution by absorption by humic substances and is therefore enriched within the humic fractions of organic matter (Bertine, 1972; Nissenbaum and Swaine, 1976; Calvert *et al.*, 1985).

The relatively large enrichment of Mo, Cr and V relative to the other organo-metallic elements in the two near-shore cores is evidence of accumulation under reducing conditions within the sediment. Shaw *et al.* (1990) reported that near-anoxic conditions produce increased accumulation of the above three metals and low accumulation of Co and Ni.

In a study of sediments in the anoxic environment of the Saanich Inlet, British Columbia by Francois (1988), Mo showed the largest enrichment of all the metals studied. This was due to additional enrichment by sulphide co-precipitation reactions occurring at the sediment/water interface (Bertine, 1972; Shaw *et al.*, 1990).

The presence of naturally metal-stained organic matter in reducing sediments, as investigated by Ittenkkot and Degens (1983) using electron microscope techniques, can help in the preservation of distinct organic matter structures upon burial. If certain organic structures, such as filamentous bacterial mats (Reimers and Suess, 1983A), are characteristic of coastal upwelling sediments, then metal staining could allow them to survive burial and become diagnostic features.

### 3.3.4. Non-anthropogenic conditions

Marine sediments in the coastal environment are susceptible to pollution from mankind's present day activities. Industrial and sewage waste outflow, land fertiliser run-off and oil tanker spillages are some of the ways in which metals can be mobilised into the marine environment in amounts equivalent to those introduced by natural weathering processes (Bruland *et al.*, 1974).

However, before the effects of anthropogenic pollution on the coastal marine environment can be examined, the complex pathways in which the metals are incorporated from the sea-water to the sediments must be fully understood and the natural, steady-state baseline for metal enrichment associated with organic matter and/or diagenetic processes needs to be quantified.

The sediments off Peru, sampled in cores CD38-09 and CD38-10, have been accumulating under natural, non-anthropogenic conditions throughout the Late Quaternary. The elevated concentrations of $C_{org}$ and its associated redox-sensitive metals found in these sediments allow for accurate quantification of the metal/$C_{org}$ ratios.

Table 3.4 lists the range, mean and standard deviation of metal/$C_{org}$ and $E.F._{metal}/C_{org}$ ratios for Mo, U, Ni, Cr, V and Cu for both CD38-09 and CD38-10, and these values could be used in any future studies in a polluted coastal environment as the natural baseline flux for comparison with any additional, anthropogenic input (Bruland *et al.*, 1974). There is generally a very good agreement between the two cores for the mean values of the ratios, implying that the values could be used for sediment sites over a range of water depths on a continental shelf. It would have to be

remembered that these sediments are from a reducing environment (6.2.3). However, according to Bertine and Goldberg (1977) coastal marine pollution records can most easily be found in undisturbed, non-bioturbated, anoxic sediments.

| | CD38-09 | | | | CD38-10 | | | |
|---|---|---|---|---|---|---|---|---|
| | Min. | Max. | Mean | S.D. | Min. | Max. | Mean | S.D. |
| Mo/Corg | 7.4 | 32.6 | 12.2 | 3.2 | 4.9 | 47.6 | 11.4 | 5.8 |
| U/Corg | 0.9 | 91.05 | | | 1.0 | 31.3 | 3.5 | 4.4 |
| Ni/Corg | 9.1 | 26.6 | 12.0 | 2.4 | 9.9 | 34.9 | 14.0 | 4.4 |
| Cr/Corg | 15.3 | 75.5 | 27.2 | 7.6 | 11.5 | 69.0 | 22.6 | 10.3 |
| V/Corg | 14.2 | 53.3 | 29.8 | 9.2 | 15.0 | 69.0 | 29.4 | 9.9 |
| Cu/Corg | 3.6 | 16.4 | 6.5 | 2.1 | 2.8 | 11.2 | 5.7 | 1.8 |
| E.F.Mo/Corg | 0.29 | 3.93 | 0.70 | 0.40 | 0.28 | 2.58 | 0.73 | 0.38 |
| E.F.U/Corg | 0.98 | 228.0 | 4.70 | 27.0 | 1.55 | 35.2 | 4.35 | 4.96 |
| E.F.Ni/Corg | 0.05 | 0.38 | 0.081 | 0.04 | 0.06 | 0.23 | 0.106 | 0.03 |
| E.F.Cr/Corg | 0.24 | 2.73 | 0.46 | 0.27 | 0.26 | 1.19 | 0.41 | 0.16 |
| E.F.V/Corg | 0.17 | 1.45 | 0.38 | 0.17 | 0.18 | 0.89 | 0.41 | 0.13 |
| E.F.Cu/Corg | 0.02 | 0.08 | 0.038 | 0.01 | 0.02 | 0.06 | 0.038 | 0.01 |

Table 3.4. Metal/$C_{org}$ and E.F.$_{metal}$/$C_{org}$ ratios :all values are x $10^{-4}$.

### 3.3.5. Fish bones and faecal pellets

High fish production in the plankton-rich waters of a coastal upwelling zone, results in hard-part fish-remains, i.e. bones and scales, being found in the sediments accumulating below in much higher concentrations than in non-upwelling regions (Frankenberg and Menzies, 1968; Diester-Haass, 1979). DeVries and Pearcy (1982) found that anchovy scales and vertebrae (*E. ringens*) were the most abundant constituent of fish debris (79.4%) in Peruvian continental slope sediments.

A semi-quantitative analysis of fish debris content in cores CD38-09 and CD38-10 was carried out on the sieved (> 63μm) samples used for foraminifera picking (Appendix A.2). The quantity of fish-remains seen in the samples were termed absent (0), rare (1), common (2) or abundant (3), and Fig. 3.12 displays this information plotted against depth for both cores. The fish-remains are well-preserved and easily identified as dark brown, thin scales and small vertebrae.

Figure 3.12A displays some similarity to the $C_{org}$ profile for core CD38-09 (Fig. 3.5) with fish bones consistently in the sediment above 530cm but rare or absent

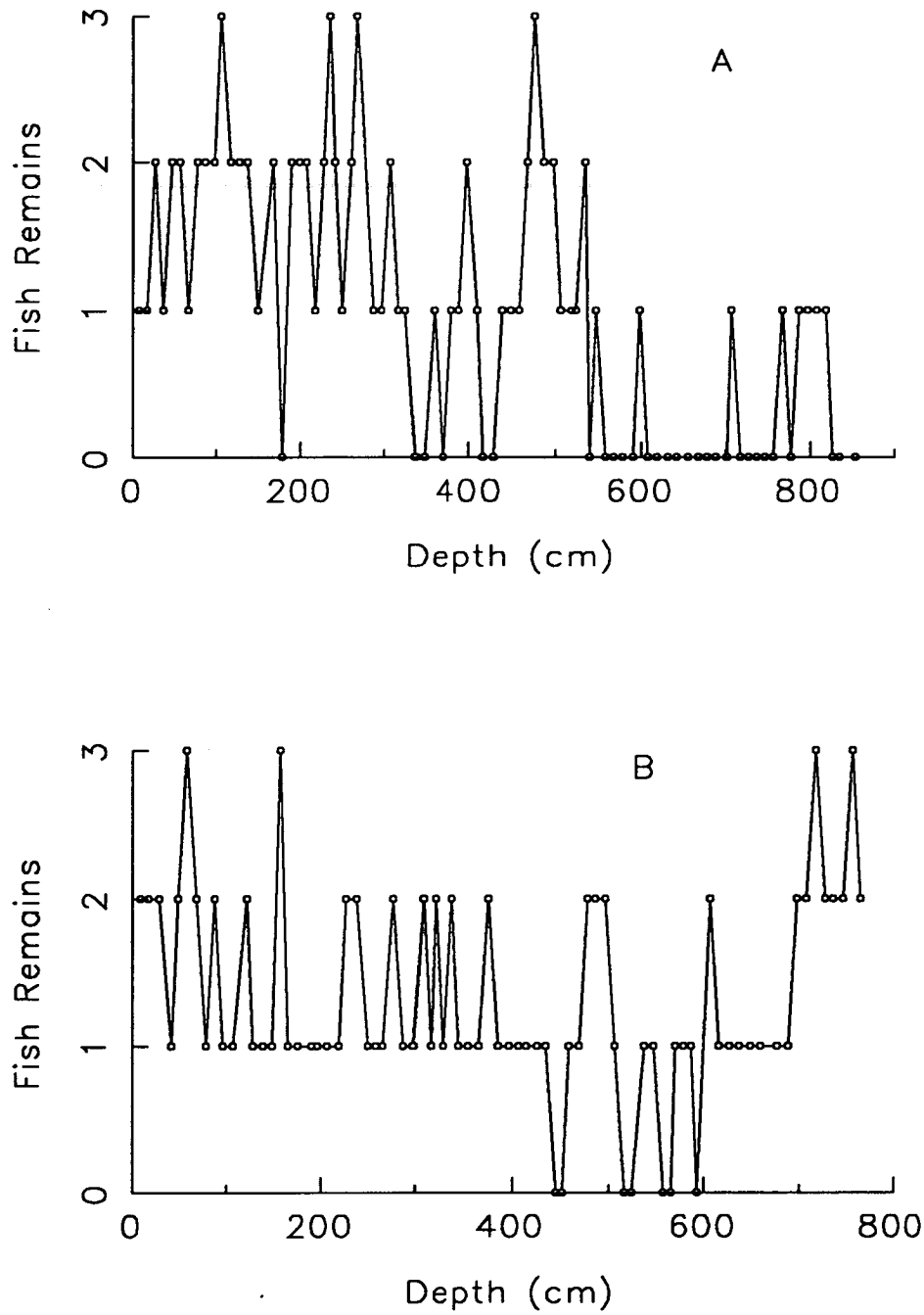


Figure 3.12. Semi-quantitative analysis of fish-remains, A) CD38-09 (148m) and B) CD38-10 (257m). Scale equivalent to: 0 = Absent, 1 = Rare, 2 = Common, 3= Abundant.

below this depth, corresponding to the drop in $C_{org}$ from about 6 to only 3 wt.%. This fish debris-$C_{org}$ relationship is to be expected for a continental margin area such as off Peru because more organic matter falling into the sediment may be the result of higher biological productivity in the surface waters and therefore, more fish should produce more fish-remains which will sink rapidly into the sediment.

The plot for core CD38-10 (Fig. 3.12.B) however illustrates a slightly different story because it does not seem to correlate with the $C_{org}$ content of the core so well (Fig. 3.6). At depths where the $C_{org}$ concentration is very low (e.g. at 30, 80-110, 500 and 735-770cm) the fish-remains are still common or abundant. This is probably due to the fact that fish bones are relatively dense and large in size and therefore, if the sediment is reworked by bottom-water currents, the less-dense, soft organic matter will be resuspended along with fine-grained clays and moved further down the continental slope. This will leave behind a concentration of fish debris (DeVries and Pearcy, 1982) and other heavy minerals.

A high flux of fish debris in continental margin areas can supply a high concentration of phosphorus (P) and uranium to the sediment. Baturin (1982) states that the P content of fish bones and scales can be up to 16 wt.% and dissolution of these fish-remains off Peru can regenerate dissolved phosphate within pore waters in quantities comparable with those regenerated from decomposition of organic matter (Suess, 1981). The utilisation of this phosphate, and the associated uranium, in phosphorite diagenesis is discussed in Chapter 4.

Faecal pellets were seen at various depths down core CD38-09 (during foraminifera picking). These pellets are covered by a protective, surface membrane (Honjo and Roman, 1978) which makes them resistant to decomposition within the water column. They are most commonly the waste products of herbivorous zooplanktonic copepods and are known to contain about 20-30% of the organic carbon from ingested phytoplankton (Eppley and Peterson, 1979) as well as the actual shells of diatoms and silicoflagellates (Schrader, 1971). Many studies have measured the very fast sinking rates of faecal pellets (up to 400m $day^{-1}$, Smayda, 1969; 126-862m $day^{-1}$, Fowler and Small, 1972) which are responsible for the rapid transport of organic matter, trace metals and fine-grained clays (Scheidegger and Krissek, 1982) to the sea-floor.

## 3.4. CONCLUSIONS

The following conclusions can be made with regards to the geochemical record of coastal upwelling contained within cores CD38-09 and CD38-10.

(1) High concentrations of $C_{org}$, averaging over a magnitude of order greater than those found in deep-sea sediments, can be found in Peruvian continental margin sediments. This is a reflection of the consistently high biological productivity in the oceanic, surface waters as a result of the physical upwelling of nutrient-rich water into the euphotic zone.

(2) Variations in the strength of coastal upwelling, which has fluctuated as the along-shore and equator-ward trade winds responded to global climate changes during the Late Quaternary, will alter the fluxes of organic matter, silicate- and carbonate- planktonic shell-remains down through the water column and into the sediment.

The concentrations of $C_{org}$, biogenic silica and $CaCO_3$ in the two shallow-water cores do vary considerably with depth (Figs 3.5 and 3.6) but the interpretation of such changes requires accurate age modelling and the effects of preservation and dilution to the productivity signal have to be taken into account.

(3) Redox-sensitive metals are scavenged from sea-water by organic matter as particles and faecal pellets sink through the water column and hence their concentrations within the sediments of off-shore Peruvian basins are elevated above that expected from a solely terrigenous-association input.

Strong organo-metallic associations are suggested by the high and positive correlation coefficients of the metal enrichment factors with $C_{org}$. The post-depositional decomposition of organic matter results in the preferential release of U, Mo and V compared with Ni and Cu (taken from the order of correlation coefficients) which implies that the former metals are incorporated into labile organic compounds whereas the latter are associated with more refractory organic fractions.

(4) Anthropogenic pollution in the marine, coastal environment may result in heavy metal contamination of continental margin sediments. The metal/$C_{org}$ or $E.F._{metal}/C_{org}$ ratios presented for cores CD38-09 and CD38-10 (Table 3.4) could be used as the natural, baseline flux in any future geochemical analysis of polluted, coastal sediments.

An oxygen-minimum zone impinges onto the Peruvian continental margin and the sediments have been accumulating under reducing conditions. Therefore, in any comparative study, the record of marine pollution would have to be taken from similar non-bioturbated, anoxic sediments.

# CHAPTER 4

# PHOSPHORITES AND EUSTACY

# 4.1. INTRODUCTION

"Phosphatic nodules are apparently more abundant in the deposits along coasts where there are great and rapid changes of temperature, arising from the meeting of cold and warm waters."

Murray and Renard (1881)

## 4.1.1. Why study phosphorites?

The first systematic study of marine sediments, during the *Challenger* Expedition of 1872-1876, included the collection and scientific observation of phosphorites. It is from the *Challenger* cruise report that the above quote was taken.

Due to its underwater location, marine phosphorite was discovered nearly a century after the first land deposits were described (Boules, 1782; cited by Daubeny and Widdrington, 1845). During the nineteenth century, phosphorite land deposits were used as agricultural fertilisers and when Lawes dissolved phosphate rock in sulphuric acid, to produce a more soluble phosphatic fertiliser (Buckland, 1843) the phosphate industry began. In order to supply this growing industry, exploration for, and investigation of, phosphorites has continued ever since (Cook *et al.*, 1990).

Today, phosphate is still a principal component in the manufacture of fertilisers and due to intensive farming techniques in the developed world, phosphorite ore deposits are of great economic importance. It is therefore vital to study the chemical and environmental processes which are involved during phosphorite diagenesis, in order to gain more understanding of the mineral's formation and perhaps aid in future exploration of further ore deposits.

Although phosphorites have been found in sediments throughout the world, spanning all geological ages from the Precambrian to the Holocene (Cook *et al.*, 1990), it is only along the narrow zones off the south west coasts of Africa, California and South America that Recent phosphorite formation is known to occur (Manheim *et al.*, 1975; Price and Calvert, 1978; Burnett *et al.*, 1980; Baturin, 1982; Jahnke *et al.*, 1983).

Therefore, examination of the core material from the *R.R.S. Charles Darwin* Leg 38 cruise may reveal the presence of phosphorites and, if so, this mineralogical, geochemical and palæoceanographical study will attempt to interpret some of the complex processes involved in phosphorite formation.

### 4.1.2. Phosphorite mineralogy

Though the name phosphorite suggests that the principal element in this mineral is phosphorus, this is not always true because in some cases there is more calcium present (on a weight percent basis) compared with phosphorus. It is probably only because of the economic value of phosphorus in fertilising farmland, that the mineral is so named.

Sedimentary phosphorite is composed principally of the mineral **carbonate fluorapatite** (CFA) (McClellan and Van Kauwenbergh, 1990) and due to its complex mineral structure and an unusually large proportion of ionic substitution, the main elemental components can vary widely between and within phosphorite samples. The composition of phosphorites measured by Baturin and Bezrukov (1979) varied as follows: $P_2O_5$ from several to 33 wt.%, CaO from 7 to 52 wt.% and fluorine from <1 to 3 wt.%.

Fluorapatite has a hexagonal structure with a unit cell of $Ca_{10}(PO_4)_6F_2$ (Manheim and Gulbrandsen, 1979). CFA is formed by the substitution of $CO_3^{2-}$ for $PO_4^{3-}$. Ionic substitution is the rule rather than the exception in CFA (McClellan, 1980) and the two factors that influence the stability of an ion in a structure are its ionic radius and its electron charge. The process of carbonate substitution also requires substitution of cations in order to maintain electron-neutrality within the mineral. There is also the effect of lattice deformation to consider, as the planar $CO_3^{2-}$ group substitutes for the tetrahedral $PO_4^{3-}$ group on a 1:1 basis (McClellan and Van Kauwenbergh, 1990).

The most common substitutions which help to accommodate the carbonate ion in the mineral lattice are $Na^+$ and $Mg^{2+}$ replacement of $Ca^{2+}$. Presence of a sodium ion reduces the total cationic charge by one electron and although magnesium has the same ionic charge as the calcium that it replaces, it allows for the CFA structure to physically compensate for the carbonate substitution. This is because $Mg^{2+}$ has a much smaller ionic radius than $Ca^{2+}$ ($Mg^{2+}$ = 0.66Å, $Ca^{2+}$ = 0.99Å; Ahrens, 1952).

Many other trace element substitutions occur within the lattice framework of the CFA mineral and these can include the incorporation of Ba, Sr, U, S, Y and some rare earth elements (REE) into the mineral structure (Price and Calvert, 1978; Baturin, 1982; Manheim and Gulbrandsen, 1979; Lucas *et al.*, 1990). This variability in the chemical composition of the CFA mineral allows for an enrichment in the concentration of these trace elements to be found in phosphorites, above that of normal marine sediments.

### 4.1.3. Phosphorite research in the marine environment

The bulk of the world's resources of phosphorus on land, estimated at 67 x $10^9$ tonnes (Stowasser, 1979), occurs in the form of bedded sedimentary phosphorites of marine origin. Therefore, the study of phosphorite formation must be carried out on modern samples from the marine environment.

After the discovery of marine phosphorites during the *Challenger* Expedition and during the early 20th Century, many theories on the origin of phosphorites were proposed. It was accepted that there was some relationship between the biomass and phosphorites and that the mineral diagenesis occurred within the sediments and not in the water column (Murray and Renard, 1891; Blackwelder, 1916; Mansfield, 1918).

Kazakov (1937) proposed that the formation of phosphorites resulted from "direct inorganic precipitation of apatite, from ascending, phosphorus-rich, deep ocean waters and took place in the upper and middle portions of the continental shelf" (approximately 50 to 200m water depth). Kazakov's "Upwelling Hypothesis" received the backing of McKelvey *et al.* (1953) who worked on the US Western Phosphate Field (as a result of the increased interest in uranium-bearing sediments). The facies and chemical composition of this ore deposit reflected "marine deposition of phosphorites controlled primarily by depth, temperature, pH and $CO_2$ content of the water".

Some recent studies have used experimental and theoretical approaches and concluded that the solubility behaviour of apatite in sea-water can only be described by a complex reaction on the mineral surface (Atlas and Pytkowicz, 1977), that initial apatite precipitation from sea-water is strongly inhibited by magnesium ions (Martens and Harris, 1970) and most importantly, that abundant organic matter must be present (Nathan and Lucas, 1976) to supply high levels of phosphorus to the sediment.

### 4.1.4. Phosphorus and marine organisms

The phosphate ion is one of the most important nutrients present in the ocean (3.1.2). Phosphorus is vital to both the genetic and metabolic aspects of living organisms because it is a structural element in enzymes, adenosine triphosphate (ATP), ribonucleic acid (RNA), deoxyribonucleic acid (DNA) and phospholipids (Baturin, 1982). The dry weight phosphorus content of terrestrial organisms ranges from 0.1 to 1% but in marine phytoplankton, particularly diatomaceous algae, this can be as high as 3%. Sverdrup *et al.* (1946) give an average C:P weight ratio of 42:1 for

phytoplankton and 40:1 for zooplankton, and this can be recalculated to a C:P molar ratio in marine plankton of 106:1 (Redfield *et al.*, 1963).

The highest concentration of P (up to 16 wt.%) in marine animals is to be found in chitin, scales and fish bones (Baturin, 1982), and it occurs mainly as inorganic phosphorus.

As with all biogenic elements in the ocean, P takes part in an intensive biological cycle and nearly all of the organic-associated P in marine organisms is recycled back into the water column by bacterial decomposition of the organic matter (Baturin, 1982). If sufficient P is to accumulate in marine sediments in order to achieve substantial phosphorite diagenesis, then there must be a high flux of organic matter to the sediment. This situation is known to occur under zones of coastal upwelling (Chapter 3).

Not only is primary productivity vastly increased in these areas and hence organic matter flux, but there is also a high fish bone (DeVries and Pearcy, 1982) and faecal pellet input, both of which supply a certain amount of P to the sediment. Taking the average P content of raw fish as 1wt.% and an area of 200,000 square miles for both the south-west African and Peruvian coastal upwelling zones, Baturin (1982) calculated that up to 50,000 tonnes of P per year is supplied to the sediments as bone detritus.

### 4.1.5. CFA diagenesis

The supply of high levels of organic-P to a marine sediment is only the precursor to CFA formation. There are many other processes, both chemical and physical, that are needed to bring about phosphorite diagenesis.

Upon bacterial degradation of organic matter within the accumulating sediment, the labile organo-phosphorus compounds, e.g. phospholipids, will release P into the surrounding pore-waters, thus converting particulate P to dissolved P (Froelich *et al.*, 1988). The dissolution of fish debris has been suggested to be the dominant source of pore-water phosphate in Peru margin sediments (Suess, 1981). A third possible source of P is from phosphate released during reduction of iron oxyhydroxide complexes contained within detrital clay particles (Froelich *et al.*, 1988).

Kazakov (1937) originally proposed that apatite precipitated directly from the oceanic bottom waters under an upwelling zone. However, this is unlikely since the

reaction would be in competition with calcium carbonate precipitation and therefore would not occur to any significant degree (Gulbrandsen, 1969; Froelich *et al.*, 1982). A far more likely model is that of CFA precipitating out of the interstitial pore-waters of anoxic sediments which contain elevated concentrations of dissolved phosphate (Baturin and Shishinka, 1973; Manheim *et al.*, 1975; Burnett, 1977; Bremner, 1980; Froelich *et al.*, 1988). Low oxygen levels are required because if the sediments were accumulating under oxic conditions, the dissolved phosphate released from organic matter would form complexes with Fe and Mn ions to become insoluble (Berner, 1973).

Baturin and Bezrukov (1979) quote values of 5-9 mg $l^{-1}$ phosphorus in pore-waters from both the Peru-Chile and south west African margins, and at such high concentrations supersaturation with respect to CFA is induced and precipitation occurs on the surfaces of mineral grains, diatom frustules, organic detritus etc.

As CFA diagenesis continues, the euhedral apatite crystals can surround the matrix upon which they grow (Burnett, 1977) or even replace the carbonate foraminifera or silica diatoms by slow phosphatisation (Manheim *et al.*, 1975). Phosphatic gels form into small pellets which are usually round or ovule-shaped grains about 125-500μm in diameter (Baker and Burnett, 1988) and include the various sedimentary components upon which diagenesis occurred (Baturin and Bezrukov, 1979). Variation in the chemical composition of phosphorite deposits occur because of large variability not only in the composition of the CFA mineral itself, but also in the composition of the enclosed, non-phosphatic material.

Pellet formation occurs at, or just below, the sediment-water interface (Baker and Burnett, 1988) and, based on fluoride and phosphate uptake rates, Froelich *et al.* (1988) concluded that diagenesis of CFA pellets on the Peru margin takes between 3 and 12 years.

### 4.1.6. Sea-level change and phosphorite lithification

Authigenic formation of phosphatic material in marine sediments occurs initially as small, disseminated pellets throughout a soft diatom ooze or clay matrix (Baker and Burnett, 1988). The phosphorite minerals are denser than the fine-grained diatoms and clays, and so they can be physically concentrated within the sediment column by any simple sorting process. Reworking of the sediment by bottom-water currents can easily winnow away the less dense, non-phosphatic grains leaving behind a concentrated deposit of heavy minerals (Burnett, 1977; Baturin and Bezrukov, 1979;

Jahnke *et al.*, 1983). Other heavy minerals which can be associated with phosphorites are zircon, rutile and illmenite.

Reworking of a sediment can be caused by a change in the speed or direction of the bottom-water current, which will be most likely to occur because of fluctuations of sea-level (Veeh *et al.*, 1974; Baturin and Bezrukov, 1979). These eustatic variations have the greatest influence on the continental shelf and slope, where a drop in sea-level of between 50 and 100m can dramatically alter the along-shore current systems affecting a particular area. This range in eustacy is known to have occurred throughout the Quaternary (Fairbanks, 1989) associated with glacial/interglacial periodicity.

Baturin (1982) suggests a model of formation for phosphatic muds found off Namibia, which involves precipitation of CFA within organic-rich muds during periods of high sea-level, then winnowing occurring during a regressive period which concentrates the phosphatic pellets.

---

A) Physical upwelling brings nutrient-rich waters to surface-productivity, coastal zone. Phosphate taken up by marine biomass. High flux of organic-P to the sea-floor upon death of marine organisms.

B) Organic matter decomposition, fish debris dissolution and/or Fe oxyhydroxide reduction in surface sediment. Release of P into interstitial pore-waters.

C) High concentration of pore-water phosphate induces precipitation of CFA. Authigenic mineral growth on surfaces of diatoms, foraminifera and other mineral grains. Uptake of U, Ba, Sr, Y and REE into mineral lattice.

D) Phosphorite initially forms as soft nodules and small pellets which need concentration to form deposit. Onset of glacial period in Late Quaternary, brings a lowering of sea-level and stronger bottom-water currents on continental shelf. This winnows away fine grained clays and leaves behind denser phosphatic grains and other heavy minerals.

Figure 4.1. Four stages of phosphorite formation (after Baturin, 1982)

Figure 4.1 summarises the four basic stages of biogenic, chemical and physical processes necessary, under the right oceanographic conditions, for phosphorite

formation (Baturin, 1982). These conditions are to be found at the present day in the waters and sediments on the continental shelf and slope off Peru.

### 4.1.7. Phosphorites off Peru

A number of previous studies have been carried out on the presence and formation of phosphorites under the coastal upwelling zone off Peru (Veeh *et al.*, 1973; Manheim *et al.*, 1975; Burnett, 1977, 1980; Baturin, 1982; Burnett and Froelich, 1988; Lamboy, 1990) from geochemical, mineralogical and radiometric points of view. Manheim *et al.* (1975) concluded that the four simultaneous requirements for phosphorite diagenesis were found in this off-shore area, i.e. (1) sediments which are rich in organic matter and, (2) covered by bottom water with a low concentration of dissolved oxygen, in an area of, (3) low rates of inorganic (terrigenous) sedimentation and (4) low, but not zero, concentrations of $CaCO_3$ in the sediment.

U/Th radiometric age determinations of Recent Peru-Chile phosphorite nodules by Burnett (1974, 1980) and Burnett *et al.* (1980) suggest that formation was during high stands of sea-level, i.e. during interglacial, warm periods there is a higher organic-P flux to the sediment and so more phosphorite diagenesis is possible. It may, however, be due to less terrigenous input and lower sedimentation rates. It is only during glacial periods, when a drop in sea-level caused by ice-sheet formation occurs, that reworking of the sediment column concentrates the phosphatic minerals into a phosphorite deposit or hardground (Baturin and Bezrukov, 1979).

The term "hardground" generally refers to an interbedded phosphorite unit which shows signs of burrowing, abrasion and polishing and can be from only a few millimetres up to 1m thick (Cook *et al.*, 1990). Phosphatic hardgrounds are often subsequently broken up by biological or storm activity into shallow-water intraclastic gravel which can be seen on land as "pebble phosphates" (Kennedy and Garrison, 1975; Southgate, 1986).

Phosphatic hardgrounds found off Peru are often irregularly shaped, burrowed and show little internal zonation. They are usually flattened in one dimension with colour variation from pale green to dark grey (Burnett, 1977; Baturin, 1982) and occur in the 120-385m water depth range (Burnett, 1980) which is roughly equivalent to the OMZ depth in this area (Veeh et al., 1973).

A large proportion of such a phosphatic concretion is made up of non-phosphate components such as quartz and feldspar clastic grains and biogenic remains

(Baturin, 1982). Microscopic examination reveals CFA forming a homogeneous cement between the clastic minerals and filling diatom valves. The carbonate tests of foraminifera found, within Peruvian nodules, are sometimes completely replaced by phosphatisation (Manheim *et al.*, 1975).

In 1982, the *R.V. Robert D. Conrad* cruise 23-06 collected many cores from the Peruvian continental margin and results from many studies of both the sediments and pore waters were published in Burnett and Froelich (1988).

One of the most important findings of the cruise was the discovery of small, spherical phosphate pellets, whose distribution and concentration in the surface sediments had not been the result of sediment reworking (Baker and Burnett, 1988). Extensive grain-size analyses by Baker and Burnett (1988) showed that these pellets resided in a poor to very poorly-sorted matrix, which suggested *in situ* production under steady-state conditions, with significant differences in pellet concentration occurring as a result of varying influx rates of detrital sediment. Radiometric age dating by Burnett *et al.* (1988) suggested that some pellets are modern (3 ka) and some were previously formed (250 ka). These pellets from a modern, marine environment are of great interest because most ancient, land phosphate deposits are formed from similar pelletal material.

Factor analysis of the chemical composition of phosphatic pellets and ooids indicated some mineralogical differences (Glenn and Arthur, 1988) and petrographic observations, by these authors, allowed for interpretation of the sequence of authigenic mineral diagenesis, involving glauconite, carbonate fluorapatite and pyrite growth in the suboxic/anoxic environment of Peruvian margin sediments.

Froelich *et al.* (1988) measured pore-water and solid-phase chemical concentrations and found pore-water phosphate levels close to the sediment/water interface which were much higher than that expected if organic matter regeneration was the only source. Other potential sources for the interfacial phosphate release into pore waters are from (1) dissolution of fish debris (Suess, 1981), (2) degradation of microbial mats (*Thiopolca sp.*, Henrichs and Farrington, 1984) and (3) reduction of iron oxyhydroxides (Froelich *et al.*, 1988). Downward-decreasing pore water profiles of fluoride imply diffusion from overlying sea-water into the interstitial pores followed by removal into the sediment column by incorporation into CFA (Froelich *et al.*, 1983; Jahnke *et al.*, 1983).

## 4.2. ANALYTICAL METHODS AND ELEMENT PARTITIONING

Concentrations of the major and trace elements involved in this geochemical study of phosphorites from off-shore Peru basins, were determined by X-ray fluorescence techniques (Appendix A.5). An actual phosphorite hardground nodule from core CD38-09, found at a depth of 273cm, was sampled and its composition analysed by both X-ray fluorescence and X-ray diffraction. The age of this nodule was determined using U/Th alpha-spectrometry as outlined in Appendix A.8.

To examine the possibility of the presence of phosphorite within each core, particular elemental concentrations in the bulk sediment samples had to be partitioned into various end-member sources. To allow for calculation of the extent of fractionation into terrigenous, organic or phosphorite phases, aluminium (Al) was assumed to be solely present in terrigenous material and organic carbon ($C_{org}$) levels were assumed to be representative of the amount of organic matter present. Fractionation equations for phosphorus, uranium, yttrium and strontium can be found in Appendix B.4.

## 4.3. RESULTS AND DISCUSSIONS

### 4.3.1. Phosphorite hardgrounds

Two zones of coarse-grained pebbles and nodules were seen when the two shallow-water Peruvian continental shelf cores were split open for subsampling. These "hardgrounds" occur at 270-277cm depth in core CD38-09 and at 87-91cm in core CD38-10.

The largest nodule was found at 273cm in core CD38-09; it measured 6x4x1cm and sat horizontally within the core like a 2-dimensional slab. Its outer coating is very dark, olive green in colour with a flat, polished top and base, and small burrows on the top side. One edge is a paler olive green colour with a rough texture indicating that the nodule may have been part of a larger hardground slab.

Due to the similarity with previous phosphorite nodules from the Peru margin (Baturin, 1982; Glenn and Arthur, 1988) the nodule, and others found in cores CD38-09 and CD38-10, were assumed to be phosphorites. The following mineralogical and geochemical analyses were used to test this assumption.

**X-ray diffraction**

Four samples were obtained by filing away a small amount of material from two nodules and thin smear slides were prepared for X-ray diffraction analysis (Appendix A.9). One sample (GM/HG3) was taken from a small nodule in core CD38-10 (87cm) and three from the large nodule in CD38-09 (273cm) at the top (GM/HG1A), middle (GM/HG1B) and base (GM/HG1C).

X-ray diffraction provided a qualitative identification of the minerals present in the nodules and the spectral patterns shown in Fig. 4.2 illustrate the similarity in mineralogical composition between all four samples. The main minerals that account for the peaks in the diffraction pattern are carbonate fluorapatite (CFA), quartz and calcite (there may also be a small amount of pyrite present). There also seems to be no major mineralogical differences between the dark, outer surfaces and paler centre of the large nodule.

**X-ray fluorescence**

A slice of the large nodule (CD38-09, 273cm) was cut into two samples (09HG/Top and 09HG/Base), which were finely ground and made into pressed pellets for X-ray fluorescence analysis (Appendix A.5). The major and trace element concentrations for both samples are presented in Table 4.1 and from this it can be seen that the bulk chemical compositions of the top and lower halves of the nodule are very similar.

| Sample | $SiO_2$ | $Al_2O_3$ | $Fe_2O_3$ | MgO | CaO | $Na_2O$ | $K_2O$ | $P_2O_5$ | Total |
|---|---|---|---|---|---|---|---|---|---|
| 09HG/Top | 12.7 | 2.49 | 2.30 | 1.03 | 32.3 | 1.39 | 0.35 | 19.3 | 71.85 |
| 09HG/Base | 16.6 | 3.31 | 2.06 | 1.03 | 31.6 | 1.49 | 0.47 | 18.7 | 75.23 |

| | Nb | Zr | Y | Ba | U | Rb | Th | Pb | Zr | Cu | Ni |
|---|---|---|---|---|---|---|---|---|---|---|---|
| 09HG/Top | 0 | 67 | 7 | 58 | 112 | 20 | 0 | 2 | 36 | 12 | 15 |
| 09HG/Base | 0 | 81 | 9 | 110 | 153 | 24 | 2 | 3 | 37 | 12 | 14 |

| | Cr | Ce | Nd | La | V | Sc | I | Br | Mo | Sr |
|---|---|---|---|---|---|---|---|---|---|---|
| 09HG/Top | 41 | 25 | 3 | 7 | 48 | 5 | 0 | 40 | 68 | 1692 |
| 09HG/Base | 44 | 19 | 7 | 24 | 56 | 7 | 0 | 35 | 64 | 1556 |

Table 4.1. X-ray fluorescence analysis of phosphorite nodule.
(Major element oxides in wt.% and trace elements in ppm.)

The two most abundant chemical elements (apart from oxygen) found in the nodule are phosphorus and calcium, which supports the theory that the nodule is

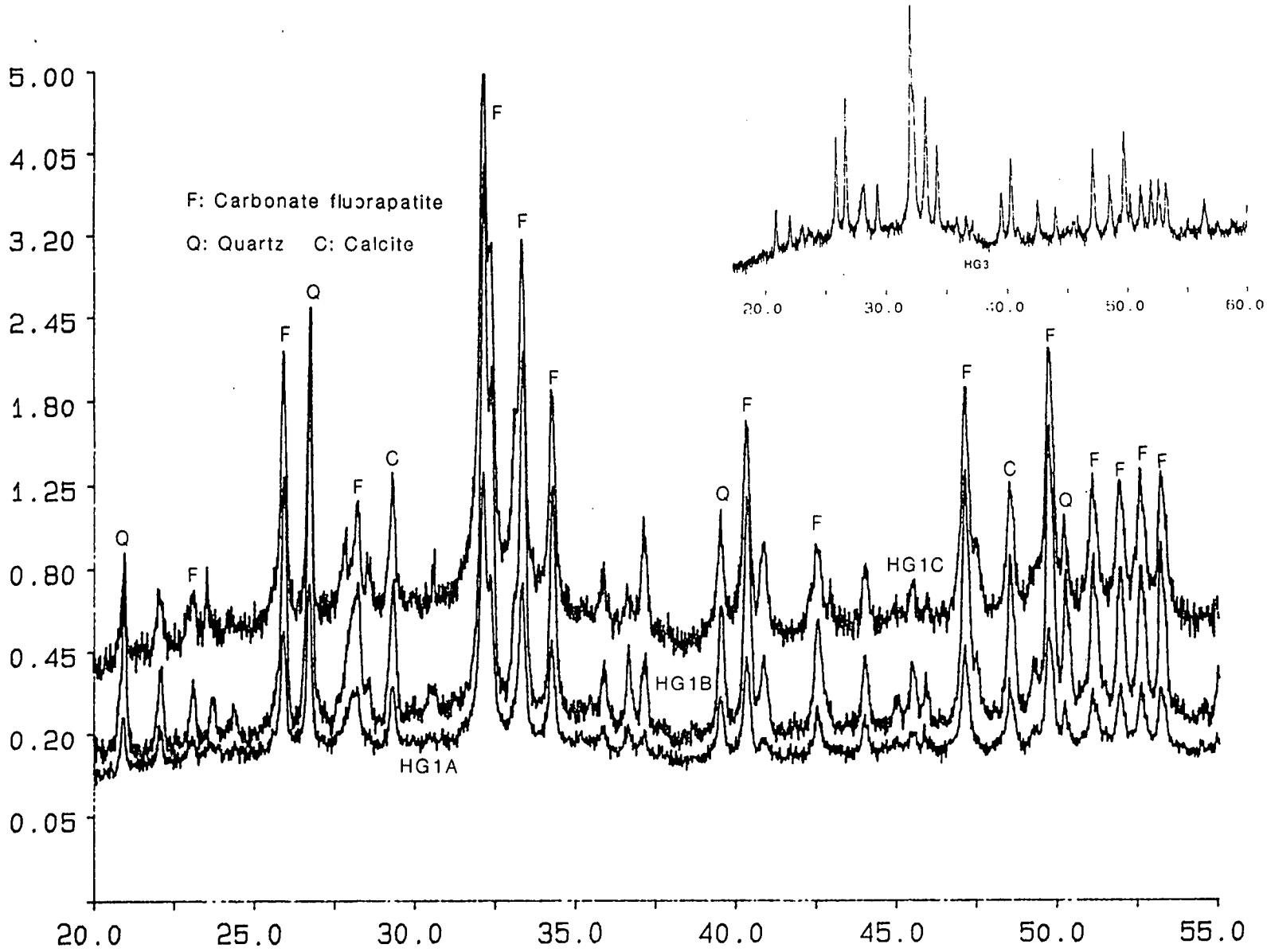


Figure 4.2. X-ray diffraction spectra of phosphorite samples.

dominantly composed of carbonate fluorapatite (CFA). The totals for the major element oxides only add up to 70-75 wt.% because both carbonate and fluorine are not analysed by XRF and they will make up most of the remaining 25-30 wt.%.

Glenn and Arthur (1988) used linear programming to estimate the concentrations of various minerals in a Peru margin nodule using electron microprobe data. Using the end-member mineral compositions from Glenn and Arthur (1988) and following the partitioning steps detailed in Appendix B.3, the above major element oxide concentrations were recalculated into mineral phases (Table 4.2) so that their relative abundances in the nodule from CD38-09 could be studied.

From the mineral data in Table 4.2. it can be seen that CFA is the dominant mineral in the large nodule by a factor of 5-6, over minerals such as feldspars, quartz and opal. The latter minerals form the terrigenous clay and sand particles and diatom frustules around which the CFA originally formed. Pyrite and dolomite are authigenic minerals which are also incorporated into phosphorite nodules (Baturin, 1982). Glenn and Arthur (1988) noted in their study of mineral paragenesis in Peru margin sediments that precipitation of CFA and pyrite appeared to be coincident and often replaced glauconite grains during sediment burial into more strongly reducing conditions.

| | CFA | Dolomite | Calcite | Pyrite | Plag. | Orthoc. | Opal/Qtz. |
|---|---|---|---|---|---|---|---|
| 09HG/Top | 67.35 | 3.41 | 3.43 | 3.20 | 9.93 | 3.21 | 9.54 |
| 09HG/Base | 62.35 | 3.26 | 3.49 | 2.74 | 12.56 | 4.12 | 11.72 |

Table 4.2. Mineral percentage composition of phosphorite nodule
(Plag. = Plagioclase, Orth. = Orthoclase and Qtz. = Quartz.)

The trace element concentrations of the large nodule (Table 4.1.) are anomalously high in uranium, strontium, molybdenum, barium and cerium because it is these elements which are most easily incorporated into the CFA mineral lattice as substitutes for calcium (Price and Calvert, 1978; Manheim and Gulbrandsen, 1979; Lucas *et al.*, 1990). The trace element enrichments (and depletions) in this hardground nodule will be interpreted, along with those for the bulk sediment samples, in 4.3.4.

### 4.3.2. Pore-water phosphate

The presence of phosphatic, hardground nodules in cores CD38-09 and CD38-10 indicates that on the continental shelf and upper slope at 11°S off Peru, the

biogeochemical and environmental conditions are suitable for phosphorite diagenesis. A second line of evidence to support the mineralogical work in 4.3.1 comes from study of the levels of dissolved phosphate ($PO_4^{2-}$) anions present in the pore-waters near the sediment/water interface (Baturin and Bezrukov, 1979; Baturin, 1982; Jahnke *et al.*, 1983; Froelich *et al.*, 1988).

Phosphate concentrations in pore-waters from box core material were measured onboard the *R.R.S. Charles Darwin* by G.B. Shimmield, T. Shimmield and A.J. Patience (following the methods described in Appendix A.7). The results for box cores CD38-09, CD38-10 and CD38-11 are tabulated in Appendix C.4. Box cores are used for pore-water analysis because the sediment/water interface can be preserved and sampled, and this is vital for the study of diagenetic processes, such as phosphorite formation, which operate in this zone.

Pore-water $PO_4$ concentrations from core CD38-11 (3835m) fall in the range 3.9-5.7μM, which are normal for sediments from the deep-sea. In comparison, the two shallow-water sites are highly enriched in their level of pore-water $PO_4$: CD38-09 (148m) = 66-134μM and CD38-10 (257m) = 38-86μM. Figure 4.3 illustrates the pore-water $PO_4$ concentrations for these three cores plotted against depth, along with two profiles from the *R.V. Robert D. Conrad* cruise 23-06 (Froelich *et al.*, 1988) for comparison.

Core CD38-09 has a depth profile which is greatly enriched from bottom-water $PO_4$ (2.5μM, Froelich *et al.*, 1988) with levels about 75μM over the first two centimetres, then displaying a maximum of 134μM at 4.5cm before slowly decreasing with increasing depth. The profile from CD38-09 is very similar to RC23-06 BX2 (Fig. 4.3) which is from a water depth of 216m and was interpreted by Froelich *et al.* (1988) as resulting from regeneration of organic matter in the upper 5cm and precipitation of phosphate into a solid phase, presumably CFA, below 5cm. It is therefore likely that the same pore-water/solid-phase interactions are occurring at present in the near-surface sediments at site CD38-09 on the Peru margin.

Core CD38-10 also has pore-water $PO_4$ levels which are greatly enriched from the bottom-water concentration, with a depth profile which peaks directly below the sediment/water interface (86μM) before sharply dropping to a minimum at 1-1.5cm of 38μM then levelling out below 5cm at around 50μM. This unusual profile is virtually identical to that of RC23-06 BX4 (Fig. 4.3) which is from a more southerly site (15°S) on the Peru margin at a water depth of 133m (Burnett and Froelich, 1988). The presence of a phosphate maximum at the sediment/water interface and a minimum just

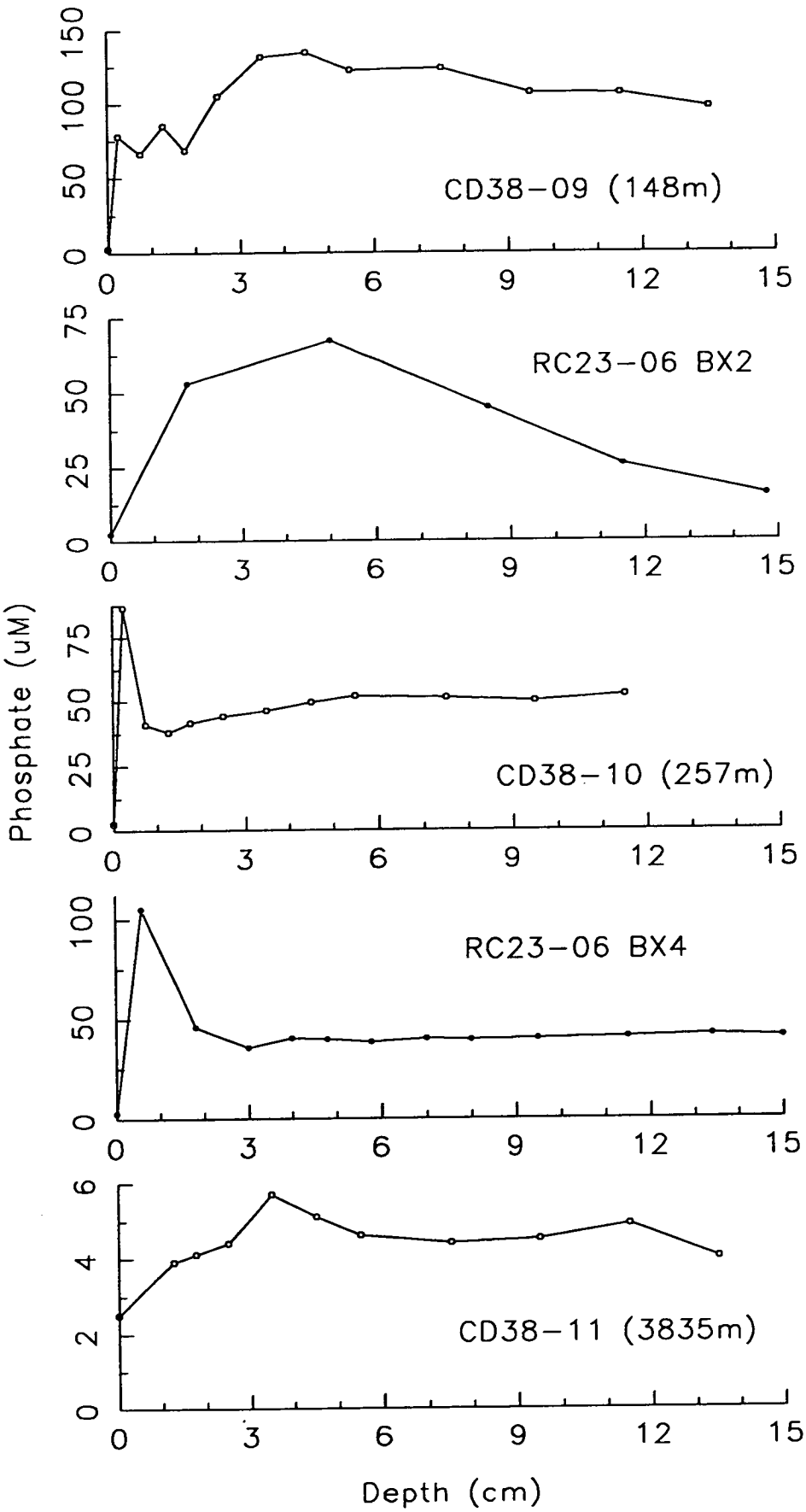


Figure 4.3. Pore-water phosphate ($PO_4$) concentrations against depth. RC23 cores and bottom-water concentration of 2.7 μmol $l^{-1}$ from Froelich *et al.*(1988).

below, requires the precipitation of an inorganic phosphate phase within the upper 5cm of the sediment column and also prevents the diffusion of $PO_4$ back into the bottom-water, when it is released from organic matter and/or fish debris at depth in the sediment (Froelich *et al.*, 1988).

Froelich *et al.* (1988) also studied other pore-water signals (e.g. silicate, sulphate and nitrate) from core RC23-06 BX4 which displayed suboxic to anoxic diagenetic trends with depth. However, the pore-water fluoride profile did not decrease with depth, as expected if CFA formation is occurring (Froelich *et al.*, 1983). The results of Froelich *et al.* (1988) suggested a two-step process of CFA precipitation, of which only the first step was occurring at site RC23-06 BX4. The two-stage diagenetic sequence involves the formation of amorphous calcium phosphate (ACP) by precipitation of pore-water $Ca^{2+}$ and $PO_4^{2-}$ ions near the sediment/water interface, as the first step, followed by uptake of fluoride and carbonate ions to convert ACP to the more stable mineral, carbonate fluorapatite (CFA).

Step 1. $3Ca^{2+} + 2PO_4^{3-} \longrightarrow Ca_3(PO_4)_2$ (ACP formation)

Step 2. $3Ca_3(PO_4)_2 + Ca^{2+} + xCO_3^{-} + (2+x)F^{-} \longrightarrow Ca_{10}(PO_4)_{6-x}(CO_3)_xF_{2+x}$ (CFA formation)

If the similarity between the phosphate depth profiles of CD38-10 and RC23-06 BX4 is indicative of a similar diagenetic and redox environment at both sites, then at the present day it is possible that CFA is not forming at site CD38-10 due to insufficient ACP-precursor formation (Froelich *et al.*, 1988). This interpretation, however, does not rule out formation of CFA in the recent past, when levels of $PO_4$ released into the pore-waters, by organic matter decomposition or fish debris dissolution (Suess, 1981), may have been slightly more enhanced.

The model of phosphorite pellet formation proposed by Froelich *et al.* (1988) invokes a steady-state diagenesis, where CFA precipitation is a sediment/water interface-linked process, which occurs in the upper centimetres of the sediment column and continuously moves upwards as more sediment accumulates in order to maintain its near-surface position. This is in contrast to the non-steady-state model proposed by Jahnke *et al.* (1983) for station 145-17 on the Mexican continental margin (off Baja California) which involves the precipitation of apatite only beginning when oxic respiration in the sediments becomes important. However,

Shimmield (1985) related the lower surface levels of organic carbon at this site to grain-size changes and concluded that the lithology change from mud to silt provided a more open-sediment matrix for diagenetic phosphorite precipitation.

The pore-water phosphate profiles of box cores CD38-09 and CD38-10 (Fig. 4.3) support the steady-state model (Froelich *et al.*, 1988) of CFA precipitation, which represents continuous phosphorite formation just below the sediment/water interface and allows for pelletal phosphorite concentrations of up to 5wt.% throughout the sediment column (Baker and Burnett, 1988). This will be shown to be the case for the phosphorite (wt.%) in the piston cores CD38-09 and CD38-10 (4.3.3).

The pore-water $PO_4$ profile from CD38-11 (Fig. 4.3) is relatively flat and not elevated very much above bottom-water concentrations. It is therefore unlikely that phosphorite formation is occurring at this site to any significant degree at the present day.

### 4.3.3. Phosphorite zones

Now that the possibility of modern phosphorite diagenesis on the Peruvian continental margin has been examined, it is of great interest in this geochemical study to investigate any variation in phosphorite concentration with depth (i.e. qualitative time-series analysis) occurring in the cores collected on the *R.R.S. Charles Darwin* cruise 38 from off Peru. Using the phosphorus fractionation equation (Eqn 4.1 and Appendix B.4) the distribution and extent of phosphorite diagenesis was examined in the bulk sediment samples for all the cores by calculating $P_{phos}$ (wt.%).

Equation 4.1. Phosphorus fractionation

$$P_{phos} = P_{total} - (P_{terr} + P_{org})$$

where, $P_{phos}$ = excess phosphorus incorporated into phosphorite,
$P_{total}$ = concentration from XRF,
$P_{terr}$ = terrigenous phosphorus = Al (wt.%) x 0.0875
(average shale, Turekian and Wedepohl, 1961),
$P_{org}$ = organic phosphorus = $C_{org}$ x 0.0053 (Mach *et al.*, 1987).

A C:P weight ratio of 41:1 in organic matter (Sverdrup *et al.*, 1946; Redfield *et al.*, 1963) is the average value for modern marine plankton and will increase upon

bacterial decomposition of the organic matter due to preferential release of organic phosphorus as dead marine organisms sink down through the water column (Bishop *et al.*, 1980). Therefore, the $C_{org}/P_{org}$ ratio in organic-rich marine sediments is much greater than the Redfield ratio (Froelich *et al.*, 1982). If the organic matter is, however, incorporated in faecal pellets or large aggregates then it will sink rapidly to the sediment surface and phosphorus-deficiency may not occur (Knauer *et al.*, 1979).

Froelich *et al.* (1982) proposed that the $P_{org}$ content of marine sediments is independent of the $C_{org}$ concentration. However, the data set of Froelich *et al.* (1982) was reviewed and updated by Mach *et al.* (1987) who fitted a best-fit straight line with the following relationship: $P_{org} = C_{org} \times 0.0053$. This C:P ratio for organic matter in marine sediments of 190 ±20 is supported by the results of Ramirez and Rose (1992) who reviewed the analytical procedures used in determining $P_{org}$ in soils and marine and fluvial sediments. The C:P ratio of Mach *et al.* (1987) has therefore been used in calculations of $P_{org}$ from the measured concentrations of $C_{org}$ in Equation 4.1.

The work of Mach *et al.* (1987) indicated no preferential loss of $P_{org}$ or $C_{org}$ associated with organic matter regeneration upon burial in the sediment column. However, Froelich *et al.* (1988) suggest that phospholipids and other labile organo-phosphorus compounds will preferentially decompose in marine sediments and therefore, the calculated $P_{org}$ concentrations may be slightly less accurate towards the base of each core.

The concentrations of the phosphorus fractions for cores CD38-09, CD38-10 and CD38-11 plotted against depth are displayed in Fig. 4.4 (the data is listed in Appendix C.13). For the box and piston cores of CD38-02 and CD38-03, all the $P_{total}$ concentration can be accounted for by the $P_{terr}$ and $P_{org}$ fractions, implying that no phosphorite is present in these cores. Core CD38-09 displays a $P_{phos}$ peak of about 6 wt.% and CD38-10 has three peaks between 2 and 3 wt.% (and 2 other possible peaks at 0.6-0.7 wt.%). However, in core CD38-11 the $P_{phos}$ peaks are no more than 0.5 wt.% which implies that phosphorite formation is only present to any significant degree in the shallow-water shelf environment.

It should be noted that fish bones and scales are enriched in P (Suess, 1981) and therefore, some of the $P_{phos}$ calculated for cores CD38-09 and CD38-10 may in fact, only be concentrations of fish debris and not P in phosphorite minerals. Study of trace metal enrichments will help to solve this problem.

Using the average concentration of P measured in the phosphorite hardground from CD38-09 (8.29 wt.%, Table 4.1) as the end-member concentration for all

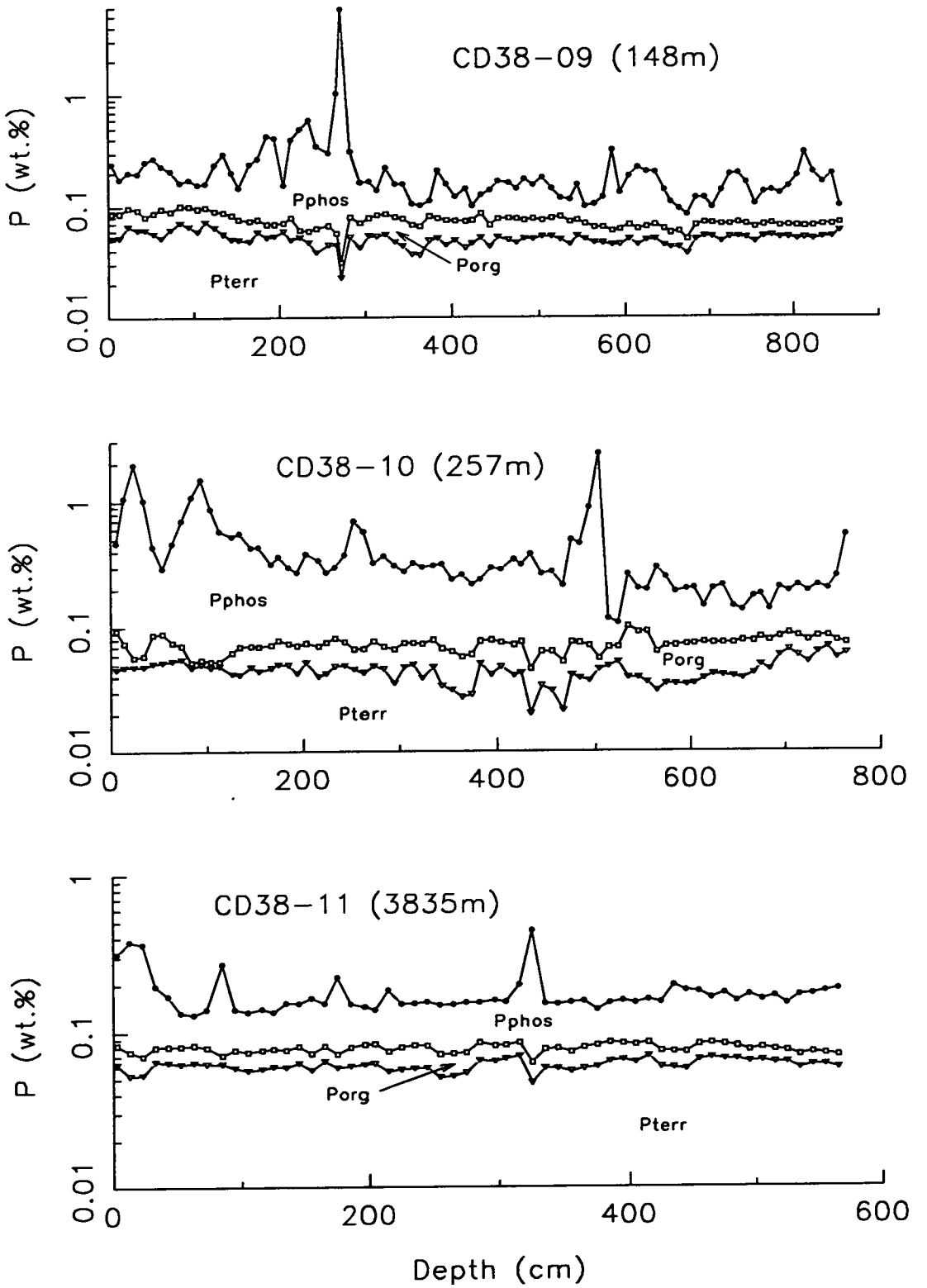


Figure 4.4. Partitioned phosphorus concentration against depth (note the log scale on the P (wt.%) axis). The area under each line represents the fraction of P where, $P_{terr} = Al \times 0.00875$ (Turekian and Wedepohl, 1961)
$P_{org} = C_{org} \times 0.0053$ (Mach *et al.*, 1987)
$P_{phos} = P_{total} - (P_{terr} + P_{org})$.

phosphorites formed in this area off Peru, the percentage amount of phosphorite (CFA and its associated non-phosphatic phases) present in each bulk sediment sample was calculated using Eqn 4.2.

Equation 4.2.

$$\text{Phosphorite (wt.\%)} = P_{phos} \times (100 / 8.29)$$

It can be seen from Fig. 4.5, which plots the calculated phosphorite percentage against depth for CD38-09, CD38-10 and CD38-11, that in core CD38-09 the background concentration is about 1wt.% but from 170 to 280cm depth there is some phosphorite enrichment. This peaks sharply at 273cm with just under 70 wt.% phosphorite in the sediment sampled and corresponds to the depth at which the hardground nodule was found.

In core CD38-10, the background phosphorite concentration is between 1 and 3wt.%, except in the region between 520 and 680cm where it falls below 1wt.% (this may be due to variability of the $C_{org}/P_{org}$ ratio with depth). The background level possibly indicates the presence of disseminated phosphorite gels and small pellets throughout the core. There are five zones in core CD38-10 where there has been enrichment of the phosphatic pellets by some sorting process (Fig. 4.5). These are at 30cm, 80-110cm, 250cm, 480-505cm and 770cm but it was only at the second of these depths that actual hardground nodules were observed during the logging of the core.

In core CD38-11 the phosphorite peaks are much smaller than in the two shallow-water cores, with more than 3 wt.% phosphorite occurring only at 10-30cm (a turbidite zone) and 330cm.

If zones in the sediment column where the phosphorite is greater than 10 wt.% are interpreted as being significant concentration events associated with periods of sediment reworking caused by stronger bottom-water currents during times of low sea-level, then core CD38-09 contains one such event and CD38-10 three events.

However, it must be emphasised that the calculated phosphorite (wt.%) depends greatly on the subsampling procedure: for instance, in core CD38-10 the phosphorite peak at 30cm is about 5% greater than the one at 90cm but it was only at 90cm that any phosphorite nodules were seen. It must also be remembered that if there is a large concentration of undissolved fish debris within the core, then it will be seen as a phosphorite-enriched horizon (Fig. 4.5).

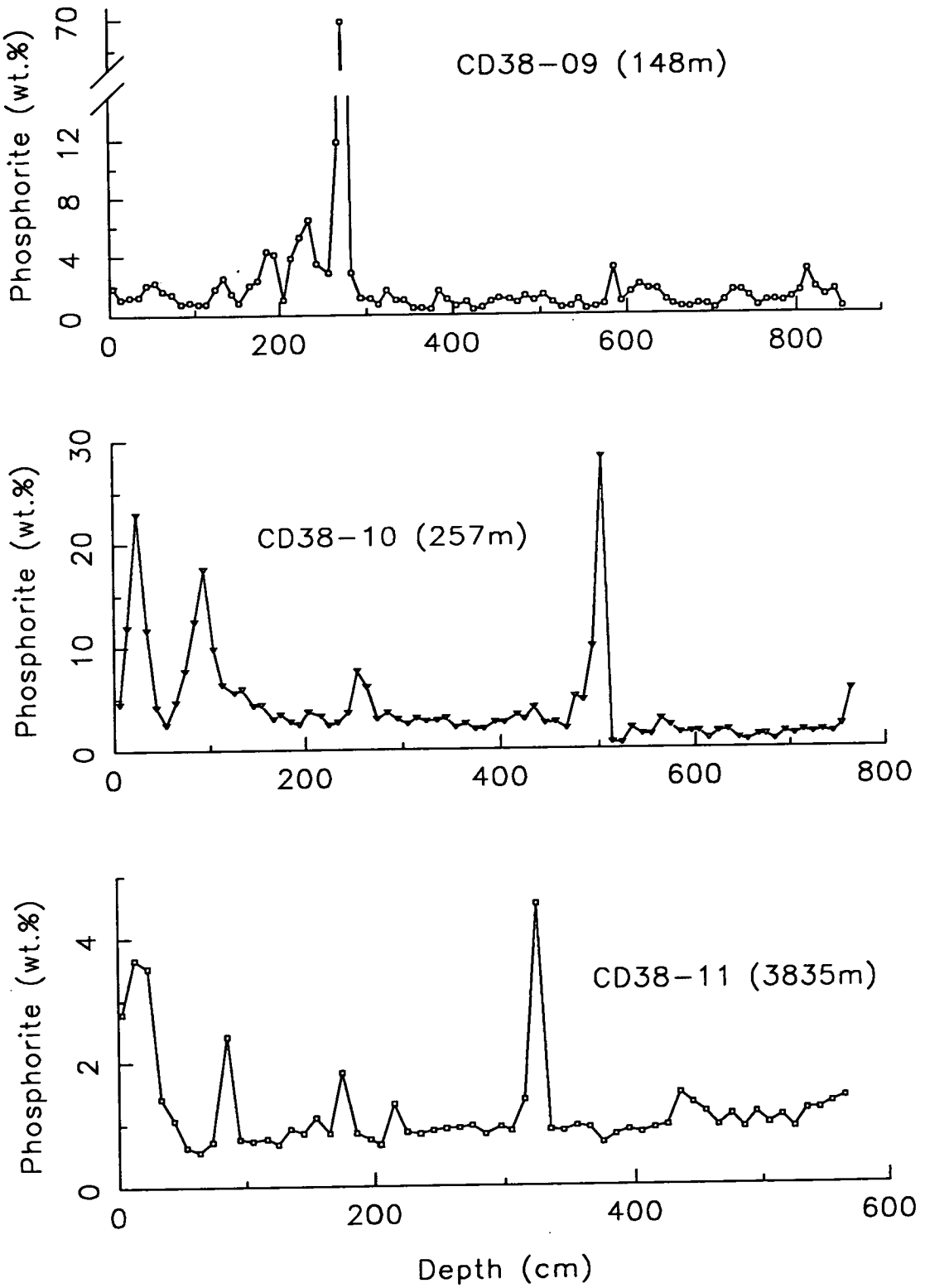


Figure 4.5. Phosphorite concentration against depth, where,

$$\text{Phosphorite} = P_{phos} \times (100 / 8.29) \qquad \text{(Eqn. 3.2)}$$

### 4.3.4. Trace element and phosphorite associations

The trace elements which have high concentrations in the X-ray fluorescence analysis of the large, hardground nodule (Table 4.1) should also be enriched, relative to the normal marine sediment concentrations, in the phosphorite-rich zones found in cores CD38-09 and CD38-10. Many previous studies have focused on the trace element composition of land phosphorites (Altschuler, 1980), marine phosphorites (Price and Calvert, 1978; Baturin, 1982; Piper *et al.*, 1988) and synthetically-grown apatite (Lucas et al., 1990) in which enrichments of uranium (U), molybdenum (Mo), strontium (Sr), barium (Ba), cadmium (Cd), yttrium (Y) and the rare earth elements are common.

The following section will look at a selection of the above trace elements with respect to their concentrations in the sediment column of cores CD38-09 and CD38-10, and interpretations of their distribution, source and association with CFA will be made. Figures 4.6 and 4.7 illustrate the concentrations of U, Sr, Ba and Y, all expressed as element/Al ratios in order to eliminate any variation in concentration resulting from terrigenous input dilution, for both the shallow-water cores. The phosphorite depth profiles are plotted below each set of trace element profiles to allow for easy comparison. Table 4.3 lists the concentrations of trace elements measured in phosphorites from a wide variety of locations and includes the large nodule found in core CD38-09 and the bulk sediment from 273cm.

**Uranium**

In addition to the small amount incorporated in terrigenous clay particles, organic matter is known to scavenge uranium (as $U^{VI}$) from sea-water and then transport it to the accumulating sediments (Baturin *et al.*, 1971; Bertine and Turekian, 1973; Baturin, 1982; Shimmield and Pedersen, 1990). It was seen in Chapter 3 that U is anomalously enriched in the suboxic/anoxic marine shelf sediments off Peru due to its association with the high flux of organic matter down the water column. However, within the sediments of cores CD38-09 and CD38-10, the U concentration displayed poor correlation with $C_{org}$ levels (Table 3.3) as a result of post-depositional decomposition of organic matter and release of U into the surrounding pore-waters.

The U ions dissolved in the near-surface pore-waters (as $U^{IV}$) are therefore readily available to be incorporated in the authigenic diagenesis of CFA by substitution of calcium in the mineral lattice (Veeh *et al.*, 1974; Price and Calvert, 1978; Manheim and Gulbrandsen, 1979).

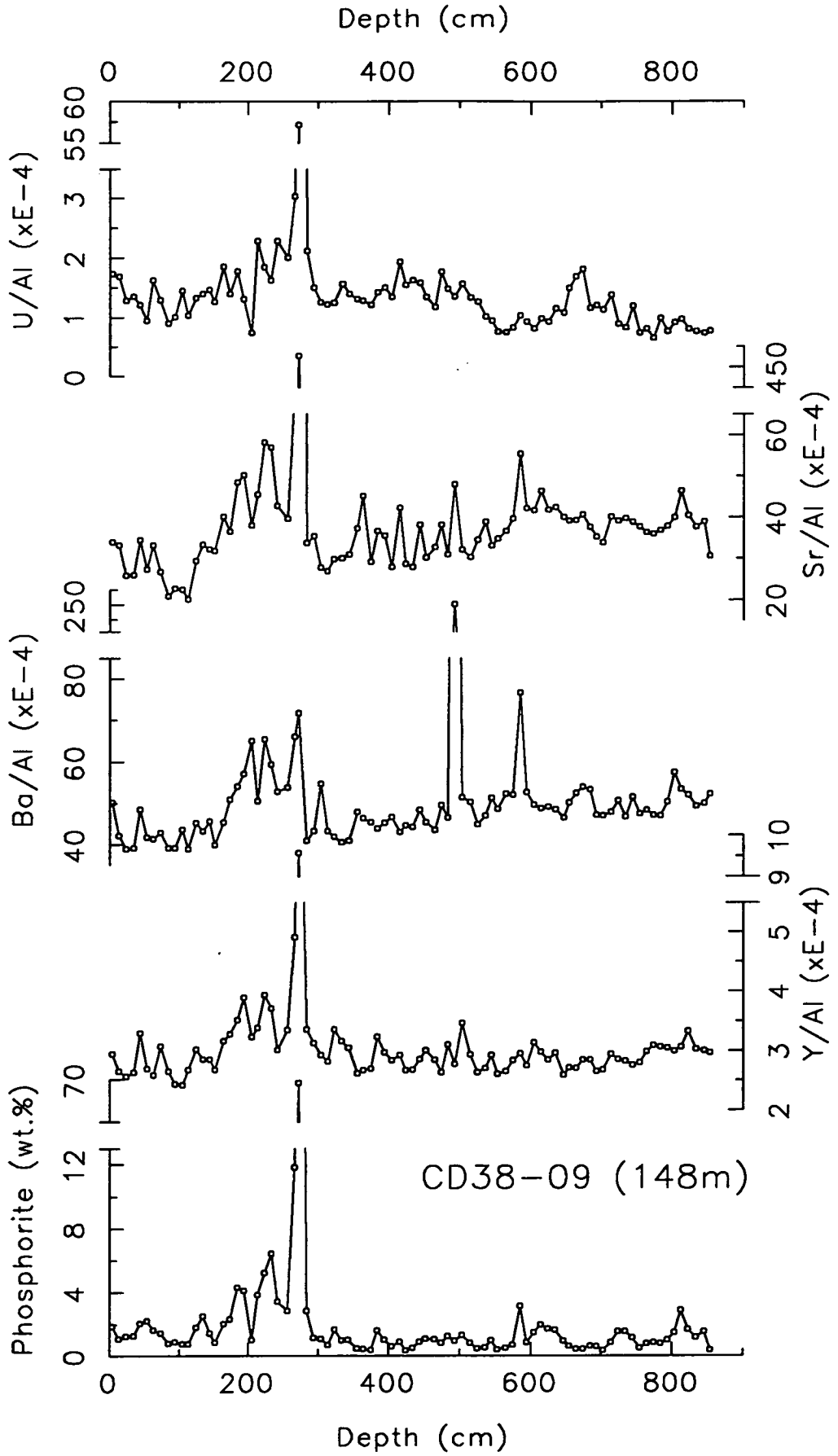


Figure 4.6. Trace element/Al ratios (U/Al, Sr/Al, Ba/Al and Y/Al) and phosphorite concentration against depth for core CD38-09 (148m).

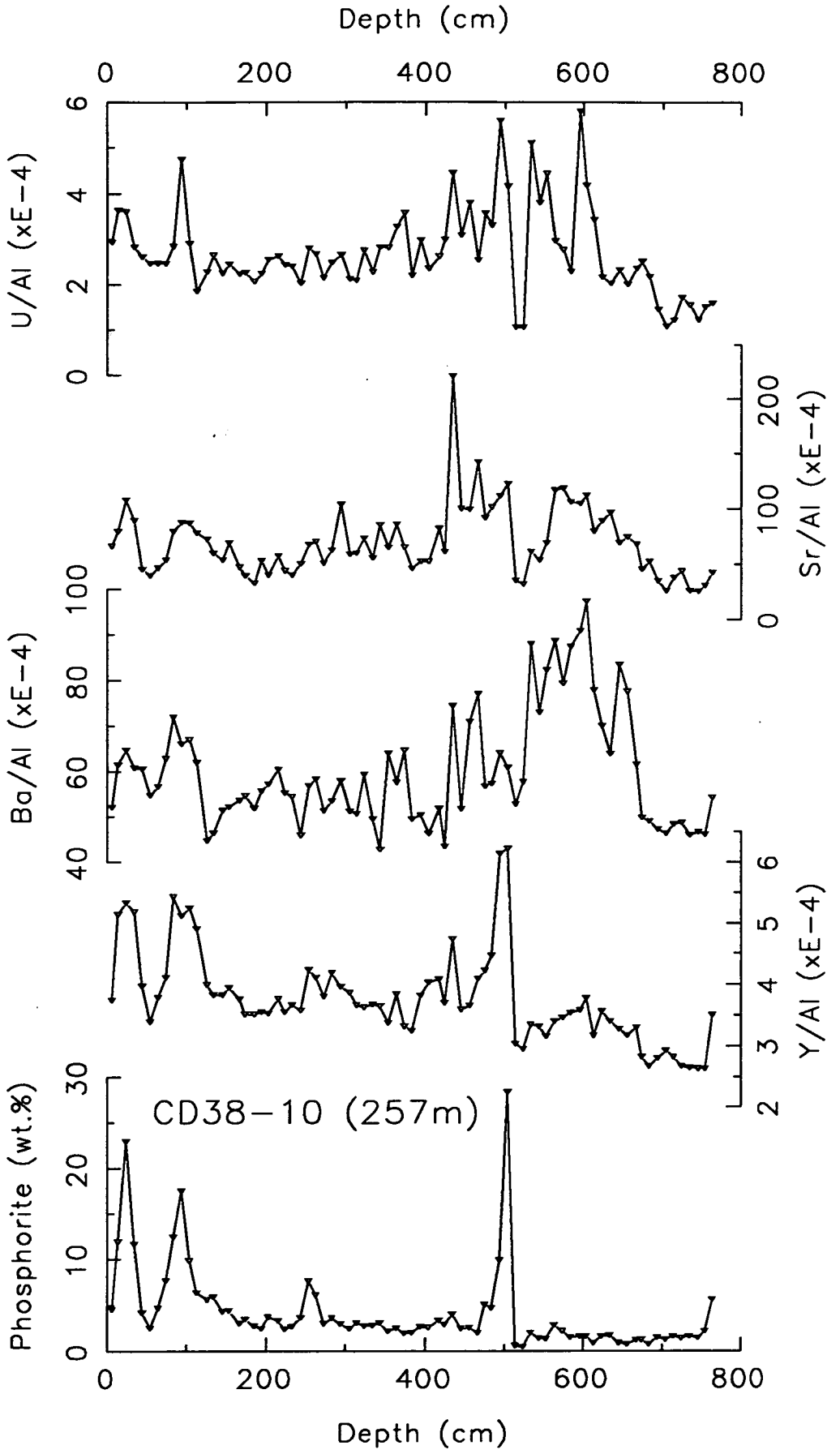


Figure 4.7. Trace element/Al ratios (U/Al, Sr/Al, Ba/Al and Y/Al) and phosphorite concentration vs. depth for core CD38-10 (257m).

| Author | Year | Location | U (ppm) | Sr (ppm) | Ba (ppm) | Mo (ppm) | Y (ppm) |
|---|---|---|---|---|---|---|---|
| Kolodny & | 1970 | Marine environment | 6-254 | | | | |
| Kaplan | | California Borderland | 36-149 | | | | |
| Veeh *et al.* | 1974 | SW African margin | 79-158 | | | | |
| Price & | 1978 | Namibian shelf | 40-130 | 470-2080 | 200-1100 | 15-45 | 5-302 |
| Calvert | | (Fish-bones) | (140) | (1640) | | (65) | (128) |
| McArthur | 1978 | Morocco sea-floor | | 53-2130 | | | |
| Manheim & | 1979 | Marine environment | 5-600 | 800-5000 | 10-900 | 2-30 | |
| Gulbrandsen | | | | | | | |
| Altschuler | 1980 | Average land deposits | 120 | 750 | 350 | 9 | 260 |
| Baturin | 1982 | Peru/Chile margin | 26-219 | | | | |
| Piper *et al.* | 1988 | Peru shelf | 51-459 | | | | 120-150 |
| | | (Fish remains) | | | | | (16) |
| This study | | CD38-09 hardground | 112-153 | 1556-1692 | 58-110 | 64-68 | 7-9 |
| | | Sediment (273cm) | 148 | 1195 | 185 | 53 | 25 |
| Turekian & | 1961 | (Deep-sea clay) | 1.3 | 180 | 2300 | 27 | 90 |
| Wedepohl | | | | | | | |

Table 4.3. Trace element concentrations of phosphorites (and fish remains)

The bulk sediment sample at the location of the large hardground nodule in CD38-09, i.e. a phosphorite-rich zone, has a U-enriched concentration of 148ppm (Table 4.3). This U-phosphorite association is illustrated in Figs 4.6 and 4.7 by the similarity between the U/Al and phosphorite depth profiles. The normal, background U/Al level ($1.55 \times 10^{-5}$, deep-sea clay, Turekian and Wedepohl, 1961) is elevated to about $1\text{-}4 \times 10^{-4}$ down both cores by the continuous presence of high organic matter concentrations. However, the phosphorite-rich zones at 270-280cm in CD38-09 and 30, 80-110 and 490-500cm in CD38-10, all correspond to peaks in U/Al (with a maximum of $57.5 \times 10^{-4}$ at 273cm in core CD38-09) which is due to the incorporation of U into phosphatic pellets and nodules (Price and Calvert, 1978).

One possible problem in this interpretation of the U-phosphorite correlation is brought about by the presence of fish remains. Fish bones and scales are also enriched in uranium (700ppm, Baturin *et al.*, 1971; 140ppm, Price and Calvert, 1978) and, although they can act as an extra source of U by dissolution in marine sediments, if a large concentration of fish debris is buried within the sediment column then its geochemical signal will be an anomalous U (and P) peak.

A correlation plot of the total U content against the calculated $P_{phos}$ content of bulk sediment samples in the phosphorite-rich zones of both CD38-09 and CD38-10, as shown in Figure 4.8, gives a regression line of:

$$U\ (ppm) = [P_{phos}\ (wt.\%) \times 14.1] + 4.3 \qquad (r = 0.905).$$

This relationship is supported by the XRF data of the large, phosphorite nodule which has an average U/P ratio of 16.0 (Table 4.1). The above regression equation accounts for the U enrichment in phosphorite zones and allows for the quantitative partitioning of U into its terrigenous, phosphatic and organic phases for all the sediments from the Peruvian margin cores (Eqn 4.3 and Appendices B.4 and C.13).

Equation 4.3. Uranium partitioning (all in ppm)

$$U_{org} = U_{total} - [U_{terr} + U_{phos}]$$

where, $U_{org}$ = excess U associated with organic matter
$U_{total}$ = salt-corrected XRF data
$U_{terr}$ = [Al (wt.%) x 0.4625]
(average shale, Turekian and Wedepohl, 1961)
$U_{phos}$ = [$P_{phos}$ x 14.1].

The down-core variations of the three U-phases are displayed in Fig. 4.9 and from this it can be seen that for core CD38-09 the $U_{phos}$-phase is dominant over the 160-300cm depth range but that $U_{org}$ is significant elsewhere. In core CD38-10, the $U_{org}$ concentrations are high throughout the core reflecting the high organic matter content, but very low (or zero) in the three phosphorite-rich zones. It should be noted that at 30 and 500cm the calculated $U_{phos}$ concentration is greater than the $U_{total}$ as measured by XRF, and this may be an indication that these zones are not composed entirely of phosphorite but that there is a significant concentration of fish debris present, which will have a lower U/P ratio (Price and Calvert, 1978).

In the semi-quantitative analysis of fish-remains in sieved samples from core CD38-10, fish bones and scales were seen to be common in these two zones (3.3.5, Fig. 3.12.B).

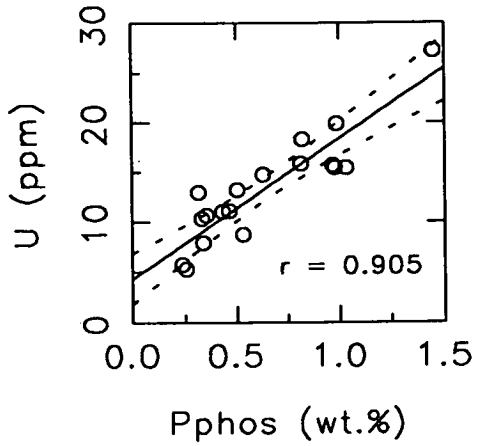


Figure 4.8. Correlation plot of U against $P_{phos}$ for the phosphatic-rich zones in CD38-09 and CD38-10. With a best-fit straight line (showing 95% confidence limits) of:
U (ppm) = ($P_{phos}$ x 14.1) + 4.3 (r = 0.905)

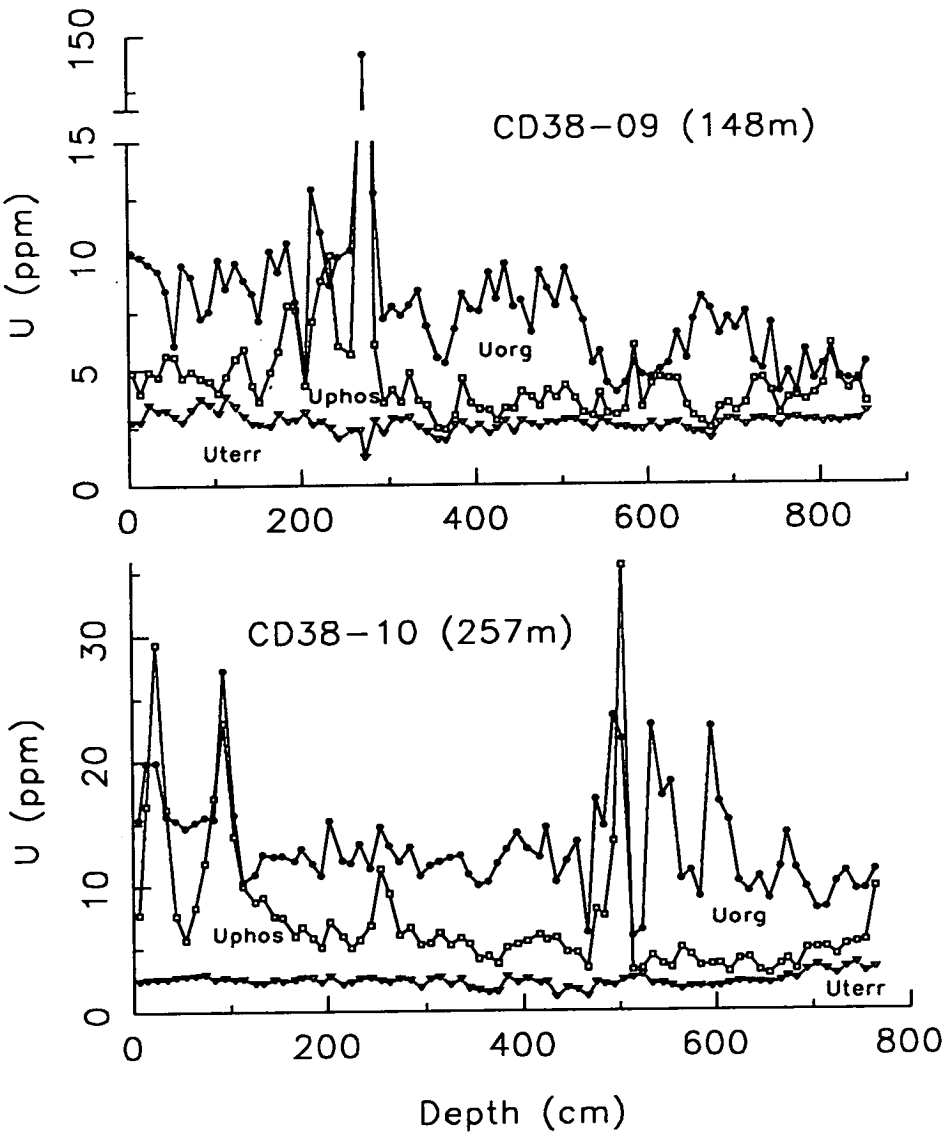


Figure 4.9. Partitioned uranium concentration against depth for CD38-09 and CD38-10 (note the break in scale on the U (ppm) axis for CD38-09). The area under each line represents the fraction of U where,

$U_{terr}$ = Al x 0.4625 (Turekian and Wedepohl, 1961),

$U_{phos}$ = $P_{phos}$ x 14.1 (Fig. 3.8),

$U_{org}$ = $U_{total}$ − ($U_{terr}$ + $U_{phos}$).

The organo-metallic relationship for $C_{org}$ and calculated $U_{org}$ has correlation coefficients of 0.655 for CD38-09 (after eliminating the sample at 273cm) and 0.813 for CD38-10, which are much higher than the original $U_{total}$-$C_{org}$ coefficients (see Table 3.3).

**Strontium**

Sr is a group II element which occurs in the same column of the periodic table as calcium. It is most stable as the $Sr^{2+}$ cation and has a very similar ionic radius compared with $Ca^{2+}$ ($Sr^{2+}$ = 1.12Å, $Ca^{2+}$ = 0.99Å, Ahrens, 1952) and therefore Sr easily substitutes for Ca in mineral structures. This is true not only for the $CaCO_3$ shells of foraminifera and coccoliths (Emiliani, 1955; Krinsley, 1960) but also for carbonate fluorapatite (McArthur, 1978; Price and Calvert, 1978; Lucas *et al.*, 1990).

Price and Calvert (1978) quote a ratio of CaO/Sr = 266 in phosphorites on the Namibian shelf and interpret the consistency of the relationship as caused by Sr incorporation into the CFA structure at the time of formation. McArthur (1978) studied the Sr content of both land and marine phosphorite deposits and concluded that because Sr substitution requires no balancing-anion replacement, it is relatively easy for Sr to be incorporated into CFA and also for it to leave the mineral upon weathering. The concentrations of Sr in phosphorites are tabulated in Table 4.3. and from this it can be seen that the large nodule in CD38-09 has an average Sr content for phosphorites but that it is greatly enriched over normal, deep-sea clay values (Turekian and Wedepohl, 1961).

Figures 4.6 and 4.7 display the Sr/Al depth profiles for cores CD38-09 and CD38-10 which are fairly similar in appearance to the phosphorite profiles. In core CD38-09, the correlation is very good over the 160-300cm depth range but elsewhere the variation in Sr/Al is controlled by changes in $CaCO_3$ concentrations (compare with Fig. 3.5). This carbonate control is also evident in core CD38-10 (compare Figs 4.7 and 3.6) especially at depths below 400cm. The two phosphorite peaks in the top metre of CD38-10 are reflected by elevations in the Sr/Al but there is not such a distinct peak at 500cm. This latter zone may be mainly an enrichment of fish debris, which is characterised by a different Sr/Al ratio.

By selecting the same bulk sediment samples as used for the U:$P_{phos}$ regression analysis, a Sr:$P_{phos}$ relationship in the phosphorite zones can be quantified (Fig. 4.10):

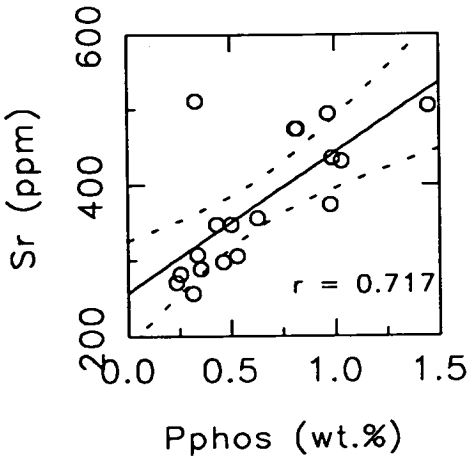


Figure 4.10. Correlation plot of Sr against $P_{phos}$ for the phosphatic-rich zones in CD38-09 and CD38-10. With a best-fit straight line (showing 95% confidence limits) of:
$Sr\ (ppm) = (P_{phos} \times 186) + 257$ $(r = 0.717)$

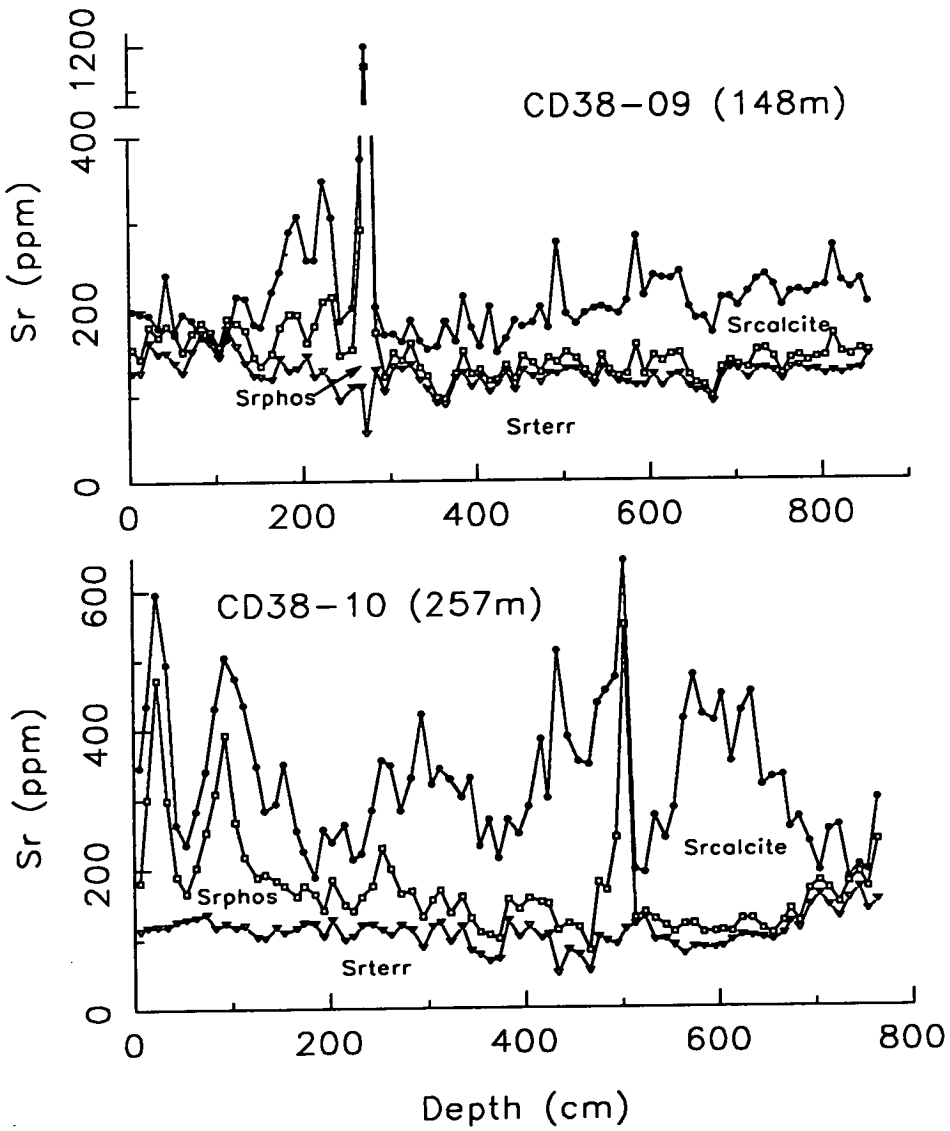


Figure 4.11. Partitioned strontium concentration against depth for CD38-09 and CD38-10 (note the break in scale on the Sr (ppm) axis for CD38-09). The area under each line represents the fraction of Sr where,

$Sr_{terr} = Al \times 21.43$ (Turekian and Wedepohl, 1961),

$Sr_{phos} = P_{phos} \times 186$ (Fig. 3.10),

$Sr_{calcite} = Sr_{total} - (Sr_{terr} + Sr_{phos})$.

$$Sr\ (ppm) = [P_{phos}\ (wt.\%) \times 186] + 257 \qquad (r = 0.717).$$

The intercept of this regression line is equivalent to the concentration of Sr from terrigenous debris and biogenic $CaCO_3$ shells found within the phosphorite-rich zones. The $Sr/P_{phos}$ ratio of 186 corresponds well to the measured Sr/P ratio of 190-200 for the hardground nodule in core CD38-09 (Table 4.1). Shimmield (1985) calculated the quantity of Sr uptake in diagenetic apatite, within sediments from Baja California, as 124ppm Sr per wt.% P.

The above regression equation allows for partitioning of the $Sr_{total}$ concentration into three phases; namely, terrigenous, phosphatic and an excess concentration which is the content associated with biogenic $CaCO_3$ (Eqn 4.4 and Appendices B.4 and C.13).

Equation 4.4. Strontium partitioning (all in ppm)

$$Sr_{calcite} = Sr_{total} - [Sr_{terr} + Sr_{phos}]$$

where, $Sr_{calcite}$ = excess Sr associated with $CaCO_3$
$Sr_{total}$ = salt-corrected XRF data
$Sr_{terr}$ = [Al (wt.%) x 21.43] (Turekian and Wedepohl, 1961)
$Sr_{phos}$ = [$P_{phos}$ x 186].

The depth profiles of the three Sr-phases (ppm) are plotted in Fig. 4.11 and this illustrates that, for both CD38-09 and CD38-10, $Sr_{terr}$ accounts for about 100ppm of the total Sr content and that there is always a significant amount of $Sr_{calcite}$ present even in the phosphorite-rich zones. This is because of the presence of both biogenic $CaCO_3$ and secondary-calcite cement within and around phosphorite pellets and nodules (Table 4.2).

The calculated $Sr_{calcite}$ and $CaCO_3$ concentrations correlate extremely well (in cores CD38-09 and CD38-10, r = 0.723 and 0.924 respectively) and the weight ratio of these two biogeochemical components will be discussed in Chapter 6.

**Barium**

Lucas *et al.* (1990) studied both Ba and Sr enrichments within synthetic apatites and concluded that $Ba^{2+}$ is a less suitable substituant for $Ca^{2+}$ compared with $Sr^{2+}$ even though the ionic charges are all equal. This is simply because the Ba cation

is much larger (1.34Å, Ahrens, 1952) than the Ca cation. Lucas *et al.* (1990) obtained a continuous solid-solution series for Sr replacement of Ca but could only achieve Ba replacement in apatites at less than 10% by weight.

It is therefore to be expected that in phosphorites from the natural, marine environment, Ba concentrations are significantly lower than the Sr content (Price and Calvert, 1978) and this be seen in the summary table of trace element concentrations in phosphorites (Table 4.3). The hardground nodule from CD38-09 has levels of Ba which are about the average for previously published results of marine phosphorites but much less than the average calculated by Altschuler (1980) for land deposits. This may be an indication that post-depositional weathering can enrich the Ba content of phosphorites.

The Ba ions which are incorporated into CFA minerals (Lucas *et al.*, 1990) must be present in the interstitial pore-waters of surface margin sediments and their flux from sea-water is via a residual solid-phase associated with organic debris and, most commonly, the biogenic silica frustules of diatoms (Dymond *et al.*, 1992 and references therein). In sediments accumulating under oxic conditions the Ba component can be well-preserved, but under reducing conditions, such as found in phosphorite-rich continental margin sediments, low Ba concentrations can occur due to the dissolution of barite and loss of dissolved Ba back into bottom-waters (Dymond *et al.*, 1992).

The Ba/Al depth profiles for the two shallow-water cores (Figs 4.6 and 4.7) display some similarities to the phosphorite profiles but the peaks at 273cm in CD38-09 and at 500cm in CD38-10 are not very pronounced. There are also large peaks in Ba/Al (at 500cm in CD38-09 and 530-650cm in CD38-10) which do not correspond to phosphorite-rich horizons. These may be due to enhanced biogenic flux to the sediment (compare with the biogenic silica profiles in Figs 3.5 and 3.6) and/or enhanced barite preservation (6.3.1).

**Molybdenum**

Molybdenum is a heavy metal which is known to be associated with organic matter enrichments in suboxic/anoxic sediments accumulating under a zone of coastal upwelling (Chapter 3). Study of the Mo-$C_{org}$ correlation coefficients for the organic-rich sediments of cores CD38-09 and CD38-10 indicated that Mo is released relatively easily upon degradation of organic matter. Therefore, there should be a high concentration of Mo dissolved in pore-waters available for incorporation into any authigenic minerals, such as CFA, or onto the mineral surfaces.

However, possibly because of its high valence state of +6, Mo uptake and enrichment in phosphorites is not common. Although the Mo concentration in the hardground nodule from CD38-09 represents an enrichment of twice the average deep-sea clay (Turekian and Wedepohl, 1961) it only represents a fairly average value for the organic-rich, reducing sediments which surround the phosphorite pellets and nodules (Table 3.1). Therefore, the enrichments seen by Price and Calvert (1978) and Altschuler (1980) are not really due to the authigenic mineral diagenesis of CFA.

**Yttrium**

One group of elements which can successfully substitute for calcium in the CFA of marine phosphorites are the rare earth elements (REE) (Manheim and Gulbrandsen, 1979; Henderson, 1984) and although Y is not classified as a REE, it does have very similar chemical characteristics to the REE and therefore is found enriched in phosphorites (Price and Calvert, 1978; Piper *et al.*, 1988; Table 4.3).

Y and the REE can be removed from sea-water into marine sediments by association with either terrigenous, hydrogenous or biogenic particles (Henderson, 1984) or, more importantly in the coastal zones such as Peru and south west Africa, incorporated in phosphatic fish-remains (Blokh, 1961; Arrhenius and Bonatti, 1965; Price and Calvert, 1978).

The hardground nodule from CD38-09 does not contain a high concentration of Y (8ppm) and yet the Y/Al depth profiles of the bulk sediment samples show extremely strong similarity to the phosphorite profiles (Figs 4.6 and 4.7). This can be explained either by an inaccurate X-ray fluorescence determination of Y in the hardground (which seems highly unlikely) or by the fact that the Y is still associated with undissolved fish bones and scales which are concentrated in the phosphorite-rich zones, especially at 500cm in core CD38-10.

As for U and Sr, the total Y concentration in these phosphatic horizons can be plotted against $P_{phos}$ (Fig. 4.12) and a regression analysis gives the following relationship:

$$Y\ (ppm) = [P_{phos}\ (wt.\%) \times 12.1] + 15.2 \qquad (r = 0.800).$$

The regression line intercepts the Y-axis at 15ppm which is the average amount of Y associated with terrigenous particles within and around the phosphatic minerals. It is now possible to separate the total Y concentration into two phases; namely the phosphatic and terrigenous associations, using Eqn 4.5 (Appendices B.4 and C.13). It

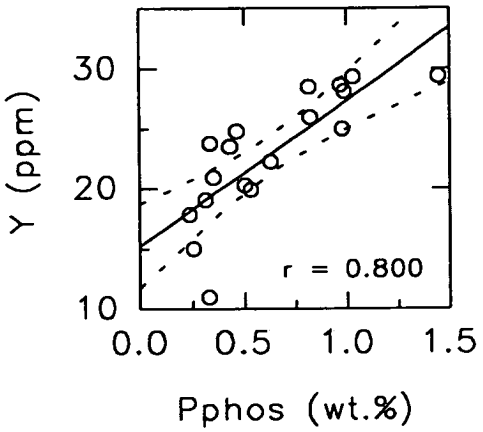


Figure 4.12. Correlation plot of Y against $P_{phos}$ for the phosphatic-rich zones in CD38-09 and CD38-10. With a best-fit straight line (showing 95% confidence limits) of:
$Y\ (ppm) = (P_{phos} \times 12.1) + 15.2$ $(r = 0.800)$

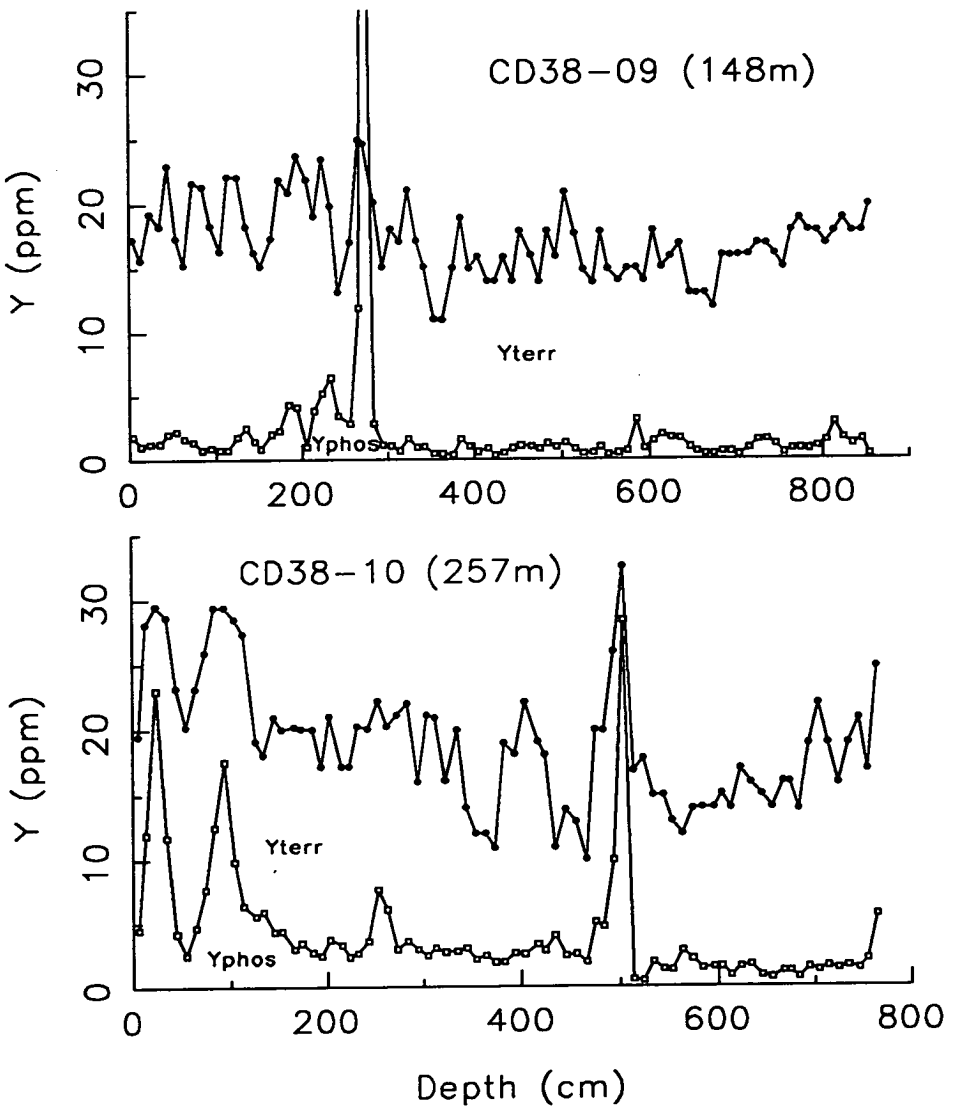


Figure 4.13. Partitioned yttrium concentration against depth for CD38-09 and CD38-10. The area under each line represents the fraction of Y where,
$Y_{phos} = P_{phos} \times 12.1$ (Fig. 3.12),
$Y_{terr} = Y_{total} - Y_{phos}$.

is not possible, however, to state how much of the $Y_{phos}$ is associated with either CFA and/or fish debris.

Equation 4.5. Yttrium partitioning (all in ppm)

$$Y_{terr} = Y_{total} - Y_{phos}$$

where, $Y_{terr}$ = excess Y associated with terrigenous clay particles
$Y_{total}$ = salt-corrected XRF data
$Y_{phos} = [P_{phos} \times 12.1]$.

Figure 4.13 illustrates the concentrations of the two phases of Y down both cores CD38-09 and CD38-10 and it can be seen that $Y_{terr}$ is the most abundant phase. Correlation coefficients of 0.879 for CD38-09 and 0.726 for CD38-10 between $Y_{terr}$ and Al (which is found only in terrigenous clays) gives support to the accuracy of the above partitioning equation.

### 4.3.5. U/Th age dating of the phosphorite nodule

Before the timing of the phosphorite hardground nodules found in the near-shore cores on the Peruvian continental margin can be interpreted with respect to changes in sea-level during the Late Quaternary, the phosphatic material has to be accurately dated.

The analytical technique which is best suited for age determination of phosphorite material is the uranium-series disequilibrium method (Ivanovich and Harmon, 1982; and references therein). This involves measurement of the activity of uranium and thorium radiochemical isotopes and calculation of the $^{234}U/^{238}U$ and $^{230}Th/^{234}U$ ratios. A brief outline of the analytical methods involved in U-series disequilibrium determinations by α-spectrometry are given in Appendix A.8 and the equations for calculation of the age of the phosphorite and the initial $^{234}U/^{238}U$ ratio are given in Appendix B.5.

The theory behind this method of age determination relies on the natural radiogenic decay of $^{238}U$ and its daughter isotopes. Following the reaction steps shown in Eqn 4.6, $^{238}U$ decays by α-particle emission (loss of $^{4}He$) and ß-particle emission to $^{234}U$ and which subsequently loses an alpha-particle to produce $^{230}Th$.

Each reaction has a known half-life ($t_{½}$) which is the time for one half of the original amount of the parent isotope to decay to its respective daughter isotope.

Equation 4.6. $^{238}U$ natural radiogenic decay series (Henderson, 1986)

$$^{238}U_{92} - \alpha \rightarrow {}^{234}Th_{90} - 2\beta \rightarrow {}^{234}U_{92} - \alpha \rightarrow {}^{230}Th_{90}.$$

Upon formation of phosphatic material at the sediment/water interface, uranium is incorporated into the CFA mineral lattice (4.3.4) with a $^{234}U/^{238}U$ ratio equal to that of sea-water (Veeh, 1967; Veeh *et al.*, 1973; Burnett *et al.*, 1988). It is assumed that the $^{234}U/^{238}U$ ratio in sea-water during the last few hundred thousand years has not significantly differed from its present value (1.14 ±0.014, Ku *et al.*, 1977) and that the phosphorite has remained a closed system with respect to U and Th since the time of formation (Veeh *et al.*, 1973).

Thus, the $^{238}U$ in the phosphorite will decay to $^{234}U$ but at a slower rate (larger $t_{½}$) than the rate at which the $^{234}U$ decays to $^{230}Th$, i.e. the $^{234}U/^{238}U$ ratio will exponentially decrease (from the initial sea-water value) with increasing age of the phosphatic material and the $^{230}Th/^{234}U$ ratio will exponentially increase. If the $^{230}Th$ content of the phosphatic material at the time of formation is assumed to be zero (i.e. all the $^{230}Th$ has been formed by U-series decay since formation) then the calculated age, from determination of the $^{234}U/^{238}U$ and $^{230}Th/^{234}U$ ratios at present in the phosphorite, can be said to be an absolute age. However, if some $^{230}Th$ was incorporated into the phosphorite during initial formation then the calculated age can only be said to be a maximum age.

The only phosphorite sample that was measured using the U-series disequilibrium methods was a bulk-sample from the base of the large nodule in core CD38-09 (273cm). From Table 4.1 it can be seen that the Th concentration of this sample is only 2ppm (of which 99.9% is $^{232}Th$, G.B. Shimmield, Pers. Comm.). Therefore, although the age calculated below cannot definitely be said to be an absolute age, the low Th content suggests that virtually all the $^{230}Th$ present in the sample will have been formed by *in situ* radiogenic decay and that the calculated age is probably very close to an absolute age.

The data in Table 4.4 gives the results of the U and Th isotopic determination by α-spectrometry on duplicate samples taken from the base of the large nodule from CD38-09, the calculated age and the original $^{234}U/^{238}U$ ratio. The raw data of number

of counts for each isotope and length of counting time are presented in Appendix C.15.

| | Sample H | (Error) | Sample I | (Error) |
|---|---|---|---|---|
| $^{238}U$ (dpm/g) | 81.95 | ±0.58 | 82.51 | ±0.47 |
| $^{234}U$ (dpm/g) | 90.68 | ±0.64 | 92.55 | ±0.52 |
| $^{230}Th$ (dpm/g) | 58.53 | ±0.41 | 62.53 | ±0.76 |
| $^{232}Th$ (dpm/g) | 0.61 | ±0.03 | 1.56 | ±0.10 |
| $^{234}U/^{238}U$ | 1.1065 | ±0.011 | 1.1216 | ±0.009 |
| $^{230}Th/^{234}U$ | 0.6454 | ±0.006 | 0.6756 | ±0.009 |
| Age (years) | 109895 | ±1500 | 118595 | ±2570 |
| Initial $^{234}U/^{238}U$ | 1.145 | | 1.169 | |

Table 4.4. U/Th isotope results for base of phosphorite nodule found at 273cm depth in CD38-09 (dpm/g = disintegration per minute/gram). Samples H and I are duplicates.

| Author | Sample and location | $^{234}U/^{238}U$ | $^{230}Th/^{234}U$ | Age (kyr) | Method |
|---|---|---|---|---|---|
| Kolodny & Kaplan (1970) | Dredged from sea-floor | < 1.00 | | > 800 | U |
| Baturin *et al.* (1972) | S.W. African shelf | 1.163 | | 24 | U |
| | Chilean shelf | 1.143 | | 55 | U |
| Veeh *et al.* (1973) | Peru - A183 - surface | 1.11 | 0.61 | <100 | U/Th |
| | Peru - A183 - core | 1.10 | 0.70 | <125 | U/Th |
| | Peru - KK77161 - surface | 1.09 | 0.46 | <66 | U/Th |
| | Peru - KK77161 - core | 1.10 | 0.62 | <102 | U/Th |
| | California (15 samples) | 0.95-1.02 | 1.00-1.12 | >200 | U/Th |
| Veeh *et al.* (1974) | S.W. African shelf | 0.87-1.02 | 1.00-1.09 | | |
| Jahnke *et al.* (1983) | Mexican margin apatite | | | <113 | |
| Kim & Burnett (1985) | Peru shelf nodules | | | <300 | U/Th |
| Burnett *et al.* (1988) | Peru shelf pellets | 1.05-1.12 | 0.15-0.73 | 3-254 | U/Th |
| This study | Peru CD38-09 nodule | 1.11-1.12 | 0.64-0.675 | 114 | U/Th |

Table 4.5. U/Th age determinations for phosphorites from Peru, S.W. Africa and Baja California.

The results in Table 4.4 for the large phosphorite nodule can now be compared with the work of previous authors (summarised in Table 4.5) for a range of phosphorite nodules and pellets from the only three sites of modern phosphorite formation; namely, off Peru, S.W. Africa and Baja California. The $^{234}U/^{238}U$ and

$^{230}Th/^{234}U$ ratios for the CD38-09 nodule seem to have fairly typical values for Recent phosphatic material found in sediments under an upwelling zone. The calculated age, when averaged for the two duplicate samples, of 114.2 ±6.4 thousand years (kyr) also falls within quite a common age range for phosphorite formation.

Calculation of the original $^{234}U/^{238}U$ ratio (using the equation in Appendix B.5) gives an average value of 1.157 which is very close to the present day sea-water $^{234}U/^{238}U$ ratio of 1.14 ±0.014 (Ku *et al.*, 1977). Not only does this give extra confidence to the accuracy of the U-series disequilibrium results but it also supports the theory that formation of the phosphatic material, from which the hardground nodule found at 273cm in core CD38-09 is composed, was initially formed at the sediment/water interface approximately 114 thousand years age (ka).

### 4.3.6 Phosphorites and eustatic variation off Peru

Given that the large phosphorite nodule in core CD38-09 has a U/Th average age of 114 (±6) ka and was found at a water depth of 148m and sediment depth of 273cm, what are the possible interpretations for the growth history of this nodule?

The phosphorite nodule is likely to have initially formed as small pellets just below the sediment/water interface (Baker and Burnett, 1988; Burnett *et al.*, 1988). Although each pellet may have only taken between 3 and 12 years to grow (Froelich *et al.*, 1988) from a nucleation point into a grain about 125-500μm in diameter (Baker and Burnett, 1988), the nodule is likely to consist of thousands of pelletal grains whose ages of diagenetic formation will range over quite a few thousand years. This means that the age of 114kyr is just a mean age for the phosphatic material, some of which may be as old as about 125kyr and some as young as about 100kyr.

One hypothesis may be that this nodule actually consists of pellets (and other non-phosphatic material) which initially formed around 114ka, whereupon it became a closed system with respect to uranium and thorium. In terms of global glacial/interglacial periodicity, 114ka occurs within interglacial stage 5, just after the peak of substage 5e when climatic conditions were very similar to the present day (Imbrie *et al.*, 1984). If the phosphorite nodule formed at this time and has remained *in situ*, slowly being buried under the accumulating sediment since 114ka, then this hypothesis requires an average sediment accumulation rate of only 2.4 cm $kyr^{-1}$. This rate is exceptionally slow for a shallow-water continental margin site, especially as it lies under a zone of coastal upwelling and the sediment receives a high biogenic flux

(Chapter 3). Also during the period since 114ka, the global climate went through a full glacial cycle which probably means that far more terrigenous material than at present was being weathered off the Andes and being deposited on the Peruvian continental shelf (7.2.3).

It is therefore highly unlikely that sediment at the site of core CD38-09 has been accumulating over the last 114kyr at an average rate of only 2.4 cm $kyr^{-1}$. Initial formation of the phosphatic material contained in the nodule 114ka may still be possible if, as well as sediment accumulation, the site has also suffered sediment loss. This is very likely due to the shallow water depth of the core and the fact that such fine-grained sediment with high organic matter content will be easily eroded upon a change in direction or strengthening of bottom-water currents. This almost certainly occurred during the last glacial period when the sea-level dropped by up to 120m in response to the global increase in ice-volume (Fairbanks, 1989).

The shape of the nodule (flattened in one dimension) and its horizontal position in the core (4.3.1) point towards a two-phase diagenetic history for this phosphorite hardground deposit, of initial pellet formation followed by a later event of mineral concentration. The radiometric age of the nodule and its depth in core CD38-09, give further proof and support for the established theory of phosphorite hardground formation (Baturin and Bezrukov, 1979; Baturin, 1982; Burnett *et al.*, 1980; Burnett and Froelich, 1988).

The phosphatic material of which the nodule is composed was probably originally introduced to the sediment as organic matter and other biogenic detritus between 125 and 100 ka, during the early stages of interglacial stage 5. At this time, the oceanographic and sedimentological conditions were ideal for diagenetic phosphorite pellet formation, upon bacterial decay of the organic matter (4.1.5), in a reducing pore-water environment (Burnett *et al.*, 1988; Froelich *et al.*, 1988). Thousands of these pellets formed per square metre of ocean floor but it was not until the onset of the next glacial period (stage 4) at about 75ka (Imbrie *et al.*, 1984) when sea-level dropped and bottom-water currents along the Peru shelf became stronger, that the fine-grained clay, diatom and organic matrix (in which the disseminated pellets sat) was winnowed away down the continental slope and the larger-grained, denser pellets were concentrated together (Baturin, 1982).

Although the phosphorite nodule has a U/Th diagenetic age of 114 ±6 ka, it probably only formed after reworking of the sediment column (Baturin and Bezrukov, 1979) sometime during the period from 75 to 19 ka (the latter being the maximum of the last glacial period, stage 2, and lowest sea-level stand; Imbrie *et al.*, 1984). The

nodule was probably part of a larger phosphorite hardground unit, which is suggested by the 2D slab-like appearance, the small burrows seen on its topside and the polished surfaces (Cook *et al.*, 1990). It is quite likely that the hardground unit was subsequently broken up by storm activity when the sea-level was at a minimum (18ka, Fairbanks, 1989) and since that time the nodule has been reburied under 273cm of fresh marine sediment. If this were the correct hypothesis then it would imply a Holocene (stage 1) sediment accumulation rate of about 15 cm $kyr^{-1}$ which is quite suitable for such a shallow-water site as CD38-09, under a zone of strong coastal upwelling.

## 4.4 CONCLUSIONS

This geochemical study of phosphorite nodules and pellets which have diagenetically formed in the Peruvian continental margin sediments has led to the following conclusions.

1) Hardground nodules found at 273cm in core CD38-09 and at 90cm in core CD38-10 (both cores located in a reducing environment, Chapter 6) have been shown by X-ray diffraction and X-ray fluorescence analyses to be composed of phosphorite. This is a multi-phase mineral deposit which, following the linear programming calculations of Glenn and Arthur (1988), is dominantly (about 65 wt.%) composed of carbonate fluorapatite (CFA).
2) Pore-water phosphate profiles from box core material supports the hypothesis of Froelich *et al.* (1988) that phosphorite pellet formation is presently occurring on the Peru shelf and that it is a two-stage process. This involves the initial formation of amorphous calcium phosphate (both at CD38-09 and CD38-10) followed by addition of fluoride and carbonate anions and conversion to CFA (probably presently only at CD38-09).
3) Down-core phosphorus partitioning in bulk sediment samples from piston cores allows for calculation of $P_{phos}$ (wt.%) and percentage phosphorite, which indicates the continuous presence of phosphorite pellets and zones of phosphorite concentration. One possible source of error in the phosphorite calculations occurs because fish bone horizons will also give concentrations of excess phosphorus, such as around 500cm in CD38-10.
4) The enrichment of certain trace elements (U, Sr, Ba, Mo, Y and REE) in phosphorites due to the necessity of CFA elemental substitution to achieve a stable mineral lattice, allows for the calculation of trace element/$P_{phos}$ ratios in

phosphorite zones. This leads to partitioning equations for the calculation of $U_{org}$, $Sr_{calcite}$ and $Y_{terr}$ concentrations in all bulk sediment samples, which will be used later in this thesis.

5) U-series disequilibrium techniques, used for age calculation of phosphatic material in the large nodule found in core CD38-09, measured U and Th radiogenic isotope activities equivalent to an age of 114 ±6 ka and with an initial $^{234}U/^{238}U$ ratio of 1.157 ±0.012, which is similar to that of present-day sea-water.

6) The above radiogenic data and the physical appearance and location of the nodule lead to the following interpretation of the phosphorite's diagenetic history.

Small phosphorite pellets formed from decaying biogenic material at the sediment/water interface in the vicinity of core CD38-09. This occurred over a period of time between 125 and 100 ka, which lies during the early stages of interglacial stage 5. At some time during the next glaciation period, when the sea-level dropped and bottom-water currents strengthened, fine-grained sediment was winnowed away from the site leaving behind a concentration of phosphorite pellets (and other heavy minerals) which slowly lithified into a hardground, bedded unit. This slab-like material was then broken up into flat nodules about 18ka, one of which sat horizontally on the sea-floor at the site of core CD38-09. It was then reburied under accumulating sediment during the Holocene period.

One question that arises from this theory is whether or not the nodule found at 90cm in core CD38-10 has the same diagenetic history as the one found at 273cm in core CD38-09. If it does have a similar history then it implies that, since the last glacial maximum, CD38-09 at 148m water depth has had an average of three times the sediment accumulation rate of CD38-10 at 257m. This may be possible because CD38-09 is situated closer to the source of terrigenous detritus and there may also have been a further period of sediment erosion at CD38-10 (highlighted by the phosphorite peak at 30cm, Fig. 4.5). In order to clarify this hypothesis further U/Th age determinations need to be carried out on the nodules and their surrounding sediments.

# CHAPTER 5

# STATISTICAL ANALYSIS OF THE DATASET

## 5.1. INTRODUCTION

"'Are you animal, vegetable or mineral?' he said. 'Mineral, I think' replied Alice."

Lewis Carroll

*Alice Through the Looking Glass*

Just as Alice, in the above quote, had to decide between animal, vegetable or mineral, marine geochemical studies have to interpret the down-core variation in element concentrations, identify element-phase correlations and decide whether or not particular elements are associated with marine animal or plant remains or with diagenetic mineral growth.

This chapter will use statistical analysis and mathematical computational techniques in an attempt to simplify the very large dataset of geochemical parameters (over 25 elements, calculated phases and ratios) measured for all the samples taken from the four piston cores from the Peruvian continental margin (over 250 samples). This is done so that each geochemical variable can be assigned to one or more sediment phases or components, which can be interpreted as the source(s) of that particular element.

The three methods used in this chapter are as follows:

(a) correlation matrices,

(b) R-mode factor analysis (principal component analysis - PCA),

(c) multi-component analysis (MCA).

## 5.2. CORRELATION MATRICES

### 5.2.1. Methods

Correlation analysis between each of the 30 geochemical variables was carried out using Minitab statistical programming and involved a least squares correlation of two independent variables. The results, given as r = correlation coefficient of a best-fit straight line in an X-Y plot of the two variables, are tabulated in Appendix C.16 and it is these values that are used throughout this thesis (e.g. Table 6.3).

There are five geochemical variables which are taken to represent five main phases in these marine sediments :

(1) $C_{org}$ - representative of organic matter phase - as measured (Appendix A.3),

(2) Biogenic silica - representative of biological silicate-remains phase - as measured (Appendix A.4),

(3) $CaCO_3$ - representative of biological carbonate-remains phase - as calculated (Appendix B.1),

(4) Phos. - representative of phosphorite mineral phase - as calculated (Appendix B.4),

(5) Terr. - representative of terrigenous-input phase = 100 - (sum of above four).

### 5.2.2. Interpretation of results

Figure 5.1 shows a summary table of the correlation matrix for each of the piston cores, which illustrates the strength of the correlation between the 30 geochemical variables and the five main phases. A strong, positive correlation (++) indicates that there is a probable association between an element and a phase and a positive correlation (+) indicates that an association is possible. Negative correlations (-- and -) occur when the concentration of a particular phase controls the concentration of another due to a strong dilution effect, and therefore an element which is associated with the latter phase will have a concentration which varies antithetically with the former phase.

Using Fig. 5.1 for reference, the following comments can be made about element-phase correlations and associations.

1) In all of the cores, the terrigenous phase correlates positively with a large number of elements and strongly with Al, Ti and K in CD38-10, CD38-02 and CD38-11. The association between the terrigenous phase and Al justifies the use of this element in calculations and ratios, used throughout this thesis, which normalise changes in the terrigenous phase and allow study of effects of biogenic dilution.

2) In core CD38-09, there are only a few strong correlations, i.e. Ni and Mo with organic matter and U and Sr with phosphorite phases, which may indicate that no **one** phase dominates the geochemical composition of the sediment in this core.

3) The positive correlation in core CD38-09 between the organic matter phase and Zr/Rb (which is a grain-size indicator, 7.2.3) shows that it is possible that the abundance of organic matter arriving at a shallow-water site may have

PC38-02 (2525m)

| | Corg | Bio.Sil. | CaCO3 | Phos. | Terr. |
|---|---|---|---|---|---|
| Corg | 1 | | | | |
| Bio.Sil. | | 1 | - | | |
| CaCO3 | | - | 1 | | – |
| Phos. | | | | 1 | |
| Terr. | | | – | | 1 |
| Al | | | – | | ++ |
| K | | | – | | ++ |
| Ti | | | – | | ++ |
| I | ++ | | | | |
| Br | + | | | | |
| Mo | + | | | | |
| U | | | | | |
| Ni | + | + | | | |
| Cr | | + | - | | + |
| V | | | – | | ++ |
| Cu | | | - | | + |
| Sr | | - | ++ | | – |
| Ba | | + | - | + | + |
| Zn | | + | – | | ++ |
| Rb | | | – | | ++ |
| Zr | | | – | | ++ |
| Zr/Rb | | | | | |
| Nb | | | - | | + |
| Pb | | | - | | + |
| Th | | | - | | + |
| La | | | - | | + |
| Ce | | | | | |
| Nd | | | | | |
| Y | | | – | | ++ |
| Sc | | | | | |

PC38-09 (148m)

| | Corg | Bio.Sil. | CaCO3 | Phos. | Terr. |
|---|---|---|---|---|---|
| Corg | 1 | | | | |
| Bio.Sil. | | 1 | | | |
| CaCO3 | | | 1 | | |
| Phos. | | | | 1 | - |
| Terr. | | | | - | 1 |
| Al | | | | | + |
| K | | - | | | + |
| Ti | | - | | | + |
| I | + | | - | | |
| Br | + | | | | |
| Mo | ++ | + | | | |
| U | | | | ++ | - |
| Ni | ++ | | - | | |
| Cr | + | | | | |
| V | | | | | |
| Cu | + | | | | |
| Sr | | | | ++ | - |
| Ba | | | | | |
| Zn | | | | | |
| Rb | | | | | - |
| Zr | | - | | | |
| Zr/Rb | + | | - | | |
| Nb | | - | | | |
| Pb | | | - | | + |
| Th | | | | - | + |
| La | | | | | + |
| Ce | | - | | | + |
| Nd | | - | | | + |
| Y | | – | | | |
| Sc | | | | - | + |

PC38-10 (257m)

| | Corg | Bio.Sil. | CaCO3 | Phos. | Terr. |
|---|---|---|---|---|---|
| Corg | 1 | + | | - | - |
| Bio.Sil. | + | 1 | | - | - |
| CaCO3 | | | 1 | | – |
| Phos. | - | - | | 1 | |
| Terr. | - | - | – | | 1 |
| Al | | - | - | | ++ |
| K | | - | - | | ++ |
| Ti | | - | - | | ++ |
| I | | | | | |
| Br | + | | | | |
| Mo | + | + | | - | |
| U | | | | + | |
| Ni | ++ | | | | |
| Cr | ++ | | | - | |
| V | + | | | - | |
| Cu | + | | | - | |
| Sr | | | | + | |
| Ba | | - | | | + |
| Zn | | | | | |
| Rb | | | - | | + |
| Zr | - | - | - | + | + |
| Zr/Rb | - | - | | ++ | |
| Nb | - | - | - | | ++ |
| Pb | | | | | + |
| Th | | | - | | + |
| La | | | | | + |
| Ce | - | - | - | | ++ |
| Nd | - | – | - | | ++ |
| Y | - | – | - | + | + |
| Sc | | | - | | + |

PC38-11 (3835m)

| | Corg | Bio.Sil. | CaCO3 | Phos. | Terr. |
|---|---|---|---|---|---|
| Corg | 1 | | | | |
| Bio.Sil. | | 1 | - | | |
| CaCO3 | | - | 1 | | - |
| Phos. | | | | 1 | |
| Terr. | | | - | | 1 |
| Al | | | - | | ++ |
| K | | | - | | ++ |
| Ti | | | - | | ++ |
| I | + | | | - | |
| Br | ++ | | | | |
| Mo | + | | + | | |
| U | | | | | |
| Ni | ++ | | | | |
| Cr | | | - | | |
| V | | | – | | + |
| Cu | | + | - | | |
| Sr | | - | ++ | | - |
| Ba | | ++ | - | | |
| Zn | | + | - | | |
| Rb | | | - | - | + |
| Zr | | - | | + | |
| Zr/Rb | | - | | ++ | |
| Nb | | | - | | ++ |
| Pb | | - | | | |
| Th | | | | | + |
| La | | | | | |
| Ce | | | | | |
| Nd | | | - | | + |
| Y | | + | - | | |
| Sc | | + | - | | + |

| Symbol | Max. | Min. |
|---|---|---|
| ++ | +0.999 | +0.800 |
| Symbol | Max. | Min. |
| + | +0.799 | +0.500 |

| Symbol | Max. | Min. |
|---|---|---|
| - | -0.500 | -0.799 |
| Symbol | Max. | Min. |
| – | -0.800 | -0.999 |

Figure 5.1. Summary tables of correlation coefficients for piston cores CD38-09, CD38-10, CD38-02 and CD38-11.

some control over the grain-size of the sediment. However, there may be an external component, such as bottom-water current activity, which controls both variables. In cores CD38-10 and CD38-11, the Zr/Rb ratio correlates strongly with the phosphorite mineral phase and this is indicative of the fact that bottom-water current strength has an influence on both phosphorite nodule growth and sediment grain-size (Chapter 4).

4) In cores CD38-02 and CD38-11, strong, positive correlations exist between the carbonate phase and Sr. This association is due to the uptake of $Sr^{2+}$ by substitution of $Ca^{2+}$ in the carbonate shells of zooplankton (6.4). The carbonate phase also displays in core CD38-02 strong, negative correlations between the terrigenous phase and elements such as Al, K, Ti, Zn, Zr and Y. This implies that, in this sediment, dilution by one phase is strongly controlling the other. However, correlation analysis cannot indicate whether it is the carbonate phase or the terrigenous phase which is the dominant, controlling phase in core CD38-02.

5) The halogens (I and Br) show some positive correlation to the organic matter phase in all of the cores, except for I in CD38-10. This indicates that a halogen-organic matter association exists in marine sediments but for some reason I has been lost from core CD38-10. The same may be said for a Ba-biogenic silica association, which shows a strong correlation in CD38-11, a positive one in CD38-02 but no correlation and a negative one in CD38-09 and CD38-10 respectively. Chapter 6 studies these associations in more detail.

The main problem with correlation analysis is that if one phase is dominating over all the others and therefore diluting all the elements in the other phases to the same degree, then there may be a strong, positive correlation between two elements which are not related in any true, geochemical association, e.g. Ba and Cr in CD38-02 (Appendix C.16). Also, there may be an element whose phase association changes over time due to loss upon burial and/or diagenetic remineralisation or an element which has more than one phase association. Correlation analysis will not pick up such associations because they have a low correlation coefficient.

Using a dataset-reduction technique which allows for simple, graphic representations of the element-element and element-phase associations may help to solve the above problems. This is possible with principal component analysis.

## 5.3. PRINCIPAL COMPONENT ANALYSIS

### 5.3.1. Introduction and methods

Principal component analysis (PCA) is a statistical data reduction technique which identifies a small set of variables ("principal component factors" each having "eigenvalues") which can account for a large proportion of the total variance in the dataset. A number of authors (Li, 1981, 1982; Gardner *et al.*, 1990; Hermelin and Shimmield, 1990; Shimmield and Mowbray, 1991; Patience, 1992) have used PCA to simplify large datasets from marine sediment studies in an attempt to identify a few factors or components with which various geochemical elements (variables) are associated.

PCA was carried out on the data from the piston core sediments of the Peruvian continental margin using Minitab R-mode factor analysis. This technique of data reduction has advantages over correlation analysis because of ease of graphic representation of the results and also over Q-mode factor analysis because in PCA the multiple-regression coefficient of variables is normalised to one for a perfect correlation (Li, 1982), which allows for easy inter-core comparison.

The results of PCA include the eigenvalues of the principal component factors (PCFs), their proportion (and the cumulative proportion) of the total variance and the principal component matrix. Appendix C.17 tabulates the results of the first 8 PCFs, using the same dataset used for correlation analysis (5.2) for each of the four piston cores. Any possible association of a group of geochemical elements within the dataset can usually be deduced from the coherence of these elements in the first three PCFs.

Before an interpretation of the PCA results is made, it should be noted that this technique only provides good statistical proof that elements are associated and therefore such associations should always be checked against some form of independent evidence. Errors in interpretation of PCA results can arise if an apparent correlation is caused by a systematic error in the chemical analysis or if it is an indirect one. Also, an apparent lack of correlation may exist if the natural variability is less than the uncertainty in the chemical analysis (Li, 1982). However, it is thought that such errors are likely to be low because of the high precision and accuracy of the X-ray fluorescence technique (Appendix A.5) and wet chemical methods in measuring the composition of sediments in this study and their high, natural variability (as seen in the down-core profiles).

### 5.3.2. Interpretation of results

The extracted PCFs 2 and 3 are plotted against PCF 1 in Figs 5.2 to 5.5 for cores CD38-09, CD38-10, CD38-02 and CD38-11 respectively. The plots all have the same scales for the axes so that inter-core comparisons are easy to make. Elements which plot close to each other in both the PCF diagrams are highly likely to have an association within the same sediment component phase. The same five end-member phases as used in the correlation analysis ($C_{org}$, Bio. Silica, $CaCO_3$, Phos. and Terr. - 5.2.1) are also plotted on the diagrams.

Each sediment phase will now be examined with respect to its location on the PCF plots (Figs. 5.2 to 5.5) and the elements which group around it.

**Organic matter phase**

Under a zone of high biological productivity associated with coastal upwelling (Chapter 3) the organic matter flux can vary considerably over time and therefore it may be expected that the variation in the organic matter phase down each core would play a large part in the total variation of the sediment composition.

This is certainly true for core CD38-10 (Fig 5.3), and to a lesser extent for CD38-11 (Fig. 5.5), in which $C_{org}$ plots strongly positive for both factors 1 and 2. This implies that the organic matter phase variation has a strong influence on the total variation. In core CD38-09, $C_{org}$ is positive for factors 2 and 3 but slightly negative for factor 1 (Fig. 5.2) which indicates that another phase is dominating the total variation in sediment composition of this core. Core CD38-02 has a variation in $C_{org}$ which plots in nearly the same place as core CD38-09 (compare Fig. 5.4 with 5.2) for the PCF 2 vs. 1 diagram. This means that although CD38-02 has a much lower concentration of $C_{org}$, its variation control on the sediment composition is at a similar level to core CD38-09 (which has a very high $C_{org}$ concentration).

The elements which have an organic matter phase association (i.e. they plot close to $C_{org}$) are the halogens (I and Br) and the heavy metals (Ni, Cr, V, Mo, Cu and U; 3.3.3).

Of the two halogens, Br always plots closer than I to $C_{org}$ (except for the PCF 3 vs. 1 plot for CD38-02) which implies a stronger organic-matter association for bromine (Chapter 6.2). The two cores which have the highest concentration of $C_{org}$ (CD38-09 and CD38-10) tend to have the organic matter-associated elements plotted much closer to $C_{org}$ than in the other cores. However, in some cases an element does

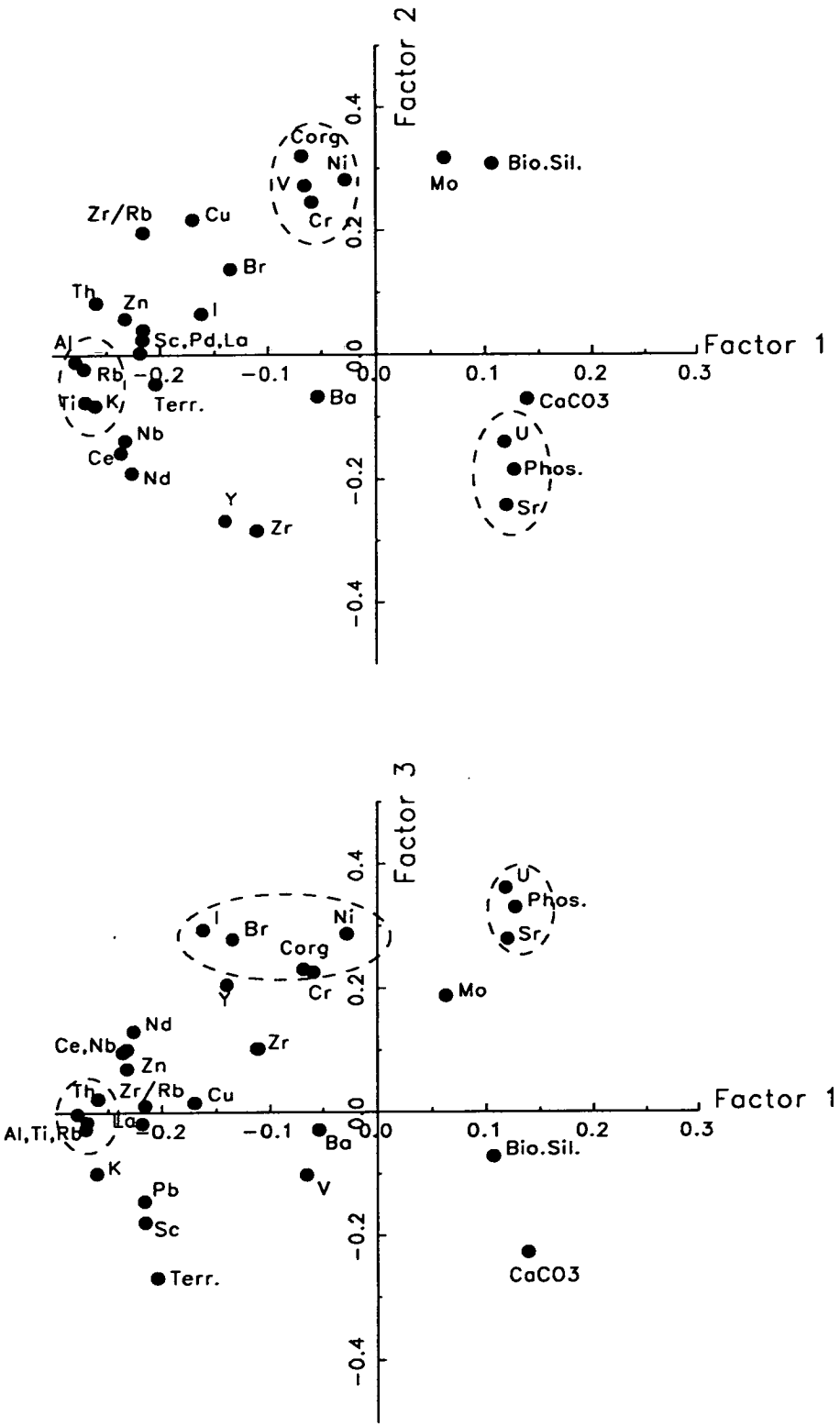


Figure 5.2. Principal component factor diagrams for core CD38-09 (148m).

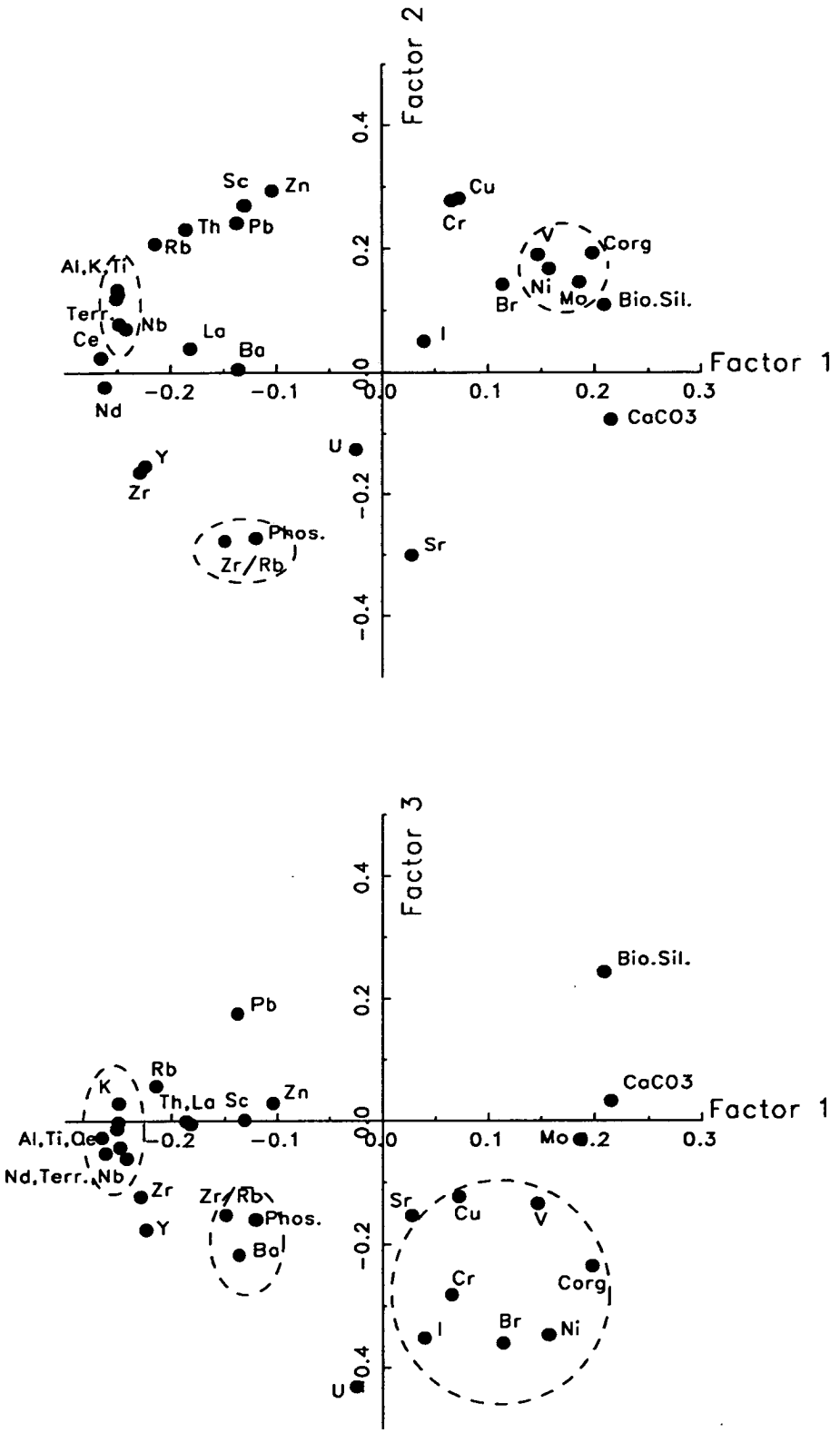


Figure 5.3. Principal component factor diagrams for core CD38-10 (257m).

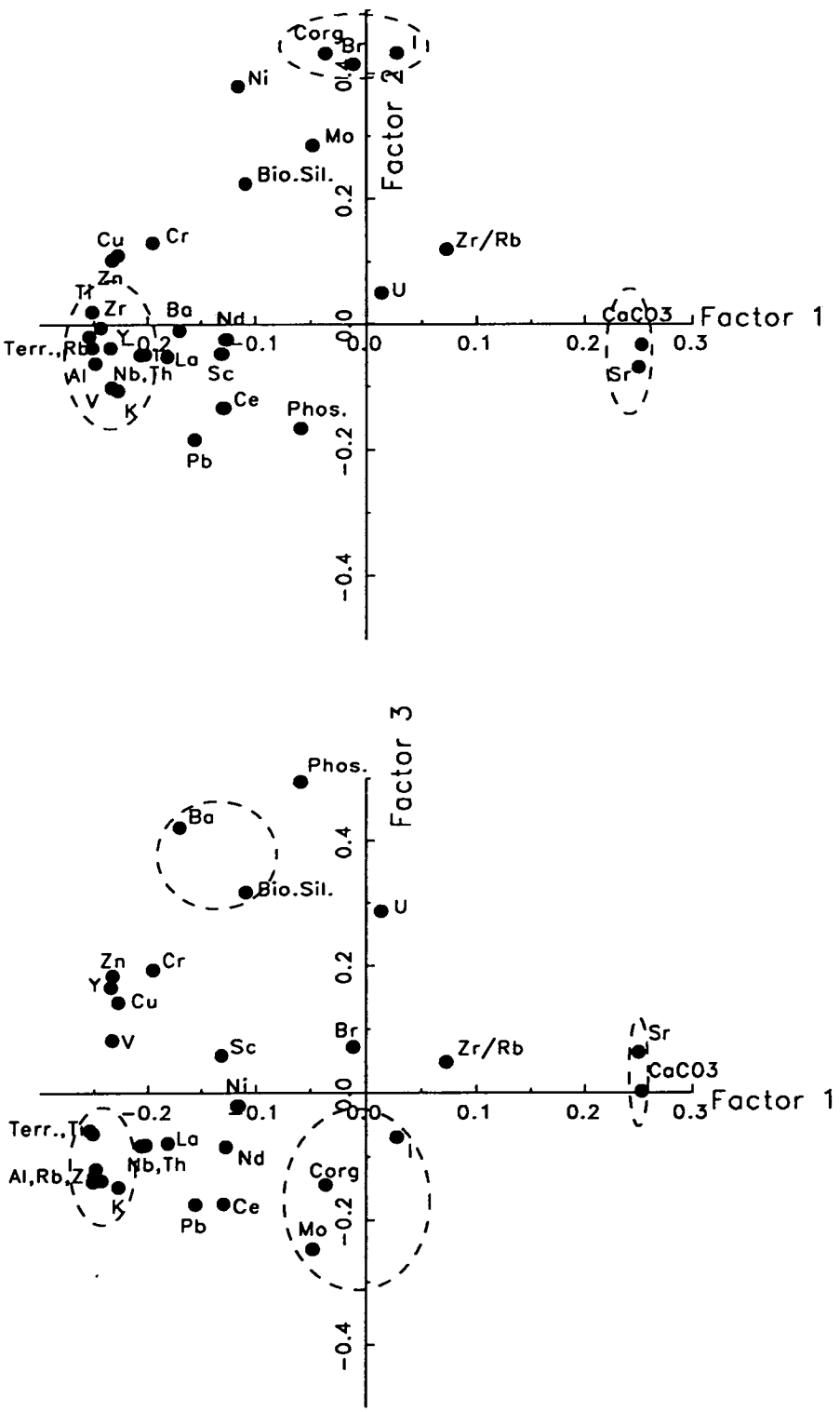


Figure 5.4. Principal component factor diagrams for core CD38-02 (2525m).

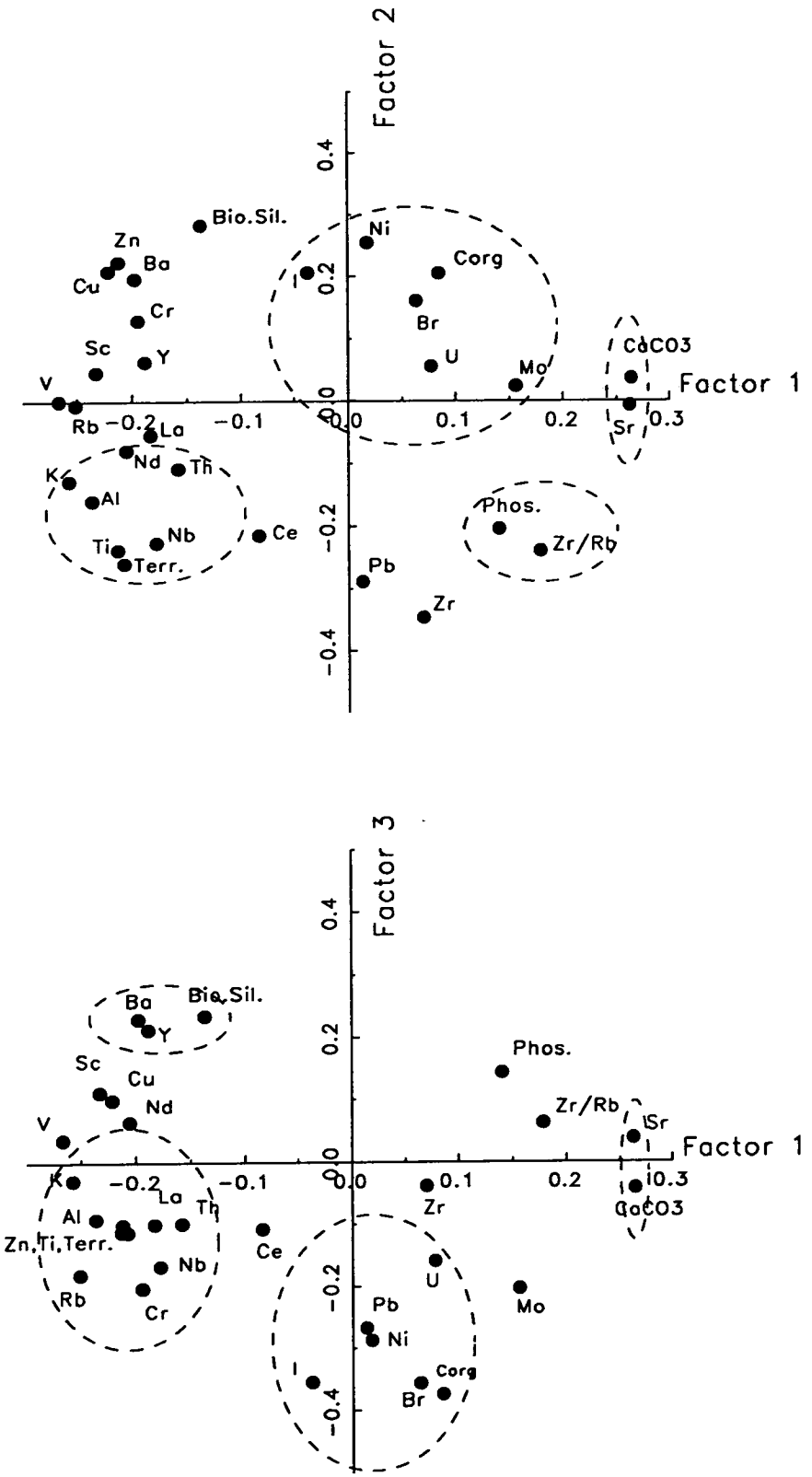


Figure 5.5. Principal component factor diagrams for core CD38-11 (3835m).

not plot close to a particular phase because it is also associated with another phase. These multi-phase elements, e.g. U, Sr, Ba, will be discussed later in this section.

**Biogenic silica phase**

The sediment phase which consists of the hard, silicate shell-remains of marine plankton is another biogenic component in marine sediments and, as for organic matter, it would be expected to influence the total variation of the sediment composition quite strongly in cores situated under high productivity zones. Cores CD38-09 and CD38-10 have strong, positive PCFs 1 and 2 for biogenic silica and the other two cores have negative values for factor 1 and positive for factors 2 and 3. The latter cores are located slightly further away from the Peruvian coastal upwelling zone and therefore the variation in biogenic silica flux would be expected to have less influence on the total sediment variation than in the two shallow-water cores.

There is little evidence from the PCF plots of any element being strongly associated with the biogenic silica phase in the sediments, except perhaps Ba and Y in CD38-11.

**Carbonate phase**

This third and final biogenic phase is composed of the hard, carbonate shell-remains of foraminifera and coccoliths, whose variation in concentration can often play a large part in the total sediment variation, especially in sediments away from the strong influence of a terrigenous input near a continental margin (Patience, 1992).

In the four piston cores studied here, the variation in $CaCO_3$ concentration is always strongly positive along the PCF 1 axis, implying that carbonate dilution is a dominating influence in sediment composition on the Peruvian continental margin. The value of the factor 1 for $CaCO_3$ and its distance away from any other sediment phases on the PCF diagrams indicates that in core CD38-02 the effects of carbonate dilution are strongest, followed by CD38-11, CD38-10 and CD38-09 in decreasing order of dominance.

In the two deeper-water cores, Sr shows a very strong association with the carbonate phase but this is the only element whose variation in PCA seems to be of a similar value to $CaCO_3$.

**Phosphorite phase**

This is an authigenic mineral phase which does not necessarily appear in all marine sediments but which may have a strong influence on the compositional variation of sediments on the Peru margin (Chapter 4).

From the PCF diagrams, it can be seen that cores CD38-09 and CD38-11 have a phosphorite variation which is positive for both factors 1 and 3 but negative for factor 2. Core CD38-10 which, like the above two cores, has zones of phosphorite pellet formation and concentration (4.3.3) is, however, negative for all three factors in terms of phosphorite variation. Accurate interpretation of the influence of phosphorite formation on total sediment compositional variation is difficult to make because its effects can be strong in some parts of the core but weak in others.

The geochemical elements which were studied in Chapter 4, i.e. U, Sr, Ba and Y, do have PCFs which plot close to, or nearby, Phos. for cores CD38-09 and CD38-10. This supports their use in the interpretation of phosphorite-trace element associations (4.3.4). It should also be noticed that Zr/Rb in cores CD38-10 and CD38-11 plots very close to Phos. which may indicate that the variation in the phosphorite phase and the variation in grain-size of the sediment are controlled by the same external influence.

Elderfield *et al.* (1981) showed that the rare earth elements (Nb, La, Ce, Nd) are mainly associated with phosphate minerals in the Wahine area sediments. However, from the PCF plots for CD38-09 and CD38-10, no such REE-phosphorite association can be seen for the sediments in this study. The REEs show closer association with the terrigenous phase.

**Terrigenous phase**

Shimmield and Mowbray (1991) used PCA to interpret sediments from ODP core 722B in the north-western Arabian Sea, and found that an "aluminosilicate, detritus factor" plotted with strong, positive values for PCF 1 and therefore its variation dominated the total sediment variation at this site. The opposite situation can be seen in the sediments from the Peruvian continental margin where the terrigenous phase (Terr.) has a strong, negative factor 1 value implying that another sediment phase is more dominant in its variation and is diluting the terrigenous phase.

The elements most closely grouped around Terr. on the PCF plots are Al, Ti, K, Zn, Rb, Zr, Ce, Nd, Th and La which are all associated strongly with aluminosilicate clay minerals. These elements are of terrigenous origin whose input to the ocean, and hence the marine sediments, is either riverine or aeolian (Chapter 7). Each of the four cores has a slightly different grouping pattern to the element-terrigenous phase association (such as an arc around Al, Ti and K in core CD38-09 and a long, thin zone in CD38-10) which may be indicative of slight differences in the mineralogical composition of the terrigenous phase.

**Mixed-phase elements**

One advantage that PCA has over simple correlation analysis is that the graphic representation of variance within a dataset allows for identification of elements which are associated with more than one end-member phase. If correlation analysis was the only statistical analysis method used on the dataset then such "mixed-phase" elements would probably have a non-significant correlation coefficient with the end-member phases, even though an association was present. Such mixed-phase associations would therefore not be noticed.

In the geochemical datasets from the four piston cores used in this study there are a few mixed-phase elements whose association with two or more end-member phases can be examined using PCA (Figs. 5.2 to 5.5). These are uranium, strontium and barium; as detailed below.

**Uranium**

In core CD38-09, uranium has a strong association with the phosphorite phase in both the PCF plots but this element is also known to be a heavy metal associated with the organic matter input to the sediment (3.3.3). For the other three piston cores, U can be seen to plot on the PCF diagrams somewhere on an imaginary line between the organic matter phase ($C_{org}$) and the phosphorite phase (Phos.) end-member components.

This mixed-phase characteristic of U can be interpreted as the variation in supply of the metal to the sediment being primarily associated with the variable organic matter input, but upon increasing organic matter decay during burial and diagenesis of phosphorite minerals (Chapter 4), the uranium becomes associated less with the $C_{org}$ phase and more with the Phos. phase. Therefore, simply from the position of U in the PCF diagrams it is possible to interpret that the uranium in core CD38-09 has undergone an almost complete remobilisation from organic matter to phosphorite minerals, whereas in core CD38-10 the remobilisation has not occurred to such a high degree.

The uranium in core CD38-11 plots closest to $C_{org}$, implying that it is still mainly associated with the organic matter which was responsible for introducing the metal into the sediment, and that very little phosphorite formation has occurred.

**Strontium**

In core CD38-10, strontium can be seen to be a mixed-phase element which, on the PCF 2 vs. 1 diagram, lies between the carbonate and phosphorite end-member phases. Cores CD38-02 and CD38-11 both show close correlation in the variance of

Sr and $CaCO_3$ (see above) which indicates a strong association between the two geochemical parameters, but in core CD38-09 the Sr is associated with the phosphorite phase only.

It is known that both carbonate and phosphorite minerals can easily incorporate Sr into their crystal lattices due to the similarity in ionic size and charge of $Ca^{2+}$ and $Sr^{2+}$ (4.3.4). Therefore, the mixed-phase characteristic of Sr in core CD38-10 indicates that both the carbonate and phosphorite phase variance are controlling the Sr concentration variance to roughly the same extent. In core CD38-09 it is the phosphorite phase which dominates the Sr variance and in CD38-02 and CD38-11 it is the carbonate phase.

The position of Sr on the PCF diagrams reflects the nature of the relative abundances, and therefore the dominance in variation control, of the carbonate and phosphorite end-member phases.

**Barium**

This mixed-phase element can be seen to plot in a variety of locations on the PCF diagrams of the four piston cores. Barium plots somewhere between the terrigenous, biogenic silica and phosphorite end-member phases which reflects its association with three possible sources, i.e. with detrital clays, diatom frustules (6.3.1) and diagenetic phosphorite mineral growth (4.3.4).

### 5.3.3. PCA Conclusion

Principal component analysis has helped to assign various elements to one (or more than one) particular end-member phase and also to indicate which phase is the most dominant in controlling the total variation in the geochemical composition of the piston cores from the Peruvian continental margin.

In cores CD38-02 and CD38-11, it is the $CaCO_3$ content of the sediment which dominates the dataset variation and, therefore, carbonate-dilution controls the down-core variation of the other four phases. This interpretation comes from the fact that for PCF 1 in CD38-02 and CD38-11, $CaCO_3$ has a high, positive value (0.253 and 0.265 respectively, C.17). Cores CD38-09 and CD38-10 do not, however, have one dominant end-member phase but seem to have three phases each whose relative abundances control the variation in the dataset. Biogenic silica, $CaCO_3$ and Phos. in core CD38-09 all have positive and roughly equal values for PCF 1 (0.107, 0.139 and 0.127 respectively, C.17) and in core CD38-10 it is the three biogenic phase

components which have high, positive values for PCF 1 ($C_{org}$ = 0.198, Bio. Sil. = 0.209 and $CaCO_3$ = 0.215, C.17).

PCA is therefore very useful in the interpretation of complex datasets such as used by marine geochemists. From examination of the proportion and cumulative percentages of the eigenvalues of each PCF (Appendix C.17) it can be seen that the highly variable chemical composition of marine sediments results in a high degree of complexity in the total variance of the dataset. It requires more than six PCFs to account for over 90% of the total variance in each of the four piston core datasets.

Also, PCA normalises the PCF eigenvalues to one for each dataset which allows for easy inter-core comparison. Of the four piston cores in this study, CD38-02 has the highest PCF 1 eigenvalue at 48.9%, which implies that the variation in carbonate concentration in this core accounts for just under half the total variation (compared with only 40.7% in core CD38-11). The cumulative variance of the first three PCF eigenvalues, which were the three used in the PCF diagrams (Figs. 5.2 to 5.5) statistically illustrates that only in core CD38-10 can over 80% of the total variance be accounted for by PCFs 1, 2 and 3. This indicates that core CD38-10 is, statistically, the least complex in its total geochemical variation of the four piston cores studied.

## 5.4. MULTI-COMPONENT ANALYSIS (MCA)

### 5.4.1. Introduction

Marine sediments are composed of a complex mixture of many chemical elements and these can be grouped into various components depending on their origin. The purpose of this section is to use multi-component analysis (MCA) in order to calculate, for each piston core sample, the relative proportions of the main components which can combine to form marine sediments. The concentration of each component and its down-core variation will then be interpreted for each piston core in this study to identify the main sources of input to the continental margin sedimentary environment.

The principles behind MCA as a computational technique used to simplify a set of geochemical data into a meaningful component composition, were set out by Heath and Dymond (1977, 1981) and Dymond (1981). These authors decided that a five-component system could be used to describe most marine sediments and allow

for estimations of the temporal variability of various depositional processes and for comparison with modern spatial variability (specifically on the Nazca plate of the Pacific Ocean). The five components defined were detritus, biogenic, authigenic, dissolved opal-solution residue and hydrothermal, and their models allowed for the simultaneous partitioning of elements using either algebraic algorithms or linear programming.

The models of Heath and Dymond (1977, 1981) and Dymond (1981) all assumed that each of the five components had a constant, end-member composition that was uniform across the Nazca plate and then converted bulk geochemical data (concentrations of Al, Si, Fe, Ni, Mn, Ba, Zn and Cu) into quantitative estimates of the mixture of components that best accounted for the measured composition of the sample.

It must be noted that the five components used in the MCA are not the same as the five end-member phases used in the regression analysis (5.2) and the principal component analysis (5.3) sections. Instead, the five components of Dymond (1981) are used so that the results of the MCA algorithm using the Peru margin sediment data can be compared to previous and/or future studies of multi-component analysis of marine sediments from other locations.

### 5.4.2. MCA methods, results and interpretations

It was decided to carry out the MCA of the four piston cores in this study by adapting the algorithms and component end-member compositions of Heath and Dymond (1977, 1981) and Dymond (1981) to create my own MCA algorithm.

The algorithm is listed in full in Appendix B.6 and uses seven geochemical variables (Al, $C_{org}$, Bio. Silica, $CaCO_3$, $P_{phos}$, Ba and Fe) to calculate the relative concentrations of five components; namely the terrigenous (TERR), biogenic (BIOG), authigenic (AUTH), residual (RESID) and hydrothermal (HYDRO) inputs to the sediment. The basic assumption used by the MCA algorithm is that the composition of each of the components is constant (in the above geochemical variables) both spatially along the Peru margin and temporally throughout the depth of each core. Also, it was assumed that each end-member component can be defined by the content of one (or more than one) characteristic geochemical variable.

For example, the algorithm assumes that all the Al present in a sample is present in the terrigenous component (5.2 and 5.3) and that the concentration of Al in a pure, end-member terrigenous sediment would be 8.40 wt.% (equivalent to the Al concentration of average deep-sea clay; Turekian and Wedepohl, 1961). The above

assumptions are, of course, not entirely accurate throughout all the marine sediment samples but in order to simplify the geochemical dataset and interpret the concentration and variation of each component present in the cores, the assumptions are justified.

The final step of the algorithm (Appendix B.6) recalculates all five components to percentages so that comparisons both within and between cores from different marine environments can be made. The results from MCA of the piston cores CD38-09, CD38-10, CD38-02 and CD38-11 are tabulated in Appendix C.18 and summarised in Table 5.1. (the hydrothermal component was absent in the MCA results for all the samples in this study).

| | TERR (%) | | BIOG (%) | | AUTH (%) | | RESID (%) | |
|---|---|---|---|---|---|---|---|---|
| Core | Range | Mean | Range | Mean | Range | Mean | Range | Mean |
| CD38-09 (148m) | 26.9-85.5 | 73.12 | 8.4-42.8 | 24.51 | 0.3-60.9 | 2.35 | | |
| CD38-10 (257m) | 31.9-88.6 | 65.69 | 32.-63.4 | 29.74 | 0.5-29.6 | 4.57 | | |
| CD38-02 (2525m) | 52.5-89.4 | 69.27 | 10.1-47.0 | 30.21 | 0.2-0.8 | 0.49 | 0-0.26 | 0.04 |
| CD38-11 (3835m) | 66.7-88.3 | 80.07 | 10.4-30.8 | 18.75 | 0.5-4.7 | 1.16 | 0-0.22 | 0.02 |

Table 5.1. Summary of MCA results for Peru margin piston cores.

The down-core profiles shown in Figs. 5.6 through to 5.9 graphically display the MCA results for cores CD38-09, CD38-10, CD38-02 and CD38-11 respectively. It can be seen from these plots that cores CD38-09 and CD38-10 contain sediments which can be described by a three-component system, and CD38-02 and CD38-11 are four-component systems. In all four cores, it is the terrigenous-source component which is the most common input (highest %) and the biogenic-source component is the second most abundant input to the sediment. This dominance of material from either a terrigenous or a biogenic origin contained within these sediments is to be expected from a marine environment which is close to a continental landmass and which is strongly influenced by high biological productivity as a result of coastal upwelling (Chapter 3). Chapter 7, which studies the environment of deposition of the Peru margin sediments, will focus on these two major components.

**CD38-09**

The MCA of CD38-09 (Fig 5.6) reveals that this core is located in an environment receiving an input of terrigenous-derived material which consistently makes up greater than 60% of the total input to the sediment, reaching a maximum of 85% (Table 5.1). The biogenic-derived material contained within the core generally

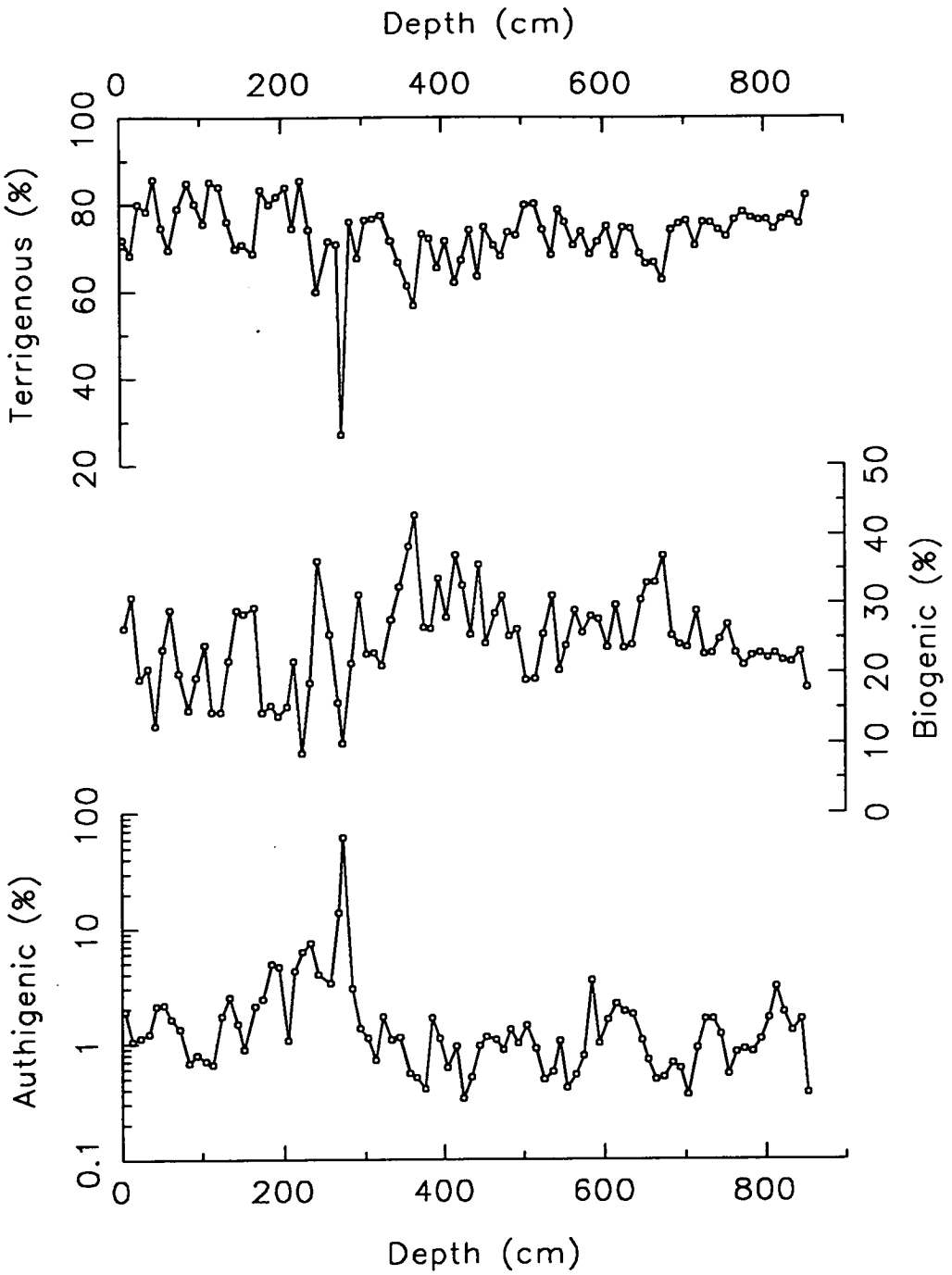


Figure 5.6. Multi-component analysis down-core profiles against depth (cm) for core CD38-09 (148m).

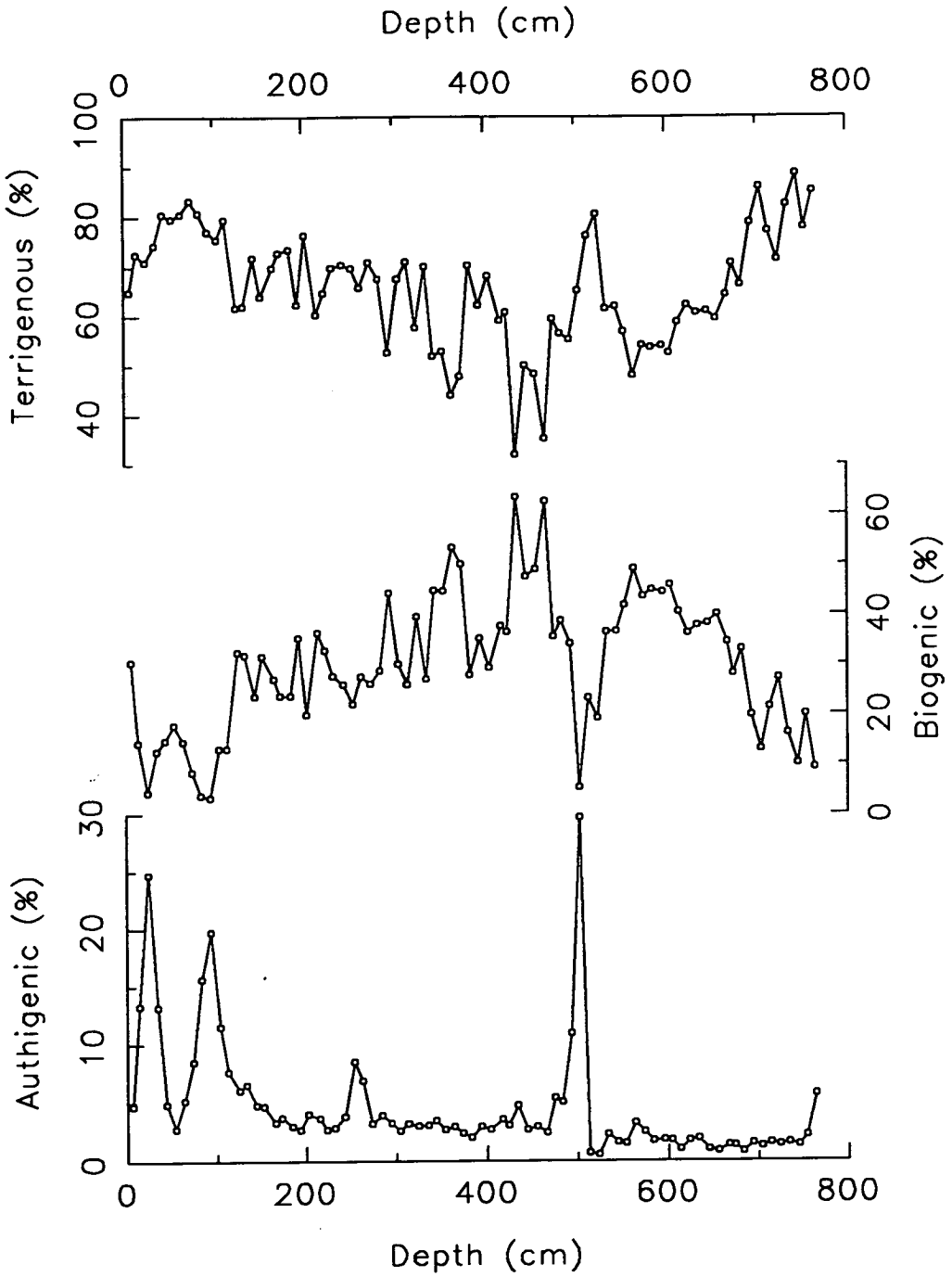


Figure 5.7. Multi-component analysis down-core profiles against depth (cm) for core CD38-10 (257m).

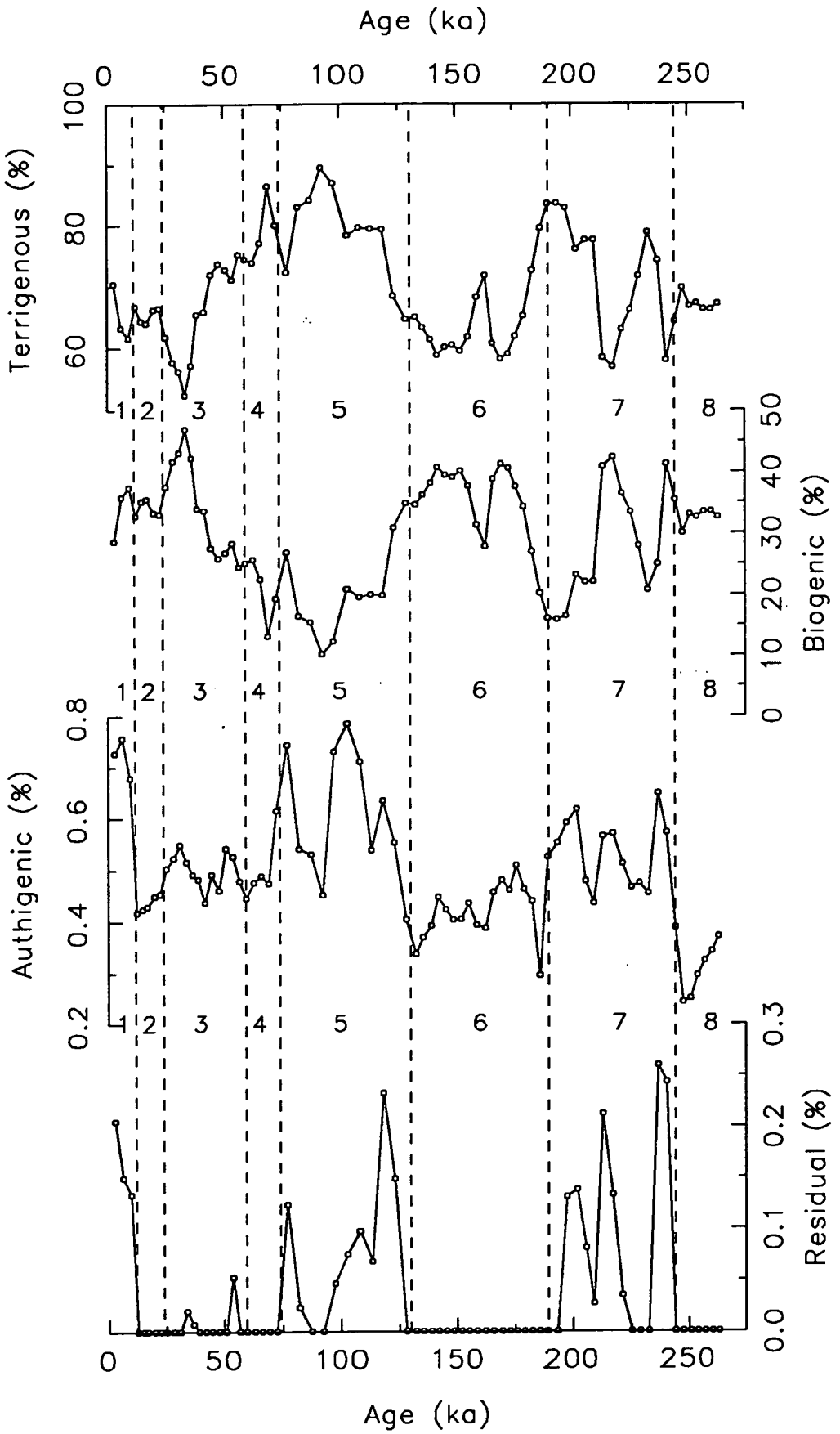


Figure 5.8. Multi-component analysis down-core profiles against age (ka) for core CD38-02 (2525m).

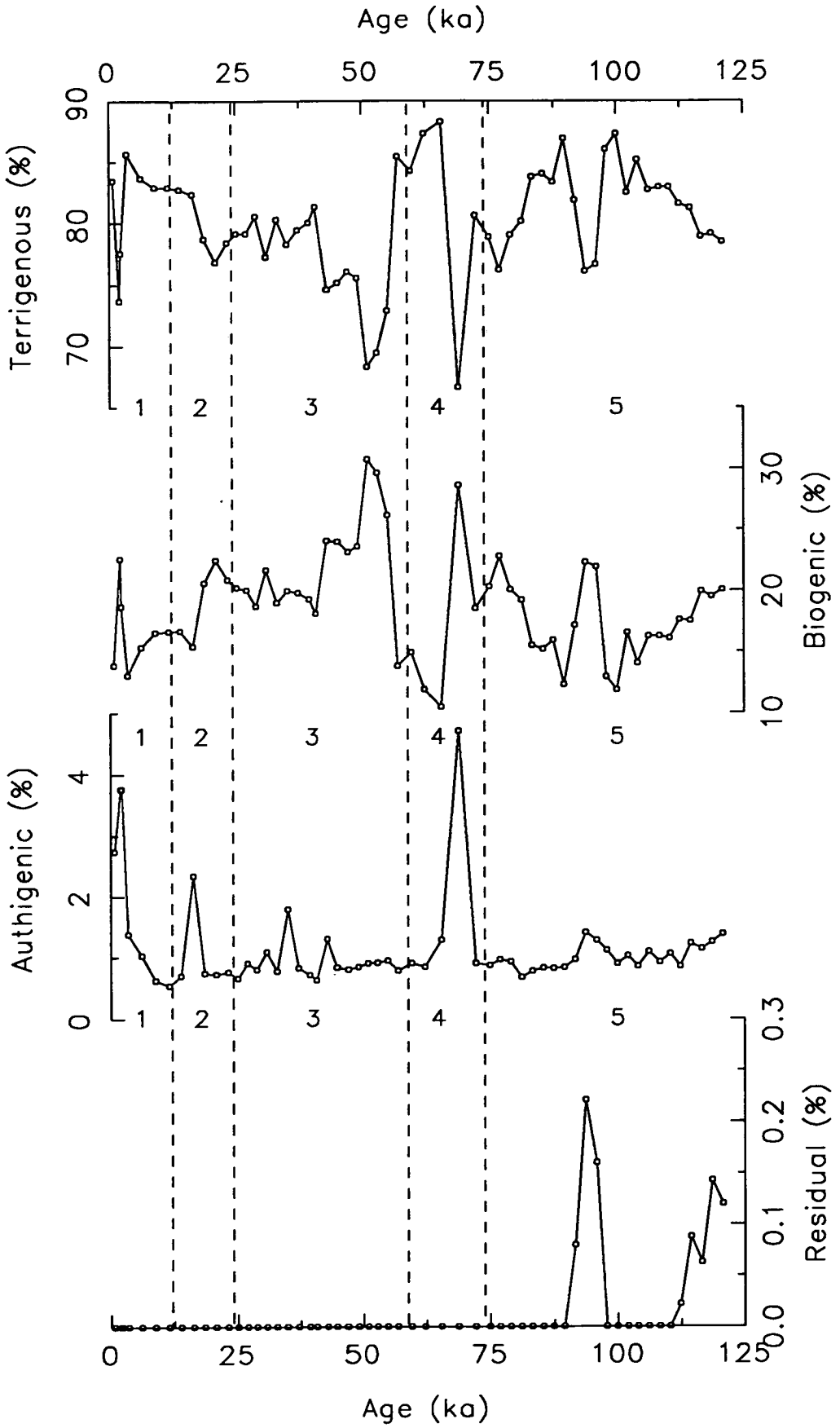


Figure 5.9. Multi-component analysis down-core profiles against age (ka) for core CD38-11 (3835m).

contributes greater than 10% of the sediment and can reach above 40%. The only other source component present in this core is the authigenic phosphorite component which is usually only a background of 1-2% but can be concentrated up to a maximum of 61% in the area around 273cm (4.3.3). It is interesting to note that below this strong authigenic zone, the terrigenous component averages 72.3% and the biogenic component averages 26.5%, but above this zone (i.e. since the last major change in sea-level at the time of phosphorite concentration; 4.3.6) the average terrigenous component has noticeably increased and the biogenic component decreased (to 76.5% and 20.7% respectively). It is, however, impossible to interpret from the MCA results whether this change in the component input to core CD38-09 is due to either increased continental weathering and input of more terrigenous material to the oceans or decreased marine biogenic productivity (and/or preservation) since the phosphorite concentration event.

**CD38-10**

The three-component system of core CD38-10 (Fig. 5.7) is essentially very similar to that of CD38-09. There is only a 100m water depth difference between the two core sites and it is therefore expected that both sets of sediment would be influenced by the same terrigenous and biogenic inputs and by zones of high authigenic input. The down-core profiles of the three components in core CD38-10 show an interesting pattern, whereby the terrigenous component is most dominant around the zones of authigenic phosphorite concentration (e.g. in the upper 100cm, between 490 to 520cm and at the base of the core) and the biogenic component is at a maximum between these zones. One possible interpretation of this pattern is that higher biogenic productivity occurred during interglacial periods and, relatively, an increased terrigenous input occurred during glacial periods (when sea-level dropped and phosphorite minerals were concentrated, 4.3.6). However, as with core CD38-09, the correct interpretation of core CD38-10 is difficult due to the lack of an accurate age model (2.3.2).

It should be noted that of the four piston cores, CD38-10 has the lowest average terrigenous-component input (Table 5.1) and yet it is situated closer to the continental landmass than both CD38-02 and CD38-11. The reason for this apparent irregularity is that CD38-10 also has high average biogenic and authigenic components (Table 5.1) and therefore the terrigenous component is relatively depleted.

**CD38-02**

Core CD38-02 is situated on the Nazca ridge and does have an accurate age model and, therefore, it is possible to interpret the four-component system (Fig. 5.8) in terms of Late Quaternary climatic changes. The terrigenous and biogenic inputs dominate the sediment composition and their down-core profiles mirror each other showing an inverse relationship of glacial/interglacial variation. The terrigenous component varies approximately ±15% about an average of 70% (Table 5.1) and is predominantly higher during the interglacial stages 1, 5 and 7 compared with the glacial stages 2, 6 and 8. The biogenic component varies to the same extent around an average of 30% (Table 5.1) and its concentration is relatively lower during the interglacial and higher during the glacial stages.

It was seen in the PCA interpretation (5.3.3) that in core CD38-02 it is the variation of $CaCO_3$ concentration which dominates the total variation and yet the MCA results show that the biogenic source component (of which $CaCO_3$ is the major contributor in this core) only makes up about one third of the total input to the sediment and is approximately half of the terrigenous component, in terms of relative concentrations. Therefore, core CD38-02 is an example of a marine sediment system in which the concentration of the major component (terrigenous) is controlled by the variation of input to the sediment of another component (biogenic).

The down-core profiles shown in Fig. 5.8 support this biogenic-dilution interpretation for core CD38-02 because when compared with the profile of the mass accumulation rate (Fig. 2.10) for the same core, it can be seen that the biogenic (and not the terrigenous) component is the most similar to the mass accumulation rate in its glacial/interglacial pattern. This implies that the variation in the biogenic component is controlling the total mass accumulation rate pattern and that the geochemical composition of core CD38-02 is strongly affected by biogenic (carbonate) dilution. A full explanation of the reasons for (i.e. productivity or preservation variation of carbonate microfossils), and the effects of, the biogenic component fluctuations over the past 250,000 years will be given in Chapter 7.

In the study of phosphorite minerals (4.3.3) it was stated that the amount of phosphorus present in core CD38-02 was not sufficient to indicate the presence of any phosphorite material. However, the algorithm used in this multi-component analysis has resulted in a small amount (<1%) of the authigenic component being required to account for the geochemical composition of the sediment. The down-core profile of this third component in core CD38-02 (Fig. 5.8) also suggests an interesting glacial/interglacial variation with slightly higher interglacial production of authigenic material. The most plausible reason for this is that the authigenic component of

CD38-02 is the result of the limitation of the algorithm, in that it assumes constant end-member compositions throughout the core (Appendix B.6). There are errors in calculating the $P_{phos}$ concentration (4.3.3) and the presence of the authigenic component in this core could easily be removed by slight adjustments to the $P_{org}/C_{org}$ ratio used in Eqn 4.1.

Core CD38-02 is, therefore, probably only really a three-component system with inputs from terrigenous, biogenic and residual sources. Inaccuracies in the MCA algorithm could also be used to explain the presence of the small percentage of the residual component but it must be stressed that this component is calculated from the barium concentration which is measured in ppm and not a weight % (as for all the other geochemical variables used in MCA). It is because a very high end-member Ba concentration of the residual component is used (equivalent to 270,000ppm; Dymond, 1981) is used, that the MCA results in a very low % residual component compared with the other more dominant components. However, it will be shown later (6.3.4) that the residual component, derived from the excess Ba concentration, is a true component whose down-core signal (Fig. 5.8) demonstrates a pattern of presence only during interglacial periods. Dymond (1981) stated that the "dissolution residual component should be high in areas of high productivity" which implies that in core CD38-02 there was higher surface biological productivity during interglacials compared with glacial stages. The use of barium as a palæo-productivity indicator will be examined later in this thesis (6.3.4)*.

**CD38-11**

The results of the MCA on core CD38-11 show it to be a true four-component system (Table 5.1 and Fig. 5.9) with high inputs of the terrigenous and biogenic components and significant quantities of the authigenic phosphorite component in a few horizons above a background level of about 1%. The residual component is not present until the lowest (and therefore oldest) region of core CD38-11 and, as in core CD38-02, it is only present during an interglacial stage.

The fact that CD38-11 has the highest average terrigenous component (80%) of the four piston cores in this study, supports the previous work of Dymond (1981) who produced a contour map of surficial sediment component concentrations on the Nazca plate and found that, except for the coastal upwelling region where biogenic

---

*It may be expected that cores CD38-09 and CD38-10 which are located under a high biological productivity zone, associated with coastal upwelling (Chapter 3), would show a strong residual component signal. However, it will be shown later that these sediments are situated in an environment which is unsuitable for the preservation of a barium-residual component (6.3.2).

dilution occurs, sediments from areas closer than 1000-1500km to the South American continent are composed of >80% terrigenous component.

### 5.4.3. MCA conclusions

The algorithm used in this multi-component analysis of the geochemical data from the four piston cores on the Peruvian continental margin obviously has its drawbacks and inaccuracies which are due to the basic assumptions made during the mathematical calculations. However, MCA does allow for the complex mixture of various components contained within marine sediments to be separated and their down-core variations and relative abundances to be examined individually.

One example of how the results of MCA can be used to help in the interpretation of geochemical and/or physical measurements is the comparison of the grain-size signals for each core (Figs 2.1, 2.2, 2.4, 2.5 and 7.7) with the respective down-core profiles of the MCA components (Figs 5.6 to 5.9). In both the shallow-water cores, CD38-09 and CD38-10, the authigenic component profile is most similar to the grain-size signal. This may indicate that the formation and concentration of authigenic phosphorites is affecting the overall grain-size of the sediment in these two cores (4.3.6). In core CD38-02, it is the biogenic component which is similar to the grain-size signal (compare Figs 2.4 and 5.8). This is because the variation in the concentration of carbonate microfossils can strongly influence the percentage of sediment which is >63 μm in grain-size. Core CD38-11 does not have any component profile which is similar to the grain-size down-core profile but it is probably the relative proportion of both the authigenic and biogenic components which is influencing the overall grain-size.

# CHAPTER 6

# GEOCHEMICAL PALÆO-PRODUCTIVITY AND PALÆO-REDOX INDICATORS

## 6.1. INTRODUCTION

"Biogeography cannot confine itself simply to describing the occurrence of living forms, arranging them regionally, investigating the ecological causes of distribution. It must also proceed historically" S. Ekman (1953)

One of the main purposes for undertaking geochemical studies of sediment core material from the marine environment, is to measure and interpret variations, cycles and anomalies of a certain element or ratio of elements in a down-core profile. If the concentration of an element in the sediment can be related to the condition of an oceanographic parameter then its profile against depth or, better still, age, can be used for palæo-reconstruction of certain physical, chemical and/or biological ocean conditions in the past.

The level of marine biological productivity in surface-waters and the concentration of dissolved oxygen in bottom- and pore-waters are two oceanographic parameters which are of utmost importance in controlling many processes operating within the water and sediment columns. Therefore, if certain geochemical elements can act as indicators of palæo-productivity and/or palæo-redox conditions, their study in marine sediments will help to broaden our understanding of the physical and biological changes which have occurred in the oceans throughout the Late Quaternary associated with glacial/interglacial periodicity. The above quote from Sven Ekman stresses the importance of using historical records, in this case marine sediment cores to study indicators of ocean productivity.

This chapter will examine four geochemical, environmental records, from the cores used in this study, in an attempt to evaluate their potential as palæo-productivity and palæo-redox indicators in the sediments from the Peruvian continental margin. This area is strongly influenced by coastal upwelling (Chapter 3) and therefore both the level of biological productivity and the strength and location of the oxygen minimum zone have affected the concentration and distribution of important geochemical indicators accumulating in the sediments through time.

The chapter will be divided into the following four sections and then conclude with a summary of the interpreted palæo-oceanographic conditions, allowing for a palæo-climatic reconstruction of Peruvian coastal upwelling.

1) Halogens: iodine and bromine and their association with organic matter.

2) Barium: Ba/Al record of biogenic silica and/or organic matter flux.

3) Strontium: variations in the Sr/Ca ratio within carbonate shell remains.

4) Molybdenum and uranium: use of the Mo/U ratio to distinguish between oxic and anoxic sediments.

## 6.2. THE HALOGEN SIGNAL

### 6.2.1. Introduction

Before an accurate interpretation of the geochemical signature from the two halogens, iodine (I) and bromine (Br), can be made for the off-shore Peruvian sediments, the basic marine chemistry of the elements and their sea-water/sediment/pore-water interactions need to be understood. This introduction will review some of the large number of marine geochemical studies of I and Br, with specific reference to their association with organic matter (Price and Calvert, 1977; Pedersen and Price, 1980; Shimmield and Pedersen, 1990) and the redox conditions within the sediment (Price and Calvert, 1973; Wong and Brewer, 1977; Kennedy and Elderfield, 1987).

The geographical locations of such studies have included the deep-sea abyssal plains of the Atlantic (Kennedy and Elderfield, 1987), anoxic basins such as the Black Sea (Wong and Brewer, 1977), shallow-water polar regions (Price *et al.*, 1970) and coastal regions such as the Panama basin (Pedersen, 1979; Pedersen and Price, 1980; Patience, 1992), off south-west Africa (Price and Calvert, 1973, 1977) and Baja California (Price and Calvert, 1973, Shimmield, 1985). However, no high-resolution study of the halogens and their organic matter-association has been published for the marine sediments from off Peru.

**Iodine**

The concentration of total dissolved I in sea-water is only 0.5μM (Wong, 1980) and it displays a nutrient-like behaviour in the oceans, being slightly depleted in surface waters (Wong and Brewer, 1974; Elderfield and Truesdale, 1980). In natural waters, I is known to exist in more than one oxidation state and the relative proportions of iodate ($IO_3^-$) and iodide ($I^-$) is strongly dependant on the redox environment (Wong, 1980). Iodate is dominant in normal, oxygenated waters (Sillen, 1961) but the opposite situation is found in anoxic basins, where high concentrations of $I^-$ and undetectable levels of $IO_3^-$ have been measured, e.g. in the Cariaco Trench and the Black Sea (Wong and Brewer, 1977). It is the interconversion between the

two species (Eqn 6.1) occurring at an Eh of +10.5 (at pH = 8.1), which makes iodine a potentially useful indicator of early diagenesis in hemipelagic sediments (Shimmield and Pedersen, 1990).

Equation 6.1. Iodate-iodide interconversion

$$IO_3^- + 6H^+ + 6e^- \longleftrightarrow I^- + 3H_2O$$

The processes responsible for the removal of iodine from sea-water into the sediment column have been studied extensively (Wong and Brewer, 1974, 1977; Truesdale, 1975; Harvey, 1980; Francois, 1987) but are still not fully understood.

| Author | Location | I (ppm) | I/Corg (x $10^{-4}$) | Br (ppm) | Br/Corg (x $10^{-4}$) |
|---|---|---|---|---|---|
| Price *et al.*, 1970 | South west Barents Sea | 60-828 | 380 | 12-257 | 120 |
| Price and Calvert, 1973 | South west Africa | 96-1990 | 90 | | |
| Price and Calvert, 1977 | South west Africa (anoxic) | 200-350 | 20 | 500-800 | 60 |
| | South west Africa (oxic) | 750-2000 | 250 | 250-500 | 72 |
| Pedersen and Price, 1980 | Panama Basin | 76-861 | 395 | 11-278 | 146 |
| Shimmield, 1985 | Baja, California | 116-569 | 173 | 71-279 | 97 |
| Pedersen *et al.*, 1992 | Oman margin | 134-870 | 140 | | |
| Patience, 1992 | Panama Basin | 37-252 | 104 | 17-182 | 49 |

Table 6.1. Iodine and bromine concentrations and their weight ratios to organic carbon, in surface sediments

As can be seen from Table 6.1, the concentration of I in surface, hemipelagic marine sediments can be greatly enriched (up to 2000 ppm) above the levels found in the open marine environment (Kennedy and Elderfield, 1987). The two most important factors in determining the level of I enrichment are the flux of organic matter to, and the redox-state of, the sediment (Price and Calvert, 1973, 1977; Shimmield and Pedersen, 1990). The association of I with organic matter was initially suggested by Vinogradov (1939) and Price *et al.* (1970) found a strong linear correlation between I and organic carbon ($C_{org}$) in the surface sediments of the Barents Sea.

Price and Calvert (1973, 1977) measured $I/C_{org}$ weight ratios of surface, oxidised sediments (about 250 x $10^{-4}$) from south west Africa and the Gulf of California which were an order of magnitude higher than in reduced sediments (20 x $10^{-4}$) from the same locations (Table 6.1), and proposed that the enrichment of iodine in an oxic environment occurred at the sediment/water interface. One possible mechanism for such an enrichment involved the sequestration of I by plankton seston using an iodide-oxidase enzyme which requires free-oxygen to perform any reaction (Shaw, 1962).

Harvey (1980) proposed that the association of I with organic matter involves nitrogenous compounds (e.g. polypeptides) which are labile upon decomposition. More recent experimental work by Francois (1987) concluded that the humic fraction of organic matter readily absorbs $IO_3^-$ which is the dominant I species in oxic bottom-waters and therefore I is enriched in oxic environments. In oxygen-deficient conditions, $I^-$ is the dominant species of I and is not adsorbed to the same extent (Pedersen *et al.*, 1992).

Shimmield and Pedersen (1990) reviewed surface $I/C_{org}$ ratios from a wide range of hemipelagic, oxic marine environments and stated that an $I/C_{org}$ molar ratio of 25 (±10) x $10^{-4}$ (equivalent to 265 ±100 x $10^{-4}$ weight ratio) was a global-average for continental margin sediments. The surface $I/C_{org}$ weight ratio can therefore be used as a redox-indicator, where values of 165-365 x $10^{-4}$ imply normal, oxic conditions and much lower values are indicative of anoxic conditions.

If organic matter did not decay upon burial within marine sediments or if I decayed at the same rate as the bulk of organic matter during decomposition, then the down-core $I/C_{org}$ ratio could easily be used as a palæo-redox signal, to indicate whether oxic or anoxic conditions were prevalent at any particular site over time. However, this is not the case, and as has been shown by many authors (Price *et al.*, 1970; Pedersen and Price, 1980; Shimmield, 1985; Kennedy and Elderfield, 1987; Patience, 1992), the $I/C_{org}$ ratio decreases exponentially down the sediment column upon preferential release of I during the post-depositional decomposition of organic matter. The complex interactions and recycling between solid-phase I incorporated with organic matter, and dissolved $IO_3^-$ and $I^-$ in bottom-waters and pore-waters has been studied by Francois (1987) and Kennedy and Elderfield (1987) and this will be looked at in more detail later, with respect to the I concentration profiles of the Peruvian continental margin sediments.

**Bromine**

This halogen occurs as one of the major anions present in sea-water at a concentration of 0.84mM (at salinity = 35 parts per thousand) and displays conservative properties (Riley and Chester, 1971). Bromine has a much more simple marine geochemical behaviour compared with I because it exists only as the bromide ion ($Br^-$) in sea-water and therefore does not display any redox-associated properties (Shimmield and Pedersen, 1990). However, as can be seen from Table 6.1, Br is present in marine surface sediments in quite high concentrations (up to 800 ppm) and is found in association with organic matter (Price *et al.*, 1970; Price and Calvert, 1977; Pedersen and Price, 1980).

Price and Calvert (1977) measured relatively low $Br/C_{org}$ ratios compared with $I/C_{org}$ in oxic sediments from the Namibian shelf and concluded that the two halogens must display different forms of association with organic matter. The fact that the I/Br ratio in Panama basin surface sediments was 3500 times greater than in sea-water, implied to Pedersen and Price (1980) that uptake of the halogens was by different organic ligands. Shimmield and Pedersen (1990) quote a $Br/C_{org}$ molar ratio of $19.6 \times 10^{-4}$ (equivalent to $131 \times 10^{-4}$ weight ratio) for surface continental margin sediments, regardless of the redox state of the water or sediment column.

Very little study has been carried out on the mechanism for, and the nature of, Br uptake by organic matter but Harvey (1980) concluded that Br exists in a large range of water-soluble and organic-soluble compounds including aliphatic molecules.

Upon burial of organic matter in marine sediments, microbial degradation will occur which should release Br to the interstitial pore-waters. Measurement of the down-core variation in $Br/C_{org}$ suggests that Br is released much slower in relation to I and this implies that Br is bound more strongly to the organic matter (Price and Calvert, 1977; Pedersen and Price, 1980; Shimmield, 1985). In Panama Basin sediments, Pedersen and Price (1980) measured $Br/C_{org}$ ratios down to depths of about 160cm which displayed zones which increased with depth. This is an indication that, in hemipelagic sediments, Br is less labile than the bulk of organic matter during diagenesis (Shimmield and Pedersen, 1990) i.e. that Br is associated with refractory organic compounds.

Of the two halogens, Br is therefore the less useful in terms of both redox and productivity signals in marine sediments. However, it is still important to study the concentrations of both halogens together, as well as their relative associations with organic matter, e.g. correlation coefficients and halogen/$C_{org}$ ratios, in the sediments on the continental margin of Peru.

### 6.2.2. Analytical methods and results

Both I and Br concentrations (ppm) were measured in all the sediment samples in this study using X-ray fluorescence techniques on pressed-pellet samples (Appendix A.5). It should be noted that there is a larger degree of error in calculating the salt-corrected concentrations of Br than for I, because there is a significant concentration of Br contained in the salt, which has to be subtracted from the raw data (Appendix A.6). As previously stated, $C_{org}$ levels were determined by combustion techniques after initial acid-removal of carbonate (Appendix A.3).

| | I (ppm) | Br (ppm) | I/Br | I/Corg ($x10^{-4}$) | Br/Corg ($x10^{-4}$) |
|---|---|---|---|---|---|
| | | | SURFACE | | |
| CD38-09 | 93 | 456 | 0.21 | 14.0 | 68.0 |
| CD38-10 | 134 | 461 | 0.29 | 14.6 | 50.0 |
| CD38-02 (Box) | 350 | 103 | 3.38 | 343.1 | 101.4 |
| CD38-02 | 222 | 132 | 1.68 | 148.7 | 88.4 |
| CD38-11 | 469 | 300 | 1.56 | 121.0 | 77.6 |
| CD38-03 (Box) | 540 | 189 | 2.87 | 314.2 | 109.6 |
| | | | RANGE | | |
| CD38-09 | 3-93 | 40-456 | 0.05-0.4 | 0.9-14.4 | 14-68 |
| CD38-10 | 3-134 | 22-461 | 0.05-0.5 | 1.4-16.8 | 16-53 |
| CD38-02 (Box) | 139-379 | 47-148 | 1.8-3.7 | 128-357 | 47-131 |
| CD38-02 | 74-355 | 47-213 | 0.8-3.2 | 67-170 | 39-101 |
| CD38-11 | 136-469 | 86-300 | 0.7-1.9 | 43-135 | 43-78 |
| CD38-03 (Box) | 174-624 | 68-266 | 1.6-3.0 | 110-330 | 46-135 |
| | | | MEAN | | |
| CD38-09 | 25.0 | 112.9 | 0.20 | 5.4 | 24.7 |
| CD38-10 | 24.1 | 132.0 | 0.19 | 4.9 | 25.0 |
| CD38-02 (Box) | 229.2 | 89.5 | 2.62 | 195.8 | 77.4 |
| CD38-02 | 161.8 | 91.9 | 1.77 | 107.1 | 62.0 |
| CD38-11 | 283.2 | 190.5 | 1.51 | 86.1 | 57.6 |
| CD38-03 (Box) | 291.3 | 140.4 | 2.12 | 162.8 | 78.0 |

Table 6.2. Iodine and bromine concentrations and weight ratios (surface, range and mean) for Peruvian margin sediments.

The data in Table 6.2 summarises the halogen concentrations (ppm), the I/Br ratio and their weight ratios to organic carbon (all surface, range and mean) for the two box cores and four piston cores used in this study (the full data set is listed in Appendix C.11). From the surface I/Corg ratios an initial interpretation of the redox environment at each core site will be made by comparison with the results of Price and Calvert (1977, Table 6.1).

Care must be taken when interpreting surface data from piston cores because these cores do not contain the sediment/water interface and the first sub-sample was taken up to 10cm down the core. In the study of a geochemical indicator whose concentration varies dramatically over the first few centimetres of the sediment column, such as the halogens, box cores give a much more detailed picture close to, and at, the sediment/water interface.

The profiles in Figs 6.1 through to 6.6 are plots of I, Br, $C_{org}$, $I/C_{org}$, $Br/C_{org}$ and I/Br against depth/age for the above cores. It can be seen that all the I and Br profiles display strong similarities to their respective $C_{org}$ profile and the strength of this halogen-$C_{org}$ relationship can be illustrated by the high correlation coefficients shown in Table 6.3, especially for the four piston cores.

| | | | Core position | |
|---|---|---|---|---|
| Iodine | 0.567 | 0.390 | CD38-09 | CD38-10 |
| | 0.120 | 0.825 | CD38-02 (Box) | CD38-02 |
| | 0.673 | 0.362 | CD38-11 | CD38-03 (Box) |
| Bromine | 0.702 | 0.745 | 0.923 | 0.732 |
| | 0.017 | 0.766 | 0.534 | 0.810 |
| | 0.815 | 0.565 | 0.724 | 0.731 |
| | Organic carbon | | Iodine | |

Table 6.3. Iodine, bromine and organic carbon correlation coefficients.

From the data presented in Figs 6.1 to 6.6 and Table 6.2, the following points should be noted.

a) The surface I concentrations are lowest in the shallow-water, shelf cores and highest at the deep-water sites, even though cores CD38-09 and CD38-10 have the highest organic matter content. This results in very low surface $I/C_{org}$ ratios for these two cores.

b) In contrast, the highest surface Br concentrations are found in the two shallow-water cores and the inter-core variation seems to be dependant on the level of

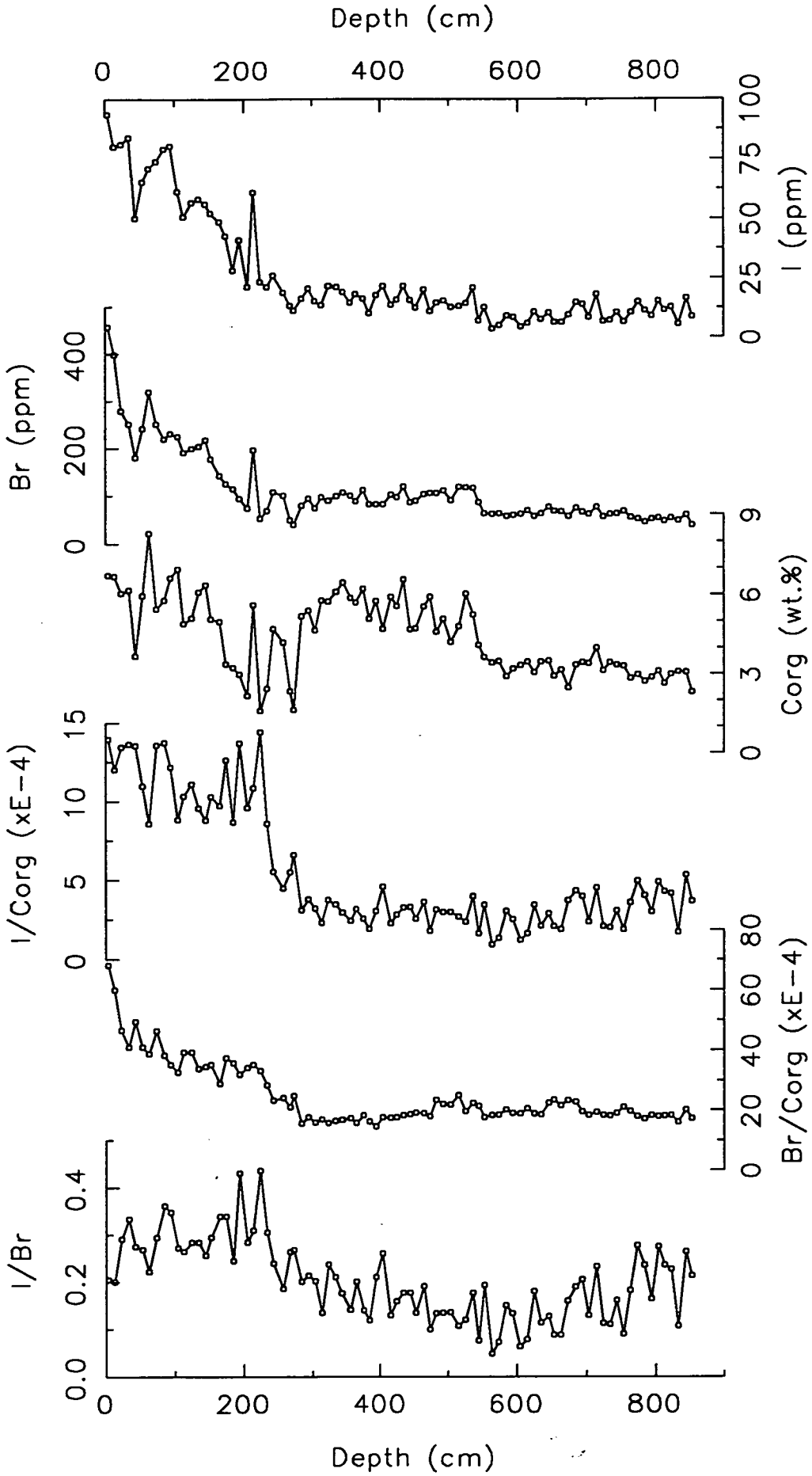


Figure 6.1. Core CD38-09 (148m) halogen depth profiles : iodine, bromine, organic carbon, $I/C_{org}$, $Br/C_{org}$ and I/Br against depth (cm).

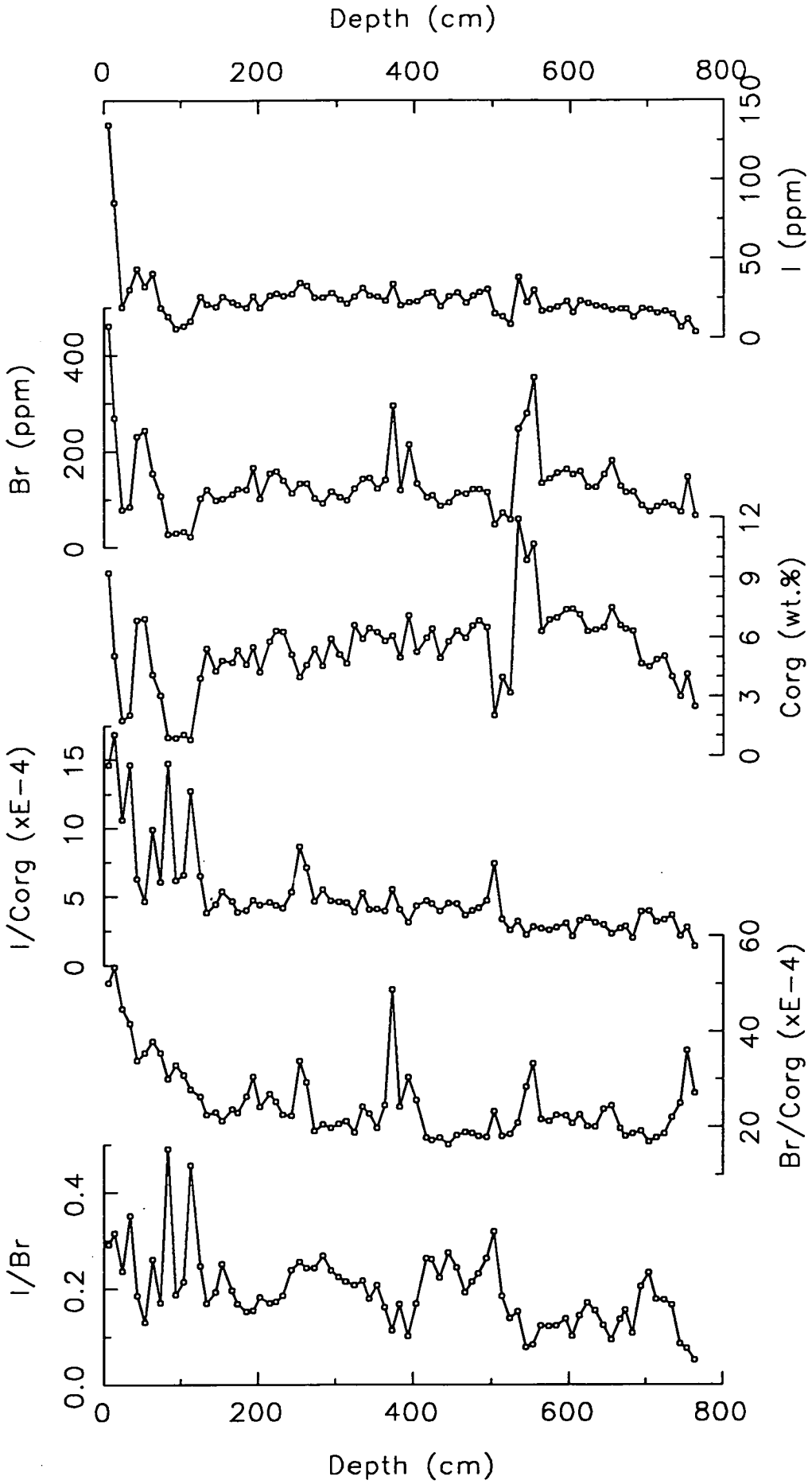


Figure 6.2. Core CD38-10 (257m) halogen depth profiles : iodine, bromine, organic carbon, $I/C_{org}$, $Br/C_{org}$ and I/Br against depth (cm).

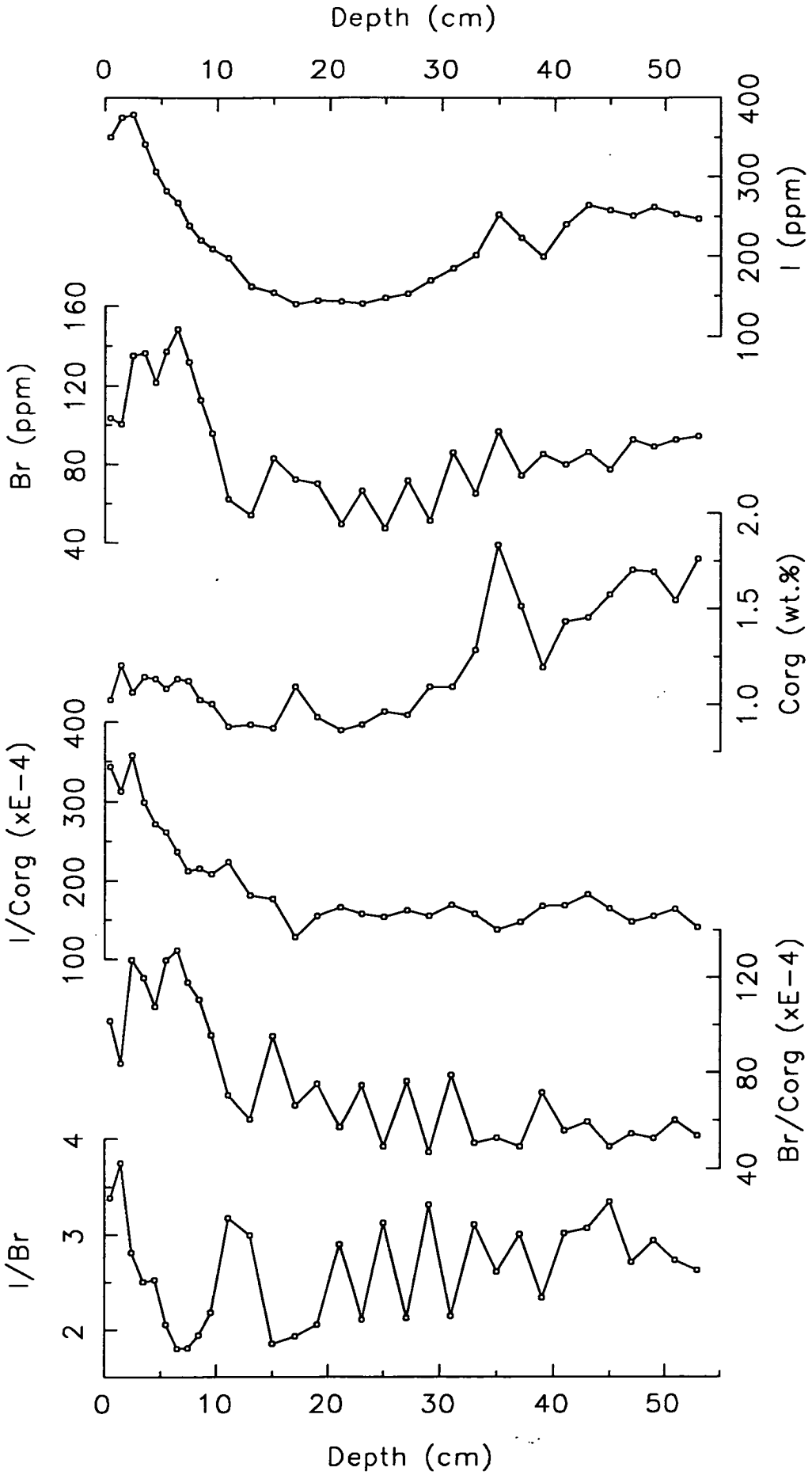


Figure 6.3. Box core CD38-02 (2530m) halogen depth profiles : iodine, bromine, organic carbon, $I/C_{org}$, $Br/C_{org}$ and I/Br against depth (cm).

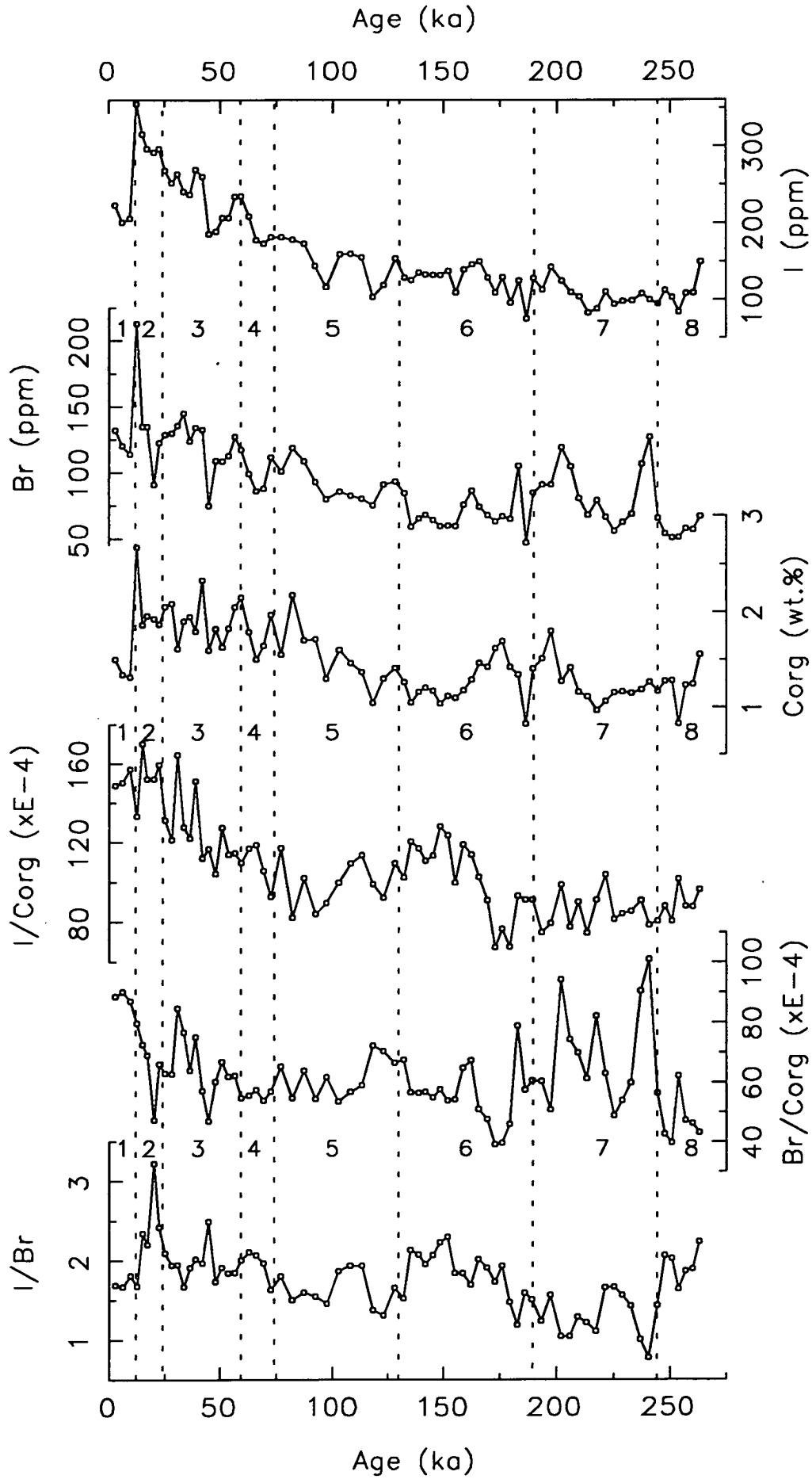


Figure 6.4. Core CD38-02 (2525m) halogen age profiles : iodine, bromine, organic carbon, $I/C_{org}$, $Br/C_{org}$ and I/Br against age (ka).

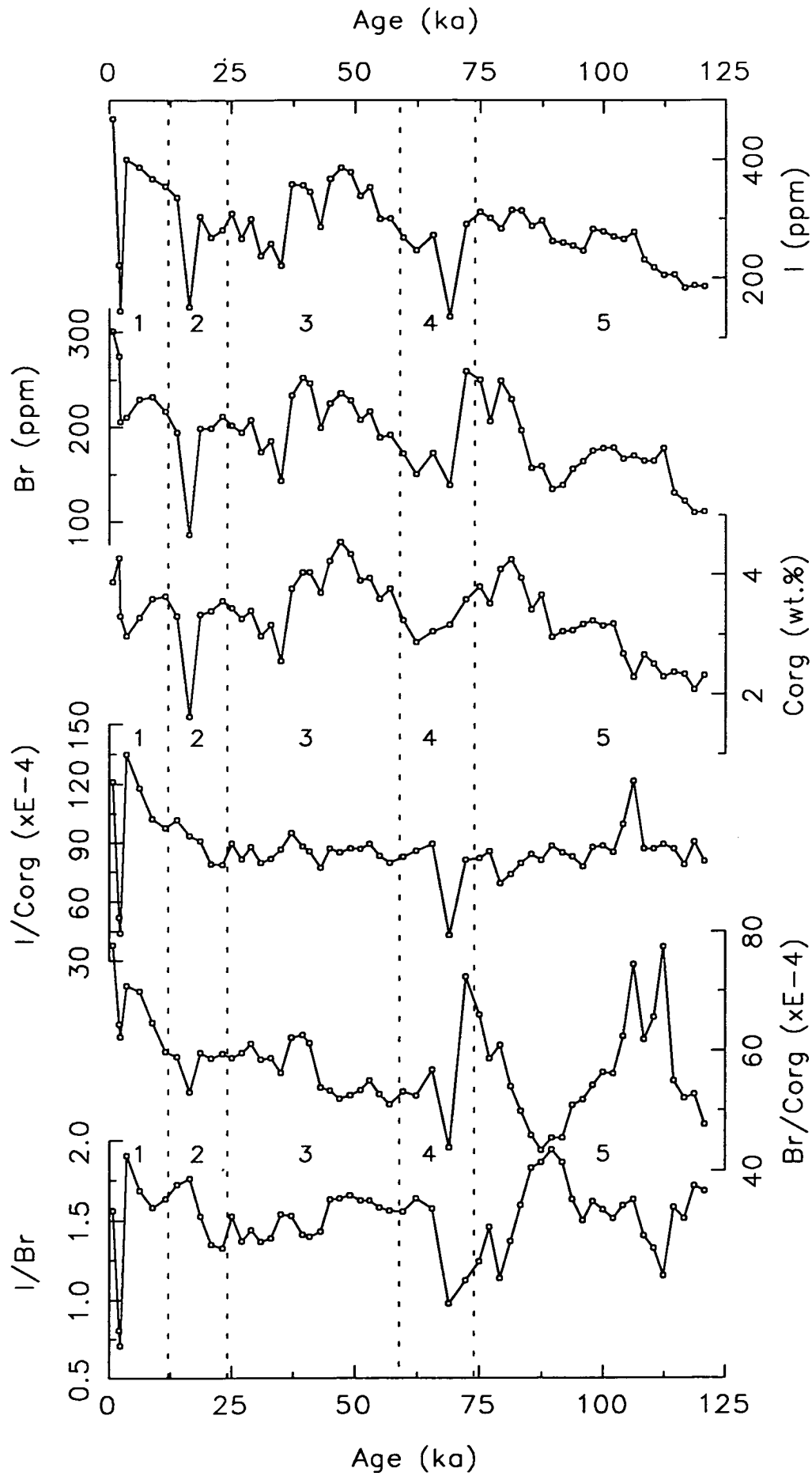


Figure 6.5. Core CD38-11 (3835m) halogen age profiles : iodine, bromine, organic carbon, $I/C_{org}$, $Br/C_{org}$ and I/Br against age (ka).

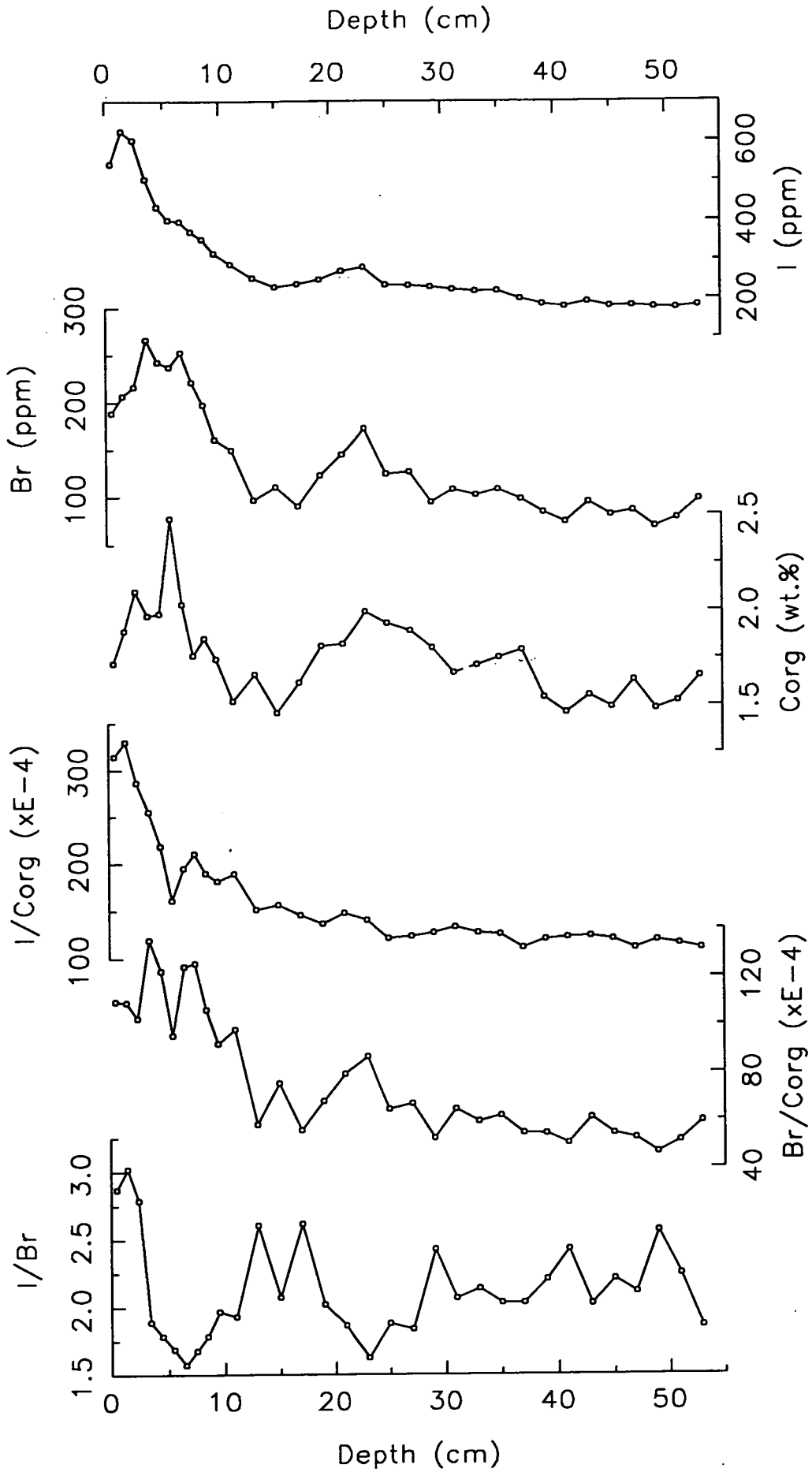


Figure 6.6. Box core CD38-03 (4289m) halogen depth profiles : iodine, bromine, organic carbon, $I/C_{org}$, $Br/C_{org}$ and I/Br against depth (cm).

$C_{org}$, resulting in fairly similar surface $Br/C_{org}$ ratios, which are within the range, 50-110 x $10^{-4}$.

c) In the two box cores (Figs 6.3 and 6.6), the peak of I (ppm) is not exactly at the sediment/water interface but is just below it, at the 1-2cm range. The pattern is similar for Br (ppm) which peaks at 2-7cm. The surface sample concentrations in the four piston cores are very dependant on the actual depth of the first sub-sample and so the near-surface peaks are not seen.

d) There is a fairly smooth exponential decrease in the $I/C_{org}$ ratios of the two box cores, which levels out within 20-30cm to an average of 160 x $10^{-4}$ for CD38-02 and 120 x $10^{-4}$ for CD38-03. The deep-water piston cores display similar profiles with a sub-surface maxima in CD38-11 at 40cm (135 x $10^{-4}$) decreasing smoothly down to a background level of 80-90 x $10^{-4}$ below 100cm. The decrease in piston core CD38-02 is not as smooth and there is a broad zone (300-500cm) where the $I/C_{org}$ increases again.

e) The two shallow-water, iodine-depleted cores have $I/C_{org}$ weight ratios which are very variable (5-15 x $10^{-4}$) above the zones of major phosphorite formation (4.3.3) but below 280cm in CD38-09 and 120cm in CD38-10 the ratio is less than 5 x $10^{-4}$ and much more steady.

f) There is a steady-state, exponential decrease in the $Br/C_{org}$ weight ratios of cores CD38-09 and CD38-10 which levels out to about 20 x $10^{-4}$. However, in all the piston cores except CD38-09, sub-surface maxima in $Br/C_{org}$ are found and the ratio is highly variable in CD38-02.

The relative enrichments of the two halogens can be expressed as an I/Br weight ratio and the lowest plot in Figs 6.1 to 6.6 displays the depth profile of I/Br for each of the cores. The four piston core I/Br profiles illustrate the difference in halogen enrichment between the shallow-water (surface I/Br = 0.2-0.3) and deep-water (surface I/Br = 1.5-1.7) environments. In core CD38-11, it is thought that a turbidite-like zone occurs at 4-24cm and the two sub-samples in this horizon (Fig. 6.5) have I/Br ratios < 1.0 (as well as anomalously low $I/C_{org}$ ratios) which may be an indication that the sediment in this zone contains organic matter which was originally deposited further up the continental slope at a much shallower depth.

The very low I/Br weight ratio in sea-water (8.5 x $E^{-4}$, Pedersen and Price, 1980) is due to the fact that Br is a major sea-salt anion (Riley and Chester, 1971). Therefore, surface sediment I/Br ratios of between 0.2 and 3.4 (Table 6.2) indicate that on the Peruvian continental margin the uptake of I is being favoured over Br by a factor of between 235 and 4000.

### 6.2.3. The halogens as palæo-indicators

The various factors which control the halogen composition of marine sediments must be examined before any interpretation of their down-core variation can be made. This discussion section will look at the two halogens separately, with respect to the results from this study, in terms of their geochemical controls and then make some interpretations about their use as palæo-indicators. Finally, their relative concentrations will be considered, using the I/Br weight ratios of piston core CD38-02 (for which a glacial/interglacial age model has been assigned; 2.4.2), for their use as indicators of global climate change.

**Iodine**

The level of organic matter flux to the sediment and its actual concentration within the sediment does not seem to control the level of I enrichment in the Peru margin sediments, even though it is the organic matter which is the vital component in the mechanism of I uptake from sea-water (Harvey, 1980; Francois, 1987). This can be seen by the inverse relationship for surface sediment concentrations of I against $C_{org}$ in Fig. 6.7.A.

If the surface sediments with the highest $C_{org}$ content have the lowest I concentration, and vice versa, and yet there is a fairly strong I-$C_{org}$ correlation in all the sediments (Table 6.3) there must be another, more dominant factor controlling the I concentration. Figure 6.7.B is a plot of the surface I concentration against water depth of the core site, which has a positive straight-line relationship [where, I (ppm) = 0.0996 x water depth (m) + 75.8 ($r = 0.956$)]. This can be interpreted either as uptake of I by organic matter within the water column (where longer sinking times allow for higher I enrichment) or uptake at the sediment/water interface by organic matter before it is buried, in which case more I enrichment would depend on slower sedimentation rates.

Previous work by Price and Calvert (1977) implies that the latter of the two, i.e. bulk sedimentation rate, is the correct interpretation, and this hypothesis is backed up by the I recycling model of Kennedy and Elderfield (1987) which is very dependant on the bulk sedimentation rate. Recycling involves initial release of I from freshly deposited organic matter in the form of the thermodynamically-unstable $I^-$ anion, which can be oxidised to $I_2$. This free iodine can then react with organic matter or be hydrolysed to HOI, which is readily sequestered by humic compounds.

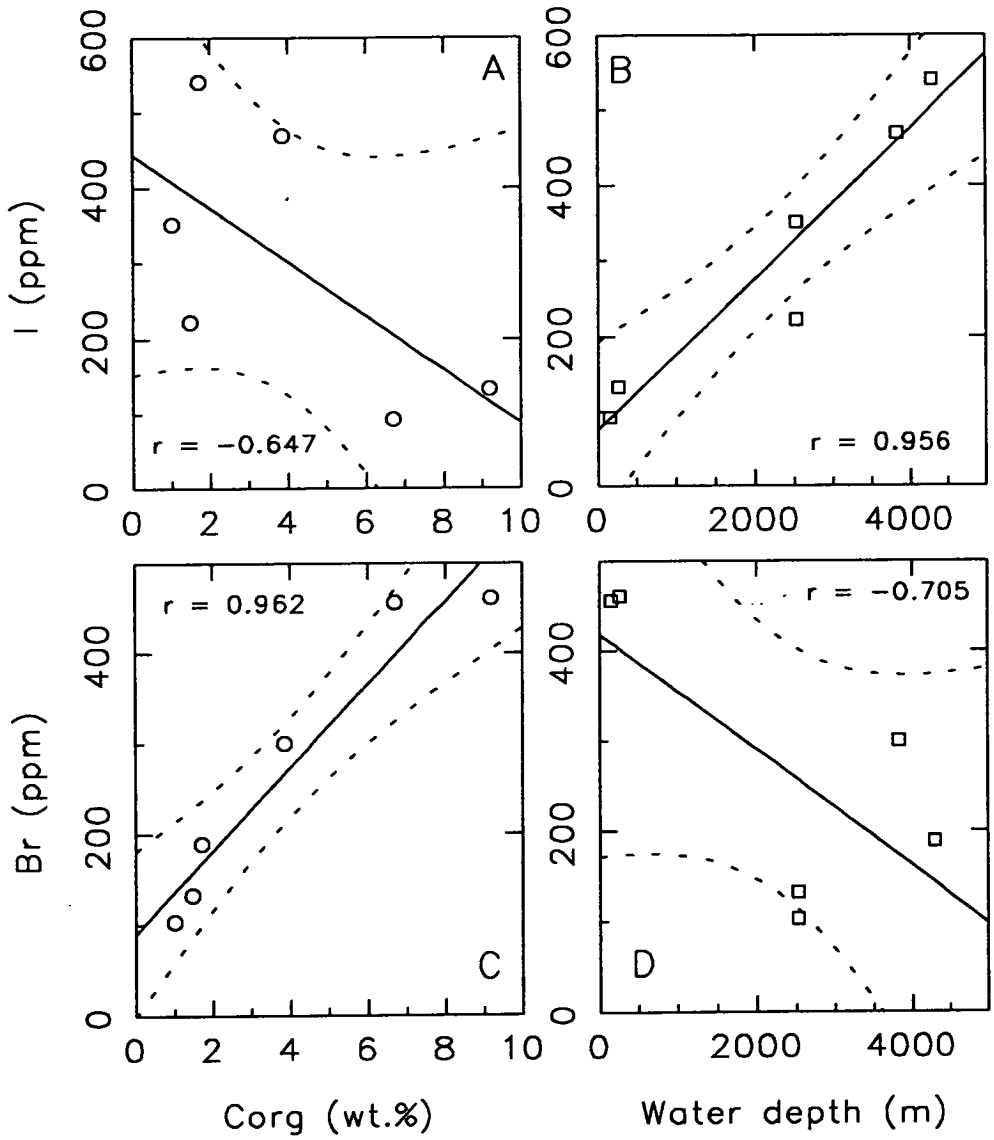


Figure 6.7. Correlation plots for surface samples in this study: A) I against $C_{org}$, B) I against water depth, C) Br against $C_{org}$ and D) Br against water depth. All show best fit straight line (full line) and 95% confidence limits (dotted lines).

Therefore, slower burial of organic matter allows for a longer residence time near the sediment/water interface and greater I enrichment by organic matter.

However, even if sedimentation rates and organic matter fluxes are similar, there is one physio-chemical property of the sediment/pore-water system which dominates the control of I concentration in marine sediments and that is the redox environment of deposition (Price and Calvert, 1973, 1977; Shimmield and Pedersen, 1990; Pedersen *et al.*, 1992).

Price and Calvert (1977) state that on the Namibian shelf, under a zone of coastal upwelling similar to that found off Peru, the $I/C_{org}$ weight ratio in surface sediments is about 250 x $10^{-4}$ in oxic sediments but only about 20 x $10^{-4}$ in reduced sediments. From the surface $I/C_{org}$ data in Table Z.2, it can therefore be interpreted that the sediments in cores CD38-09 and CD38-10 are presently accumulating under reduced, anoxic conditions, in contrast to the deeper-water cores which are situated in an oxic environment. The two shallow-water cores are located within the 100-400m water depth where the oxygen-minimum zone (OMZ) impinges on the Peruvian continental shelf (Veeh *et al.*, 1973) and therefore the bottom-waters and pore-waters at these sites are very deficient in dissolved oxygen (Chapter 1).

As previously mentioned, Price and Calvert (1973, 1977) concluded that I uptake at the sediment/water interface involves an iodide-oxidase enzyme within organic matter which requires the presence of free oxygen to react (Shaw, 1962). This I-organic matter reaction, therefore does not operate in sediments within the OMZ off Peru, resulting in the relatively low I concentrations in CD38-09 and CD38-10. Laboratory experiments by Francois (1987) suggested that humic substances can reduce iodate to electropositive iodine species, which then electrophilically substitute onto organic molecules. This reaction did not occur when humic compounds were exposed to iodide-bearing solutions, such as found in anoxic systems (Francois, 1987). Therefore, sediments accumulating under such conditions are less enriched in I than those exposed to oxic, iodate-bearing waters.

The problem with relating this redox-indicating property of I to sediments which are no longer at the surface, arises from the preferential release of I back into pore-waters upon post-depositional decay of organic matter and recycling of the halogen (Kennedy and Elderfield, 1987; Shimmield and Pedersen, 1990). The exponential decrease of the $I/C_{org}$ ratio with increasing depth, can result in sediments

which were initially deposited under oxic conditions displaying a very low $I/C_{org}$ ratio.

The iodine concentration is of limited use as a palæo-redox indicator but when applied in conjunction with $C_{org}$ measurements, it can be used to distinguish between past oxic conditions ($I/C_{org}$ = 250 down to 80 x $10^{-4}$) and anoxic conditions ($I/C_{org}$ < 20 x $10^{-4}$) existing at the sediment/water interface.

From the $I/C_{org}$ profiles in Figs 6.1 to 6.6, it can be seen that the sediments in cores CD38-09 and CD38-10 have been continuously deposited under anoxic conditions and all the other cores within an oxic environment. The shallow-water, anoxic conditions on the Peruvian continental shelf indicate that over the length of time that the sediments in cores CD38-09 and CD38-10 were deposited, the OMZ was always present. This, in turn, probably means that coastal upwelling has existed in this area throughout the Late Quaternary (Schrader, 1992).

One other application of this $I/C_{org}$ palæo-redox indicator is in the determination of possible breaks in the sedimentation pattern of a core, which can be either due to loss (i.e. erosion of the column) or gain (i.e. a turbidite) of sediment. In core CD38-11 (Fig. 6.5), the turbidite zone at 4-24cm is highlighted by anomalously low $I/C_{org}$ weight ratios (40 x $E^{-4}$) below which an exponential, steady-state decrease occurs. In cores CD38-09 and CD38-10 (Figs 6.1 and 6.2), there is a non-steady-state decrease pattern of $I/C_{org}$ in the upper part of each core, then a sharp break at the zones of phosphorite formation (220-270cm in CD38-09 and 80-110cm in CD38-10) followed by much lower $I/C_{org}$ ratios which show less variation. This unusual $I/C_{org}$ profile implies that the smooth exponential decrease of $I/C_{org}$ has been disturbed by a period of erosion of the sediment column (occurring at the same time as phosphorite concentration, 4.3.6) and that the sediment below the phosphorite horizon is relatively older than its current depth would imply.

**Bromine**

The ability of an element to act as an indicator of surface ocean productivity or bottom-water oxygen conditions in a marine sediment record depends respectively on the mechanisms of preservation of the element's original surface sediment signal and the number of valence states in which the element exists in sea-water.

As previously mentioned, bromine cannot easily be used as a palæo-indicator because,

a) the mechanisms of release of Br upon organic matter degradation are not fully understood (Harvey, 1980; Shimmield and Pedersen, 1990) and therefore a

palæo-measurement of Br concentration cannot be accurately interpolated back to an original surface Br content and thus organic matter/ocean productivity level, and,

b) bromide is the only form of Br that exists in sea-water and therefore it displays no redox behaviour (Shimmield and Pedersen, 1990).

There is a linear correlation between Br and organic carbon for the surface sediments from all the cores in this study, regardless of the redox state of the sediments or water column (Fig. 6.7.C). However, this relationship does not hold for sub-surface samples due to inter-core differences in the decay of organic matter and release of Br.

Measurement of Br and its ratio to $C_{org}$ in marine sediment cores can help to indicate possible sediment loss at the top of piston cores and possible inter-core variations in the sedimentation rate and/or the composition of organic matter present.

Shimmield and Pedersen (1990) produced a correlation plot of Br against $C_{org}$ for surface, hemipelagic sediments with a straight line molar ratio of 19.6 x $10^{-4}$, which is equivalent to a weight ratio of 131 x $10^{-4}$. The two box cores in this study have surface $Br/C_{org}$ weight ratios of 102 x $10^{-4}$ for CD38-02 and 110 x $10^{-4}$ for CD38-03 (Table 6.2), which agree well with the combined data set used by Shimmield and Pedersen (1990). In fact, the $Br/C_{org}$ weight ratios measured between 2 and 3cm, where the sub-surface peak of Br (ppm) occurs, are 130 x $10^{-4}$ and 135 x $10^{-4}$ respectively. It can also be seen from Figs 6.3 and 6.6 that within the upper 30cm in the two box cores, the $Br/C_{org}$ ratio has dropped to 50-60 x $10^{-4}$.

This information can now be used for all the piston cores to determine whether or not much of the surface sediment has been lost during the coring procedure. A surface value of 130 x $E^{-4}$ for $Br/C_{org}$ can be applied to all the Peruvian continental margin sites including the two shallow-water, anoxic cores because the redox state should not affect the surface $Br/C_{org}$ ratio (Pedersen and Price, 1980; Shimmield and Pedersen, 1990). The top samples in the four piston cores from this study fall within the range 50-90 x $10^{-4}$ for $Br/C_{org}$ (Table 6.2) which indicates that very little (up to 30cm) of the original surface sediment has been lost during coring.

The depth at which the $Br/C_{org}$ ratio reaches a background, steady level in marine sediments can suggest differences in sedimentation rates between cores. If the sedimentation rate is relatively slow, any Br associated with labile organic matter should have enough time to be released before being buried too deep. The cores CD38-02 and CD38-11 both seem to reach background $Br/C_{org}$ ratios of about 60 x

$10^{-4}$ within the upper metre of sediment (Figs 6.4 and 6.5) suggesting a slower sedimentation rate at these sites compared with CD38-09 and CD38-10 which take 3 and 1.5m respectively to reach their background $Br/C_{org}$ level of about 20 x $10^{-4}$ (Figs 6.1 and 6.2). This is as expected, since the shallow-water cores are situated on the continental shelf, close to the terrigenous-input source (7.2.3).

This picture may, however, also be influenced by differences in the type of organic matter and/or its flux to the sediment at each site. It is of interest to note that the two cores situated directly under the zone of coastal upwelling display a much lower background level of $Br/C_{org}$ when compared with the cores on the Nazca ridge and deep continental slope (20 x $E^{-4}$ compared with 60 x $E^{-4}$). This difference may be due to contrasts in the composition of organic matter at these sites, e.g. if different organic compounds take up variable quantities of Br in labile forms compared with more refractory forms, then more Br will be released upon post-depositional decomposition from the organic matter containing more labile-Br. This will result in a lower background $Br/C_{org}$ ratio.

**I/Br**

In previously published studies of marine sediments which measured both I and Br (Price *et al.*, 1970; Price and Calvert, 1977; Pedersen and Price, 1980; Patience, 1992) the concentrations of the two halogens have generally been considered separately and then conclusions drawn about their contrasting geochemical behaviours. Pedersen and Price (1980) used the surface sediment I/Br ratio to quantify the degree of enrichment of I in relation to Br in Panama Basin sediments compared with sea-water, but did not study down-core variations in I/Br. Patience (1992) plotted temporal variations in I/Br which showed a general decrease down-core indicative of preferential release of I relative to Br during burial diagenesis. The I/Br weight ratio profiles for the piston cores in this study also show this down-core decreasing trend (Figs 6.1, 6.2, 6.4 and 6.5) but these are complicated by zones of higher I/Br as well.

As described above, the two halogens are taken up at the sediment/water interface by organic matter to different degrees due to the redox state of the pore-waters, the flux of organic matter and/or the sedimentation rate. They are then released upon burial at different rates. This would seem to imply that the I/Br ratio would be of little use as a palæo-indicator of the possible changes in surface biological productivity associated with glacial/interglacial periodicity throughout the Late Quaternary.

The two near-shore cores, CD38-09 and CD38-10, have exceptionally low (<0.5) I/Br ratios due to the lack of I uptake in the anoxic environment. Although the

down-core plots of I/Br for these two cores (Figs 6.1 and 6.2) do show a possible cyclic pattern, interpretation is difficult because of the lack of accurate age models and the breaks in the sediment column caused by erosion. However, for piston core CD38-02 an accurate age model has been determined by foraminifera oxygen isotope profiling (2.4.2) and the lowest plot in Fig. 6.4, which displays the I/Br ratio plotted against calculated age, shows that on the Nazca ridge the I/Br profile does show a possible palæo-environmental record of glacial/interglacial variation. The sediments in core CD38-02 have accumulated under surface oxic, steady-state conditions resulting in I/Br ratios which vary between 0.9 and 3.1, with the interglacial stages displaying relatively lower values. This is the case both in the near-surface sediments, which contain organic matter which is still releasing the halogens during decomposition, and in the deeper sediments, which have reached a stable state with respect to organic matter decay.

Why should hemipelagic sediments from the Peruvian continental margin display I/Br ratios which seem to fluctuate in correspondence to Late Quaternary climate changes? The I/Br against age profile of CD38-02 could be interpreted as a palæo-productivity record because climate change, caused by ice-sheet build-up during glacial periods, is known to affect the strength of coastal upwelling, which in turn can alter the structure and volume of the marine biomass in the surface waters and change the organic matter flux to the sediment (Chapter 3). Variations in the quantity and/or composition of organic matter at the sediment/water interface could affect the relative amounts of uptake of the two halogens into organic compounds thus altering the I/Br ratio measured throughout the sediment column. There seems to be either a relatively greater uptake of I or less uptake of Br during glacial periods, resulting in higher I/Br ratios in core CD38-02. This interpretation is, however, very speculative and no such I/Br-climate change relationship was seen in core CD38-11. Until a more detailed understanding of the complex mechanisms of halogen incorporation in hemipelagic sediments is known, it is difficult to interpret these I/Br variations further.

### 6.2.4. Conclusions

The following conclusions can be made with regards to the use of I and Br as indicators of palæo-productivity and palæo-redox conditions in the Peru continental margin sediments.

1) I and Br are closely associated with organic carbon and with each other (Table 6.3). However, their post-depositional diagenetic mobility means that the halogens are unreliable as indicators of palæo-productivity.

2) Surface sediment concentrations of I and the $I/C_{org}$ ratio can be used to distinguish between oxic and anoxic environments of deposition. Piston cores CD38-09 and CD38-10 show very low surface $I/C_{org}$ ratios, and are therefore located in an anoxic environment, where the OMZ impinges on the sea-floor under the Peruvian coastal upwelling zone. All other cores used in this study contain much higher surface $I/C_{org}$ ratios which indicates that they are situated in a more normal, oxic marine environment.

3) Interpretation of down-core $I/C_{org}$ ratios is made complicated by the decay of organic matter and recycling of I (Kennedy and Elderfield, 1987) but they seem to imply that palæo-redox conditions at the above sites on the Peru continental margin have not changed throughout the Late Quaternary, i.e. cores CD38-09 and CD38-10 have accumulated under generally anoxic conditions, which implies that coastal upwelling has affected bottom-water oxygen levels throughout the history of sediment deposition.

4) Surface $Br/C_{org}$ ratios are independent of redox conditions (Shimmield and Pedersen, 1990) and therefore this halogen cannot be used as a palæo-redox indicator. Stronger statistical correlation in the piston cores between Br and $C_{org}$ compared with I and $C_{org}$ (Table 6.3) suggests that Br is associated with less labile compounds within marine organic matter.

5) Down-core variations in halogen content and their ratios to $C_{org}$ can help to identify breaks in the sedimentation pattern (turbidite zone in CD38-11 and erosion in CD38-09 and CD38-10), loss of sediment at the top of piston cores and inter-core variations in sedimentation rate and/or organic matter composition.

6) The I/Br ratio in sediments from an undisturbed, oxic core, such as CD38-02, may indicate changes in the composition and/or flux of organic matter associated with glacial/interglacial climate change, where glacial periods display relatively higher I/Br ratios. Until the complex interactions involved in the uptake and release of halogens by organic matter are more fully understood, this I/Br - climate change hypothesis cannot be substantiated.

## 6.3. THE BARIUM SIGNAL

### 6.3.1. Introduction

A major aim of palæo-oceanography is to find a geochemical record in marine sediments of past levels of sea-surface biological productivity and because most of the proxy indicators previously used ($C_{org}$, $CaCO_3$, biogenic silica; Chapter 7) are indicators of more than one oceanographic process, the ideal palæo-productivity indicator has still to be found (Rea *et al.*, 1991).

However, since Revelle *et al.* (1955) first noticed a link between barium (Ba), opal (biogenic silica) and biogenic sedimentation, many authors (Chow and Goldberg, 1960; Church, 1970, 1979; Schmitz, 1987; Nair *et al.*, 1989; Dehairs *et al.*, 1991; Shimmield and Mowbray, 1991; Dymond *et al.*, 1992; Patience, 1992; Von Breymann *et al.*, 1992) have studied Ba in terms of its usefulness as a palæo-productivity indicator.

Ba in sediments occurs mainly as barite ($BaSO_4$), a marine mineral which was first reported by Murray and Renard (1898) and whose production in the water column from dissolved Ba seems to be related to the marine biogeochemical cycle. There are two sets of hypotheses for the production of barite in the ocean:

1) formation in microenvironments, such as siliceous plankton tests, marine snow, faecal pellets etc., where decay of organic matter provides an enrichment of dissolved sulphate (Chan *et al.*, 1976; Dehairs *et al.*, 1980; Bishop, 1988); and
2) active precipitation by marine organisms, such as benthic foraminifera (Lea and Boyle, 1989), corals (Lea and Boyle, 1990A) and benthic protozoans (Bishop, 1988).

Church (1970, 1979) found a correlation in East Pacific Rise sediments between Ba, $CaCO_3$ and $C_{org}$ but the relationships and causes of such trends have still not been firmly established (Schmitz, 1987; Shimmield and Mowbray, 1991; Shimmield, 1992; Patience, 1992). Recently, Dymond *et al.* (1992) used sediment traps in the Atlantic and Pacific oceans to measure particulate fluxes of Ba and $C_{org}$. They found that the $C_{org}$/Ba ratio decreased with increasing water depth as a result of the simultaneous uptake of Ba in settling particles during organic matter decomposition. The results from Dymond *et al.* (1992) support the first of the above

two hypotheses as a cause of deep-sea barite production, i.e. formation of barite in microenvironments rather than secretion by specific organisms. Their water column observations imply that Ba could be used as a quantitative productivity signal in marine sediments and, because Ba can resist dissolution and/or remineralisation upon burial (Heath and Dymond, 1977, 1981; Dymond, 1981), its "residual" signal has potential for use as a palæo-productivity indicator.

### 6.3.2. Analytical methods and results

Barium is classified as a trace element and its concentration in the sediments in this study was determined by X-ray fluorescence techniques on pressed-pellet samples (Appendix A.5). As previously stated, Al determination used X-ray fluorescence analysis of fused discs (Appendix A.5) and $C_{org}$ and biogenic silica concentrations were measured using wet chemical techniques (Appendices A.3 and A.4 respectively).

A proportion of the Ba concentration present in marine sediments is associated with the terrigenous, detrital aluminosilicates and, therefore, in order to examine any variation in the "biogenic-source" Ba ($Ba_{bio}$), the total Ba concentration (ppm) can be expressed as a ratio to Al (Ba/Al x $E^{-4}$). Table 6.4 shows the range and mean values of total Ba, $Ba_{bio}$ and the Ba/Al ratio for the four piston cores, which is a summary of the Ba data in Appendices C.10, C.11 and C.14.

The Ba/Al depth/age profiles for the above piston cores are illustrated in Fig. 6.8 and this shows that even after normalising for the variation of terrigenous-Ba input, there is still a large dynamic range in the Ba/Al ratio, especially for cores CD38-02 and CD38-11. The reasons for such variation over time will be discussed shortly.

| | Ba (ppm) | | | Ba/Al (x E-4) | | | $Ba_{bio}$ (ppm) | | |
|---|---|---|---|---|---|---|---|---|---|
| | Min. | Max. | Mean | Min. | Max. | Mean | Min. | Max. | Mean |
| CD38-09 (148m) | 185 | 1438 | 292 | 38.8 | 250.1 | 51.1 | -299 | 1006 | -140 |
| CD38-10 (257m) | 164 | 397 | 296 | 42.7 | 97.2 | 59.8 | -225 | 89 | -84 |
| CD38-02 (2525m) | 1098 | 2424 | 1600 | 167.0 | 425.1 | 277.8 | 620 | 1941 | 1166 |
| CD38-11 (3835m) | 385 | 2495 | 1390 | 63.1 | 369.2 | 199.2 | -73 | 1988 | 868 |

Table 6.4. Range and mean of Ba, Ba/Al and $Ba_{bio}$ (calculated using Eqn 6.3).

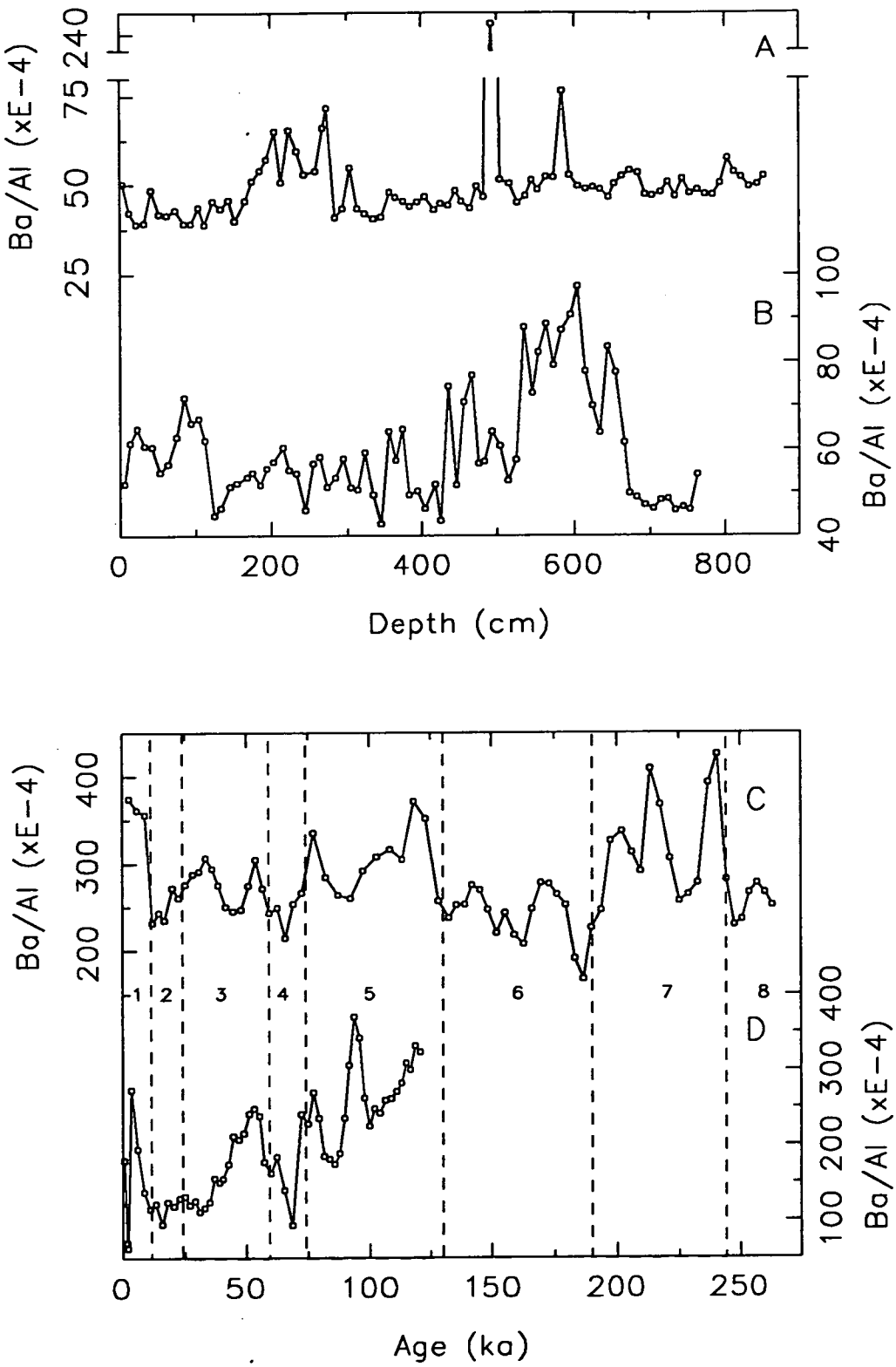


Figure 6.8 Ba/Al weight ratio down-core profiles: A) CD38-09, B) CD38-10, C) CD38-02 and D) CD38-11.

If Ba is to be a useful palæo-productivity tracer then study of the correlation coefficients between Ba and $C_{org}$ and biogenic silica (Table 6.5) may indicate the presence of any biogenic relationships (Dehairs *et al.*, 1980; Von Breymann *et al.*, 1992).

| Ba correlation | Corg | Bio. Silica |
|---|---|---|
| CD38-09 | -0.094 | -0.648 |
| CD38-10 | -0.191 | -0.171 |
| CD38-02 | -0.066 | 0.540 |
| CD38-11 | -0.357 | 0.822 |

Table 6.5. Correlation coefficients of Ba (ppm) with $C_{org}$ and biogenic silica for piston cores.

The lower concentration of Ba found in the two shallow-water cores (CD38-09 and CD38-10) compared with the deeper-water cores (Table 6.4) supports the work of Von Breymann *et al.* (1992) who found a water depth/sedimentation rate dependence on the biogenic-Ba content of many Peru shelf and slope sites. This theory might initially suggest less biogenic-Ba input at CD38-09 and CD38-10. The shallow-water cores are very near the coast, which is the source of aluminosilicate, terrigenous detritus (aeolian and riverine) and so this source of Ba can dominate over a biogenic source. However, as was seen in Chapter 3, it is these cores which are situated directly under the zone of Peruvian coastal upwelling and therefore there is also a high biogenic flux to the sediment. At these two sites a high total Ba concentration (terrigenous and biogenic) would be expected.

The main reason for the low Ba concentrations and Ba/Al ratios (and negative $Ba_{bio}$) is that Ba is being lost upon burial in the sediment during diagenetic mobilisation (Von Breymann *et al.*, 1992). This can only occur in sediments within a suboxic/anoxic environment (Dymond, 1981; Dymond *et al.*, 1992) due to pore-water undersaturation with respect to barite at the base of the sulphate reduction zone (Von Breymann *et al.*, 1992). The low Ba concentrations in cores CD38-09 and CD38-10 therefore supports the theory that the sediments at these shallow-water sites are accumulating under reducing conditions (6.2.3) and high sedimentation rates. In terms of using Ba as a palæo-productivity indicator, the cores taken at these two sites are of no use and will not be studied further in this section.

### 6.3.3. Ba and oxygen isotope profiles

On the Owen Ridge in the north-western Arabian Sea (ODP site 722B), Shimmield and Mowbray (1991) measured a Ba/Al depth profile which had a very large dynamic range and bore an almost perfect correlation with the foraminifera $\delta^{18}O$ stratigraphy. Elevated Ba contents were seen during interglacial stages in core 722B, even when considered in terms of Ba flux, which according to the authors, reflected periods of enhanced productivity (Fig. 6.9).

This remarkable capacity for Ba concentrations to parallel the SPECMAP oxygen isotope curve (2.3.1; Shimmield, 1992) is also seen in cores CD38-02 and CD38-11 from the Peruvian continental margin (compare Figs 6.8C and D with Fig. 2.9). Figure 6.9. illustrates the similarity between the Ba/Al age profiles of cores CD38-02 from the Peru margin and ODP 722B from the Arabian sea (Shimmield and Mowbray, 1991). There is the possibility that variation in the Ba content of the sediment is caused by changes in the strength of dilution by another component within the sediment, e.g. calcium carbonate. However, any carbonate dilution will affect the Ba and the Al concentrations to the same degree and therefore the variation in the Ba/Al profile is independent of such dilution effects (Figs 6.8.C and D). The Ba/Al profile could be caused simply by fluctuations in the ratio of these two elements in purely terrigenous material but it is thought that the degree of natural variation of Al (7.2.3) is much less significant than the biogenic-associated fluctuations of Ba, displayed by the Ba/Al ratios.

Use of the Ba/Al ratio for age modelling obviously needs further, detailed study and this would be possible by comparing Ba/Al ratios and foraminifera $\delta^{18}O$ records when both sets of measurements are taken from the same depth samples. Unfortunately, in this study (as in most due to the limitations in volume of sample material from a specific depth) the geochemical bulk-sediment sub-samples were taken up to 5cm away from the sieved-sediment sub-samples used for foraminifera studies. If the same sub-sample were used for both measurements then comparison of exact variations between peaks and troughs in the Ba/Al and *Uvigerina* profiles would be possible and a relationship could be established between the concentration of Ba in a sediment and the oxygen isotope signal recorded by foraminifera living at that time.

All that can be said from comparison of the Ba/Al and $\delta^{18}O$ records in CD38-02 and CD38-11 (compare Figs. 2.9 and 6.9) is that higher $Ba_{bio}$ contents are found during the interglacial periods and seem to correspond closely to heavier (more negative) values of $\delta^{18}O$ in *Uvigerina* shells. This in turn implies that during the Late

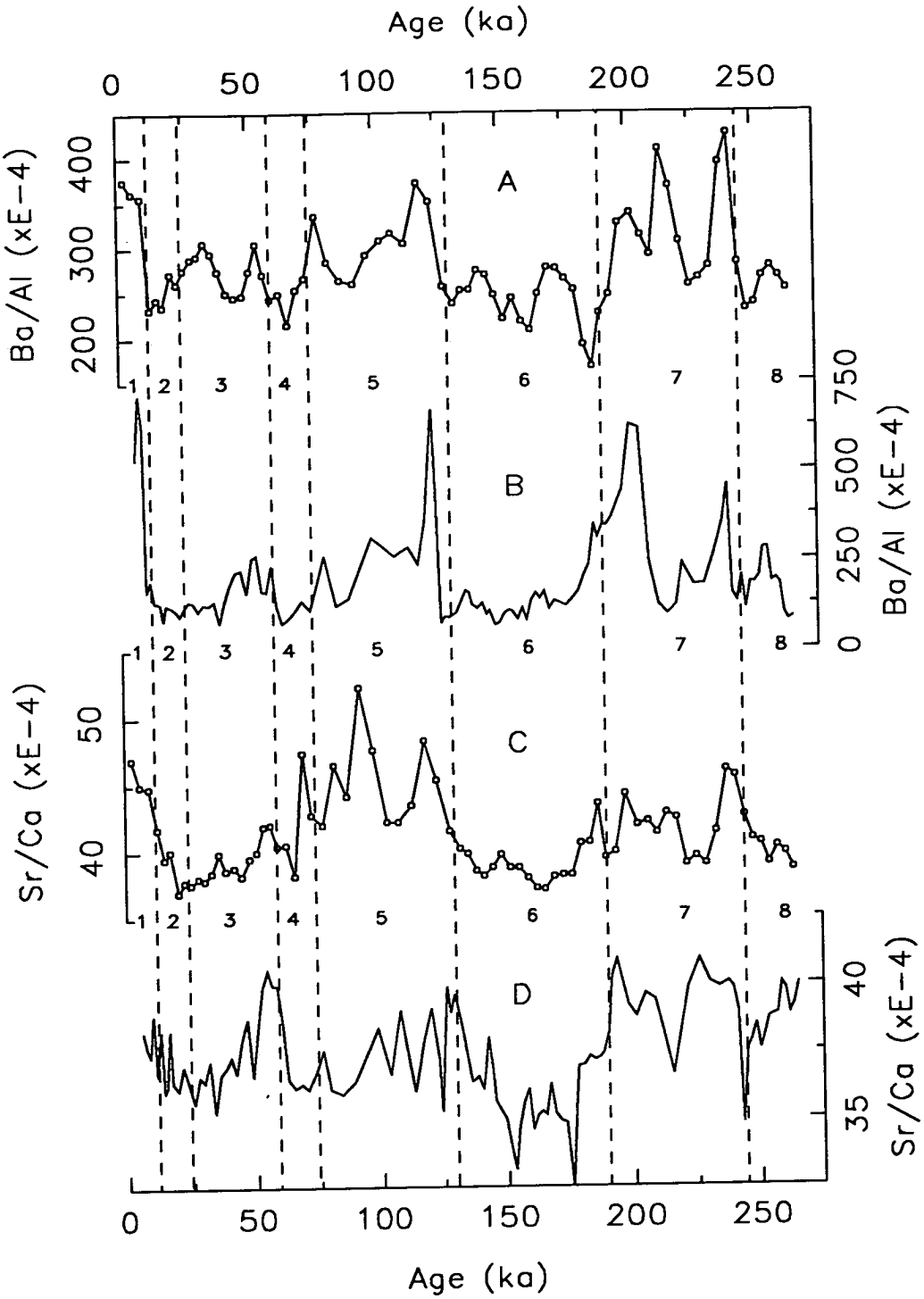


Figure 6.9. Ba/Al weight ratios against age: A) CD38-02 and B) ODP 722B (Shimmield and Mowbray, 1991). Sr/Ca weight ratios against age: C) CD38-02 and D) ODP 722B (Shimmield and Mowbray, 1991).

Quaternary at these two sites, more $Ba_{bio}$ accumulated in the sediments when the global ice-sheet volume was at a minimum. The question that then arises is; are the Ba/Al ratios in the sediment recording changes in sea-surface productivity associated with global climate changes? If so, then barium may be one of the best proxies for palæo-productivity available to marine geochemists.

### 6.3.4. Palæo-productivity from Ba fluxes

This section will review the recent paper by Dymond *et al.* (1992) which advocates the use of Ba as a palæo-productivity proxy. Once their sediment trap Ba-$C_{org}$ relationship and the $Ba_{bio}$-new production equation have been explained, the Ba data from core CD38-02 will be used to establish a proxy record of palæo-productivity in the waters off the continental margin of Peru.

Dehairs *et al.* (1980) proposed that the particulate Ba content of the upper 1000m of the water column was positively correlated with diatom productivity and further analyses of water from the Southern Ocean (Dehairs *et al.*, 1990, 1991) provided support for this theory. Dymond *et al.* (1992) takes the work of the above authors one stage further with the basic hypothesis that the flux of particulate Ba to the sea-floor (i.e. input to the sediment record) has a quantifiable relationship to the level of new productivity in the oceans. New production is defined as "the fraction of total primary production supported by the input of nutrients into the euphotic zone rather than by the recycling of nutrients from particulate organic matter within the euphotic zone" (Eppley and Petersen, 1979). Using sediment traps located in the Atlantic, Equatorial Pacific and California Current, the authors measured particulate $C_{org}$, Ba and Al fluxes and plotted $C_{org}/Ba_{bio}$ ratios against water depth for the three sites. The ratios all decreased sympathetically with increasing water depth, and the best-fit curves predicted a $C_{org}/Ba_{bio}$ ratio of 200 at the 200m base of the euphotic zone.

By converting the carbon flux-new production relationship equation of Sarnthein *et al.* (1988) and incorporating terms which depend on the dissolved Ba content of the water through which the organic debris settles, Dymond *et al.* (1992) produced an equation (Eqn 6.2) from which new production can be calculated.

The authors addressed the problem which affects all geochemical productivity indicators, i.e. the preservation factor - how much, if any, of the original signal reaches the sediment and is then retained upon burial? Marine biological systems use chemical elements and components for essential life processes which are easily

recycled, e.g. carbon, nitrogen, phosphorus. Therefore, the concentration of a productivity indicator in marine sediments is usually only a small fraction of the original signal or it can be lost altogether (completely recycled). Barium, however, has been shown to be an element which is fairly resistant to recycling and post-depositional mobilisation (Dymond, 1981) because in oxic sediments, the pore-waters are saturated with respect to barite (Church and Wolgemuth, 1972).

Equation 6.2. Calculation of new production (Dymond *et al.*, 1992)

$$P_{new} = \{[(F_{Babio}) \times (0.171 \times Ba^{2.218}) \times z^{(0.476-0.00478Ba)}] / 2056\}^{1.504}$$

where, Pnew = new production (g C $m^{-2}$ $year^{-1}$),
$F_{Babio}$ = flux of biogenic-Ba to the sea-floor (µg $m^{-2}$ $year^{-1}$),
Ba = dissolved Ba concentration at 1700m (µmol $kg^{-1}$),
z = water depth of core site (m).

Equation 6.3. Calculation of $Ba_{bio}$

$$Ba_{bio} = Ba_{total} - (Al \times Ba/Al_{aluminosilicate})$$

where, $Ba_{bio}$ = biogenic barium,
$Ba_{total}$ and Al= as measured by X-ray fluorescence,
$Ba/Al_{aluminosilicate}$ = 0.0075 (Dymond *et al.*, 1992).

Dymond *et al.* (1992) carried out a series of selective leaching experiments on sediment trap samples and found that the total Ba content consisted of a small aluminosilicate fraction (1-2%) and a barite fraction, which occurred mainly in two forms; an absorbed, calcite-bound phase (22-43%) which was soluble in acetic acid (pH = 5), and a residual phase (48-70%). The authors partitioned the total Ba concentration into aluminosilicate and biological phases using Eqn 6.3 (used to calculate $Ba_{bio}$ in Table 6.4), and then, by comparing the Ba/Al ratio in sediment traps with the $Ba_{bio}$/Al ratio in sediments directly below (using Eqn 6.4), they produced a best-fit line of approximately 30% Ba preservation (i.e. 70% $Ba_{bio}$ recycled before reaching the sea-floor) which is the highest preservation factor for any productivity proxy measured so far.

However, preservation of Ba upon burial in the sediment was seen to have a non-linear relationship with the mass accumulation rate (MAR), and Eqn 6.5 predicts the original total $Ba_{bio}$ flux to the sea-floor from the MAR and accumulation rate of $Ba_{bio}$ in the sediment (both in $\mu g\ cm^{-2}\ year^{-1}$). This work allowed Dymond *et al.* (1992) to specify a step-by-step scheme for calculating new production in the ocean from knowledge of the Ba concentration and MAR in the sediment at any particular age (Eqn 6.2), assuming that an accurate concentration of dissolved Ba in the water column (1700m) can be measured or calculated (Lea and Boyle, 1990B).

Equation 6.4. Calculation of barium preservation factor

$$\%\ Ba\ preserved = [(Ba_{bio}/Al)_{sediment} / (Ba/Al)_{sed.\ trap}] \times 100$$

Equation 6.5. Calculation of original $Ba_{bio}$ flux

$$F_{Babio} = (Ba_{bio}\ accumulation\ rate) / [(0.209 \times \log MAR) - 21.3]$$

Using the step-by-step scheme of Dymond *et al.* (1992) the Ba concentration data from piston core CD38-02 was converted to $Ba_{bio}$ (Eqn 6.3) then to $F_{Babio}$ (Eqn 6.5) and finally to the palæo-productivity signal of $P_{new}$ (Eqn 6.2).

The final calculation involved using a value of 145 nmol $kg^{-1}$ for the dissolved Ba concentration at 1700m in the water column, which is actually the level measured at the GEOSECS site in the California Current (Lea and Boyle, 1990B). The value was chosen because it was thought to be a close approximation for the Nazca ridge core since both sites are located on continental margins affected by coastal upwelling (2.1.1). In effect, this means that the values of $P_{new}$ for CD38-02 may not be completely accurate, but the calculation should give a good approximation of the new production levels at this site. The shape of the down-core palæo-productivity signal will not, however, be affected by this estimation of the dissolved Ba because each sample point uses the same value of 145 nmol $kg^{-1}$ in the calculation (Eqn 6.2).

The values of $P_{new}$ for core CD38-02 are tabulated in Appendix C.14 and range from 7 to 30 gC $m^{-2}$ $yr^{-1}$ with a mean value of 14.4 gC $m^{-2}$ $yr^{-1}$. The age profile of this new production record is shown in Fig. 6.10.C and from it can be seen an interesting glacial/interglacial pattern of palæo-productivity.

The most obvious feature of this signal is the two large peaks in interglacial stage 7 which drop sharply on either side into the glacial stages 6 and 8. There are

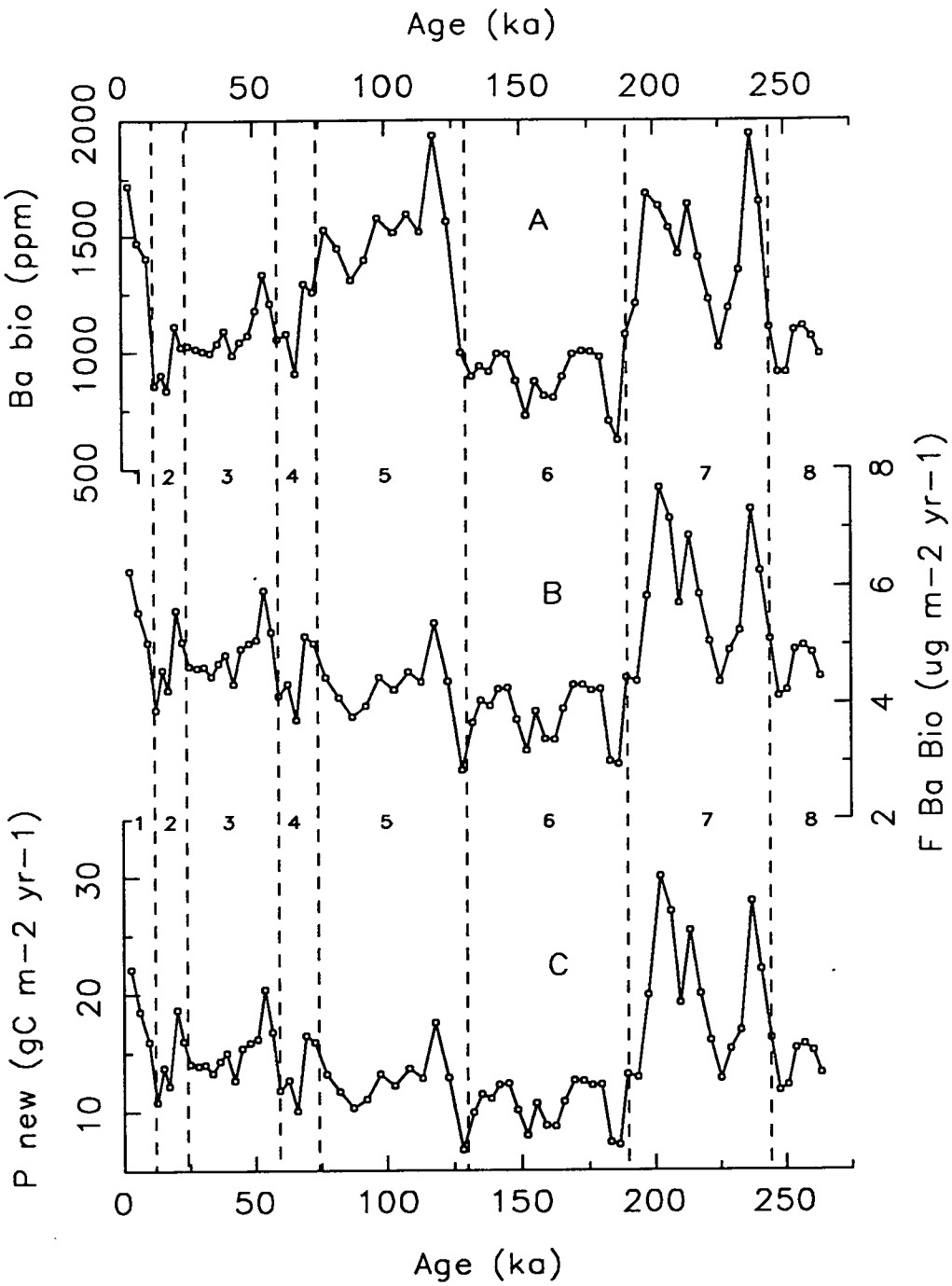


Figure 6.10. The barium palæo-productivity signal for core CD38-02 (2525m) against age: A) $Ba_{bio}$ (ppm), B) $F_{Ba_{bio}}$ ($\mu g\ m^{-2}\ yr^{-1}$) and C) $P_{new}$ (g C $m^{-2}\ yr^{-1}$).

other interglacial maxima (>16 gC $m^{-2}$ $yr^{-1}$) in the $P_{new}$ profile, which lie at the top of stage 1 and the base of stages 3 and 5, and glacial minima (<12 gC $m^{-2}$ $yr^{-1}$) which occur during stages 2, 4 and 6; all of which indicate that there is a glacial/interglacial periodicity control on the levels of new production in the waters above the Nazca ridge site. This in turn suggests that the coastal upwelling primary productivity along the Peruvian continental margin has been strongly affected by the global climate during the Late Quaternary and has been more intense during the interglacial stages.

However, the $P_{new}$ profile of CD38-02 is much more complex than the simple hypothesis above suggests. Figure 6.10 also shows maxima at the base of glacial stages 2 and 4 and the intensity of the peaks in stage 7 cannot be easily explained. The equation to calculate $P_{new}$ from Dymond *et al.* (1992) depends strongly on the mass accumulation rate. This means that the age model from the foraminifera $\delta^{18}O$ record needs to be correct. Simply moving some of the stage boundaries in the original age model for CD38-02 (Chapter 2) can significantly change the mass accumulation rates, which alters the concentrations of $P_{new}$ and can give a down-core profile which peaks strongly in glacial stages 2 and 4.

It is also wrong to assume that interglacial peaks on the $P_{new}$ profile are caused by more intense coastal upwelling and higher biological productivity on the Peruvian continental margin. It may be that lateral movement of the main coastal upwelling zone along the coast, caused by changes in the wind patterns during global climate change, brought a higher biogenic flux to the sediments accumulating on the Nazca ridge during interglacial periods. Other factors such as the dissolved Ba concentration may also have varied with time. Lea and Boyle (1989,1990A and B) have examined the Ba/Ca ratio of benthic foraminifera from many deep-sea cores in the Atlantic and Pacific oceans and concluded that because of water mass circulation variations during the Late Quaternary, the deep-waters of the Pacific during glacial conditions were about 25% lower in their dissolved Ba concentration (at about 3000m water depth) compared with today's interglacial levels.

In conclusion, it is likely that the levels of new production at CD38-02 have altered significantly over the past 250,000 years associated with the variation in global climate. However, until other cores with accurately defined age models in this area are also used for the calculation of $P_{new}$, the precise reasons for such variation in this palæo-productivity signal cannot be known. The equations of Dymond *et al.* (1992) are the first attempt to use and quantify sediment Ba concentrations as an ocean biological productivity indicator and hopefully this and many future studies (e.g. Shimmield *et al.*, 1992) will help to clarify both the relationship between Ba and

organic matter in the water column, and the variation of dissolved Ba concentrations in water masses over time.

## 6.4. THE STRONTIUM SIGNAL

### 6.4.1. Introduction

The marine biomass is a complex mixture of phytoplankton, zooplankton and many other larger marine organisms, which are all inter-related by the food chain. It has been shown that barium can be used as an indicator of the total palæo-productivity in the oceans but it is possible that other geochemical signals in the sediment record can indicate changes over time in the relative abundance of one type of marine organism compared to another. This section will examine the biological relationship of strontium (Sr) with calcium carbonate shell-remains and interpret temporal variations in the biogenic Sr/Ca ratio with respect to variation in the relative abundances of foraminifera and coccoliths; two important groups of marine plankton.

Strontium in marine sediments occurs mainly in carbonate minerals but can also be found in phosphorite, barite and aluminosilicates (El Wakeel and Riley, 1961; Church, 1970). As previously stated (4.3.4), it is because the $Sr^{2+}$ cation has a similar ionic radius as well as the same ionic charge as $Ca^{2+}$, that Sr easily substitutes for Ca in most minerals. Sr substitution for Ba in marine barite only occurs to a relatively small degree (0.2-3.4 mol% Sr, Church, 1979) which allows for a potential contribution of 30-150ppm Sr to the total Sr concentration in most marine sediments (Patience, 1992).

Table 6.6 lists the Sr concentration previously found in marine organisms and sediments and from this it can be seen that the Sr content of pelagic foraminifera (1500-1710ppm) is slightly higher than that of coccoliths (1000ppm), with the result that a foraminiferal ooze has a higher Sr/Ca ratio (33 x $10^{-4}$, Thompson and Chow, 1956) compared with a coccolith-rich ooze (26-26 x $10^{-4}$, Turekian, 1964).

### 6.4.2. Analytical methods and results

Strontium and calcium concentrations in the sediments in this study were determined using X-ray fluorescence on pressed pellet samples and fused discs respectively (Appendix A.5). The amount of $CaCO_3$ present was then calculated by

correcting for the calcium content of aluminosilicates and phosphorite present (Appendix B.1). Using the strong correlation between Sr and $P_{phos}$ in phosphorite zones (4.3.4, Fig. 4.10) the total Sr concentration can be partitioned into terrigenous ($Sr_{terr}$), phosphatic ($Sr_{phos}$) and calcium carbonate ($Sr_{calcite}$) phases using Eqn 4.4 (Appendix B.4). This then allows for the true Sr/Ca ratio in biogenic carbonate shell remains ($Sr/Ca_{bio}$) to be calculated.

| **Author** | **Organism/sediment type** | **Sr** (ppm) | **Sr/Ca** ($\times 10^{-4}$) |
|---|---|---|---|
| Emiliani (1955) | Foraminifera tests | 1200 | |
| Thompson & Chow (1956) | Foraminifera tests | 1300 | |
| | Pacific Globigerina ooze | | 33 |
| Turekian (1957) | Foraminifera tests | 1200 | |
| Krinsley (1960) | Foraminifera tests | 1150 | |
| Turekian & Wedepohl (1961) | Deep-sea clay | 180 | |
| | Deep-sea carbonate | 2000 | |
| Turekian (1964) | Pure foraminifera ooze | 1600 | |
| | Pure coccolith ooze | 1000 | 25-26 |
| Martin & Knauer (1973) | Mean marine organism | 862 | |
| Shimmield and Mowbray (1991) | NW. Arabian Sea sediments | 740-1489 | 33-45 |
| Patience (1992) | E. Equatorial Pacific sediments | 330-1207 | 32-64 |
| Carpenter & Lohmann (1992) | Foraminifera tests | 1190-1710 | |

Table 6.6. Sr concentration and Sr/Ca weight ratio of marine organisms and sediments.

Table 6.7 summarises the strontium data for the four piston cores from the Peruvian continental margin (listed in Appendices C.10 and C.13) and includes the range and mean of total Sr, the mean $CaCO_3$ concentration, the range and mean of $Sr_{calcite}$ and the $Sr/Ca_{bio}$ ratio and the correlation coefficient of total Sr with $CaCO_3$.

The $Sr_{total}$:$CaCO_3$ correlation coefficients are much lower for cores CD38-09 and CD38-10 compared with CD38-02 and CD38-11 (Table 6.7) because in the shallow-water cores there is less calcium carbonate present, more aluminosilicate detrital material and significant zones of phosphorite formation; all of which have different Sr/Ca ratios in the minerals. It is because of the complication of the phosphorite zones, that cores CD38-09 and CD38-10 will not be considered further in this section.

| | | CD38-09 (148m) | CD38-10 (257m) | CD38-02 (2525m) | CD38-11 (3835m) |
|---|---|---|---|---|---|
| Sr (ppm) | range | 149-1195 | 185-642 | 311-812 | 222-423 |
| | mean | 220 | 329 | 567 | 277 |
| $CaCO_3$ (wt.%) | mean | 2.9 | 8.2 | 26.9 | 10.7 |
| $Sr_{calcite}$ (ppm) | range | 0-138 | 7-400 | 143-700 | 43-238 |
| | mean | 61 | 156 | 434 | 110 |
| $Sr/Ca_{bio}$ ($x10^{-4}$) | range | | | 36.9-52.2 | 14.7-33.6 |
| | mean | | | 41.0 | 25.1 |
| Corr. coeff. of Sr with $CaCO_3$ | | 0.235 | 0.451 | 0.980 | 0.948 |

Table 6.7. Strontium data summary table

A plot of $Sr_{total}$ against $CaCO_3$ concentration for core CD38-02 is shown in Fig. 6.11 and has the following straight-line relationship:

$$Sr\ (ppm) = 13.01 \times CaCO_3\ (wt.\%) + 216.$$

The best-fit straight line intercepts the Y-axis of Fig. 6.11 at 216ppm Sr, which is equivalent to the average amount of Sr in each sample which has been introduced to the sediment by a non-carbonate source, i.e. associated with terrigenous, aluminosilicate material. If the sediments in core CD38-02 were to contain purely carbonate shell remains then the total Sr concentration would be 13.01 x 100 (%) = 1301ppm. This calculation of the Sr content of marine organisms in sediments on the Nazca ridge corresponds well with the Sr analyses of the foraminifera tests shown in Table 6.6. This calculation gives confidence to the use of the equation to calculate $CaCO_3$ levels from X-ray fluorescence analysis of total Ca concentration (Appendix B.1).

It is therefore of no surprise that the down-core age profiles for both CD38-02 and CD38-11 of $Sr_{total}$ and $Sr_{calcite}$ in Figs 6.12 and 6.13 show remarkable similarity to their respective $CaCO_3$ profiles.

### 6.4.3. Sr/Ca temporal variations

In sediments from the Northwest Arabian Sea (ODP core 722B), Shimmield and Mowbray (1991) found ratios of Sr/Ca which were higher than previously reported (up to 45 x $10^{-4}$, Table 6.6) and whose down-core profile showed a close similarity to the $\delta^{18}O$ foraminifera curve, although the peaks were damped or

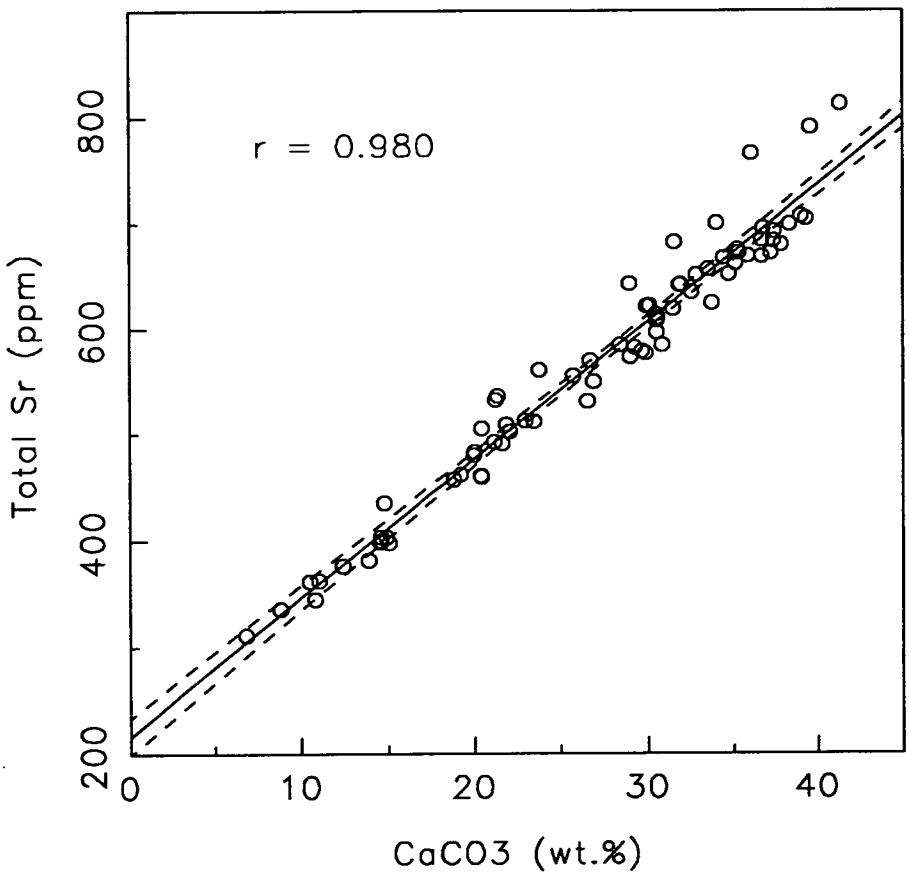


Figure 6.11. Core CD38-02 (2525m): total strontium against calcium carbonate. Shows best fit straight line (full line) and 95% confidence limits (dotted lines) representing,

$$Sr\ (ppm) = 13.01 \times CaCO_3\ (wt.\%) + 216.2 \qquad (r=0.980)$$

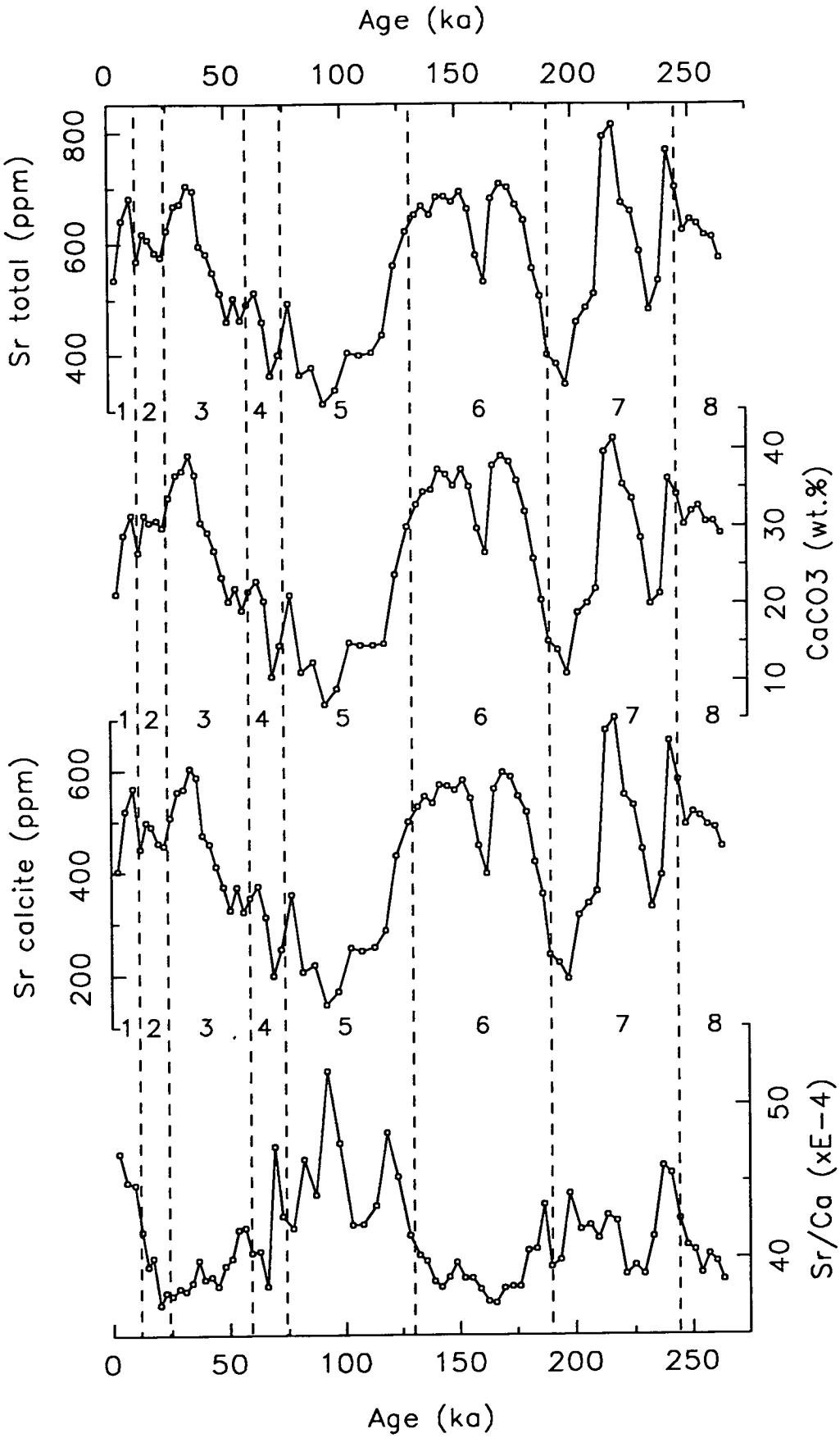


Figure 6.12. Core CD38-02 (2525m): $Sr_{total}$, $CaCO_3$, $Sr_{calcite}$ and Sr/Ca down-core profiles against age (ka).

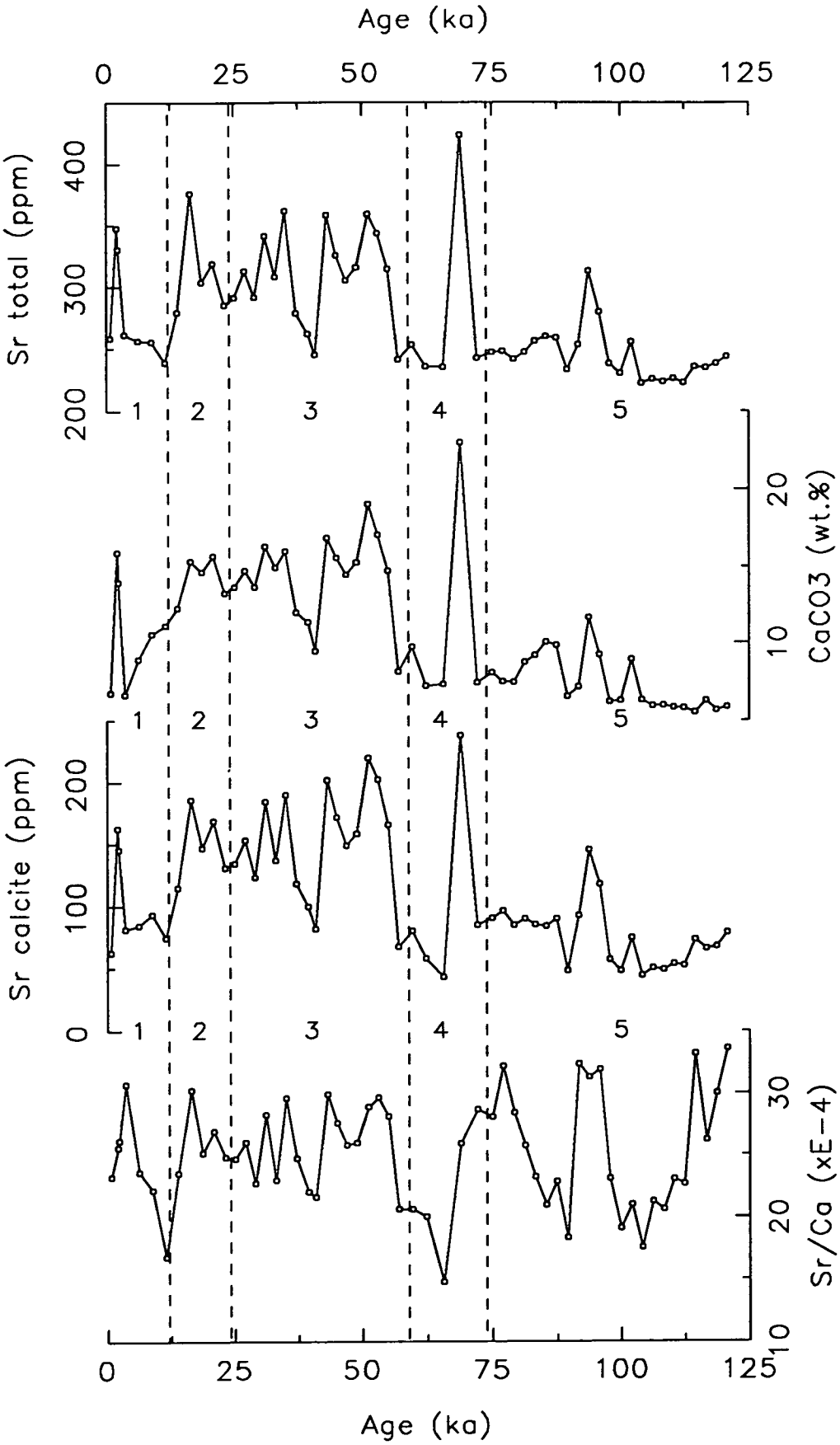


Figure 6.13. Core CD38-11 (3835m): $Sr_{total}$, $CaCO_3$, $Sr_{calcite}$ and Sr/Ca down-core profiles against age (ka).

modulated (Fig. 6.9). The authors measured elevated concentrations of Sr with respect to Ca in the interglacial stages and suggested that the Sr content of the biogenic carbonate was indicating a temperature/species/vital effect control, which fluctuated with changes in the global climate. Patience (1992) concluded that variations in the excess Sr/excess Ca ratio (similar to $Sr/Ca_{bio}$) in Eastern Equatorial Pacific sediments illustrated changes in the relative dominance of coccoliths to foraminifera in the oceanic waters.

The age profiles of biogenic Sr/Ca ratio for cores CD38-02 and CD38-11 are plotted in Figs 6.12 and 6.13, and both illustrate temporal changes which have higher ratios during the interglacial stages (most pronounced in CD38-02, shown in Fig. 6.9 with ODP 722B for comparison). The most obvious interpretation of such a geochemical signal in terms of palæo-productivity is that during interglacial periods, when the overall $CaCO_3$ concentration is lowest, the production of foraminifera is more dominant over that of coccoliths (the latter having a lower Sr content in their shells). Whereas during glacial periods, when total carbonate production (or preservation?) is much higher, coccolith production is increased at a greater rate relative to the rate of increase in foraminifera production and this results in significantly lower $Sr/Ca_{bio}$ ratios. However, this simple hypothesis may be strongly affected by increased rates of $CaCO_3$ dissolution in the sediment, increased barite production and/or diagenetic overprinting (Baker *et al.*, 1982).

Shimmield and Mowbray (1991) discounted diagenetic overprinting as being responsible for the Sr/Ca profile in core 722B due to the "shallow depth of the core". Their core was situated at a water depth (2028m) fairly similar to core CD38-02 (2525m) and therefore the same statement can be made for the Nazca ridge core. However, core CD38-11 is from much deeper water (3835m) and therefore diagenetic overprinting may be responsible for the more noisy Sr/Ca signal.

The question of variable carbonate dissolution affecting the Sr/Ca ratio profiles can be discounted because dissolution is thought to affect foraminifera shell remains more than coccoliths (Broecker, 1971; Honjo, 1977) and its influence to have been greater during the interglacial periods. This would mean that the dominance of foraminifera over coccoliths would be less significant during interglacials and the $Sr/Ca_{bio}$ ratio would be expected to decrease (Patience, 1992). This is clearly the opposite of what is seen for the $Sr/Ca_{bio}$ ratio in cores CD38-02 and CD38-11 (Figs 6.12 and 6.13).

The possibility that increased barite production during interglacial periods due to higher organic matter settling fluxes (6.3.4) may also be bringing more Sr,

incorporated within the mineral (Church, 1979), to the sediment cannot, however, be discounted. This extra source of "biogenic" Sr may be able to account for some of the variation seen in the biogenic Sr/Ca profiles.

It can only, therefore, be concluded that fluctuations in the Sr/Ca ratio of carbonate shell-remains in the sediments from cores CD38-02 and CD38-11 may be a palæo-productivity signal of temporal changes in the relative dominance of foraminifera over coccoliths off the Peruvian continental margin during global climate change. There may, however, be a temperature and/or species related control on the uptake of Sr by marine plankton and the influence of increased barite production (itself a palæo-productivity indicator, which is not accounted for in the calculation of $Sr_{calcite}$) must also be examined. Before any definite statements about the Sr/Ca palæo-productivity signal can be made more detailed studies of the Sr content of both marine organisms and diagenetic minerals need to be carried out.

## 6.5. THE MOLYBDENUM-URANIUM SIGNAL

### 6.5.1. Introduction

The final section in this palæo-indicators chapter will examine the use of the ratio of two heavy metals, molybdenum (Mo) and uranium (U), for identification of the redox environment under which deposition of marine sediments occurs. The Mo and U geochemical data of the four piston cores from the Peruvian continental margin will be used to calculate Mo/U ratios and to critically review the following hypothesis made by Bertine and Turekian (1973).

Their data of Mo and U concentrations from a wide variety of marine sediments indicated that two different chemical associations are responsible for the removal of Mo from sea-water; namely, with ferromanganese minerals under oxidising conditions and with a sulphide or high organic matter phase under reducing conditions. The authors stated that due to the different Mo/U ratios measured in samples from deep-sea, oxic sediments (Mo/U = 3-4) and from near-shore anaerobic sediments (Mo/U about unity), the two mechanisms of Mo accumulation in marine sediments could be distinguished. This means that, in terms of using the Mo/U ratio as a palæo-redox indicator, Bertine and Turekian (1973) implied that a ratio of about one is indicative of reducing conditions and a ratio above three is indicative of oxidising conditions at the sediment/water interface at the time of deposition.

### 6.5.2. Analytical methods and results

Both Mo and U concentrations were analytically determined using X-ray fluorescence techniques on pressed pellet samples and are expressed as parts per million (ppm) (Appendix A.5). In contrast, Bertine and Turekian (1973) measured Mo and U by neutron activation analysis and expressed their results as ppm on a carbonate-free basis. Since this section is examining the Mo/U ratio, it does not matter if the data has not been corrected for the carbonate content of the sample because both the metal concentrations would be affected by the recalculation to the same extent.

| | | CD38-09 (148m) | CD38-10 (257m) | CD38-02 (2525m) | CD38-11 (3835m) | Bertine & Turekian (1973) Oxic | Anoxic |
|---|---|---|---|---|---|---|---|
| Mo/U | Min. | 0.36 | 0.56 | 0.00 | 0.18 | 1.24 | 0.36 |
| | Max. | 17.29 | 13.12 | 0.62 | 2.10 | 4.92 | 2.19 |
| | Mean | 7.37 | 4.81 | 0.23 | 1.07 | 2.77 | 1.08 |
| $Mo/U_{org}$ | Min. | 0.81 | 3.76 | 0.00 | 0.27 | | |
| | Max. | 617.7 | 50.9 | 1.63 | 16.9 | | |
| | Mean | 35.3 | 11.0 | 0.39 | 2.62 | | |

Table 6.8. Summary of Mo/U and $Mo/U_{org}$ data.

The Mo/U ratios of the sediments from the four piston cores are summarised in Table 6.8 (full data listed in Appendix C.11). This table also includes the $Mo/U_{org}$ ratio data, which has been determined after calculation of the U content associated with the organic carbon fraction of the sediment (using the partitioning equation 4.3). The use of the $Mo/U_{org}$ ratio may give a more accurate indication of the true Mo-U relationship in the near-shore cores CD38-09 and CD38-10, where phosphorite mineral diagenesis can preferentially concentrate U (4.3.4) and therefore distort the original Mo/U signal. The results from Bertine and Turekian (1973) for deep-sea sediments (oxic) and near-shore sediments (anoxic) are also given in Table 6.8 for comparison.

### 6.5.3. Interpretation and discussion of Mo/U ratios

Previously in this chapter, it has been interpreted from the iodine/$C_{org}$ ratio down-core profiles that of the four piston cores, two have been collected from a depositional environment of reducing conditions (CD38-09 and CD38-10) and two from an environment of oxidising conditions (CD38-02 and CD38-11). The

knowledge of the redox state of each core throughout its depositional history can now be used to interpret the Mo/U and $Mo/U_{org}$ ratio profiles for each core (Figs 6.14 and 6.15) and determine the usefulness of these ratios as palæo-redox indicators, following the work of Bertine and Turekian (1973).

From consideration of the mean values of Mo/U and $Mo/U_{org}$ for cores CD38-09 and CD38-10 (Table 6.8) and from the depth profiles (Figs 6.14 and 6.15) it is obvious that the statement of Bertine and Turekian (1973) that near-shore reducing sediments have a Mo/U ratio close to unity (with a maximum of about two) is invalid.

It also seems that the authors were wrong in their hypothesis that oxidising sediments have a Mo/U ratio of between 3 and 4, when considering the Mo/U and $Mo/U_{org}$ mean ratios (Table 6.8) of cores CD38-02 and CD38-11. In fact, if the Mo and U data from the piston cores used in this study had been available to Bertine and Turekian then they may have arrived at a completely opposite hypothesis. They may then have stated that the two mechanisms of the removal of Mo from sea-water could be distinguished by,

1) Mo/U ratios of near unity for removal under oxidising conditions associated with ferromanganese minerals and,
2) Mo/U ratios of between 5 and 10 (or higher, if considering $Mo/U_{org}$ ratios) for removal under reducing conditions associated with a high organic matter phase.

In conclusion, the Mo and U concentration data from this study of both reduced and oxidised sediments from the Peruvian continental margin imply that the simple hypothesis of Bertine and Turekian (1973) is invalid. In fact, uptake of these two heavy metals and their relationship in marine sediments is highly complex and does not just depend on the redox state of the depositional environment. Therefore, until more detailed work into the relationship of Mo and U with organic matter, ferromanganese and phosphorite minerals and of their post-depositional mobility is carried out, the Mo/U ratio cannot be used as a reliable palæo-redox indicator in marine sediments.

## 6.6 CONCLUDING INTERPRETATIONS OF PERUVIAN PALÆO-OCEANOGRAPHIC CONDITIONS

Of the three groups of palæo-chemical tracers described by Elderfield (1990), namely tracers of oceanic (1) chemistry, (2) fluxes and (3) processes, this chapter has

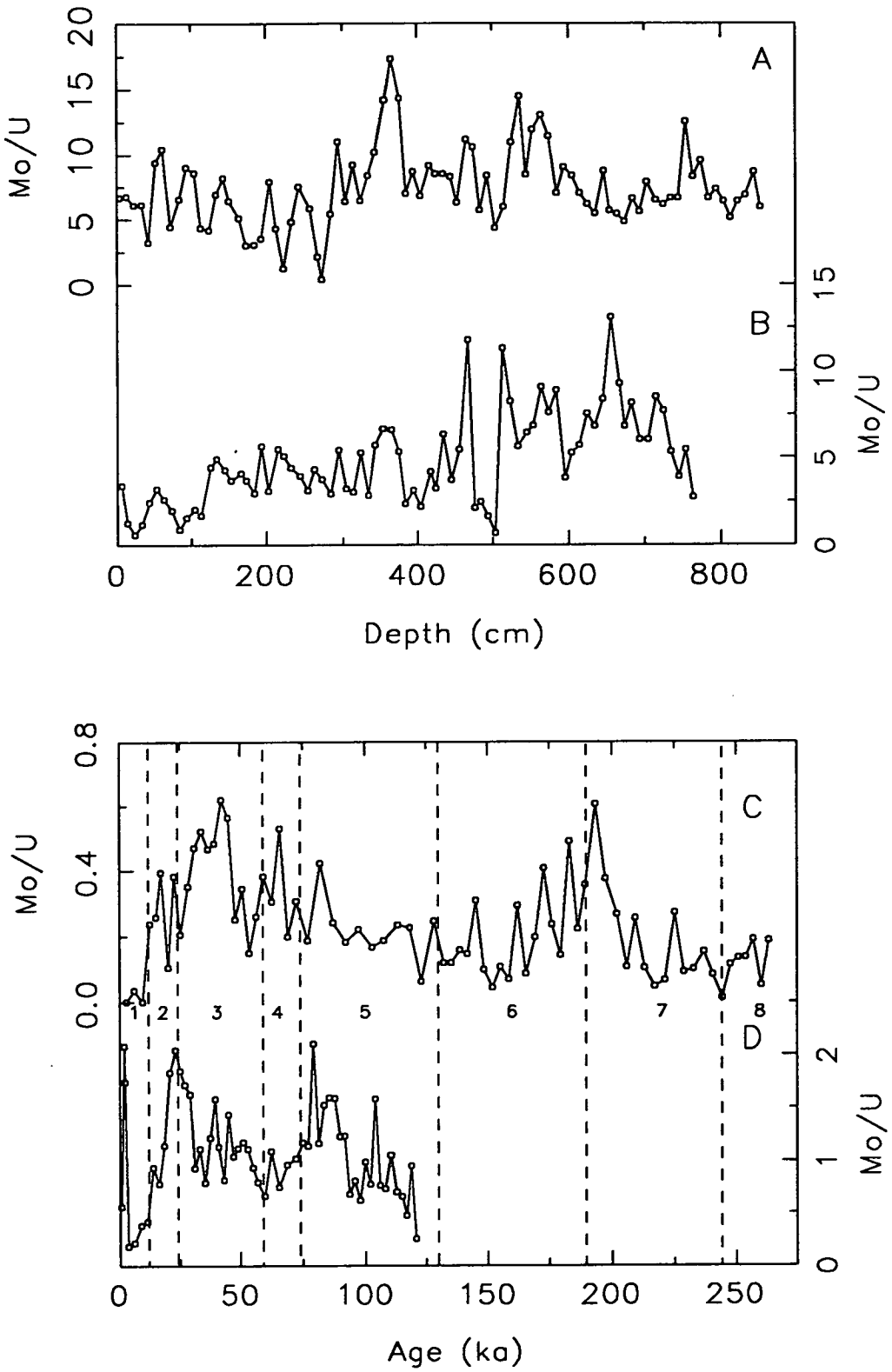


Figure 6.14. Mo/U weight ratio down-core profiles: A) CD38-09, B) CD38-10, C) CD38-02 and D) CD38-11.

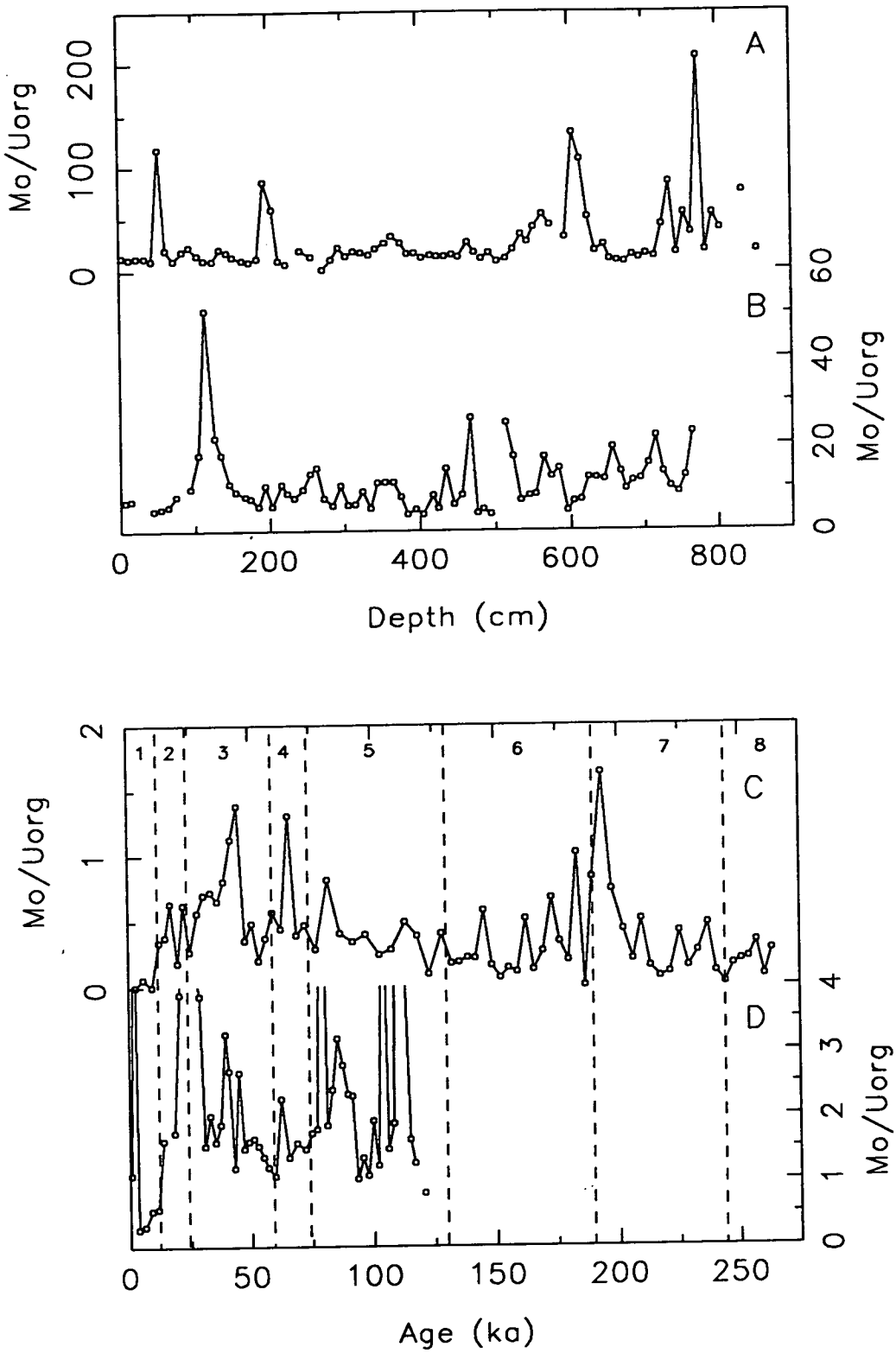


Figure 6.15. $Mo/U_{org}$ weight ratio down-core profiles: A) CD38-09, B) CD38-10, C) CD38-02 and D) CD38-11.

concentrated on the last group by examining the use of trace element geochemistry in the interpretation of two important oceanic processes. These are the level of biological productivity in the surface-waters and the state of the redox environment which exists at the sediment/water interface, each in terms of both the present day condition and the historical record contained in the box and piston cores from the Peruvian continental margin.

Elderfield (1990) stressed the importance of the above two processes by stating that chemical records can lead to "an examination of how climate-related processes such as increased production or lowered bottom-water oxygen concentrations might modify element accumulation rates." Therefore, if trace element signals can be used as palæo-productivity and palæo-redox indicators, it is necessary to study, interpret and fully understand their chemical record before other element accumulation rates can be examined. The following conclusions summarise the information that has been interpreted from the halogen, barium, strontium, molybdenum and uranium signals contained in the CD38 cores.

1) The post-depositional diagenetic mobility of the halogens renders them unreliable as palæo-productivity indicators. However, iodine concentrations, used in conjunction with organic carbon measurements, allow for the classification of marine sediments in terms of the redox state (oxic or anoxic) that existed at the sediment/water interface at the time of deposition. The sediment in piston cores CD38-09 and CD38-10 has been deposited within a reduced, anoxic environment, whereas all the other cores in this study have been sites of deposition under oxic conditions.

   The halogens may also be used to identify breaks in the sedimentation pattern, inter-core variations in sedimentation rate and/or organic matter composition and the I/Br ratio in CD38-02 (an undisturbed, oxic core site) may indicate organic matter flux changes associated with glacial/interglacial climate change.

2) The lack of Ba in cores CD38-09 and CD38-10 supports the theory of reduced conditions during their sediment deposition but this trace element can be used as a palæo-productivity signal as well as a simple palæo-redox indicator. Following the algorithm of Dymond *et al.* (1992) the level of new production above site CD38-02 has been calculated and from the age profile of this productivity signal (Fig. 6.10), it could be interpreted that the interglacial periods of the Late Quaternary were associated with more intense biological production in the surface-waters on the Peru margin.

3) Temporal variations in the Sr/Ca ratio of sediments containing a significant quantity of $CaCO_3$ shell-remains (CD38-02 and CD38-11) are a geochemical record which is more likely to be a productivity signal rather than a preservation effect. It may be interpreted as fluctuations in the degree of the dominance of foraminifera over coccoliths and seems to be related to glacial/interglacial periodicity.

4) The use of the Mo/U (and the $Mo/U_{org}$) ratio as a palæo-redox indicator in the Peruvian margin sediments contradicts the previous work of Bertine and Turekian (1973). The anoxic, shallow-water cores (CD38-09 and CD38-10) display higher Mo/U ratios compared with those in the oxic, deeper-water cores (CD38-02 and CD38-11). This implies that until more detailed work is carried out on the complex processes involved in Mo and U movement into and within marine sediments, the Mo/U ratio is highly unreliable as a palæo-redox indicator.

# CHAPTER 7

# ENVIRONMENT OF DEPOSITION

## 7.1. INTRODUCTION

> "Factors controlling element distributions in sediments are difficult to induce, because the distributions are frequently the result of non-equilibrium processes."
>
> Spencer *et al.* (1968)

It is because the environment of marine sediment deposition is both complex and highly variable, in terms of geology, chemistry, biology and physics, that the study of such sediments can reveal a great deal of information about the natural processes responsible for its composition. This study has so far attempted to interpret some of the factors controlling the geochemical element distributions in marine sediments from the Peru margin. In this chapter the overall environment of deposition will be considered in order to understand a particular element concentration and/or its down-core variation.

The cores sampled in this study have been taken from a range of depositional environments, widely varying in water depth, proximity to the Peruvian continental margin, redox potential at the sediment/water interface etc. This allows for the element distributions contained within the cores and the processes controlling them to be examined both spatially and temporally.

The marine environment contains such a complex mixture of many "non-equilibrium processes" that this chapter has had to be divided into various sections which, in effect, separate the inter-twined processes. The two main sections which follow correspond to the two most important input components to marine sediments which are accumulating on a continental margin affected by strong coastal upwelling (i.e. terrigenous and biogenic inputs, Chapter 5). The conclusions will, however, attempt to tie the various processes together again.

## 7.2. THE TERRIGENOUS INPUT

### 7.2.1. Introduction

Multi-component analysis (MCA) of the geochemical dataset from the Peru margin sediments (5.4) suggested that an average of 72% (on a weight basis) of the material was of a terrigenous origin. In some samples the abundance of the terrigenous component was as high as 90%, and on this fact alone, a detailed

examination of the major component in these marine sediments is merited. The terrigenous material is land-derived (i.e. not oceanic or biogenic) and can originate either from terrestrial (continental landmass) sources or from the alteration of oceanic basalts and/or hydrothermal exhalations (Bonatti *et al.*, 1983; Nath *et al.*, 1989). However, the results of the MCA indicated that hydrothermal deposits were completely absent from the sediments in this study and, therefore, this discussion of the depositional and environmental controls on the terrigenous input can concentrate solely on material whose source is the South American continent, in particular the Andes mountain range and the arid Peruvian coastal plain (Prospero and Bonatti, 1969; Scheidegger and Krissek, 1982; Boyle, 1983).

As well as the natural, continuous erosion and weathering of the continental rocks and soils, a second (but much less significant, in quantitative terms) source in this area, for terrigenous-derived material contained within marine sediments, is from land (and oceanic island) based volcanic activity (Ninkovitch and Shackleton, 1975; Ledbetter, 1982, 1985). Such volcanic ash deposits ("tephra") can form distinct layers which have characteristic geochemical compositions and can aid in the dating and correlation of marine sediment cores. The presence of any such ash layers within the Peru margin cores may be highlighted by the following geochemical interpretation of the terrigenous component.

There are a number of important questions which this section will try to interpret and answer, with respect to the spatial and temporal records of terrigenous material deposition in the marine environment of the Peruvian continental margin.

1) Is the composition, abundance and/or variation of terrigenous material strongly controlled by the proximity of each core site to the continental landmass?
2) Are there temporal variations which can be explained by climatic changes in sea-level, wind strength, continental aridity etc. during glacial/interglacial periodicity in the Late Quaternary (Boyle, 1983)?
3) Can the mechanism of transport of terrigenous material (wind-blown, river or ocean currents) be examined by any geochemical indicators?
4) What are the possible source differences that exist between (and within) cores from varying oceanographic locations and environments (Krissek *et al.*, 1980; Scheidegger and Krissek, 1982)?

### 7.2.2. Analyses and results

The geochemical parameters described below (namely aluminium, silicon, iron, manganese, potassium, rubidium, titanium and zirconium) were all analysed by X-ray fluorescence techniques using fused and pressed discs (Appendix A.5) and all data are presented on a salt-free basis (Appendix A.6). Regression analysis (5.2) and principal component analysis (5.3) both highlight the above elements as having strong correlations with the terrigenous phase and, therefore, they are likely to be most useful in the interpretation of this important sediment phase.

The only correction that has been made to the salt-free XRF data was for silicon (Si). The total Si concentration ($Si_{total}$) has been recalculated to remove the contribution of biogenic silica (as measured using the techniques described in Appendix A.4) which results in a terrigenous Si value ($Si_{terr}$) for all samples (using Eqn 7.1 and Appendix B.4).

Equation 7.1. Calculation of terrigenous silicon

$$Si_{terr} = Si_{total} - [Bio.\ Sil. \times 0.466]$$

where,
$Si_{terr}$ = terrigenous silicon (wt.%),
$Si_{total}$ = XRF Si concentration (wt.%),
Bio. Sil. = biogenic silica concentration (wt.%),
0.466 = atomic weight conversion from biogenic silica to biogenic silicon.

**Terrigenous element ratios**

As previously stated (e.g. 5.2.2 and 6.3.2), the element which is known to be exclusively associated with the terrigenous component is aluminium (Al) (Arrhenius, 1952; Bostrom, 1973; Bischoff *et al.*, 1979) and it has often been used in marine sediment studies as an indicator of clay detritus of terrestrial origin (e.g. Shimmield, 1985; Finney *et al.*, 1988; Shimmield and Mowbray, 1991; Patience, 1992; Pedersen *et al.*, 1992). In order to illustrate any variations in the composition of the terrigenous material, it is necessary to convert the simple elemental wt.% (which can be influenced by dilution effects of another component) into an element/Al ratio. The data and down-core profiles in this section are therefore expressed as elemental ratios to Al (or, in some cases, to Rb).

The complete dataset for $Si_{terr}$/Al, Ti/Al, Fe/Al, Mn/Al, K/Al, K/Rb and Zr/Rb for all the cores in this study can be found in Appendices C.8 and C.11. Table 7.1 summarises this large set of data by displaying the mean and range of values of the above geochemical parameters. The average deep-sea clay composition from Turekian and Wedepohl (1961) is also listed, for comparison with the Peru margin cores.

| | | $Si_{terr}$/Al | Ti/Al ($x10^{-3}$) | Fe/Al | Mn/Al ($x10^{-3}$) | K/Al | K/Rb ($x10^{-3}$) | Zr/Rb |
|---|---|---|---|---|---|---|---|---|
| CD38-09 | Range | 2.51-5.28 | 46.3-56.6 | 0.29-1.14 | 3.39-7.30 | 0.20-0.26 | 18.3-25.3 | 1.40-5.11 |
| (148m) | Mean | 3.85 | 52.29 | 0.46 | 5.48 | 0.226 | 21.48 | 1.94 |
| CD38-10 | Range | 2.99-5.79 | 43.5-55.2 | 0.26-0.49 | 1.23-6.29 | 0.22-0.27 | 17.5-25.9 | 1.26-5.17 |
| (257m) | Mean | 4.02 | 49.74 | 0.39 | 4.24 | 0.240 | 20.86 | 2.125 |
| CD38-02 | Range | 2.43-2.82 | 44.5-48.2 | 0.49-0.62 | 3.43-6.63 | 0.26-0.29 | 19.5-21.7 | 1.36-1.52 |
| (Box, 2530m) | Mean | 2.65 | 46.37 | 0.55 | 4.70 | 0.278 | 20.73 | 1.43 |
| CD38-02 | Range | 2.05-3.13 | 38.5-53.7 | 0.38-0.62 | 4.14-5.94 | 0.19-0.34 | 12.1-24.6 | 1.19-1.41 |
| (2525m) | Mean | 2.54 | 49.46 | 0.51 | 4.95 | 0.266 | 17.76 | 1.27 |
| CD38-11 | Range | 1.67-3.82 | 44.5-60.4 | 0.34-0.50 | 3.11-5.94 | 0.22-0.28 | 16.4-21.4 | 1.20-2.98 |
| (3835m) | Mean | 2.32 | 49.59 | 0.41 | 4.20 | 0.254 | 17.84 | 1.39 |
| CD38-03 | Range | 1.89-2.54 | 45.4-49.1 | 0.41-0.64 | 3.24-12.5 | 0.25-0.28 | 19.9-22.6 | 1.24-1.42 |
| (Box, 4289m) | Mean | 2.20 | 47.69 | 0.47 | 4.74 | 0.268 | 21.43 | 1.34 |
| T & W (1961) | | 2.97 | 54.76 | 0.77 | 79.7 | 0.297 | 22.72 | 1.364 |

Table 7.1. Range and mean of terrigenous ratios for all cores in this study and average deep-sea clay values from Turekian and Wedepohl (1961).

From the information contained within Table 7.1 it can be seen that there is a wide range of variation of each of the terrigenous element ratios both within and between each core in this study. When compared with the average deep-sea clay ratios (Turekian and Wedepohl, 1961) the data displays the following interesting points.

a) An enrichment (above 3.0) in the mean $Si_{terr}$/Al ratio is seen only for the two shallow-water cores, CD38-09 and CD38-10. The deeper-water sites all have mean $Si_{terr}$/Al ratios which are significantly depleted from the average clay value.

b) The majority of the Ti/Al ratios fall within the range of approximately 45-55 x $10^{-3}$, with this upper limit representing the average clay ratio. The only

exceptions to this range are the minimum in core CD38-02 (38.5 x $10^{-3}$) and the maximum in core CD38-11 (60.4 x $10^{-3}$).

c) The mean Fe/Al and Mn/Al values are all significantly depleted compared to the average deep-sea clay composition. However, Turekian and Wedepohl (1961) do not indicate whether their sediment samples are restricted to purely surface samples or if they are a mixture of surface and core samples. As will be shown later by the down-core profiles of the two box cores, this information is significant because of near-surface migration of both Mn and Fe relating to the redox environment of the sediment (Calvert and Price, 1977; Heath and Lyle, 1981; Graybeal and Heath, 1984).

d) The K/Al and K/Rb ratios from the Peru margin show only slight inter-core variation and the mean ratios are slightly depleted compared with the world average clay composition.

e) Cores CD38-09, CD38-10 and CD38-11 show Zr/Rb maxima which are 2-4 times the average deep-sea clay but of these, only the two shallow-water sites have mean Zr/Rb ratios which are enriched in Zr compared with Rb.

It is important in this examination of terrigenous input variation to study the down-core profiles of the above element ratios. Figures 7.1 through to 7.7 illustrate the temporal fluctuations of $Si_{terr}$/Al, Ti/Al, Fe/Al, Mn/Al, K/Al, K/Rb and Zr/Al (against depth or age) respectively and because each figure shows all six core profiles together, the spatial pattern of terrigenous composition can also be easily studied.

The following section (7.2.3) will give detailed interpretations of Figs 7.1 to 7.7 in terms of environmental and depositional conditions but described below are some of the most interesting features of the profiles.

a) With the knowledge that core CD38-09 contains a concentrated phosphorite horizon at 273cm and core CD38-10 contains similar zones at approximately 30, 80-110 and 500cm (4.3.3) then the down-core profiles display variations in the terrigenous composition which occur either around these zones (e.g. the Zr/Rb ratio peaks significantly at the above depths, Fig. 7.7) or between these zones. Examples of this latter variation pattern are, 1) in core CD38-10 where the Ti/Al ratio is on average around 45 x $10^{-3}$ below 500cm but above the phosphorite zone it shifts to an average of around 52 x $10^{-3}$ (Fig. 7.2) and, 2) in core CD38-09 where below the phosphorite zone (273cm) the Fe/Al and the $Si_{terr}$/Al ratios have significantly higher average ratios compared with those

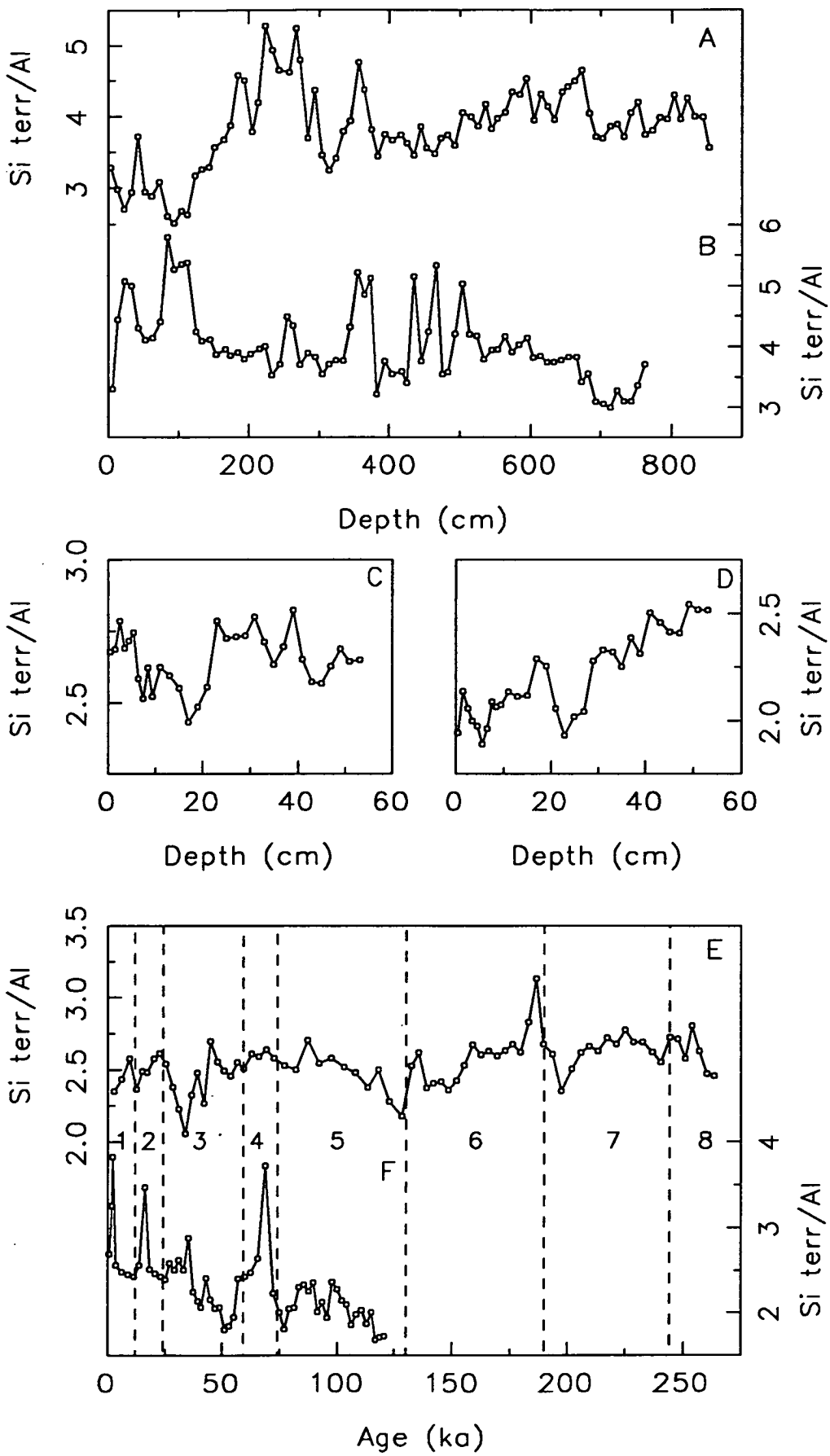


Figure 7.1. $Si_{terr}/Al$ ratio down-core profiles: A) CD38-09, B) CD38-10, C) box core CD38-02, D) box core CD38-03, E) CD38-02 and F) CD38-11.

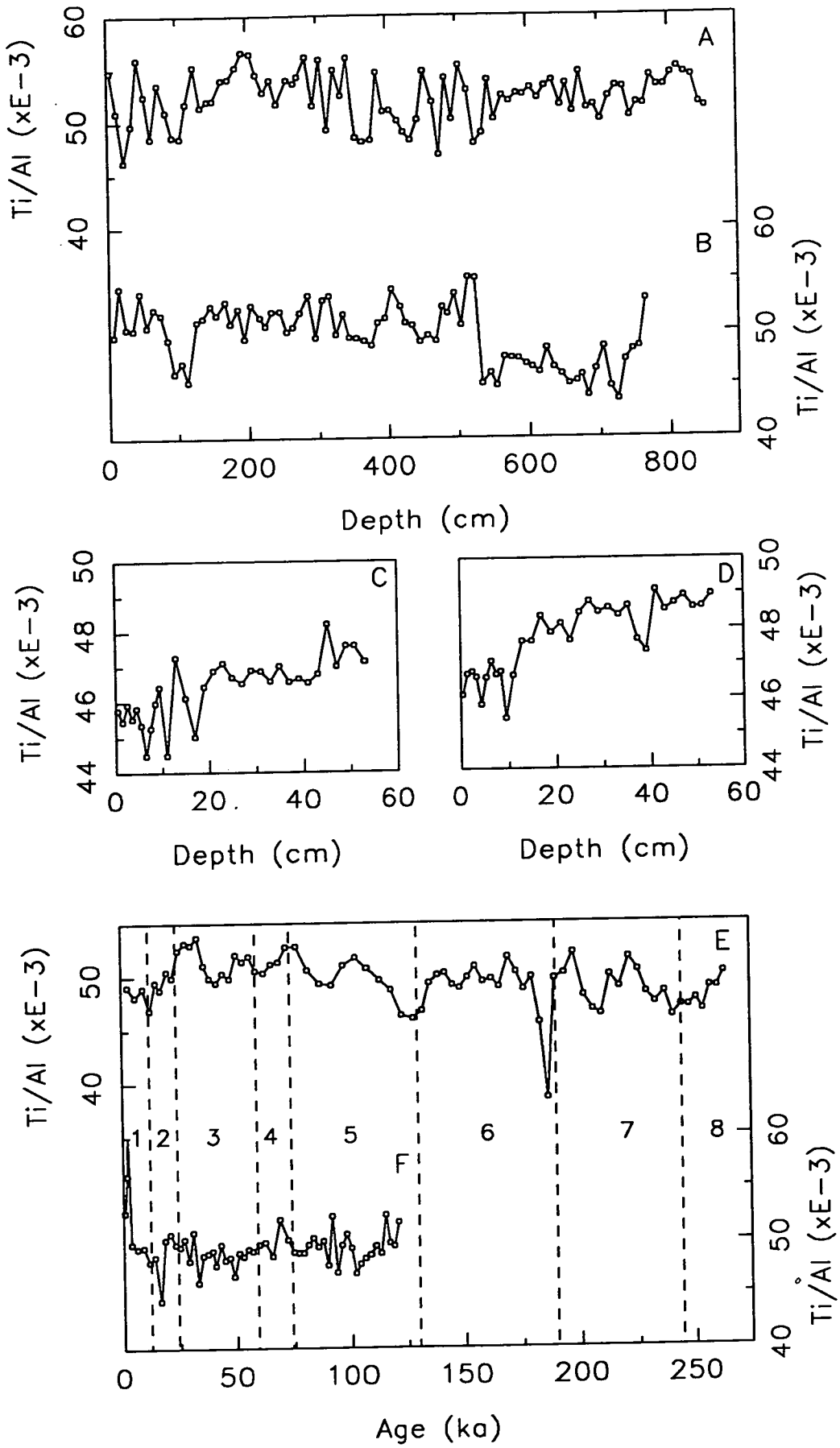


Figure 7.2. Ti/Al ratio down-core profiles: A) CD38-09, B) CD38-10, C) box core CD38-02, D) box core CD38-03, E) CD38-02 and F) CD38-11.

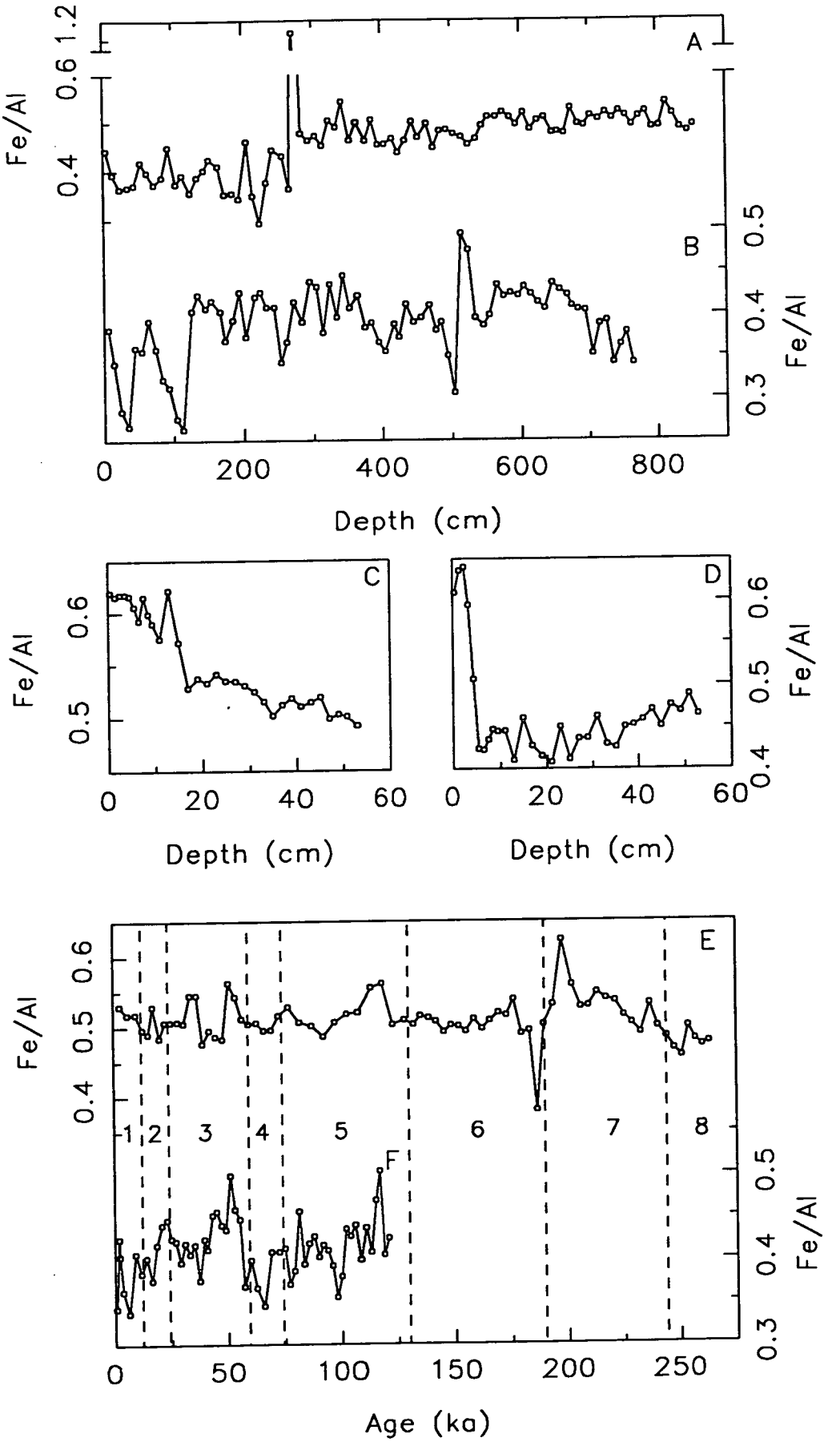


Figure 7.3. Fe/Al ratio down-core profiles: A) CD38-09, B) CD38-10, C) box core CD38-02, D) box core CD38-03, E) CD38-02 and F) CD38-11.

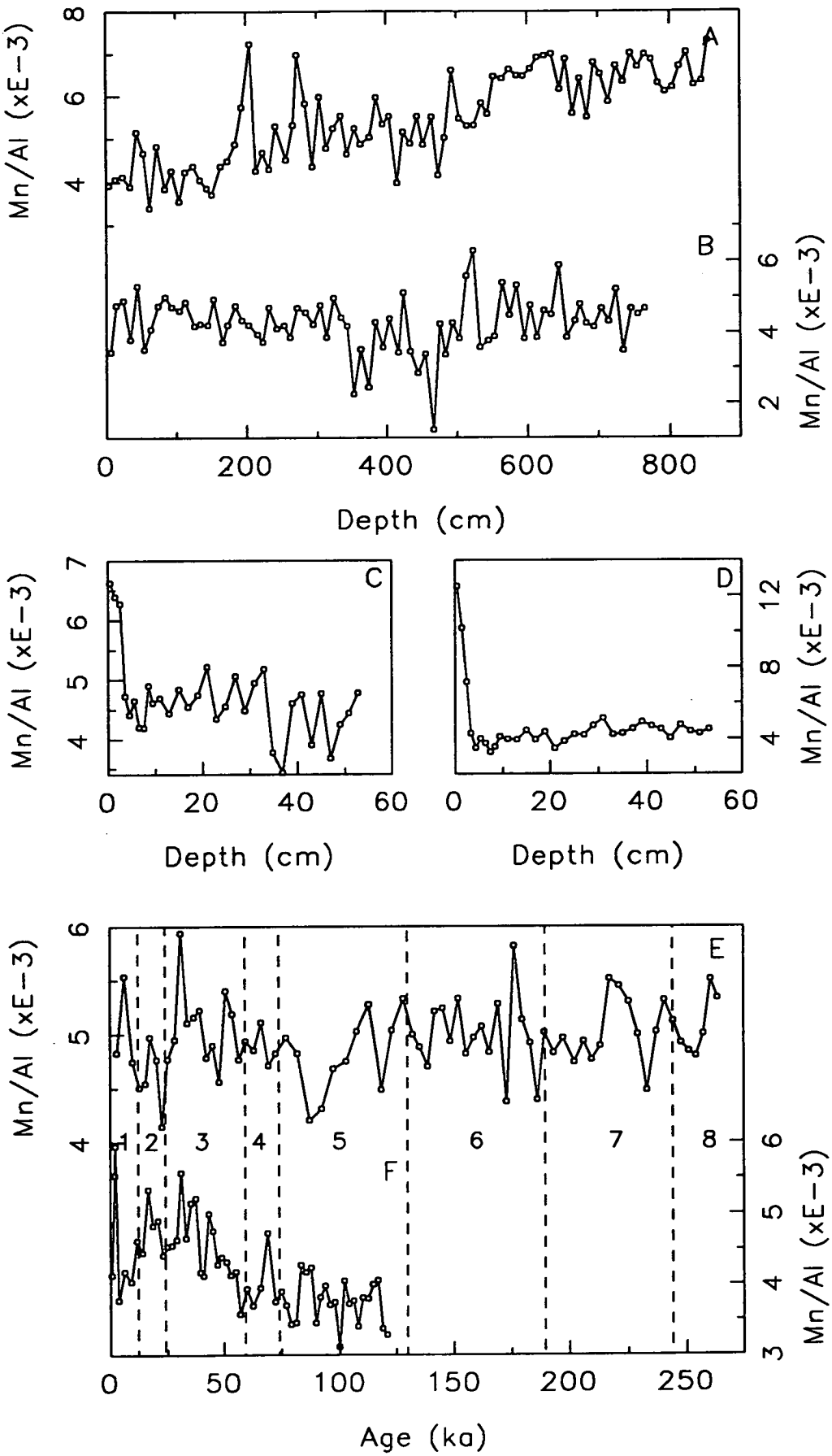


Figure 7.4. Mn/Al ratio down-core profiles: A) CD38-09, B) CD38-10, C) box core CD38-02, D) box core CD38-03, E) CD38-02 and F) CD38-11.

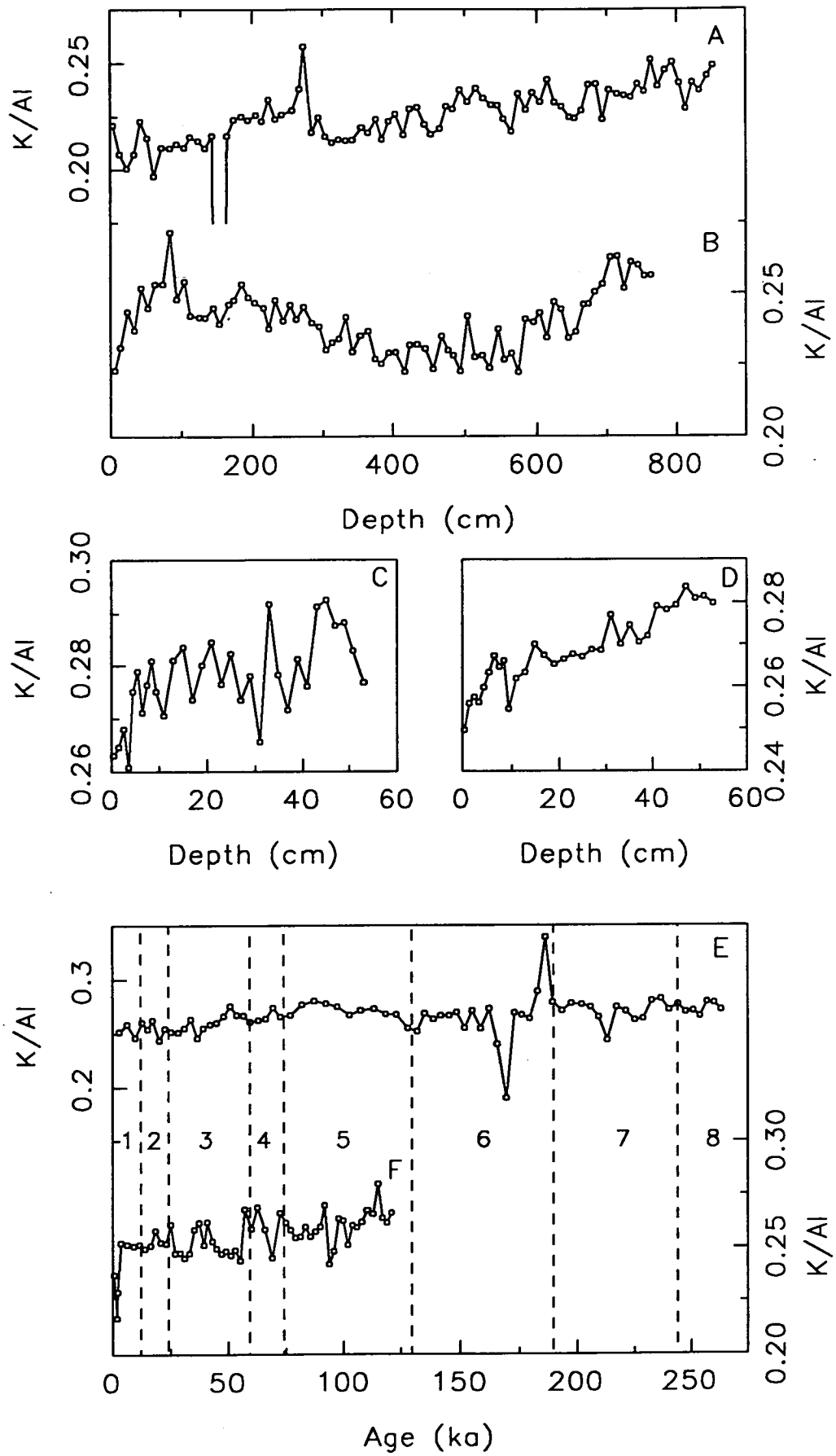


Figure 7.5. K/Al ratio down-core profiles: A) CD38-09, B) CD38-10, C) box core CD38-02, D) box core CD38-03, E) CD38-02 and F) CD38-11.

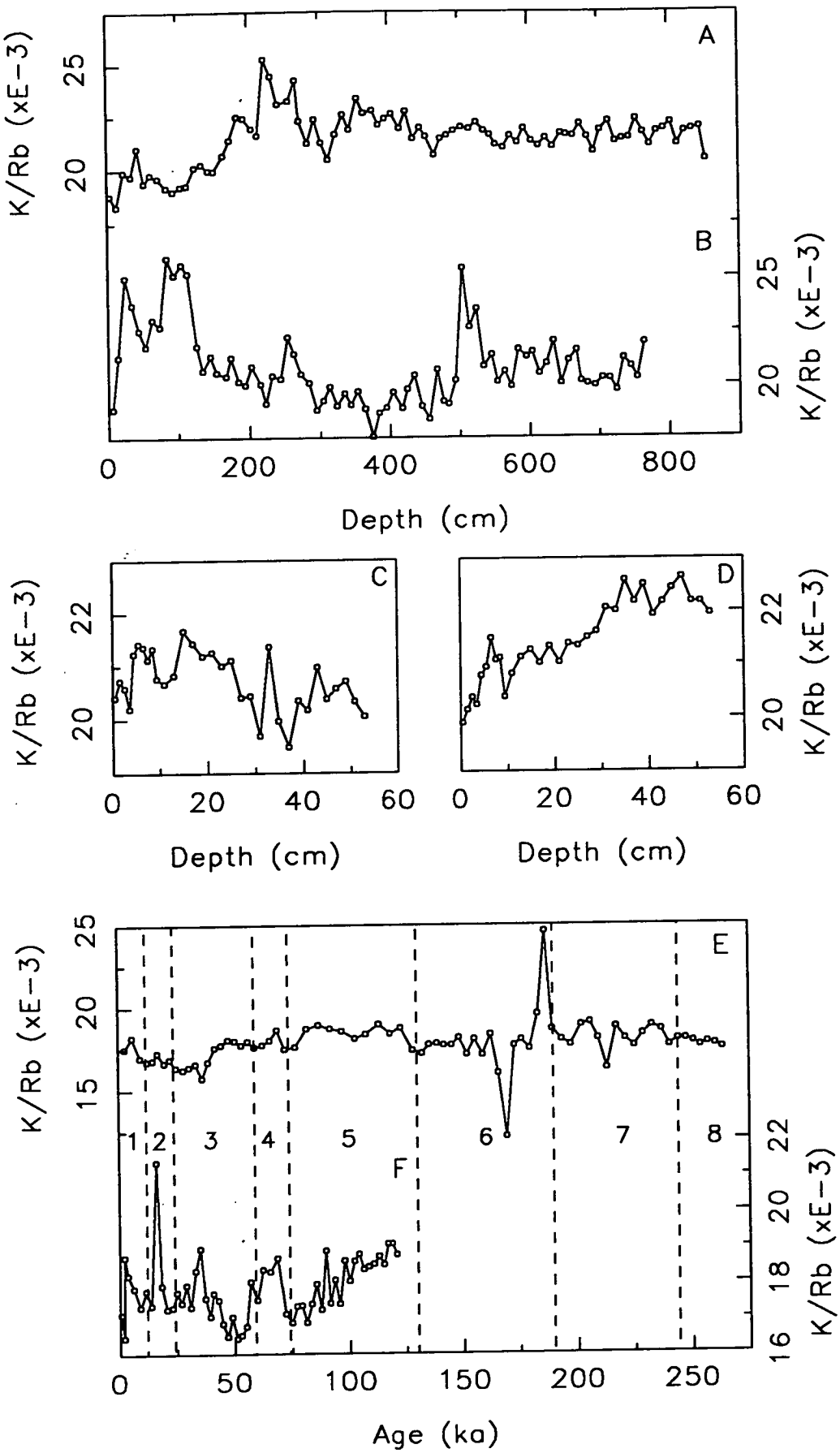


Figure 7.6. K/Rb ratio down-core profiles: A) CD38-09, B) CD38-10, C) box core CD38-02, D) box core CD38-03, E) CD38-02 and F) CD38-11.

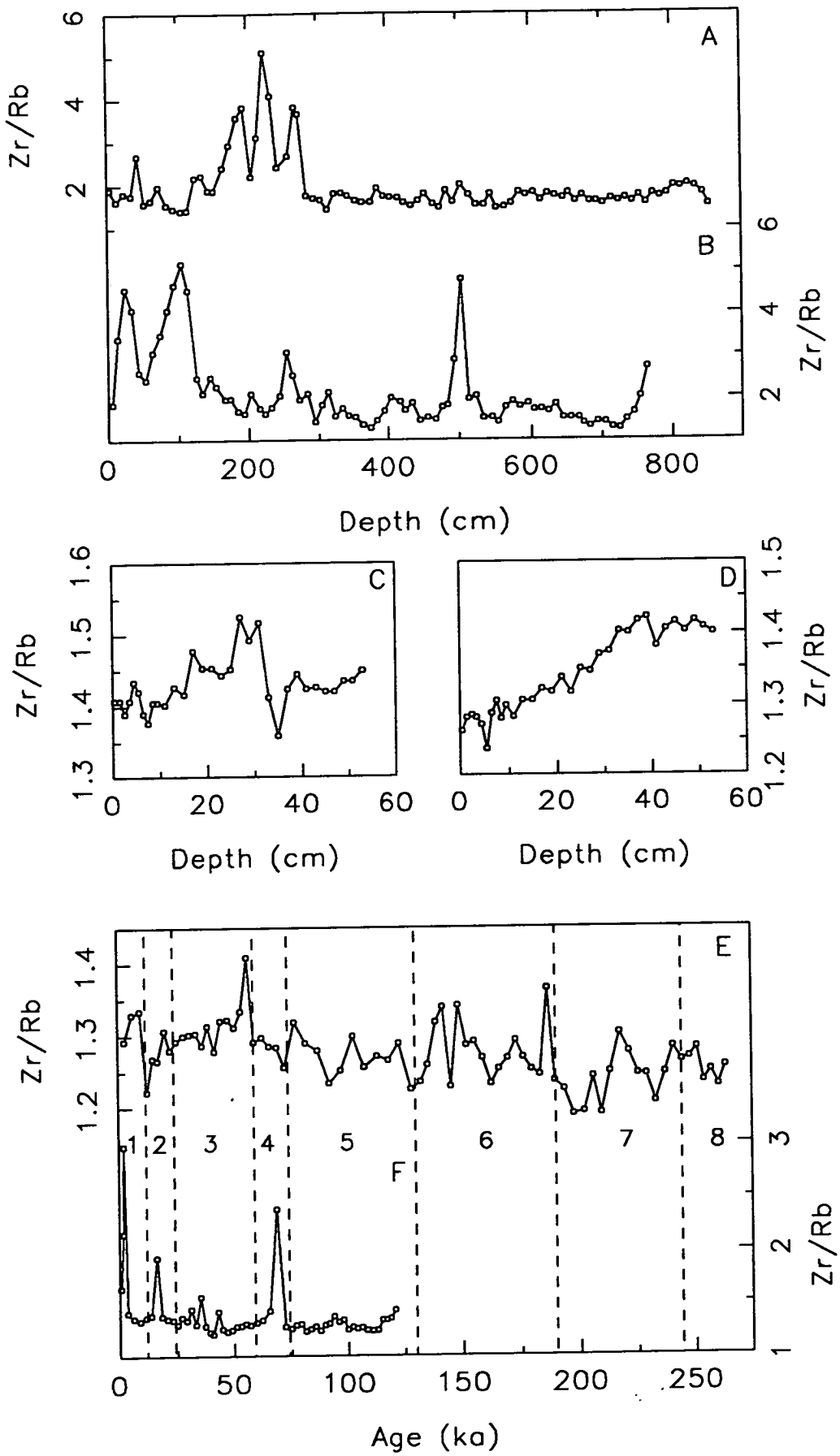


Figure 7.7. Zr/Rb ratio down-core profiles: A) CD38-09, B) CD38-10, C) box core CD38-02, D) box core CD38-03, E) CD38-02 and F) CD38-11.

above the phosphorite concentration event (from about 0.5 to 0.4 and from 4.0 to 3.0 respectively, Figs 7.3 and 7.1).

b) The two box cores (CD38-02 and CD38-03) display diagenetic, surface enrichment profiles of Fe/Al and Mn/Al (Figs 7.3 and 7.4) and in both sediment columns, it is the Mn/Al which drops at a shallower depth than the Fe/Al.

c) All the profiles for piston core CD38-02 contain anomalous troughs or peaks at about 186ka (lower stage 6); the most significant of which is the drop in Ti/Al (Fig. 7.2) down to 38.5 x $E^{-3}$.

d) The turbiditic zone in core CD38-11 (6.2.3) at about 2.5ka shows strong enrichments in $Si_{terr}$/Al, Ti/Al, Mn/Al and Zr/Rb but a depletion in K/Al compared with the rest of the sediment in this core. The glacial stages 2 and 4 also show peaks in $Si_{terr}$/Al and Zr/Rb in this core but because of the lack of a Ti/Al enrichment (and from the $I/C_{org}$ data, 6.2.3) these areas are not considered to be turbidite (secondary sedimentation) layers.

e) Accurate temporal studies are only possible using the two cores with age models, however, there seems to be very little obvious glacial/interglacial variation contained within the terrigenous composition profiles. The $Si_{terr}$/Al profile during stage 5 perhaps shows some similarity between CD38-02 and CD38-11 (Fig. 7.1) with the ratio starting low after glacial stage 6, rising steadily during interglacial stage 5 before dropping again just before the stage 4/5 boundary. The Ti/Al record of core CD38-02 displays a trend of decreasing ratios at the end of each glacial stage (2, 4, 6 and 8) followed by a double peak/trough system within the interglacial stages 3, 5 and 7. However, core CD38-11 shows no such pattern in its Ti/Al profile (Fig. 7.2).

f) Of the four piston cores, CD38-10 and CD38-02 show no obvious trend in their Mn/Al down-core profiles (Fig. 7.4) whereas core CD38-09 displays a generally increasing trend with depth (up to 7.3 x $10^{-3}$) and core CD38-11 shows a generally decreasing trend (down to 3.3 x $10^{-3}$ at the base of the core).

g) The K/Al record of core CD38-10 (Fig. 7.5) looks like it contains a smooth and continuous cycle of changing relative concentrations of K and Al in terrigenous material with time. However, it must be remembered that this is a depth profile and not an age profile and, therefore, variations in the sedimentation rate and periods of sediment erosion (2.3.2) must be taken into account. The peak in K/Al at around 80-100cm in core CD38-10 is related to the phosphorite horizon and can also be seen in core CD38-09 at 273cm (where there is a significant break in the trend of increasing K/Al with depth).

Obviously, the mineralogical composition of the terrigenous component is of concern in this study of the Peru margin sediments and Table 7.2 lists the chemical composition of some of the most common minerals (including quartz, heavy minerals, clays and feldspars) along with an indication of their density and hardness, and it will be referred to throughout the following section (7.2.3) on terrigenous environmental interpretations.

| Mineral | Chemical formula | Density | Hardness |
|---|---|---|---|
| Quartz | $SiO_2$ | 2.65 | 7 |
| Zircon | $Zr(SiO_4)$ | 4.65 | 7.5 |
| Ilmenite | $FeTiO_3$ | 4.74 | 5.5 |
| Rutile | $TiO_2$ | 4.8 | 6 |
| Anatase | $TiO_2$ | 3.9 | 5.5 |
| Magnetite | $Fe_3O_4$ | 5.2 | 7.5 |
| Haematite | $Fe_2O_3$ | 5.25 | 5.5 |
| Alkali feldspar | $(K,Na)(AlSi_3O_8)$ | 2.6 | 6 |
| Plagioclase feldspar | $Na(AlSi_3O_8) - Ca(Al_2Si_2O_8)$ | 2.6 | 6 |
| Illite | $K_{1-1.5}Al_4[(Si,Al)_8O_{20}](OH_4)$ | 2.75 | 1.5 |
| Chlorite | $(Mg,Al,Fe)12[(Si,Al)_8O_{20}](OH)_{16}$ | 3.0 | 2.5 |
| Smectite | $(0.5Ca,Na)_{0.7}(Al,Mg,Fe)_4[(Si,Al)_8O_{20}](OH_4).nH_2O$ | 2.5 | 1.5 |

Table 7.2. Terrigenous mineral composition, density and hardness (Deer *et al.*, 1966).

**Terrigenous element fluxes**

In order to examine the true variation of a particular sediment component and then to interpret the reasons for its temporal variation of input to the sediment, mass accumulation rate (MAR) fluxes need to be calculated. In this study, only piston cores CD38-02 and CD38-11 have been designated accurate age models and therefore flux data can only be calculated for these two cores (2.4.2). In this section the MAR fluxes of Al and $Si_{terr}$ will be used to display quantitative differences of terrigenous input both between the two cores (which are situated in contrasting depositional environments) and within the cores, in terms of glacial/interglacial variability.

The use of MAR fluxes does not completely solve the problem of correctly quantifying the amount of input of a particular geochemical component over time.

The method of calculation of fluxes (i.e. multiplication of the sediment accumulation rate by the dry bulk density and then by the component weight percentage) renders the result susceptible to potentially large and accumulative errors. The flux data is dependant on correct sediment accumulation rates, which in turn relies on an accurate age model. If there are any errors in the designation of the depth of the stage boundaries then the sedimentation rates (which are assumed to be linear between these points) can be significantly increased or decreased. A second problem can arise if there are errors in the dry bulk density measurement which was calculated directly from the wt.% water content of the sediment (Eqn 2.4., 2.2.1) and assumed a constant grain density of 2.6 g $cm^{-3}$. If, for example, one particular section of the core suffered from evaporation loss during transport and/or sampling then the dry bulk density calculated may be anomalously high. Unreliable flux data can also occur if the component of interest is only present as a small percentage compared with a second, more dominant component. Small variations in the abundance of the dominant component can significantly affect the concentration and flux measurement of the minor component even though the input of the latter may not have varied by much, if at all.

As a result of these problems, MAR flux data has to be interpreted with these possible errors in mind and corroborative evidence of component input variation should be looked for.

The terrigenous MAR flux data was calculated by multiplying the salt-free concentrations of Al and $Si_{terr}$ by the MAR for each sample (Eqn 7.2) and the complete dataset for cores CD38-02 and CD38-11 is listed in Appendix C.19.

Equation 7.2. Mass accumulation rate flux calculation

$$\text{MAR flux (mg/cm}^2\text{/kyr)} = \text{Element conc.} \times [\text{MAR (g/cm}^2\text{/kyr)} \times 1000]$$

where, MAR flux = mass accumulation rate flux of element,
Element conc. = concentration of element, expressed as a weight fraction of total sediment,
MAR = mass accumulation rate (from Eqn 2.5).

The range and mean of the Al and $Si_{terr}$ MAR fluxes are shown in Table 7.2, along with similar data from the Eastern Equatorial Pacific (Patience, 1992) for comparison. Figure 7.8 displays the fluxes as down-core age profiles for both CD38-02 and CD38-11.

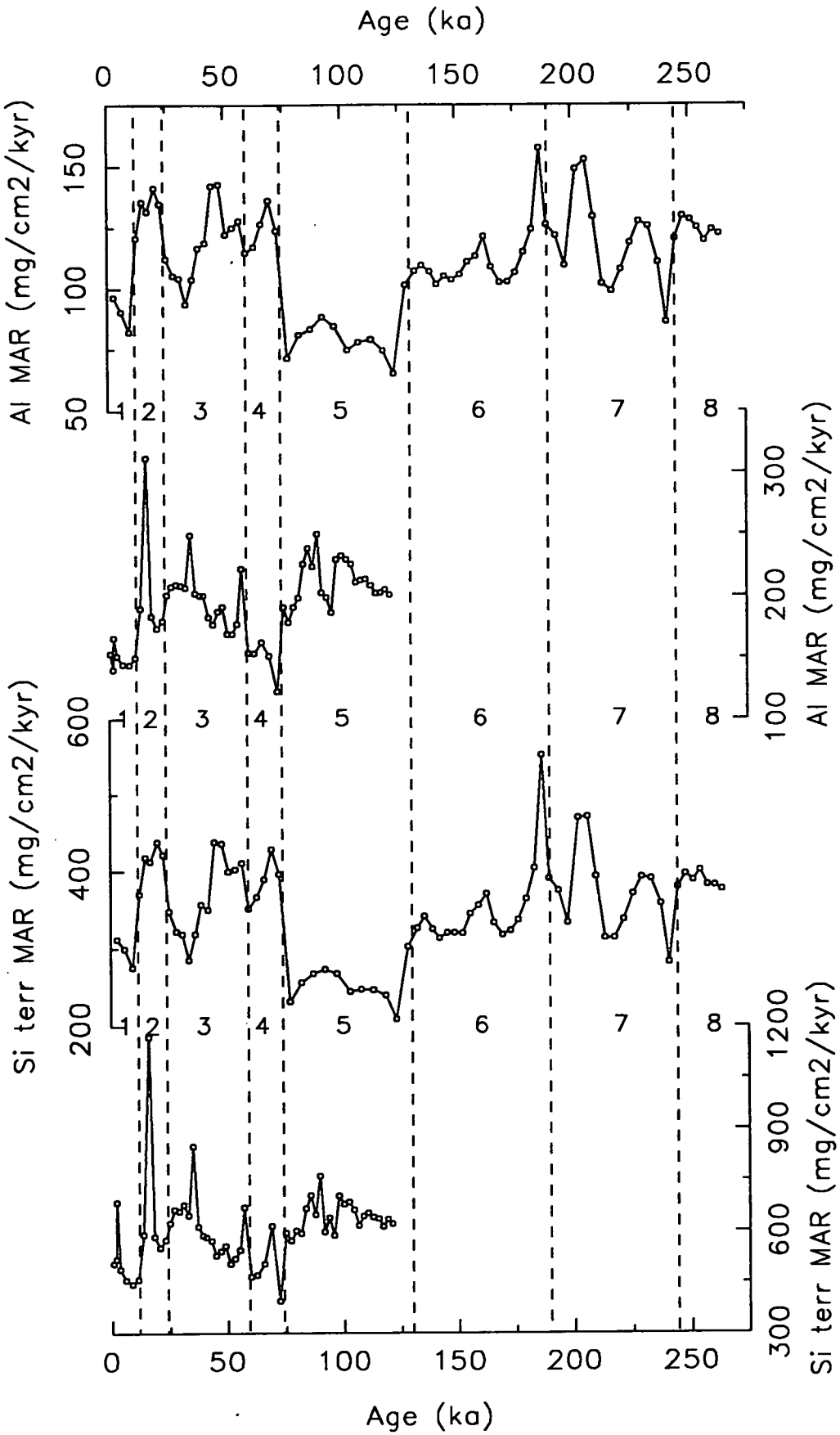


Figure 7.8. Terrigenous component Al and $Si_{terr}$ mass accumulation rate fluxes: A) and C) CD38-02, B) and D) CD38-11.

Table 7.3 reveals the basic fact that core CD38-11 has received a higher average flux of both Al and $Si_{terr}$ when compared with core CD38-02. It also shows that, as expected from the average deep-sea $Si_{terr}$/Al ratio (Table 7.1, Turekian and Wedepohl, 1961) the $Si_{terr}$ MAR is approximately three times the Al MAR. The average flux data for both cores fall within the range measured by Patience (1992) which implies that over the Late Quaternary, similar volumes of terrigenous material have been introduced to the marine sediments accumulating on the Peru margin and the Eastern Equatorial Pacific (Panama Basin).

| | | Al MAR ($mg\ cm^{-2}\ kyr^{-1}$) | Siterr MAR ($mg\ cm^{-2}\ kyr^{-1}$) |
|---|---|---|---|
| CD38-02 | Range | 65.0-157.5 | 208.5-551.7 |
| (2525m) | Mean | 112.0 | 349.7 |
| CD38-11 | Range | 122.0-312.0 | 393.7-1169 |
| (3835m) | Mean | 193.7 | 605.4 |
| Patience (1992) | | 15.2-292.1 | 85.3-754.0 |

Table 7.3. Range and mean of the mass accumulation rates of Al and $Si_{terr}$ ($mg\ cm^{-2}\ kyr^{-1}$) for cores CD38-02 and CD38-11.
Data from Patience (1992) is a range of the mean values for five cores from the Eastern Equatorial Pacific (water depth range, 1540-3225m).

The co-variation of both the fluxes of Al and $Si_{terr}$ over the past 265ka for CD38-02 and 120ka for CD38-11 is illustrated in Fig. 7.8. In the case of core CD38-02, the terrigenous fluxes are, on average, higher during glacial stages than during interglacial ones. However, high fluxes do occur during stages 3 and 7 which distort the glacial/interglacial cyclicity. No simple climatic pattern exists for core CD38-11, where interglacial stage 5 is a period of relatively high terrigenous flux, the Holocene (stage 1) contains a low flux and the period in between (from 75 to 12ka) shows a general trend of increasing flux over time. The highest fluxes of Al (312 $mg\ cm^{-2}\ kyr^{-1}$) and $Si_{terr}$ (1169 $mg\ cm^{-2}\ kyr^{-1}$) measured in this study occur in core CD38-11 during glacial stage 2 at 16.5ka.

### 7.2.3. Terrigenous environmental interpretations

This section is divided into sub-sections, each of which will discuss a particular environmental control on the deposition of terrigenous material along the Peru continental margin by interpretation of the geochemical data described above.

**Continental landmass proximity**

As stated in the introduction to this terrigenous input study (7.2.1), the terrigenous material which is found within the marine sediments in this study originates from the continental landmass of South America. Whatever the mode of transport of this material (wind-blown or fluvial input to the ocean) it is probable that the proximity of a particular core site to the continent (i.e. source area) will be the dominant control on the volume of material reaching that site. Measurement of the Al MAR and $Si_{terr}$ MAR fluxes showed that core CD38-11 has received an average of nearly twice the volume of terrigenous material compared with core CD38-02 (Table 7.3) and since the former core is situated closer to the continental landmass then this fact could be taken as evidence of the above statement. It is unfortunate that no mass accumulation rates could be calculated for cores CD38-09 and CD38-10, which are the closest sites in this study to the Peruvian coast, because it is likely that the terrigenous fluxes for these two sites would exceed those for CD38-11 by an order of magnitude or more.

However, the measured flux of terrigenous input is by no means linearly correlated with the distance from the continent. Factors such as latitudinal source differences, ocean currents and the actual oceanographic setting of the core on the continental slope, shelf or ridge, both on a regional and local scale, (all of which will be discussed fully below) can all affect the concentration of the terrigenous component in marine sediments (Scheidegger and Krissek, 1982; Clayton and Kemp, 1990).

Compositional, rather than abundance, differences in the terrigenous component of all six cores can, however, be examined and it is possible that the proximity of each site to the continent may play a role in such spatial variations. Cores CD38-09, CD38-10 and CD38-11 form a transect of increasing distance from South America at approximately 11°S and so any source-derived compositional differences will be minimal between the three sites. Therefore, the fact that the two near-shore cores contain much higher average $Si_{terr}$/Al ratios compared with CD38-11 (3.85 and 4.02 compared with 2.32, Table 7.1) may be interpreted as a proximity-controlled compositional difference. Increased $Si_{terr}$/Al ratios can be obtained by a higher than average quartz concentration compared to clays (Table 7.2, Shimmield and Mowbray, 1991; Patience, 1992). The $Si_{terr}$/Al data from this study imply that

cores CD38-09 and CD38-10 are accumulating greater quantities of quartz detritus, relative to aluminosilicate clays, due to their proximity to the continental margin.

In a study of the distribution of opal and quartz in the southeastern Pacific, Molina-Cruz and Price (1977) found that along the Peruvian and northern Chilean coast, quartz distribution (principally controlled by aeolian transport) decreased rapidly seaward and quartz/feldspar ratios measured by Scheidegger and Krissek (1982) confirmed this finding. The source of the quartz is thought to be the arid coastal plains of Peru and Chile, including the Atacama desert (Prospero and Bonatti, 1969; Molina-Cruz and Price, 1977).

If the enrichment of quartz within the terrestrial-derived assemblage at near-shore sites is due to shorter transport times for larger quartz grains compared to fine-grained clays, then any indicator of sediment grain-size (physical or geochemical) should also show differences between sediments deposited at different distances from the continental landmass. In marine sediments zirconium (Zr) occurs almost exclusively in zircon; a mineral which is highly resistant to weathering upon erosion of continental rocks and therefore tends to occur in the coarse-grained fraction of the sediment (Table 7.2, Hill and Parker, 1970). On the other hand, rubidium (Rb) is found associated mainly with the fine-grained fraction of marine sediments (Calvert, 1976) since it can easily substitute for potassium (ionic radius of $Rb^+$ = 1.47Å and $K^+$ = 1.33Å, Ahrens, 1952) in clays, such as illite (potassic-mica), and feldspars (Pedersen, 1979). Therefore, the ratio of Zr/Rb can be used as an indication of the average sediment grain-size, where the higher the Zr/Rb ratio, the coarser-grained the sediment (compare Fig. 7.7 with the % sediment > 63μm profiles in Figs 2.1 and 2.2).

It was highlighted in the results of this terrigenous input study (Table 7.1) that the only sites with an average Zr/Rb ratio appreciably enriched compared with the average deep-sea clay (Turekian and Wedepohl, 1961) were the near-shore cores, CD38-09 and CD38-10. This indication that coarser (and denser) grained terrigenous material is more abundant in samples from close to the Peruvian coast supports the $Si_{terr}$/Al results and implies that the proximity to the continental margin (i.e. source of terrigenous material) is a controlling influence on the geochemical and sedimentological composition of the total sediment.

**Volcanic activity**

The only sedimentary component which originates from the terrestrial environment but which has not been produced by continuous weathering of

continental rocks is tephra. Volcanic ash deposits in the eastern Pacific, transported to the ocean by atmospheric winds, are the result of andesitic to rhyolitic continental volcanism associated with the subduction of the oceanic Nazca and Cocos plates under the central and south American continent (Rose *et al.*, 1979; Wright, 1981; Pouclet *et al.*, 1990). Kennett and Thunell (1975) evaluated the distribution of ash layers contained within the deep-drilled cores of the Deep Sea Drilling Project from throughout the world's oceans and their results indicated a global increase of explosive volcanism within the Quaternary (over the last 2 million years) compared with the previous 20 million years. In a study of the distribution and age of ash layer "L" (Bowles *et al.*, 1973) in the Panama Basin region, Ninkovich and Shackleton (1975) also found the layer present in core V15-39 (4cm thick), located at 10°S at 2545m off the Peru margin. From its geochemical composition, the source of this particular ash deposit was interpreted as the andesitic volcanoes between 5°N and 2°S (i.e. Colombia and Equador) and the extreme southerly distribution was thought to be controlled initially by high-altitude winds which deposited the ash in the ocean between 5°N and 5°S, followed by ocean current transport (i.e. the Peru poleward undercurrent, 3.1.1).

Many authors have used volcanic ash layers as stratigraphic markers (Ninkovich and Shackleton, 1975; Drexler *et al.*, 1980, Ledbetter, 1982, Patience, 1992) and a study by Ledbetter (1985) attempted to integrate the tephrachronology of the eastern Pacific with microprobe geochemical analyses, which designated particular tephra layers using their characteristic chemical compositions. In terms of the recognition of ash layers using bulk-sediment geochemical analysis, the most striking characteristic is a low Ti/Al ratio compared with the surrounding alumino-silicate clays (Finney *et al.*, 1988; Patience, 1992). The only sample in all of the cores from this study to contain an anomalously low Ti/Al ratio is in core CD38-02 at an age of 186ka (38.5 x $E^{-3}$, Fig. 7.2). During the process of foraminifera picking (Appendix A.2) by microscopic study of the > 63μm fraction of the sediment, the sample from this depth in core CD38-02 was found to contain abundant small, dark brown crystals. These were subsequently picked out of the sample, analysed by X-ray diffraction (Appendix A.9) and found to be biotite minerals (Fig. 7.9). The interpretation that the biotite flakes at 186ka in core CD38-02 are part of a volcanic ash deposit (with a low Ti/Al ratio) is supported by the evidence of the tephra study of the ODP Leg 112 (Pouclet *et al.*, 1990) which found biotite flakes present in Quaternary andesitic-ash layers in core 687A.

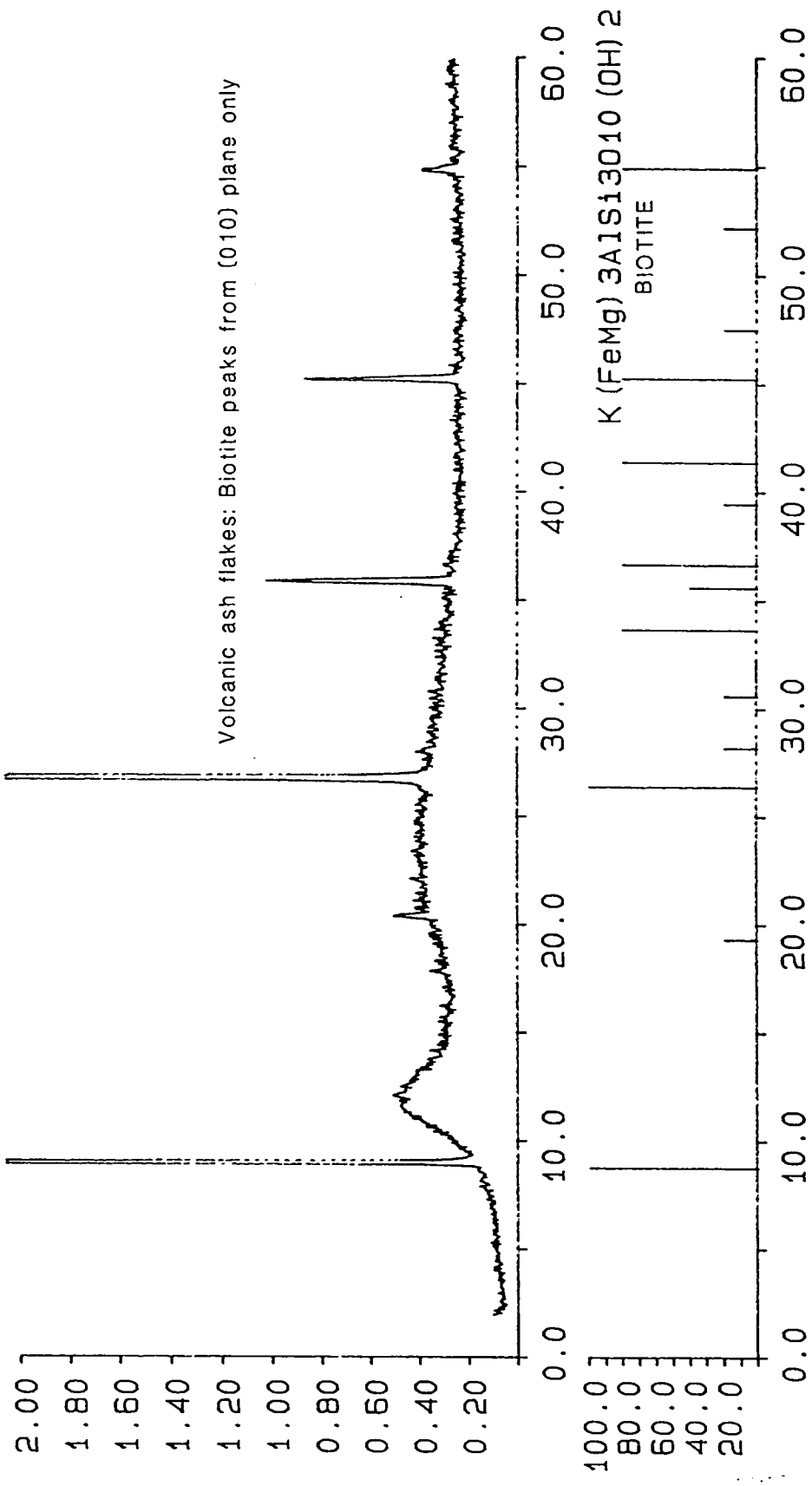


Figure 7.9. X-ray diffraction spectrum of biotite flakes of the ash layer at 186ka in core CD38-02.

The presence of a volcanic ash layer in the Nazca ridge site at 186ka leads to the question of the timing and origin of the volcanic activity that produced it, with respect to the regional temporal and spatial pattern of central and south American volcanism. Ash layer "G" was dated by Ledbetter (1985) at 190 ±11ka but was only seen in cores to the north of 10°N. It is possible that, by atmospheric wind and then sea current transport, the ash layer seen at 16°S in core CD38-02 was erupted from the same central American volcanoes. However, it is more likely that there was an eruption within the Central Andean volcanic arc of Peru (Pouclet *et al.*, 1990) at a similar time to the ash layer G eruption event, which produced this andesitic, biotite-rich ash deposit.

**Wind strength/continental aridity variations**

Throughout the Late Quaternary, climatic conditions have fluctuated relatively rapidly between glacial and interglacial periods and environmental factors such as wind strength and continental aridity have varied accordingly. During glacial periods it is thought that stronger atmospheric winds were produced by the growth of ice caps and latitudinal shrinking of the pressure cells in the Pacific and Atlantic oceans (Sarnthein *et al.*, 1988) around which the wind-systems move (anti-clockwise around the S. Pacific and therefore equator-ward up the western coast of S. America, 3.1.1). In addition to stronger glacial winds eroding more terrigenous detritus and transporting it to the oceans, the tropical regions were apparently more arid during glacial periods (and the sea-level dropped) and therefore, the source regions should have expanded (Sarnthein, 1978; Boyle, 1983).

The record of depositional variation of the terrigenous input contained within the Peru margin cores should therefore illustrate this glacial/interglacial periodicity of wind strength and aridity. There are two geochemical methods available in order to study such fluctuations; measurement of either the flux of the total terrigenous component (Al MAR and $Si_{terr}$ MAR) or the ratio of two particular elements which can indicate terrigenous grain-density/size and may be dependant on wind strength.

The terrigenous mass accumulation rate fluxes for cores CD38-02 and CD38-11 show quite large variations in their down-core age profiles (Fig. 7.8). For CD38-02, the cyclic pattern of low Al and $Si_{terr}$ fluxes during stages 5 and 1 compared with higher (about a 50% increase) fluxes during stages 2, 4, 6 and 8 could be interpreted as a climatic control on the volume of terrigenous material deposition on the Nazca ridge, where stronger winds during glacial stages have brought more clay, quartz and

feldspar detritus to this area of the Pacific Ocean. Although the highest terrigenous flux in core CD38-11 is seen during a glacial period, there seems to be no particular cyclic pattern and it is interpreted that this continental slope site receives a high input of terrigenous material from further up the slope and shelf which is not controlled simply by wind strength or aridity. At this site there is a more complex interplay of the above factors and also fluvial-transport input, sea-level eustatic variations and ocean current direction/strength need to be considered; all of which vary on different scales of glacial/interglacial change.

In his work on sediment accumulation off Peru, Boyle (1983) developed the use of high precision Ti/Al ratios as an indicator of climate change and attributed "fluctuations of Ti/Al in core V19-29 to changes in the intensity of aeolian transport associated with glacial/interglacial climate oscillations". His reasons for this are that the occurrence of Ti in the terrigenous component is principally in coarse-grained, dense minerals such as anatase, rutile and ilmenite (Table 7.2, Chester and Aston, 1976) and therefore the Ti/Al ratio of a sediment should increase if stronger winds are carrying more coarse grains to a particular depositional location (Shimmield and Mowbray, 1991). Boyle (1983) measured Ti/Al ratios which varied between 44 and 46 x $E^{-3}$ with higher ratios associated with glacial periods, and in this study the Ti/Al ratios show strong down-core variations between 44 and 55 x $E^{-3}$ (Fig. 7.2). The exceptionally low Ti/Al ratio in core CD38-02 at 186ka has been interpreted as a volcanic ash deposit and the anomalous peak in core CD38-11 occurs within the turbidite zone (a deposit of sediment washed down from the continental slope which is enriched in coarse-grained material) and therefore these two horizons can be excluded from this wind strength interpretation. For these two cores (in which the Ti/Al signal is plotted against age) CD38-11 shows no obvious glacial/interglacial pattern and CD38-02 varies on a sub-stage scale which is characterised by a drop in Ti/Al at the end of each glacial stage. This latter feature could be interpreted as an indication of a reduction in wind strength and/or continental aridity during the change from glacial to interglacial climatic conditions.

Of the four other cores (Ti/Al plotted against depth), the two box cores contain increasing ratios with depth (most noticeable in CD38-03) which may imply that both contain sediments which represent Holocene deposition at the surface down to the last glacial stage at the base of the cores. This would give these two sites an average sediment accumulation rate of about 3cm $kyr^{-1}$ (55cm in approximately 18kyr) which is roughly similar to the average SAR for piston core CD38-02 (Table 2.2).

There is also a marked variation in the Ti/Al record of the two near-shore cores on a fairly rapid scale and on a longer time-scale in core CD38-10, where lower Ti/Al ratios below 500cm, compared with those above this depth (where phosphorite enrichment occurs), may represent deposition of terrigenous matter during an interglacial stage. Interpretations of this nature are prone to errors because of the lack of an accurate age model (2.3.2) and, as will be discussed later, the influence of sea-level variations at such a shallow-water site.

It should be noted here that if both the Ti/Al ratio and the Zr/Rb ratio are indicators of sediment grain-size then, in these Peruvian continental margin sediments, they must be representative of different fractions of the grain-size (i.e. Zr-rich coarse-grained minerals are not the same as the Ti-rich ones) because the down-core profiles (compare Figs 7.2 and 7.7) are not very similar (except perhaps for box core CD38-03). One reason for this difference between Ti/Al and Zr/Rb may be that the Ti-rich minerals are dominated by aeolian transport (Parkin and Shackleton, 1973; Boyle, 1983) whereas the input of zircon to the oceans is principally by fluvial transport.

**Terrigenous source variation**

The six cores in this study can be split on a geographical basis into a northerly group at about 11°S (CD38-09, CD38-10 and CD38-11) and a southerly group between 14 and 16°S (piston and box cores CD38-02 and CD38-03). There is a strong possibility that compositional differences in the terrigenous components between these two locations will be influenced by variations in the original composition of the source rocks from which the quartz, clay, feldspar and other minerals have been eroded. In order to examine this spatial variability in the composition of the sediments, the geochemical signal will have to be one which is not strongly affected by grain-size variations and/or mode of transport to the ocean. If the ratios of two elements which occur predominantly in fine-grained clays display inter-core and down-core variation, then it is possible that such geochemical variation is caused by differences in the ratio of one clay to another which, in turn, may give an indication of spatial and temporal source variations.

Both iron (Fe) and potassium (K) are mostly contained within aluminosilicate clays and can be strongly controlled by the illite/chlorite/smectite mineralogy of the terrigenous component of the sediment (Table 7.2, Boyle, 1983; Shankar *et al.*, 1987;

Shimmield and Mowbray, 1991). Boyle (1983) measured an average Fe/Al ratio in core V19-29 (at 3°S) of about 0.45 and concluded that this value was probably representative of aluminosilicate material in the region of the Peru margin. If the average Fe/Al ratios of the cores in this study are examined, with respect to their northerly/southerly groupings, it can be seen that the cores located around 11°S have ratios around 0.45 or less, but the southerly group have higher ratios (0.47-0.55, Table 7.1) and this may be an indication of clay variation between the two groups. However, all the Fe/Al data show a depletion of iron (7.2.2) when compared to the average deep-sea clay (Turekian and Wedepohl, 1961) and Patience (1992) interpreted similar, low Fe/Al ratios in Panama Basin sediments as representing higher feldspar content in the terrigenous component relative to ferro-magnesium minerals.

It can be seen from the mineralogical composition data (Table 7.2) that Fe in terrigenous-derived sediments is present in dense minerals such as haematite, ilmenite, pyrite and magnetite as well as the fine-grained clays (mainly chlorite and perhaps nontronite). Therefore, the apparent spatial difference in Fe/Al ratios could be due to either one of two environmental influences (or a mixture of both). If the variation is due solely to the contrast in the source of the terrestrial detritus then, perhaps there is an increase in the illite/chlorite clay ratio from south to north along the Peruvian continent. However, if the variation is simply controlled by the relative concentrations of Fe-rich, dense minerals (compared to feldspars) then, perhaps the north/south variation is simply caused by grain-size differences due to the contrasting proximity to the continent and/or mode of transport of sediment to the cores.

One further interesting feature of the Fe/Al ratios is seen in the shallow-water core CD38-09, where there is a marked difference between the average Fe/Al ratio above and below the phosphorite-rich zone at 273cm. As with the spatial differences described above, this temporal difference could be caused by either a change in the source of the terrigenous matter (over a glacial/interglacial boundary) or a change in the average grain-size of sediment deposited at this site (due to sea-level increase since the last glacial maximum).

The Fe/Al ratio does not give conclusive evidence of north/south source variation along the Peru margin but the K/Al and K/Rb ratios can perhaps act as indicators of clay composition variation contained within the marine sediments. Whilst Al is present in all clay minerals (as suggested by the name, aluminosilicates) K occurs mainly in illite (Table 7.2) and it is therefore likely that variations in K/Al reflect the abundance of illite compared with other clay minerals (Boyle, 1983).

Rubidium can substitute for K in illite and the K/Rb ratio may also indicate differences in clay composition along the Peru margin.

There is a north/south difference present in the average K/Al ratios of the six cores but no such variation is shown by the K/Rb ratios (Table 7.1). The northerly group have a K/Al range from 0.226 to 0.254 and the southerly group from 0.266 to 0.278, which may be an indication of a source clay variation with increased illite concentrations (relative to chlorite and smectite) to the south. However, Scheidegger and Krissek (1983) undertook a comprehensive study of the clay mineralogy of fluvial sediments from 41 rivers along the Peruvian coastline from 3°S down to 17°S, which showed that illite was generally more abundant towards the north with relative increases of smectite south of 14°S. The explanation for this difference was related to the continental geology of the area resulting in latitudinal source variation of the clay composition. On the western slopes of the Andes and the coastal cordillera of Peru, the igneous rocks vary from gabbroic batholiths and basaltic volcanics south of approximately 14°S to more granitic igneous complexes and less-basic to intermediate volcanics to the north (Noble *et al.*, 1974; Pitcher, 1974). As well as influencing the clay composition, erosion of the northern province produces sediments which are two or three times more quartz-rich than those from the southern province (Scheidegger and Krissek, 1983) which may explain the very high $Si_{terr}$/Al ratios measured in cores CD38-09 and CD38-10.

The clay mineralogy work of ODP Leg 112 sediments (Clayton and Kemp, 1991) found Quaternary assemblages in the Salaverry, Lima and Trujillo basins (all between 6 and 12°S) which contained abundant illite compared to expandable clay minerals (smectite and vermiculite) and the opposite relative concentrations in core 686 located in the West Pisco basin at 13.5°S, and this supports the source variation control theory of Scheidegger and Krissek (1983).

The north/south variation measured in the K/Al ratio of the marine sediments in this study, therefore, contradicts the clay composition variation of the above authors. This is possibly due to a north/south source change in the feldspar content of the terrigenous component, with the more northerly group containing a lower alkali/plagioclase feldspar ratio compared with the southerly group (being more dominant than a clay variation). There are down-core variations of K/Al present in the sediments (Fig. 7.5) which may result from localised changes in either the clay and/or the feldspar composition over time. There is no glacial/interglacial cyclicity seen in this geochemical signal in cores CD38-02 and CD38-11 but in the box core CD38-03 there is a general increase in K/Al with depth which may be caused by decreased illite concentrations at this site since the last glacial stage. This interpretation is very

speculative because the sediments in CD38-03 have not been dated, as is the interpretation (for similar reasons) that the K/Al profiles of CD38-09 and CD38-10 represent increasing illite concentrations from the present day composition (surface sediments) down to a phosphorite concentration horizon (glacial stage?) where the K/Al (and K/Rb) is at a maximum. This is followed by a change in the clay composition (sharp decrease in illite in CD38-09, gentler in CD38-10) which once again becomes enriched in illite towards the base of each core.

This section about terrigenous source variations has shown that the geochemical signals of Fe/Al, K/Al and K/Rb are all, to varying degrees, controlled by the north/south variation in the igneous rock composition of the South American continent. However, the geochemical results are of limited use because of the multi-phase mineralogical composition of the above elements (Table 7.2). A purely mineralogical study of cores from a wider distribution along the continental shelf and slope would be required for a more detailed and accurate interpretation of source differences in the Peru margin sediments.

**Sea-level, ocean currents and other oceanographic influences**

The actual oceanographic setting of each of the sediment cores can strongly influence the volume and composition of the terrigenous component present (Rosato and Kulm, 1981; Scheidegger and Krissek, 1983). In near-shore locations, the supply of terrigenous material over time may be dependant on the eustatic variation of the global sea-level during glacial/interglacial periods. In contrast, the terrigenous component input to deeper-water sites will not be strongly influenced by such sea-level changes, but may be dependant on the precise location and environment within the continental margin.

The Zr/Rb ratio can be used as an indicator of average sediment grain-size because of the contrasting affinity of the two trace elements for coarse- and fine-grained minerals. The down-core profiles of Zr/Rb for cores CD38-09 and CD38-10 (both extremely shallow-water sites) illustrate a pattern of variation which can be interpreted by sea-level variations. The broad peak in CD38-09 and the five sharp peaks in CD38-10 of Zr/Rb all correspond to zones of phosphorite enrichment (compare Fig. 7.7 with Fig. 4.5). These are thought to be periods of lower sea-level on the Peru margin which resulted in stronger bottom-water currents sweeping the continental shelf and, therefore, fine-grained clays (Rb-rich) were winnowed off down

the continental slope leaving behind a lag deposit, which includes a concentration of heavy minerals (Zr-rich) and phosphorite pellets and nodules. If the sea-level drop in this area during maximum glacial periods of the Late Quaternary was as much as estimated by Fairbanks (1989) who analysed submerged coral terraces on Barbados (i.e. 100-120m) then this would give core CD38-10 a glacial water depth of about 150m and CD38-09 only about 30-50m. The drop in sea-level would expose a large area of freshly-deposited marine sediments along the Peru coast and cores CD38-09 and CD38-10 would be sites for increased terrigenous input of a preferentially clay-depleted composition during glacial periods.

Rosato and Kulm (1981) carried out factor analysis on the clay mineralogy of surface sediments from the Nazca plate and concluded that various environments of terrigenous-sediment deposition existed, whose spatial distribution could be characterised by the degree of mixing between two continental-factor assemblages and an oceanic-factor assemblage. More detailed examination of the clay mineral assemblages on either side of the Peru-Chile Trench was undertaken by Scheidegger and Krissek (1983) who concluded that the trench was "an imposing physiographic barrier to the seaward near-bottom advection of suspended particulates". This limits the influence of hemipelagic sedimentation to the relatively narrow continental margin and therefore, on the seaward side of the trench the deposition of terrigenous material is dominated by aeolian (rather than fluvial) transport.

It is highly probable, therefore, that the Peru-Chile Trench has a very strong influence on the differences between cores CD38-11 and CD38-03 (located on the continental slope) and CD38-02 (located on the seaward side of the trench) both in the volume (Al and $Si_{terr}$ MAR fluxes) and in the composition (Fe/Al, K/Al and Zr/Rb) of the terrigenous material being deposited at each site.

**Sediment redox potential**

Both iron (Fe) and manganese (Mn) can be incorporated into marine sediments by a variety of pathways. Initial introduction to the ocean from a terrigenous source can be fluvial (Sholkovitz, 1978; Martin and Whitfield, 1983), aeolian (Hodge *et al.*, 1978) or from hydrothermal/volcanic activity (Klinkhammer *et al.*, 1985). Deposition of these two redox-sensitive metals can occur by either direct clay mineral accumulation or, after desorbtion from clays in sea-water, the dissolved metals are re-adsorbed by biogenic and faecal particles or form oxyhydroxide coatings on particle surfaces (Shimmield and Pedersen, 1990). Patience (1992) states that these latter

methods of Fe and Mn accumulation in continental margin sediments are quantitatively less important relative to the input from terrigenous clay minerals. However, the latter Fe- and Mn-oxyhydroxide formation is sensitive to the redox potential of the sediments and surrounding pore-waters and has, therefore, been the focus of attention for many marine geochemical studies (e.g. Calvert and Price, 1977; Heath and Lyle, 1981; Graybeal and Heath, 1984; Thomson *et al.*, 1990).

The complex chemical processes between dissolved and particulate Fe and Mn under oxic or reduced conditions have been extensively reviewed in Shimmield and Pedersen (1990) and involve the following redox-controlled cyclic process. The oxyhydroxide minerals are stable in surface, oxic sediments and upon burial into a reduced-sediment zone, the metals are preferentially reduced to their dissolved-phase within the pore-waters. Upward migration of these pore-waters, upon compaction of the sediment, transports the metals back into the oxic-sediment zone and reprecipitation of solid-phase oxyhydroxide minerals occurs.

This natural, recycling process results in an enrichment in surficial sediments of solid-phase Mn and Fe, which decreases with depth across the redox boundary layer, and the pore-water concentrations of the dissolved metals display the opposite profile (Lynn and Bonatti, 1965). The driving forces for such cyclic processes are the continuous accumulation of fresh sediments and the diagenetic breakdown of organic matter (Patience, 1992). Therefore, the controlling factors on the extent of surface Fe and Mn enrichment are the sediment accumulation rate and the input flux of organic matter.

The data from the six cores on the Peru margin show a depletion of both average Fe/Al and Mn/Al ratios, relative to the average deep-sea clay which must be the result of Turekian and Wedepohl (1961) analysing only surface (oxic) sediment samples compared with the down-core samples measured in this study. When interpreting surface redox processes, it is vital that the true sediment/water interface is sampled and therefore, only the down-core Fe/Al and Mn/Al profiles of the box cores CD38-02 and CD38-03 (Figs 7.3 and 7.4) can be used to study Fe and Mn redox recycling.

It was shown in the halogen/$C_{org}$ interpretation (6.2.3) that these two cores are accumulating under surface-oxic conditions and the Mn/Al and Fe/Al profiles display strong surface enrichments, which are up to three times that of the ratio for the reduced-sediments which lie below the redox boundary layer. In both cores, the depth of the enrichment is shallower for Mn/Al compared to Fe/Al indicating that, although the processes of Fe and Mn redox-cycling are essentially similar for the two metals,

they do occur at slightly different Eh levels (Shimmield and Pedersen, 1990). There are also oxic-layer depth differences between the two cores (shallower for CD38-03) that may be related to different rates of sediment accumulation and/or organic matter flux between the Nazca ridge site and the continental slope site.

The Fe/Al enrichment in both cores (Fig. 7.3) displays a maximum which is below the actual sediment/water interface (at about 12cm in CD38-02 and 3cm in CD38-03) and this can be interpreted as resulting from the fact that precipitation of Fe is occurring from both above (from fresh terrigenous deposition) and below (from upward migration of dissolved-Fe) the oxic zone, which produces the maximum concentration of solid-phase Fe (relative to Al) towards the base of the oxic layer rather than at the top of it.

## 7.3. THE BIOGENIC INPUT

### 7.3.1. Introduction

Marine sediments, deposited in a range of environments along the Peru continental margin, can contain a relatively high concentration of material which originated from a biogenic source. In terms of wt.%, the biogenic component measured by multi-component analysis (Table 5.1) constitutes an average of 25.8% in the piston core sediments of this study, and can be as high as 47%. The biogenic component is composed of:

1) organic matter from the decaying remains of phytoplankton, zooplankton and other marine life (as well as their faecal pellets) - represented by organic carbon ($C_{org}$),
2) skeletal remains of diatoms, radiolaria and silicoflagellates which consist of amorphous silica - represented by biogenic silica (bio.sil),
3) skeletal remains of foraminifera and coccoliths which consist of hard, carbonate shells - represented by calcium carbonate ($CaCO_3$),
4) fish remains which are highly resistant to decomposition, i.e. scales and bones.

The first three of the above biogenic components are present in most marine sediments and have often been interpreted in marine geochemical studies as tracers of oceanic palæo-productivity (Arrhenius, 1952; Molina-Cruz and Price, 1977; Müller and Suess, 1979). The actual concentrations of $C_{org}$, bio.sil and $CaCO_3$, and the relative concentrations to each other, can vary considerably and depend on the

complex interplay between a number of factors and, therefore, the spatial and temporal variation of the biogenic input to the sediment can be interpreted in terms of the environment of biogenic production, transport and deposition.

This section will present the biogenic component data from all six cores along the Peru margin as individual concentrations of $C_{org}$, bio.sil and $CaCO_3$ and as mass accumulation rate fluxes for the two cores with accurate age models. The interpretations of this data will then be given, with respect to the following environmental factors which control the composition and the volume of biogenic input to continental margin sediments.

1) Primary productivity in the overlying water column which, in turn, is dependant on the location and strength of the coastal upwelling zone off Peru (3.1.1).
2) Faunal variations of the marine biomass which can fluctuate on many time scales from seasonal up to glacial/interglacial periodicity.
3) Decomposition of organic matter and dissolution of silica and carbonate, as the biogenic material falls to the sea-floor and within the sediment column, which is dependant on ocean chemistry, redox environment and water mass circulation. This results in the recycling of most of the elements vital to further marine life and the preservation of only a small fraction of the original biogenic signal.
4) Dilution by non-biogenic material, which is principally the terrigenous component along the continental margin.

### 7.3.2. Analyses and results

The concentration of organic carbon, biogenic silica and calcium carbonate have been analytically determined using the techniques detailed in Appendices A.3, A.4 and A.5 (and $CaCO_3$ calculated using the equation in Appendix B.1), respectively.

#### Biogenic component concentrations

The biogenic component dataset, presented on a salt-free basis, is tabulated in full in Appendix C.12 and is summarised in Table 7.4, which lists the range, mean and surface values of $C_{org}$, bio.sil and $CaCO_3$ (all wt.%) for all six cores in this study.

| | | Corg (wt.%) | Bio.Sil (wt.%) | CaCO3 (wt.%) |
|---|---|---|---|---|
| CD38-09 | Range | 1.59-8.26 | 3.10-25.82 | 0-6.40 |
| (148m) | Mean | 4.38 | 15.45 | 2.93 |
| | Surface | 6.70 | 16.85 | 2.16 |
| CD38-10 | Range | 0.79-11.92 | 0.48-28.61 | 0-25.71 |
| (257m) | Mean | 5.37 | 13.37 | 8.25 |
| | Surface | 9.21 | 9.38 | 10.58 |
| CD38-02 | Range | 0.86-1.83 | 4.58-8.90 | 11.58-36.15 |
| (Box, 2530m) | Mean | 1.20 | 6.53 | 24.75 |
| | Surface | 1.02 | 8.48 | 12.34 |
| CD38-02 | Range | 0.82-2.67 | 3.52-9.83 | 0.60-37.54 |
| (2525m) | Mean | 1.48 | 6.28 | 22.25 |
| | Surface | 1.49 | 9.54 | 16.84 |
| CD38-11 | Range | 1.62-4.55 | 3.46-18.09 | 0-20.92 |
| (3835m) | Mean | 3.31 | 10.59 | 5.42 |
| | Surface | 3.87 | 7.99 | 2.19 |
| CD38-03 | Range | 1.46-2.48 | 11.97-17.86 | 0-0.94 |
| (Box, 4289m) | Mean | 1.76 | 14.80 | 0.38 |
| | Surface | 1.72 | 17.86 | 0.04 |

Table 7.4. Range, mean and surface values of organic carbon, biogenic silica and calcium carbonate (all wt.%) in Peru margin cores.

There are a number of features of the data in Table 7.4, which will be fully interpreted in the following section (7.3.3).

a) The mean $C_{org}$ concentrations of the two near-shore, shallow-water cores (CD38-09 and CD38-10) are two to three times higher than those of the deeper-water cores.

b) The Nazca ridge site (box and piston cores CD38-02) contains sediment with the largest mean and individual $CaCO_3$ concentrations of all the cores in this study.

c) The deepest-water core at 4289m (CD38-03) contains negligible quantities of $CaCO_3$ but has a bio.sil content which is consistently above 10wt.% of the total sediment.

d) All the sediments contain reasonable concentrations of bio.sil (> 3wt.%) except for within core CD38-10, which has a minimum of only 0.5wt.% (due to strong terrigenous dilution).

Included in Table 7.4 are the surface-sediment biogenic concentrations but, as was explained in the halogen section (6.2.2), care must be taken in the interpretation of this surface data because it is only the two box cores which are from true surface samples. The piston core surface samples are actually from up to 10cm depth in the core but they may still be useful in the interpretation of spatial variance of the three biogenic components along the Peru margin.

Figure 7.10 illustrates this variation by graphically representing the water depth of each core site plotted against the surface wt.% of the biogenic components. It can be seen that the maximum surface sediment concentrations of $C_{org}$ are found in the shallow-water sites (CD38-09 and CD38-10), that the surface bio.sil concentration is high in both the shallowest (CD38-09) and the deepest (CD38-03) sites and that the intermediate water core (CD38-02) contains the highest concentration of surface $CaCO_3$. These surface-sediment concentrations are similar to the overall mean sediment contents of the Peru cores, however, none of the plots (Fig. 7.10) display a simple concentration pattern with respect to the depth of water through which the $C_{org}$, bio.sil and $CaCO_3$ biogenic-remains have fallen before reaching the accumulating sediment. This implies that, as well as water depth, there are a number of other factors influencing the spatial pattern of biogenic input to marine sediments.

The down-core, temporal variation of the total biogenic input was demonstrated by the MCA results (Figs 5.6 to 5.9) for the four piston cores. Here, the individual down-core profiles of $C_{org}$, bio.sil and $CaCO_3$ are illustrated for all six cores in Figs 7.11, 7.12 and 7.13 respectively. Each of the biogenic components, when expressed as a wt.%, is susceptible to down-core fluctuations in its concentration as a result of dilution effects either from another of the biogenic components or from a non-biogenic component. Therefore, it will be impossible to be certain of any environmental interpretations made from the profiles in Figs 7.11 to 7.13. However, the following features are of interest and the biological/oceanographic factors controlling them need to be examined (7.3.3).

a) Of the two near-shore cores, CD38-10 demonstrates a possible down-core correlation between the three biogenic components; characterised by low concentrations at 30, 80-110 and 500cm and decreasing concentrations with

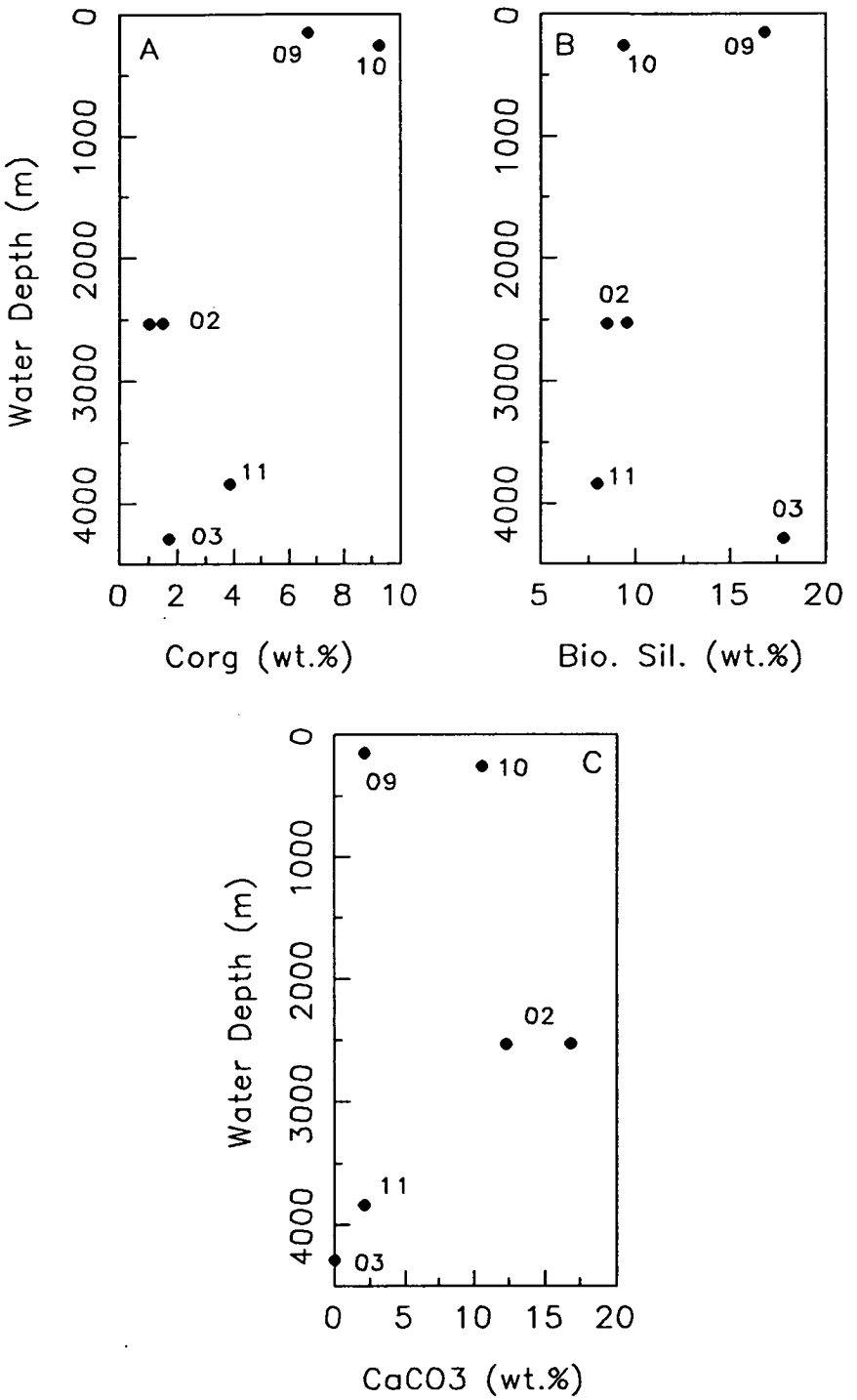


Figure 7.10. Core site water depth against the concentrations of A) organic carbon, B) biogenic silica and C) calcium carbonate of the surface samples from cores CD38–09, CD38–10, CD38–02 (piston and box), CD38–11 and CD38–03 (box).

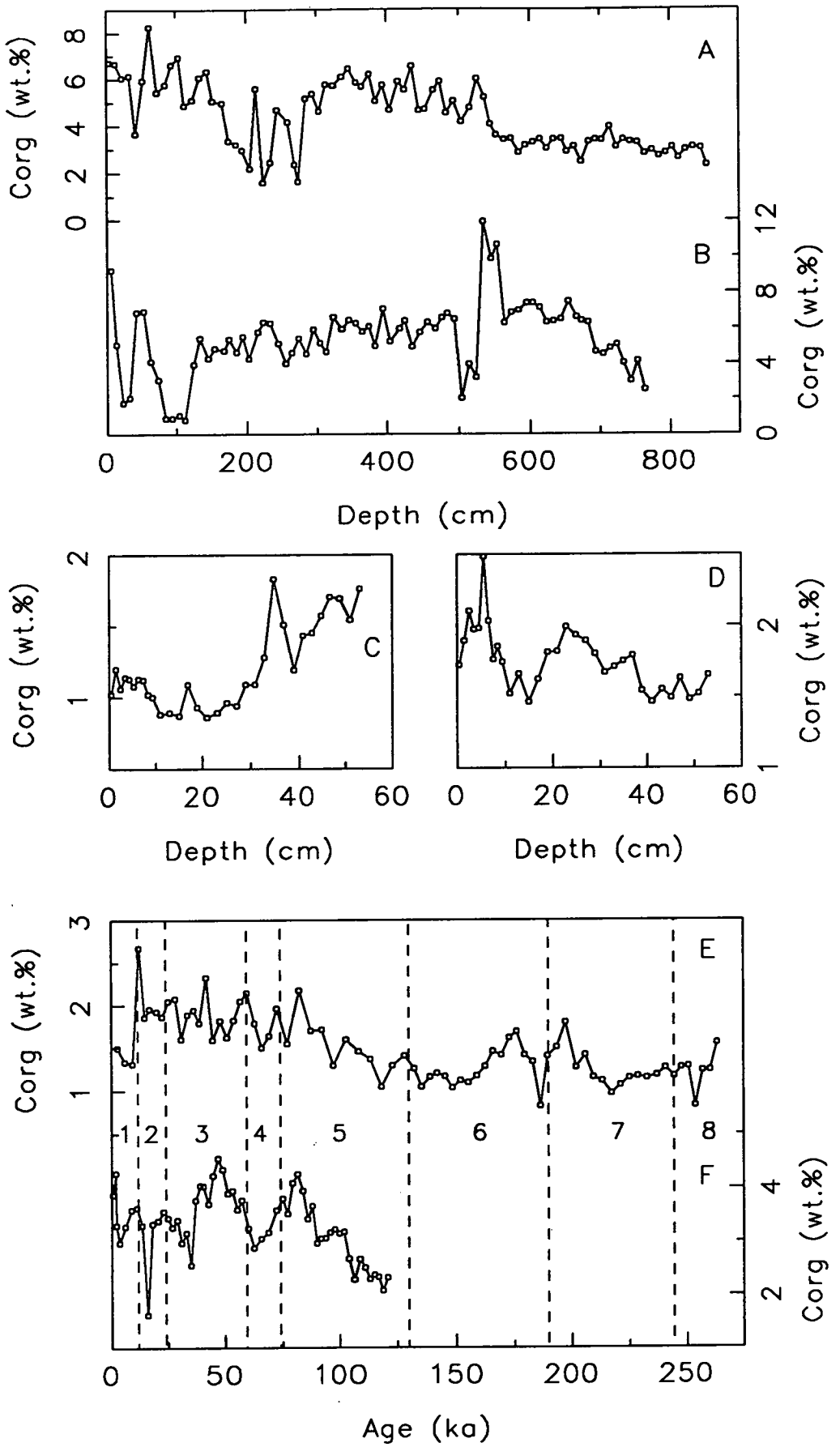


Figure 7.11. Organic carbon (wt.%) down-core profiles: A) CD38-09, B) CD38-10, C) box core CD38-02, D) box core CD38-03, E) CD38-02 and F) CD38-11.

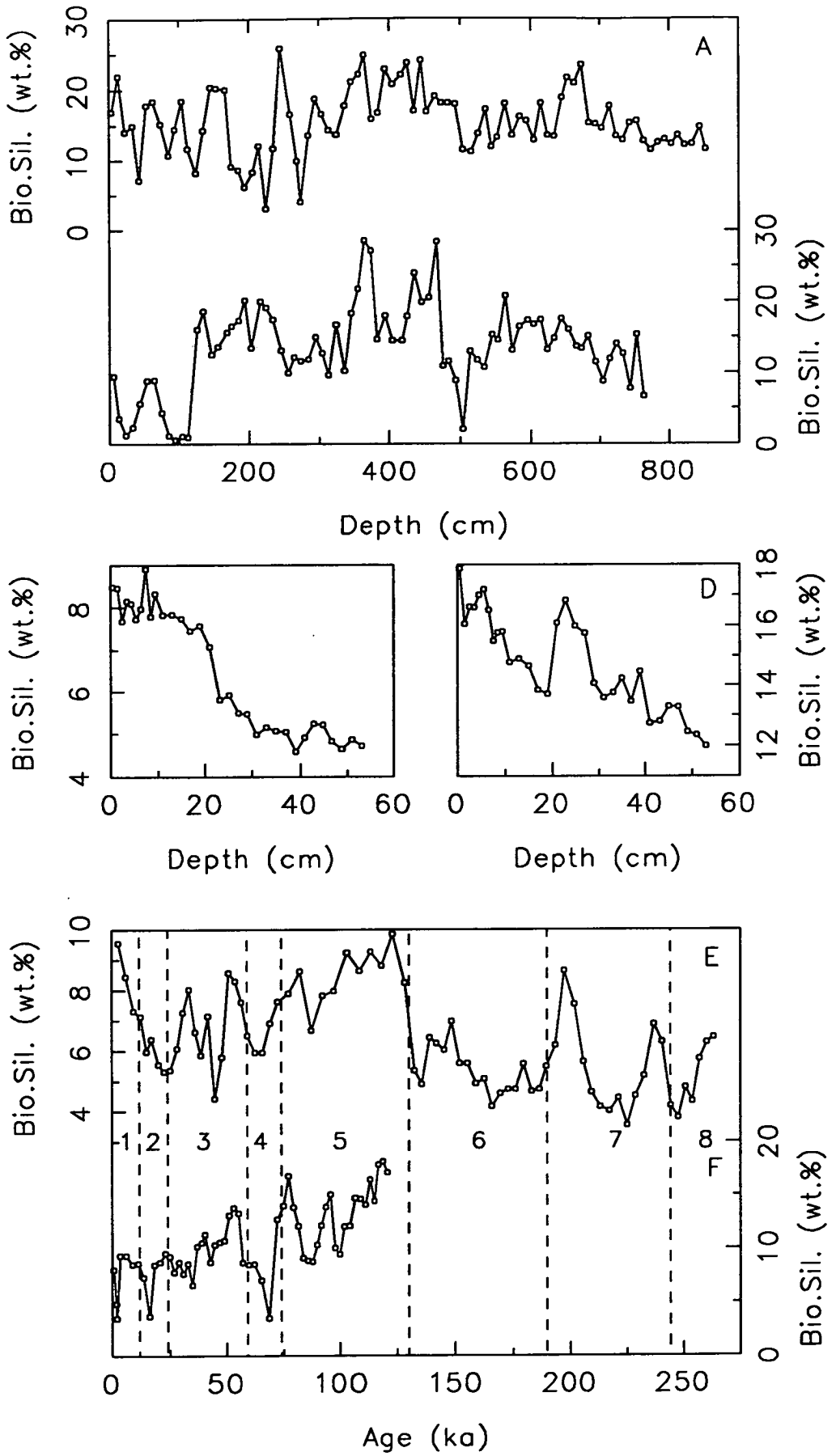


Figure 7.12. Biogenic silica (wt.%) down-core profiles: A) CD38-09, B) CD38-10, C) box core CD38-02, D) box core CD38-03, E) CD38-02 and F) CD38-11.

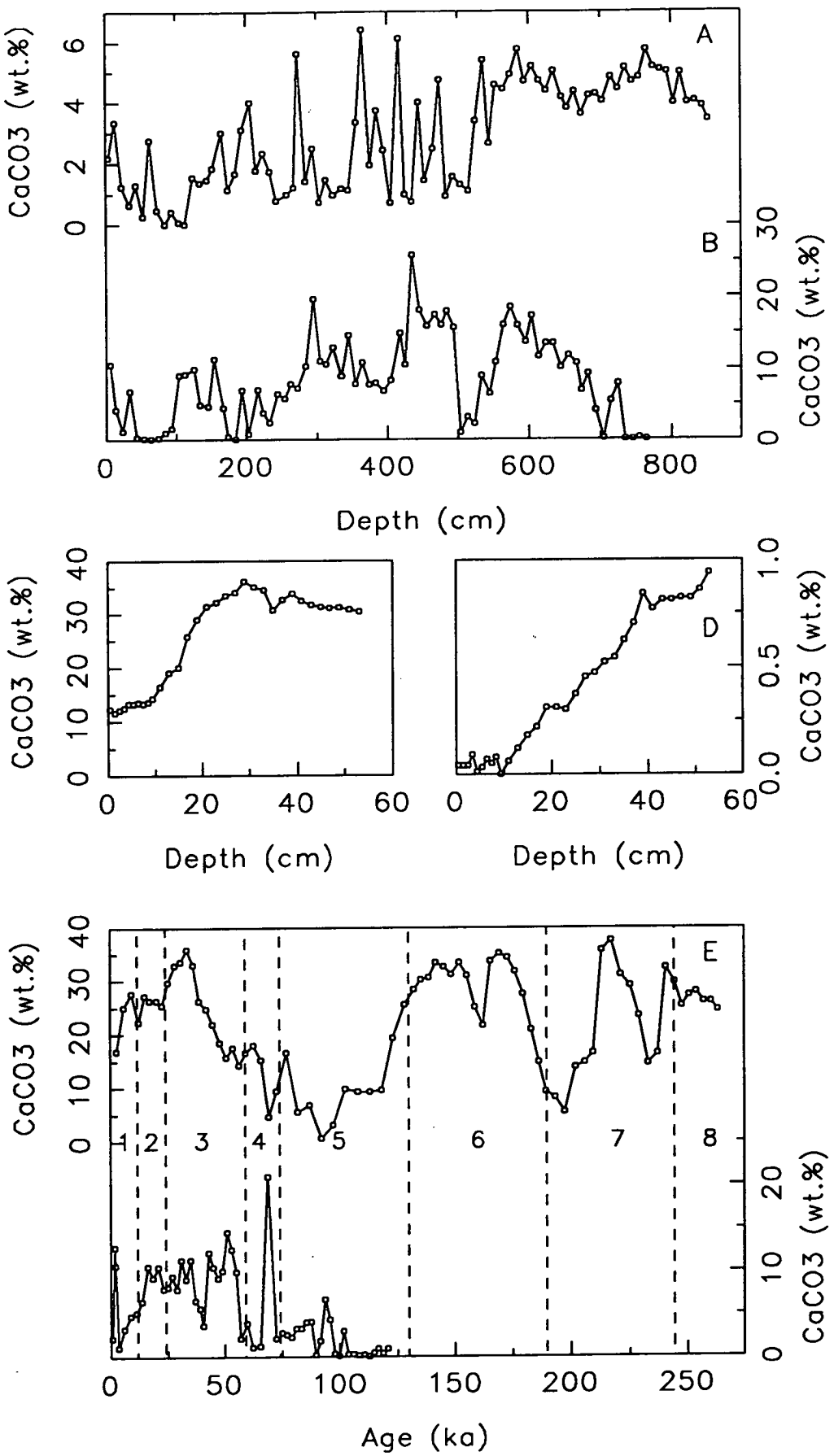


Figure 7.13. Calcium carbonate (wt.%) down-core profiles: A) CD38-09, B) CD38-10, C) box core CD38-02, D) box core CD38-03, E) CD38-02 and F) CD38-11.

depth from 550cm to the base of the core (most pronounced in $C_{org}$ and $CaCO_3$). In contrast, CD38-09 demonstrates very little correlation between $C_{org}$, bio.sil and $CaCO_3$ and, in fact, by comparing the average concentrations both above and below a transition zone about 530cm, it can be seen that the $C_{org}$ and $CaCO_3$ contents in CD38-09 are possibly inversely correlated.

b) In the box cores, there is a noticeable inverse relationship between the bio.sil and $CaCO_3$ concentrations, with the former showing a generally decreasing trend with depth whilst the latter increases. The reason for this variation is unlikely to be simply caused by dilution because core CD38-02 has a dramatically higher $CaCO_3$ content (and slightly lower bio.sil) compared with CD38-03.

c) More accurate temporal fluctuation interpretations can be made for piston cores CD38-02 and CD38-11, which have their biogenic concentrations plotted against age (ka) in Figs 7.11 to 7.13. The general trend of decreasing $C_{org}$ contents with increasing sediment age, due to decomposition of organic matter upon burial, does not show a smooth exponential profile in cores CD38-02 or CD38-11 but is distorted by peaks and troughs. These show no obvious glacial/interglacial pattern except for the general increase of $C_{org}$ (wt.%) from the earlier to the later parts of interglacial stage 5.

d) The bio.sil and $CaCO_3$ signals in core CD38-02 are, at first sight, inversely related with relatively higher bio.sil during interglacial stages 1, 3, 5 and 7 and higher $CaCO_3$ during glacial stages 2, 6 and 8. However, closer examination of the down-core profiles (Figs 7.12 and 7.13) shows that the magnitude and timing of each of the glacial/interglacial cycles of bio.sil and $CaCO_3$ are not exactly similar. This indicates that the concentration of the biogenic components are controlled by factors which affect the amplitude of variation and the relative lag of each individual component to different degrees, which may, or may not, be related to global climatic changes.

e) Core CD38-11 contains approximately half the $CaCO_3$, but double the bio.sil, content when compared with CD38-02. Although there are spatial differences in the biogenic input to the sediment at these two sites (Fig. 7.10), the temporal variations shown within CD38-11 are coincident with those in CD38-02, with generally higher interglacial bio.sil and glacial $CaCO_3$.

f) The ash band found at 186ka in core CD38-02 (7.2.3) is characterised by a low $C_{org}$ concentration but by normal levels of bio.sil and $CaCO_3$. In contrast, the turbidite zone in core CD38-11 at about 2-3ka contains an enrichment

(compared with the surrounding sediments) of $C_{org}$ and $CaCO_3$ but a depletion of bio.sil.

**Biogenic component fluxes**

The problem of dilution which affects the above down-core profiles of the biogenic components expressed as a wt.%, can be removed by the calculation of mass accumulation rate (MAR) fluxes. As was the case in the terrigenous input section (7.2), the MAR fluxes of $C_{org}$, bio.sil and $CaCO_3$ have only be calculated for cores CD38-02 and CD38-11. The fluxes have been calculated using Eqn 7.2, and it must be remembered that, because of the possible errors involved (7.2.2), MAR fluxes are not the perfect solution to the representation of the true biogenic flux input.

The biogenic flux data is presented in full in Appendix C.19 and summarised below in Table 7.5, giving the range and mean values of $C_{org}$, bio.sil and $CaCO_3$ MAR fluxes. The average fluxes for four piston cores from the Eastern Equatorial Pacific (Patience, 1992) are also given in Table 7.5, for comparison with the Peru margin cores.

| (MAR = mg $cm^{-2}$ $kyr^{-1}$) | | Corg MAR | Bio.Sil MAR | CaCO3 MAR |
|---|---|---|---|---|
| CD38-02 | Range | 11.8-59.0 | 75.0-179.8 | 7.0-781.7 |
| (2525m) | Mean | 29.2 | 119.7 | 457.1 |
| CD38-11 | Range | 57.3-127.2 | 94.3-530.6 | 0-586.0 |
| (3835m) | Mean | 91.4 | 295.7 | 154.5 |
| Patience (1992) | | 60 | 133 | 1948 |

Table 7.5. Biogenic component mass accumulation rate fluxes (all in mg $cm^{-2}$ $kyr^{-1}$) for the Peru margin cores CD38-02 and CD38-11 and an average for four cores from the Eastern Equatorial Pacific (Patience, 1992).

From the data in Table 7.5, it can be seen that both CD38-02 and CD38-11 display large fluctuations in the flux of all three of the biogenic component inputs, with mean values which are higher in $C_{org}$ and bio.sil for CD38-11 but higher in $CaCO_3$ for CD38-02. Comparisons between the Peru margin and E. Equatorial Pacific (Patience, 1992) show rough agreement for the flux of organic carbon to the sediments but contrasting fluxes for the other two biogenic components, with core CD38-11 receiving over double the flux of bio.sil and the mean $CaCO_3$ flux of the E. Equatorial Pacific being four times that of core CD38-02.

The down-core profiles of the above biogenic MAR fluxes plotted against age (ka) are illustrated in Fig. 7.14 for cores CD38-02 and CD38-11. The $C_{org}$ MAR at the Nazca ridge site (CD38-02) is relatively stable during stages 6, 7 and 8 at about 20-30 mg $cm^{-2}$ $kyr^{-1}$ followed by a drop at the beginning of interglacial stage 5 to only 12 mg $cm^{-2}$ $kyr^{-1}$, which steadily rises up to a maximum of 60 mg $cm^{-2}$ $kyr^{-1}$ during glacial stage 2. This glacial maximum, however, is not seen in the $C_{org}$ MAR flux of the Peru continental slope (CD38-11) where maxima are seen during interglacial stages 3 and 5.

The bio.sil MAR profiles also contrast between the two cores, where from stage 5 up to the present Holocene, core CD38-02 displays a generally increasing trend and core CD38-11, a generally decreasing trend. The actual pattern of $CaCO_3$ variation has not been affected by the change from wt.% to MAR fluxes (compare Figs 7.13 and 7.14) especially for CD38-02. The glacial/interglacial cyclicity of relatively higher glacial flux to the sediment of $CaCO_3$ shells (complicated by the peaks during stages 3 and 7) gives rise to the question of whether this signal is produced by surface-water productivity variations or by preservation changes (dissolution effects) or by a complex interplay of both environmental factors (7.3.3).

### 7.3.3. Biogenic environmental interpretations

This section will discuss the biological and oceanographic environmental controls on the deposition of biogenic material along the Peru continental margin by interpretation of the geochemical data described above (7.3.2). Since the concentration of each component is critically dependant on the complex (and ever changing) interactions of the four factors described in the introduction above (7.3.1), this discussion section cannot be easily split into separate sections which will each interpret one particular environmental condition (as was done for 7.2.3). Therefore, the organic carbon, biogenic silica and calcium carbonate geochemical data will each be interpreted in turn and then, in the conclusions the overall palæo-oceanographic history of the Peru margin will be discussed.

#### Organic carbon

This thesis has already shown that the upwelling movement of nutrient-rich water (which replaces the nutrient-poor surface water pushed off-shore by Ekman transport) helps to sustain high levels of biological productivity, resulting in an

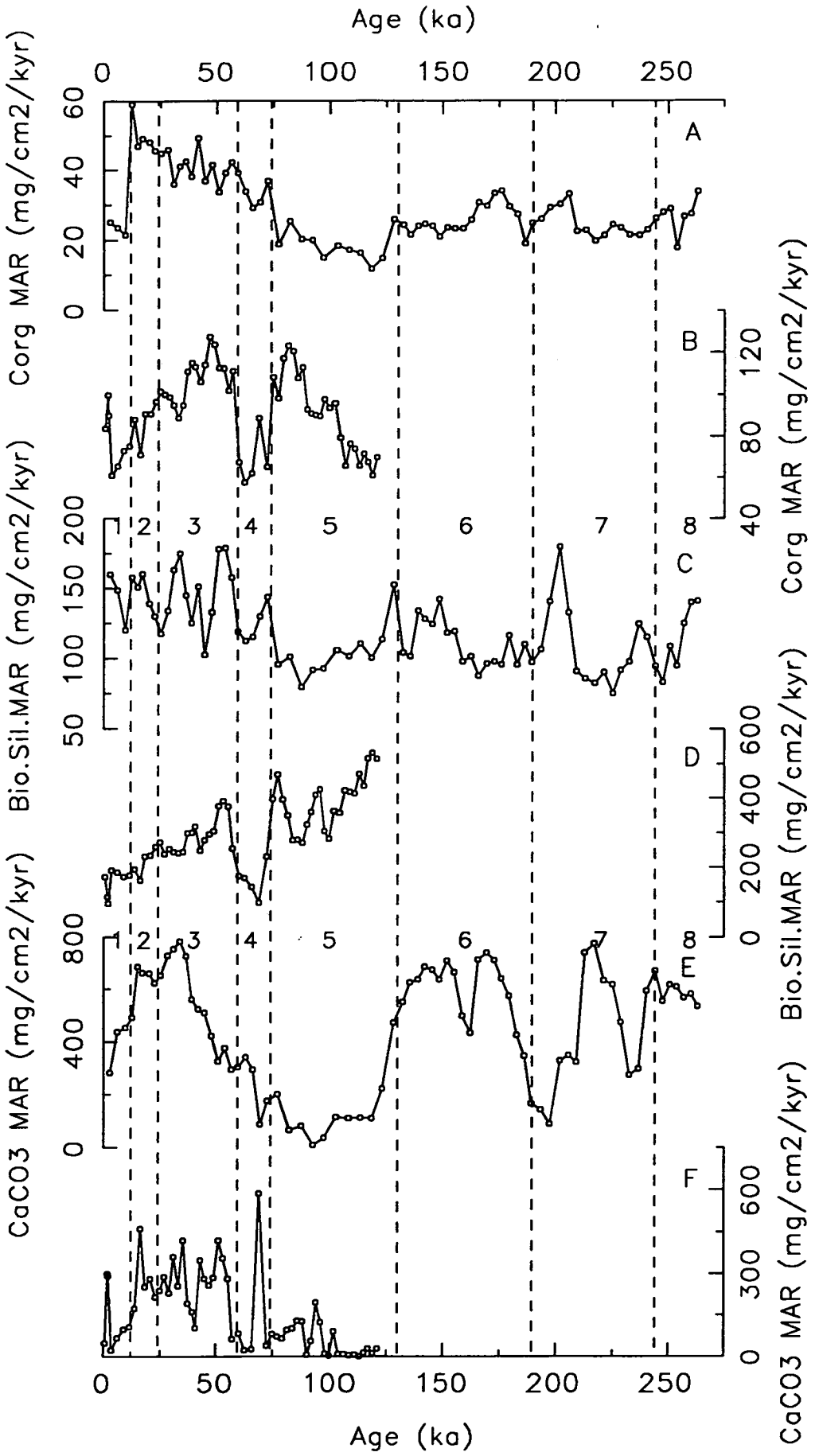


Figure 7.14. Organic carbon, biogenic silica and calcium carbonarte flux (mg $cm^{-2}$ $kyr^{-1}$) profiles against age for cores CD38-02 (A, C and E) and CD38-11 (B, D and F).

anomalously high flux of organic matter in the water column and high concentrations of $C_{org}$ in the sediment below (Chapter 3; Reimers and Suess, 1983A; Henrichs and Farrington, 1984).

Thus, the productivity control of coastal upwelling is the initial environmental factor which influences the concentrations of $C_{org}$ measured in these marine sediments. Its dominance over other possible factors, in terms of the spatial variance of the $C_{org}$ concentrations along the Peru margin, is supported by the mean and surface data for the sediments in this study (Table 7.4) which shows higher $C_{org}$ contents in the two near-shore core sites (CD38-09 and CD38-10) which are located within the main coastal upwelling zone, compared to the other sites which occur either seaward or at a more southerly location from the upwelling zone.

The plot of water depth against $C_{org}$ (Fig. 7.10) which indicates a decrease in the $C_{org}$ concentration of surface sediments with increasing water depth is, therefore, showing the near-shore proximity to the coastal upwelling zone rather than a pattern of equal $C_{org}$ surface-water levels with the degree of organic matter decomposition dependant on the depth of water through which it falls.

This simple spatial control on the depositional differences in the input of organic matter between the core sites does not explain the temporal variation of $C_{org}$ (wt.%) seen within each core (Fig. 7.11). If a particular sediment site was receiving a constant flux of organic matter over a period of time (and all the other component inputs remained constant as well) then the level of organic matter (measured as $C_{org}$) would not be at a constant concentration but would exponentially decrease with depth/age due to the natural decomposition of the organic matter upon burial (Reimers and Suess, 1983B; Calvert, 1987). Of course, this ideal scenario is unlikely to exist in the marine environment due to one or more of the following factors:

1) changes in the surface-water productivity levels on a range of time scales from seasonal to glacial/interglacial periodicity,
2) variations in the degree of organic matter recycling in the water column,
3) changes in the strength of the dilution effects from one or more components, mainly terrigenous and other biogenic inputs,
4) differences in the redox environment at the sediment/water interface and the depth of the oxic layer within the sediment column,
5) variations in the sediment accumulation rate over time.

The down-core profiles of $C_{org}$ for the six cores all show a large degree of variation over time; very little of which can be easily explained by only one of the above and most of which is open to the question of a productivity and/or preservation control (Shimmield, 1992).

In core CD38-10, the prominent depletions of $C_{org}$ coincide exactly with the zones of phosphorite concentration (4.3.3), increased terrigenous input (7.2.3) and coarser sediment grain-size (Fig. 7.7). It is possible that this dilution control has occurred because of a decrease in the organic matter input relative to the authigenic and terrigenous component inputs to the sediment. However, it is far more likely that these phosphorite-rich zones correspond to periods of erosion of the sediment column by bottom-water currents, which have resuspended the organic matter (along with the fine-grained clays) and swept it down the continental slope to be redeposited at greater water depths. This theory is supported Walsh (1981) who studied the influence of modern-day Peru margin bottom-water currents on $C_{org}$ transport in relation to the Peruvian anchovy fishery, and can also explain the broad band of low $C_{org}$ contents found in core CD38-09 between 190 and 270cm.

The preservation and accumulation of $C_{org}$ was originally thought to have been strongly influenced by the redox environment of deposition, which allowed for faster decomposition of organic matter within oxic sediments compared with suboxic or anoxic sediments due to the differing pathways of degradation utilised (following the equations set out in Froelich *et al.*, 1979, Emerson, 1985). However, recent work has shown that organic matter decomposes as readily under anoxic as oxic conditions as a result of bacterial activity (Canfield, 1989; Pedersen and Calvert, 1990; Lee, 1992; Pedersen *et al.*, 1992).

The increase in $C_{org}$ concentration seen in core CD38-09 from about 3wt.% below 530cm to nearly 6wt.% above this zone may, a few years ago, have been interpreted as relating to the movement of this core site from above the oxygen minimum zone (OMZ) during a glacial stage to within the OMZ as the sea-level rose during an interglacial stage, producing increased preservation of organic matter under stronger anoxic conditions (Emerson, 1985). However, this cannot be the correct explanation because it was shown by using the halogen/$C_{org}$ ratios (6.2.3) that the sediment in CD38-09 has accumulated under continuous suboxic/anoxic conditions and also it is now generally believed that the OMZ plays only a small part in the preferential preservation of a high $C_{org}$ concentration record. In fact the opposite occurs, with the high rates of primary productivity in the surface waters off Peru producing the low benthic oxygen levels (Pedersen and Calvert, 1990).

The $C_{org}$ biogenic component input is therefore dominantly controlled by the rate of primary productivity (Pedersen *et al.*, 1992) along the Peru continental margin and, in order to avoid the effects of non-biogenic dilution, the $C_{org}$ MAR flux data can be interpreted to study possible palæo-productivity signals.

The average $C_{org}$ MAR flux at CD38-11 is approximately three times that of CD38-02 (Table 7.5) simply because of the position of the upwelling zone with respect to the two core sites. If it had been possible to calculate MAR flux data for cores CD38-09 and CD38-10, then the $C_{org}$ MAR would probably have needed to be expressed as g $cm^{-2}$ $kyr^{-1}$ instead of only mg $cm^{-2}$ $kyr^{-1}$ (Henrichs and Farrington, 1984).

Sarnthein *et al.* (1988) observed a marked increase in biological productivity at low- and mid-latitude upwelling zones during the last glacial maximum. This conforms to the hypothesis that polar ice-sheet growth reduced the latitudinal-size of the atmospheric pressure cells which increased the wind strength during glacial periods, causing more coastal and equatorial upwelling and thereby increasing the productivity of the marine biomass (Müller *et al.*, 1983; Pedersen, 1983; Lyle *et al.*, 1988). The $C_{org}$ MAR flux profile of CD38-02 (Fig. 7.14) does possibly show this glacial/interglacial pattern with relatively high $C_{org}$ input during glacial stages 2, 4 and 6 compared with the interglacial stages 1 and 5. However, core CD38-11 does not conform to the above hypothesis since it displays considerably higher $C_{org}$ MAR flux during stages 3 and 5 compared with stage 4. It is quite possible that the coastal upwelling off Peru has varied in its strength in time with the global climatic changes. However, these two core sites have received contrasting $C_{org}$ flux inputs over time, which is possibly due to the movement of the main upwelling zone along-shore and/or off-shore caused by sea-level and wind strength variations over glacial/interglacial periods.

The flux of biogenic barium to the sediment has already been used (for core CD38-02) to calculate a palæo-productivity signal of new production ($P_{new}$) levels in the surface-waters during the Late Quaternary (6.3.4, Dymond *et al.*, 1992). If the flux of organic carbon to the sediment can be used to estimate the levels of ocean productivity in the past, does it compare or contrast with the Ba calculations? In order to answer this question, the level of surface productivity must firstly be calculated and this can be done using the formula shown in Eqn 7.3, which is taken from the work by Müller and Suess (1979).

The relationship between $C_{org}$ and palæo-productivity (R) was thought to be dependant on the sediment accumulation rate, sediment porosity and dry bulk density (Müller and Suess, 1979) and although future studies tried to improve the equation (e.g. incorporation of a water depth factor, Sarnthein *et al.*, 1987) the original equation is still used to calculate palæo-productivity for cores CD38-02 and CD38-11.

Equation 7.3. Palæo-productivity from $C_{org}$ concentrations (Müller and Suess, 1979)

$$R = [C_{org} \times fs \times (1 - \phi)] / [0.0030 \times S^{0.30}]$$

where, R = Palæo-productivity (gC $m^{-2}$ $yr^{-1}$),
$C_{org}$ = organic carbon (wt.%),
fs = sediment density (g $cm^{-2}$),
$\phi$ = sediment porosity (% water / 100),
S = sediment accumulation rate (cm $kyr^{-1}$).

The results of this palæo-productivity calculation are presented in Appendix C.19, and Fig. 7.15 displays the down-core profiles of R against age for both cores. It is apparent from the results that, even once the differences in sedimentation rate and the physical properties of the sediments between the two cores sites (Chapter 2) have been taken into account, core CD38-11 still contains a higher palæo-productivity record compared with core CD38-02. However, neither cores achieve the levels of productivity that were measured by Müller and Suess (1979) at two sites on the Peru margin (330 gC $m^{-2}$ $yr^{-1}$) but this is simply due to the fact that these levels were measured at shallow water sites within the coastal upwelling zone, whereas cores CD38-11 and CD38-02 are located at some distance from this very high productivity zone.

The down-core profiles of palæo-productivity (Fig. 7.15) show no obvious glacial/interglacial pattern as would be expected if the high glacial productivity scenario of Sarnthein *et al.* (1988) was operating. However, the limitations of the calculation of R must be remembered, i.e. there is no mention in Eqn 7.3 of the depth/age of each sample which therefore ignores the effects of the natural decomposition of organic matter upon burial. The only similarity between the two core sites is the shape of the profile during interglacial stage 5, which displays a generally increasing level of R from 120ka up to 80ka, followed by a sharp drop over the transition from stage 5 into stage 4. This implies that after glacial stage 6, the productivity of the surface waters along the Peru margin dropped to a minimum and

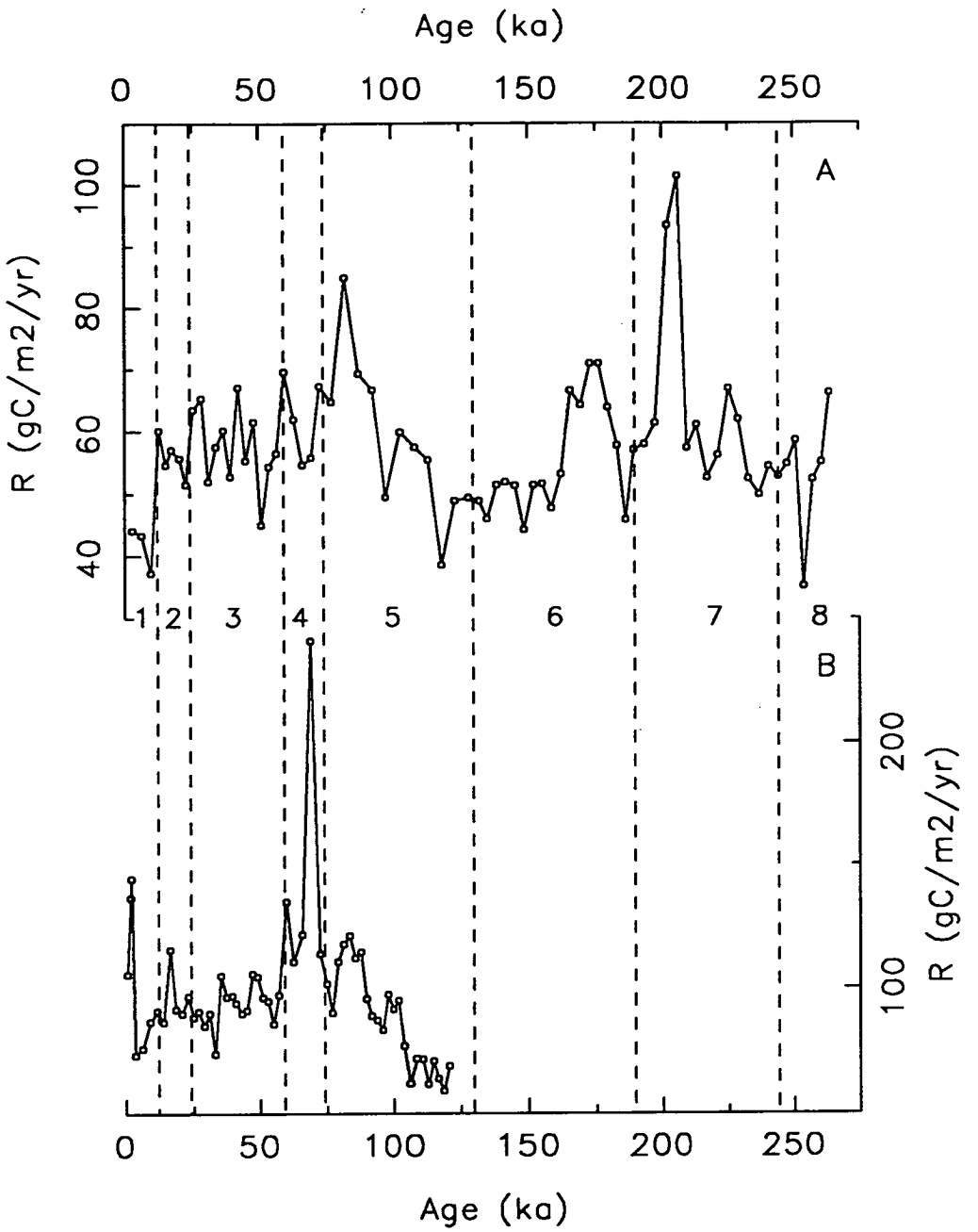


Figure 7.15. Palæo-productivity measurements calculated from Equation 7.3 (Müller and Suess, 1979) for cores CD38-02 (A) and CD38-11 (B).

then gradually (as the warm, interglacial stage continued) the productivity increased until it reached maximum levels, after which the productivity levels crashed with the onset of glacial climatic conditions. Perhaps the same scenario is occurring at both core sites during interglacial stage 1, which sees a drop from high, glacial stage 2 levels and shows signs of the start of an increase up to the present-day productivity levels.

The palæo-productivity profile of CD38-02 (Fig. 7.15) can be compared with the $P_{new}$ profile calculated from the Ba content of the same core (Fig. 6.10.C). The latter productivity record is a signal of new production in the water column, i.e. the amount of organic matter falling out of the euphotic zone (Dymond *et al.*, 1992). This is perhaps the reason why the levels of $P_{new}$ are considerably lower than those of R, which is an indicator of the surface-water levels of primary productivity. However, the two profiles do not really match in terms of the timing and magnitude of variations in productivity, except perhaps for the peak during stage 7 (about 200ka) and the trough during stage 4 (about 65ka). The reasons for the differences must be either due to the errors involved in the two palæo-productivity calculations (Eqns 6.2 and 7.3) or, more likely, caused by the contrasting geochemical behaviours of $C_{org}$ and Ba upon burial in the sediment column, i.e. the degradation of the former compared with the residual nature of the latter.

**Biogenic Silica**

The planktonic organisms which form their skeletons from silica (diatoms, radiolaria and silicoflagellates; Diester-Haass, 1988) are primary producers and their productivity should increase dramatically in fertile, upwelling areas (Chapter 3). If the record of their existence in marine sediments as biogenic silica, was controlled purely by the level of primary productivity in the overlying surface-waters, then the pattern of highest productivity above core sites CD38-09 and CD38-10 compared with the other sites in this study would be expected to show a similar surface-sediment wt.% bio.sil distribution to the one seen for organic carbon. However, in the plot of water depth against bio.sil (Fig. 7.10) the cores with the highest concentration are CD38-09 and CD38-03 and therefore the spatial distribution of bio.sil along the Peru margin must be controlled by more than one of the environmental factors listed in the introduction to this biogenic input section (7.3.1).

Sea-water and interstitial pore-waters are undersaturated with respect to silica (Wollast, 1974) and therefore the siliceous parts of marine organisms will be susceptible to dissolution as soon as they die. This recycles most of the silica within the euphotic zone (Calvert, 1968; Berger, 1976) as dissolved silicate; an essential nutrient for marine life. Murray (1987) estimated that, in the Pacific, only 8-11% of the biogenic silica which actually escapes from the euphotic zone survives to be incorporated into marine sediments. This dissolution means that under normal primary productivity levels all, or nearly all, the bio.sil is dissolved before reaching the sediment column (Diester-Haass, 1988) and so the very high mean bio.sil concentrations measured in the Peru cores (> 6wt.%, Table 7.4) can only be produced as a result of high productivity from coastal upwelling.

Other environmental factors to be considered include dilution effects by the $CaCO_3$ content of the sediment. This is probably dominating the variation in the down-core wt.% bio.sil profile of the box and piston cores CD38-02 (Fig. 7.12) but is definitely absent in the box core CD38-03, resulting in the high bio.sil concentration at this deep-water site (Table 7.4).

Dilution by terrigenous material is possibly the cause of the extreme fluctuations in the concentration of bio.sil seen in core CD38-10 (Fig. 7.12) which ranges from virtually zero up to nearly 30wt.% of the total sediment. The erosion and winnowing which explained the very low $C_{org}$ contents at certain horizons in this core has also produced the lowest bio.sil concentrations. The high energy environment of strong bottom-water currents along the continental shelf will tend to fragment the fragile diatom and radiolarian skeletons with the result that a greater surface area of bio.sil will be exposed to the undersaturated waters and will cause greater dissolution (Patience, 1992).

However, despite these environmental influences affecting the original bio.sil signal, many authors have considered the bio.sil concentration in marine sediments to be a rough reflection of the levels of primary productivity and upwelling (e.g. Molina-Cruz and Price, 1977; Broecker and Peng, 1982; Leinen *et al.*, 1986). As for the $C_{org}$ discussion above, it is easier to remove the influence of dilution caused by other sediment components and study the MAR flux of bio.sil, when interpreting the possible palæo-productivity signal.

The weight of bio.sil input which has been deposited at sites CD38-02 and CD38-11 is, on average , four to five times that of $C_{org}$ (Table 7.5) and its down-core profile (Fig. 7.14) has varied considerably over (although not exactly in phase with) the interglacial/glacial cycles of the Late Quaternary. Generally higher bio.sil fluxes

are associated with the interglacial periods (stages 3 and 7 in CD38-02 and stages 3 and 5 in CD38-11) but the timing and magnitude of these peaks are not consistent. If this is a purely productivity controlled signal then the bio.sil MAR broadly agrees with the Ba flux data (6.3.4) and implies that the palæo-productivity signals from bio.sil and $C_{org}$ are perhaps representing relative changes in the faunal composition of the marine biomass over time periods which are longer than just a simple seasonal fluctuation (Lyle *et al.*, 1988; Rea *et al.*, 1991). If, for example, the organic matter flux resulting from a predominantly diatom-based plankton biomass is considerably different from that of a predominantly foram-based biomass than the signal recorded in the sediment column would display contrasting bio.sil and $C_{org}$ MAR flux patterns (Patience, 1992).

Some marine sediment studies have examined the varying species-assemblage of the diatoms found in coastal sediments as a function of the levels of primary productivity and, hence, the strength of coastal upwelling (Abrantes, 1988; Schrader and Sorkness, 1991; Schrader, 1992). However, the changes in diatom assemblage over time are not reflected in the overall total bio.sil abundance measured in a sediment (pers. comm., H. Schrader, 1991) and therefore the results found by the above authors in terms of the palæo-productivity of the Peru and other upwelling ecosystems can not be directly compared with the bio.sil wt.% and MAR flux records presented in this thesis.

**Calcium Carbonate**

The carbonate shell-remains of foraminifera and coccoliths which are incorporated into marine sediments, have been measured in many cores as variations in the wt.% $CaCO_3$ which form cycles relating to the glacial/interglacial periodicity of the Late Quaternary (e.g. Pisias and Rea, 1988; Farrell and Prell, 1989, 1991; Rea *et al.*, 1991; Patience, 1992). Originally a relationship between the $CaCO_3$ content of oceanic sediments and climate was established by Murray and Philippi (1908) and this theory was supported by Arrhenius (1952) who concluded that Pleistocene climate changes increased the glacial trade winds and upwelling strength which was recorded by higher glacial $CaCO_3$ concentrations. It is possible that, as with the $C_{org}$ and bio.sil contents, the $CaCO_3$ input to a sediment is controlled by variations of palæo-productivity but there is also the environmental factors of faunal variations, dilution effects from the terrigenous detritus and dissolution of the carbonate shells within the water column to be considered.

Of the above, the latter is now generally accepted as being the most important factor in the variation of $CaCO_3$ content measured in marine sediments. The dissolution of $CaCO_3$ is thoroughly reviewed by Volat *et al.* (1980) but before the carbonate record of the Peru margin cores can be interpreted, the following brief explanation of carbonate dissolution is required.

Berger (1971) proposed a carbonate-solution ocean model which requires an equilibrium between the amount of carbonate being supplied to the oceans (from terrestrial weathering) and the amount taken out by organisms. If the latter exceeds the former, dissolution of carbonate is required to return the dissolved carbonate levels to equilibrium. Dissolution of $CaCO_3$ generally increases with water depth due to the thermodynamic effects at lower temperature and higher hydrostatic pressure which both increase the solubility of carbonate in water.

Therefore a simple model of carbonate dissolution can be envisaged within which a number of depth-boundaries have been defined. Dissolution increases dramatically below the "lysocline" (Berger, 1971), a depth defined as where the *in situ* carbonate ion concentration of the water is equal to the saturation level (Broecker and Takahashi, 1978). Below the lysocline lies a transition zone within which the majority of all dissolution occurs, down to the "calcite critical depth" (CCrD, Farrell and Prell, 1989) which is the shallowest pelagic depth where the sediments contain <10wt.% $CaCO_3$ (Lisitzin and Peltelin, 1967). The actual depth at which sediments contain no $CaCO_3$ because the rate of dissolution equals the rate of deposition (Farrell and Prell, 1989) is termed the calcite compensation depth (CCD) and although this lies only slightly deeper than the CCrD, the two should not be confused.

The above theory of increasing dissolution with water depth can explain the contrasting mean and surface $CaCO_3$ concentrations measured in cores CD38-02, CD38-11 and CD38-03 (Table 7.4 and Fig. 7.10). Core CD38-02 at less than 2500m water depth must lie above or very close to the lysocline in order to receive its high carbonate input.* In contrast, core CD38-11 at 3835m lies towards the lower end of the transition zone, possibly at the CCrD, resulting in much lower $CaCO_3$ levels and core CD38-03 at 4289m lies on or below the CCD resulting in minimal carbonate

*It should be noted that the high terrigenous flux along a continental margin (7.2.3) will prevent the $CaCO_3$ concentration from achieving the levels (up to 90wt.%) measured in cores at similar water depths but away from a strong terrigenous source.

deposition (the less than 1% $CaCO_3$ measured in this core may just be the result of errors in the Ca/Al ratio used in the calculation of wt.% $CaCO_3$, Appendix B.1).

However, if the $CaCO_3$ concentration was controlled only by the above dissolution theory then it would be expected that the shallow-water core sites would contain the highest wt.% $CaCO_3$ content. The data in Table 7.4 and Figs 7.10 and 7.13 show that this is not the case and cores CD38-09 and CD38-10 are sites of lower $CaCO_3$ concentration than site CD38-02. There are a few possible reasons for this anomaly. Firstly, the low carbonate concentrations may just be the result of dilution by the strong terrigenous input in these near-shore sediments. There may also be a preferential winnowing effect on the foraminifera and coccolith shells, which means they are swept down the continental slope by bottom-water current activity. This is illustrated in core CD38-10 as the virtual lack of carbonate content within the phosphorite-rich horizons. One final explanation could be that the presence of the oxygen minimum zone, impinging on the continental shelf at water depths within which CD38-09 and CD38-10 are located, lowers the pH of the water which increases the solubility of carbonate and, therefore increases the carbonate dissolution at these very shallow water depths (Steens *et al.*, 1991).

Thus, the spatial variance of carbonate concentrations in the Peru margin sediments can be explained as a function of the water depth of each core site influencing the degree of dissolution affecting the original productivity levels of calcium carbonate (Volat *et al.*, 1980). Does the same oceanographic process control the temporal fluctuations of $CaCO_3$ wt.% (Fig. 7.13) and MAR flux (Fig. 7.14) seen in the down-core profiles or do productivity and/or dilution variations play a more dominant role?

In sediments above the lysocline and under zones of high primary production, it is thought that variation in the volume of biogenic carbonate from the euphotic zone will be represented by similar changes in the input of carbonate to the sediment and recorded in the sediment column. Unfortunately, the two cores which could be examined to study this hypothesis (CD38-09 and CD38-10) because they are shallow-water cores located under the coastal upwelling zone are the ones for which MAR fluxes cannot be calculated (2.3.2). Therefore, their down-core signal (Fig. 7.13) is susceptible to an interpretation of variation in the strength of the terrigenous-dilution effect.

Recalculation of $CaCO_3$ wt.% into $CaCO_3$ MAR flux, in order to avoid these dilution effects, is possible for cores CD38-02 and CD38-11. The similarity of the profiles in Figs 7.13 and 7.14 for these two cores implies that dilution effects are, in

fact, minimal and that the variation in the bulk-sediment MAR is being principally controlled by the carbonate flux to the sediment and its variation over time. This interpretation is supported by comparison of the carbonate MAR down-core profile (Fig. 7.14) and the bulk-sediment MAR profile (Fig. 2.10).

The variations of $CaCO_3$ MAR flux during the Late Quaternary are quite smooth for core CD38-02 but very erratic for core CD38-11 (Fig. 7.14). This may be due to the fact that CD38-11 is located well within the carbonate transition zone and is therefore susceptible to changes in the degree of carbonate dissolution over shorter time scales than core CD38-02, which changes gradually over glacial/interglacial periods. This points towards a possible dissolution control on the temporal fluctuations of $CaCO_3$ flux in both these cores and leads on to the question of how the depth positions of the lysocline, CCrD and CCD have varied over time.

The depth of the lysocline is thought to have changed markedly during the global climatic cycles (shallowing by up to 800m in the central Pacific during interglacials) whilst the CCrD has remained relatively constant (Farrell and Prell, 1989). Therefore, significant variations in the thickness of the transition zone between the lysocline and the CCrD are envisaged over this time (Farrell and Prell, 1989, 1991; Rea *et al.*, 1991). The reasons for this variation are thought to be linked to circulation patterns of the ocean water masses (Berger, 1968; Broecker, 1971; Farrell and Prell, 1991) which brought more "corrosive" water to shallower depths during interglacial periods and increased the dissolution of carbonate material (Luz and Shackleton, 1975; Farrell and Prell, 1989). Therefore, if core CD38-02 on the Nazca ridge lies at the present day, and during previous interglacial periods, somewhere about the lysoclinal depth but well above it during glacial periods, this environmental fluctuation could produce the $CaCO_3$ MAR flux pattern displayed in Fig. 7.14. This interpretation is not ideal because it does not explain the peaks of carbonate input (lower dissolution periods?) during interglacial stages 3 and 7. It is possible that the strong down-core dissolution pattern is being overprinted on top of fluctuations of $CaCO_3$ input caused by changes in the primary production of carbonate microfossils over time.

## 7.4. OVERALL PALÆO-ENVIRONMENTAL CONCLUSIONS

This chapter has examined the deposition of the terrigenous and biogenic components on the Peruvian continental margin in terms of the spatial and temporal environmental parameters, which are recorded in the bulk geochemical signals of the

four piston and two box cores in this study. It would be more constructive to conclude and summarise the findings of this chapter by bringing together the various processes (climatic, oceanographic and biological) into an overall palæo-environmental picture of sediment deposition on the margin, rather than just simply summarise the results of each section above (7.2.3 and 7.3.3) individually.

The quote which began this chapter (7.1) has been shown to be quite true because, although the many processes which can control and affect the chemical composition of the various sediment components can be easily described, the correct interpretation of the strength and influence of each individual component is "difficult to induce because the [element] distributions are frequently the result of non-equilibrium processes" (Spencer *et al.*, 1968). However, it is safe to conclude that the two most important factors which affect the composition of these Peru margin sediments are the extreme closeness of the core sites to the continent and the high surface-water biological productivity which results from coastal upwelling.

The two environmental features above manifest themselves in the following geochemical signals:

A) Continental proximity

1) High mass accumulation rates of terrigenous derived clay and quartz detritus, seen in cores CD38-02 and CD38-11 as Al and $Si_{terr}$ MAR fluxes which are consistently above 75 and 200 mg $cm^{-2}$ $kyr^{-1}$ respectively (Table 7.2 and Fig. 7.8).

2) Terrigenous elemental ratios which are anomalously high compared with the average deep-sea clay (Turekian and Wedepohl, 1961), e.g. Si/Al and Zr/Rb in the two near-shore cores CD38-09 and CD38-10 indicate very high quartz and heavy mineral deposition compared with clays. These minerals tend to be coarse-grained and denser than alumino-silicate clays (Table 7.3) and therefore have a shorter history of transport from source (Andes and Peru coastal plain) to depositional environment.

3) The generally high terrigenous component input can produce strong dilution-effects when examining other geochemical records on a wt.% basis.

B) Coastal upwelling

1) High mass accumulation rates of organic carbon, biogenic silica and calcium carbonate calculated for cores CD38-02 and CD38-11 (Table 7.5 and Fig. 7.14) which are situated south and sea-ward from the strong upwelling zone respectively.

2) Anomalously high organic carbon concentrations (on average >5 times the normal for marine sediments) in cores CD38-09 and CD38-10, which are located directly under the main upwelling zone and at shallow-water depths. These cores are situated within the water-depth boundaries (100-400m; Veeh *et al.*, 1973) of the oxygen-minimum zone, which results from the intense bottom-water microbial decomposition of the high organic matter input (Pedersen and Calvert, 1990; Pedersen *et al.*, 1992).

3) The high biogenic component input can also produce strong dilution-effects (especially from $CaCO_3$) when examining other geochemical signals on a wt.% basis.

The spatial and oceanographic location of each core produce latitudinal and water-depth variations in the terrigenous and biogenic inputs and are highlighted by:

1) Possible source rock compositional differences in the Fe/Al and K/Al ratios measured in the northerly group of cores compared to the southerly ones.

2) The degree of dissolution of carbonate- and silicate-shelled planktonic organisms within the water column indicated by the water-depth against surface sediment $CaCO_3$ and bio.sil concentration plots (Fig. 7.10).

3) Differences between the fluvial- and aeolian-dominated transport on the land-ward and sea-ward sides of the Peru-Chile Trench respectively, as shown by both the volumetric (Al and $Si_{terr}$ MAR fluxes) and compositional (Fe/Al, Ti/Al and Zr/Rb) variation in the terrigenous components of cores CD38-03, CD38-11 and CD38-02.

On a temporal basis, the global climatic variations of the Late Quaternary have influenced the sediment terrigenous and biogenic compositional input over time. The following are just a few environmental factors which have affected the Peru margin during glacial/interglacial periodicity.

1) Sea-level change, caused by polar ice-sheet growth, results in extreme shallowing of the water-depths at CD38-09 and CD38-10 during glacial periods, which altered the terrigenous supply to these sites (Si/Al ratio; Fig. 7.1) and may have produced stronger bottom-water current activity and preferential erosion of fine-grained clays compared with heavy minerals (Zr/Rb ratio; Fig. 7.7). The strong coastal upwelling zone may also have moved off-shore and/or along-shore due to sea-level fluctuation which may, in turn, have altered the palæo-productivity pattern of the region and produced the $C_{org}$, bio.sil and $CaCO_3$ variation seen in the above two cores (Figs 7.11 to 7.13).

2) Movement of $CaCO_3$ dissolution depths occurs as a result of variation in the circulation pattern of the oceanic water masses in the Pacific (Farrell and Prell, 1989). This environmental process is probably the controlling factor on the carbonate profile (wt.% and MAR flux) of core CD38-02 (Figs 7.13 and 7.14). This site lies at 2525m at the present day on the Nazca Ridge which is probably just below the lysocline. However, during glacial periods, the depth of the lysocline deepened in the Pacific Ocean (Farrell and Prell, 1989) and CD38-02 would have sat well above the lysocline. In terms of carbonate dissolution and preservation, the $CaCO_3$ record of CD38-02 can be explained by interglacial stages as periods of relatively higher dissolution of $CaCO_3$ microfossils and hence lower preservation of the carbonate production signal compared with glacial periods, without the need for any significant variation in the surface-water production levels.

3) Fluctuations in the average wind strength during global climate change is caused by ice-sheet growth and latitudinal shrinking of the atmospheric pressure cells during glacial periods, resulting in stronger glacial winds (Sarnthein *et al.*, 1988). This natural process can significantly affect the strength of coastal upwelling and hence an increase of biological productivity along the Peru margin during the glacial periods is displayed in the sediment record as higher concentrations of the biogenic components (Fig. 7.11 and 7.12). Stronger winds can also transport greater volumes of terrigenous debris as airborne dust to the oceans and deposit it further from the continental source area. For this reason, and because the continents were more arid during the cold climatic stages, the glacial signal of terrigenous input shows higher mass accumulation rates (Fig. 7.8) and variation in some of the terrigenous element/Al ratios (Si/Al and Ti/Al; Figs 7.1 and 7.2).

However, the complex interplay of the climatic, oceanographic and biological systems results in marine sediment geochemical records which do not simply automatically switch between glacial and interglacial global conditions, and therefore they do not display down-core profiles which fluctuate in perfect timing with the stage boundaries.* There is a general tendency for the environmental processes to increase and/or decrease their influences and strengths to varying degrees within the climatic stages and to do so with differing lengths of lag or lead in relation to the glacial/interglacial periods. This results in terrigenous and biogenic component inputs which vary with non-linear relationships to time, such as seen in the Peru margin cores studied in this thesis.

*Of course, the global climate does not switch between the two extremes of glacial and interglacial stages instantly, but can take thousands of years to build up or remove glacial conditions. It is a gradual process over time, upon which the lines of stage boundaries have been placed as indicators of movement from a dominantly glacial period into a dominantly interglacial period, or vice versa.

# CHAPTER 8

# CONCLUSIONS

## 8.1. SCIENTIFIC RELEVANCE OF MARINE SEDIMENT STUDIES

"Nothing is rich but the inexhaustible wealth of nature.
She shows us only surfaces, but she is a million fathoms deep."
Ralph Waldo Emerson (1957)

The above quote brings to mind some aspects of this marine sediment geochemical study in terms of its scientific relevance. Firstly, there is the implication that nature is an extremely complex system, which depends on the interplay between marine life, terrestrial life, meteorology, climate conditions, ocean water movement and many other parameters. No science-based, environmental project is able to study all aspects of these processes, let alone interpret and understand all of them, and therefore each study must be biased towards attempting to understand just one small part of the "wealth of nature". This thesis has concentrated on the interpretation of the oceanographic conditions (biological, chemical and physical) which occurred along the Peruvian continental margin over the latter stages of the Quaternary period.

The second part of the quote could be interpreted as man's view of the oceans. From the land we can see only the surface of the sea but we know that it is within the deep, ocean waters and on the sea-floor that some of the most important natural processes occur, e.g. photosynthesis by marine phytoplankton, $CO_2$ uptake from the atmosphere and storage of the carbon (as $C_{org}$) in marine sediments below. It is only relatively recently that man has been able to study the deep-sea environment and to collect marine sediment cores, in order to analyse the important historical records contained within them. However, it must be remembered that in a study of such sediments, the cores analysed represent only a minute fraction of the total area of sea-floor in the region of interest. Therefore, any interpretations and conclusions made from cores (such as the CD38 ones) may be representative of only localised features and not of the overall regional palæo-environmental picture.

Finally, the quote is a reminder of the fact that nature supplies man with many resources, some of which are regarded as riches, e.g. gold and diamonds. Natural oil and gas could nowadays be included in the above category and this study has concentrated on a particular type of marine sediment which can be a precursor, source-rock to these important fossil fuels. The coastal upwelling region of Peru supplies a high flux of biogenic debris to the accumulating sediment column which, under the correct geological conditions, may be regenerated as an oil or gas deposit in the future (Calvert, 1987). Unfortunately, the petroleum-forming process takes millions of years to occur, but if studies, such as this, can lead to a greater

understanding of the environmental controls on the formation of organic-rich sediments, then perhaps this will result in the location and recovery of further fossil fuel deposits at the present day. Another natural resource studied in this thesis is the mineral phosphorite, found as hardgrounds, nodules and pellets within the sediments of the Peru margin. Phosphorites are formed by a complex series of diagenetic processes at the sediment/water interface (Froelich *et al.*, 1988). Present-day formation occurs along continental margins under zones of strong coastal upwelling and, in time, may produce large phosphate ore deposits such as those of economic importance in the agricultural fertiliser industry today (Cook *et al.*, 1990).

## 8.2. THE GEOCHEMICAL PALÆO-OCEANOGRAPHY AND MINERALOGY OF MARINE SEDIMENTS FROM THE PERUVIAN CONTINENTAL MARGIN

Each of the preceding chapters has sections contained within it (2.5, 3.4, 4.4, 5.3.3, 5.4.3, 6.6 and 7.4) in which the main conclusions of this study are individually presented. However, by bringing together the interpretations and hypotheses that have been drawn from this geochemical analysis of the Peru margin sediments, it is possible to present the following general statements regarding the palæo-environmental and palæo-oceanographic features of the area and their influence upon the sediment composition.

### Oceanographic setting

The specific location of the CD38 cores, on the shelf and slope of the Peruvian continental margin, has produced marine sediments which can be distinguished from deep-sea sediments by the following features.

1) The proximity of the continental land-mass of South America results in a strong, but highly variable, input of terrigenous, detrital material. The terrigenous component supplies up to 90 wt.% of the total sediment composition. This results in high concentrations of elements such as Si, Al, Fe, Ti and K, from quartz, clays, feldspars and heavy minerals.

2) The high rate of sediment accumulation along the Peru margin produces sediment cores which preserve a high resolution signal of sediment input. Cores CD38-02 and CD38-11 have sediment accumulation rates which have been measured

at between 2 and 5 cm $kyr^{-1}$ and it is expected that the shallower-water cores, CD38-09 and CD38-10, have accumulated at faster rates. Unfortunately, these near-shore sediments have suffered from periods of sediment erosion and/or turbidite deposition resulting in depth/age models which are distorted and susceptible to errors in their interpretation.

3) A wide range of water-depths and environments of sediment deposition can be achieved for cores taken on a continental margin from a relatively small area, compared with the deep-ocean floor. This allows for inter-core comparison of the effects of many geochemical processes, such as carbonate dissolution and terrigenous transport patterns, to be examined. The carbonate profile of core CD38-02 from an intermediate water-depth has been interpreted as representing its position relative to variation of the lysoclinal-depth at the Nazca Ridge. This same core was shown to have a terrigenous component which varies in its Fe/Al, K/Al, Ti/Al and Zr/Rb element ratios compared with cores CD38-03 and CD38-11. The oceanic setting of the Nazca Ridge (on the sea-ward side of the Peru-Chile Trench) limits its terrigenous input to only that from aeolian transport, in comparison with the latter cores (on the land-ward side of the trench) which receive a mixture of fluvial- and aeolian-transported terrigenous material.

**Coastal upwelling**

The continental margin of Peru is a region of the Pacific Ocean which is strongly influenced by the physical phenomena of persistent coastal upwelling of cold, nutrient-rich water into the euphotic zone and the resultant high marine biological productivity (Suess and Thiede, 1983). Even though the majority of the organic matter and other biogenic-remains is recycled within the water column, an enhanced flux of this material reaches the sediment/water interface for incorporation into the sediment column. This manifests itself as an enrichment of the following geochemical components.

1) Organic carbon: within cores CD38-09 and CD38-10, the $C_{org}$ concentration was measured as over an order of magnitude greater than that found in deep-sea sediments. Down-core variation of the organic matter concentration may be a result of off-shore and/or along-shore movement of the main coastal upwelling zone in response to shifting wind patterns (the atmospheric driving-force behind upwelling).

2) Biogenic-remains: the hard-part shells of plankton which survive water-column dissolution were measured geochemically as enrichments of biogenic silica and calcium carbonate. During the microscopic examination of the >63μm sediment fraction of cores CD38-09 and CD38-10, strong preservation of fish bones and scales was also recorded.

3) Barium: this trace element is associated with biogenic productivity within the water column but survives dissolution to be measured as a residual component in oxic, marine sediments. By using the present-day relationship between Ba and organic matter (Dymond *et al.*, 1992) palæo-productivity levels at core site CD38-02 were calculated, which suggest that intense surface-water biological production occurred during interglacial periods.

4) Halogens: uptake of iodine by organic matter occurs at a rate which is dependent on the redox state at the sediment/water interface. Anoxic (lack of oxygen) conditions exist at sites CD38-09 and CD38-10, resulting in lower $I/C_{org}$ compared with the other oxic cores in this study. Organic matter flux changes may be recorded by I/Br ratio variations in oxic environments (CD38-02) though the exact chemical mechanisms of the halogen-organic carbon relationships are still poorly understood (Shimmield and Pedersen, 1990).

5) Trace metals: within the water column, the high flux of organic matter along the Peru margin can scavenge large quantities of metals, such as Mo, U, Cr, V, Cu and Ni, and incorporate them in the sediment column. In cores CD38-09 and CD38-10, the down-core profiles of the metal enrichment factors resemble the respective $C_{org}$ profile, supporting a hypothesis of strong organo-metallic relationships in anoxic marine sediments (McNeill and Shimmield, 1991). The metal/$C_{org}$ ratios show good agreement between the two shallow-water cores and may be useful in future studies of an anthropogenic, metal-polluted environment.

**Chemical diagenesis**

The concentration of organic matter, which was introduced to the Peru margin sediments as a direct result of coastal upwelling, is the main reason for the following chemical conditions and diagenetic processes.

1) Redox environment: bottom-water dissolved oxygen levels are reduced to a minimum in zones where the high flux of organic matter produces intense benthic activity by microbial bacteria, which utilise oxygen in decompositional processes. An oxygen minimum zone (OMZ) exists between 100 and 400m water-depth off Peru under coastal upwelling zones (Veeh *et al.*, 1971) and impinges on the sea-floor at sites CD38-09 and CD38-10. As a result, these sediments are accumulating under a reduced, anoxic environment, which is geochemically represented by low $I/C_{org}$ and Ba/Al ratios compared with the oxic cores of CD38-02 and CD38-11. The Mo/U ratios from the CD38 cores contradict the established palæo-redox theory of Bertine and Turekian (1973) due to their complex organo-metallic relationships and diagenetic mobility.

2) Phosphorite pellets: carbonate fluorapatite (CFA) mineral growth occurs as a result of the release of phosphorus from decaying organic matter into near-surface pore-waters in a suboxic/anoxic environment. Authigenic precipitation of CFA is a two-stage process from the pore-water phosphate onto the surfaces of other mineral grains and diatom/foraminifera shells (Froelich *et al.*, 1988). This formation of phosphorite pellets can incorporate many elements into its crystal lattice, including U, Sr, Ba and Y. The presence of disseminated phosphorite pellets throughout the sediments of cores CD38-09, CD38-10 and CD38-11 has been demonstrated using pore-water phosphate profiles and sediment phosphorus partitioning equations.

3) Trace element partitioning: the concentrations of multi-phase elements (U, Sr and Y) are partitioned into their organic, terrigenous, phosphorite and/or carbonate phases using a series of geochemical-relationship equations. The trace element/$P_{phos}$ ratios in the Peru margin phosphorites are quantified to allow for the calculation of the $U_{org}$, $Sr_{calcite}$ and $Y_{terr}$ concentrations in the CD38 piston cores.

**Climate change**

The period of time during which the cores studied in this thesis accumulated on the Peru margin, was one of relatively intense and frequent variation between glacial and interglacial conditions of the global climate. These Late Quaternary climate changes are due to the orbital position of the Earth relative to the Sun (Imbrie *et al.*, 1984) and have resulted in polar and continental ice-sheet growth during glacial periods. Glacial/interglacial periodicity has affected the Peru margin in the following manner.

1) Wind-strength variation: latitudinal shrinking of the pressure-cells around which the Pacific wind-systems move resulted in stronger glacial winds. This may have induced more intense coastal upwelling off Peru and increased the biological production of the area and/or moved the main zone of primary productivity off-shore and along-shore. Both of the above scenarios could be responsible for the variation of the biogenic components recorded in the Peruvian marine sediment cores. Stronger winds and continental aridity during glacial periods (Sarnthein *et al.*, 1984) may also have blown more terrigenous detritus into the ocean, to produce the increased terrigenous mass accumulation rates (Al and $Si_{terr}$) measured in cores CD38-02 and CD38-11.

2) Eustatic variation: the global sea-level has fluctuated by about 50-100m in response to ice-sheet growth/decay during the glacial/interglacial stages of the Late Quaternary (Fairbanks, 1989). A drop in glacial sea-level of this magnitude at the near-shore core sites, CD38-09 and CD38-10, is thought to be responsible for the zones of sediment erosion, when stronger bottom-water currents winnowed down-slope the fine-grained clays, leaving behind a concentration of phosphorite pellets and other heavy minerals. The phosphorite formed hardground beds which subsequently broke up into flat nodules. Such nodules have been found in a position in the sediment column (273cm in CD38-09) which indicates a younger age than their actual U/Th radiochemical age of formation (114ka) suggests. The contrasting geochemical behaviour of Rb (in fine-grained clays) and Zr (in coarse-grained zircon) results in a Zr/Rb ratio, whose down-core profile displays peaks during these glacial, erosion events, illustrating its use as a sediment grain-size indicator.

3) Water mass circulation: glacial/interglacial variation in the pattern of water mass movement around the Pacific can alter the water-depth of the lysocline, below which the majority of carbonate dissolution occurs (Farrell and Prell, 1989). Strong variation in the concentration and flux of $CaCO_3$ presented for the Nazca Ridge site, CD38-02, can be explained by dissolution variation due to lysoclinal-depth movement resulting in a glacial/interglacial preservation signal rather than a productivity one (better preservation during glacial periods).

The hypothesis above of stronger upwelling during glacial periods contradicts the results from the barium-productivity calculations for CD38-02 (which peaked during interglacials) and therefore, further and more detailed work is required in order

to solve this enigma. It is thought that the impact of wind strength variation on productivity in the oceans is probably decoupled over the 100,000 year glacial/interglacial periodicity. The barium signal is probably also affected by changes in the deep-ocean circulation (Lea and Boyle, 1990B, Dymond *et al.*, 1992) over this long term climate change. However, at this moment not enough is known about the exact mechanisms and strengths of these complex palæo-oceanographic processes.

## 8.3. SUGGESTED FUTURE WORK

This geochemical study has measured the concentrations and fluxes of many elements and sediment components from the marine sediments of the Peruvian continental margin. However, there are some geochemical parameters whose results and down-core profiles merit a more thorough examination. The following could be studied in the future in order to expand on the hypotheses presented and/or to determine the exact causes of various marine geochemical relationships.

1) Organo-metallic ratios: organic matter has been shown to have a strong relationship with particular metals. The exact mechanisms/bonding structures of organo-metallic scavenging in sea-water could be examined by a detailed organic geochemical study of the sediments from cores CD38-09 and CD38-10.

2) Barium and palæo-productivity relationship: core CD38-02 contains a Ba flux signal which matches that of the glacial/interglacial oxygen isotope profile from foraminifera microfossils. It would be interesting to measure closely the timing of these profiles with respect to each other in order to determine if there is a consistent lead or lag of the increased productivity in the surface waters around the Nazca Ridge relative to the onset of an interglacial period. This future work could closely examine a glacial/interglacial stage boundary using very high resolution Ba and oxygen isotope analyses from closely-spaced (every 1-2cm) sub-samples from core CD38-02.

3) I/Br and Sr/Ca ratios: these two geochemical ratios show down-core variation (in cores CD38-02 and CD38-11) which may be linked to changes in the structure of the marine biomass over glacial/interglacial periodicity. The sediments of the Peruvian margin could be used in an in-depth study of the close, but highly variable, relationship between various types of organic matter and the halogens; which is known to be dependant on both the redox environment of deposition and the depth of sediment burial. Inductively-coupled plasma mass spectrometry (ICP-MS) could

possibly be used to examine any differences in the Sr/Ca ratio of foraminifera microfossils compared with that of coccoliths, and to determine if this signal changes over time.

4) U/Th radiochemistry of phosphorites: the average age of 114ka for the phosphorite material of the nodule in CD38-09 supported the prevailing hypothesis of initial pellet formation during an interglacial period under a coastal upwelling zone followed by concentration and conglomeration into a hardground nodule during a glacial period. However, more evidence for this theory could be gained by carrying out further U-series disequilibrium radiochemical measurements of the Peruvian phosphorites. Such work may also help in the calculation of sedimentation rates for the two near-shore cores, if the phosphorite zones at 273cm in CD38-09 and at about 90cm in CD38-10 are shown to contain phosphatic material of the same age.

The following are possible future areas of study which would be able to use some of the results and interpretations presented in this thesis.

1) Time-series spectral analysis of the geochemical signals (such as Ba/Al, $CaCO_3$, Ti/Al, $Si_{terr}$/Al) measured in core CD38-02 may generate results which would demonstrate which of the Milankovitch orbital frequencies (eccentricity, tilt or precession) is dominating the variation in input of the biogenic and terrigenous components to the sediment at the Nazca Ridge. This core would need to be used because, of the four piston cores in this study, CD38-02 has the most accurate age model.

2) A more detailed mineralogical examination of the down-core changes in both terrigenous and authigenic minerals in cores CD38-09 and CD38-10 may reveal more evidence of continental margin erosion events. Of most interest would be the diagenetic formation of phosphorite pellets and the mineralogical associations of the nodules in the phosphorite-rich zones. This work could involve both thin-section studies and scanning electron microscopy.

3) The Zr/Rb ratio has been used in this thesis as a trace element indicator of the average grain-size of marine sediments. Detailed particle size profiles of the terrigenous component in cores CD38-09 and CD38-10 could be obtained using a laser particle size analyser. This would provide a means of proving the existence of

(and perhaps allow for the quantification of) such a geochemical/physical sediment relationship.

Finally, now that most of the co-workers (1.5) in this multi-disciplined study have completed their respective projects, there is a need for all the results, interpretations and conclusions to be drawn together. The process of scientific discussion between geochemists, sedimentologists and micro-palæontologists may lead to a greater understanding of each individual's results, regarding the marine sediments recovered by *R.R.S. Charles Darwin* Leg 38 from the Peruvian continental margin.

# REFERENCES

Abrantes, F. (1988) Diatom assemblages as upwelling indicators in surface sediments off Portugal. *Mar. Geol.* **85**, 15-39.

Ahrens, L.H. (1952) The use of ionization potentials. Part 1. Ionic radii of the elements. *Geochim. Cosmochim. Acta* **2**, 155-169.

Altschular, Z.S. (1980) The geochemistry of trace elements in marine phosphorites, Part 1. Characteristic abundances and enrichment. In *Marine Phosphorites: A Symposium* Society of Economic Paleontologists and Mineralogists, Special Publication Vol. 29 (Ed. Y.K. Bentor), pp.19-30.

Arrhenius, G.O. (1952) Sediment cores from the East Pacific. In *Reports of the Swedish Deep-Sea Expedition* (Ed. H. Pettersen), Vol. 5, pp.1-227.

Arrhenius, G and Bonatti, E. (1965) Neptunism and vulcanism in the ocean. *Progress in Oceanography* (Ed. M. Sears), Vol. 3, pp.7-22. Pergamon Press, Oxford.

Atlas, E. and Pytkowicz, R.M. (1977) Solubility behaviour of apatites in seawater. *Limnol. Oceanog.*, **22**, 290-300.

Baker, K.B. and Burnett, W.C. (1988) Distribution, texture and composition of modern phosphate pellets in Peru shelf muds. *Mar. Geol.* **80**, 195-213.

Bakun, A. (1990) Global climate change and intensification of coastal ocean upwelling. *Science* **247**, 198-201.

Balistreri, L.S., Brewer, P.G. and Murray, J.W. (1981) Scavenging residence times of trace metals and surface chemistry of sinking particles in the deep ocean. *Deep-Sea Res.* **28**, 101-121.

Balistrieri, L.S. and Murray, J.W. (1986) The surface chemistry of sediments from the Panama Basin: the influence of Mn oxides on metal adsorption. *Geochim. Cosmochim. Acta* **50**, 2235-2243.

Barber, R.T. and Smith, R.L. (1981) Coastal upwelling ecosystems. In *Analysis of Marine Ecosystems* (Ed. A.R.Longhurst), pp.31-68. Academic Press, New York.

Baturin, G.N. (1982) *Phosphorites on the Sea Floor - Origin, Composition and Distribution. Developments in Sedimentology*, Vol. 33, 343pp. Elsevier, Amsterdam.

Baturin, G.N. and Bezrukov, P.L. (1979) Phosphorites on the sea floor and their origin. *Mar. Geol.* **31**, 317-332.

Baturin, G.N., Kochenov, A.V. and Senin, Y.M. (1971) Uranium concentration in Recent ocean sediments in zones of rising currents. *Geochem. Int.* **8**, 281-286.

Baturin, G.N. and Shishkina, O.V. (1973) Fluorine in the course of phosphorite formation in the ocean. *Okeanologiya* **4**.

Berger, W.H. (1968) Radiolarian skeletons: solution at depth. *Science* **159**, 1237-1238.

Berger, W.H. (1971) Sedimentation of planktonic foraminifera. *Mar. Geol.* **11**, 325-358.

Berger, W.H. (1976) Biogenous deep-sea sediments: production, preservation and interpretation. In *Chemical Oceanography* (Eds J.P. Riley and R. Chester), Vol. 5, pp.265-374. Academic Press, New York.

Berger, W.H. and Vincent, E. (1986) Deep-sea carbonates: reading the carbon-isotope signal. *Geologische Rundschau* **75**, 249-269.

Berner, R.A. (1973) Phosphate removal from sea water by absorption on volcanic ferric oxides. *Earth Planet. Sci. Lett.* **18**, 77-86.

Bertine, K.K. (1972) The deposition of molybdenum in anoxic waters. *Mar. Chem.* **1**, 43-53.

Bertine, K.K. and Goldberg, E.D. (1977) History of heavy metal pollution in Southern California coastal zone - Reprise. *Environ. Sci. Technol.* **11**, 297-299.

Bertine, K.K. and Turekian, K.K. (1973) Molybdenum in marine deposits. *Geochim. Cosmochim. Acta* **37**, 1415-1434.

Bischoff, J.L., Heath, G.R. and Leinen, M. (1979) Geochemistry of deep-sea sediments from the Pacific manganese nodule province: DOMES sites A, B and C. In *Marine Geology and Oceanography of the Pacific Manganese Nodule Province* (Eds J.L. Bischoff and D.Z. Piper), pp.397-473. Plenum Press, New York.

Bishop, J.K. (1988) The barite-opal-organic carbon association in oceanic paticulate matter. *Nature* **332**, 341-343.

Bishop, J.K., Edmond, J.M., Ketten, D.R., Bacon, M.P. and Silker, W.B. (1980) The chemistry, biology and vertical flux of particulate matter from the upper 1500m of the Panama Basin. *Deep-Sea Res.* **27A**, 615-640.

Blackwelder, E. (1916) The geological role of phosphorus. *Amer. J. Sci.* **42**, 282-298.

Blokh, A.M. (1961) Rare earths in the remains of Palæzoic fishes of the Russian platform. *Geokh.* **5**, 390-400 (translated into English, *Geochem. Int.* 404-415).

Bonatti, E., Craig Simmons, E., Breger, D., Hamlyn, P.R. and Lawrence, J. (1983) Ultramafic rock/seawater interactions in the oceanic crust: Mg-silicate (sepiolite) deposit from the Indian ocean floor. *Earth Planet. Sci. Lett.* **62**, 229-238.

Bostrom, K. (1973) The origin and fate of metalliferous active ridge sediments. *Stockholm Contribut. Geol.* **27**, 149-243.

Bowles, F.A., Jack, R.N. and Carmichael, I.S.E. (1973) Investigation of deep-sea volcanic ash layers from Equatorial Pacific cores. *Geol. Soc. Amer. Bull.* **84**, 2371-2388.

Boyle, E.A. (1983) Chemical accumulation variations under the Peru current during the past 130,000 years. *J. Geophys. Res.* **88 (C12)**, 7667-7680.

Bremner, J.M. (1980) Concretionary phosphorite from S.W. Africa. *J. Geol. Soc. London* **137**, 773-786.

Brink, K.H., Halperk, D., Huyer, A. and Smith, R.L. (1983) The physical environment of the Peruvian upwelling system. *Prog. Oceanog.* **12**, 285-305.

Brockmann, C., Fahrbach, E., Huyer, A. and Smith, R.L. (1980) The poleward undercurrent along the Peru coast: 5 to 15°S. *Deep-Sea Res.* **27A**, 847-856.

Broecker, W.S. (1971) Calcite accumulation rates and glacial to interglacial changes in oceanic mixing. In *The Late Cenozoic Glacial Ages* (Ed. K.K. Turekian), pp.239-265. Yale Univ. Press.

Broecker, W.S. (1984) Carbon dioxide circulation through ocean and atmosphere. *Nature* **308**, 602-604.

Broecker, W.S. and Peng, T.H. (1982) *Tracers in the Sea,* 690pp. Eldigio, Palisades.

Broecker, W.S. and Takahashi, T. (1978) The relationship between lysochine depth and *in situ* carbonate ion concentration. *Deep-Sea Res.* **27**,591-613.

Bruland, K.W., Bertine, K., Koide, M. and Goldberg, E.D. (1974) History of metal pollution in Southern California coastal zone. *Environ. Sci. Technol.* **8**, 425-532.

Brusmack, H.J. and Gieskes, J.M. (1983) Interstitial water trace-metal chemistry of laminated sediments from the Gulf of California. *Mar. Chem.* **14**, 86-106.

Buchanan, (1886) *Proc. Royal Geographical Soc.* **8,** 753-770.

Buckland, W. (1843) On the causes of the general presence of phosphates in the strata on the earth and in all fertile soils. *J. Royal Agri. Soc.* **10**, 520-525.

Burnett, W.C. (1974) Phosphorite deposits from the sea floor off Peru and Chile; radiochemical and geochemical investigations concerning their origin. *Hawaii Inst. Geophys. Rep.* **HIG-74-3**, 164pp.

Burnett, W.C. (1977) Geochemistry and origin of phosphorite deposits from off Peru and Chile. *Geol. Soc. Amer. Bull.* **88**, 813-823.

Burnett, W.C. (1980) Apatite-glauconite associations off Peru and Chile: palaeo-oceanographic implications. *J. Geol. Soc.* **137**, 757-764.

Burnett, W.C., Baker, K.B., Chin, P.A., McCabe, W. and Ditchburn, R. (1988) Uranium-series and AMS $^{14}C$ studies of modern phosphatic pellets from Peru shelf muds. *Mar. Geol.* **80**, 215-230.

Burnett, W.C. and Froelich, P.N. (1988) The origin of marine phosphorite. The results of the *R.V. Robert D. Conrad* cruise 23-06 to the Peru shelf. *Mar. Geol. Special Issue* **80**, 343pp.

Burnett, W.C., Veeh, H.H. and Soutar, A. (1980) U-series, oceanographic and sedimentary evidence in support of Recent formation of phosphorite nodules off Peru. In *Marine Phosphorites: A Symposium* Society of Economic Paleontologists and Mineralogists, Special Publication Vol. 29 (Ed. Y.K. Bentor), pp.61-71.

Burt, W.V., Enfield, D.B., Smith R.L. and Crew, H. (1973) The surface wind over an upwelling area near Pisco, Peru. *Boundary Layer Meteor.* **3**, 385-391.

Busch, W.H. and Keller, G.H. (1981) The physical properties of Peru-Chile continental margin sediments - the influence of coastal upwelling on sediment properties. *J. Sed. Pet.* **51**, 705-719.

Calvert, S.E. (1968) Silica balance in the oceans and diagenesis. *Nature* **219**, 919-920.

Calvert, S.E. (1976) The mineralogy and geochemistry of near-shore sediments. In *Chemical Oceanography* (Eds J.P. Riley and R. Chester), Vol. 6, pp.187-280.

Calvert, S.E. (1987) Oceanographic controls on the accumulation of organic matter in marine sediments. In *Marine Petroleum Source Rocks* Geology Society Special Publication, No. 26 (Eds J.Brooks and A.J.Fleet), pp.137-151.

Calvert, S.E., Mukherjee, S. and Morris, R.J. (1985) Trace metals in fulvic and humic acids from modern organic-rich sediments. *Oceanologica Acta* **8**, 167-173.

Calvert, S.E. and Price, N.B. (1970) Minor metal contents of Recent organic-rich sediments off South West Africa. *Nature* **227**, 593-595.

Calvert, S.E. and Price, N.B. (1977) Geochemical variation in ferromanganese nodules and associated sediments from the Pacific. *Mar. Chem.* **5**, 43-74.

Canfield, D.E. (1989) Sulphate reduction and oxic respiration in marine sediments: implications for organic carbon preservation in euxinic environments. *Deep-Sea Res.* **36**, 121-138.

Carpenter, S.J. and Lohmann, K.C. (1992) Sr/Mg ratios of modern marine calcite: empirical indicators of ocean chemistry and precipitation rate. *Geochim. Cosmochim. Acta* **56**, 1837-1849.

Chan, L.H., Edmond, J.M., Stallard, R.F., Broecker, W.S., Chung, Y.C., Weiss, R.F. and Ku, T.L. (1976) Radium and barium at GEOSECS stations in the Atlantic and Pacific. *Earth Planet. Sci. Lett.* **32**, 258-267.

Chavez, F.P. and Barber, R.T. (1987) An estimate of new production in the equatorial Pacific. *Deep-Sea Res.* **34A**, 1229-1243.

Chester, R. and Aston, S.R. (1976) The geochemistry of deep-sea sediments. In *Chemical Oceanography* (Eds J.P. Riley and R. Chester), Vol. 6, pp.281-390. Academic Press, London.

Chow, T.J. and Goldberg, E.D. (1960) On the marine geochemistry of barium. *Geochim. Cosmochim. Acta* **20**, 192-198.

Church, T.M. (1970) Marine Barite. *Unpubl. Ph.D. Thesis*, 100pp. University of California.

Church, T.M. (1979) Marine Barite. In *Marine Minerals,* Min. Soc. Amer. Short Course Notes (Ed. R.G. Burns), Vol. 6, pp.175-209.

Church, T.M. and Woglemuth, K. (1972) Marine barite saturation. *Earth Planet. Sci. Lett.* **15**, 35-44.

Clayton, T. and Kemp, A.E.S. (1990) Clay mineralogy of the Cenozoic sediments from the Peruvian continental margin: Leg 112. In *Proc. of the Ocean Drilling Program* (Eds E. Suess *et al.*), Leg 112, pp.59-86.

Codispoti, L.A. (1983) On nutrient variability and sediments in upwelling regions. In *Coastal Upwelling* (Eds E.Suess and J.Thiede), Part A, pp.125-145. Plenum Press, New York.

Cook, P.J., Shergold, J.H., Burnett, W.C. and Riggs, S.R. (1990) Phosphorite research: a historical overview. In *Phosphorite Research and Development* Geological Society Special Publication, No. 52 (Eds A.J.G. Notholt and I. Jarvis), pp.1-22.

Corliss, B.H. and Chen, C. (1988) Morphotype patterns of Norwegian Sea deep-sea benthic foraminifera and ecological implications. *Geology* **16**, 716-719.

Couch, R. and Whitsett, R.M. (1981) Structures of the Nazca Ridge and continental shelf and slope of southern Peru. In*Nazca Plate: Crustal Formation and Andean Convergence* Geological Society of America, Memoir 154 (Eds L.D. Kulm, J. Dymond, E.J. Dasch and D.M. Hussong), pp.569-586.

Craig, H. (1974) A scavenging model of trace elements in the deep sea. *Earth Planet. Sci. Lett.* **23**, 149-159.

Croll, J. (1867A) On the excentricity of the earth's orbit, and its physical relations to the glacial epoch. *Phil. Mag.* **33**, 119-131.

Croll, J. (1867B) On the change in the obliquity of the ecliptic, its influence on the climate of the polar regions and on the level of the sea. *Phil. Mag.* **33**, 426-445.

Daubeny, C. and Widdrington, C. (1845) On the occurrence of phosphorite in Estremadura. *J. Geol. Soc. London* **31**, 357-364.

De Mendiola, B.R. (1981) Seasonal phytoplankton distribution along the Peruvian coast. In *Coastal Upwelling (Coastal and Esturine Sciences 1.)*, (Ed. F.A.Richards), pp.348-356. Amer. Geophys. Union.

Deer, W.A., Howie, R.A. and Zussman, J. (1966) *An Introduction to the Rock Forming Minerals,* 528pp.Longman, London.

Dehairs, F., Chesselet, R. and Jedwab, J. (1980) Discrete suspended particles of barite and the barium cycle in the ocean. *Earth Planet. Sci. Lett.* **49**, 528-550.

Dehairs, F., Stroobants, N. and Goeyens, L. (1991) Suspended barite as a tracer of biological activity in the Southern Ocean. *Mar. Chem.* **35**, 399-410.

Demaison, G.J., Holck, A.J., Jones, R.W. and Moore, G.T. (1984) Predictive source bed stratigraphy: a guide to regional petroleum occurrence. In *Proc. 11th World Petroleum Congress, Volume 2: Geology, Exploration, Reserves* pp.17-29. J. Wiley, New York.

Demaster, D.J. (1981) The supply and accumulation of silica in the marine environment. *Geochim. Cosmochim. Acta* **45**, 1715-1732.

DeVries, T.J. and Pearcy, W.G. (1982) Fish debris in sediments of the upwelling zone off central Peru: a Late Quaternary record. *Deep-Sea Res.* **28A**, 87-109.

Diester-Haass, L. (1978) Sediments as indicators of upwelling. In *Upwelling Ecosystems* (Eds R.Boje and M.Tomczak), pp.261-281. Springer, New York.

Dobbie, K.E. (1988) Determination of the biogenic silica content of sediments off the coast of Southern Oman. *Unpub. B.Sc. Thesis*, 67pp. University of Edinburgh.

Dougan, W.K. and Wilson, A.L. (1974) The absorptiometric determination of aluminium in water. *Analyst* **99**, 413-430.

Drexler, J.W., Rose, W.I., Sparks, R.S. and Ledbetter, M.T. (1980) The Los Chocoyos Ash, Guatemala: a major stratigraphic marker in Middle America and in three ocean basins. *Quat. Res.* **13**, 327-345.

Dunbar, R.B. and Wefer, G. (1984) Stable isotope fractionation in benthic foraminifera from the Peruvian continental margin. *Mar. Geol.* **59**, 215-225.

Dymond, J. (1981) Geochemistry of Nazca plate surface sediments: an evaluation of hydrothermal, biogenic, detrital and hydrogenous sources. In*Nazca Plate: Crustal Formation and Andean Convergence* Geological Society of America, Memoir 154 (Eds L.D. Kulm, J. Dymond, E.J. Dasch and D.M. Hussong), pp.133-173.

Dymond, J., Suess, E. and Lyle, M. (1992) Barium in deep-sea sediment: a geochemical proxy for paleoproductivity. *Paleocean.* **7**, 163-181.

Eggimann, D.W., Manheim, F.T. and Betzer, P.R. (1980) Dissolution and analysis of amorphous silica in marine sediments. *J. Sed. Pet.* **50**, 215-225.

Ekman, S. (1953) *Zoogeography of the Sea,* 417pp. Sidgwick and Jackson, London.

Ekman, V.W. (1905) On the influence of the Earth's rotation on ocean currents. *Ark. Math. Astrom. Fys.* **2**.

El Wakeel, S.K. and Riley, J.P. (1961) Chemical and mineralogical studies of deep-sea sediments. *Geochim. Cosmochim. Acta* **25**, 110-146.

Elderfield, H. (1990) Tracers of ocean paleoproductivity and paleochemistry: an introduction. *Paleocean.* **5**, 711-717.

Elderfield, H., Hawkesworth, C.J., Greaves, M.J. and Calvert, S.E. (1981) REE geochemistry of oceanic ferromanganese nodule and associated sediments. *Geochim. Cosmochim. Acta* **45**, 513-528.

Elderfield, H. and Truesdale, V.W. (1980) On the biophilic nature of iodine in seawater. *Earth Planet. Sci. Lett.* **50**, 105-114.

Emerson, R.W. (1957) *An Organic Anthology* (Ed. S. E. Whicher), 517pp. Riverside Press, Cambridge, MA.

Emerson, S. (1985) Organic carbon preservation in marine sediments. In *The Carbon Cycle and Atmospheric $CO_2$: Natural Variations, Archean to Present* American Geophysical Union, Monograph 32 (Eds E.T. Sunquist and W.S. Broecker), pp.78-87.

Emiliani, C. (1955A) Mineralogical and chemical composition of the tests of certain pelagic foraminfera. *Micropalaeontology* **1**, 377-380.

Emiliani, C. (1955B) Pleistocene palaeotemperatures. *J. Geol.* **63**, 539-578.

Emiliani, C. and Shackleton, N.J. (1974) The Bruhnes epoch: Isotope palaeotemperatures and geochronology. *Science* **183**, 511-514.

Eppley, R.W. and Peterson, B.J. (1979) Particulate organic matter flux and planktonic new production in the deep ocean. *Nature* **282**, 677-680.

Fairbanks, R.G. (1989) A 17,000-year glacio-eustatic sea level record: influence of glacial melting rates on the Younger Dryas event and deep-ocean circulation. *Nature* **342**, 637-642.

Farrell, J.W. and Prell, W.L. (1989) Climatic change and $CaCO_3$ preservation: an 800,000 year bathymetric reconstruction from the Central Equatorial Pacific ocean. *Paleocean.* **4**, 447-466.

Farrell, J.W. and Prell, W.L. (1991) Pacific $CaCO_3$ preservation and $\delta^{18}O$ since 4Ma: paleoceanic and paleoclimatic implications. *Paleocean.* **6**, 485-498.

Finney, B.P., Lyle, M.W. and Heath, G.R. (1988) Sedimentation at MANOP site H (Eastern Equatorial Pacific) over the past 400,000 years: climatically induced redox variations and their effect on transition metal cycling. *Paleocean.* **3**, 169-189.

Fowler, S.W. and Small, L.F. (1972) Sinking rates for euphasid fecal pellets. *Limnol. Oceanog.* **17**, 293-296.

Francois, R. (1987) The influence of humic substances on the geochemistry of iodine in nearshore and hemipelagic marine sediments. *Geochim. Cosmochim. Acta* **51**, 2417-2427.

Francois, R. (1988) A study on the regulation of the concentrations of some trace metals (Rb, Sr, Zn, Pb, Cu, V, Cr, Ni, Mn and Mo) in Saanich Inlet sediments, British Columbia, Canada. *Mar. Geol.* **83**, 285-308.

Frankenberg, D. and Menzies, R.J. (1968) Some quantatative analyses of deep-sea benthos off Peru. *Deep-Sea Res.* **15**, 623-626.

Froelich, P.N., Arthur, M., Burnett, W.C., Deakin, M., Hensley, V., Jahnke, R., Kaul, L., Roe, K., Soutar, A. and Vathakanon, C. (1988) Early diagenesis of organic matter in Peru continental margin sediments: phosphorite precipitation. *Mar. Geol.* **80**, 309-343.

Froelich, P.N., Bender, M.L., Luedtke, N.A., Heath, G.R. and DeVries, T. (1982) The marine phosphorus cycle. *Amer. J. Sci.* **282**, 474-511.

Froelich, P.N., Kim, K.H., Jahnke, R., Burnett, W.C., Soutar, A. and Deakin, M. (1983) Pore water fluoride in Peru continental margin sediments: uptake from seawater. *Geochim. Cosmochim. Acta* **47**, 1605-1612.

Froelich, P.N., Klinkhammer, G.P., Bender, M.L., Luedtke, N.A., Heath, G.R., Cullen, D., Dauphin, P., Hammond, D., Hartman, B. and Maynard, V. (1979) Early oxidation of organic matter in pelagic sediments of the eastern equatorial Atlantic: suboxic diagenesis. *Geochim. Cosmochim. Acta* **43**, 1075-1090.

Ganssen, G. and Sarnthein, M. (1983) Stable isotope composition of foraminifers - the surface and bottom water record of coastal upwelling. In *Coastal Upwelling* (Eds E.Suess and J.Thiede), Part A, pp.99-121. Plenum Press, New York.

Gardner, J.V., Dean, W.E. and Alonso, B. (1990) Inorganic geochemistry of surface sediments of the Ebro shelf and slope, north-western Mediterranean. *Mar. Geol.* **95**, 225-245.

Glenn, C.R. and Arthur, M.A. (1988) Petrology and major element geochemistry of Peru margin phosphorites and associated diagenetic minerals: authigenesis in modern orgainic-rich sediments. *Mar. Geol.* **80**, 231-267.

Goldberg, E.D. (1954) Marine geochemistry 1.Chemical scavengers of the sea. *J. Geol.* **62**, 249-265.

Graybeal, A.L. and Heath, G.R. (1984) Remobilisation of transition metals in surficial pelagic sediments from the eastern Pacific. *Geochim. Cosmochim. Acta* **48**, 965-975.

Gulbrandsen, R.A. (1969) Physical and chemical factors in the formation of marine apatite. *Econ. Geol.* **64**, 365-382.

Gunther, E.R. (1936) A report on oceanographical investigations in the Peru coastal current. *Discovery Rep.* **13**.

Hartline, B.K. (1980) Coastal upwelling: physical factors feed fish. *Science* **208**, 38-40.

Harvey, G.R. (1980) A study of the chemistry of iodine and bromine in marine sediments. *Mar. Chem.* **8**, 327-332.

Heath, G.R. and Dymond, J. (1977) Genesis and transformation of metalliferous sediments from the East Pacific Rise, Bauer Deep and Central Basin, northwest Nazca plate. *Geol. Soc. Amer. Bull.* **88**, 723-733.

Heath, G.R. and Dymond, J. (1981) Metalliferous-sediment deposition in time and space: East Pacific Rise and Bauer Basin, northern Nazca plate. In*Nazca Plate: Crustal Formation and Andean Convergence* Geological Society of America, Memoir 154 (Eds L.D. Kulm, J. Dymond, E.J. Dasch and D.M. Hussong), pp.175-197.

Heath, G.R. and Lyle, M. (1981) Profiles of solid phase manganese at MANOP sites M and H. *Trans. Amer. Geophys. Union (EOS)* **62**, 905.

Heinze, P.M. and Wefer, G. (1992) The history of coastal upwelling off Peru (11°S, ODP Leg 112, Site 680B) over the past 650,000 years. In *Upwelling Ecosystems: Evolution Since the Early Miocene* Geological Society Special Publication, No. 64 (Eds C.P. Summerhayes *et al.*), pp.451-462.

Henderson, P. (Ed.) (1984) *Rare Earth Element Geochemistry.* Developments in Geochemistry, Vol. 2, 510pp. Elsevier, Amsterdam.

Henrichs, S.M. and Farrington, J.W. (1984) Peru upwelling region sediments near 15°S 1.Remineralization and accumulation of organic matter. *Limnol. Oceanog.* **29**, 1-19.

Hermelin, J.O.R. and Shimmield, G.B. (1990) The importance of the oxygen minimum zone and sediment geochemistry in the distribution of Recent benthic foraminifera in the Northwest Indian Ocean. *Mar. Geol.* **91**, 1-29.

Hey, R., Johnson, G.L. and Lowrie, A. (1977) Recent plate motions in the Galapagos area. *Geol. Soc. Amer. Bull.* **88**, 1385-1403.

Hill, P.A. and Parker, A. (1970) Tin and zirconium in sediments around the British Isles: a preliminary reconnaisance. *Econ. Geol.* **65**, 409-416.

Hodge, V. *et al.* (1978) Influence of atmospherically transported aerosols on surface ocean water composition. *Geochem. J.* **12**, 7.

Holland, H.H. (1978) *The Chemistry of the Atmosphere and Oceans*. J.Wiley, New York.

Honjo, S (1977) Biogenic carbonate particles in the ocean: do they dissolve in the water column. In *The Fate of Fossil Fuel $CO_2$ in the Oceans* Marine Science, Vol. 6 (Eds N.R. Anderson and A. Malahoff), pp.269-294. Plenum Press, New York.

Honjo, S. and Roman, M.R. (1978) Marine copepod fecal pellets: production, preservation and sedimentation. *J. Mar. Res.* **36**, 45-57.

Horne, R.A. (1969) *Marine Chemistry*, 568pp.Wiley, London.

Hurlburt, H.E. (1974) The influence of coastline geometry and bottom topography on the eastern ocean circulation. In *Technical Report, Mesoscale Air-Sea Interaction Group,* Florida State University.

Huyer, A., Knoll, M., Paluszkiewicz, T. and Smith, R.L. (1991) The Peru undercurrent: a study in variability. *Deep-Sea Res.* **38**, S247-271.

Imbrie, J., Hays, J.D., Martinson, D.G., McIntyre, A., Mix, A.C., Morley, J.J., Pisias, N.G., Prell, W.L. and Shackleton, N.J. (1984) The orbital theory of Pleistocene climate: support from a revised chronology of the marine $\delta^{18}O$ record. In *Milankovitch and Climate, Part 1.* (Eds. A. Berger *et al.*), pp.269-305. Hingman, MA.

Imbrie, J. and Imbrie, K.P. (1979) *Ice Ages - Solving the Mystery* 224pp. Macmillan, London.

Ittekkot, V. and Degens, E.T. (1983) Metal-staining of sedimentary organic matter by natural processes. In *Coastal Upwelling* (Eds E.Suess and J.Thiede), Part A, pp.573-588. Plenum Press, New York.

Ivanovich, M and Harmon, R.S. (1982) *U-series Disequilibrium Applications to Environmental Problems* 571pp.Clarendon Press, Oxford.

Jahnke, R.A., Emerson, S.R., Roe, K.K. and Burnett, W.C. (1983) The present day formation of apatite in Mexican continental margin sediments. *Geochim. Cosmochim. Acta* **47**, 259-266.

Kazakov, A.V. (1937) The phosphorite facies and the genesis of phosphorites. In *Geological Investigations of Agricultural Ores, Trans. Sci. Inst. Fertilizers and Insectofungicides* **142,** 93-113.

Kennedy, H.A. and Elderfield, H. (1987) Iodine diagenesis in pelagic deep-sea sediments. *Geochim. Cosmochim. Acta* **51**, 2489-2504.

Kennedy, W.J. and Garrison, R.E. (1975) Morpholgy and genesis of nodular chalks and hardgrounds in the Upper Cretaceous of southern England. *Sedimentology* **22**, 311-386.

Kennett, J.P. and Thunell, R.C. (1975) Global increase in Quaternary explosive volcanism. *Science* **187**, 497-503.

Kim, K.H. and Burnett, W.C. (1986) Uranium-series growth history of a Quaternary phosphatic crust from the Peruvian continental margin. *Chem. Geol.* **58**, 227-244.

Klinkhammer, G.P., Rona, P., Greaves, M. and Elderfield, H. (1985) Hydrothermal manganese plumes in the Mid-Atlantic Ridge rift valley. *Nature* **314**, 727-731.

Knauer, G.A., Martin, J.H. and Bruland, K.W. (1979) Fluxes of particulate carbon, nitrogen and phosphorus in the upper water column of the northeast Pacific. *Deep-Sea Res.* **26A**, 97-108.

Kolodny, Y. and Kaplan, I.R. (1970) Uranium isotopes in sea-floor phosphorites. *Geochim. Cosmochim. Acta* **34**, 3-24.

Krinsley, D. (1960) Trace elements in the tests of planktonic foraminifera. *Micropalaeontology* **6**, 297-300.

Krissek, L.A., Scheidegger, K.F. and Kulm, L.D. (1980) Surface sediments of the Peru-Chile continental margin and the Nazca plate. *Geol. Soc. Amer. Bull.* **91**, 321-331.

Ku, T.-L., Knauss, K.G. and Mathieu, G. (1977) Uranium in open oceans: concentration and isotopic composition. *Deep-Sea Res.* **24**, 1005.

Kulm, L.D., Dymond, J., Dasch, E.J. and Hussong, D.M. (Eds) (1981) *Nazca Plate Crustal Formation and Andean Convergence.* Geological Society of America, Memoir 154, 824pp.

Labracherie, M., Barde, M.F., Moyes, J. and Pujos-Lamy, A. (1983) Variability of upwelling regimes (northwest Africa, south Arabia) during the latest Pleistocene: a comparison. In *Coastal Upwelling* (Eds E.Suess and J.Thiede), Part B, pp.347-364. Plenum Press, New York.

Lamboy, M. (1990) Microstructures of a phosphatic crust from the Peruvian continental margin: phosphatized bacteria and associated phenomena. *Oceanologica Acta* **13**, 439-451.

Lea, D. and Boyle, E. (1989) Barium content of benthic foraminifera controlled by bottom water composition. *Nature* **388**, 751-753.

Lea, D. and Boyle, E. (1990A) A 21,000 year record of barium variability in the deep northwest Atlantic ocean. *Nature* **397**, 269-272.

Lea, D. and Boyle, E. (1990B) Foraminiferal reconstruction of barium distributions in water masses of the glacial oceans. *Paleocean.* **5**, 719-742.

Ledbetter, M.T. (1982) Tephrachronology at sites 502 and 503. In *Initial Reports of the Deep-Sea Drilling Project* (Eds W.Prell *et al.*), Vol. 68, pp.403-408. U.S. Government Printing Office, Washington D.C.

Ledbetter, M.T. (1985) Tephrachronology of marine tephra adjacent to Central America. *Geol. Soc. Amer. Bull.* **96**, 77-82.

Lee, C. (1992) Controls on organic carbon preservation: the use of stratified water bodies to compare intrinsic rates of decomposition in oxic and anoxic systems. *Geochim. Cosmochim. Acta* **56**, 3323-3335.

Leinen, M., Cwienk, D., Heath, G.R., Biscaye, P.E., Kolla, V., Theide, J. and Dauphin, J.P. (1986) Distribution of biogenic silica and quartz in Recent deep-sea sediments. *Geology* **14**, 199-203.

Li, Y-H. (1981) Geochemical cycles of elements and human pertubation. *Geochim. Cosmochim. Acta* **45**, 2073-2084.

Li, Y-H. (1982) Interelement relationship in abyssal Pacific ferromanganese nodules and associated pelagic sediments. *Geochim. Cosmochim. Acta* **46**, 1053-1060.

Lisitzin, A.P. and Peltelin, V.P. (1967) Features of distribution and modification of $CaCO_3$ in bottom sediments of the Pacific ocean. *Lithol. Miner. Resour. Engl. Transl.* **5**, 565-578.

Lonsdale, P.F. (1976) Abyssal circulation of the south-eastern Pacific and some geological implications. *J. Geophys. Res.* **81**, 1163-1146.

Lucas, J., El Faleh, E.M. and Prevot, L. (1990) Experimental study of the substitution of Ca by Sr and Ba in synthetic apatites. In *Phosphorite Research and Development* Geological Society Special Publication, No. 52 (Eds A.J.G. Notholt and I. Jarvis), pp.33-47.

Luz, B. and Shackleton, N.J. (1975) $CaCO_3$ solution in the tropical East Pacific during the past 130,000 years. *Cushman Found. Foraminiferal Res. Spec. Publ.* **13**, 142-150.

Lyle, M. (1988) Climatically forced organic carbon burial in equatorial Atlantic and Pacific Oceans. *Nature* **335**, 529-532.

Lyle, M., Heath, G.R., Murray, D.W., Finney, B.P., Dymond, J., Robbins, J.M. and Brooksforce, K. (1988) The record of Late Pleistocene sedimentation in the eastern equatorial Pacific ocean. *Paleocean.* **3**, 39-59.

Lynn, D.C. and Bonatti, E. (1965) Mobility of manganese in diagenesis of deep sea sediments. *Mar. Geol.* **3**, 457-474.

Mach, D.L., Ramirez, A. and Holland, H.D. (1987) Organic phosphorus and carbon in marine sediments. *Amer. J. Sci.* **287**, 429-441.

Manheim, F.T. and Gulbrandsen, R.A. (1979) Marine phosphorites. In *Marine Minerals,* Min. Soc. Amer. Short Course Notes (Ed. R.G. Burns), Vol. 6, pp.151-173.

Manheim, F.T., Rowe, G.T. and Jipa, D. (1975) Marine phosphorite formation off Peru. *J. Sed. Pet.* **45**, 243-251.

Mansfield, G.R. (1918) Origin of the Western phosphates of the United States. *Amer. J. Sci.* **46**, 592-598.

Martens, C.S. and Harris, R.C. (1970) Inhibition of apatite precipitation in the marine environment by magnesium ions. *Geochim. Cosmochim. Acta* **34**, 621-625.

Martin, J.H. (1987) VERTEX: carbon cycling in the northeast Pacific. *Deep-Sea Res.* **34**, 267-285.

Martin, J.H. and Knauer, G.A. (1973) The elemental composition of plankton. *Geochim. Cosmochim. Acta* **37**, 1639-1653.

Martin, J.M. and Whitfield, M. (1983) River input of trace elements to the ocean. In *Trace Metals in Seawater, NATO Conference Series IV: Marine Science,* (Eds C.S. Wong *et al.*), Vol. 9, p.265. Plenum Press, New York.

Martinson, D.G., Pisias, N.G., Hays, J.D., Imbrie, J., Moore, T.C. and Shackleton, N.J. (1987) Age dating and the orbital theory of the Ice Ages: development of a high resolution 0 to 300,000 year chronostratigraphy. *Quat. Res.* **27**, 1-29.

McArthur, J.M. (1978) Systematic variations in the contents of Na, Sr, $CO_3$ and $SO_4$ in marine carbonate fluorapatite and their relation to weathering. *Chem. Geol.* **21**, 89-112.

McClellan, G.H. (1980) Mineralogy of carbonate fluorapatites. *J. Geol. Soc. London* **137**, 675-681.

McClellan, G.H. and Van Kauwenbergh, S. J. (1990) Mineralogy of sedimentary apatites. In *Phosphorite Research and Development*, Geological Society Special Publication, No. 52 (Eds A.J.G. Notholt and I. Jarvis), pp.23-31.

McCorkle, D.C., Keigwin, L.D., Corliss, B.H. and Emerson, S.R. (1990), Influence of microhabitats on th carbon isotope composition of deep-sea benthic foraminifera. *Paleocean.* **5**, 161-185.

McKelvey, V.E., Swanson, R.W. and Sheldon, R.P. (1953) The Permian phosphorite deposits of western United States. *19th Session of the International Geological Congress*, Algers, 1952, Vol. 11, pp.45-64.

McNeill, G.W. and Shimmield, G.B. (1991) Diagenetic controls on uranium, molybdenum and vanadium enrichment in organic-rich marine shelf sediments. In *Proc. 8th International Conference on Heavy Metals in the Environment* (Ed. J.G. Farmer), pp.436-439. CEP Consultants, Edinburgh.

Milankovitch, M. (1941) *Théorie mathématique des phénomènes thermiques produits par la radiation solaire*. Royal Serb. Acad. Special Publication, Vol. 133, pp.1-633. Gauthiers-Villars, Paris.

Molina-Cruz, A. and Price, P. (1977) Distribution of opal and quartz on the ocean floor of the subtropical, southeastern Pacific. *Geology* **5**, 81-84.

Müller, P.J., Erlenkeuser, H. and Von Grafenstein, R. (1983) Glacial-interglacial cycles in oceanic productivity inferred from organic carbon contents in eastern North Atlantic sediment cores. In *Coastal Upwelling* (Eds E.Suess and J.Thiede), Part B, pp.365-398. Plenum Press, New York.

Müller, P.J. and Suess, E. (1979) Productivity, sedimentation rate and sedimentary organic matter in the oceans - 1.Organic carbon preservation. *Deep-Sea Res.* **26A**, 1347-1362.

Murray, D.W. (1987) Spatial and temporal variations in sediment accumulation in the Central Tropical Pacific. *Unpub. Ph.D. Thesis*,343pp. Oregon State University.

Murray, J. and Philippi, E. (1908) Die Grundproben der Deutschen Tiefsee Expedition 1898-1899. *Wiss. Ergeb. Dtsch. Tiefsee Exped. Valdivia* **10**, 77-206.

Murray, J. and Renard, A.F. (1891) *Scientific Results, H.M.S. Challenger, Deep Sea Deposits*, pp.391-400.Longmans London.

Murray, J. and Renard, A.F. (1898) *Deep-Sea Deposits, Challenger Reports*, 525pp. Longmans, London.

Nair, R.R., Ittekot, V., Manganini, S.J., Ramaswamy, V., Haake, B., Degens, E.T., Desai, B.N. and Honjo, S. (1989) Increased particulate flux to the deep ocean related to monsoons. *Nature* **338**, 749-751.

Nath, B.G., Rao, V.P. and Becker, K.P. (1989) Geochemical evidence of terrigenous influence in deep-sea sediments up to 8°S in the central Indian ocean. *Mar. Geol.* **87**, 301-313.

Nathan, Y. and Lucas, J. (1976) Experiences sur la precipitation directe de l'apatite dans l'eau de mer: implication dans la genese des phosphorites. *Chem. Geol.* **18**.

Ninkovich, D. and Shackleton, N.J. (1975) Distribution, stratigraphic position and age of ash layer "L", in the Panama Basin region. *Earth Planet. Sci. Lett.* **27**, 20-34.

Nissenbaum, A. and Swaine, D.J. (1976) Organic matter-metal interactions in Recent sediments: the role of humic substances. *Geochim. Cosmochim. Acta* **40**, 809-816.

Noble, D.C., McKee, E.H., Farmer, E. and Petersen, U. (1974) Eposodic Cenozoic volcanism and tectonism in the Andes of Peru. *Earth Planet. Sci. Lett.* **21**, 213-220.

Norrish, K and Hutton, J.T. (1969) An accurate X-ray spectrographic method for the analysis of a wide range of geological samples. *Geochim. Cosmochim. Acta* **33**, 431-453.

Osterberg, C., Carey, A.G. and Curl, H. (1963) Acceleration of sinking rates of radionucleides in the ocean. *Nature* **200**, 1276-1277.

Parkin, D.W.and Shackleton, N.J. (1973) Trade wind and temperature correlations down a deep sea core off the Saharan coast. *Nature* **245**, 455-457.

Patience, A.J. (1992) Geochemical indicators of palaeoproductivity and palaeoclimate in Eastern Equatorial Pacific sediments. *Unpub. Ph.D. Thesis*, 473pp. University of Edinburgh.

Patience, A.J. and Kroon, D. (1991) Oxygen isotope chronostratigraphy. In *Quaternary Dating Methods - A User's Guide* Quaternary Res. Assoc., Tech. Guide No. 4, (Eds P.L. Smart and P.D. Frances), pp.199-228.Cambridge, U.K.

Pedersen, T.F. (1979) The geochemistry of sediments of the Panama Basin, Eastern Equatorial Pacific Ocean. *Unpub. Ph.D. Thesis*, 235pp. University of Edinburgh.

Pedersen, T.F. (1983) Increased productivity in the eastern equatorial Pacific during the last glacial maximum (19,000 to 14,000 yr B.P.). *Geology* **11**, 16-19.

Pedersen, T.F. and Calvert, S.E. (1990) Anoxia vs productivity: what controls the formation of organic-carbon-rich sediments and sedimentary rocks? *Amer. Assoc. Pet. Geol. Bull.* **74**, 454-466.

Pedersen, T.F. and Price, N.B. (1980) The geochemistry of iodine and bromine in sediments of the Panama Basin. *J. Mar. Res.* **38**, 397-411.

Pedersen, T.F., Shimmield, G.B. and Price, N.B. (1992) Lack of enhanced preservation of organic matter in sediments under the oxygen minimum on the Oman margin. *Geochim. Cosmochim. Acta* **56**, 545-551.

Pickard, G.L. and Emery, W.J. (1982) *Descriptive Physical Oceanography, An Introduction*, 249pp. Pergamon Press, Oxford.

Piper, D.Z., Baedecker, P.A., Crock, J.G., Burnett, W.C. and Loebner, B.J. (1988) Rare earth elements in phosphatic-enriched sediment of the Peru shelf. *Mar. Geol.* **88**, 269-285.

Pisias, N.G. and Rea, D.K. (1988) Late Pleisocene paleoclimatology of the Central Equatorial Pacific: sea surface response to the southeast trade winds. *Paleocean.* **3**, 21-37.

Pitcher, W.S. (1974) The Mesozoic and Cenozoic batholiths of Peru. *Pacific Geology* **8**, 51-62.

Poole, A.J. (1992) Sedimentology, neotectonics and geomorphology related to tectonic uplift and sea-level change: Quaternary of Cyprus. *Unpub. Ph.D. Thesis*, 235pp.University of Edinburgh.

Pouclet, A., Cambray, H., Cadet, J.P., Bourgois, J. and De Wever, P. (1991) Volcanic ash from Leg 112 off Peru. In *Proc. of the Ocean Drilling Program* (Eds E. Suess *et al.*), Leg 112, pp.465-480.

Price, N.B. and Calvert, S.E. (1973) The geochemistry of iodine in oxidised and reduced Recent marine sediments. *Geochim. Cosmochim. Acta* **37**, 2149-2158.

Price, N.B. and Calvert, S.E. (1977) The contrasting geochemical behaviours of iodine and bromine in recent sediments from the Namibian shelf. *Geochim. Cosmochim. Acta* **41**, 1769-1775.

Price, N.B. and Calvert, S.E. (1978) The geochemistry of phosphorites from the Namibian shelf. *Chem. Geol.* **23**, 151-170.

Price, N.B., Calvert, S.E. and Jones, P.G.W. (1970) The distribution of iodine and bromine in the sediments of the Southwestern Barents Sea. *J. Mar. Res.* **28**, 22-34.

Price, N.B. *et al.* (1989) *Report of* R.R.S. Charles Darwin *Cruise 38: Peru Margin and Eastern Equatorial Pacific.*University of Edinburgh.

Prospero, J.M. and Bonatti, E. (1969) Continental dust in the atmosphere of the Eastern Equatorial Pacific. *J. Geophys. Res.* **74**, 3362-3371.

Ramirez, A.J. and Rose, A.W. (1992) Analytical geochemistry of organic phosphorus and its correlation with organic carbon in marine and fluvial sediments and soils. *Amer. J. Sci.* **292**, 421-454.

Rea, D.K., Pisias, N.G. and Newberry, T. (1991) Late Pleistocene paleoclimatology of the Central Equatorial Pacific: flux patterns of biogenic sediments. *Paleocean.* **6**, 227-244.

Redfield, A.C., Ketchum, B.H. and Richards, F.A. (1963) The influence of organisms on the composition of seawater. In *The Sea* (Ed. M.N. Hill), Vol. 2, pp.26-77. J. Wiley, New York.

Reimers, C.E. and Suess, E. (1983A) Spatial and temporal patterns of organic matter accumulation on the Peru continental margin. In *Coastal Upwelling* (Eds E.Suess and J.Thiede), Part B, pp.311-337. Plenum Press, New York.

Reimers, C.E. and Suess, E. (1983B) The partitioning of organic carbon fluxes and sediment organic carbon decomposition rates in the ocean. *Mar. Chem.* **13**, 141-168.

Revelle, R.R., Bramlette, M., Arrhenius, G. and Goldberg, E.D. (1955) Pelagic sediments of the Pacific. *Geol. Soc. Amer. Spec. Paper* **62**, 221-236.

Riley, J.P. and Chester, R. (1971) *Introduction to Marine Chemistry*, 465pp.Academic Press, London.

Rosato, V.J. and Kulm, L.D. (1981) Clay mineralogy of the Peru continental margin and adjacent Nazca plate: implications for provenance, sea-level changes and continental accretion. In *Nazca Plate: Crustal Formation and Andean Convergence*, Geol. Soc. Amer. Mem., Vol. 154 (Eds L.D. Kulm *et al.*), pp.545-568.

Rose, W.I.,Jr., Grant, N.K. and Easter, J. (1979) Geochemistry of the Los Chocoyos Ash, Quezaltenango valley ash flow tuffs. *Geol. Soc. Amer. Spec. Paper* **180**, 87-99.

Rutland, R.W.R. (1971) Andean orogeny and ocean floor spreading. *Nature* **223**, 252-255.

Ryther, J.H. (1969) Photosynthesis and fish production in the sea. *Science* **166**, 72-76.

Sarnthein, M. (1978) Sand deserts during glacial maximum and clatic optimum. *Nature* **271**, 43-46.

Sarnthein, M., Winn, K., Duplessy, J.-D. and Fontugne, M.R. (1988) Global variations of surface ocean productivity in low and mid latitudes: influence on $CO_2$ reservoirs of the deep ocean and atmosphere during the last 21,000 years. *Paleocean.* **3**, 361-399.

Scheidegger, K.F. and Krissek, L.A. (1982) Dispersal and deposition of eolian and fluvial sediments off Peru and northern Chile. *Geol. Soc. Amer. Bull.* **93**, 150-162.

Schmitz, B. (1987) Barium, equatorial high productivity, and the northward wandering of the Indian continent. *Paleocean.* **2**, 63-77.

Scholl, D.W., Christensen, M.N., von Huene, R. and Marlowe, M. (1970) Peru-Chile Trench sediments and sea-floor spreading. *Geol. Soc. Amer. Bull.* **81**, 1339-1360.

Schrader, H. (1971) Fecal pellets: role in sedimentation of pelagic diatoms. *Science* **174**, 55-57.

Schrader, H. (1992) Comparison of Quaternary coastal upwelling proxies off central Peru. *Mar. Micropal.* **19**, 29-47.

Schrader, H. and Sorknes, R. (1991) Peruvian coastal upwelling: Late Quaternary productivity changes revealed by diatoms. *Mar. Geol.* **97**, 233-249.

Schweller, W.J., Kulm, L.D. and Prince, R.A. (1981) Tectonics, structure and sedimentary framework of the Peru-Chile Trench. In*Nazca Plate: Crustal Formation and Andean Convergence* Geological Society of America, Memoir 154 (Eds L.D. Kulm, J. Dymond, E.J. Dasch and D.M. Hussong), pp.323-349.

Sclater, F.R., Boyle, E. and Edmond, J.M. (1976) On the marine geochemistry of nickel. *Earth Planet. Sci. Lett.* **31**, 119-128.

Semina, G.I. (1971) Distribution of plankton in the south-eastern part of the Pacific Ocean. *Tr. Inst. Okeanol. Akad. Nauk SSSR* **89**.

Shankar, R., Subbarao, K.V. and Kolla, V. (1987) Geochemistry of surface sediments from the Arabian Sea. *Mar. Geol.* **76**, 253-279.

Shaw, T.I. (1962) Halogens in algae. In *Physiology and Biochemistry of Algae* (Ed. R.A.Lewin), pp.247-253. Academic Press, London.

Shaw, T.J., Gieskes, J.M. and Jahnke, R.A. (1990) Early diagenesis in differing depositional environments: the response of transition metals in pore water. *Geochim. Cosmochim. Acta* **54**, 1233-1246.

Shimmield, G.B. (1985) The geochemistry and mineralogy of Pacific sediments, Baja California. *Unpub. Ph.D. Thesis*, 323pp. University of Edinburgh.

Shimmield, G.B. (1992) Can sediment geochemistry record changes in coastal upwelling palaeoproductivity? Evidence from northwest Africa and the Arabian Sea. In *Upwelling Ecosystems* Geological Society Special Publication, No. 64 (Eds C.P. Summerhayes *et al.*), pp.29-46.

Shimmield, G.B., Derrick, S., Kroon, D., Lloyd, J., McNeill, G. and Matthewson, A. (1992) Barium palæoproductivity records from mesotrophic ocean margin provinces recorded over the last 250,000 years. In *Proc. 4th International Conference of Paleoceanography*, Kiel Germany.

Shimmield, G.B. and Mowbray, S.R. (1991) The inorganic geochemical record of the northwest Arabian Sea: a history of productivity variation over the last 400 ky from sites 722 and 724. In *Proc. ODP Sci. Results*,(Eds W.L. Prell *et al.*), Vol. 117, pp.409-429.

Shimmield, G.B. and Pedersen, T.F. (1990) The geochemistry of reactive trace metals and halogens in hemi-pelagic continental margin sediments. *Aquatic Sciences* **3**, 255-279.

Sholkovitz, E.R. (1978) The flocculation of dissolved Fe, Mn, Al, Cu, Ni, Co and Cd during esturine mixing. *Earth Planet. Sci. Lett.* **41**, 77-86.

Sillen, L.G. (1961) The physical chemistry of seawater. In *Oceanography* (Ed. M.Seers), pp.549-581. Amer. Assoc. Advanc. Sci., Washington D.C.

Smayda, T.J. (1969) Some measurements of the sinking rate of fecal pellets. *Limnol. Oceanog.* **14**, 621-625.

Smith, R.L. (1968) Upwelling. *Oceanog. Mar. Biol. Ann. Rev.* **6**, 11-46.

Smith, R.L. (1983) Circulation patterns in upwelling regions. In *Coastal Upwelling* (Eds E.Suess and J.Thiede), Part A, pp.13-36. Plenum Press, New York.

Southgate, P.N. (1986) Cambrian phoscrete profiles, coated grains and microbial processes in phosphogenesis: Georgina Basin, Australia. *J. Sed. Pet.* **56**, 429-441.

Spencer D.W., Degens, E.T. and Kulbicki, G. (1968) Factors affecting element distributions in sediments. In *Origin and Distribution of the Elements* (Ed. L.H. Ahrens), pp.981-998.Pergamon Press, Oxford.

Ssaidova, H.M. (1971) Recent sediments off the Pacific coast of South America. *Ac. Science U.S.S.R. Invest. P.P. Shirschov-Inst. of Oceanologie* **89**, 139-145 (in Russian).

Staresnic, N., Farrington, J., Gagosian, R.B., Clifford, C.H. and Hulburt, E.M. (1983) Downward transport of particulate matter in the Peru coastal upwelling: role of the anchoveta, *Engraulis ringens*. In *Coastal Upwelling* (Eds E.Suess and J.Thiede), Part A, pp.225-240. Plenum Press, New York.

Steens, T.N.F., Kroon, D., Ten Kate, W.G. and Sprenger, A. (1991) Late Pleistocene periodicities of oxygen isotpoe ratios, calcium carbonate contents and magnetic susceptibilities of Western Arabian Sea margin Hole 728A. In *Proc. Ocean Drilling Program, Scientific Res.* (Eds W.L. Prell *et al.*), Vol. 117, pp.309-320.

Stowasser, W.F. (1979) Phosphate: mineral commodity profiles. *U.S. Bur. Mines* Pittsburgh, 19pp.

Strickland, J.D.H. and Parsons, T.R. (1968) A Handbook of Seawater Analysis. *Bull. Fish. Res. Bd.* Canada, **167**, 65-70.

Suess, E. (1981) Phosphate regeneration from sediments of the Peru continantal margin by dissolution of fish debris. *Geochim. Cosmochim. Acta* **45**, 577-588.

Suess, E. and Thiede, J. (1983) Coastal upwelling : Introduction. In *Coastal Upwelling* (Eds E.Suess and J.Thiede), Part A, pp.1-10. Plenum Press, New York.

Suess, E., von Huene, R. *et al.* (1988) *Proc. ODP, Init. Rep.*, Leg 112, 1015pp.

Suess, E., von Huene, R. *et al.* (1990) *Proc. ODP, Sci. Res.*, Leg 112, 738pp.

Summerhayes, C.P., Prell, W.L. and Emeis, K.-C. (Eds) (1992) *Upwelling Systems: Evolution Since the Early Miocene*, Geological Society Special Publication, No. 64, 511pp.

Sverdrup, H.U., Johnson, M.W. and Fleming, R.H. (1946) *The Oceans: their Physics, Chemistry and General Biology*, 1088pp. Prentice-Hall, New York.

Theisen, R. and Vollach, D. (1967) *Tables of X-ray Mass Absorption Coefficients.* Varlag Stahleisen M.B.H., Dusseldorf.

Thiede, J. (1975) Distribution of foraminifera in surface waters of a coastal upwelling area. *Nature* **253**, 712-714.

Thiede, J. and Suess, E. (1983) Coastal upwelling :Introduction. In *Coastal Upwelling* (Eds E.Suess and J.Thiede), Part B, pp.1-7. Plenum Press, New York.

Thompson, T.G. and Chow, J.J. (1956) The strontium-calcium atom ratio in carbonate secreting marine organisms. *Deep-Sea Res. Supplement* **3**, 20-39.

Thomson, J., Wallace, H.E., Colley, S. and Toole, J. (1990) Authigenic uranium in Atlantic sediments of the last glacial stage - a diagenetic phenomenon. *Earth Planet. Sci. Lett.* **98**, 222-232.

Thornburg, T.M. and Kulm, L.D. (1981) Sedimentary basins of the Peru continental margin: structure, stratigraphy and Cenozoic tectonics from 6°S to 16°S latitude. In*Nazca Plate: Crustal Formation and Andean Convergence* Geological Society of America, Memoir 154 (Eds L.D. Kulm, J. Dymond, E.J. Dasch and D.M. Hussong), pp.469-508.

Truesdale, V.W. (1975) "Reactive" and "unreactive" iodine in seawater - a possible indication of an organically bound iodine fraction. *Mar. Chem.* **3**, 111-119.

Turekian, K.K. (1957) The significance of variations in the strontium content of deep-sea cores. *Limnol. Oceanogr.* **2**, 309-314.

Turekian, K.K. (1964) The marine geochemistry of strontium. *Geochim. Cosmochim. Acta* **28**, 1479-1496.

Turekian, K.K. and Wedepohl, K.H. (1961) Distribution of the elements in some major units of the Earth's crust. *Geol. Soc. Amer. Bull.* **72**, 175-192.

Veeh, H.H., Burnett, W.C. and Soutar, A. (1973) Contempoary phosphorites on the continental margin of Peru. *Science* **181**, 844-845.

Veeh, H.H., Calvert, S.E. and Price, N.B. (1974) Accumulation of uranium in sediments and phosphorites on the S.W. African shelf. *Mar. Chem.* **2**, 189-202.

Vinogradov, A.P. (1939) Iodine in marine muds: to the problems of the origin of iodine-bromine waters in petroliferous regions (in Russian). *Tr. Biogeokhim. Lab. Akad. Nauk. SSSR.* **5**, 19-22 (English trans. 33-46).

Volat, J-L., Pastouret, L. and Vergnaud-Grazzini, C. (1980) Dissolution and carbonate fluctuations in Pleistocene deep-sea cores: a review. *Mar. Geol.* **34**, 1-28.

Von Breymann, M.T., Emeis, K.-C. and Camerlenghi (1990) Geochemistry of sediments from the Peru upwelling area: results from ODP sites 680, 682, 685 and 688. In *Proc. ODP Results* (Eds E. Suess *et al.*), Vol. 112, pp.491-503.

Von Breymann, M.T., Emeis, K.-C. and Suess, E. (1992) Water depth and diagenetic constraints on the use of barium as a palaeoproductivity indicator. In *Upwelling Ecosystems* Geological Society Special Publication, No. 64 (Eds C.P Summerhayes *et al.*), pp.273-284.

Walsh, J.J. (1975) A spatial simulation model of the Peru upwelling ecosystem. *Deep-Sea Res.* **22**, 201-236.

Walsh, J.J. (1981) A carbon budget for overfishing off Peru, *Nature* **298**, 300-304.

Walsh, J.J. (1991) Importance of continental margins in the marine biogeochemical cycling of carbon and nitrogen. *Nature* **350**, 53-55.

Wefer, G., Dunbar, P.B. and Suess, E. (1983) Stable isotopes of foraminifers off Peru recording high fertility and changes in upwelling history. In *Coastal Upwelling* (Eds E.Suess and J.Thiede), Part B, pp.295-308. Plenum Press, New York.

Wollast, R. (1974) The silica problem. In *The Sea* (Ed. E.D. Goldberg), Vol. 5, pp.359-392. J. Wiley, New York.

Wong, G.T.F. (1980) The stability of dissolved inorganic species of iodine in seawater. *Mar. Chem.* **9**, 13-24.

Wong, G.T.F. and Brewer, P.G. (1974) The determination and distribution of iodate in South Atlantic waters. *J. Mar. Res.* **32**, 25-36.

Wong, G.T.F. and Brewer, P.G. (1977) The marine chemistry of iodine in anoxic basins. *Geochim. Cosmochim. Acta* **41**, 151-159.

Wright, J.V. (1981) The Caliente ignimbrite: analysis of a compound intraplinian ignimbrite from a major Quaternary Mexican eruption. *Bull. Volvanologique* **44**, 198-212.

Wyrtki,K. (1963) The horizontal and vertical field of motion in the Peru Current. *Bull. Scripps Inst. Oceanography* **8**, 13-346.

Zuta, S., Rivera, T. and Bustamante, A. (1978) Hydrologic aspects of the main upwelling areas off Peru. In *Upwelling Ecosystems* (Eds R.Boje and M.Tomczak), pp.235-257.Springer, New York.

# APPENDIX A

# ANALYTICAL METHODS

# APPENDIX A.1. SEDIMENT COLLECTION AND SAMPLING

Four piston cores and two box cores recovered from the Peruvian continental margin during the *R.R.S. Charles Darwin* Leg 38 cruise (April-May 1989) were selected and sampled for analysis (Table 1.1).

The piston cores (in sections of about 1m in length) and the box cores (sliced at 1-2cm intervals onboard ship and stored in sealed polythene bags) were transported in a sealed container at 4°C to the Grant Institute, University of Edinburgh.

Sub-sampling of the piston cores was carried out after the sections had been sliced in half lengthwise and one half stored for archive. Using $10cm^3$ polythene plugs (2cm diameter), samples were taken at approximately 10cm intervals down to the base of each core. The intervals varied slightly due to irregularities in the core and also due to the fact that, for some of the cores, S. King from Southampton University was also taking samples.

The wet sediment samples (from both piston and box cores) were placed on watchglasses, weighed and then dried in an oven at 50°C for up to 5 days. Reweighing after drying allowed for calculation of the sample water content, and from this value the sample salt content was also calculated (Appendix A.6). Water and salt content data are tabulated in Appendix C.1.

Dried sediment samples were ground to a very fine powder (<2μm) using a tungsten-carbide TEMA mill for 1 minute. These samples are the dried bulk sediment samples used for XRF and other geochemical analyses.

# APPENDIX A.2.

# SAMPLING, CLEANING AND ANALYSIS OF FORAMINIFERA

## A.2.1. Sample Preparation

The four piston cores (Table 1.1) were resampled at about 10cm intervals using the same techniques as for the bulk sediment samples (Appendix A.1). However, instead of being dried after weighing, the samples were sieved through a 63μm mesh using a fine spray of warm tap water. The >63μm fraction remaining contained foraminifera, radiolaria, diatoms, fish bones and coarse-grained material, and this was dried overnight at 40°C in an oven and then reweighed. This enabled

determination of the weight percent >63μm fraction for each sample (data are given in Appendix C.2).

Under a microscope and using a very fine paintbrush, up to 40 individual and intact tests of particular foraminifera species were picked from each sample; species, numbers and size fractions are detailed in Appendix C.2. The foraminifera were placed in labelled plastic vials, ultrasonicated in methanol for up to 1 min and dried prior to analysis of their stable isotope ratios at the Scottish Universities' Research and Reactor Centre (SURRC), East Kilbride. During foraminifera picking, each sample was semi-quantitatively examined for the presence of diatom frustules, fish remains and quartz and clay grains using a simple scaling of : 0 = absent, 1 = rare, 2 = common and 3 = abundant. The results of this examination are detailed in Appendix C.2.

### A.2.2. Stable Isotope Analysis

Determination of the carbon and oxygen stable isotope ratios of the foraminifera $CaCO_3$ tests was carried out on a VG Isotech PRISM isotope mass spectrometer, under the supervision of A.E. Fallick and T. Donnelly. Between 3 and 20 individual tests per sample (depending on size and species) were weighed into tiny buckets. The optimum weight for analysis was about 0.1mg. Both SM calcite and MBL1 standards were run with each autorun batch of samples.

The mass spectrometer autorun procedure was as follows: the sample is dropped from the rotating carousel into the reaction vessel containing 10ml phosphoric acid (at 90°C and continuously stirred). The $CO_2$ gas given off from the reaction between the calcium carbonate and the acid, is pumped via a water trap (at -100°C) over to a cold finger (at -196°C) under high vacuum. The cold finger is then heated back to room temperature and the $CO_2$ gas moved through a series of valves and a second cold finger, until it reaches the mass spectrometer. The reference ion beam current is matched to that of the sample ion beam by the use of variable-volume bellows. The mass spectrometer then measures the difference between the $^{13}C/^{12}C$ and the $^{18}O/^{16}O$ ratios of the sample and those of the reference gas, and gives the results as $\delta 1$ and $\delta 2$ values (Eqn A.2.1).

These values are then recalculated into $\delta^{13}C$ (‰) and $\delta^{18}O$ (‰) by comparison with the average $\delta 1$ and $\delta 2$ values for the SM calcite standards in the autorun and then, using Eqn A.2.2, converted into the standard nomenclature for

foraminifera isotope results. Results of $\delta^{13}C$ (PDB, ‰) and $\delta^{18}O$ (PDB, ‰) for all the foraminifera samples are tabulated in Appendix C.2.

Equation A.2.1. Delta Calculation

$$\delta 1\ (‰) = (({}^{13}C/{}^{12}C_{sam} - {}^{13}C/{}^{12}C_{ref}) / {}^{13}C/{}^{12}C_{ref}) \times 1000$$

$$\delta 2\ (‰) = (({}^{18}O/{}^{16}O_{sam} - {}^{18}O/{}^{16}O_{ref}) / {}^{18}O/{}^{16}O_{ref}) \times 1000$$

where, sam = sample gas
ref = reference gas

Equation A.2.2. $\delta^{13}C$ and $\delta^{18}O$ calculations

$$\delta^{13}C\ (PDB, ‰) = (\delta^{13}C_{sample} - \delta^{13}C_{PDB\ standard}) / \delta^{13}C_{PDB\ standard} \times 1000$$

$$\delta^{18}O\ (PDB, ‰) = (\delta^{18}O_{sample} - \delta^{18}O_{PDB\ standard}) / \delta^{18}O_{PDB\ standard} \times 1000$$

| | | |
|---|---|---|
| Target major ion beam | $6.00 \times 10^{-9}$ A | |
| Maximum reference ion beam | $1.64 \times 10^{-8}$ A | |
| Minimum reference ion beam | $2.49 \times 10^{-9}$ A | |
| Ion gauge base pressure | $7.60 \times 10^{-10}$ Torr | |
| Cold finger ambient temperature | 25°C | |
| | $\delta^{18}O$ | $\delta^{13}C$ |
| Std. dev. for SM1 standard (n = 100) | 0.085% | 0.115% |

Table A.2.1. Normal operating conditions of the PRISM mass spectrometer and the typical standard deviation values for the SM calcite standard.

## APPENDIX A.3. ORGANIC CARBON

Carbon occurs in marine sediments from two main sources; carbonate carbon ($CaCO_3$ shells of zooplankton) and organic carbon (from the remains of marine organisms). Before the concentration of organic carbon ($C_{org}$) can be measured, the carbonate carbon within the sample must be preferentially removed. Acid digestion of the carbonate is the common way to remove this phase. Care must be taken to avoid

loss of $C_{org}$ by hydrolysis if the sample is washed after acid attack, and so the entire analytical procedure is carried out with the sample in a LECO ceramic crucible.

The dried bulk sediment sample was accurately weighed (0.2-0.5g ±0.01mg) into a LECO crucible and dampened with deionised water. This ensured no loss of sample from splashing, upon addition of the first few drops of 50% solution HCl (aq). The strength of effervescence was dependant upon the concentration of carbonate and so extra care was taken with carbonate-rich samples. Further drops of acid were added only once the fizzing had ceased each time, and then when no more effervescence occurred the crucible was placed on a hotplate set at about 60°C for 2 hours to allow for evaporation of the excess water. After cooling, more acid was added and the sample stirred with a glass rod to ensure complete digestion of the carbonate. The glass rod was washed with deionised water into the crucible after each stirring. All work was carried out in a fume cupboard.

Samples were evaporated to dryness on the hotplate overnight before analysis. $C_{org}$ concentration was analysed by combustion in an induction furnace, in an oxygen atmosphere, followed by potassium hydroxide absorption of the $CO_2$ produced. Combustion of the sample was performed using a LECO 521-200 induction furnace fitted with a dust trap, sulphur trap ($MnO_2$ powder) and catalyst furnace. The sample crucible was put into the furnace straight from the hotplate (to minimise loss of $CaCl_2$), with tin and iron chip accelerators and at an oxygen flow rate of 1.5 l $min^{-1}$.

The furnace was connected to a LECO 572-100 carbon analyser which has a glass burette to measure the change in volume that results when the $CO_2$-$O_2$ mixture from combustion is flushed through the $CO_2$-absorbing KOH solution. The burette reading was then corrected for air pressure, temperature and the original weight of sample to calculate the percentage weight of organic carbon.

These values were then corrected for salt dilution (see Appendix A.6) and the results are tabulated in Appendix C.12.

Steel rings were run as standards after every fifth sample and one (high carbonate) sample was replicated to assess analytical precision.

Sample 3803-29 : n = 48, mean = 1.50 wt.% $C_{org}$
$\sigma$ = 0.07, standard deviation = 4.66%.

## APPENDIX A.4. BIOGENIC SILICA

Analytical determination of the concentration of biogenic silica was based on a wet chemical leaching technique (Eggimann *et al.*, 1980) which is more sensitive than

other methods, e.g. X-ray diffraction or infra-red spectroscopy. Exact procedures follow the work by Dobbie (1988) and involve initial digestion of the sample in sodium carbonate, and then colorimetric spectrophotometry of both silica and alumina in the filtered solution.

### A.4.1. Sample Digestion

Into a PTFE beaker, approximately 50mg of bulk sediment sample was accurately weighed, 20ml of 2M $NaCO_3$ (aq) was added and the beaker sealed in a steel bomb. The bomb was then placed in an oven at 90-100°C for 4 hours; leaching conditions which are sufficient to allow for complete digestion of biogenic, amorphous silica whilst keeping aluminosilicate (clays) and quartz attack to a minimum. The increase in pressure with heating raised the boiling point of the solution and ensured no loss of solution at the lid, and the closed-system reaction required no stirring and prevented evaporation and concentration of the sodium carbonate solution.

After cooling, the contents of the beaker were vacuum filtered through a 0.4μm polycarbonate membrane filter, using a plastic filtering system. Plastic apparatus was used to prevent contamination caused by silica leaching from glassware. The filtrate and washings (always using deionised water) were diluted to 100ml in a volumetric flask and then the solution was stored in a plastic bottle, prior to silica and alumina analysis.

### A.4.2. Silica Determination

Measurement of the silica content of the filtrate by colorimetric analysis depends on the formation of yellow, unreduced silicomolybdate acid, followed by selective reduction to molybdate blue using excess molybdate (Strickland and Parsons, 1968). Methods of reagent preparation follow those of Dobbie (1988).

The procedure was carried out in a 100ml glass volumetric flask and silica contamination was avoided by initially adding dilute HCl (aq) : enough to neutralise the sodium carbonate plus 1ml in excess to obtain the correct pH (1.0-1.4). The aliquot of sample (or standard or blank) that was added depended on the rough percentage of biogenic silica, and this was followed by deionised water to make the volume up to 15ml. After addition of 1ml ammonium molybdate reagent the flask was shaken and left for exactly 10 min to allow the colour to develop. Then 5ml oxalic acid (which decomposes any yellow phosphomolybdate and prevents iron

interference) and 2ml reducing solution were added in quick succession along with deionised water to make up to the 100ml mark.

After 1 hour, the absorption of the solution was measured at 812nm using 2cm cells in a Perkin Elmer 550 spectrophotometer.

A calibration graph of absorption against concentration gave a linear co-relation for a range of standards and so with each batch of samples only one standard needed to be measured. One blank per batch was also required to allow for interference from NaCl in solution.

Silica concentration of the sample was calculated by direct comparison with the known standard and then weight percent from the known weight of sample digested (Eqn A.4.1.). This weight % silica is termed apparent biogenic silica because some of the silica in solution may be derived from non-amorphous sources. The final stage of the analytical procedure is therefore to measure the alumina content of the sample solution so that corrections can be made to allow for any digestion of aluminosilicates. The presence of quartz-derived silica is thought to be negligible and is ignored because it would require a second-order correction.

Equation A.4.1. Apparent Biogenic Silica Calculation

$$\text{App. Bio. Sil. (wt.\%)} = [(R-B) \times k] / [(S-B) \times wt.]$$

where,

R = Absorption of sample
B = Absorption of blank
S = Absorption of standard
wt. = Sample weight (mg)
k = [(No. of ml standard in 100ml) x (100%)
x (wt. of Specpure $SiO_2$ in standard stock solution)].

### A.4.3. Alumina Determination

This colorimetric method (Dougan and Wilson, 1974) involved the formation of an aluminium catechol violet complex. All standards and reagents were stored in plastic bottles to avoid leaching of $Al_2O_3$ from Pyrex glassware. Once again, the methods of reagent preparation follow those of Dobbie (1988).

A 5ml aliquot of sample, standard or blank was added to a 50ml plastic volumetric flask, followed by dilute HCl (enough to neutralise the sodium carbonate

plus 1.24ml in excess) and dilution to 35ml with deionised water. Then 1ml of 10% phenanthroline solution was added to prevent iron interference, followed by 2ml of the catechol violet reagent and 10ml hexamine solution (this acts as a buffer to obtain pH = 5.9-6.2). The flask was shaken after each addition and the solution made up to the 50ml mark with deionised water.

After 10 min, the absorption of the solution was measured at 585nm using 1cm cells in a Perkin Elmer 550 spectrophotometer.

The standard calibration graph (absorption against concentration) was linear and so only one standard (and one blank) was measured per batch of samples. The calculation of $Al_2O_3$ content of the sample solutions was by comparison with the standard and use of the known sample weight (Eqn A.4.2.).

Equation A.4.2. Alumina Calculation

$$Al_2O_3 \text{ (wt.\%)} = [(R-B) \times k] / [(S-B) \times wt.]$$

where,
R = Absorption of sample
B = Absorption of blank
S = Absorption of standard
wt. = Weight of sample (mg)
k = [(No. of ml of standard in 100ml) x (No. of ml $Al_2O_3$ standard) x (weight of $Al_2O_3$ in stock standard) x (100%)].

Equation A.4.3. was used to calculate the weight percent biogenic silica, and then these values were corrected for salt dilution (Appendix A.6.) and the results are tabulated in Appendix C.12.

Equation A.4.3. Biogenic Silica Calculation

$$\text{Biogenic Silica (wt.\%)} = \text{Apparent Biogenic Silica (wt.\%)} - [2 \times Al_2O_3 \text{ (wt.\%)}]$$

where, 2 = $SiO_2$ / $Al_2O_3$ ratio of marine clays (Dobbie, 1988).

### A.4.4. Analytical Precision

One sediment sample was replicated to assess analytical precision.

Sample BC 3803-32 : n = 7, mean = 11.25 wt.% biogenic silica
$\sigma$ = 0.193, standard deviation = 1.71%.

# APPENDIX A.5.

## X-RAY FLUORESCENCE (XRF) SPECTROMETRY

XRF spectrometry was used to measure a wide range of major and minor (trace) elements in the sediment samples, using a Phillips PW 1480 sequential automatic X-ray spectrometer and a PW 1510 sample changer.

### A.5.1. Major Element Disc Preparation

Fused glass discs (45mm diameter) were prepared following methods similar to those of Norrish and Hutton (1969). Approximately 1.5g of dried bulk sediment sample was dried overnight at 50°C in an oven and then about 0.9g of the sample was accurately weighed (±0.0001g) into a platinum crucible. The crucible, with Pt lid, was then placed in a muffle furnace at 1100°C for 5 min ignition. This length of time was chosen after a test was run to examine the loss of volatile alkali metals (K and Na) with varying ignition times (Table A.5.1.). Over five minutes ignition resulted in loss of Na and K but at less than 5 min. ignition time, the furnace did not return to 1100°C.

| Ignition time (mins) | Na2O (wt.%) | K2O (wt.%) |
|---|---|---|
| 0 | 3.08 | 1.775 |
| 0 | 3.00 | 1.761 |
| 2 | 3.25 | 1.794 |
| 5 | 2.92 | 1.680 |
| 10 | 2.75 | 1.501 |
| 15 | 2.69 | 1.402 |
| 20 | 2.49 | 1.115 |
| 60 | 2.32 | 0.934 |

Table A.5.1. Loss of Na and K upon increasing ignition times.

After cooling and reweighing, to calculate a loss on ignition percentage, an ultrapure flux (Spectroflux 105, Johnson Matthey Chemicals Ltd.) was added in a ratio to the pre-ignited sample weight of exactly 5:1. The crucible was covered again

and placed back in the furnace to fuse the sample and flux for 20 min. Working with batches of four crucibles was most suitable.

The flux is composed of $Li_2B_4O_2$, $La_2O_2$ and $Li_2CO_3$; the tetraborate helps to dissolve the sediment and the lanthinum acts as a heavy absorber of the X-rays and helps to minimise matrix effects. The effect of the matrix differences between samples and standards is also corrected for by using theoretical absorption coefficients (Theisen and Vollach, 1967).

Once the crucible had cooled back to room temperature, it was reweighed. A small amount of flux was added to make up to the correct total weight (±0.0002g) and the sample was fused again over a Meker burner. The molten glass was then poured into a disc-shaped graphite mould, placed in a brass sleeve and on a hot-plate at 220°C. With an aluminium plunger, also at 220°C, the glass was quickly pressed into a 1mm thick disc, the upper surface of which had an "orange peel" texture. The disc was allowed to anneal on the hot-plate, cooled slowly and then stored in a sealed polythene bag in a desiccator prior to analysis.

### A.5.2. Major Element Analysis

International rock and sediment standards which cover the wide range in composition of major elements found in marine sediments were used for calibration of the X-ray spectrometer (Table A.5.2). For all the major elements (Si, Al, Fe, K, P, Na, Ti, Mn, Mg and Ca) measured, calibration lines were found to be linear.

Analytical conditions for the XRF major element analysis are given in Table A.5.3 and the precision and accuracy for each element in Table A.5.4. The raw data in the form of major element oxides (Appendix C.5) were then recalculated into major element concentrations (Appendix C.6) and corrected for the effects of the presence of salt (Appendix A.6) and the resulting data are tabulated in Appendix C.7.

| Standards |
|---|
| Ba-1 (I-III), Ba-2 (I-III), Ba-3 (I-III), Ba-4 (I-III), Ba-5 (I-III), Ba-6 (I-III) |
| BRIMO-1 (I-III), BRIMO-2 (I-III), BRIMO-3 (I-III), BRIMO-4 (I-III) BRIMO-5 (I-III), BRIMO-6 (I-III), BRIMO-7 (I-III) |
| MAG-1, BCR-1, AGV-1, GA, BR, GH, SY-2, SY-3, JB-1, PCC-1, SGR-1, GSP-1 |

Table A.5.2. Internal and international rock standards used in XRF calibration.

Ba- and BRIMO- standards are a synthetic dilution series made from the following SPECPURE compounds: $Ba(IO_3)_2$, $KBrO_3$, $(NH_4)Mo_7O_{24}.4H_2O$ and

Table A.5.3. Analytical conditions for X-ray fluorescence

| Element | Line | Tube | kV | mA | Crystal | Peak (°) | + Offset | - Offset | Detector | Pulse Height | Collimator | Sample | Count (s) |
|---|---|---|---|---|---|---|---|---|---|---|---|---|---|
| Al | k-alpha | Rh | 40 | 60 | PE | 144.955 | 0.60 | 0.00 | FL | 28 76 | Coarse | FD | 50 |
| Ba | L-alpha | Rh | 50 | 50 | Ge220 | 87.970 | 1.60 | 2.70 | FL | 32 70 | Fine | PP | 100 |
| Br | k-alpha | Rh | 80 | 30 | LiF200 | 29.940 | 0.00 | 0.60 | FS | 27 75 | Fine | PP | 20 |
| Ca | k-alpha | Rh | 50 | 50 | LiF200 | 113.145 | 0.00 | 4.00 | FL | 30 75 | Fine | FD | 20 |
| Ce | L-beta | Rh | 50 | 50 | LiF200 | 71.625 | 0.00 | 0.00 | FL | 32 70 | Fine | PP | 100 |
| Cr | k-alpha | Rh | 50 | 50 | LiF200 | 69.375 | 1.62 | 0.88 | FL | 32 70 | Fine | PP | 40 |
| Cu | k-alpha | Rh | 50 | 50 | LiF200 | 45.040 | 1.70 | 0.70 | FL | 40 70 | Fine | PP | 40 |
| Fe | k-alpha | Rh | 50 | 50 | LiF200 | 57.530 | 0.00 | 2.50 | FL | 18 68 | Fine | FD | 10 |
| I | k-alpha | Rh | 80 | 30 | LiF200 | 12.375 | 0.50 | 0.50 | SC | 25 75 | Fine | PP | 20 |
| K | k-alpha | Rh | 50 | 50 | LiF200 | 136.720 | 0.00 | 5.00 | FL | 32 75 | Fine | FD | 20 |
| La | L-alpha | Rh | 50 | 50 | LiF200 | 82.950 | 1.20 | 1.20 | FL | 32 70 | Fine | PP | 100 |
| Mg | k-alpha | Rh | 40 | 60 | PX1 | 22.605 | 3.10 | 0.00 | FL | 25 80 | Coarse | FD | 50 |
| Mn | k-alpha | Rh | 50 | 50 | LiF200 | 63.000 | 2.50 | 0.00 | FL | 14 72 | Fine | FD | 10 |
| Mo | k-alpha | Rh | 80 | 30 | LiF200 | 20.300 | 0.44 | 0.44 | SC | 28 70 | Fine | PP | 100 |
| Na | k-alpha | Rh | 40 | 60 | PX1 | 27.275 | 0.00 | 0.00 | FL | 25 75 | Coarse | FD | 50 |
| Ni | k-alpha | Rh | 50 | 50 | LiF200 | 48.685 | 1.30 | 0.00 | FL | 40 70 | Fine | PP | 40 |
| Nb | k-alpha | Rh | 80 | 30 | LiF200 | 21.360 | 0.40 | 0.70 | FS | 20 75 | Fine | PP | 40 |
| Nd | k-alpha | Rh | 40 | 50 | LiF200 | 72.160 | 2.30 | 0.00 | FL | 32 70 | Fine | PP | 100 |
| P | k-alpha | Rh | 50 | 60 | Ge111 | 140.915 | 3.00 | 0.00 | FL | 34 75 | Coarse | FD | 50 |
| Pb | L-beta | Rh | 80 | 30 | LiF200 | 28.245 | 0.30 | 0.30 | FS | 20 75 | Fine | PP | 100 |
| Rb | k-alpha | Rh | 80 | 30 | LiF200 | 26.585 | 0.54 | 0.00 | FS | 20 75 | Fine | PP | 40 |
| Sc | k-alpha | Rh | 50 | 50 | LiF200 | 97.750 | 0.00 | 2.00 | FL | 30 70 | Fine | PP | 40 |
| Si | k-alpha | Rh | 40 | 60 | PE | 109.070 | 4.00 | 0.00 | FL | 30 75 | Coarse | FD | 50 |
| Sr | k-alpha | Rh | 80 | 30 | LiF200 | 21.111 | 0.76 | 0.76 | FS | 20 75 | Fine | PP | 40 |
| Ti | k-alpha | Rh | 50 | 50 | LiF200 | 86.185 | 3.50 | 0.00 | FL | 28 72 | Fine | FD | 20 |
| Th | L-alpha | Rh | 80 | 30 | LiF200 | 27.465 | 0.00 | 0.30 | FS | 20 75 | Fine | PP | 100 |
| U | L-alpha | Rh | 80 | 30 | LiF200 | 26.130 | 0.00 | 0.36 | FS | 20 75 | Fine | PP | 100 |
| V | k-alpha | Rh | 50 | 50 | LiF200 | 123.260 | 0.00 | 1.30 | FL | 32 70 | Fine | PP | 40 |
| Y | k-alpha | Rh | 80 | 30 | LiF200 | 23.760 | 0.00 | 0.00 | FS | 20 75 | Fine | PP | 40 |
| Zn | k-alpha | Rh | 50 | 50 | LiF200 | 41.795 | 0.66 | 0.66 | FS | 22 75 | Fine | PP | 40 |
| Zr | k-alpha | Rh | 80 | 30 | LiF200 | 22.500 | 0.66 | 0.76 | FS | 20 75 | Fine | PP | 40 |

Detectors : FL = Flow, SC = Scintilation and FS = Flow and Scintilation

Samples : FD = Fused disc and PP = Pressed pellet

Table A.5.4. XRF analytical precision and accuracy

| Oxide | Mean (n=8) | S.D. | % S.D. | Accuracy |
|---|---|---|---|---|
| SiO2 | 52.137 | 0.061 | 0.117 | 0.147 |
| Al2O3 | 15.619 | 0.033 | 0.211 | 0.124 |
| Fe2O3 | 8.894 | 0.021 | 0.236 | 0.157 |
| MgO | 3.407 | 0.02 | 0.582 | 0.037 |
| CaO | 1.852 | 0.01 | 0.523 | 0.086 |
| Na2O | 3.111 | 0.031 | 0.996 | 0.062 |
| K2O | 1.439 | 0.007 | 0.486 | 0.017 |
| TiO2 | 0.824 | 0.003 | 0.314 | 0.017 |
| MnO | 0.054 | 0.002 | 4.444 | 0.01 |
| P2O5 | 0.11 | 0.003 | 2.573 | 0.014 |

| Element | Mean (n=8) | S.D. | % S.D. | Accuracy |
|---|---|---|---|---|
| Ba | 2615.1 | 11.1 | 0.4 | 27.66 |
| Br | 160.1 | 1.7 | 1.1 | 2.4 |
| Ce | 26.4 | 3.5 | 13.4 | 7.89 |
| Cr | 71.8 | 1 | 1.4 | 55.48 |
| Cu | 89.9 | 0.7 | 0.8 | 5.69 |
| I | 84.9 | 3.5 | 4.1 | 3.7 |
| La | 13.9 | 2.2 | 15.9 | 4.3 |
| Mo | 4.4 | 0.3 | 6.4 | 0.6 |
| Nb | 3.5 | 0.2 | 6.4 | 2.42 |
| Nd | 19.5 | 2.3 | 11.7 | 3.14 |
| Ni | 153.4 | 0.9 | 0.6 | 4.45 |
| Pb | 7 | 0.8 | 11.4 | 2.02 |
| Rb | 26.7 | 0.2 | 0.7 | 3.08 |
| Sc | 16.7 | 1.5 | 9 | 3.19 |
| Sr | 528.2 | 3.2 | 0.6 | 8.46 |
| Th | 0.4 | 0.4 | 100 | 1.77 |
| U | 10.2 | 0.9 | 9.2 | 4.73 |
| V | 198.4 | 1.2 | 0.6 | 6.37 |
| Y | 23.7 | 0.5 | 2.3 | 1.28 |
| Zn | 285.2 | 1.2 | 0.4 | 3.27 |
| Zr | 58.8 | 0.5 | 0.8 | 10.49 |

Major element oxides measured in wt.%

Minor elements measured in ppm

% S.D. is total precision including counting error, disc reproducibility, error. in regression line and error in matrix mass absorption determinations.

Accuracy determined from r.m.s.d. of international standards about the regresion line.

Repeat analysis carried out by A.J.Patience on a marine sediment sample from the Eastern Equatorial Pacific (Patience, 1992), who ran XRF samples at same time as the CD38 samples in this study.

$BaCO_3$. Each was prepared using $CaCO_3$ (I), Salisbury Crag Dolomite (II) and Shap Granite (III) matrices, to represent a wide range of possible sediment compositions and mass absorption effects. Calibration lines were periodically revised and some standards changed, depending on what concentrations of each element were required.

### A.5.3. Minor Element Disc Preparation

Pressed powder discs (32mm diameter) were used for minor element analysis. Approximately 3g (±0.1g) of dried bulk sediment sample was placed onto a polished tungsten carbide disc, enclosed in a stainless steel inner sleeve (which itself was enclosed in a larger cylinder). A perspex plunger was inserted down the inner sleeve, carefully compacting the sediment under hand pressure. After removal of both the plunger and inner sleeve, boric acid powder was added to cover the sample disc. Then a large, stainless steel plunger was lowered onto the boric acid and, using a hydraulic press at 10 tons for 1 min, the disc was fully compacted. The pressed powder disc was then stored in a sealed polythene bag and within a desiccator prior to analysis (this prevented loss of halogens and movement of salt to the surface).

### A.5.4. Minor Element Analysis

The international rock and sediment standards used gave linear calibration lines for all the minor elements (Ba, Sc, V, Ni, Cu, Zn, Sr, Nb, Cr, Zr, Pb, Th, U, Rb, Mo, I, Br, Y, La, Ce and Nd) measured over their wide range in concentrations (Table A.5.2). Analytical conditions for XRF minor element analysis are given in Table A.5.3, with the precision and accuracy for each element in Table A.5.4. Minor element raw data (Appendix C.9) was then corrected for salt dilution (Appendix A.6) and the results are tabulated in Appendix C.10.

## APPENDIX A.6. SALT CORRECTIONS

Upon drying the bulk sediment samples (Appendix A.1) the sea salt that is contained within the pore-waters is incorporated within the sediment. This salt contains significant amounts of Na, Mg, Ca, K and Br and thus the measured concentration of these elements needs to be corrected for the contribution that the salt makes to the sample. All XRF elemental, $C_{org}$ and biogenic silica measurements of the bulk sediment sample must then be corrected for the dilution effect of the salt.

The salinity of pore-waters is assumed to be constant and the same as that of normal sea-water, i.e. about 35 parts per thousand. Using this assumed value and the water contents measured for each sample (Appendix C.1), the salt content in the sediment was calculated using Eqn A.6.1.

Equation A.6.1. Salt Content

$$Salt = (3.513 \times W) / (100 - W)$$

where, W = Water content (% wet weight).

Salt contribution corrections for Na, Mg, Ca, K and Br were calculated using the following equations:

$$Na_{sed}\ (wt.\%) = Total\ Na_{sed}\ (wt.\%) - (0.306 \times Salt)$$
$$Mg_{sed}\ (wt.\%) = Total\ Mg_{sed}\ (wt.\%) - (0.037 \times Salt)$$
$$Ca_{sed}\ (wt.\%) = Total\ Ca_{sed}\ (wt.\%) - (0.012 \times Salt)$$
$$K_{sed}\ (wt.\%) = Total\ K_{sed}\ (wt.\%) - (0.011 \times Salt)$$
$$Br_{sed}\ (ppm) = Total\ Br_{sed}\ (ppm) - (19 \times Salt)$$

where, Total wt.% or ppm are from XRF raw data,
Salt is from Eqn A.6.1,
Multiplication factors are from Horne (1969).

Then, all elemental concentrations were corrected for salt dilution using Eqn A.6.2 to obtain salt-free values.

Equation A.6.2. Salt dilution correction

$$Element\ (salt\text{-}free) = Element_{meas} \times (100 / (100 \times Salt))$$

where, $Element_{meas}$ is from XRF, $C_{org}$ and biogenic silica raw data or from above for Na, Mg, Ca, K and Br,
Salt is from Eqn A.6.1.

## APPENDIX A.7. PORE-WATER PHOSPHATE

Pore-water phosphate concentrations were measured on samples from thin slices of box core material which had been centrifuged and filtered through 0.4μm membrane filters into acid-washed vials. Analyses were carried out using a FIATRON flow injection analysis system following methods based on Strickland and Parsons (1968) and results were found to be very precise but may contain ±5-10% errors in accuracy due to matrix interference. Analysis was carried out onboard the *R.R.S. Charles Darwin* by G.B. Shimmield, T. Shimmield and A.J. Patience. The results for cores CD38-09, CD38-10 and CD38-11 are listed in Appendix C.4.

## APPENDIX A.8. URANIUM-SERIES DISEQUILIBRIUM METHODS

The uranium-series dating of the large phosphorite nodule from core CD38-09 was carried out under the supervision of Dr G.B. Shimmield. Although I carried out a large number of test samples to try to increase the efficiency of the procedure, the actual phosphorite sample determination was done by Colin Chilcott, a research assistant, in the new clean laboratory at the Department of Geology and Geophysics. The data of the count rates and activities of the U and Th isotopes can be seen in Appendix C.15.

The following is a short description of the analytical methods used. Full details can be found in Poole (1992).

1) The sample was ground to a fine powder using a TEMA mill and then divided into two duplicate samples of between 0.3 and 0.4g in weight. Both samples were then run in parallel to check for precision of results.
2) The sample was transferred to a PTFE crucible and completely digested in conc. $HNO_3$ and conc. HF acids, then fumed to dryness.
3) In order to allow the yield of the procedure to be deduced, a mixed spike of $^{228}Th$ and $^{232}U$ was added using an Eppendorf pipette.
4) $^{230}Th$ and $^{234}U$ have very similar peak α-particle energies and therefore the U and Th radionucleides were chemically separated using an anion exchange column filled with Bio-Rad AG1-X8 resin.
5) Once separated, the U and Th solutions were electroplated onto different stainless steel planchets, in order to obtain a mono-atomic layer suitable for counting.

6) Samples were counted using α-spectrometry on a silicon surface barrier counter for about $10^4$ counts or a time equivalent to the background counting time (measured for 2 days prior to the sample and used to correct for detector contamination).

7) $^{238}U$, $^{234}U$, $^{232}Th$ and $^{230}Th$ activity rates were calculated using knowledge of sample weight, unknown isotope corrected-counts, spike corrected-counts and spike activity.

8) $^{234}U/^{238}U$ and $^{230}Th/^{234}U$ ratios were then calculated, along with their errors, and from an isochron plot and the formula in Appendix B.5, the (maximum) age of the sample was calculated.

## APPENDIX A.9. X-RAY DIFFRACTION ANALYSIS

Sample preparation for X-ray diffraction analysis involved placing a small amount (about 0.1g) of the bulk-sediment sample in a mortar, adding a few drops of acetone and gently grinding with a pestle.

| | |
|---|---|
| Generator settings | 40kV, 50mA |
| Cu kα 1,2 wavelengths | 1.54060, 1.554439 |
| Step size, sample time | 15 sec / ° |
| Monochromator used | Yes |
| Divergence slit | Automatic |
| Analysis program number | 8 |
| Peak angle range | 2° to 60° (2θ°) |
| Range in D-spacing | 2.25221 to 44.1372 Å |
| Crystal peak width range | 0 to 2° |
| Minimum peak significance | 0.75 |

Table A.9.1. X-ray diffraction analytical conditions

The resulting solution was drawn up in a pipette and dispersed onto a 2cm diameter glass slide. The acetone was allowed to evaporate off, leaving a thin, even film of the sample on the glass disc. The mineral identification analysis was carried out using a Phillips PW 1011/1050 diffractometer, under the analytical conditions set out in Table A.9.1.

# APPENDIX B

# CALCULATION OF SEDIMENT PARAMETERS

## APPENDIX B.1. Calcium carbonate

$$CaCO_3\ (wt.\%) = [Ca - \{(Ca/Al^* \times Al) + (Ca/P \times P_{phos})\}] \times (100/40)$$

where, Ca, Al and P are XRF data (salt corrected and in wt.%),
Ca/Al* = Ca/Al ratio from average shale (Turekian and Wedepohl, 1961) or minimum Ca/Al ratio for core,
Ca/P = Ca/P ratio in phosphorite nodule :CD38-09 (273cm),
(100/40) = molecular weight conversion factor.

## APPENDIX B.2. Enrichment factors of metals

$$E.F._{metal} = [Metal_{sample}/Al_{sample}] / [Metal_{clay}/Al_{clay}]$$

where values from Turekian and Wedepohl (1961) for deep-sea clay are as follows (all in ppm):

Al = 84,000, Mo = 27, U = 1.3, Ni = 225, Cr = 90, V = 120 and Cu = 250.

$E.F._{metal} > 1.0$ = Enrichment above that expected from terrigenous input
$E.F._{metal} < 1.0$ = Depletion below that expected from terrigenous input.

## APPENDIX B.3. Phosphorite mineral composition calculation

Algorithm for calculation of mineral composition in phosphorite nodules (uses end-member compositions from Table B.1.)

Step 1. Recalculate XRF major element oxides to total 100%.

Step 2. Put all $P_2O_5$ available into CFA

$$(P_2O_5 / 39.85) \times 100 = CFA\ (\%)$$

Step 3. Put all MgO available into dolomite

$$(MgO / 42.0) \times 100 = Dolomite\ (\%)$$

Step 4. Calculate how much CaO is left over from CFA and dolomite

$$CaO - ((CFA / 100) \times 58.77) - ((Dolomite / 100) \times 58.0) = CaO\ left$$

Step 5. Put all CaO left into calcite

(CaO left /100) x 100 = Calcite (%)

Step 6. Put all $Fe_2O_3$ available into pyrite

($Fe_2O_3$ / 100) x 100 = Pyrite (%)

Step 7. Put all $K_2O$ available into orthoclase

($K_2O$ / 15.16) x 100 = Orthoclase (%)

Step 8. Calculate how much $Al_2O_3$ is left over from orthoclase

$Al_2O_3$ - ((Orthoclase / 100) x 26.74) = $Al_2O_3$ left

Step 9. Put all $Al_2O_3$ left into plagioclase

($Al_2O_3$ left / 25.26) x 100 = Plagioclase (%)

Step 10. Calculate how much $SiO_2$ is left over from orthoclase and plagioclase

$SiO_2$ - ((Orthoclase / 100) x 59.6) - ((Plagioclase / 100) x 62.38) = $SiO_2$ left

Step 11. Put all $SiO_2$ left into opal/quartz

($SiO_2$ left / 100) x 100 = Opal/Quartz (%)

| | CFA | Dolom. | Calcite | Pyrite | Orth. | Plag. | Opal/Qtz |
|---|---|---|---|---|---|---|---|
| $SiO_2$ | 0 | 0 | 0 | 0 | 59.60 | 62.38 | 100 |
| $Al_2O_3$ | 0 | 0 | 0 | 0 | 25.26 | 26.74 | 0 |
| $Fe_2O_3$ | 0 | 0 | 0 | 100 | 0 | 0 | 0 |
| MgO | 0 | 42.0 | 0 | 0 | 0 | 0 | 0 |
| CaO | 58.77 | 58.0 | 100 | 0 | 0 | 0 | 0 |
| $Na_2O$ | 1.00 | 0 | 0 | 0 | 0 | 10.90 | 0 |
| $K_2O$ | 0 | 0 | 0 | 0 | 15.16 | 0 | 0 |
| $P_2O_5$ | 39.85 | 0 | 0 | 0 | 0 | 0 | 0 |

Table B.1. End-member mineral compositions (Glenn and Arthur, 1988)

## APPENDIX B.4. Partitioning Equations

### B.4.1. Phosphorus

$$P_{phos} = P_{total} - (P_{terr} + P_{org})$$

where, $P_{total}$ = salt-corrected XRF data,

$P_{terr} = Al \times 0.00875$ (Turekian and Wedepohl, 1961),

$P_{org} = C_{org} \times 0.0053$ (Mach *et al.*, 1987)

and, phosphorite concentration,

$$\text{Phosphorite} = P_{phos} \times (100 / 8.29)$$

**B.4.2. Uranium**

$$U_{org} = U_{total} - (U_{terr} + U_{phos})$$

where, $U_{total}$ = salt-corrected XRF data,

$U_{terr} = Al \times 0.4625$ (Turekian and Wedepohl, 1961),

$U_{phos} = P_{phos} \times 14.1$ (Fig. 3.8).

**B.4.3. Strontium**

$$Sr_{calcite} = Sr_{total} - (Sr_{terr} + Sr_{phos})$$

where, $Sr_{total}$ = salt-corrected XRF data,

$Sr_{terr} = Al \times 21.43$ (Turekian and Wedepohl, 1961),

$Sr_{phos} = P_{phos} \times 186$ (Fig. 3.10).

**B.4.4. Yttrium**

$$Y_{terr} = Y_{total} - Y_{phos}$$

where, $Y_{total}$ = salt-corrected XRF data,

$Y_{phos} = P_{phos} \times 12.1$ (Fig. 3.12).

**B.4.5. Silicon**

$$Si_{terr} = Si_{total} - [\text{Bio. Sil.} \times 0.466]$$

where, $Si_{terr}$ = terrigenous silicon (wt.%),

$Si_{total}$ = XRF Si concentration (wt.%),

Bio. Sil. = biogenic silica concentration (wt.%),

0.466 = atomic weight conversion from silica to silicon.

## APPENDIX B.5. U-series disequilibrium age and initial $^{234}U/^{238}U$ calculation

Using the measured $^{234}U/^{238}U$ and $^{230}Th/^{234}U$ ratios, the age of the sample can either be graphically estimated using a U/Th isochron plot or accurately calculated using the equation below (Ivanovich and Harmon, 1982).

### B.5.1. Age calculation

$$^{230}Th/^{234}U = [\{1 - \exp - (\lambda^{230}Th \times t)\} / {}^{234}U/^{238}U] + [\{1 - (1 / {}^{234}U/^{238}U)\} \times \{\lambda^{230}Th / (\lambda^{230}Th - \lambda^{234}U)\} \times \{1 - \exp - (\lambda^{230}Th - \lambda^{234}U) \times t\}]$$

where, $^{234}U/^{238}U$ = ratio calculated from $\alpha$-spectrometry results,
$^{230}Th/^{234}U$ = ratio calculated from $\alpha$-spectrometry results,
$\lambda^{230}Th = 9.2154 \times E^{-6} = 0.693 / {}^{230}Th_{half\text{-}life}$,
$\lambda^{234}U = 2.7943 \times E^{-6} = 0.693 / {}^{234}U_{half\text{-}life}$,
t = age of sample (years).

### B.5.2. Initial $^{234}U/^{238}U$ calculation

$$^{234}U/^{238}U_{initial} = (^{234}U/^{238}U_t - 1) / \exp - (\lambda^{234}U \times t)$$

where, $^{234}U/^{238}U_{initial}$ = initial ratio (as incorporated from sea-water),
$^{234}U/^{238}U_t$ = ratio at time (t),
$\lambda^{234}U = 2.7943 \times E^{-6}$,
t = age of sample (years).

## APPENDIX B.6. Multi-component analysis (MCA) algorithm

Algorithm for calculation of relative concentrations of 5 components (terrigenous, biogenic, authigenic, residual and hydrothermal) in marine sediments. Adapted from Dymond and Heath (1979) and Dymond (1981).

Step 1. Assume all Al (wt.%) is present only in the terrigenous component. Calculate TERR using the Al content of average clay composition (Turekian and Wedepohl, 1961).

$$TERR = (Al / Al_{clay}) \times 100 \qquad \text{where, } Al_{clay} = 8.40$$

Step 2. Calculate biogenic component by adding calcium carbonate, biogenic silica and organic carbon concentrations (all wt.%).

$$BIOG = CaCO_3 + Bio.Sil. + C_{org}$$

Step 3. Phosphorite is the dominant authigenic mineral in Peru margin sediments and therefore, calculate authigenic component as equal to wt.% phosphorite.

$$AUTH = (P_{phos} / P_{nodule}) \times 100$$

where, $P_{phos}$ = calculated from Eqn 4.1,
$P_{nodule}$ = average P concentration of phosphorite nodule in core CD38-09 = 8.29 wt.% (Table 4.1).

Step 4. Calculate the concentration of Ba (ppm) in excess to that required by the TERR, BIOG and AUTH components.

$$Ba_{xs} = Ba_{total} - (Ba_{TERR} + Ba_{BIOG} + Ba_{AUTH})$$

where, $Ba_{TERR}$ = Al (wt.%) x $Ba/Al_{clay}$ = Al x 273.41,
$Ba_{BIOG}$ = $CaCO_3$ (wt.%) x (40/100) x $Ba/Ca_{carbonate}$
= $CaCO_3$ x 0.4 x 6.082,
$Ba_{AUTH}$ = $P_{phos}$ (wt.%) x $Ba/P_{nodule}$ = $P_{phos}$ x 10.133.
($Ba/Al_{clay}$ and $Ba/Ca_{carbonate}$ from Turekian and Wedepohl, 1961. $Ba/P_{nodule}$ from Table 4.1)

Step 5. Calculate the concentration of Fe (wt.%) in excess to that required by the TERR component.

$$Fe_{xs} = Fe_{total} - [Al (wt.\%) \times Fe/Al_{clay}]$$

where, $Fe/Al_{clay}$ = 0.774 (Turekian and Wedepohl, 1961)

Step 6. If $Ba_{xs}$ is non-negative, calculate the residual component by assuming concentration of pure residual phase = 270,000 ppm Ba (Dymond, 1981).

$$RESID = (Ba_{xs} / 270{,}000) \times 100$$

Step 7. If $Fe_{xs}$ is non-negative, calculate the hydrothermal component by assuming concentration of pure hydrothermal phase = 34.8 wt.% Fe (Dymond, 1981).

$$HYDRO = (Fe_{xs} / 34.8) \times 100$$

Step. 8 Recalculate all five components to % by dividing by the sum of components and multiplying by 100.

e.g. TERR % = [TERR/ (TERR + BIOG + AUTH + RESID + HYDRO)] x100

# APPENDIX C

# DATA TABLES

| APPENDIX C.1. SEDIMENT PHYSICAL PARAMETERS | | | | | | | | | | | | |
|---|---|---|---|---|---|---|---|---|---|---|---|---|
| CD38-03 | | | | | | | CD38-02 | | | | | |
| Sample | Depth (cm.) | Water (%) | Salt | Porosity | D.B.D. | | Sample | Depth (cm.) | Water (%) | Salt | Porosity | D.B.D. |
| BC3803-01 | 0.5 | 81.6 | 15.58 | 0.921 | 0.218 | | BC3802-01 | 0.5 | 72.1 | 9.08 | 0.872 | 0.351 |
| BC3803-02 | 1.5 | 77.0 | 11.76 | 0.898 | 0.281 | | BC3802-02 | 1.5 | 73.0 | 9.50 | 0.877 | 0.338 |
| BC3803-03 | 2.5 | 78.1 | 12.53 | 0.904 | 0.264 | | BC3802-03 | 2.5 | 67.4 | 7.26 | 0.845 | 0.427 |
| BC3803-04 | 3.5 | 72.7 | 9.36 | 0.875 | 0.358 | | BC3802-04 | 3.5 | 67.4 | 7.26 | 0.845 | 0.426 |
| BC3803-05 | 4.5 | 73.9 | 9.95 | 0.882 | 0.325 | | BC3802-05 | 4.5 | 68.4 | 7.60 | 0.851 | 0.411 |
| BC3803-06 | 5.5 | 73.1 | 9.55 | 0.877 | 0.338 | | BC3802-06 | 5.5 | 64.7 | 6.44 | 0.828 | 0.470 |
| BC3803-07 | 6.5 | 68.7 | 7.71 | 0.853 | 0.405 | | BC3802-07 | 6.5 | 61.5 | 5.61 | 0.808 | 0.527 |
| BC3803-08 | 7.5 | 69.1 | 7.86 | 0.855 | 0.399 | | BC3802-08 | 7.5 | 59.7 | 5.20 | 0.796 | 0.559 |
| BC3803-09 | 8.5 | 70.9 | 8.56 | 0.865 | 0.370 | | BC3802-09 | 8.5 | 59.6 | 5.18 | 0.795 | 0.562 |
| BC3803-10 | 9.5 | 68.6 | 7.67 | 0.852 | 0.407 | | BC3802-10 | 9.5 | 59.4 | 5.14 | 0.794 | 0.564 |
| BC3803-11 | 11.0 | 68.9 | 7.78 | 0.854 | 0.411 | | BC3802-11 | 11.0 | 59.7 | 5.20 | 0.796 | 0.559 |
| BC3803-12 | 13.0 | 68.6 | 7.67 | 0.852 | 0.406 | | BC3802-12 | 13.0 | 59.5 | 5.16 | 0.795 | 0.562 |
| BC3803-13 | 15.0 | 66.6 | 7.00 | 0.840 | 0.447 | | BC3802-13 | 15.0 | 58.8 | 5.01 | 0.790 | 0.576 |
| BC3803-14 | 17.0 | 66.8 | 7.07 | 0.841 | 0.436 | | BC3802-13A | 17.0 | 57.2 | 4.69 | 0.779 | 0.606 |
| BC3803-15 | 19.0 | 65.6 | 6.70 | 0.834 | 0.463 | | BC3802-14 | 19.0 | 54.9 | 4.28 | 0.762 | 0.649 |
| BC3803-16 | 21.0 | 64.5 | 6.38 | 0.827 | 0.474 | | BC3802-15 | 21.0 | 54.5 | 4.21 | 0.759 | 0.658 |
| BC3803-17 | 23.0 | 65.8 | 6.76 | 0.835 | 0.456 | | BC3802-16 | 23.0 | 54.7 | 4.24 | 0.761 | 0.655 |
| BC3803-18 | 25.0 | 65.1 | 6.55 | 0.831 | 0.463 | | BC3802-17 | 25.0 | 54.4 | 4.19 | 0.759 | 0.661 |
| BC3803-19 | 27.0 | 63.9 | 6.22 | 0.823 | 0.487 | | BC3802-18 | 27.0 | 54.1 | 4.14 | 0.756 | 0.667 |
| BC3803-20 | 29.0 | 63.7 | 6.16 | 0.822 | 0.488 | | BC3802-19 | 29.0 | 55.4 | 4.36 | 0.766 | 0.642 |
| BC3803-21 | 31.0 | 63.6 | 6.14 | 0.822 | 0.499 | | BC3802-20 | 31.0 | 55.1 | 4.31 | 0.764 | 0.645 |
| BC3803-22 | 33.0 | 62.3 | 5.81 | 0.813 | 0.512 | | BC3802-21 | 33.0 | 55.9 | 4.45 | 0.770 | 0.630 |
| BC3803-23 | 35.0 | 62.6 | 5.88 | 0.815 | 0.510 | | BC3802-21A | 35.0 | 56.4 | 4.54 | 0.773 | 0.621 |
| BC3803-24 | 37.0 | 60.9 | 5.47 | 0.804 | 0.538 | | BC3802-22 | 37.0 | 56.1 | 4.49 | 0.771 | 0.644 |
| BC3803-25 | 39.0 | 64.5 | 6.38 | 0.827 | 0.478 | | BC3802-23 | 39.0 | 56.6 | 4.58 | 0.775 | 0.616 |
| BC3803-26 | 41.0 | 63.7 | 6.16 | 0.822 | 0.488 | | BC3802-24 | 41.0 | 56.0 | 4.47 | 0.770 | 0.638 |
| BC3803-27 | 43.0 | 61.4 | 5.59 | 0.807 | 0.528 | | BC3802-25 | 43.0 | 56.3 | 4.53 | 0.772 | 0.631 |
| BC3803-28 | 45.0 | 61.6 | 5.64 | 0.809 | 0.525 | | BC3802-26 | 45.0 | 56.6 | 4.58 | 0.775 | 0.618 |
| BC3803-29 | 47.0 | 62.3 | 5.81 | 0.813 | 0.515 | | BC3802-27 | 47.0 | 56.4 | 4.54 | 0.773 | 0.621 |
| BC3803-30 | 49.0 | 62.3 | 5.81 | 0.813 | 0.512 | | BC3802-28 | 49.0 | 56.0 | 4.47 | 0.770 | 0.630 |
| BC3803-31 | 51.0 | 63.5 | 6.11 | 0.821 | 0.496 | | BC3802-29 | 51.0 | 55.7 | 4.42 | 0.768 | 0.635 |
| BC3803-32 | 53.0 | 62.9 | 5.96 | 0.817 | 0.502 | | BC3802-30 | 53.0 | 56.5 | 4.56 | 0.774 | 0.620 |

| APPENDIX C.1. SEDIMENT PHYSICAL PARAMETERS | | | | | | | | | | | | |
|---|---|---|---|---|---|---|---|---|---|---|---|---|
| | | | | | | | | | | | | |
| CD38-09 | | | | | | | CD38-09 | | | | | |
| Sample | Depth | Water | Salt | Porosity | D.B.D. | | Sample | Depth | Water | Salt | Porosity | D.B.D. |
| | (cm.) | (%) | | | | | | (cm.) | (%) | | | |
| PC3809G01 | 4.0 | 67.7 | 7.36 | 0.847 | 0.421 | | PC3809G33 | 324.0 | 59.8 | 5.23 | 0.797 | 0.556 |
| PC3809G02 | 13.0 | 74.7 | 10.37 | 0.886 | 0.323 | | PC3809G34 | 335.0 | 65.0 | 6.52 | 0.830 | 0.465 |
| PC3809G03 | 23.0 | 65.2 | 6.58 | 0.832 | 0.462 | | PC3809G35 | 344.0 | 66.9 | 7.10 | 0.842 | 0.433 |
| PC3809G04 | 34.0 | 66.1 | 6.85 | 0.837 | 0.448 | | PC3809G36 | 355.0 | 71.5 | 8.81 | 0.869 | 0.360 |
| PC3809G05 | 43.0 | 54.3 | 4.17 | 0.758 | 0.662 | | PC3809G37 | 364.0 | 71.0 | 8.60 | 0.866 | 0.369 |
| PC3809G06 | 53.0 | 68.4 | 7.60 | 0.851 | 0.410 | | PC3809G38 | 375.0 | 65.3 | 6.61 | 0.832 | 0.461 |
| PC3809G07 | 62.0 | 69.8 | 8.12 | 0.859 | 0.386 | | PC3809G39 | 384.0 | 58.5 | 4.95 | 0.788 | 0.581 |
| PC3809G08 | 73.0 | 68.3 | 7.57 | 0.850 | 0.412 | | PC3809G40 | 394.0 | 64.9 | 6.50 | 0.830 | 0.468 |
| PC3809G09 | 84.0 | 64.2 | 6.30 | 0.825 | 0.480 | | PC3809G41 | 404.0 | 61.3 | 5.56 | 0.807 | 0.530 |
| PC3809G10 | 94.0 | 66.9 | 7.10 | 0.842 | 0.433 | | PC3809G42 | 416.0 | 66.0 | 6.82 | 0.836 | 0.449 |
| PC3809G11 | 104.0 | 69.7 | 8.08 | 0.858 | 0.388 | | PC3809G43 | 424.0 | 66.2 | 6.88 | 0.838 | 0.446 |
| PC3809G12 | 113.0 | 59.4 | 5.14 | 0.794 | 0.564 | | PC3809G44 | 434.0 | 60.5 | 5.38 | 0.801 | 0.544 |
| PC3809G13 | 124.0 | 58.1 | 4.87 | 0.785 | 0.589 | | PC3809G45 | 444.0 | 66.0 | 6.82 | 0.836 | 0.448 |
| PC3809G14 | 134.0 | 66.3 | 6.91 | 0.838 | 0.445 | | PC3809G46 | 453.0 | 58.6 | 4.97 | 0.789 | 0.578 |
| PC3809G15 | 144.0 | 68.7 | 7.71 | 0.853 | 0.404 | | PC3809G47 | 465.0 | 63.4 | 6.09 | 0.820 | 0.493 |
| PC3809G16 | 152.0 | 68.2 | 7.53 | 0.850 | 0.413 | | PC3809G48 | 474.0 | 64.7 | 6.44 | 0.828 | 0.470 |
| PC3809G17 | 165.0 | 68.8 | 7.75 | 0.853 | 0.403 | | PC3809G49 | 483.0 | 58.9 | 5.03 | 0.791 | 0.574 |
| PC3809G18 | 174.0 | 53.8 | 4.09 | 0.754 | 0.672 | | PC3809G50 | 493.0 | 61.6 | 5.64 | 0.809 | 0.524 |
| PC3809G19 | 185.0 | 55.3 | 4.35 | 0.765 | 0.642 | | PC3809G51 | 504.0 | 54.3 | 4.17 | 0.758 | 0.661 |
| PC3809G20 | 194.0 | 46.8 | 3.09 | 0.699 | 0.783 | | PC3809G52 | 515.0 | 52.8 | 3.93 | 0.747 | 0.692 |
| PC3809G21 | 205.0 | 53.0 | 3.96 | 0.748 | 0.687 | | PC3809G53 | 525.0 | 61.7 | 5.66 | 0.809 | 0.522 |
| PC3809G22 | 214.0 | 60.9 | 5.47 | 0.804 | 0.537 | | PC3809G54 | 536.0 | 64.1 | 6.27 | 0.825 | 0.481 |
| PC3809G23 | 224.0 | 36.9 | 2.05 | 0.606 | 1.070 | | PC3809G55 | 544.0 | 56.2 | 4.51 | 0.772 | 0.625 |
| PC3809G24 | 234.0 | 55.6 | 4.40 | 0.767 | 0.636 | | PC3809G56 | 553.0 | 63.0 | 5.98 | 0.818 | 0.500 |
| PC3809G25 | 243.0 | 70.3 | 8.32 | 0.862 | 0.379 | | PC3809G57 | 564.0 | 67.3 | 7.23 | 0.844 | 0.427 |
| PC3809G26 | 257.0 | 63.8 | 6.19 | 0.823 | 0.486 | | PC3809G58 | 574.0 | 64.5 | 6.38 | 0.827 | 0.473 |
| PC3809G27 | 267.0 | 52.7 | 3.91 | 0.746 | 0.695 | | PC3809G59 | 585.0 | 65.5 | 6.67 | 0.833 | 0.456 |
| PC3809G28 | 273.0 | 43.3 | 2.68 | 0.668 | 0.903 | | PC3809G60 | 594.0 | 67.0 | 7.13 | 0.842 | 0.432 |
| PC3809G29 | 284.0 | 62.4 | 5.83 | 0.814 | 0.510 | | PC3809G61 | 605.0 | 59.3 | 5.12 | 0.793 | 0.565 |
| PC3809G30 | 294.0 | 66.9 | 7.10 | 0.842 | 0.433 | | PC3809G62 | 615.0 | 66.5 | 6.97 | 0.839 | 0.441 |
| PC3809G31 | 304.0 | 62.4 | 5.83 | 0.814 | 0.510 | | PC3809G63 | 625.0 | 61.9 | 5.71 | 0.811 | 0.518 |
| PC3809G32 | 314.0 | 64.4 | 6.35 | 0.827 | 0.476 | | PC3809G64 | 635.0 | 60.0 | 5.27 | 0.798 | 0.554 |

APPENDIX C.1. SEDIMENT PHYSICAL PARAMETERS

| CD38-09 | | | | | | | CD38-10 | | | | | |
|---|---|---|---|---|---|---|---|---|---|---|---|---|
| Sample | Depth (cm.) | Water (%) | Salt | Porosity | D.B.D. | | Sample | Depth (cm.) | Water (%) | Salt | Porosity | D.B.D. |
| PC3809G65 | 646.0 | 68.8 | 7.75 | 0.853 | 0.402 | | PC3810A08 | 74.0 | 50.1 | 3.53 | 0.726 | 0.748 |
| PC3809G66 | 654.0 | 68.2 | 7.53 | 0.850 | 0.413 | | PC3810A09 | 84.0 | 25.6 | 1.21 | 0.475 | 1.415 |
| PC3809G67 | 664.0 | 68.9 | 7.78 | 0.854 | 0.401 | | PC3810A10 | 94.0 | 26.2 | 1.25 | 0.483 | 1.396 |
| PC3809G68 | 674.0 | 69.3 | 7.93 | 0.856 | 0.394 | | PC3810A11 | 104.0 | 31.5 | 1.62 | 0.548 | 1.225 |
| PC3809G69 | 684.0 | 63.8 | 6.19 | 0.823 | 0.485 | | PC3810A12 | 113.0 | 26.5 | 1.27 | 0.487 | 1.386 |
| PC3809G70 | 694.0 | 62.8 | 5.93 | 0.816 | 0.503 | | PC3810A13 | 126.0 | 62.8 | 5.93 | 0.816 | 0.502 |
| PC3809G71 | 703.0 | 63.8 | 6.19 | 0.823 | 0.485 | | PC3810A14 | 134.0 | 62.7 | 5.91 | 0.816 | 0.505 |
| PC3809G72 | 714.0 | 64.4 | 6.35 | 0.827 | 0.476 | | PC3810A15 | 146.0 | 56.3 | 4.53 | 0.772 | 0.623 |
| PC3809G73 | 724.0 | 60.7 | 5.43 | 0.803 | 0.541 | | PC3810A16 | 154.0 | 58.6 | 4.97 | 0.789 | 0.578 |
| PC3809G74 | 734.0 | 60.3 | 5.34 | 0.800 | 0.548 | | PC3810A17 | 167.0 | 63.1 | 6.01 | 0.818 | 0.499 |
| PC3809G75 | 744.0 | 65.5 | 6.67 | 0.833 | 0.457 | | PC3810A18 | 174.0 | 60.6 | 5.40 | 0.802 | 0.542 |
| PC3809G76 | 754.0 | 66.4 | 6.94 | 0.839 | 0.442 | | PC3810A19 | 185.0 | 59.1 | 5.08 | 0.792 | 0.570 |
| PC3809G77 | 764.0 | 59.7 | 5.20 | 0.796 | 0.558 | | PC3810A20 | 194.0 | 66.5 | 6.97 | 0.839 | 0.440 |
| PC3809G78 | 774.0 | 56.8 | 4.62 | 0.776 | 0.613 | | PC3810A21 | 203.0 | 57.3 | 4.71 | 0.779 | 0.603 |
| PC3809G79 | 784.0 | 59.8 | 5.23 | 0.797 | 0.557 | | PC3810A22 | 216.0 | 66.1 | 6.85 | 0.837 | 0.447 |
| PC3809G80 | 794.0 | 58.5 | 4.95 | 0.788 | 0.581 | | PC3810A23 | 224.0 | 66.3 | 6.91 | 0.838 | 0.444 |
| PC3809G81 | 804.0 | 59.3 | 5.12 | 0.793 | 0.567 | | PC3810A24 | 233.0 | 63.9 | 6.22 | 0.823 | 0.485 |
| PC3809G82 | 813.0 | 56.4 | 4.54 | 0.773 | 0.621 | | PC3810A25 | 244.0 | 60.2 | 5.31 | 0.799 | 0.551 |
| PC3809G83 | 823.0 | 57.1 | 4.68 | 0.778 | 0.608 | | PC3810A26 | 254.0 | 60.7 | 5.43 | 0.803 | 0.541 |
| PC3809G84 | 834.0 | 57.1 | 4.68 | 0.778 | 0.606 | | PC3810A27 | 263.0 | 63.5 | 6.11 | 0.821 | 0.490 |
| PC3809G85 | 845.0 | 58.7 | 4.99 | 0.789 | 0.577 | | PC3810A28 | 273.0 | 59.4 | 5.14 | 0.794 | 0.565 |
| PC3809G86 | 854.0 | 56.1 | 4.49 | 0.771 | 0.626 | | PC3810A29 | 284.0 | 56.7 | 4.60 | 0.775 | 0.615 |
| | | | | | | | PC3810A30 | 295.0 | 64.1 | 6.27 | 0.825 | 0.480 |
| CD38-10 | | | | | | | PC3810A31 | 305.0 | 59.2 | 5.10 | 0.793 | 0.568 |
| | | | | | | | PC3810A32 | 314.0 | 55.3 | 4.35 | 0.765 | 0.642 |
| PC3810A01 | 6.0 | 69.1 | 7.86 | 0.855 | 0.398 | | PC3810A33 | 324.0 | 65.7 | 6.73 | 0.835 | 0.454 |
| PC3810A02 | 14.0 | 52.7 | 3.91 | 0.746 | 0.695 | | PC3810A34 | 335.0 | 58.3 | 4.91 | 0.786 | 0.585 |
| PC3810A03 | 24.0 | 32.1 | 1.66 | 0.555 | 1.207 | | PC3810A35 | 344.0 | 66.9 | 7.10 | 0.842 | 0.433 |
| PC3810A04 | 34.0 | 39.0 | 2.25 | 0.627 | 1.013 | | PC3810A36 | 354.0 | 70.4 | 8.36 | 0.862 | 0.378 |
| PC3810A05 | 44.0 | 59.6 | 5.18 | 0.795 | 0.561 | | PC3810A37 | 364.0 | 70.4 | 8.36 | 0.862 | 0.378 |
| PC3810A06 | 54.0 | 63.3 | 6.06 | 0.820 | 0.494 | | PC3810A38 | 374.0 | 69.6 | 8.04 | 0.858 | 0.392 |
| PC3810A07 | 64.0 | 57.7 | 4.79 | 0.782 | 0.596 | | PC3810A39 | 383.0 | 59.5 | 5.16 | 0.795 | 0.561 |

APPENDIX C.1. SEDIMENT PHYSICAL PARAMETERS

| CD38-10 Sample | Depth (cm.) | Water (%) | Salt | Porosity | D.B.D. | CD38-10 Sample | Depth (cm.) | Water (%) | Salt | Porosity | D.B.D. |
|---|---|---|---|---|---|---|---|---|---|---|---|
| PC3810A40 | 394.0 | 63.9 | 6.22 | 0.823 | 0.483 | PC3810A72 | 714.0 | 58.5 | 4.95 | 0.788 | 0.580 |
| PC3810A41 | 404.0 | 58.5 | 4.95 | 0.788 | 0.581 | PC3810A73 | 724.0 | 60.3 | 5.34 | 0.800 | 0.548 |
| PC3810A42 | 417.0 | 61.1 | 5.52 | 0.805 | 0.533 | PC3810A74 | 734.0 | 57.8 | 4.81 | 0.783 | 0.594 |
| PC3810A43 | 424.0 | 62.6 | 5.88 | 0.815 | 0.506 | PC3810A75 | 745.0 | 52.6 | 3.90 | 0.745 | 0.698 |
| PC3810A44 | 434.0 | 70.7 | 8.48 | 0.864 | 0.373 | PC3810A76 | 754.0 | 59.4 | 5.14 | 0.794 | 0.564 |
| PC3810A45 | 445.0 | 64.5 | 6.38 | 0.827 | 0.475 | PC3810A77 | 764.0 | 46.4 | 3.04 | 0.695 | 0.833 |
| PC3810A46 | 456.0 | 67.2 | 7.20 | 0.844 | 0.429 | | | | | | |
| PC3810A47 | 467.0 | 73.3 | 9.64 | 0.879 | 0.481 | CD38-02 | | | | | |
| PC3810A48 | 476.0 | 57.5 | 4.75 | 0.781 | 0.600 | | | | | | |
| PC3810A49 | 484.0 | 55.9 | 4.45 | 0.770 | 0.631 | PC3802P01 | 8.0 | 58.71 | 4.99 | 0.79 | 0.58 |
| PC3810A50 | 494.0 | 50.8 | 3.63 | 0.731 | 0.733 | PC3802P02 | 18.0 | 57.20 | 4.69 | 0.78 | 0.61 |
| PC3810A51 | 504.0 | 31.5 | 1.62 | 0.548 | 1.227 | PC3802P03 | 28.0 | 59.27 | 5.11 | 0.79 | 0.57 |
| PC3810A52 | 514.0 | 58.9 | 5.03 | 0.791 | 0.574 | PC3802P04 | 38.0 | 61.14 | 5.53 | 0.81 | 0.53 |
| PC3810A53 | 524.0 | 55.7 | 4.42 | 0.768 | 0.633 | PC3802P05 | 48.0 | 57.06 | 4.67 | 0.78 | 0.61 |
| PC3810A54 | 534.0 | 64.9 | 6.50 | 0.830 | 0.468 | PC3802P06 | 57.5 | 57.18 | 4.69 | 0.78 | 0.61 |
| PC3810A55 | 545.0 | 63.9 | 6.22 | 0.823 | 0.485 | PC3802P07 | 70.0 | 57.30 | 4.71 | 0.78 | 0.60 |
| PC3810A56 | 554.0 | 67.9 | 7.43 | 0.848 | 0.418 | PC3802P08 | 79.0 | 58.02 | 4.86 | 0.78 | 0.59 |
| PC3810A57 | 564.0 | 70.1 | 8.24 | 0.861 | 0.384 | PC3802P09 | 89.0 | 56.92 | 4.64 | 0.78 | 0.61 |
| PC3810A58 | 574.0 | 64.8 | 6.47 | 0.829 | 0.469 | PC3802P10 | 100.0 | 56.70 | 4.60 | 0.78 | 0.62 |
| PC3810A59 | 584.0 | 66.9 | 7.10 | 0.842 | 0.434 | PC3802P11 | 110.0 | 56.21 | 4.51 | 0.77 | 0.63 |
| PC3810A60 | 596.0 | 67.3 | 7.23 | 0.844 | 0.428 | PC3802P12 | 120.0 | 57.20 | 4.70 | 0.78 | 0.61 |
| PC3810A61 | 604.0 | 66.3 | 6.91 | 0.838 | 0.444 | PC3802P13 | 130.0 | 56.92 | 4.64 | 0.78 | 0.61 |
| PC3810A62 | 614.0 | 66.6 | 7.00 | 0.840 | 0.440 | PC3802P14 | 139.0 | 57.68 | 4.79 | 0.78 | 0.60 |
| PC3810A63 | 624.0 | 62.0 | 5.73 | 0.811 | 0.517 | PC3802P15 | 150.0 | 58.05 | 4.86 | 0.78 | 0.59 |
| PC3810A64 | 634.0 | 62.0 | 5.73 | 0.811 | 0.518 | PC3802P16 | 160.0 | 55.08 | 4.31 | 0.76 | 0.65 |
| PC3810A65 | 645.0 | 66.0 | 6.82 | 0.836 | 0.449 | PC3802P17 | 171.0 | 55.45 | 4.37 | 0.77 | 0.64 |
| PC3810A66 | 655.0 | 66.8 | 7.07 | 0.841 | 0.436 | PC3802P18 | 181.0 | 58.67 | 4.99 | 0.79 | 0.58 |
| PC3810A67 | 667.0 | 64.0 | 6.25 | 0.824 | 0.471 | PC3802P19 | 191.0 | 57.51 | 4.75 | 0.78 | 0.60 |
| PC3810A68 | 674.0 | 62.8 | 5.93 | 0.816 | 0.504 | PC3802P20 | 201.0 | 58.71 | 4.99 | 0.79 | 0.58 |
| PC3810A69 | 683.0 | 63.3 | 6.06 | 0.820 | 0.494 | PC3802P21 | 211.0 | 57.01 | 4.66 | 0.78 | 0.61 |
| PC3810A70 | 694.0 | 57.2 | 4.69 | 0.779 | 0.605 | PC3802P22 | 221.0 | 55.94 | 4.46 | 0.77 | 0.63 |
| PC3810A71 | 704.0 | 54.4 | 4.19 | 0.759 | 0.659 | PC3802P23 | 231.0 | 55.12 | 4.32 | 0.76 | 0.65 |

| APPENDIX C.1. SEDIMENT PHYSICAL PARAMETERS | | | | | | | | | | | | |
|---|---|---|---|---|---|---|---|---|---|---|---|---|
| | | | | | | | | | | | | |
| CD38-02 | | | | | | | CD38-02 | | | | | |
| Sample | Depth | Water | Salt | Porosity | D.B.D. | | Sample | Depth | Water | Salt | Porosity | D.B.D. |
| | (cm.) | (%) | | | | | | (cm.) | (%) | | | |
| PC3802P24 | 241.0 | 56.23 | 4.51 | 0.77 | 0.62 | | PC3802P56 | 560.0 | 56.79 | 4.62 | 0.78 | 0.61 |
| PC3802P25 | 251.0 | 56.13 | 4.50 | 0.77 | 0.63 | | PC3802P57 | 572.0 | 43.54 | 2.71 | 0.67 | 0.90 |
| PC3802P26 | 261.0 | 55.22 | 4.33 | 0.76 | 0.64 | | PC3802P58 | 582.0 | 44.01 | 2.76 | 0.67 | 0.89 |
| PC3802P27 | 271.0 | 56.30 | 4.53 | 0.77 | 0.62 | | PC3802P59 | 591.0 | 50.57 | 3.59 | 0.73 | 0.74 |
| PC3802P28 | 281.0 | 55.60 | 4.40 | 0.77 | 0.64 | | PC3802P60 | 601.0 | 48.79 | 3.35 | 0.72 | 0.78 |
| PC3802P29 | 291.0 | 56.35 | 4.53 | 0.77 | 0.62 | | PC3802P61 | 611.0 | 48.96 | 3.37 | 0.72 | 0.77 |
| PC3802P30 | 301.0 | 56.62 | 4.58 | 0.77 | 0.62 | | PC3802P62 | 621.0 | 49.42 | 3.43 | 0.72 | 0.76 |
| PC3802P31 | 312.0 | 56.97 | 4.65 | 0.78 | 0.61 | | PC3802P63 | 631.0 | 47.80 | 3.22 | 0.71 | 0.80 |
| PC3802P32 | 322.0 | 56.17 | 4.50 | 0.77 | 0.63 | | PC3802P64 | 641.0 | 49.36 | 3.42 | 0.72 | 0.77 |
| PC3802P33 | 332.0 | 55.67 | 4.41 | 0.77 | 0.64 | | PC3802P65 | 651.0 | 51.99 | 3.80 | 0.74 | 0.71 |
| PC3802P34 | 342.0 | 57.20 | 4.70 | 0.78 | 0.61 | | PC3802P66 | 662.0 | 53.32 | 4.01 | 0.75 | 0.68 |
| PC3802P35 | 352.0 | 56.82 | 4.62 | 0.78 | 0.61 | | PC3802P67 | 671.0 | 53.02 | 3.96 | 0.75 | 0.69 |
| PC3802P36 | 362.0 | 55.88 | 4.45 | 0.77 | 0.63 | | PC3802P68 | 681.0 | 51.33 | 3.71 | 0.74 | 0.72 |
| PC3802P37 | 372.0 | 54.20 | 4.16 | 0.76 | 0.66 | | PC3802P69 | 691.0 | 52.22 | 3.84 | 0.74 | 0.71 |
| PC3802P38 | 381.0 | 52.13 | 3.82 | 0.74 | 0.71 | | PC3802P70 | 701.0 | 51.17 | 3.68 | 0.73 | 0.73 |
| PC3802P39 | 391.0 | 51.99 | 3.80 | 0.74 | 0.71 | | PC3802P71 | 711.0 | 52.40 | 3.87 | 0.74 | 0.70 |
| PC3802P40 | 400.0 | 52.43 | 3.87 | 0.74 | 0.70 | | PC3802P72 | 721.0 | 52.42 | 3.87 | 0.74 | 0.70 |
| PC3802P41 | 410.0 | 52.16 | 3.83 | 0.74 | 0.71 | | PC3802P73 | 731.0 | 51.69 | 3.76 | 0.74 | 0.72 |
| PC3802P42 | 420.0 | 52.61 | 3.90 | 0.75 | 0.70 | | PC3802P74 | 741.0 | 52.37 | 3.86 | 0.74 | 0.70 |
| PC3802P43 | 430.0 | 51.33 | 3.71 | 0.74 | 0.72 | | | | | | | |
| PC3802P44 | 440.0 | 50.94 | 3.65 | 0.73 | 0.73 | | CD38-11 | | | | | |
| PC3802P45 | 450.0 | 53.44 | 4.03 | 0.75 | 0.68 | | | | | | | |
| PC3802P46 | 460.0 | 53.19 | 3.99 | 0.75 | 0.69 | | PC3811P01 | 3.0 | 58.76 | 5.01 | 0.79 | 0.58 |
| PC3802P47 | 470.0 | 51.51 | 3.73 | 0.74 | 0.72 | | PC3811P02 | 13.0 | 56.25 | 4.52 | 0.77 | 0.62 |
| PC3802P48 | 481.0 | 51.64 | 3.75 | 0.74 | 0.72 | | PC3811P03 | 23.0 | 51.05 | 3.66 | 0.73 | 0.73 |
| PC3802P49 | 491.0 | 52.18 | 3.83 | 0.74 | 0.71 | | PC3811P04 | 33.0 | 60.27 | 5.33 | 0.80 | 0.55 |
| PC3802P50 | 501.0 | 52.94 | 3.95 | 0.75 | 0.69 | | PC3811P05 | 43.0 | 61.22 | 5.55 | 0.81 | 0.53 |
| PC3802P51 | 511.0 | 51.75 | 3.77 | 0.74 | 0.71 | | PC3811P06 | 53.0 | 60.62 | 5.41 | 0.80 | 0.54 |
| PC3802P52 | 521.0 | 52.43 | 3.87 | 0.74 | 0.70 | | PC3811P07 | 63.0 | 60.08 | 5.29 | 0.80 | 0.55 |
| PC3802P53 | 531.0 | 47.96 | 3.24 | 0.71 | 0.80 | | PC3811P08 | 73.0 | 58.45 | 4.94 | 0.79 | 0.58 |
| PC3802P54 | 540.0 | 53.93 | 4.11 | 0.76 | 0.67 | | PC3811P09 | 85.0 | 41.18 | 2.46 | 0.65 | 0.96 |
| PC3802P55 | 550.0 | 54.90 | 4.28 | 0.76 | 0.65 | | PC3811P10 | 95.0 | 57.70 | 4.79 | 0.78 | 0.60 |

| APPENDIX C.1. SEDIMENT PHYSICAL PARAMETERS | | | | | | | | | | | | |
|---|---|---|---|---|---|---|---|---|---|---|---|---|
| | | | | | | | | | | | | |
| CD38-11 | | | | | | | CD38-11 | | | | | |
| Sample | Depth | Water | Salt | Porosity | D.B.D. | | Sample | Depth | Water | Salt | Porosity | D.B.D. |
| | (cm.) | (%) | | | | | | (cm.) | (%) | | | |
| PC3811P11 | 105.0 | 58.22 | 4.90 | 0.79 | 0.59 | | PC3811P43 | 425.0 | 56.53 | 4.57 | 0.77 | 0.62 |
| PC3811P12 | 116.0 | 57.88 | 4.83 | 0.78 | 0.59 | | PC3811P44 | 435.0 | 56.88 | 4.63 | 0.78 | 0.61 |
| PC3811P13 | 125.0 | 58.28 | 4.91 | 0.79 | 0.59 | | PC3811P45 | 445.0 | 58.14 | 4.88 | 0.79 | 0.59 |
| PC3811P14 | 135.0 | 57.07 | 4.67 | 0.78 | 0.61 | | PC3811P46 | 455.0 | 55.95 | 4.46 | 0.77 | 0.63 |
| PC3811P15 | 145.0 | 58.71 | 4.99 | 0.79 | 0.58 | | PC3811P47 | 465.0 | 56.51 | 4.57 | 0.77 | 0.62 |
| PC3811P16 | 155.0 | 55.71 | 4.42 | 0.77 | 0.63 | | PC3811P48 | 475.0 | 56.09 | 4.49 | 0.77 | 0.63 |
| PC3811P17 | 165.0 | 59.75 | 5.21 | 0.80 | 0.56 | | PC3811P49 | 485.0 | 56.71 | 4.60 | 0.78 | 0.62 |
| PC3811P18 | 175.0 | 50.60 | 3.60 | 0.73 | 0.74 | | PC3811P50 | 495.0 | 57.64 | 4.78 | 0.78 | 0.60 |
| PC3811P19 | 186.0 | 58.33 | 4.92 | 0.79 | 0.58 | | PC3811P51 | 505.0 | 57.70 | 4.79 | 0.78 | 0.60 |
| PC3811P20 | 197.0 | 59.33 | 5.13 | 0.79 | 0.57 | | PC3811P52 | 515.0 | 56.85 | 4.63 | 0.78 | 0.61 |
| PC3811P21 | 204.0 | 59.77 | 5.22 | 0.80 | 0.56 | | PC3811P53 | 525.0 | 57.80 | 4.81 | 0.78 | 0.59 |
| PC3811P22 | 215.0 | 59.15 | 5.09 | 0.79 | 0.57 | | PC3811P54 | 535.0 | 56.07 | 4.48 | 0.77 | 0.63 |
| PC3811P23 | 225.0 | 60.95 | 5.48 | 0.80 | 0.54 | | PC3811P55 | 545.0 | 57.49 | 4.75 | 0.78 | 0.60 |
| PC3811P24 | 235.0 | 59.82 | 5.23 | 0.80 | 0.56 | | PC3811P56 | 555.0 | 56.94 | 4.64 | 0.78 | 0.61 |
| PC3811P25 | 245.0 | 59.30 | 5.12 | 0.79 | 0.57 | | PC3811P57 | 565.0 | 56.18 | 4.50 | 0.77 | 0.63 |
| PC3811P26 | 255.0 | 58.90 | 5.03 | 0.79 | 0.57 | | | | | | | |
| PC3811P27 | 265.0 | 59.31 | 5.12 | 0.79 | 0.57 | | | | | | | |
| PC3811P28 | 275.0 | 59.47 | 5.15 | 0.79 | 0.56 | | | | | | | |
| PC3811P29 | 285.0 | 58.23 | 4.90 | 0.79 | 0.59 | | | | | | | |
| PC3811P30 | 297.0 | 52.97 | 3.96 | 0.75 | 0.69 | | | | | | | |
| PC3811P31 | 305.0 | 54.28 | 4.17 | 0.76 | 0.66 | | | | | | | |
| PC3811P32 | 315.0 | 53.70 | 4.07 | 0.75 | 0.67 | | | | | | | |
| PC3811P33 | 325.0 | 42.27 | 2.57 | 0.66 | 0.93 | | | | | | | |
| PC3811P34 | 335.0 | 57.38 | 4.73 | 0.78 | 0.60 | | | | | | | |
| PC3811P35 | 345.0 | 57.86 | 4.82 | 0.78 | 0.59 | | | | | | | |
| PC3811P36 | 355.0 | 58.54 | 4.96 | 0.79 | 0.58 | | | | | | | |
| PC3811P37 | 365.0 | 57.68 | 4.79 | 0.78 | 0.60 | | | | | | | |
| PC3811P38 | 375.0 | 57.34 | 4.72 | 0.78 | 0.60 | | | | | | | |
| PC3811P39 | 385.0 | 55.68 | 4.41 | 0.77 | 0.64 | | | | | | | |
| PC3811P40 | 395.0 | 54.63 | 4.23 | 0.76 | 0.66 | | | | | | | |
| PC3811P41 | 405.0 | 55.38 | 4.36 | 0.77 | 0.64 | | | | | | | |
| PC3811P42 | 415.0 | 54.82 | 4.26 | 0.76 | 0.65 | | | | | | | |

| APPENDIX C.2 SEDIMENT >63µm DESCRIPTION AND FORAMINIFERA STABLE ISOTOPES | | | | | | | | | | | | | | | |
|---|---|---|---|---|---|---|---|---|---|---|---|---|---|---|---|
| CD38-02 | | | Description (0=absent, 1=rare, 2=common, 3=abundant) | | | | | Number of forams picked | | | Isotopic composition of Uvigerina | | | |
| Sample | Depth | Sed.>63um | Forams | Qtz. | Clays | Diatoms | Fish bits | Uvig. | Cibicid. | Glob. | Sample | Depth | d18O | d13C |
| | (cm) | (%) | (0-10) | (0-3) | (0-3) | (0-3) | (0-3) | | | | | (cm) | (PDB) | (PDB) |
| 3802F1 | 5.0 | 0.64 | 9 | 0 | 0 | 0 | 1 | 24 | 2 | 18 | 3802F1 | 5.0 | 2.833 | -0.827 |
| 3802F2 | 14.0 | 0.72 | 9 | 0 | 1 | 1 | 1 | 26 | 5 | 22 | 3802F2 | 14.0 | 3.004 | -0.960 |
| 3802F3 | 24.0 | 1.39 | 10 | 0 | 0 | 2 | 1 | 22 | 10 | 22 | 3802F3 | 24.0 | 3.770 | -1.065 |
| 3802F4 | 35.0 | 1.10 | 7 | 0 | 2 | 1 | 0 | 21 | 11 | 33 | 3802F4 | 35.0 | 3.955 | -1.293 |
| 3802F5 | 45.0 | 1.25 | 8 | 0 | 1 | 1 | 1 | 33 | 9 | 31 | 3802F5 | 45.0 | 4.921 | -1.217 |
| 3802F6 | 54.0 | 1.08 | 8 | 0 | 1 | 2 | 1 | 29 | 5 | 26 | 3802F6 | 54.0 | 4.924 | -1.275 |
| 3802F7 | 67.0 | 1.49 | 9 | 0 | 1 | 1 | 1 | 31 | 21 | 30 | 3802F7 | 67.0 | 4.939 | -1.379 |
| 3802F8 | 76.0 | 1.03 | 7 | 0 | 1 | 1 | 2 | 25 | 19 | 26 | 3802F8 | 76.0 | 4.586 | -1.423 |
| 3802F9 | 86.0 | 1.34 | 9 | 0 | 1 | 1 | 1 | 28 | 15 | 30 | 3802F9 | 86.0 | 4.997 | -1.179 |
| 3802F10 | 96.0 | 1.48 | 10 | 0 | 1 | 1 | 0 | 28 | 9 | 25 | 3802F10 | 96.0 | 3.694 | -1.265 |
| 3802F11 | 106.0 | 1.91 | 8 | 0 | 1 | 3 | 0 | 22 | 8 | 33 | 3802F11 | 106.0 | 4.689 | -1.302 |
| 3802F12 | 116.0 | 1.68 | 9 | 0 | 1 | 2 | 0 | 26 | 9 | 28 | 3802F12 | 116.0 | 4.695 | -1.440 |
| 3802F13 | 126.0 | 1.77 | 6 | 0 | 1 | 3 | 1 | 29 | 15 | 38 | 3802F13 | 126.0 | 4.746 | -1.499 |
| 3802F14 | 136.0 | 1.50 | 7 | 0 | 1 | 2 | 1 | 29 | 10 | 26 | 3802F14 | 136.0 | 4.403 | -1.284 |
| 3802F15 | 146.0 | 1.91 | 7 | 0 | 1 | 2 | 1 | 24 | 5 | 28 | 3802F15 | 146.0 | 4.463 | -1.272 |
| 3802F16 | 156.0 | 1.20 | 9 | 0 | 1 | 1 | 1 | 28 | 10 | 34 | 3802F16 | 156.0 | 4.471 | -1.263 |
| 3802F17 | 164.5 | 1.05 | 8 | 0 | 1 | 2 | 1 | 36 | 15 | 23 | 3802F17 | 164.5 | 4.460 | -1.252 |
| 3802F18 | 178.0 | 0.86 | 9 | 0 | 0 | 3 | 0 | 32 | 14 | 22 | 3802F18 | 178.0 | 4.402 | -1.159 |
| 3802F19 | 188.0 | 0.69 | 9 | 0 | 1 | 2 | 0 | 29 | 7 | 23 | 3802F19 | 188.0 | 4.516 | -1.228 |
| 3802F20 | 198.0 | 0.73 | 6 | 0 | 2 | 3 | 0 | 30 | 4 | 26 | 3802F20 | 198.0 | 4.350 | -1.260 |
| 3802F21 | 208.0 | 0.70 | 7 | 0 | 1 | 2 | 0 | 34 | 7 | 20 | 3802F21 | 208.0 | 4.583 | -1.197 |
| 3802F22 | 218.0 | 0.90 | 9 | 0 | 1 | 1 | 0 | 38 | 5 | 26 | 3802F22 | 218.0 | 4.630 | -1.407 |
| 3802F23 | 228.0 | 0.68 | 9 | 0 | 1 | 0 | 0 | 33 | 11 | 30 | 3802F23 | 228.0 | 4.634 | -1.329 |
| 3802F24 | 238.0 | 0.80 | 8 | 2 | 2 | 0 | 0 | 35 | 17 | 22 | 3802F24 | 238.0 | 4.272 | -1.175 |
| 3802F25 | 248.0 | 0.58 | 8 | 2 | 1 | 1 | 1 | 26 | 2 | 16 | 3802F25 | 248.0 | 4.418 | -0.559 |
| 3802F26 | 258.0 | 0.69 | 9 | 0 | 1 | 2 | 1 | 36 | 15 | 23 | 3802F26 | 258.0 | 4.122 | -0.946 |
| 3802F27 | 268.0 | 0.62 | 9 | 1 | 1 | 2 | 0 | 33 | 7 | 24 | 3802F27 | 268.0 | 4.059 | -0.992 |
| 3802F28 | 278.0 | 0.64 | 8 | 1 | 2 | 1 | 0 | 35 | 1 | 11 | 3802F28 | 278.0 | 4.281 | -1.223 |
| 3802F29 | 288.0 | 0.79 | 7 | 1 | 1 | 2 | 1 | 38 | 3 | 26 | 3802F29 | 288.0 | 4.417 | -1.040 |
| 3802F30 | 299.0 | 0.35 | 6 | 2 | 3 | 1 | 0 | 33 | 0 | 0 | 3802F30 | 299.0 | 4.082 | -0.998 |
| 3802F31 | 309.0 | 0.57 | 8 | 0 | 2 | 2 | 0 | 34 | 5 | 12 | 3802F31 | 309.0 | 4.228 | -0.958 |
| 3802F32 | 319.0 | 0.73 | 8 | 1 | 1 | 1 | 1 | 25 | 7 | 17 | 3802F32 | 319.0 | 4.437 | -0.994 |
| 3802F33 | 329.0 | 0.82 | 8 | 1 | 1 | 1 | 2 | 37 | 4 | 29 | 3802F33 | 329.0 | 4.480 | -0.998 |
| 3802F34 | 339.0 | 0.63 | 7 | 0 | 1 | 2 | 1 | 33 | 5 | 19 | 3802F34 | 339.0 | 4.025 | -0.943 |
| 3802F35 | 349.0 | 0.93 | 5 | 0 | 1 | 3 | 0 | 23 | 5 | 23 | 3802F35 | 349.0 | 3.728 | -0.981 |
| 3802F36 | 359.0 | 1.38 | 5 | 0 | 1 | 3 | 0 | 23 | 5 | 27 | 3802F36 | 359.0 | 4.051 | -1.048 |
| 3802F37 | 369.0 | 0.94 | 8 | 0 | 1 | 0 | 1 | 20 | 15 | 37 | 3802F37 | 369.0 | 5.038 | -0.758 |
| 3808F38 | 378.0 | 1.16 | 9 | 0 | 1 | 0 | 0 | 29 | 16 | 46 | 3808F38 | 378.0 | 4.636 | -1.083 |

| APPENDIX C.2 SEDIMENT >63µm DESCRIPTION AND FORAMINIFERA STABLE ISOTOPES | | | | | | | | | | | | | | | |
|---|---|---|---|---|---|---|---|---|---|---|---|---|---|---|---|
| CD38-02 | | | Description (0=absent, 1=rare, 2=common, 3=abundant) | | | | | Number of forams picked | | | Isotopic composition of Uvigerina | | | |
| Sample | Depth | Sed.>63um | Forams | Qtz. | Clays | Diatoms | Fish bits | Uvig. | Cibicid. | Glob. | Sample | Depth | d18O | d13C |
| | (cm) | (%) | (0-10) | (0-3) | (0-3) | (0-3) | (0-3) | | | | | (cm) | (PDB) | (PDB) |
| 3802F39 | 388.0 | 1.43 | 9 | 0 | 1 | 0 | 0 | 27 | 21 | 45 | 3802F39 | 388.0 | 5.049 | -1.350 |
| 3802F40 | 398.0 | 1.76 | 9 | 0 | 1 | 0 | 0 | 34 | 26 | 32 | 3802F40 | 398.0 | 4.876 | -1.412 |
| 3802F41 | 407.0 | 0.94 | 9 | 0 | 1 | 0 | 1 | 20 | 3 | 25 | 3802F41 | 407.0 | 4.863 | -1.295 |
| 3802F42 | 417.0 | 0.96 | 10 | 0 | 1 | 0 | 0 | 24 | 12 | 44 | 3802F42 | 417.0 | 4.930 | -1.464 |
| 3802F43 | 427.0 | 1.77 | 10 | 0 | 1 | 0 | 0 | 23 | 13 | 45 | 3802F43 | 427.0 | 4.632 | -1.554 |
| 3802F44 | 437.0 | 1.39 | 10 | 0 | 1 | 0 | 0 | 29 | 7 | 38 | 3802F44 | 437.0 | 4.772 | -1.351 |
| 3802F45 | 447.0 | 0.76 | 9 | 0 | 1 | 0 | 1 | 29 | 9 | 37 | 3802F45 | 447.0 | 4.739 | -1.318 |
| 3802F46 | 457.0 | 0.95 | 8 | 0 | 2 | 0 | 1 | 19 | 13 | 30 | 3802F46 | 457.0 | 4.826 | -1.301 |
| 3802F47 | 468.0 | 0.82 | 8 | 0 | 2 | 0 | 1 | 20 | 6 | 28 | 3802F47 | 468.0 | 4.779 | -1.513 |
| 3802F48 | 478.0 | 1.30 | 10 | 0 | 1 | 1 | 0 | 19 | 12 | 39 | 3802F48 | 478.0 | 4.642 | -1.407 |
| 3802F49 | 488.0 | 0.99 | 8 | 0 | 1 | 1 | 0 | 22 | 10 | 37 | 3802F49 | 488.0 | 4.449 | -1.268 |
| 3802F50 | 498.0 | 0.88 | 9 | 0 | 1 | 1 | 1 | 22 | 9 | 29 | 3802F50 | 498.0 | 4.618 | -1.573 |
| 3802F51 | 508.0 | 1.09 | 10 | 0 | 1 | 1 | 0 | 22 | 22 | 39 | 3802F51 | 508.0 | 4.664 | -1.282 |
| 3802F52 | 518.0 | 1.15 | 9 | 0 | 1 | 1 | 1 | 19 | 6 | 28 | 3802F52 | 518.0 | 4.582 | -1.779 |
| 3802F53 | 528.0 | 2.01 | 6 | 2 | 1 | 0 | 1 | 16 | 8 | 28 | 3802F53 | 528.0 | 4.615 | -1.191 |
| 3802F54 | 537.0 | 1.28 | 7 | 2 | 2 | 0 | 1 | 19 | 3 | 24 | 3802F54 | 537.0 | 4.527 | -1.370 |
| 3802F55 | 547.0 | 0.75 | 7 | 3 | 2 | 0 | 0 | 23 | 0 | 37 | 3802F55 | 547.0 | 3.510 | -1.266 |
| 3802F56 | 557.0 | 0.53 | 6 | 1 | 2 | 1 | 0 | 15 | 1 | 20 | 3802F56 | 557.0 | 4.075 | -1.209 |
| 3802F57 | 568.0 | 0.64 | 8 | 0 | 1 | 1 | 0 | 20 | 3 | 19 | 3802F57 | 568.0 | 3.538 | -1.107 |
| 3802F58 | 578.0 | 0.77 | 8 | 0 | 2 | 1 | 1 | 30 | 3 | 26 | 3802F58 | 578.0 | 3.468 | -1.013 |
| 3802F59 | 588.0 | 1.00 | 9 | 0 | 2 | 1 | 1 | 28 | 5 | 27 | 3802F59 | 588.0 | 3.518 | -1.253 |
| 3802F60 | 598.0 | 1.03 | 10 | 0 | 2 | 1 | 1 | 33 | 10 | 36 | 3802F60 | 598.0 | 3.549 | -1.112 |
| 3802F61 | 608.0 | 0.85 | 9 | 0 | 1 | 1 | 0 | 20 | 2 | 34 | 3802F61 | 608.0 | 3.123 | -1.095 |
| 3802F62 | 618.0 | 1.08 | 10 | 0 | 1 | 0 | 0 | 34 | 8 | 24 | 3802F62 | 618.0 | 4.167 | -1.636 |
| 3802F63 | 628.0 | 0.85 | 10 | 0 | 1 | 0 | 0 | 27 | 15 | 32 | 3802F63 | 628.0 | 4.260 | -1.483 |
| 3802F64 | 638.0 | 1.01 | 10 | 1 | 1 | 0 | 0 | 33 | 22 | 34 | 3802F64 | 638.0 | 4.818 | -1.373 |
| 3802F65 | 648.0 | 0.86 | 9 | 0 | 1 | 1 | 1 | 31 | 10 | 22 | 3802F65 | 648.0 | 4.348 | -1.238 |
| 3802F66 | 660.0 | 0.79 | 7 | 1 | 2 | 1 | 1 | 32 | 12 | 22 | 3802F66 | 660.0 | 4.055 | -1.310 |
| 3802F67 | 668.0 | 0.93 | 8 | 0 | 2 | 1 | 1 | 30 | 8 | 26 | 3802F67 | 668.0 | 4.149 | -1.263 |
| 3802F68 | 678.0 | 0.94 | 10 | 0 | 1 | 0 | 0 | 25 | 15 | 37 | 3802F68 | 678.0 | 4.333 | -1.360 |
| 3802F69 | 688.0 | 1.67 | 9 | 1 | 2 | 0 | 1 | 26 | 14 | 30 | 3802F69 | 688.0 | 4.459 | -1.351 |
| 3802F70 | 698.0 | 1.38 | 10 | 0 | 1 | 1 | 1 | 30 | 8 | 44 | 3802F70 | 698.0 | 4.804 | -1.423 |
| 3802F71 | 708.0 | 0.83 | 9 | 0 | 3 | 0 | 1 | 19 | 8 | 36 | 3802F71 | 708.0 | 4.927 | -1.297 |
| 3802F72 | 718.0 | 0.84 | 8 | 1 | 2 | 0 | 0 | 27 | 9 | 45 | 3802F72 | 718.0 | 4.744 | -1.426 |
| 3802F73 | 728.0 | 1.07 | 8 | 1 | 3 | 1 | 1 | 23 | 10 | 41 | 3802F73 | 728.0 | 4.272 | -1.519 |
| 3802F74 | 738.0 | 1.20 | 7 | 1 | 3 | 1 | 1 | 21 | 7 | 33 | 3802F74 | 738.0 | 4.850 | -1.720 |
| 3802F75 | 748.0 | 1.13 | 8 | 0 | 2 | 1 | 0 | 18 | 2 | 34 | 3802F75 | 748.0 | 4.653 | -1.708 |

APPENDIX C.2 SEDIMENT >63µm DESCRIPTION AND FORAMINIFERA STABLE ISOTOPES

| CD38-09 | | | Description (0=absent, 1=rare, 2=common, 3=abundant) | | | | | Number of forams picked | Isotopic composition of B.sem. | | | |
|---|---|---|---|---|---|---|---|---|---|---|---|---|
| Sample | Depth | Sed.>63um | Forams | Qtz. | Clays | Diatoms | Fish bits | Bolivina seminuda | Sample | Depth | d18O | d13C |
| | (cm) | (%) | (0-10) | (0-3) | (0-3) | (0-3) | (0-3) | | | (cm) | (PDB) | (PDB) |
| 3809F1 | 7.5 | 0.69 | 0 | 2 | 3 | 2 | 1 | 0 | 3809F2 | 18.0 | 0.568 | -0.962 |
| 3809F2 | 18.0 | 0.22 | 1 | 0 | 0 | 3 | 1 | 24 | 3809F19 | 199.0 | 0.993 | -1.547 |
| 3809F3 | 28.0 | 0.27 | 1 | 2 | 2 | 2 | 2 | 17 | 3809F20 | 208.0 | 0.928 | -1.006 |
| 3809F4 | 38.0 | 0.39 | 0 | 1 | 2 | 3 | 1 | 0 | 3809F29 | 297.0 | 1.004 | -4.556 |
| 3809F5 | 47.5 | 0.58 | 1 | 2 | 3 | 2 | 2 | 20 | 09-349SK | 349.0 | 0.719 | -1.863 |
| 3809F6 | 57.0 | 0.30 | 3 | 2 | 3 | 2 | 2 | 31 | 3809F35 | 358.5 | 1.543 | -1.676 |
| 3809F7 | 67.0 | 0.18 | 0 | 2 | 2 | 3 | 1 | 0 | 3809F37 | 379.0 | 1.153 | -3.661 |
| 3809F8 | 77.5 | 0.35 | 1 | 3 | 2 | 2 | 2 | 11 | 3809F42 | 428.0 | 1.287 | -2.005 |
| 3809F9 | 87.0 | 0.16 | 0 | 2 | 3 | 3 | 2 | 0 | 3809F43 | 438.0 | 1.278 | -6.562 |
| 3809F10 | 98.0 | 0.32 | 3 | 2 | 3 | 2 | 2 | 26 | 3809F47 | 476.5 | 1.369 | -4.453 |
| 3809F11 | 106.5 | 0.35 | 0 | 2 | 2 | 2 | 3 | 0 | 3809F52 | 523.0 | 1.056 | -1.188 |
| 3809F12 | 118.0 | 0.61 | 0 | 3 | 2 | 1 | 2 | 0 | 09-530SK | 530.0 | 0.533 | -1.902 |
| 3809F13 | 128.0 | 0.72 | 0 | 3 | 2 | 1 | 2 | 0 | 3809F54 | 539.0 | 1.046 | -3.652 |
| 3809F14 | 137.5 | 0.45 | 2 | 1 | 2 | 2 | 2 | 26 | 09-540SK | 540.0 | 1.145 | -4.434 |
| 3809F15 | 149.5 | 0.43 | 4 | 1 | 2 | 2 | 1 | 23 | 3809F55 | 547.0 | 1.223 | -4.081 |
| 3809F16 | 167.0 | 1.69 | 0 | 2 | 2 | 2 | 2 | 0 | 09-550SK | 550.0 | 1.099 | -2.344 |
| 3809F17 | 177.5 | 4.47 | 0 | 3 | 2 | 1 | 0 | 0 | 3809F63 | 631.5 | 1.248 | -2.634 |
| 3809F18 | 189.0 | 1.85 | 0 | 3 | 2 | 2 | 2 | 0 | 3809F68 | 688.0 | 0.640 | -3.526 |
| 3809F19 | 199.0 | 1.68 | 4 | 2 | 3 | 2 | 2 | 26 | 09-740SK | 740.0 | 1.137 | -3.755 |
| 3809F20 | 208.0 | 2.86 | 6 | 2 | 2 | 1 | 2 | 31 | 3809F74 | 747.0 | 1.810 | -2.580 |
| 3809F21 | 218.0 | 8.47 | 3 | 3 | 3 | 1 | 1 | 22 | 09-750SK | 750.0 | 1.123 | -2.718 |
| 3809F22 | 228.0 | 18.94 | 0 | 3 | 2 | 1 | 2 | 0 | 3809F76 | 768.0 | 1.315 | -1.394 |
| 3809F23 | 236.0 | 8.21 | 0 | 3 | 2 | 1 | 3 | 0 | 09-780SK | 780.0 | 0.944 | -3.374 |
| 3809F24 | 241.0 | 1.89 | 0 | 2 | 2 | 3 | 2 | 0 | 3809F79 | 797.0 | 1.464 | -3.268 |
| 3809F25 | 249.5 | 0.27 | 0 | 1 | 1 | 3 | 1 | 0 | 09-800SK | 800.0 | 1.097 | -3.441 |
| 3809F26 | 260.5 | 0.33 | 0 | 1 | 1 | 3 | 2 | 0 | 3809F82 | 827.5 | 1.434 | -3.268 |
| 3809F27 | 267.0 | 9.80 | 0 | 2 | 3 | 2 | 3 | 0 | | | | |
| 3809F28 | 287.0 | 0.28 | 0 | 0 | 1 | 3 | 1 | 0 | (SK samples from S.King - Southampton) | | | |
| 3809F29 | 297.0 | 0.06 | 2 | 0 | 2 | 2 | 1 | 23 | | | | |
| 3809F30 | 308.0 | 0.26 | 0 | 0 | 2 | 2 | 2 | 0 | | | | |
| 3809F31 | 317.5 | 0.13 | 2 | 0 | 2 | 2 | 1 | 25 | | | | |
| 3809F32 | 326.0 | 0.13 | 1 | 0 | 2 | 2 | 1 | 13 | | | | |
| 3809F33 | 337.5 | 0.14 | 0 | 0 | 1 | 3 | 0 | 0 | | | | |
| 3809F34 | 347.0 | 0.14 | 1 | 0 | 2 | 3 | 0 | 22 | | | | |
| 3809F35 | 358.5 | 0.29 | 6 | 0 | 1 | 3 | 1 | 35 | | | | |
| 3809F36 | 369.0 | 0.62 | 2 | 0 | 0 | 3 | 0 | 22 | | | | |
| 3809F37 | 379.0 | 0.33 | 7 | 1 | 2 | 2 | 1 | 33 | | | | |
| 3809F38 | 388.0 | 0.17 | 2 | 0 | 2 | 2 | 1 | 27 | | | | |

APPENDIX C.2 SEDIMENT >63μm DESCRIPTION AND FORAMINIFERA STABLE ISOTOPES

| CD38-09 | | | Description (0=absent, 1=rare, 2=common, 3=abundant) | | | | | Number of forams picked |
|---|---|---|---|---|---|---|---|---|
| Sample | Depth | Sed.>63um | Forams | Qtz. | Clays | Diatoms | Fish bits | Bolivina seminuda |
| | (cm) | (%) | (0-10) | (0-3) | (0-3) | (0-3) | (0-3) | |
| 3809F39 | 398.0 | 0.11 | 0 | 1 | 2 | 2 | 2 | 0 |
| 3809F40 | 410.0 | 0.19 | 1 | 0 | 2 | 3 | 1 | 20 |
| 3809F41 | 416.5 | 0.33 | 2 | 0 | 1 | 3 | 0 | 23 |
| 3809F42 | 428.0 | 0.25 | 6 | 0 | 1 | 3 | 0 | 35 |
| 3809F43 | 438.0 | 0.33 | 8 | 0 | 2 | 1 | 1 | 37 |
| 3809F44 | 448.0 | 0.34 | 2 | 0 | 2 | 2 | 1 | 20 |
| 3809F45 | 458.0 | 0.12 | 1 | 0 | 2 | 2 | 1 | 20 |
| 3809F46 | 468.0 | 0.06 | 4 | 0 | 2 | 2 | 2 | 25 |
| 3809F47 | 476.5 | 0.13 | 5 | 0 | 2 | 2 | 3 | 31 |
| 3809F48 | 487.0 | 0.14 | 3 | 1 | 2 | 1 | 2 | 17 |
| 3809F49 | 498.0 | 0.18 | 1 | 1 | 3 | 1 | 2 | 16 |
| 3809F50 | 506.5 | 0.23 | 0 | 1 | 3 | 1 | 1 | 0 |
| 3809F51 | 518.0 | 0.12 | 0 | 0 | 2 | 2 | 1 | 0 |
| 3809F52 | 523.0 | 0.22 | 5 | 0 | 2 | 2 | 1 | 30 |
| 3809F53 | 534.0 | 0.12 | 5 | 0 | 2 | 1 | 2 | 27 |
| 3809F54 | 539.0 | 0.18 | 9 | 0 | 1 | 1 | 0 | 30 |
| 3809F55 | 547.0 | 0.15 | 5 | 0 | 2 | 2 | 1 | 29 |
| 3809F56 | 558.0 | 0.72 | 3 | 0 | 1 | 3 | 0 | 15 |
| 3809F57 | 568.0 | 0.44 | 1 | 0 | 2 | 3 | 0 | 12 |
| 3809F58 | 579.0 | 0.14 | 3 | 0 | 1 | 3 | 0 | 27 |
| 3809F59 | 591.0 | 0.19 | 1 | 0 | 1 | 3 | 0 | 20 |
| 3809F60 | 599.0 | 0.45 | 5 | 0 | 2 | 2 | 1 | 23 |
| 3809F61 | 608.0 | 0.61 | 4 | 0 | 2 | 2 | 0 | 22 |
| 3809F62 | 618.5 | 0.44 | 1 | 0 | 1 | 3 | 0 | 0 |
| 3809F63 | 631.5 | 0.86 | 2 | 0 | 2 | 3 | 0 | 22 |
| 3809F64 | 642.0 | 0.39 | 1 | 0 | 2 | 3 | 0 | 0 |
| 3809F65 | 656.5 | 1.10 | 1 | 0 | 2 | 3 | 0 | 10 |
| 3809F66 | 668.0 | 0.65 | 1 | 0 | 1 | 3 | 0 | 0 |
| 3809F67 | 678.5 | 0.27 | 1 | 0 | 2 | 3 | 0 | 0 |
| 3809F68 | 688.0 | 0.23 | 4 | 0 | 2 | 2 | 0 | 34 |
| 3809F69 | 701.0 | 0.57 | 1 | 0 | 1 | 3 | 0 | 0 |
| 3809F70 | 707.0 | 0.27 | 5 | 0 | 2 | 2 | 1 | 25 |
| 3809F71 | 717.5 | 0.31 | 2 | 0 | 2 | 2 | 0 | 0 |
| 3809F72 | 727.5 | 0.50 | 2 | 0 | 2 | 2 | 0 | 27 |
| 3809F73 | 737.0 | 0.63 | 1 | 0 | 1 | 3 | 0 | 13 |
| 3809F74 | 747.0 | 0.20 | 2 | 0 | 2 | 2 | 0 | 28 |
| 3809F75 | 757.0 | 0.24 | 6 | 0 | 2 | 2 | 0 | 24 |
| 3809F76 | 768.0 | 0.37 | 4 | 0 | 2 | 2 | 1 | 26 |

APPENDIX C.2 SEDIMENT >63µm DESCRIPTION AND FORAMINIFERA STABLE ISOTOPES

| CD38-09 | | | Description (0=absent, 1=rare, 2=common, 3=abundant) | | | | | Number of forams picked | |
|---|---|---|---|---|---|---|---|---|---|
| Sample | Depth | Sed.>63um | Forams | Qtz. | Clays | Diatoms | Fish bits | Bolivina seminuda | |
| | (cm) | (%) | (0-10) | (0-3) | (0-3) | (0-3) | (0-3) | | |
| 3809F77 | 778.0 | 0.45 | 2 | 0 | 2 | 2 | 0 | 22 | |
| 3809F78 | 787.0 | 0.63 | 2 | 0 | 2 | 2 | 1 | 10 | |
| 3809F79 | 797.0 | 0.21 | 7 | 0 | 2 | 2 | 1 | 34 | |
| 3809F80 | 807.5 | 0.35 | 3 | 0 | 2 | 3 | 1 | 24 | |
| 3809F81 | 819.5 | 0.44 | 2 | 0 | 2 | 3 | 1 | 22 | |
| 3809F82 | 827.5 | 0.47 | 4 | 0 | 2 | 3 | 0 | 30 | |
| 3809F83 | 836.0 | 0.41 | 2 | 0 | 2 | 3 | 0 | 20 | |
| 3809F84 | 855.0 | 0.75 | 3 | 0 | 2 | 2 | 0 | 24 | |
| CD38-10 | | | | | | | | | |
| 3810F1 | 9.0 | 1.64 | 4 | 1 | 3 | 2 | 2 | 19 | |
| 3810F2 | 18.0 | 4.81 | 2 | 2 | 2 | 0 | 2 | 9 | |
| 3810F3 | 29.0 | 5.08 | 3 | 3 | 1 | 0 | 2 | 5 | |
| 3810F4 | 42.0 | 0.82 | 8 | 2 | 1 | 0 | 1 | 17 | |
| 3810F5 | 49.0 | 1.66 | 0 | 2 | 3 | 2 | 2 | 0 | |
| 3810F6 | 58.0 | 1.88 | 0 | 2 | 3 | 2 | 3 | 0 | |
| 3810F7 | 68.0 | 4.07 | 0 | 1 | 3 | 2 | 2 | 0 | |
| 3810F8 | 78.5 | 33.62 | 0 | 2 | 2 | 0 | 1 | 0 | |
| 3810F9 | 88.0 | 54.40 | 0 | 2 | 2 | 0 | 2 | 0 | |
| 3810F10 | 97.0 | 19.17 | 6 | 3 | 1 | 0 | 1 | 16 | |
| 3810F11 | 108.0 | 20.88 | 7 | 2 | 2 | 0 | 1 | 21 | |
| 3810F12 | 122.0 | 6.80 | 8 | 2 | 1 | 0 | 2 | 26 | |
| 3810F13 | 128.0 | 1.76 | 9 | 2 | 2 | 1 | 1 | 29 | |
| 3810F14 | 138.0 | 0.72 | 6 | 2 | 1 | 3 | 1 | 33 | |
| 3810F15 | 148.0 | 0.68 | 6 | 2 | 2 | 1 | 1 | 26 | |
| 3810F16 | 157.0 | 0.61 | 5 | 2 | 1 | 2 | 3 | 33 | |
| 3810F17 | 165.0 | 0.63 | 10 | 0 | 0 | 1 | 1 | 35 | |
| 3810F18 | 176.0 | 0.36 | 4 | 3 | 0 | 3 | 1 | 23 | |
| 3810F19 | 190.5 | 0.20 | 6 | 2 | 2 | 2 | 1 | 37 | |
| 3810F20 | 197.0 | 0.54 | 10 | 0 | 0 | 1 | 1 | 31 | |
| 3810F21 | 207.0 | 0.32 | 5 | 2 | 1 | 2 | 1 | 20 | |
| 3810F22 | 219.0 | 0.19 | 4 | 2 | 1 | 2 | 1 | 19 | |
| 3810F23 | 226.5 | 0.66 | 2 | 1 | 2 | 3 | 2 | 13 | |
| 3810F24 | 238.0 | 0.39 | 1 | 3 | 1 | 2 | 2 | 2 | |
| 3810F25 | 250.0 | 0.29 | 3 | 3 | 1 | 1 | 1 | 21 | |
| 3810F26 | 259.0 | 0.41 | 7 | 3 | 0 | 1 | 1 | 36 | |
| 3810F27 | 266.5 | 0.53 | 9 | 2 | 0 | 0 | 1 | 31 | |

Isotopic composition of B.sem.

| Sample | Depth (cm) | d18O (PDB) | d13C (PDB) |
|---|---|---|---|
| 3810F1 | 9.0 | 1.809 | -0.455 |
| 3810F4 | 42.0 | 1.262 | -2.645 |
| 3810F11 | 108.0 | 1.687 | -1.903 |
| 3810F12 | 122.0 | 2.503 | -1.646 |
| 3810F13 | 128.0 | 2.148 | -1.394 |
| 3810F14 | 138.0 | 2.028 | -1.461 |
| 3810F15 | 148.0 | 1.795 | -0.812 |
| 3810F16 | 157.0 | 2.013 | -1.268 |
| 3810F17 | 165.0 | 2.048 | -2.168 |
| 3810F18 | 176.0 | 2.048 | -1.055 |
| 3810F19 | 190.5 | 2.440 | -1.186 |
| 3810F20 | 197.0 | 1.984 | -1.880 |
| 3810F21 | 207.0 | 1.612 | -1.821 |
| 3810F22 | 219.0 | 1.845 | -1.035 |
| 3810F25 | 250.0 | 1.710 | -1.050 |
| 3810F26 | 259.0 | 1.456 | -1.026 |
| 3810F27 | 266.5 | 2.011 | -1.204 |
| 3810F29 | 289.0 | 1.788 | -1.598 |
| 3810F30 | 299.0 | 1.989 | -1.949 |
| 3810F31 | 308.0 | 2.143 | -1.589 |
| 3810F32 | 316.0 | 2.159 | -1.872 |
| 3810F33 | 320.5 | 2.009 | -1.589 |
| 3810F34 | 329.0 | 2.140 | -1.924 |
| 3810F36 | 346.0 | 2.014 | -2.331 |
| 3810F37 | 356.0 | 0.863 | -2.074 |
| 3810F38 | 367.0 | 1.948 | -1.805 |
| 3810F39 | 376.0 | 1.849 | -1.755 |

APPENDIX C.2 SEDIMENT >63µm DESCRIPTION AND FORAMINIFERA STABLE ISOTOPES

| CD38-10 | | | Description (0=absent, 1=rare, 2=common, 3=abundant) | | | | | Number of forams picked | Isotopic composition of B.sem. | | | |
|---|---|---|---|---|---|---|---|---|---|---|---|---|
| Sample | Depth | Sed.>63um | Forams | Qtz. | Clays | Diatoms | Fish bits | Bolivina seminuda | Sample | Depth | d18O | d13C |
| | (cm) | (%) | (0-10) | (0-3) | (0-3) | (0-3) | (0-3) | | | (cm) | (PDB) | (PDB) |
| 3810F28 | 278.0 | 0.53 | 7 | 1 | 1 | 1 | 2 | 23 | 3810F41 | 397.0 | 1.645 | -1.393 |
| 3810F29 | 289.0 | 0.13 | 5 | 2 | 2 | 1 | 1 | 32 | 3810F42 | 407.0 | 1.371 | -1.497 |
| 3810F30 | 299.0 | 0.53 | 10 | 0 | 1 | 0 | 1 | 30 | 3810F43 | 415.0 | 1.903 | -1.640 |
| 3810F31 | 308.0 | 0.20 | 4 | 2 | 2 | 2 | 2 | 24 | 3810F44 | 427.0 | 1.677 | -1.962 |
| 3810F32 | 316.0 | 0.17 | 9 | 0 | 2 | 0 | 1 | 29 | 3810F45 | 436.0 | 1.930 | -2.110 |
| 3810F33 | 320.5 | 0.36 | 10 | 1 | 1 | 0 | 2 | 30 | 3810F47 | 452.0 | 1.837 | -2.064 |
| 3810F34 | 329.0 | 0.45 | 10 | 1 | 1 | 0 | 1 | 28 | 3810F48 | 459.0 | 1.662 | -1.481 |
| 3810F35 | 338.0 | 0.29 | 4 | 2 | 2 | 0 | 2 | 23 | 3810F49 | 469.0 | 1.530 | -1.987 |
| 3810F36 | 346.0 | 0.40 | 8 | 0 | 1 | 2 | 1 | 25 | 3810F50 | 478.0 | 1.392 | -1.831 |
| 3810F37 | 356.0 | 0.87 | 8 | 0 | 1 | 2 | 1 | 27 | 3810F51 | 486.0 | 1.427 | -1.814 |
| 3810F38 | 367.0 | 0.76 | 9 | 0 | 2 | 1 | 1 | 26 | 3810F52 | 497.0 | 0.876 | -1.223 |
| 3810F39 | 376.0 | 0.56 | 8 | 0 | 2 | 1 | 2 | 21 | 3810F53 | 507.0 | 1.333 | -1.863 |
| 3810F40 | 386.0 | 0.13 | 5 | 1 | 2 | 0 | 1 | 24 | 3810F54 | 517.0 | 0.829 | -2.003 |
| 3810F41 | 397.0 | 0.65 | 6 | 1 | 2 | 0 | 1 | 29 | 3810F55 | 525.0 | 1.066 | -2.106 |
| 3810F42 | 407.0 | 0.19 | 4 | 2 | 3 | 0 | 1 | 22 | 3810F56 | 537.5 | 0.999 | -3.045 |
| 3810F43 | 415.0 | 0.29 | 10 | 1 | 0 | 0 | 1 | 27 | 3810F57 | 547.0 | -0.296 | -1.988 |
| 3810F44 | 427.0 | 0.56 | 8 | 1 | 1 | 1 | 1 | 22 | 3810F58 | 557.0 | 1.551 | -5.166 |
| 3810F45 | 436.0 | 0.66 | 9 | 1 | 1 | 1 | 1 | 25 | 3810F59 | 565.5 | 1.516 | -3.176 |
| 3810F46 | 446.0 | 0.63 | 8 | 1 | 2 | 2 | 0 | 26 | 3810F60 | 570.0 | 1.644 | -7.899 |
| 3810F47 | 452.0 | 0.33 | 9 | 0 | 1 | 3 | 0 | 32 | 3810F61 | 579.0 | 1.468 | -3.313 |
| 3810F48 | 459.0 | 2.20 | 10 | 0 | 1 | 1 | 1 | 33 | 3810F62 | 587.5 | 1.454 | -3.066 |
| 3810F49 | 469.0 | 0.82 | 9 | 0 | 1 | 2 | 1 | 34 | 3810F63 | 593.5 | 1.432 | -3.943 |
| 3810F50 | 478.0 | 0.75 | 4 | 2 | 2 | 1 | 2 | 24 | 3810F64 | 607.0 | 1.676 | -3.331 |
| 3810F51 | 486.0 | 0.84 | 4 | 2 | 2 | 1 | 2 | 25 | 3810F65 | 616.0 | 1.657 | -2.958 |
| 3810F52 | 497.0 | 1.71 | 2 | 3 | 3 | 0 | 2 | 22 | 3810F66 | 627.0 | 1.653 | -3.495 |
| 3810F53 | 507.0 | 6.74 | 7 | 2 | 2 | 0 | 1 | 29 | 3810F67 | 637.0 | 2.022 | -2.969 |
| 3810F54 | 517.0 | 0.81 | 4 | 1 | 1 | 3 | 0 | 20 | 3810F68 | 649.0 | 1.891 | -2.693 |
| 3810F55 | 525.0 | 0.54 | 4 | 1 | 1 | 3 | 0 | 22 | 3810F69 | 660.0 | 2.081 | -2.618 |
| 3810F56 | 537.5 | 0.75 | 9 | 0 | 2 | 0 | 1 | 29 | 3810F70 | 678.0 | 2.210 | -2.095 |
| 3810F57 | 547.0 | 0.29 | 7 | 0 | 2 | 0 | 1 | 26 | 3810F71 | 689.0 | 2.304 | -1.983 |
| 3810F58 | 557.0 | 1.20 | 7 | 0 | 1 | 2 | 0 | 27 | 3810F72 | 698.0 | 2.587 | -1.921 |
| 3810F59 | 565.5 | 0.54 | 7 | 0 | 1 | 2 | 0 | 28 | 3810F73 | 708.0 | 2.453 | -2.538 |
| 3810F60 | 570.0 | 2.40 | 9 | 0 | 1 | 2 | 1 | 32 | 3810F74 | 718.0 | 2.412 | -2.068 |
| 3810F61 | 579.0 | 0.92 | 8 | 0 | 1 | 2 | 1 | 23 | 3810F75 | 728.0 | 2.519 | -1.899 |
| 3810F62 | 587.5 | 1.12 | 8 | 0 | 1 | 2 | 1 | 26 | 3810F76 | 737.0 | 2.761 | -1.330 |
| 3810F63 | 593.5 | 0.63 | 5 | 0 | 1 | 3 | 0 | 23 | | | | |
| 3810F64 | 607.0 | 1.18 | 8 | 0 | 2 | 1 | 2 | 24 | | | | |
| 3810F65 | 616.0 | 0.87 | 6 | 0 | 1 | 2 | 1 | 24 | | | | |

APPENDIX C.2 SEDIMENT >63µm DESCRIPTION AND FORAMINIFERA STABLE ISOTOPES

| CD38-10 | | | Description (0=absent, 1=rare, 2=common, 3=abundant) | | | | | Number of forams picked |
|---|---|---|---|---|---|---|---|---|
| Sample | Depth | Sed.>63um | Forams | Qtz. | Clays | Diatoms | Fish bits | Bolivina seminuda |
| | (cm) | (%) | (0-10) | (0-3) | (0-3) | (0-3) | (0-3) | |
| 3810F66 | 627.0 | 0.64 | 9 | 0 | 2 | 2 | 1 | 26 |
| 3810F67 | 637.0 | 1.36 | 7 | 0 | 2 | 3 | 1 | 26 |
| 3810F68 | 649.0 | 1.47 | 9 | 0 | 1 | 1 | 1 | 37 |
| 3810F69 | 660.0 | 0.52 | 3 | 0 | 3 | 3 | 1 | 22 |
| 3810F70 | 678.0 | 0.59 | 10 | 0 | 1 | 1 | 1 | 39 |
| 3810F71 | 689.0 | 0.61 | 7 | 0 | 2 | 1 | 1 | 40 |
| 3810F72 | 698.0 | 0.36 | 6 | 0 | 2 | 1 | 2 | 37 |
| 3810F73 | 708.0 | 0.52 | 8 | 0 | 2 | 1 | 2 | 39 |
| 3810F74 | 718.0 | 4.27 | 7 | 0 | 2 | 2 | 3 | 45 |
| 3810F75 | 728.0 | 0.44 | 5 | 0 | 3 | 2 | 2 | 33 |
| 3810F76 | 737.0 | 0.48 | 5 | 0 | 3 | 3 | 2 | 32 |
| 3810F77 | 748.0 | 0.70 | 0 | 2 | 2 | 2 | 2 | 0 |
| 3810F78 | 758.0 | 1.02 | 0 | 2 | 2 | 1 | 3 | 0 |
| 3810F79 | 766.0 | 14.53 | 0 | 3 | 2 | 1 | 2 | 0 |
| CD38-11 | | | | | | | | Uvigerina |
| 3811F01 | 6.0 | 1.37 | 1 | 3 | 2 | 1 | 1 | 1 |
| 3811F02 | 16.0 | 0.88 | 3 | 3 | 2 | 1 | 1 | 0 |
| 3811F03 | 26.0 | 0.77 | 0 | 2 | 1 | 1 | 3 | 0 |
| 3811F04 | 36.0 | 0.40 | 1 | 2 | 1 | 1 | 3 | 0 |
| 3811F05 | 46.0 | 0.44 | 4 | 2 | 1 | 1 | 2 | 17 |
| 3811F06 | 56.0 | 0.21 | 5 | 2 | 1 | 2 | 2 | 21 |
| 3811F07 | 66.0 | 0.32 | 4 | 2 | 1 | 2 | 3 | 23 |
| 3811F08 | 76.0 | 1.95 | 5 | 2 | 1 | 2 | 2 | 29 |
| 3811F09 | 88.0 | 2.65 | 6 | 3 | 1 | 1 | 1 | 34 |
| 3811F10 | 102.0 | 0.90 | 6 | 3 | 2 | 2 | 2 | 36 |
| 3811F11 | 111.0 | 0.53 | 4 | 3 | 2 | 2 | 2 | 20 |
| 3811F12 | 121.0 | 0.31 | 6 | 3 | 1 | 1 | 2 | 22 |
| 3811F13 | 131.0 | 1.93 | 7 | 3 | 2 | 1 | 1 | 37 |
| 3811F14 | 141.0 | 1.80 | 3 | 2 | 1 | 2 | 1 | 14 |
| 3811F15 | 151.0 | 1.43 | 7 | 3 | 1 | 2 | 2 | 29 |
| 3811F16 | 161.0 | 1.16 | 5 | 3 | 2 | 1 | 2 | 31 |
| 3811F17 | 171.0 | 2.66 | 5 | 3 | 2 | 1 | 2 | 30 |
| 3811F18 | 181.0 | 0.68 | 7 | 3 | 1 | 1 | 2 | 30 |
| 3811F19 | 191.0 | 0.41 | 4 | 2 | 2 | 1 | 2 | 20 |
| 3811F20 | 200.0 | 0.60 | 6 | 2 | 2 | 1 | 2 | 31 |
| 3811F21 | 211.0 | 3.44 | 4 | 2 | 2 | 1 | 2 | 21 |

Isotopic composition of Uvigerina

| Sample | Depth (cm) | d18O (PDB) | d13C (PDB) |
|---|---|---|---|
| 3811F01 | 6.0 | 4.762 | -1.338 |
| 3811F05 | 46.0 | 4.913 | -1.243 |
| 3811F06 | 56.0 | 5.189 | -1.210 |
| 3811F07 | 66.0 | 5.254 | -1.184 |
| 3811F08 | 76.0 | 5.006 | -1.284 |
| 3811F09 | 88.0 | 5.326 | -1.467 |
| 3811F10 | 102.0 | 5.336 | -1.534 |
| 3811F11 | 111.0 | 5.283 | -1.360 |
| 3811F12 | 121.0 | 5.386 | -1.259 |
| 3811F13 | 131.0 | 5.358 | -1.451 |
| 3811F14 | 141.0 | 5.261 | -1.388 |
| 3811F15 | 151.0 | 5.303 | -1.397 |
| 3811F16 | 161.0 | 5.213 | -1.418 |
| 3811F17 | 171.0 | 5.348 | -1.481 |
| 3811F18 | 181.0 | 5.327 | -1.323 |
| 3811F19 | 191.0 | 5.332 | -1.322 |
| 3811F20 | 200.0 | 5.066 | -1.350 |
| 3811F21 | 211.0 | 5.085 | -1.463 |
| 3811F22 | 222.0 | 5.176 | -1.498 |
| 3811F23 | 231.0 | 5.083 | -1.405 |
| 3811F24 | 241.0 | 5.115 | -1.326 |

APPENDIX C.2 SEDIMENT >63μm DESCRIPTION AND FORAMINIFERA STABLE ISOTOPES

| CD38-11 | | | Description (0=absent, 1=rare, 2=common, 3=abundant) | | | | | Number of forams picked | Isotopic composition of Uvigerina | | | |
|---|---|---|---|---|---|---|---|---|---|---|---|---|
| Sample | Depth | Sed.>63um | Forams | Qtz. | Clays | Diatoms | Fish bits | Uvigerina | Sample | Depth | d18O | d13C |
| | (cm) | (%) | (0-10) | (0-3) | (0-3) | (0-3) | (0-3) | | | (cm) | (PDB) | (PDB) |
| 3811F22 | 222.0 | 1.02 | 4 | 2 | 2 | 1 | 2 | 23 | 3811F26 | 261.0 | 4.723 | -1.216 |
| 3811F23 | 231.0 | 0.27 | 6 | 2 | 2 | 1 | 3 | 25 | 3811F27 | 271.0 | 4.701 | -1.345 |
| 3811F24 | 241.0 | 0.26 | 8 | 2 | 1 | 1 | 3 | 33 | 3811F28 | 281.0 | 4.794 | -1.299 |
| 3811F25 | 251.0 | 0.28 | 7 | 1 | 1 | 2 | 3 | 21 | 3811F29 | 291.0 | 4.589 | -1.361 |
| 3811F26 | 261.0 | 0.24 | 6 | 1 | 1 | 2 | 3 | 22 | 3811F30 | 301.0 | 4.432 | -1.379 |
| 3811F27 | 271.0 | 0.31 | 7 | 1 | 2 | 2 | 3 | 27 | 3811F33 | 331.0 | 4.692 | -1.175 |
| 3811F28 | 281.0 | 0.28 | 5 | 2 | 2 | 1 | 3 | 26 | 3811F35 | 351.0 | 3.659 | -1.483 |
| 3811F29 | 291.0 | 0.37 | 5 | 2 | 2 | 2 | 3 | 17 | 3811F36 | 361.0 | 4.459 | -1.351 |
| 3811F30 | 301.0 | 0.46 | 4 | 2 | 2 | 1 | 3 | 20 | 3811F37 | 371.0 | 4.715 | -1.316 |
| 3811F31 | 311.0 | 0.68 | 2 | 2 | 2 | 1 | 3 | 0 | 3811F38 | 381.0 | 4.752 | -1.470 |
| 3811F32 | 321.0 | 2.76 | 3 | 2 | 2 | 1 | 3 | 0 | 3811F39 | 391.0 | 4.708 | -1.480 |
| 3811F33 | 331.0 | 0.32 | 2 | 2 | 2 | 2 | 3 | 5 | 3811F40 | 401.0 | 4.549 | -1.521 |
| 3811F34 | 341.0 | 0.25 | 2 | 1 | 2 | 1 | 3 | 1 | 3811F41 | 411.0 | 4.533 | -1.298 |
| 3811F35 | 351.0 | 0.17 | 1 | 2 | 2 | 1 | 3 | 9 | 3811F42 | 421.0 | 4.201 | -1.278 |
| 3811F36 | 361.0 | 0.19 | 2 | 2 | 1 | 1 | 3 | 11 | 3811F43 | 431.0 | 4.138 | -1.285 |
| 3811F37 | 371.0 | 0.11 | 2 | 2 | 2 | 1 | 3 | 8 | 3811F44 | 441.0 | 4.190 | -1.315 |
| 3811F38 | 381.0 | 0.08 | 3 | 2 | 1 | 1 | 3 | 9 | 3811F45 | 451.0 | 3.673 | |
| 3811F39 | 391.0 | 0.22 | 5 | 2 | 2 | 1 | 3 | 26 | 3811F47 | 471.0 | 4.411 | -1.256 |
| 3811F40 | 401.0 | 0.12 | 4 | 1 | 2 | 1 | 3 | 16 | 3811F48 | 481.0 | 4.762 | -0.996 |
| 3811F41 | 411.0 | 0.17 | 3 | 1 | 1 | 1 | 3 | 16 | 3811F50 | 501.0 | 4.276 | -0.923 |
| 3811F42 | 421.0 | 0.24 | 2 | 1 | 2 | 1 | 2 | 20 | 3811F51 | 511.0 | 4.150 | -0.729 |
| 3811F43 | 431.0 | 0.23 | 5 | 1 | 1 | 1 | 3 | 21 | 3811F57 | 571.0 | 3.639 | -1.164 |
| 3811F44 | 441.0 | 0.27 | 3 | 1 | 1 | 1 | 3 | 12 | | | | |
| 3811F45 | 451.0 | 0.13 | 1 | 1 | 1 | 1 | 3 | 1 | | | | |
| 3811F46 | 461.0 | 0.08 | 1 | 1 | 1 | 1 | 3 | 2 | | | | |
| 3811F47 | 471.0 | 0.17 | 4 | 0 | 1 | 1 | 3 | 24 | | | | |
| 3811F48 | 481.0 | 0.20 | 2 | 1 | 2 | 1 | 3 | 8 | | | | |
| 3811F49 | 491.0 | 0.10 | 0 | 1 | 2 | 1 | 3 | 0 | | | | |
| 3811F50 | 501.0 | 0.14 | 1 | 1 | 1 | 1 | 3 | 3 | | | | |
| 3811F51 | 511.0 | 0.10 | 1 | 1 | 2 | 1 | 3 | 2 | | | | |
| 3811F52 | 521.0 | 0.18 | 0 | 0 | 2 | 1 | 3 | 0 | | | | |
| 3811F53 | 531.0 | 0.25 | 0 | 0 | 2 | 1 | 3 | 0 | | | | |
| 3811F54 | 541.0 | 0.15 | 0 | 0 | 2 | 1 | 3 | 0 | | | | |
| 3811F55 | 551.0 | 0.38 | 1 | 1 | 1 | 1 | 3 | 0 | | | | |
| 3811F56 | 561.0 | 0.33 | 1 | 1 | 1 | 1 | 3 | 2 | | | | |
| 3811F57 | 571.0 | 0.20 | 2 | 1 | 1 | 1 | 3 | 7 | | | | |

APPENDIX C.3. SEDIMENT ACCUMULATION RATES, DRY BULK DENSITIES, MASS ACCUMULATION RATES AND DEPTH/AGE CORRELATION

| CD38-02 | 2525m | | | | | CD38-11 | 3835m | | | |
|---|---|---|---|---|---|---|---|---|---|---|
| Depth (cm) | SAR (cm/kyr) | DBD (g/cm2) | MAR (g/cm2/kyr) | Age (ka) | | Depth (cm) | SAR (cm/kyr) | DBD (g/cm2) | MAR g/cm2/kyr | Age (ka) |
| 8.0 | 2.90 | 0.58 | 1.67 | 2.76 | | 3.0 | 3.73 | 0.58 | 2.16 | 0.80 |
| 18.0 | 2.90 | 0.61 | 1.76 | 6.21 | | 13.0 | 3.73 | 0.62 | 2.33 | 2.00 |
| 28.0 | 2.90 | 0.57 | 1.64 | 9.66 | | 23.0 | 3.73 | 0.73 | 2.72 | 2.20 |
| 38.0 | 4.15 | 0.53 | 2.21 | 12.77 | | 33.0 | 3.73 | 0.55 | 2.05 | 3.49 |
| 48.0 | 4.15 | 0.61 | 2.53 | 15.18 | | 43.0 | 3.73 | 0.53 | 1.98 | 6.17 |
| 57.5 | 4.15 | 0.61 | 2.52 | 17.47 | | 53.0 | 3.73 | 0.54 | 2.02 | 8.85 |
| 70.0 | 4.15 | 0.60 | 2.51 | 20.48 | | 63.0 | 3.73 | 0.55 | 2.06 | 11.53 |
| 79.0 | 4.15 | 0.59 | 2.45 | 22.65 | | 73.0 | 4.56 | 0.58 | 2.66 | 13.80 |
| 89.0 | 3.59 | 0.61 | 2.19 | 25.22 | | 85.0 | 4.56 | 0.96 | 4.37 | 16.44 |
| 100.0 | 3.59 | 0.62 | 2.21 | 28.29 | | 95.0 | 4.56 | 0.60 | 2.72 | 18.63 |
| 110.0 | 3.59 | 0.63 | 2.24 | 31.07 | | 105.0 | 4.56 | 0.59 | 2.67 | 20.82 |
| 120.0 | 3.59 | 0.61 | 2.18 | 33.86 | | 116.0 | 4.56 | 0.59 | 2.70 | 23.23 |
| 130.0 | 3.59 | 0.61 | 2.19 | 36.64 | | 125.0 | 5.02 | 0.59 | 2.94 | 25.11 |
| 139.0 | 3.59 | 0.60 | 2.14 | 39.15 | | 135.0 | 5.02 | 0.61 | 3.05 | 27.10 |
| 150.0 | 3.59 | 0.59 | 2.12 | 42.22 | | 145.0 | 5.02 | 0.58 | 2.90 | 29.09 |
| 160.0 | 3.59 | 0.65 | 2.32 | 45.00 | | 155.0 | 5.02 | 0.63 | 3.19 | 31.08 |
| 171.0 | 3.59 | 0.64 | 2.30 | 48.07 | | 165.0 | 5.02 | 0.56 | 2.80 | 33.07 |
| 181.0 | 3.59 | 0.58 | 2.08 | 50.85 | | 175.0 | 5.02 | 0.74 | 3.71 | 35.07 |
| 191.0 | 3.59 | 0.60 | 2.15 | 53.64 | | 186.0 | 5.02 | 0.58 | 2.93 | 37.26 |
| 201.0 | 3.59 | 0.58 | 2.07 | 56.42 | | 197.0 | 5.02 | 0.57 | 2.84 | 39.45 |
| 211.0 | 3.01 | 0.61 | 1.83 | 59.29 | | 204.0 | 5.02 | 0.56 | 2.80 | 40.84 |
| 221.0 | 3.01 | 0.63 | 1.90 | 62.61 | | 215.0 | 5.02 | 0.57 | 2.86 | 43.03 |
| 231.0 | 3.01 | 0.65 | 1.95 | 65.94 | | 225.0 | 5.02 | 0.54 | 2.69 | 45.03 |
| 241.0 | 3.01 | 0.62 | 1.88 | 69.26 | | 235.0 | 5.02 | 0.56 | 2.80 | 47.02 |
| 251.0 | 3.01 | 0.63 | 1.89 | 72.58 | | 245.0 | 5.02 | 0.57 | 2.84 | 49.01 |
| 261.0 | 1.88 | 0.64 | 1.21 | 76.96 | | 255.0 | 5.02 | 0.57 | 2.88 | 51.00 |
| 271.0 | 1.88 | 0.62 | 1.17 | 82.03 | | 265.0 | 5.02 | 0.57 | 2.84 | 52.99 |
| 281.0 | 1.88 | 0.64 | 1.20 | 87.11 | | 275.0 | 5.02 | 0.56 | 2.83 | 54.99 |
| 291.0 | 1.88 | 0.62 | 1.17 | 92.18 | | 285.0 | 5.02 | 0.59 | 2.94 | 56.98 |
| 301.0 | 1.88 | 0.62 | 1.16 | 97.26 | | 297.0 | 3.01 | 0.69 | 2.08 | 59.62 |
| 312.0 | 1.88 | 0.61 | 1.15 | 102.84 | | 305.0 | 3.01 | 0.66 | 2.00 | 62.28 |
| 322.0 | 1.88 | 0.63 | 1.18 | 107.92 | | 315.0 | 3.01 | 0.67 | 2.03 | 65.60 |
| 332.0 | 1.88 | 0.64 | 1.19 | 113.00 | | 325.0 | 3.01 | 0.93 | 2.80 | 68.93 |
| 342.0 | 1.88 | 0.61 | 1.14 | 118.07 | | 335.0 | 3.01 | 0.60 | 1.81 | 72.25 |
| 352.0 | 1.88 | 0.61 | 1.15 | 123.15 | | 345.0 | 4.80 | 0.59 | 2.85 | 74.95 |
| 362.0 | 2.93 | 0.63 | 1.85 | 128.22 | | 355.0 | 4.80 | 0.58 | 2.79 | 77.04 |
| 372.0 | 2.93 | 0.66 | 1.95 | 132.23 | | 365.0 | 4.80 | 0.60 | 2.86 | 79.12 |
| 381.0 | 2.93 | 0.71 | 2.07 | 135.30 | | 375.0 | 4.80 | 0.60 | 2.90 | 81.20 |
| 391.0 | 2.93 | 0.71 | 2.08 | 138.71 | | 385.0 | 4.80 | 0.64 | 3.05 | 83.29 |
| 400.0 | 2.93 | 0.70 | 2.05 | 141.79 | | 395.0 | 4.80 | 0.66 | 3.15 | 85.37 |
| 410.0 | 2.93 | 0.71 | 2.07 | 145.20 | | 405.0 | 4.80 | 0.64 | 3.08 | 87.45 |
| 420.0 | 2.93 | 0.70 | 2.04 | 148.61 | | 415.0 | 4.80 | 0.65 | 3.13 | 89.54 |
| 430.0 | 2.93 | 0.72 | 2.12 | 152.02 | | 425.0 | 4.80 | 0.62 | 2.97 | 91.62 |
| 440.0 | 2.93 | 0.73 | 2.14 | 155.44 | | 435.0 | 4.80 | 0.61 | 2.94 | 93.70 |
| 450.0 | 2.93 | 0.68 | 1.99 | 158.85 | | 445.0 | 4.80 | 0.59 | 2.82 | 95.79 |
| 460.0 | 2.93 | 0.69 | 2.01 | 162.26 | | 455.0 | 4.80 | 0.63 | 3.02 | 97.87 |
| 470.0 | 2.93 | 0.72 | 2.11 | 165.68 | | 465.0 | 4.80 | 0.62 | 2.97 | 99.95 |
| 481.0 | 2.93 | 0.72 | 2.10 | 169.43 | | 475.0 | 4.80 | 0.63 | 3.01 | 102.04 |
| 491.0 | 2.93 | 0.71 | 2.07 | 172.84 | | 485.0 | 4.80 | 0.62 | 2.95 | 104.12 |
| 501.0 | 2.93 | 0.69 | 2.02 | 176.26 | | 495.0 | 4.80 | 0.60 | 2.87 | 106.20 |
| 511.0 | 2.93 | 0.71 | 2.09 | 179.67 | | 505.0 | 4.80 | 0.60 | 2.86 | 108.29 |
| 521.0 | 2.93 | 0.70 | 2.05 | 183.08 | | 515.0 | 4.80 | 0.61 | 2.94 | 110.37 |
| 531.0 | 2.93 | 0.80 | 2.33 | 186.50 | | 525.0 | 4.80 | 0.59 | 2.85 | 112.45 |
| 540.0 | 2.66 | 0.67 | 1.78 | 189.57 | | 535.0 | 4.80 | 0.63 | 3.01 | 114.54 |
| 550.0 | 2.66 | 0.65 | 1.73 | 193.52 | | 545.0 | 4.80 | 0.60 | 2.88 | 116.62 |
| 560.0 | 2.66 | 0.61 | 1.63 | 197.42 | | 555.0 | 4.80 | 0.61 | 2.93 | 118.70 |
| 572.0 | 2.66 | 0.90 | 2.39 | 202.11 | | 565.0 | 4.80 | 0.63 | 3.00 | 120.79 |
| 582.0 | 2.66 | 0.89 | 2.36 | 206.02 | | | | | | |
| 591.0 | 2.66 | 0.74 | 1.97 | 209.53 | | | | | | |
| 601.0 | 2.66 | 0.78 | 2.07 | 213.44 | | | | | | |
| 611.0 | 2.66 | 0.77 | 2.06 | 217.34 | | | | | | |
| 621.0 | 2.66 | 0.76 | 2.03 | 221.25 | | | | | | |
| 631.0 | 2.66 | 0.80 | 2.13 | 225.16 | | | | | | |
| 641.0 | 2.66 | 0.77 | 2.04 | 229.06 | | | | | | |
| 651.0 | 2.66 | 0.71 | 1.89 | 232.97 | | | | | | |
| 662.0 | 2.66 | 0.68 | 1.82 | 237.27 | | | | | | |
| 671.0 | 2.66 | 0.69 | 1.83 | 240.78 | | | | | | |
| 681.0 | 3.12 | 0.72 | 2.26 | 244.50 | | | | | | |
| 691.0 | 3.12 | 0.71 | 2.20 | 247.71 | | | | | | |
| 701.0 | 3.12 | 0.73 | 2.27 | 250.91 | | | | | | |
| 711.0 | 3.12 | 0.70 | 2.19 | 254.12 | | | | | | |
| 721.0 | 3.12 | 0.70 | 2.19 | 257.32 | | | | | | |
| 731.0 | 3.12 | 0.72 | 2.23 | 260.53 | | | | | | |
| 741.0 | 3.12 | 0.70 | 2.19 | 263.73 | | | | | | |

APPENDIX C.4. WATER COLUMN AND PORE-WATER DATA

| CD38-03 | Water column | | | CD38-10 | Water column | | | CD38-09 | Water column | | |
|---|---|---|---|---|---|---|---|---|---|---|---|
| Water | | Dissolved | | Water | | Dissolved | | Water | | Dissolved | |
| Depth | Temp. | Salinity | Oxygen | Depth | Temp. | Salinity | Oxygen | Depth | Temp. | Salinity | Oxygen |
| (m) | (°C) | (o/oo) | (ml/l) | (m) | (°C) | (o/oo) | (ml/l) | (m) | (°C) | (o/oo) | (ml/l) |
| 5 | 20.25 | 34.975 | 6.23 | 5 | 17.64 | 34.948 | 1.86 | 5 | 16.71 | 34.882 | 3.45 |
| 50 | 14.79 | 34.977 | 0.32 | 25 | 14.83 | 35.003 | 0.43 | 10 | 16.52 | 34.984 | 2.85 |
| 101 | 13.31 | 34.934 | 0.19 | 50 | 14.06 | 34.988 | 0.17 | 19 | 15.33 | 34.988 | 0.46 |
| 201 | 12.05 | 34.866 | 0.20 | 80 | 13.84 | 34.975 | 0.36 | 40 | 14.16 | 34.981 | 0.35 |
| 549 | 7.83 | 34.612 | 0.23 | 110 | 13.71 | 34.966 | 0.26 | 60 | 14.04 | 34.979 | 0.19 |
| 900 | 5.16 | 34.521 | | 140 | 13.55 | 34.956 | 0.20 | 80 | 13.99 | 34.975 | |
| 1101 | 4.21 | 34.538 | 0.50 | 171 | 13.50 | 34.953 | 0.20 | 100 | 13.95 | 34.975 | |
| 1299 | 3.63 | 34.558 | 1.80 | 201 | 13.48 | 34.951 | 0.20 | 120 | 13.92 | 34.975 | 0.04 |
| 1601 | 2.88 | 34.597 | 2.19 | 241 | 13.35 | 34.945 | 0.22 | 130 | 13.88 | 34.973 | 0.16 |
| 1801 | 2.49 | 34.625 | 2.47 | 264 | 13.05 | 34.927 | 0.24 | 140 | 13.62 | 34.959 | 0.46 |
| 1998 | 2.29 | 34.637 | 2.80 | | | | | | | | |
| 2248 | 2.05 | 34.653 | | | | | | | | | |
| 2351 | 1.96 | 34.657 | 3.12 | | | | | | | | |
| 2502 | 1.88 | 34.666 | | | | | | | | | |
| 2751 | 1.82 | 34.671 | 3.35 | | | | | | | | |
| 2999 | 1.79 | 34.676 | 3.35 | | | | | | | | |
| 3348 | 1.79 | 34.679 | | | | | | | | | |
| 3648 | 1.76 | 34.684 | 3.65 | | | | | | | | |
| 4000 | 1.75 | 34.687 | 3.74 | | | | | | | | |
| 4295 | 1.75 | 34.689 | 3.80 | | | | | | | | |

| CD38-09 | Pore-water | CD38-10 | Pore-water | CD38-11 | Pore-water |
|---|---|---|---|---|---|
| Depth | Phosphate | Depth | Phosphate | Depth | Phosphate |
| (cm) | (µmol/l) | (cm) | (µmol/l) | (cm) | (µmol/l) |
| 0.00 | 2.7 | 0.00 | 2.7 | 0.00 | 2.7 |
| 0.25 | 77.9 | 0.25 | 86.4 | 1.25 | 3.9 |
| 0.75 | 66.2 | 0.75 | 40.9 | 1.75 | 4.1 |
| 1.25 | 84.8 | 1.25 | 37.8 | 2.50 | 4.4 |
| 1.75 | 68.2 | 1.75 | 41.5 | 3.50 | 5.7 |
| 2.50 | 104.7 | 2.50 | 44.2 | 4.50 | 5.1 |
| 3.50 | 131.0 | 3.50 | 46.3 | 5.50 | 4.6 |
| 4.50 | 133.7 | 4.50 | 49.4 | 7.50 | 4.4 |
| 5.50 | 121.6 | 5.50 | 51.7 | 9.50 | 4.5 |
| 7.50 | 123.2 | 7.50 | 51.1 | 11.50 | 4.9 |
| 9.50 | 106.7 | 9.50 | 49.9 | 13.50 | 4.0 |
| 11.50 | 106.5 | 11.50 | 52.2 | | |
| 13.50 | 96.7 | | | | |

Bottom-water concentration of 2.7 µmol/l taken from Froelich et al. (1988).

| APPENDIX C.5. UNCORRECTED MAJOR ELEMENT DATA : OXIDES (XRF) | | | | | | | | | | | | | |
|---|---|---|---|---|---|---|---|---|---|---|---|---|---|
| | | | | | | | | | | | | | |
| BC38-03 | 4289m | | | | | | | | | | | | |
| Sample | Depth | | SiO2 | Al2O3 | Fe2O3 | MgO | CaO | Na2O | K2O | TiO2 | MnO2 | P2O5 | LOI | Total |
| | (cm) | | (wt.%) | (wt.%) | (wt.%) | (wt.%) | (wt.%) | (wt.%) | (wt.%) | (wt.%) | (wt.%) | (wt.%) | (%) | (%) |
| | | | | | | | | | | | | | | |
| BC3803-01 | 0.5 | | 57.53 | 11.45 | 5.27 | 0.25 | 1.44 | 5.47 | 2.039 | 0.466 | 0.098 | 0.251 | 10.13 | 94.39 |
| BC3803-02 | 1.5 | | 58.48 | 11.60 | 5.57 | 0.24 | 1.41 | 4.86 | 2.074 | 0.478 | 0.081 | 0.257 | 10.74 | 95.80 |
| BC3803-03 | 2.5 | | 57.99 | 11.52 | 5.57 | 0.25 | 1.41 | 4.92 | 2.079 | 0.476 | 0.056 | 0.252 | 10.73 | 95.25 |
| BC3803-04 | 3.5 | | 58.62 | 11.64 | 5.23 | 0.24 | 1.41 | 4.89 | 2.057 | 0.479 | 0.034 | 0.233 | 10.95 | 95.79 |
| BC3803-05 | 4.5 | | 60.20 | 12.25 | 4.68 | 0.26 | 1.44 | 5.03 | 2.193 | 0.496 | 0.029 | 0.210 | 10.81 | 97.60 |
| BC3803-06 | 5.5 | | 59.08 | 12.03 | 3.85 | 0.24 | 1.42 | 4.83 | 2.179 | 0.495 | 0.033 | 0.205 | 11.00 | 95.36 |
| BC3803-07 | 6.5 | | 59.67 | 12.15 | 3.88 | 0.24 | 1.42 | 4.65 | 2.211 | 0.505 | 0.031 | 0.203 | 10.65 | 95.61 |
| BC3803-08 | 7.5 | | 59.81 | 12.34 | 4.05 | 0.24 | 1.44 | 4.74 | 2.224 | 0.509 | 0.027 | 0.198 | 10.93 | 96.51 |
| BC3803-09 | 8.5 | | 59.66 | 12.30 | 4.15 | 0.24 | 1.46 | 4.68 | 2.236 | 0.508 | 0.030 | 0.199 | 10.78 | 96.26 |
| BC3803-10 | 9.5 | | 62.22 | 13.17 | 4.42 | 0.26 | 1.50 | 4.76 | 2.279 | 0.528 | 0.037 | 0.205 | 10.68 | 100.07 |
| BC3803-11 | 11.0 | | 60.09 | 12.77 | 4.29 | 0.26 | 1.49 | 4.90 | 2.274 | 0.526 | 0.035 | 0.207 | 10.32 | 97.17 |
| BC3803-12 | 13.0 | | 60.36 | 12.89 | 4.00 | 0.25 | 1.53 | 4.30 | 2.305 | 0.542 | 0.035 | 0.205 | 10.27 | 96.69 |
| BC3803-13 | 15.0 | | 59.57 | 12.65 | 4.40 | 0.25 | 1.53 | 4.72 | 2.312 | 0.532 | 0.038 | 0.211 | 9.54 | 95.74 |
| BC3803-14 | 17.0 | | 61.07 | 12.92 | 4.17 | 0.25 | 1.58 | 4.15 | 2.339 | 0.552 | 0.035 | 0.219 | 10.13 | 97.42 |
| BC3803-15 | 19.0 | | 60.42 | 12.92 | 4.05 | 0.27 | 1.62 | 4.55 | 2.316 | 0.546 | 0.039 | 0.227 | 10.49 | 97.44 |
| BC3803-16 | 21.0 | | 61.13 | 12.38 | 3.81 | 0.25 | 1.56 | 4.14 | 2.229 | 0.526 | 0.029 | 0.217 | 10.82 | 97.08 |
| BC3803-17 | 23.0 | | 60.74 | 12.38 | 4.21 | 0.25 | 1.55 | 4.52 | 2.243 | 0.521 | 0.032 | 0.220 | 10.36 | 97.03 |
| BC3803-18 | 25.0 | | 60.68 | 12.53 | 3.90 | 0.25 | 1.61 | 4.09 | 2.262 | 0.536 | 0.036 | 0.227 | 10.62 | 96.73 |
| BC3803-19 | 27.0 | | 59.99 | 12.24 | 4.03 | 0.25 | 1.62 | 4.54 | 2.221 | 0.527 | 0.035 | 0.226 | 10.26 | 95.94 |
| BC3803-20 | 29.0 | | 61.25 | 12.76 | 4.21 | 0.25 | 1.67 | 4.02 | 2.311 | 0.546 | 0.041 | 0.234 | 10.00 | 97.30 |
| BC3803-21 | 31.0 | | 60.28 | 12.48 | 4.36 | 0.26 | 1.67 | 4.70 | 2.330 | 0.535 | 0.044 | 0.228 | 9.75 | 96.64 |
| BC3803-22 | 33.0 | | 60.91 | 12.61 | 4.09 | 0.26 | 1.70 | 4.22 | 2.293 | 0.539 | 0.036 | 0.235 | 9.86 | 96.76 |
| BC3803-23 | 35.0 | | 60.43 | 12.43 | 3.99 | 0.26 | 1.71 | 4.40 | 2.297 | 0.534 | 0.036 | 0.231 | 9.60 | 95.91 |
| BC3803-24 | 37.0 | | 62.43 | 13.00 | 4.42 | 0.27 | 1.82 | 4.22 | 2.361 | 0.547 | 0.040 | 0.240 | 9.75 | 99.10 |
| BC3803-25 | 39.0 | | 63.03 | 12.96 | 4.43 | 0.28 | 1.90 | 4.51 | 2.377 | 0.542 | 0.044 | 0.319 | 9.57 | 99.96 |
| BC3803-26 | 41.0 | | 60.95 | 12.46 | 4.32 | 0.26 | 1.81 | 4.02 | 2.343 | 0.540 | 0.040 | 0.230 | 9.72 | 96.68 |
| BC3803-27 | 43.0 | | 61.12 | 12.64 | 4.49 | 0.27 | 1.85 | 4.38 | 2.362 | 0.542 | 0.039 | 0.234 | 9.65 | 97.57 |
| BC3803-28 | 45.0 | | 60.90 | 12.44 | 4.23 | 0.26 | 1.82 | 4.03 | 2.334 | 0.535 | 0.034 | 0.233 | 9.70 | 96.52 |
| BC3803-29 | 47.0 | | 60.57 | 12.37 | 4.44 | 0.26 | 1.82 | 4.30 | 2.358 | 0.534 | 0.040 | 0.233 | 9.34 | 96.26 |
| BC3803-30 | 49.0 | | 61.18 | 12.53 | 4.43 | 0.26 | 1.85 | 3.92 | 2.365 | 0.537 | 0.038 | 0.237 | 9.20 | 96.53 |
| BC3803-31 | 51.0 | | 61.38 | 12.80 | 4.72 | 0.27 | 1.88 | 4.30 | 2.423 | 0.550 | 0.038 | 0.249 | 8.92 | 97.55 |
| BC3803-32 | 53.0 | | 60.03 | 12.59 | 4.42 | 0.27 | 1.91 | 4.39 | 2.371 | 0.544 | 0.039 | 0.241 | 9.91 | 96.73 |

| APPENDIX C.5. UNCORRECTED MAJOR ELEMENT DATA : OXIDES (XRF) | | | | | | | | | | | | | | |
|---|---|---|---|---|---|---|---|---|---|---|---|---|---|---|
| | | | | | | | | | | | | | | |
| BC38-02 | 2530m | | | | | | | | | | | | | |
| Sample | Depth | | SiO2 | Al2O3 | Fe2O3 | MgO | CaO | Na2O | K2O | TiO2 | MnO2 | P2O5 | LOI | Total |
| | (cm) | | (wt.%) | (wt.%) | (wt.%) | (wt.%) | (wt.%) | (wt.%) | (wt.%) | (wt.%) | (wt.%) | (wt.%) | (%) | (%) |
| | | | | | | | | | | | | | | |
| BC3802-01 | 0.5 | | 50.36 | 11.15 | 5.22 | 0.24 | 8.71 | 4.29 | 2.021 | 0.450 | 0.050 | 0.306 | 12.10 | 94.89 |
| BC3802-02 | 1.5 | | 50.65 | 11.25 | 5.24 | 0.25 | 8.32 | 4.14 | 2.055 | 0.451 | 0.049 | 0.290 | 12.07 | 94.76 |
| BC3802-03 | 2.5 | | 50.58 | 11.18 | 5.22 | 0.24 | 8.70 | 3.95 | 2.042 | 0.453 | 0.048 | 0.285 | 12.15 | 94.84 |
| BC3802-04 | 3.5 | | 50.14 | 11.12 | 5.19 | 0.24 | 8.92 | 3.81 | 1.980 | 0.447 | 0.036 | 0.289 | 13.02 | 95.20 |
| BC3802-05 | 4.5 | | 50.15 | 11.08 | 5.16 | 0.24 | 9.24 | 3.88 | 2.081 | 0.449 | 0.033 | 0.286 | 12.22 | 94.82 |
| BC3802-06 | 5.5 | | 49.84 | 11.03 | 5.05 | 0.24 | 9.34 | 3.86 | 2.084 | 0.442 | 0.035 | 0.298 | 12.62 | 94.84 |
| BC3802-07 | 6.5 | | 49.72 | 11.46 | 5.14 | 0.25 | 9.56 | 3.99 | 2.096 | 0.450 | 0.033 | 0.275 | 12.93 | 95.91 |
| BC3802-08 | 7.5 | | 49.81 | 11.12 | 5.17 | 0.25 | 9.39 | 3.81 | 2.068 | 0.444 | 0.032 | 0.282 | 12.83 | 95.20 |
| BC3802-09 | 8.5 | | 49.54 | 11.34 | 5.13 | 0.26 | 9.61 | 3.80 | 2.140 | 0.460 | 0.038 | 0.293 | 12.45 | 95.06 |
| BC3802-10 | 9.5 | | 49.15 | 11.27 | 5.03 | 0.25 | 9.94 | 3.61 | 2.085 | 0.462 | 0.036 | 0.276 | 12.71 | 94.81 |
| BC3802-11 | 11.0 | | 51.13 | 11.84 | 5.15 | 0.28 | 11.22 | 3.58 | 2.152 | 0.465 | 0.038 | 0.282 | 13.28 | 99.40 |
| BC3802-12 | 13.0 | | 46.80 | 10.50 | 4.93 | 0.24 | 12.32 | 3.21 | 1.988 | 0.438 | 0.032 | 0.269 | 14.24 | 94.98 |
| BC3802-13 | 15.0 | | 45.82 | 10.39 | 4.49 | 0.25 | 12.85 | 3.86 | 1.983 | 0.423 | 0.034 | 0.270 | 14.32 | 94.68 |
| BC3802-13A | 17.0 | | 42.56 | 9.92 | 3.96 | 0.23 | 15.82 | 3.50 | 1.827 | 0.394 | 0.031 | 0.253 | 16.58 | 95.08 |
| BC3802-14 | 19.0 | | 41.33 | 9.15 | 3.72 | 0.21 | 17.44 | 3.25 | 1.724 | 0.375 | 0.030 | 0.254 | 17.67 | 95.15 |
| BC3802-15 | 21.0 | | 40.68 | 9.03 | 3.64 | 0.21 | 18.78 | 2.81 | 1.728 | 0.374 | 0.032 | 0.252 | 18.56 | 96.09 |
| BC3802-16 | 23.0 | | 39.58 | 8.75 | 3.58 | 0.21 | 19.12 | 3.20 | 1.631 | 0.364 | 0.026 | 0.250 | 19.00 | 95.72 |
| BC3802-17 | 25.0 | | 39.21 | 8.76 | 3.54 | 0.20 | 19.83 | 2.69 | 1.664 | 0.361 | 0.027 | 0.252 | 19.24 | 95.78 |
| BC3802-18 | 27.0 | | 37.92 | 8.60 | 3.48 | 0.20 | 20.12 | 3.06 | 1.586 | 0.353 | 0.030 | 0.244 | 20.05 | 95.64 |
| BC3802-19 | 29.0 | | 37.48 | 8.47 | 3.40 | 0.20 | 21.19 | 2.65 | 1.591 | 0.351 | 0.026 | 0.245 | 20.74 | 96.34 |
| BC3802-20 | 31.0 | | 36.91 | 8.40 | 3.34 | 0.20 | 20.62 | 3.12 | 1.510 | 0.348 | 0.028 | 0.243 | 20.88 | 95.60 |
| BC3802-21 | 33.0 | | 37.37 | 8.72 | 3.40 | 0.20 | 20.34 | 2.73 | 1.714 | 0.359 | 0.031 | 0.236 | 20.52 | 95.61 |
| BC3802-21A | 35.0 | | 37.50 | 9.09 | 3.45 | 0.21 | 18.61 | 3.18 | 1.705 | 0.377 | 0.023 | 0.201 | 19.85 | 94.18 |
| BC3802-22 | 37.0 | | 37.68 | 8.95 | 3.47 | 0.20 | 19.38 | 2.73 | 1.641 | 0.368 | 0.021 | 0.214 | 20.54 | 95.19 |
| BC3802-23 | 39.0 | | 36.95 | 8.62 | 3.38 | 0.21 | 19.91 | 3.29 | 1.637 | 0.355 | 0.027 | 0.234 | 20.20 | 94.81 |
| BC3802-24 | 41.0 | | 37.46 | 9.11 | 3.52 | 0.20 | 19.33 | 3.00 | 1.696 | 0.374 | 0.030 | 0.203 | 20.45 | 95.38 |
| BC3802-25 | 43.0 | | 37.70 | 9.25 | 3.60 | 0.21 | 18.91 | 3.24 | 1.813 | 0.382 | 0.025 | 0.203 | 19.64 | 94.97 |
| BC3802-26 | 45.0 | | 37.11 | 9.08 | 3.57 | 0.20 | 18.67 | 2.91 | 1.789 | 0.387 | 0.030 | 0.203 | 19.77 | 93.73 |
| BC3802-27 | 47.0 | | 37.64 | 9.32 | 3.52 | 0.22 | 18.64 | 3.27 | 1.805 | 0.387 | 0.023 | 0.208 | 19.61 | 94.63 |
| BC3802-28 | 49.0 | | 38.03 | 9.37 | 3.56 | 0.21 | 18.69 | 3.05 | 1.816 | 0.394 | 0.027 | 0.208 | 19.62 | 94.98 |
| BC3802-29 | 51.0 | | 38.05 | 9.37 | 3.55 | 0.21 | 18.47 | 3.16 | 1.783 | 0.394 | 0.028 | 0.208 | 19.64 | 94.87 |
| BC3802-30 | 53.0 | | 38.02 | 9.45 | 3.52 | 0.22 | 18.26 | 3.16 | 1.761 | 0.393 | 0.031 | 0.221 | 19.38 | 94.41 |

| APPENDIX C.5. UNCORRECTED MAJOR ELEMENT DATA : OXIDES (XRF) | | | | | | | | | | | | | |
|---|---|---|---|---|---|---|---|---|---|---|---|---|---|
| PC38-09 Sample | 148m Depth (cm) | | SiO2 (wt.%) | Al2O3 (wt.%) | Fe2O3 (wt.%) | MgO (wt.%) | CaO (wt.%) | Na2O (wt.%) | K2O (wt.%) | TiO2 (wt.%) | MnO2 (wt.%) | P2O5 (wt.%) | LOI (%) | Total (%) |
| PC3809-01 | 4.0 | | 53.88 | 10.29 | 3.44 | 0.19 | 2.84 | 4.52 | 1.573 | 0.498 | 0.028 | 0.509 | 15.62 | 93.38 |
| PC3809-02 | 13.0 | | 53.45 | 10.01 | 2.97 | 0.18 | 3.17 | 5.02 | 1.476 | 0.450 | 0.028 | 0.361 | 16.58 | 93.69 |
| PC3809-03 | 23.0 | | 53.91 | 13.31 | 3.66 | 0.20 | 2.48 | 4.49 | 1.821 | 0.544 | 0.037 | 0.430 | 14.63 | 95.50 |
| PC3809-04 | 34.0 | | 54.53 | 12.21 | 3.38 | 0.20 | 2.08 | 4.68 | 1.735 | 0.536 | 0.032 | 0.425 | 15.87 | 95.68 |
| PC3809-05 | 43.0 | | 60.09 | 12.65 | 3.55 | 0.17 | 2.68 | 3.69 | 1.890 | 0.625 | 0.045 | 0.549 | 10.46 | 96.39 |
| PC3809-06 | 53.0 | | 54.01 | 11.24 | 3.55 | 0.20 | 2.06 | 4.55 | 1.669 | 0.521 | 0.036 | 0.576 | 15.68 | 94.10 |
| PC3809-07 | 62.0 | | 50.42 | 10.24 | 3.07 | 0.20 | 3.07 | 4.97 | 1.414 | 0.438 | 0.024 | 0.486 | 19.56 | 93.90 |
| PC3809-08 | 73.0 | | 57.12 | 12.33 | 3.46 | 0.18 | 2.05 | 3.86 | 1.784 | 0.583 | 0.041 | 0.440 | 13.84 | 95.68 |
| PC3809-09 | 84.0 | | 52.41 | 14.30 | 4.18 | 0.20 | 1.57 | 4.05 | 2.038 | 0.644 | 0.037 | 0.354 | 15.14 | 94.91 |
| PC3809-10 | 94.0 | | 51.04 | 13.20 | 4.47 | 0.19 | 1.94 | 4.25 | 1.913 | 0.567 | 0.038 | 0.370 | 15.73 | 93.71 |
| PC3809-11 | 104.0 | | 52.73 | 11.74 | 3.31 | 0.19 | 1.59 | 4.51 | 1.710 | 0.503 | 0.028 | 0.333 | 16.98 | 93.63 |
| PC3809-12 | 113.0 | | 55.39 | 14.85 | 4.39 | 0.25 | 1.73 | 3.94 | 2.151 | 0.679 | 0.043 | 0.350 | 14.81 | 98.59 |
| PC3809-13 | 124.0 | | 55.12 | 13.17 | 3.53 | 0.18 | 2.79 | 3.56 | 1.895 | 0.643 | 0.039 | 0.521 | 14.71 | 96.17 |
| PC3809-14 | 134.0 | | 55.10 | 11.29 | 3.30 | 0.18 | 2.71 | 4.55 | 1.633 | 0.512 | 0.031 | 0.631 | 14.61 | 94.54 |
| PC3809-15 | 144.0 | | 56.01 | 9.95 | 3.02 | 0.17 | 2.32 | 4.54 | 1.497 | 0.457 | 0.026 | 0.429 | 15.34 | 93.76 |
| PC3809-16 | 152.0 | | 58.75 | 9.90 | 3.17 | 0.17 | 2.33 | 4.37 | 1.518 | 0.455 | 0.025 | 0.311 | 12.35 | 93.36 |
| PC3809-17 | 165.0 | | 58.45 | 9.58 | 2.97 | 0.16 | 3.25 | 4.54 | 1.445 | 0.457 | 0.029 | 0.509 | 13.01 | 94.40 |
| PC3809-18 | 174.0 | | 61.99 | 12.12 | 3.22 | 0.15 | 2.62 | 3.53 | 1.817 | 0.579 | 0.037 | 0.587 | 10.18 | 96.83 |
| PC3809-19 | 185.0 | | 64.17 | 10.77 | 2.88 | 0.13 | 3.38 | 3.78 | 1.634 | 0.525 | 0.036 | 0.935 | 9.24 | 97.49 |
| PC3809-20 | 194.0 | | 63.09 | 11.18 | 2.89 | 0.14 | 4.15 | 3.40 | 1.668 | 0.559 | 0.044 | 0.908 | 8.87 | 96.90 |
| PC3809-21 | 205.0 | | 60.83 | 12.30 | 4.28 | 0.21 | 3.79 | 3.90 | 1.859 | 0.614 | 0.061 | 0.341 | 8.62 | 96.80 |
| PC3809-22 | 214.0 | | 59.43 | 10.09 | 2.66 | 0.15 | 3.21 | 3.98 | 1.534 | 0.486 | 0.029 | 0.862 | 13.87 | 96.31 |
| PC3809-23 | 224.0 | | 69.26 | 11.06 | 2.45 | 0.10 | 4.08 | 3.20 | 1.706 | 0.516 | 0.035 | 1.108 | 5.20 | 98.73 |
| PC3809-24 | 234.0 | | 65.55 | 9.70 | 2.76 | 0.12 | 3.95 | 3.76 | 1.471 | 0.462 | 0.028 | 1.296 | 8.64 | 97.74 |
| PC3809-25 | 243.0 | | 63.40 | 7.53 | 2.53 | 0.16 | 2.30 | 4.80 | 1.212 | 0.344 | 0.027 | 0.729 | 11.21 | 94.24 |
| PC3809-26 | 257.0 | | 63.02 | 9.05 | 2.95 | 0.15 | 2.38 | 4.06 | 1.423 | 0.432 | 0.028 | 0.647 | 12.32 | 96.47 |
| PC3809-27 | 267.0 | | 64.45 | 9.24 | 2.54 | 0.12 | 5.28 | 3.52 | 1.482 | 0.438 | 0.033 | 2.280 | 6.34 | 95.72 |
| PC3809-28 | 273.0 | | 29.70 | 4.74 | 4.07 | 0.28 | 25.20 | 2.48 | 0.831 | 0.227 | 0.023 | 12.921 | 13.71 | 94.18 |
| PC3809-29 | 284.0 | | 57.65 | 10.71 | 3.86 | 0.21 | 2.78 | 4.08 | 1.591 | 0.531 | 0.043 | 0.677 | 13.27 | 95.40 |
| PC3809-30 | 294.0 | | 59.40 | 8.48 | 2.96 | 0.17 | 2.61 | 4.66 | 1.328 | 0.386 | 0.025 | 0.351 | 13.96 | 94.33 |
| PC3809-31 | 304.0 | | 58.76 | 11.01 | 3.93 | 0.21 | 1.92 | 4.14 | 1.620 | 0.544 | 0.045 | 0.362 | 12.80 | 95.35 |
| PC3809-32 | 314.0 | | 52.86 | 10.74 | 3.67 | 0.22 | 2.17 | 4.09 | 1.568 | 0.467 | 0.035 | 0.300 | 15.55 | 91.66 |

| APPENDIX C.5. UNCORRECTED MAJOR ELEMENT DATA : OXIDES (XRF) | | | | | | | | | | | | | |
|---|---|---|---|---|---|---|---|---|---|---|---|---|---|
| PC38-09 | 148m | | | | | | | | | | | | |
| Sample | Depth | | SiO2 | Al2O3 | Fe2O3 | MgO | CaO | Na2O | K2O | TiO2 | MnO2 | P2O5 | LOI | Total |
| | (cm) | | (wt.%) | (wt.%) | (wt.%) | (wt.%) | (wt.%) | (wt.%) | (wt.%) | (wt.%) | (wt.%) | (wt.%) | (%) | (%) |
| PC3809-33 | 324.0 | | 56.60 | 11.28 | 4.29 | 0.21 | 2.25 | 3.79 | 1.640 | 0.547 | 0.040 | 0.482 | 14.55 | 95.67 |
| PC3809-34 | 335.0 | | 57.77 | 9.59 | 3.55 | 0.18 | 1.99 | 4.15 | 1.416 | 0.444 | 0.036 | 0.343 | 15.39 | 94.86 |
| PC3809-35 | 344.0 | | 58.45 | 8.70 | 3.57 | 0.19 | 1.88 | 4.36 | 1.302 | 0.431 | 0.028 | 0.340 | 14.34 | 93.59 |
| PC3809-36 | 355.0 | | 59.19 | 7.23 | 2.53 | 0.17 | 2.71 | 5.23 | 1.144 | 0.310 | 0.026 | 0.219 | 13.88 | 92.65 |
| PC3809-37 | 364.0 | | 57.90 | 7.10 | 2.68 | 0.17 | 4.27 | 4.68 | 1.110 | 0.302 | 0.024 | 0.214 | 14.53 | 92.96 |
| PC3809-38 | 375.0 | | 57.27 | 9.83 | 3.43 | 0.19 | 2.23 | 4.42 | 1.514 | 0.419 | 0.034 | 0.240 | 15.24 | 94.82 |
| PC3809-39 | 384.0 | | 57.07 | 10.54 | 4.02 | 0.19 | 3.63 | 3.72 | 1.533 | 0.509 | 0.043 | 0.459 | 13.77 | 95.49 |
| PC3809-40 | 394.0 | | 59.37 | 8.94 | 3.06 | 0.17 | 2.59 | 4.21 | 1.377 | 0.402 | 0.033 | 0.340 | 14.89 | 95.37 |
| PC3809-41 | 404.0 | | 61.24 | 10.03 | 3.44 | 0.18 | 1.66 | 3.96 | 1.547 | 0.452 | 0.038 | 0.264 | 12.73 | 95.54 |
| PC3809-42 | 416.0 | | 56.31 | 8.43 | 2.97 | 0.18 | 4.42 | 4.25 | 1.274 | 0.373 | 0.023 | 0.309 | 16.40 | 94.94 |
| PC3809-43 | 424.0 | | 59.98 | 9.22 | 3.05 | 0.17 | 1.66 | 4.36 | 1.458 | 0.399 | 0.032 | 0.215 | 13.31 | 93.85 |
| PC3809-44 | 434.0 | | 57.66 | 10.62 | 3.70 | 0.19 | 1.71 | 3.99 | 1.653 | 0.453 | 0.035 | 0.275 | 15.74 | 96.04 |
| PC3809-45 | 444.0 | | 60.16 | 8.62 | 3.26 | 0.17 | 3.34 | 4.34 | 1.329 | 0.382 | 0.032 | 0.299 | 12.80 | 94.75 |
| PC3809-46 | 453.0 | | 59.22 | 10.72 | 3.79 | 0.19 | 2.27 | 3.72 | 1.575 | 0.518 | 0.036 | 0.363 | 13.62 | 96.02 |
| PC3809-47 | 465.0 | | 57.31 | 9.99 | 3.74 | 0.19 | 2.73 | 3.90 | 1.503 | 0.457 | 0.038 | 0.351 | 15.28 | 95.49 |
| PC3809-48 | 474.0 | | 56.14 | 9.35 | 3.15 | 0.18 | 3.79 | 4.14 | 1.480 | 0.387 | 0.027 | 0.311 | 15.39 | 94.35 |
| PC3809-49 | 483.0 | | 61.15 | 10.37 | 3.77 | 0.18 | 2.01 | 3.83 | 1.607 | 0.496 | 0.036 | 0.383 | 13.00 | 96.83 |
| PC3809-50 | 493.0 | | 58.68 | 10.25 | 3.75 | 0.18 | 2.24 | 3.98 | 1.657 | 0.455 | 0.046 | 0.335 | 13.33 | 94.90 |
| PC3809-51 | 504.0 | | 61.28 | 10.93 | 3.93 | 0.18 | 2.28 | 3.50 | 1.705 | 0.534 | 0.041 | 0.399 | 12.53 | 97.31 |
| PC3809-52 | 515.0 | | 60.46 | 10.96 | 3.88 | 0.19 | 2.03 | 3.63 | 1.751 | 0.513 | 0.040 | 0.319 | 12.70 | 96.47 |
| PC3809-53 | 525.0 | | 57.15 | 10.07 | 3.45 | 0.18 | 3.05 | 4.10 | 1.603 | 0.426 | 0.037 | 0.255 | 15.37 | 95.69 |
| PC3809-54 | 536.0 | | 59.25 | 9.12 | 3.20 | 0.19 | 4.02 | 4.24 | 1.448 | 0.394 | 0.036 | 0.247 | 14.12 | 96.27 |
| PC3809-55 | 544.0 | | 59.18 | 11.00 | 4.09 | 0.20 | 2.91 | 3.67 | 1.708 | 0.524 | 0.042 | 0.339 | 13.11 | 96.77 |
| PC3809-56 | 553.0 | | 58.33 | 10.18 | 3.92 | 0.20 | 3.66 | 4.08 | 1.560 | 0.452 | 0.045 | 0.215 | 11.98 | 94.62 |
| PC3809-57 | 564.0 | | 59.48 | 9.29 | 3.58 | 0.20 | 3.52 | 4.48 | 1.409 | 0.430 | 0.041 | 0.221 | 12.62 | 95.26 |
| PC3809-58 | 574.0 | | 58.74 | 9.34 | 3.66 | 0.18 | 3.84 | 4.31 | 1.515 | 0.428 | 0.042 | 0.257 | 12.07 | 94.38 |
| PC3809-59 | 585.0 | | 58.96 | 8.97 | 3.45 | 0.18 | 4.97 | 4.23 | 1.418 | 0.417 | 0.040 | 0.682 | 12.64 | 95.95 |
| PC3809-60 | 594.0 | | 60.50 | 8.95 | 3.34 | 0.17 | 3.73 | 4.51 | 1.465 | 0.415 | 0.040 | 0.281 | 11.09 | 94.49 |
| PC3809-61 | 605.0 | | 58.19 | 10.25 | 4.01 | 0.18 | 4.33 | 3.70 | 1.613 | 0.481 | 0.047 | 0.409 | 13.18 | 96.40 |
| PC3809-62 | 615.0 | | 60.34 | 8.89 | 3.26 | 0.17 | 4.06 | 4.35 | 1.491 | 0.410 | 0.042 | 0.477 | 10.75 | 94.24 |
| PC3809-63 | 625.0 | | 59.73 | 9.99 | 3.80 | 0.18 | 3.95 | 4.08 | 1.580 | 0.470 | 0.047 | 0.443 | 11.85 | 96.11 |
| PC3809-64 | 635.0 | | 58.69 | 10.24 | 3.94 | 0.18 | 4.30 | 3.82 | 1.598 | 0.487 | 0.049 | 0.440 | 12.87 | 96.61 |

| APPENDIX C.5. UNCORRECTED MAJOR ELEMENT DATA : OXIDES (XRF) | | | | | | | | | | | | | |
|---|---|---|---|---|---|---|---|---|---|---|---|---|---|
| | | | | | | | | | | | | | |
| PC38-09 | 148m | | | | | | | | | | | | |
| Sample | Depth | | SiO2 | Al2O3 | Fe2O3 | MgO | CaO | Na2O | K2O | TiO2 | MnO2 | P2O5 | LOI | Total |
| | (cm) | | (wt.%) | (wt.%) | (wt.%) | (wt.%) | (wt.%) | (wt.%) | (wt.%) | (wt.%) | (wt.%) | (wt.%) | (%) | (%) |
| | | | | | | | | | | | | | | |
| PC3809-65 | 646.0 | | 60.63 | 8.76 | 3.16 | 0.17 | 3.45 | 4.60 | 1.378 | 0.399 | 0.037 | 0.294 | 12.97 | 95.85 |
| PC3809-66 | 654.0 | | 62.06 | 8.38 | 3.04 | 0.17 | 3.13 | 4.44 | 1.318 | 0.396 | 0.039 | 0.231 | 12.35 | 95.56 |
| PC3809-67 | 664.0 | | 62.23 | 8.41 | 3.03 | 0.16 | 3.36 | 4.61 | 1.345 | 0.378 | 0.032 | 0.199 | 12.37 | 96.13 |
| PC3809-68 | 674.0 | | 60.23 | 7.32 | 2.92 | 0.16 | 2.86 | 4.35 | 1.243 | 0.353 | 0.032 | 0.177 | 11.32 | 90.96 |
| PC3809-69 | 684.0 | | 60.25 | 9.99 | 3.74 | 0.18 | 3.53 | 4.19 | 1.641 | 0.452 | 0.038 | 0.254 | 12.52 | 96.78 |
| PC3809-70 | 694.0 | | 59.57 | 10.73 | 3.99 | 0.19 | 3.62 | 4.09 | 1.639 | 0.488 | 0.050 | 0.256 | 13.23 | 97.86 |
| PC3809-71 | 703.0 | | 58.08 | 10.60 | 4.10 | 0.19 | 3.41 | 4.22 | 1.717 | 0.469 | 0.047 | 0.211 | 10.27 | 93.30 |
| PC3809-72 | 714.0 | | 58.86 | 9.64 | 3.68 | 0.18 | 3.88 | 4.32 | 1.559 | 0.445 | 0.039 | 0.296 | 11.90 | 94.80 |
| PC3809-73 | 724.0 | | 59.68 | 10.63 | 4.16 | 0.20 | 3.99 | 3.99 | 1.695 | 0.500 | 0.049 | 0.420 | 9.91 | 95.22 |
| PC3809-74 | 734.0 | | 57.40 | 10.73 | 4.11 | 0.19 | 4.38 | 3.87 | 1.703 | 0.504 | 0.046 | 0.429 | 11.50 | 94.87 |
| PC3809-75 | 744.0 | | 61.74 | 10.31 | 4.07 | 0.18 | 3.95 | 4.47 | 1.696 | 0.459 | 0.049 | 0.346 | 11.44 | 98.71 |
| PC3809-76 | 754.0 | | 59.60 | 9.46 | 3.66 | 0.17 | 3.73 | 4.34 | 1.545 | 0.432 | 0.043 | 0.222 | 11.87 | 95.08 |
| PC3809-77 | 764.0 | | 57.79 | 10.76 | 4.01 | 0.18 | 4.48 | 3.72 | 1.830 | 0.490 | 0.051 | 0.289 | 11.03 | 94.63 |
| PC3809-78 | 774.0 | | 58.54 | 11.03 | 4.25 | 0.18 | 4.21 | 3.57 | 1.776 | 0.528 | 0.052 | 0.301 | 12.09 | 96.52 |
| PC3809-79 | 784.0 | | 59.42 | 10.51 | 4.13 | 0.18 | 4.09 | 3.69 | 1.755 | 0.495 | 0.045 | 0.282 | 10.76 | 95.36 |
| PC3809-80 | 794.0 | | 59.86 | 10.57 | 3.90 | 0.18 | 4.14 | 3.63 | 1.787 | 0.498 | 0.044 | 0.327 | 10.99 | 95.92 |
| PC3809-81 | 804.0 | | 61.03 | 10.11 | 3.74 | 0.17 | 3.67 | 3.73 | 1.650 | 0.486 | 0.043 | 0.406 | 10.28 | 95.32 |
| PC3809-82 | 813.0 | | 60.10 | 10.49 | 4.28 | 0.19 | 4.68 | 3.63 | 1.622 | 0.510 | 0.048 | 0.665 | 11.23 | 97.45 |
| PC3809-83 | 823.0 | | 61.09 | 10.24 | 3.99 | 0.17 | 3.76 | 3.61 | 1.667 | 0.493 | 0.049 | 0.443 | 10.40 | 95.92 |
| PC3809-84 | 834.0 | | 60.01 | 10.62 | 3.91 | 0.17 | 3.68 | 3.57 | 1.701 | 0.509 | 0.046 | 0.360 | 11.32 | 95.90 |
| PC3809-85 | 845.0 | | 62.58 | 10.71 | 3.88 | 0.18 | 3.70 | 3.84 | 1.767 | 0.488 | 0.047 | 0.424 | 10.34 | 97.96 |
| PC3809-86 | 854.0 | | 60.05 | 12.11 | 4.50 | 0.20 | 3.25 | 3.70 | 2.019 | 0.548 | 0.060 | 0.221 | 10.37 | 97.03 |
| | | | | | | | | | | | | | | |
| PC38-10 | 257m | | | | | | | | | | | | | |
| | | | | | | | | | | | | | | |
| PC3810-01 | 6.0 | | 42.71 | 9.10 | 2.63 | 0.17 | 8.25 | 4.60 | 1.421 | 0.400 | 0.021 | 0.990 | 22.15 | 92.45 |
| PC3810-02 | 14.0 | | 53.31 | 9.93 | 2.57 | 0.14 | 7.45 | 3.58 | 1.545 | 0.476 | 0.032 | 2.337 | 14.52 | 95.89 |
| PC3810-03 | 24.0 | | 60.10 | 10.27 | 2.22 | 0.11 | 9.36 | 3.06 | 1.652 | 0.458 | 0.034 | 4.412 | 5.98 | 97.66 |
| PC3810-04 | 34.0 | | 59.93 | 10.21 | 2.07 | 0.11 | 8.92 | 3.13 | 1.606 | 0.453 | 0.026 | 2.299 | 8.80 | 97.55 |
| PC3810-05 | 44.0 | | 56.40 | 10.48 | 2.86 | 0.16 | 3.04 | 4.02 | 1.786 | 0.498 | 0.038 | 0.945 | 15.00 | 95.23 |
| PC3810-06 | 54.0 | | 57.61 | 10.59 | 2.86 | 0.16 | 2.45 | 4.35 | 1.767 | 0.473 | 0.025 | 0.633 | 15.52 | 96.44 |
| PC3810-07 | 64.0 | | 60.10 | 11.01 | 3.26 | 0.15 | 3.16 | 3.99 | 1.877 | 0.508 | 0.031 | 1.007 | 11.19 | 96.28 |

| APPENDIX C.5. UNCORRECTED MAJOR ELEMENT DATA : OXIDES (XRF) | | | | | | | | | | | | | | |
|---|---|---|---|---|---|---|---|---|---|---|---|---|---|---|
| | | | | | | | | | | | | | | |
| PC38-10 | 257m | | | | | | | | | | | | | |
| Sample | Depth | | SiO2 | Al2O3 | Fe2O3 | MgO | CaO | Na2O | K2O | TiO2 | MnO2 | P2O5 | LOI | Total |
| | (cm) | | (wt.%) | (wt.%) | (wt.%) | (wt.%) | (wt.%) | (wt.%) | (wt.%) | (wt.%) | (wt.%) | (wt.%) | (%) | (%) |
| | | | | | | | | | | | | | | |
| PC3810-08 | 74.0 | | 61.67 | 11.52 | 3.13 | 0.14 | 4.20 | 3.64 | 1.946 | 0.526 | 0.037 | 1.558 | 9.90 | 98.26 |
| PC3810-09 | 84.0 | | 67.40 | 10.10 | 2.47 | 0.10 | 5.95 | 2.69 | 1.801 | 0.440 | 0.034 | 2.457 | 3.92 | 97.36 |
| PC3810-10 | 94.0 | | 64.41 | 10.71 | 2.54 | 0.10 | 7.96 | 2.88 | 1.747 | 0.437 | 0.034 | 3.404 | 4.17 | 98.39 |
| PC3810-10 | 104.0 | | 62.17 | 10.09 | 2.11 | 0.10 | 9.59 | 2.94 | 1.692 | 0.420 | 0.032 | 1.954 | 6.74 | 97.82 |
| PC3810-11 | 113.0 | | 64.27 | 10.41 | 2.07 | 0.09 | 8.63 | 2.82 | 1.659 | 0.417 | 0.034 | 1.309 | 6.33 | 98.04 |
| PC3810-12 | 126.0 | | 56.08 | 8.53 | 2.61 | 0.14 | 8.25 | 3.83 | 1.418 | 0.384 | 0.024 | 1.129 | 13.40 | 95.80 |
| PC3810-13 | 134.0 | | 56.43 | 8.41 | 2.69 | 0.15 | 5.65 | 3.74 | 1.397 | 0.381 | 0.024 | 1.205 | 14.82 | 94.90 |
| PC3810-14 | 146.0 | | 57.92 | 9.88 | 3.04 | 0.15 | 5.33 | 3.59 | 1.635 | 0.459 | 0.028 | 0.936 | 12.71 | 95.67 |
| PC3810-15 | 154.0 | | 52.76 | 9.10 | 2.86 | 0.15 | 8.77 | 3.43 | 1.482 | 0.415 | 0.031 | 0.942 | 16.27 | 96.22 |
| PC3810-16 | 167.0 | | 57.44 | 9.55 | 2.91 | 0.17 | 4.71 | 3.85 | 1.608 | 0.447 | 0.024 | 0.685 | 13.58 | 94.98 |
| PC3810-17 | 174.0 | | 60.19 | 10.22 | 2.85 | 0.17 | 2.80 | 3.82 | 1.718 | 0.459 | 0.029 | 0.789 | 13.03 | 96.07 |
| PC3810-18 | 185.0 | | 61.53 | 10.22 | 3.04 | 0.17 | 2.05 | 3.51 | 1.751 | 0.472 | 0.033 | 0.650 | 13.31 | 96.73 |
| PC3810-19 | 194.0 | | 55.26 | 8.51 | 2.74 | 0.16 | 5.67 | 3.99 | 1.464 | 0.371 | 0.025 | 0.582 | 15.25 | 94.02 |
| PC3810-20 | 203.0 | | 59.87 | 10.71 | 3.02 | 0.17 | 3.16 | 3.58 | 1.782 | 0.498 | 0.031 | 0.832 | 12.50 | 96.15 |
| PC3810-21 | 216.0 | | 54.65 | 8.04 | 2.55 | 0.15 | 5.91 | 4.08 | 1.369 | 0.365 | 0.022 | 0.728 | 16.11 | 93.98 |
| PC3810-22 | 224.0 | | 56.33 | 8.51 | 2.74 | 0.16 | 3.99 | 3.98 | 1.404 | 0.380 | 0.022 | 0.580 | 15.60 | 93.71 |
| PC3810-23 | 233.0 | | 55.56 | 9.81 | 3.03 | 0.18 | 3.55 | 3.96 | 1.662 | 0.451 | 0.031 | 0.644 | 14.64 | 93.52 |
| PC3810-24 | 244.0 | | 54.50 | 10.03 | 3.10 | 0.17 | 6.04 | 3.68 | 1.639 | 0.461 | 0.028 | 0.811 | 14.65 | 95.11 |
| PC3810-25 | 254.0 | | 57.13 | 9.38 | 2.43 | 0.14 | 6.81 | 3.94 | 1.573 | 0.415 | 0.027 | 1.512 | 11.65 | 95.01 |
| PC3810-26 | 263.0 | | 54.42 | 8.74 | 2.43 | 0.14 | 7.30 | 4.06 | 1.450 | 0.390 | 0.023 | 1.228 | 14.14 | 94.33 |
| PC3810-27 | 273.0 | | 52.71 | 9.94 | 3.12 | 0.16 | 6.28 | 3.57 | 1.654 | 0.456 | 0.032 | 0.700 | 15.41 | 94.04 |
| PC3810-28 | 284.0 | | 53.19 | 9.50 | 2.81 | 0.15 | 8.05 | 3.24 | 1.542 | 0.449 | 0.030 | 0.802 | 15.76 | 95.52 |
| PC3810-29 | 295.0 | | 44.97 | 7.15 | 2.37 | 0.15 | 12.32 | 3.46 | 1.190 | 0.313 | 0.021 | 0.661 | 21.67 | 94.27 |
| PC3810-30 | 305.0 | | 51.35 | 9.79 | 3.20 | 0.17 | 8.09 | 3.34 | 1.533 | 0.459 | 0.032 | 0.602 | 16.64 | 95.20 |
| PC3810-31 | 314.0 | | 52.57 | 10.33 | 2.95 | 0.16 | 8.17 | 3.24 | 1.622 | 0.488 | 0.027 | 0.712 | 15.57 | 95.85 |
| PC3810-32 | 324.0 | | 49.03 | 7.82 | 2.57 | 0.16 | 8.79 | 3.77 | 1.277 | 0.344 | 0.026 | 0.637 | 19.65 | 94.07 |
| PC3810-33 | 335.0 | | 51.53 | 9.79 | 2.93 | 0.17 | 7.07 | 3.44 | 1.604 | 0.447 | 0.029 | 0.673 | 16.77 | 94.45 |
| PC3810-34 | 344.0 | | 49.97 | 6.74 | 2.27 | 0.15 | 9.58 | 3.87 | 1.096 | 0.294 | 0.019 | 0.677 | 20.70 | 95.36 |
| PC3810-35 | 354.0 | | 56.32 | 6.16 | 1.90 | 0.14 | 5.66 | 4.36 | 1.047 | 0.269 | 0.009 | 0.504 | 17.04 | 93.40 |
| PC3810-36 | 364.0 | | 55.97 | 5.42 | 1.73 | 0.13 | 7.17 | 4.28 | 0.939 | 0.235 | 0.013 | 0.550 | 17.48 | 93.91 |
| PC3810-37 | 374.0 | | 58.01 | 5.70 | 1.66 | 0.13 | 5.48 | 4.07 | 0.942 | 0.245 | 0.009 | 0.463 | 17.66 | 94.36 |
| PC3810-38 | 383.0 | | 52.03 | 10.48 | 3.09 | 0.18 | 6.44 | 3.35 | 1.604 | 0.471 | 0.031 | 0.521 | 17.29 | 95.49 |

| APPENDIX C.5. UNCORRECTED MAJOR ELEMENT DATA : OXIDES (XRF) | | | | | | | | | | | | | | |
|---|---|---|---|---|---|---|---|---|---|---|---|---|---|---|
| | | | | | | | | | | | | | | |
| PC38-10 | 257m | | | | | | | | | | | | | |
| Sample | Depth | | SiO2 | Al2O3 | Fe2O3 | MgO | CaO | Na2O | K2O | TiO2 | MnO2 | P2O5 | LOI | Total |
| | (cm) | | (wt.%) | (wt.%) | (wt.%) | (wt.%) | (wt.%) | (wt.%) | (wt.%) | (wt.%) | (wt.%) | (wt.%) | (%) | (%) |
| | | | | | | | | | | | | | | |
| PC3810-39 | 394.0 | | 52.69 | 8.41 | 2.33 | 0.15 | 5.70 | 3.68 | 1.334 | 0.382 | 0.021 | 0.638 | 18.66 | 94.01 |
| PC3810-40 | 404.0 | | 53.38 | 9.86 | 2.65 | 0.16 | 6.71 | 3.34 | 1.536 | 0.471 | 0.029 | 0.627 | 16.66 | 95.41 |
| PC3810-41 | 417.0 | | 47.62 | 8.33 | 2.44 | 0.15 | 10.17 | 3.31 | 1.278 | 0.386 | 0.020 | 0.751 | 20.45 | 94.90 |
| PC3810-42 | 424.0 | | 50.40 | 8.69 | 2.45 | 0.15 | 7.75 | 3.59 | 1.388 | 0.391 | 0.030 | 0.677 | 18.87 | 94.39 |
| PC3810-43 | 434.0 | | 45.20 | 3.99 | 1.24 | 0.12 | 15.07 | 4.01 | 0.708 | 0.179 | 0.009 | 0.797 | 22.17 | 93.51 |
| PC3810-44 | 445.0 | | 47.81 | 6.84 | 2.02 | 0.14 | 11.31 | 3.51 | 1.108 | 0.297 | 0.013 | 0.573 | 20.45 | 94.07 |
| PC3810-45 | 456.0 | | 48.86 | 6.21 | 1.86 | 0.14 | 10.04 | 3.76 | 0.993 | 0.272 | 0.014 | 0.587 | 21.55 | 94.27 |
| PC3810-46 | 467.0 | | 50.87 | 4.16 | 1.29 | 0.12 | 10.11 | 4.47 | 0.755 | 0.181 | 0.003 | 0.445 | 20.14 | 92.55 |
| PC3810-47 | 476.0 | | 44.62 | 8.51 | 2.45 | 0.15 | 11.41 | 3.14 | 1.336 | 0.394 | 0.025 | 1.080 | 21.95 | 95.06 |
| PC3810-48 | 484.0 | | 43.73 | 8.05 | 2.38 | 0.14 | 12.27 | 2.90 | 1.254 | 0.368 | 0.019 | 1.015 | 22.67 | 94.80 |
| PC3810-49 | 494.0 | | 45.25 | 7.70 | 2.04 | 0.13 | 12.69 | 2.85 | 1.164 | 0.365 | 0.022 | 1.969 | 20.86 | 95.02 |
| PC3810-50 | 504.0 | | 57.32 | 9.72 | 2.25 | 0.11 | 10.88 | 2.88 | 1.554 | 0.435 | 0.025 | 5.417 | 7.34 | 97.94 |
| PC3810-51 | 514.0 | | 59.81 | 9.97 | 3.73 | 0.18 | 3.39 | 3.75 | 1.543 | 0.486 | 0.038 | 0.254 | 11.97 | 95.13 |
| PC3810-52 | 524.0 | | 62.78 | 10.90 | 3.92 | 0.19 | 2.97 | 3.69 | 1.677 | 0.531 | 0.047 | 0.236 | 10.50 | 97.45 |
| PC3810-53 | 534.0 | | 44.04 | 7.91 | 2.36 | 0.17 | 6.54 | 3.97 | 1.236 | 0.315 | 0.019 | 0.565 | 23.30 | 90.43 |
| PC3810-54 | 545.0 | | 50.08 | 7.99 | 2.33 | 0.16 | 5.07 | 4.01 | 1.315 | 0.325 | 0.021 | 0.438 | 21.45 | 93.19 |
| PC3810-55 | 554.0 | | 45.78 | 7.20 | 2.17 | 0.17 | 7.17 | 4.22 | 1.157 | 0.286 | 0.019 | 0.422 | 24.40 | 93.00 |
| PC3810-56 | 564.0 | | 47.96 | 6.12 | 2.01 | 0.17 | 10.08 | 4.37 | 1.014 | 0.257 | 0.023 | 0.628 | 20.08 | 92.71 |
| PC3810-57 | 574.0 | | 43.79 | 7.10 | 2.26 | 0.18 | 11.47 | 3.69 | 1.111 | 0.298 | 0.022 | 0.538 | 23.60 | 94.06 |
| PC3810-58 | 584.0 | | 47.08 | 6.95 | 2.23 | 0.17 | 9.84 | 4.09 | 1.180 | 0.291 | 0.025 | 0.409 | 21.12 | 93.38 |
| PC3810-59 | 596.0 | | 48.35 | 6.87 | 2.19 | 0.16 | 8.68 | 4.22 | 1.164 | 0.285 | 0.018 | 0.429 | 20.85 | 93.21 |
| PC3810-60 | 604.0 | | 46.00 | 7.02 | 2.29 | 0.17 | 10.60 | 4.15 | 1.198 | 0.289 | 0.023 | 0.437 | 20.35 | 92.51 |
| PC3810-61 | 614.0 | | 50.02 | 7.76 | 2.48 | 0.16 | 7.57 | 4.01 | 1.273 | 0.316 | 0.020 | 0.313 | 20.32 | 94.26 |
| PC3810-62 | 624.0 | | 48.46 | 8.49 | 2.65 | 0.17 | 8.92 | 3.52 | 1.439 | 0.363 | 0.027 | 0.440 | 19.73 | 94.22 |
| PC3810-63 | 634.0 | | 49.29 | 8.33 | 2.56 | 0.16 | 8.93 | 4.50 | 1.400 | 0.343 | 0.026 | 0.466 | 20.13 | 96.14 |
| PC3810-64 | 645.0 | | 50.90 | 8.08 | 2.66 | 0.17 | 6.84 | 4.04 | 1.318 | 0.328 | 0.032 | 0.312 | 19.30 | 93.97 |
| PC3810-65 | 655.0 | | 48.55 | 7.76 | 2.51 | 0.16 | 7.60 | 4.16 | 1.284 | 0.308 | 0.020 | 0.289 | 20.21 | 92.86 |
| PC3810-66 | 667.0 | | 50.10 | 8.61 | 2.75 | 0.16 | 7.32 | 3.92 | 1.459 | 0.344 | 0.025 | 0.378 | 18.29 | 93.35 |
| PC3810-67 | 674.0 | | 51.44 | 10.04 | 3.10 | 0.18 | 5.59 | 3.68 | 1.685 | 0.406 | 0.033 | 0.394 | 18.17 | 94.72 |
| PC3810-68 | 683.0 | | 51.25 | 9.21 | 2.82 | 0.17 | 6.51 | 3.73 | 1.578 | 0.357 | 0.027 | 0.299 | 14.98 | 90.94 |
| PC3810-69 | 694.0 | | 53.53 | 12.19 | 3.72 | 0.20 | 4.48 | 3.44 | 2.070 | 0.499 | 0.034 | 0.450 | 18.24 | 98.84 |
| PC3810-70 | 704.0 | | 55.29 | 13.57 | 3.61 | 0.22 | 2.52 | 3.23 | 2.376 | 0.582 | 0.043 | 0.424 | 14.24 | 96.11 |

| APPENDIX C.5. UNCORRECTED MAJOR ELEMENT DATA : OXIDES (XRF) | | | | | | | | | | | | | |
|---|---|---|---|---|---|---|---|---|---|---|---|---|---|
| PC38-10 | 257m | | | | | | | | | | | | |
| Sample | Depth | | SiO2 | Al2O3 | Fe2O3 | MgO | CaO | Na2O | K2O | TiO2 | MnO2 | P2O5 | LOI | Total |
| | (cm) | | (wt.%) | (wt.%) | (wt.%) | (wt.%) | (wt.%) | (wt.%) | (wt.%) | (wt.%) | (wt.%) | (wt.%) | (%) | (%) |
| PC3810-71 | 714.0 | | 52.24 | 12.08 | 3.54 | 0.21 | 5.24 | 3.41 | 2.133 | 0.477 | 0.036 | 0.468 | 14.81 | 94.66 |
| PC3810-72 | 724.0 | | 52.66 | 10.64 | 3.15 | 0.19 | 6.23 | 3.35 | 1.813 | 0.409 | 0.038 | 0.418 | 16.42 | 95.32 |
| PC3810-74 | 734.0 | | 57.18 | 12.89 | 3.33 | 0.21 | 2.16 | 3.52 | 2.253 | 0.538 | 0.031 | 0.469 | 13.87 | 96.44 |
| PC3810-75 | 745.0 | | 57.89 | 14.38 | 3.94 | 0.22 | 2.18 | 3.45 | 2.484 | 0.612 | 0.046 | 0.445 | 10.99 | 96.63 |
| PC3810-76 | 754.0 | | 58.32 | 11.52 | 3.29 | 0.19 | 2.54 | 3.67 | 1.988 | 0.494 | 0.036 | 0.552 | 13.03 | 95.64 |
| PC3810-77 | 764.0 | | 60.88 | 12.95 | 3.34 | 0.18 | 3.61 | 3.24 | 2.200 | 0.607 | 0.041 | 1.197 | 9.53 | 97.76 |
| PC38-02 | 2525m | | | | | | | | | | | | | |
| PC3802-01 | 8.0 | | 46.91 | 10.31 | 4.13 | 2.31 | 11.68 | 3.70 | 1.76 | 0.447 | 0.034 | 0.254 | 15.75 | 97.29 |
| PC3802-02 | 18.0 | | 42.77 | 9.25 | 3.62 | 2.14 | 15.75 | 3.41 | 1.62 | 0.393 | 0.035 | 0.246 | 15.66 | 94.90 |
| PC3802-03 | 28.0 | | 40.99 | 8.95 | 3.51 | 2.09 | 17.04 | 3.49 | 1.50 | 0.387 | 0.029 | 0.228 | 19.06 | 97.27 |
| PC3802-04 | 38.0 | | 40.57 | 9.75 | 3.66 | 2.20 | 14.35 | 3.70 | 1.73 | 0.404 | 0.030 | 0.207 | 19.64 | 96.22 |
| PC3802-05 | 48.0 | | 39.45 | 9.66 | 3.58 | 2.11 | 17.02 | 3.29 | 1.66 | 0.422 | 0.030 | 0.200 | 19.72 | 97.15 |
| PC3802-06 | 57.5 | | 39.51 | 9.42 | 3.77 | 2.07 | 16.51 | 3.37 | 1.67 | 0.406 | 0.032 | 0.198 | 19.53 | 96.49 |
| PC3802-07 | 70.0 | | 40.91 | 10.14 | 3.71 | 2.15 | 16.69 | 2.61 | 1.67 | 0.452 | 0.033 | 0.212 | 19.62 | 98.18 |
| PC3802-08 | 79.0 | | 40.10 | 9.89 | 3.79 | 2.22 | 16.15 | 3.19 | 1.70 | 0.436 | 0.028 | 0.207 | 19.08 | 96.80 |
| PC3802-09 | 89.0 | | 37.47 | 9.21 | 3.53 | 2.09 | 18.26 | 3.18 | 1.57 | 0.427 | 0.030 | 0.211 | 20.71 | 96.68 |
| PC3802-10 | 100.0 | | 35.55 | 8.58 | 3.29 | 1.97 | 19.83 | 3.19 | 1.47 | 0.403 | 0.029 | 0.208 | 22.04 | 96.55 |
| PC3802-11 | 110.0 | | 35.99 | 8.38 | 3.20 | 1.94 | 20.15 | 3.11 | 1.45 | 0.392 | 0.034 | 0.205 | 21.83 | 96.68 |
| PC3802-12 | 120.0 | | 34.41 | 7.74 | 3.19 | 1.81 | 21.22 | 3.15 | 1.39 | 0.367 | 0.027 | 0.195 | 22.71 | 96.20 |
| PC3802-13 | 130.0 | | 35.92 | 8.51 | 3.51 | 1.93 | 19.87 | 3.08 | 1.42 | 0.384 | 0.030 | 0.200 | 23.21 | 98.08 |
| PC3802-14 | 139.0 | | 39.47 | 9.81 | 3.53 | 2.14 | 16.52 | 3.42 | 1.69 | 0.432 | 0.035 | 0.211 | 19.80 | 97.06 |
| PC3802-15 | 150.0 | | 40.46 | 10.10 | 3.78 | 2.20 | 15.82 | 3.55 | 1.77 | 0.441 | 0.033 | 0.214 | 19.55 | 97.92 |
| PC3802-16 | 160.0 | | 42.84 | 11.06 | 4.07 | 2.30 | 14.64 | 3.09 | 1.93 | 0.491 | 0.037 | 0.226 | 16.86 | 97.54 |
| PC3802-17 | 171.0 | | 44.39 | 11.23 | 4.10 | 2.37 | 12.79 | 3.43 | 2.01 | 0.494 | 0.035 | 0.224 | 15.80 | 96.87 |
| PC3802-18 | 181.0 | | 47.29 | 10.57 | 4.50 | 2.34 | 11.10 | 3.70 | 1.96 | 0.486 | 0.039 | 0.225 | 15.39 | 97.60 |
| PC3802-19 | 191.0 | | 45.98 | 10.44 | 4.29 | 2.33 | 12.02 | 3.54 | 1.88 | 0.474 | 0.037 | 0.224 | 16.33 | 97.54 |
| PC3802-20 | 201.0 | | 47.47 | 11.06 | 4.28 | 2.44 | 10.45 | 3.73 | 1.99 | 0.507 | 0.036 | 0.225 | 15.86 | 98.03 |
| PC3802-21 | 211.0 | | 45.29 | 11.27 | 4.30 | 2.40 | 11.78 | 3.50 | 1.98 | 0.503 | 0.038 | 0.225 | 16.58 | 97.87 |
| PC3802-22 | 221.0 | | 45.14 | 11.16 | 4.27 | 2.42 | 12.52 | 3.50 | 1.96 | 0.496 | 0.037 | 0.225 | 15.77 | 97.50 |
| PC3802-23 | 231.0 | | 46.68 | 11.75 | 4.40 | 2.50 | 11.19 | 3.55 | 2.07 | 0.531 | 0.041 | 0.231 | 14.49 | 97.45 |

| APPENDIX C.5. UNCORRECTED MAJOR ELEMENT DATA : OXIDES (XRF) | | | | | | | | | | | | | | |
|---|---|---|---|---|---|---|---|---|---|---|---|---|---|---|
| PC38-02 | 2525m | | | | | | | | | | | | | |
| Sample | Depth | | SiO2 | Al2O3 | Fe2O3 | MgO | CaO | Na2O | K2O | TiO2 | MnO2 | P2O5 | LOI | Total |
| | (cm) | | (wt.%) | (wt.%) | (wt.%) | (wt.%) | (wt.%) | (wt.%) | (wt.%) | (wt.%) | (wt.%) | (wt.%) | (%) | (%) |
| PC3802-24 | 241.0 | | 53.18 | 13.05 | 4.89 | 2.79 | 5.85 | 3.92 | 2.39 | 0.592 | 0.042 | 0.243 | 11.85 | 98.79 |
| PC3802-25 | 251.0 | | 50.22 | 11.84 | 4.62 | 2.58 | 8.07 | 3.74 | 2.11 | 0.552 | 0.039 | 0.257 | 13.92 | 97.95 |
| PC3802-26 | 261.0 | | 46.62 | 10.61 | 4.24 | 2.34 | 11.65 | 3.55 | 1.90 | 0.495 | 0.036 | 0.261 | 15.95 | 97.66 |
| PC3802-27 | 271.0 | | 52.91 | 12.45 | 4.77 | 2.64 | 6.18 | 3.90 | 2.31 | 0.556 | 0.041 | 0.254 | 13.08 | 99.08 |
| PC3802-28 | 281.0 | | 52.08 | 12.53 | 4.75 | 2.57 | 6.89 | 3.73 | 2.35 | 0.546 | 0.036 | 0.247 | 12.94 | 98.66 |
| PC3802-29 | 291.0 | | 55.20 | 13.59 | 5.00 | 2.75 | 3.87 | 3.84 | 2.52 | 0.590 | 0.040 | 0.246 | 11.26 | 98.91 |
| PC3802-30 | 301.0 | | 54.72 | 13.13 | 5.03 | 2.74 | 5.03 | 3.78 | 2.41 | 0.592 | 0.042 | 0.286 | 10.85 | 98.62 |
| PC3802-31 | 312.0 | | 52.29 | 11.71 | 4.59 | 2.56 | 8.29 | 3.68 | 2.10 | 0.535 | 0.038 | 0.283 | 12.52 | 98.60 |
| PC3802-32 | 322.0 | | 51.18 | 11.94 | 4.70 | 2.66 | 8.08 | 3.65 | 2.17 | 0.535 | 0.041 | 0.271 | 12.89 | 98.11 |
| PC3802-33 | 332.0 | | 51.11 | 11.93 | 5.01 | 2.57 | 8.05 | 3.56 | 2.18 | 0.523 | 0.043 | 0.239 | 13.10 | 98.32 |
| PC3802-34 | 342.0 | | 51.30 | 11.75 | 4.99 | 2.62 | 8.17 | 3.70 | 2.12 | 0.505 | 0.036 | 0.249 | 12.52 | 97.95 |
| PC3802-35 | 352.0 | | 46.33 | 10.17 | 3.87 | 2.21 | 12.94 | 3.49 | 1.84 | 0.416 | 0.035 | 0.221 | 15.61 | 97.13 |
| PC3802-36 | 362.0 | | 41.28 | 9.89 | 3.81 | 2.14 | 16.24 | 3.25 | 1.70 | 0.402 | 0.036 | 0.195 | 18.37 | 97.32 |
| PC3802-37 | 372.0 | | 39.50 | 9.96 | 3.79 | 2.12 | 17.80 | 3.15 | 1.69 | 0.411 | 0.034 | 0.182 | 19.34 | 97.97 |
| PC3802-38 | 381.0 | | 38.59 | 9.60 | 3.74 | 2.10 | 18.73 | 2.94 | 1.73 | 0.418 | 0.032 | 0.181 | 19.26 | 97.32 |
| PC3802-39 | 391.0 | | 38.38 | 9.34 | 3.62 | 2.06 | 18.90 | 2.89 | 1.65 | 0.413 | 0.030 | 0.184 | 20.41 | 97.87 |
| PC3802-40 | 400.0 | | 37.34 | 8.99 | 3.45 | 2.01 | 20.33 | 2.98 | 1.61 | 0.399 | 0.032 | 0.191 | 20.92 | 98.25 |
| PC3802-41 | 410.0 | | 37.65 | 9.22 | 3.43 | 1.95 | 19.95 | 3.05 | 1.65 | 0.400 | 0.033 | 0.189 | 20.18 | 97.71 |
| PC3802-42 | 420.0 | | 38.90 | 9.20 | 3.49 | 1.95 | 19.16 | 3.10 | 1.67 | 0.397 | 0.031 | 0.183 | 18.72 | 96.79 |
| PC3802-43 | 430.0 | | 36.41 | 9.07 | 3.43 | 1.97 | 20.37 | 2.88 | 1.56 | 0.399 | 0.033 | 0.183 | 19.53 | 95.82 |
| PC3802-44 | 440.0 | | 38.52 | 9.42 | 3.51 | 2.04 | 19.16 | 2.98 | 1.71 | 0.423 | 0.031 | 0.192 | 19.74 | 97.73 |
| PC3802-45 | 450.0 | | 41.35 | 10.31 | 3.98 | 2.24 | 16.14 | 3.16 | 1.76 | 0.450 | 0.035 | 0.194 | 17.86 | 97.49 |
| PC3802-46 | 460.0 | | 42.75 | 10.97 | 4.12 | 2.32 | 14.48 | 3.42 | 2.00 | 0.481 | 0.038 | 0.202 | 16.23 | 97.03 |
| PC3802-47 | 470.0 | | 36.54 | 9.39 | 3.61 | 2.02 | 20.62 | 2.87 | 1.52 | 0.406 | 0.031 | 0.201 | 21.37 | 98.57 |
| PC3802-48 | 481.0 | | 35.55 | 8.87 | 3.48 | 1.94 | 21.27 | 2.56 | 1.15 | 0.405 | 0.032 | 0.198 | 23.37 | 98.82 |
| PC3802-49 | 491.0 | | 36.66 | 9.03 | 3.52 | 1.95 | 20.87 | 2.82 | 1.63 | 0.401 | 0.027 | 0.199 | 20.79 | 97.90 |
| PC3802-50 | 501.0 | | 38.72 | 9.56 | 3.89 | 2.05 | 19.53 | 3.04 | 1.72 | 0.411 | 0.038 | 0.215 | 21.11 | 100.28 |
| PC3802-51 | 511.0 | | 41.09 | 9.98 | 3.69 | 2.06 | 17.38 | 3.03 | 1.76 | 0.439 | 0.035 | 0.207 | 18.25 | 97.93 |
| PC3802-52 | 521.0 | | 44.92 | 11.01 | 4.11 | 2.15 | 14.06 | 3.38 | 2.12 | 0.443 | 0.037 | 0.212 | 15.00 | 97.45 |
| PC3802-53 | 531.0 | | 53.57 | 12.33 | 3.54 | 1.84 | 11.23 | 3.80 | 2.77 | 0.419 | 0.037 | 0.195 | 12.26 | 101.99 |
| PC3802-54 | 540.0 | | 50.17 | 12.84 | 4.88 | 2.65 | 8.33 | 3.56 | 2.38 | 0.563 | 0.044 | 0.249 | 13.03 | 98.70 |
| PC3802-55 | 550.0 | | 50.24 | 12.73 | 5.11 | 2.69 | 7.71 | 3.53 | 2.30 | 0.564 | 0.042 | 0.253 | 13.75 | 98.92 |

| APPENDIX C.5. UNCORRECTED MAJOR ELEMENT DATA : OXIDES (XRF) | | | | | | | | | | | | | |
|---|---|---|---|---|---|---|---|---|---|---|---|---|---|
| PC38-02 | 2525m | | | | | | | | | | | | |
| Sample | Depth | | SiO2 | Al2O3 | Fe2O3 | MgO | CaO | Na2O | K2O | TiO2 | MnO2 | P2O5 | LOI | Total |
| | (cm) | | (wt.%) | (wt.%) | (wt.%) | (wt.%) | (wt.%) | (wt.%) | (wt.%) | (wt.%) | (wt.%) | (wt.%) | (%) | (%) |
| PC3802-56 | 560.0 | | 49.85 | 12.09 | 5.69 | 2.65 | 6.06 | 3.55 | 2.25 | 0.556 | 0.041 | 0.252 | 13.69 | 96.67 |
| PC3802-57 | 572.0 | | 48.13 | 11.43 | 4.83 | 2.62 | 10.47 | 3.93 | 2.10 | 0.485 | 0.037 | 0.247 | 14.00 | 98.28 |
| PC3802-58 | 582.0 | | 46.92 | 11.87 | 4.73 | 2.49 | 11.09 | 3.46 | 2.16 | 0.490 | 0.040 | 0.230 | 13.95 | 97.42 |
| PC3802-59 | 591.0 | | 45.66 | 11.98 | 4.79 | 2.51 | 12.00 | 3.33 | 2.12 | 0.490 | 0.039 | 0.221 | 14.43 | 97.55 |
| PC3802-60 | 601.0 | | 35.32 | 8.98 | 3.72 | 1.97 | 21.65 | 2.69 | 1.47 | 0.396 | 0.030 | 0.212 | 21.32 | 97.76 |
| PC3802-61 | 611.0 | | 35.30 | 8.76 | 3.57 | 2.01 | 22.61 | 2.86 | 1.61 | 0.378 | 0.033 | 0.209 | 21.69 | 99.03 |
| PC3802-62 | 621.0 | | 38.56 | 9.68 | 3.92 | 2.16 | 19.32 | 2.89 | 1.75 | 0.441 | 0.036 | 0.209 | 19.00 | 97.98 |
| PC3802-63 | 631.0 | | 39.45 | 10.22 | 3.98 | 2.21 | 18.36 | 2.88 | 1.79 | 0.455 | 0.037 | 0.208 | 18.49 | 98.09 |
| PC3802-64 | 641.0 | | 44.11 | 11.42 | 4.35 | 2.41 | 15.58 | 3.04 | 2.01 | 0.487 | 0.039 | 0.225 | 16.10 | 99.77 |
| PC3802-65 | 651.0 | | 47.51 | 12.09 | 4.48 | 2.53 | 10.96 | 3.30 | 2.26 | 0.506 | 0.037 | 0.225 | 13.65 | 97.55 |
| PC3802-66 | 662.0 | | 47.04 | 11.08 | 4.45 | 2.44 | 11.70 | 3.59 | 2.09 | 0.473 | 0.038 | 0.247 | 13.99 | 97.14 |
| PC3802-67 | 671.0 | | 37.64 | 8.54 | 3.22 | 1.92 | 19.64 | 3.09 | 1.57 | 0.348 | 0.031 | 0.206 | 19.46 | 95.66 |
| PC3802-68 | 681.0 | | 38.64 | 9.72 | 3.56 | 2.06 | 18.54 | 2.98 | 1.80 | 0.404 | 0.034 | 0.187 | 17.95 | 95.87 |
| PC3802-69 | 691.0 | | 40.74 | 10.71 | 3.78 | 2.14 | 16.37 | 3.11 | 1.94 | 0.445 | 0.036 | 0.173 | 17.50 | 96.93 |
| PC3802-70 | 701.0 | | 39.93 | 10.28 | 3.55 | 2.09 | 17.34 | 2.92 | 1.86 | 0.433 | 0.034 | 0.170 | 18.25 | 96.86 |
| PC3802-71 | 711.0 | | 41.87 | 10.37 | 3.91 | 2.34 | 17.69 | 3.17 | 1.85 | 0.427 | 0.034 | 0.174 | 18.34 | 100.18 |
| PC3802-72 | 721.0 | | 41.43 | 9.95 | 3.61 | 2.14 | 16.59 | 3.07 | 1.86 | 0.429 | 0.034 | 0.178 | 17.72 | 97.02 |
| PC3802-73 | 731.0 | | 41.21 | 10.10 | 3.60 | 2.13 | 16.65 | 3.01 | 1.88 | 0.435 | 0.038 | 0.184 | 17.90 | 97.14 |
| PC3802-74 | 741.0 | | 41.54 | 10.16 | 3.66 | 2.17 | 15.79 | 3.04 | 1.85 | 0.450 | 0.037 | 0.193 | 17.97 | 96.85 |
| PC38-11 | 3835m | | | | | | | | | | | | | |
| PC3811-01 | 3.0 | | 55.33 | 12.78 | 3.31 | 2.11 | 2.59 | 3.61 | 2.040 | 0.596 | 0.036 | 0.682 | 14.35 | 97.43 |
| PC3811-02 | 13.0 | | 50.01 | 10.84 | 3.48 | 1.75 | 8.07 | 3.35 | 1.591 | 0.539 | 0.041 | 0.827 | 16.67 | 97.17 |
| PC3811-03 | 23.0 | | 55.25 | 11.09 | 3.39 | 1.63 | 7.00 | 3.21 | 1.704 | 0.591 | 0.045 | 0.800 | 12.63 | 97.34 |
| PC3811-04 | 33.0 | | 57.24 | 13.20 | 3.62 | 2.45 | 2.04 | 3.77 | 2.237 | 0.581 | 0.034 | 0.428 | 12.51 | 98.10 |
| PC3811-05 | 43.0 | | 55.37 | 12.97 | 3.31 | 2.40 | 3.18 | 3.83 | 2.195 | 0.566 | 0.037 | 0.366 | 13.70 | 97.92 |
| PC3811-06 | 53.0 | | 52.50 | 12.70 | 3.91 | 2.23 | 3.96 | 3.59 | 2.143 | 0.555 | 0.035 | 0.289 | 14.81 | 96.73 |
| PC3811-07 | 63.0 | | 53.17 | 13.01 | 3.78 | 2.28 | 4.18 | 3.69 | 2.200 | 0.553 | 0.041 | 0.280 | 14.86 | 98.04 |
| PC3811-08 | 73.0 | | 52.14 | 12.83 | 3.90 | 2.24 | 4.89 | 3.52 | 2.149 | 0.551 | 0.039 | 0.304 | 15.77 | 98.34 |
| PC3811-09 | 85.0 | | 59.53 | 13.16 | 3.74 | 1.90 | 7.19 | 3.60 | 2.182 | 0.517 | 0.048 | 0.606 | 9.13 | 101.61 |
| PC3811-10 | 95.0 | | 51.70 | 12.13 | 3.83 | 2.32 | 6.28 | 3.52 | 2.100 | 0.538 | 0.040 | 0.304 | 16.47 | 99.23 |

| APPENDIX C.5. UNCORRECTED MAJOR ELEMENT DATA : OXIDES (XRF) | | | | | | | | | | | | | | |
|---|---|---|---|---|---|---|---|---|---|---|---|---|---|---|
| PC38-11 Sample | 3835m Depth (cm) | | SiO2 (wt.%) | Al2O3 (wt.%) | Fe2O3 (wt.%) | MgO (wt.%) | CaO (wt.%) | Na2O (wt.%) | K2O (wt.%) | TiO2 (wt.%) | MnO2 (wt.%) | P2O5 (wt.%) | LOI (%) | Total (%) |
| PC3811-11 | 105.0 | | 50.24 | 11.65 | 3.88 | 2.25 | 6.90 | 3.46 | 1.979 | 0.522 | 0.039 | 0.293 | 16.01 | 97.24 |
| PC3811-12 | 116.0 | | 52.28 | 11.94 | 4.03 | 2.28 | 5.56 | 3.49 | 2.022 | 0.525 | 0.036 | 0.306 | 15.47 | 97.93 |
| PC3811-13 | 125.0 | | 51.98 | 12.27 | 3.94 | 2.35 | 5.70 | 3.55 | 2.149 | 0.537 | 0.038 | 0.291 | 14.90 | 97.72 |
| PC3811-14 | 135.0 | | 51.69 | 12.23 | 3.90 | 2.27 | 6.38 | 3.48 | 2.030 | 0.543 | 0.038 | 0.334 | 15.51 | 98.39 |
| PC3811-15 | 145.0 | | 54.47 | 12.96 | 3.89 | 2.54 | 5.64 | 3.81 | 2.154 | 0.552 | 0.041 | 0.330 | 15.95 | 102.34 |
| PC3811-16 | 155.0 | | 50.72 | 11.82 | 3.75 | 2.16 | 7.36 | 3.36 | 1.944 | 0.531 | 0.045 | 0.359 | 15.07 | 97.12 |
| PC3811-17 | 165.0 | | 54.89 | 13.21 | 4.06 | 2.58 | 6.28 | 3.94 | 2.195 | 0.539 | 0.042 | 0.329 | 14.81 | 102.87 |
| PC3811-18 | 175.0 | | 53.48 | 12.23 | 3.86 | 2.07 | 7.43 | 3.41 | 2.104 | 0.526 | 0.043 | 0.493 | 12.89 | 98.54 |
| PC3811-19 | 186.0 | | 52.08 | 12.36 | 3.51 | 2.26 | 4.85 | 3.50 | 2.170 | 0.534 | 0.044 | 0.328 | 17.87 | 99.52 |
| PC3811-20 | 197.0 | | 51.91 | 12.63 | 4.05 | 2.35 | 4.42 | 3.51 | 2.133 | 0.548 | 0.036 | 0.316 | 11.87 | 93.77 |
| PC3811-21 | 204.0 | | 52.79 | 12.80 | 3.99 | 2.32 | 3.37 | 3.64 | 2.251 | 0.540 | 0.036 | 0.301 | 14.46 | 96.51 |
| PC3811-22 | 215.0 | | 48.83 | 11.43 | 3.91 | 2.13 | 7.73 | 3.53 | 1.948 | 0.502 | 0.039 | 0.402 | 16.93 | 97.38 |
| PC3811-23 | 225.0 | | 49.40 | 11.71 | 4.04 | 2.28 | 6.84 | 3.68 | 1.975 | 0.499 | 0.038 | 0.328 | 17.09 | 97.87 |
| PC3811-24 | 235.0 | | 49.15 | 11.97 | 3.99 | 2.20 | 6.21 | 3.38 | 1.995 | 0.513 | 0.035 | 0.329 | 18.43 | 98.21 |
| PC3811-25 | 245.0 | | 49.80 | 12.03 | 3.96 | 2.33 | 6.65 | 3.55 | 2.011 | 0.497 | 0.036 | 0.337 | 17.34 | 98.54 |
| PC3811-26 | 255.0 | | 47.98 | 10.52 | 3.97 | 1.96 | 8.90 | 3.26 | 1.753 | 0.455 | 0.031 | 0.322 | 18.76 | 97.92 |
| PC3811-27 | 265.0 | | 50.17 | 10.64 | 3.69 | 2.04 | 7.83 | 3.30 | 1.791 | 0.457 | 0.030 | 0.325 | 18.77 | 99.04 |
| PC3811-28 | 275.0 | | 51.64 | 11.21 | 3.79 | 2.04 | 6.52 | 3.29 | 1.848 | 0.488 | 0.032 | 0.334 | 17.31 | 98.52 |
| PC3811-29 | 285.0 | | 54.44 | 13.54 | 3.77 | 2.23 | 2.63 | 3.50 | 2.427 | 0.587 | 0.033 | 0.336 | 13.97 | 97.47 |
| PC3811-30 | 297.0 | | 54.20 | 13.41 | 4.05 | 2.20 | 3.57 | 3.19 | 2.309 | 0.589 | 0.036 | 0.352 | 14.21 | 98.12 |
| PC3811-31 | 305.0 | | 56.41 | 13.90 | 3.85 | 2.25 | 2.12 | 3.34 | 2.487 | 0.613 | 0.035 | 0.341 | 12.81 | 98.17 |
| PC3811-32 | 315.0 | | 57.61 | 14.46 | 3.77 | 2.33 | 2.24 | 3.41 | 2.487 | 0.621 | 0.039 | 0.440 | 15.39 | 102.80 |
| PC3811-33 | 325.0 | | 49.08 | 9.92 | 3.07 | 1.57 | 12.50 | 2.52 | 1.616 | 0.456 | 0.032 | 0.980 | 16.57 | 98.32 |
| PC3811-34 | 335.0 | | 56.38 | 12.10 | 3.74 | 2.10 | 2.48 | 3.35 | 2.160 | 0.536 | 0.031 | 0.332 | 14.39 | 97.59 |
| PC3811-35 | 345.0 | | 55.73 | 12.04 | 3.76 | 2.13 | 2.83 | 3.45 | 2.115 | 0.521 | 0.032 | 0.330 | 14.90 | 97.83 |
| PC3811-36 | 355.0 | | 57.63 | 11.48 | 3.22 | 2.08 | 2.63 | 3.61 | 1.996 | 0.496 | 0.029 | 0.335 | 14.59 | 98.09 |
| PC3811-37 | 365.0 | | 55.80 | 11.97 | 3.50 | 2.11 | 2.53 | 3.59 | 2.047 | 0.517 | 0.028 | 0.342 | 15.15 | 97.58 |
| PC3811-38 | 375.0 | | 53.19 | 12.31 | 4.25 | 2.12 | 3.10 | 3.33 | 2.107 | 0.540 | 0.029 | 0.303 | 16.37 | 97.64 |
| PC3811-39 | 385.0 | | 53.40 | 13.37 | 3.99 | 2.30 | 3.22 | 3.30 | 2.318 | 0.594 | 0.039 | 0.335 | 15.75 | 98.61 |
| PC3811-40 | 395.0 | | 54.31 | 13.70 | 4.34 | 2.46 | 3.66 | 3.34 | 2.331 | 0.599 | 0.039 | 0.346 | 14.84 | 99.96 |
| PC3811-41 | 405.0 | | 51.42 | 13.13 | 4.24 | 2.39 | 3.62 | 3.26 | 2.259 | 0.580 | 0.038 | 0.335 | 15.71 | 96.99 |
| PC3811-42 | 415.0 | | 59.64 | 14.45 | 4.40 | 2.54 | 1.68 | 3.56 | 2.498 | 0.609 | 0.034 | 0.353 | 13.52 | 103.30 |

APPENDIX C.5. UNCORRECTED MAJOR ELEMENT DATA : OXIDES (XRF)

| PC38-11 Sample | 3835m Depth (cm) | | SiO2 (wt.%) | Al2O3 (wt.%) | Fe2O3 (wt.%) | MgO (wt.%) | CaO (wt.%) | Na2O (wt.%) | K2O (wt.%) | TiO2 (wt.%) | MnO2 (wt.%) | P2O5 (wt.%) | LOI (%) | Total (%) |
|---|---|---|---|---|---|---|---|---|---|---|---|---|---|---|
| PC3811-43 | 425.0 | | 52.63 | 12.28 | 3.87 | 2.19 | 2.34 | 3.31 | 2.217 | 0.568 | 0.032 | 0.338 | 13.59 | 93.36 |
| PC3811-44 | 435.0 | | 57.62 | 12.17 | 3.78 | 2.35 | 4.90 | 3.49 | 1.980 | 0.506 | 0.033 | 0.432 | 14.95 | 102.22 |
| PC3811-45 | 445.0 | | 56.63 | 11.86 | 3.52 | 2.13 | 3.61 | 3.43 | 1.981 | 0.520 | 0.030 | 0.399 | 14.31 | 98.42 |
| PC3811-46 | 455.0 | | 57.08 | 13.70 | 3.68 | 2.44 | 1.68 | 3.47 | 2.410 | 0.613 | 0.035 | 0.394 | 13.48 | 98.98 |
| PC3811-47 | 465.0 | | 55.71 | 14.11 | 4.05 | 2.43 | 1.59 | 3.51 | 2.471 | 0.615 | 0.030 | 0.358 | 13.56 | 98.43 |
| PC3811-48 | 475.0 | | 57.93 | 13.75 | 4.53 | 2.45 | 3.11 | 3.51 | 2.306 | 0.570 | 0.038 | 0.386 | 13.83 | 102.40 |
| PC3811-49 | 485.0 | | 57.26 | 13.77 | 4.45 | 2.38 | 1.65 | 3.55 | 2.394 | 0.582 | 0.035 | 0.342 | 13.35 | 99.76 |
| PC3811-50 | 495.0 | | 57.73 | 13.23 | 4.40 | 2.34 | 1.59 | 3.48 | 2.297 | 0.565 | 0.034 | 0.375 | 13.90 | 99.94 |
| PC3811-51 | 505.0 | | 59.61 | 13.37 | 4.04 | 2.38 | 1.53 | 3.54 | 2.342 | 0.575 | 0.031 | 0.349 | 12.85 | 100.61 |
| PC3811-52 | 515.0 | | 58.65 | 13.07 | 4.32 | 2.32 | 1.55 | 3.42 | 2.336 | 0.572 | 0.034 | 0.367 | 12.17 | 98.81 |
| PC3811-53 | 525.0 | | 61.31 | 13.12 | 4.05 | 2.39 | 1.46 | 3.58 | 2.334 | 0.566 | 0.034 | 0.329 | 12.51 | 101.68 |
| PC3811-54 | 535.0 | | 56.86 | 12.09 | 4.29 | 2.18 | 1.57 | 3.29 | 2.261 | 0.560 | 0.033 | 0.373 | 11.29 | 94.80 |
| PC3811-55 | 545.0 | | 60.38 | 12.63 | 4.81 | 2.33 | 1.89 | 3.43 | 2.231 | 0.556 | 0.035 | 0.379 | 13.08 | 101.75 |
| PC3811-56 | 555.0 | | 61.41 | 12.60 | 3.86 | 2.34 | 1.59 | 3.56 | 2.208 | 0.551 | 0.029 | 0.395 | 12.38 | 100.92 |
| PC3811-57 | 565.0 | | 58.52 | 12.05 | 3.87 | 2.25 | 1.82 | 3.46 | 2.147 | 0.551 | 0.027 | 0.408 | 11.35 | 96.45 |

APPENDIX C.6. UNCORRECTED MAJOR ELEMENTS

| BC38-03 | 4289m | | | | | | | | | | |
|---|---|---|---|---|---|---|---|---|---|---|---|
| Sample | Depth | Si | Al | Fe | Mg | Ca | Na | K | Ti | Mn | P |
| | (cm) | (wt.%) | (wt.%) | (wt.%) | (wt.%) | (wt.%) | (wt.%) | (wt.%) | (wt.%) | (wt.%) | (wt.%) |
| BC3803-01 | 0.5 | 26.85 | 6.06 | 3.69 | 0.15 | 1.03 | 4.06 | 1.657 | 0.279 | 0.076 | 0.110 |
| BC3803-02 | 1.5 | 27.29 | 6.14 | 3.90 | 0.15 | 1.01 | 3.61 | 1.686 | 0.287 | 0.063 | 0.112 |
| BC3803-03 | 2.5 | 27.06 | 6.10 | 3.90 | 0.15 | 1.01 | 3.65 | 1.690 | 0.285 | 0.044 | 0.110 |
| BC3803-04 | 3.5 | 27.36 | 6.16 | 3.66 | 0.15 | 1.01 | 3.63 | 1.672 | 0.287 | 0.026 | 0.102 |
| BC3803-05 | 4.5 | 28.10 | 6.48 | 3.28 | 0.15 | 1.03 | 3.73 | 1.782 | 0.297 | 0.023 | 0.092 |
| BC3803-06 | 5.5 | 27.57 | 6.37 | 2.70 | 0.14 | 1.02 | 3.58 | 1.771 | 0.297 | 0.025 | 0.090 |
| BC3803-07 | 6.5 | 27.84 | 6.43 | 2.71 | 0.15 | 1.02 | 3.45 | 1.798 | 0.303 | 0.024 | 0.089 |
| BC3803-08 | 7.5 | 27.91 | 6.53 | 2.84 | 0.15 | 1.03 | 3.52 | 1.808 | 0.305 | 0.021 | 0.087 |
| BC3803-09 | 8.5 | 27.84 | 6.51 | 2.91 | 0.15 | 1.04 | 3.47 | 1.818 | 0.304 | 0.023 | 0.087 |
| BC3803-10 | 9.5 | 29.04 | 6.97 | 3.09 | 0.16 | 1.07 | 3.53 | 1.852 | 0.317 | 0.029 | 0.090 |
| BC3803-11 | 11.0 | 28.04 | 6.76 | 3.01 | 0.16 | 1.06 | 3.63 | 1.849 | 0.315 | 0.027 | 0.090 |
| BC3803-12 | 13.0 | 28.17 | 6.82 | 2.80 | 0.15 | 1.09 | 3.19 | 1.874 | 0.325 | 0.027 | 0.090 |
| BC3803-13 | 15.0 | 27.80 | 6.70 | 3.08 | 0.15 | 1.09 | 3.50 | 1.880 | 0.319 | 0.030 | 0.092 |
| BC3803-14 | 17.0 | 28.50 | 6.84 | 2.92 | 0.15 | 1.13 | 3.08 | 1.901 | 0.331 | 0.027 | 0.096 |
| BC3803-15 | 19.0 | 28.20 | 6.84 | 2.84 | 0.16 | 1.16 | 3.38 | 1.883 | 0.327 | 0.030 | 0.099 |
| BC3803-16 | 21.0 | 28.53 | 6.55 | 2.67 | 0.15 | 1.11 | 3.07 | 1.812 | 0.315 | 0.022 | 0.095 |
| BC3803-17 | 23.0 | 28.34 | 6.55 | 2.95 | 0.15 | 1.11 | 3.36 | 1.823 | 0.312 | 0.025 | 0.096 |
| BC3803-18 | 25.0 | 28.32 | 6.63 | 2.73 | 0.15 | 1.15 | 3.03 | 1.839 | 0.321 | 0.028 | 0.099 |
| BC3803-19 | 27.0 | 27.99 | 6.48 | 2.82 | 0.15 | 1.16 | 3.37 | 1.806 | 0.316 | 0.027 | 0.098 |
| BC3803-20 | 29.0 | 28.58 | 6.76 | 2.95 | 0.15 | 1.20 | 2.98 | 1.878 | 0.328 | 0.032 | 0.102 |
| BC3803-21 | 31.0 | 28.13 | 6.61 | 3.05 | 0.15 | 1.20 | 3.49 | 1.894 | 0.321 | 0.034 | 0.099 |
| BC3803-22 | 33.0 | 28.43 | 6.68 | 2.86 | 0.15 | 1.21 | 3.13 | 1.864 | 0.323 | 0.028 | 0.103 |
| BC3803-23 | 35.0 | 28.20 | 6.58 | 2.80 | 0.15 | 1.22 | 3.27 | 1.867 | 0.320 | 0.028 | 0.101 |
| BC3803-24 | 37.0 | 29.13 | 6.88 | 3.09 | 0.16 | 1.30 | 3.13 | 1.919 | 0.328 | 0.031 | 0.105 |
| BC3803-25 | 39.0 | 29.42 | 6.86 | 3.10 | 0.17 | 1.35 | 3.34 | 1.932 | 0.325 | 0.034 | 0.139 |
| BC3803-26 | 41.0 | 28.44 | 6.60 | 3.02 | 0.15 | 1.29 | 2.98 | 1.905 | 0.324 | 0.031 | 0.100 |
| BC3803-27 | 43.0 | 28.52 | 6.69 | 3.14 | 0.16 | 1.32 | 3.25 | 1.920 | 0.325 | 0.030 | 0.102 |
| BC3803-28 | 45.0 | 28.42 | 6.59 | 2.96 | 0.16 | 1.30 | 2.99 | 1.898 | 0.321 | 0.026 | 0.102 |
| BC3803-29 | 47.0 | 28.27 | 6.55 | 3.11 | 0.16 | 1.30 | 3.19 | 1.917 | 0.320 | 0.031 | 0.102 |
| BC3803-30 | 49.0 | 28.55 | 6.63 | 3.10 | 0.16 | 1.32 | 2.91 | 1.922 | 0.322 | 0.029 | 0.104 |
| BC3803-31 | 51.0 | 28.65 | 6.78 | 3.30 | 0.16 | 1.35 | 3.19 | 1.970 | 0.330 | 0.029 | 0.109 |
| BC3803-32 | 53.0 | 28.01 | 6.67 | 3.09 | 0.17 | 1.37 | 3.26 | 1.927 | 0.326 | 0.030 | 0.105 |
| BC38-02 | 2530m | | | | | | | | | | |
| BC3802-01 | 0.5 | 23.50 | 5.90 | 3.65 | 0.15 | 6.22 | 3.18 | 1.643 | 0.270 | 0.039 | 0.134 |
| BC3802-02 | 1.5 | 23.64 | 5.95 | 3.67 | 0.15 | 5.94 | 3.07 | 1.670 | 0.271 | 0.038 | 0.127 |
| BC3802-03 | 2.5 | 23.60 | 5.92 | 3.65 | 0.15 | 6.21 | 2.93 | 1.660 | 0.272 | 0.037 | 0.124 |
| BC3802-04 | 3.5 | 23.40 | 5.89 | 3.64 | 0.14 | 6.37 | 2.83 | 1.610 | 0.268 | 0.028 | 0.126 |
| BC3802-05 | 4.5 | 23.40 | 5.87 | 3.61 | 0.14 | 6.60 | 2.88 | 1.691 | 0.269 | 0.026 | 0.125 |
| BC3802-06 | 5.5 | 23.26 | 5.84 | 3.54 | 0.15 | 6.67 | 2.86 | 1.694 | 0.265 | 0.027 | 0.130 |
| BC3802-07 | 6.5 | 23.20 | 6.07 | 3.60 | 0.15 | 6.83 | 2.96 | 1.703 | 0.270 | 0.025 | 0.120 |
| BC3802-08 | 7.5 | 23.24 | 5.89 | 3.62 | 0.15 | 6.70 | 2.83 | 1.681 | 0.266 | 0.025 | 0.123 |
| BC3802-09 | 8.5 | 23.12 | 6.00 | 3.59 | 0.15 | 6.87 | 2.82 | 1.740 | 0.276 | 0.029 | 0.128 |
| BC3802-10 | 9.5 | 22.94 | 5.97 | 3.52 | 0.15 | 7.10 | 2.68 | 1.695 | 0.277 | 0.028 | 0.120 |
| BC3802-11 | 11.0 | 23.86 | 6.27 | 3.60 | 0.17 | 8.01 | 2.66 | 1.749 | 0.279 | 0.029 | 0.123 |
| BC3802-12 | 13.0 | 21.84 | 5.56 | 3.45 | 0.15 | 8.80 | 2.38 | 1.616 | 0.263 | 0.025 | 0.118 |
| BC3802-13 | 15.0 | 21.38 | 5.50 | 3.14 | 0.15 | 9.18 | 2.86 | 1.612 | 0.254 | 0.027 | 0.118 |
| BC3802-13A | 17.0 | 19.86 | 5.25 | 2.77 | 0.14 | 11.30 | 2.60 | 1.485 | 0.236 | 0.024 | 0.111 |
| BC3802-14 | 19.0 | 19.29 | 4.84 | 2.60 | 0.13 | 12.45 | 2.41 | 1.401 | 0.225 | 0.023 | 0.111 |
| BC3802-15 | 21.0 | 18.99 | 4.78 | 2.55 | 0.12 | 13.41 | 2.09 | 1.405 | 0.224 | 0.025 | 0.110 |
| BC3802-16 | 23.0 | 18.47 | 4.63 | 2.51 | 0.13 | 13.66 | 2.37 | 1.326 | 0.218 | 0.020 | 0.109 |
| BC3802-17 | 25.0 | 18.30 | 4.64 | 2.48 | 0.12 | 14.16 | 1.99 | 1.353 | 0.217 | 0.021 | 0.110 |
| BC3802-18 | 27.0 | 17.70 | 4.55 | 2.43 | 0.12 | 14.37 | 2.27 | 1.289 | 0.212 | 0.023 | 0.106 |
| BC3802-19 | 29.0 | 17.49 | 4.49 | 2.38 | 0.12 | 15.13 | 1.96 | 1.293 | 0.210 | 0.020 | 0.107 |
| BC3802-20 | 31.0 | 17.22 | 4.45 | 2.33 | 0.12 | 14.73 | 2.31 | 1.227 | 0.209 | 0.022 | 0.106 |
| BC3802-21 | 33.0 | 17.44 | 4.62 | 2.38 | 0.12 | 14.53 | 2.03 | 1.393 | 0.215 | 0.024 | 0.103 |
| BC3802-21A | 35.0 | 17.50 | 4.81 | 2.42 | 0.13 | 13.29 | 2.36 | 1.386 | 0.226 | 0.018 | 0.088 |
| BC3802-22 | 37.0 | 17.58 | 4.74 | 2.43 | 0.12 | 13.84 | 2.03 | 1.334 | 0.221 | 0.016 | 0.094 |
| BC3802-23 | 39.0 | 17.24 | 4.56 | 2.37 | 0.12 | 14.22 | 2.44 | 1.331 | 0.213 | 0.021 | 0.102 |
| BC3802-24 | 41.0 | 17.48 | 4.82 | 2.46 | 0.12 | 13.81 | 2.22 | 1.379 | 0.224 | 0.023 | 0.089 |
| BC3802-25 | 43.0 | 17.60 | 4.90 | 2.52 | 0.13 | 13.50 | 2.40 | 1.474 | 0.229 | 0.019 | 0.089 |
| BC3802-26 | 45.0 | 17.32 | 4.81 | 2.50 | 0.12 | 13.33 | 2.16 | 1.455 | 0.232 | 0.023 | 0.089 |
| BC3802-27 | 47.0 | 17.56 | 4.94 | 2.46 | 0.13 | 13.31 | 2.42 | 1.467 | 0.232 | 0.018 | 0.091 |
| BC3802-28 | 49.0 | 17.75 | 4.96 | 2.49 | 0.13 | 13.35 | 2.26 | 1.476 | 0.236 | 0.021 | 0.091 |
| BC3802-29 | 51.0 | 17.76 | 4.96 | 2.49 | 0.13 | 13.19 | 2.34 | 1.450 | 0.236 | 0.022 | 0.091 |
| BC3802-30 | 53.0 | 17.74 | 5.00 | 2.46 | 0.13 | 13.04 | 2.34 | 1.432 | 0.236 | 0.024 | 0.096 |

APPENDIX C.6. UNCORRECTED MAJOR ELEMENTS

| PC38-09 | 148m | | | | | | | | | | |
|---|---|---|---|---|---|---|---|---|---|---|---|
| Sample | Depth | Si | Al | Fe | Mg | Ca | Na | K | Ti | Mn | P |
| | (cm) | (wt.%) | (wt.%) | (wt.%) | (wt.%) | (wt.%) | (wt.%) | (wt.%) | (wt.%) | (wt.%) | (wt.%) |
| PC3809-01 | 4.0 | 25.14 | 5.45 | 2.41 | 0.11 | 2.03 | 3.36 | 1.278 | 0.298 | 0.021 | 0.222 |
| PC3809-02 | 13.0 | 24.94 | 5.30 | 2.08 | 0.11 | 2.26 | 3.72 | 1.200 | 0.270 | 0.022 | 0.158 |
| PC3809-03 | 23.0 | 25.16 | 7.04 | 2.56 | 0.12 | 1.77 | 3.33 | 1.480 | 0.326 | 0.029 | 0.188 |
| PC3809-04 | 34.0 | 25.45 | 6.46 | 2.37 | 0.12 | 1.48 | 3.47 | 1.411 | 0.321 | 0.025 | 0.185 |
| PC3809-05 | 43.0 | 28.04 | 6.70 | 2.48 | 0.10 | 1.92 | 2.74 | 1.536 | 0.375 | 0.034 | 0.240 |
| PC3809-06 | 53.0 | 25.21 | 5.95 | 2.49 | 0.12 | 1.47 | 3.38 | 1.357 | 0.312 | 0.028 | 0.251 |
| PC3809-07 | 62.0 | 23.53 | 5.42 | 2.15 | 0.12 | 2.19 | 3.69 | 1.150 | 0.263 | 0.018 | 0.212 |
| PC3809-08 | 73.0 | 26.66 | 6.53 | 2.42 | 0.11 | 1.46 | 2.86 | 1.450 | 0.349 | 0.031 | 0.192 |
| PC3809-09 | 84.0 | 24.46 | 7.57 | 2.92 | 0.12 | 1.12 | 3.01 | 1.657 | 0.386 | 0.029 | 0.155 |
| PC3809-10 | 94.0 | 23.82 | 6.99 | 3.13 | 0.12 | 1.39 | 3.15 | 1.555 | 0.340 | 0.030 | 0.162 |
| PC3809-11 | 104.0 | 24.61 | 6.21 | 2.32 | 0.12 | 1.14 | 3.35 | 1.390 | 0.301 | 0.022 | 0.145 |
| PC3809-12 | 113.0 | 25.85 | 7.86 | 3.07 | 0.15 | 1.23 | 2.92 | 1.749 | 0.407 | 0.033 | 0.153 |
| PC3809-13 | 124.0 | 25.72 | 6.97 | 2.47 | 0.11 | 2.00 | 2.64 | 1.541 | 0.385 | 0.030 | 0.227 |
| PC3809-14 | 134.0 | 25.71 | 5.98 | 2.31 | 0.11 | 1.94 | 3.37 | 1.327 | 0.307 | 0.024 | 0.276 |
| PC3809-15 | 144.0 | 26.14 | 5.27 | 2.11 | 0.10 | 1.65 | 3.37 | 1.217 | 0.274 | 0.020 | 0.187 |
| PC3809-16 | 152.0 | 27.42 | 5.24 | 2.22 | 0.10 | 1.66 | 3.24 | 1.234 | 0.273 | 0.019 | 0.136 |
| PC3809-17 | 165.0 | 27.28 | 5.07 | 2.08 | 0.10 | 2.32 | 3.37 | 1.175 | 0.274 | 0.022 | 0.222 |
| PC3809-18 | 174.0 | 28.93 | 6.42 | 2.25 | 0.09 | 1.87 | 2.62 | 1.477 | 0.347 | 0.029 | 0.256 |
| PC3809-19 | 185.0 | 29.95 | 5.70 | 2.02 | 0.08 | 2.41 | 2.80 | 1.328 | 0.315 | 0.028 | 0.408 |
| PC3809-20 | 194.0 | 29.44 | 5.92 | 2.03 | 0.08 | 2.96 | 2.53 | 1.356 | 0.335 | 0.034 | 0.396 |
| PC3809-21 | 205.0 | 28.39 | 6.51 | 3.00 | 0.12 | 2.71 | 2.89 | 1.511 | 0.368 | 0.047 | 0.149 |
| PC3809-22 | 214.0 | 27.74 | 5.34 | 1.86 | 0.09 | 2.29 | 2.95 | 1.247 | 0.291 | 0.023 | 0.376 |
| PC3809-23 | 224.0 | 32.32 | 5.86 | 1.71 | 0.06 | 2.91 | 2.38 | 1.387 | 0.310 | 0.027 | 0.484 |
| PC3809-24 | 234.0 | 30.59 | 5.13 | 1.93 | 0.07 | 2.82 | 2.79 | 1.195 | 0.277 | 0.022 | 0.566 |
| PC3809-25 | 243.0 | 29.59 | 3.99 | 1.77 | 0.10 | 1.64 | 3.56 | 0.985 | 0.206 | 0.021 | 0.318 |
| PC3809-26 | 257.0 | 29.41 | 4.79 | 2.06 | 0.09 | 1.70 | 3.02 | 1.157 | 0.259 | 0.022 | 0.282 |
| PC3809-27 | 267.0 | 30.08 | 4.89 | 1.78 | 0.07 | 3.77 | 2.61 | 1.205 | 0.262 | 0.026 | 0.995 |
| PC3809-28 | 273.0 | 13.86 | 2.51 | 2.85 | 0.17 | 18.00 | 1.84 | 0.676 | 0.136 | 0.018 | 5.642 |
| PC3809-29 | 284.0 | 26.90 | 5.67 | 2.70 | 0.12 | 1.99 | 3.03 | 1.293 | 0.318 | 0.033 | 0.296 |
| PC3809-30 | 294.0 | 27.72 | 4.49 | 2.07 | 0.10 | 1.86 | 3.46 | 1.080 | 0.231 | 0.020 | 0.153 |
| PC3809-31 | 304.0 | 27.42 | 5.83 | 2.75 | 0.12 | 1.37 | 3.07 | 1.317 | 0.326 | 0.035 | 0.158 |
| PC3809-32 | 314.0 | 24.67 | 5.68 | 2.57 | 0.13 | 1.55 | 3.04 | 1.274 | 0.280 | 0.027 | 0.131 |
| PC3809-33 | 324.0 | 26.41 | 5.97 | 3.00 | 0.12 | 1.60 | 2.82 | 1.333 | 0.328 | 0.031 | 0.210 |
| PC3809-34 | 335.0 | 26.96 | 5.08 | 2.49 | 0.11 | 1.42 | 3.08 | 1.151 | 0.266 | 0.028 | 0.150 |
| PC3809-35 | 344.0 | 27.28 | 4.61 | 2.50 | 0.11 | 1.34 | 3.24 | 1.058 | 0.258 | 0.021 | 0.149 |
| PC3809-36 | 355.0 | 27.62 | 3.83 | 1.77 | 0.10 | 1.94 | 3.88 | 0.930 | 0.186 | 0.020 | 0.096 |
| PC3809-37 | 364.0 | 27.02 | 3.76 | 1.87 | 0.10 | 3.05 | 3.47 | 0.903 | 0.181 | 0.018 | 0.093 |
| PC3809-38 | 375.0 | 26.73 | 5.20 | 2.40 | 0.11 | 1.60 | 3.28 | 1.231 | 0.251 | 0.026 | 0.105 |
| PC3809-39 | 384.0 | 26.63 | 5.58 | 2.81 | 0.12 | 2.59 | 2.76 | 1.247 | 0.305 | 0.033 | 0.201 |
| PC3809-40 | 394.0 | 27.70 | 4.73 | 2.14 | 0.10 | 1.85 | 3.12 | 1.120 | 0.241 | 0.025 | 0.149 |
| PC3809-41 | 404.0 | 28.58 | 5.31 | 2.41 | 0.11 | 1.19 | 2.94 | 1.257 | 0.271 | 0.029 | 0.115 |
| PC3809-42 | 416.0 | 26.28 | 4.46 | 2.08 | 0.11 | 3.16 | 3.16 | 1.035 | 0.224 | 0.018 | 0.135 |
| PC3809-43 | 424.0 | 27.99 | 4.88 | 2.13 | 0.10 | 1.19 | 3.24 | 1.185 | 0.239 | 0.025 | 0.094 |
| PC3809-44 | 434.0 | 26.91 | 5.62 | 2.59 | 0.12 | 1.22 | 2.96 | 1.344 | 0.272 | 0.027 | 0.120 |
| PC3809-45 | 444.0 | 28.08 | 4.57 | 2.28 | 0.10 | 2.39 | 3.22 | 1.080 | 0.229 | 0.025 | 0.130 |
| PC3809-46 | 453.0 | 27.63 | 5.67 | 2.65 | 0.11 | 1.62 | 2.76 | 1.281 | 0.311 | 0.028 | 0.159 |
| PC3809-47 | 465.0 | 26.75 | 5.29 | 2.62 | 0.11 | 1.95 | 2.90 | 1.222 | 0.274 | 0.029 | 0.153 |
| PC3809-48 | 474.0 | 26.20 | 4.95 | 2.21 | 0.11 | 2.71 | 3.07 | 1.203 | 0.232 | 0.021 | 0.136 |
| PC3809-49 | 483.0 | 28.54 | 5.49 | 2.64 | 0.11 | 1.43 | 2.84 | 1.306 | 0.297 | 0.028 | 0.167 |
| PC3809-50 | 493.0 | 27.38 | 5.43 | 2.62 | 0.11 | 1.60 | 2.95 | 1.347 | 0.273 | 0.036 | 0.146 |
| PC3809-51 | 504.0 | 28.60 | 5.79 | 2.75 | 0.11 | 1.63 | 2.59 | 1.386 | 0.320 | 0.032 | 0.174 |
| PC3809-52 | 515.0 | 28.22 | 5.80 | 2.72 | 0.11 | 1.45 | 2.69 | 1.423 | 0.307 | 0.031 | 0.139 |
| PC3809-53 | 525.0 | 26.67 | 5.33 | 2.42 | 0.11 | 2.18 | 3.04 | 1.303 | 0.256 | 0.028 | 0.111 |
| PC3809-54 | 536.0 | 27.65 | 4.83 | 2.24 | 0.11 | 2.87 | 3.15 | 1.177 | 0.236 | 0.028 | 0.108 |
| PC3809-55 | 544.0 | 27.62 | 5.82 | 2.86 | 0.12 | 2.08 | 2.72 | 1.388 | 0.314 | 0.032 | 0.148 |
| PC3809-56 | 553.0 | 27.22 | 5.39 | 2.75 | 0.12 | 2.62 | 3.03 | 1.268 | 0.271 | 0.035 | 0.094 |
| PC3809-57 | 564.0 | 27.76 | 4.92 | 2.50 | 0.12 | 2.51 | 3.32 | 1.145 | 0.258 | 0.032 | 0.096 |
| PC3809-58 | 574.0 | 27.41 | 4.94 | 2.57 | 0.11 | 2.74 | 3.19 | 1.231 | 0.257 | 0.033 | 0.112 |
| PC3809-59 | 585.0 | 27.51 | 4.75 | 2.42 | 0.11 | 3.55 | 3.14 | 1.153 | 0.250 | 0.031 | 0.298 |
| PC3809-60 | 594.0 | 28.23 | 4.74 | 2.34 | 0.10 | 2.66 | 3.34 | 1.191 | 0.249 | 0.031 | 0.123 |
| PC3809-61 | 605.0 | 27.15 | 5.43 | 2.81 | 0.11 | 3.09 | 2.75 | 1.312 | 0.288 | 0.036 | 0.178 |
| PC3809-62 | 615.0 | 28.16 | 4.71 | 2.28 | 0.10 | 2.90 | 3.23 | 1.212 | 0.246 | 0.033 | 0.208 |
| PC3809-63 | 625.0 | 27.87 | 5.29 | 2.66 | 0.11 | 2.82 | 3.02 | 1.284 | 0.282 | 0.037 | 0.193 |
| PC3809-64 | 635.0 | 27.39 | 5.42 | 2.76 | 0.11 | 3.07 | 2.83 | 1.299 | 0.292 | 0.038 | 0.192 |
| PC3809-65 | 646.0 | 28.29 | 4.64 | 2.21 | 0.10 | 2.47 | 3.41 | 1.120 | 0.239 | 0.029 | 0.128 |
| PC3809-66 | 654.0 | 28.96 | 4.44 | 2.13 | 0.10 | 2.24 | 3.30 | 1.072 | 0.238 | 0.031 | 0.101 |
| PC3809-67 | 664.0 | 29.04 | 4.45 | 2.12 | 0.10 | 2.40 | 3.42 | 1.093 | 0.227 | 0.025 | 0.087 |

| APPENDIX C.6. UNCORRECTED MAJOR ELEMENTS | | | | | | | | | | | |
|---|---|---|---|---|---|---|---|---|---|---|---|
| | | | | | | | | | | | |
| PC38-09 | 148m | | | | | | | | | | |
| Sample | Depth | Si | Al | Fe | Mg | Ca | Na | K | Ti | Mn | P |
| | (cm) | (wt.%) | (wt.%) | (wt.%) | (wt.%) | (wt.%) | (wt.%) | (wt.%) | (wt.%) | (wt.%) | (wt.%) |
| | | | | | | | | | | | |
| PC3809-68 | 674.0 | 28.11 | 3.88 | 2.04 | 0.09 | 2.04 | 3.23 | 1.010 | 0.212 | 0.025 | 0.077 |
| PC3809-69 | 684.0 | 28.11 | 5.29 | 2.62 | 0.11 | 2.52 | 3.11 | 1.334 | 0.271 | 0.029 | 0.111 |
| PC3809-70 | 694.0 | 27.80 | 5.68 | 2.79 | 0.12 | 2.59 | 3.03 | 1.332 | 0.293 | 0.039 | 0.112 |
| PC3809-71 | 703.0 | 27.10 | 5.61 | 2.87 | 0.12 | 2.43 | 3.13 | 1.396 | 0.281 | 0.037 | 0.092 |
| PC3809-72 | 714.0 | 27.47 | 5.10 | 2.58 | 0.11 | 2.77 | 3.21 | 1.267 | 0.267 | 0.030 | 0.129 |
| PC3809-73 | 724.0 | 27.85 | 5.63 | 2.91 | 0.12 | 2.85 | 2.96 | 1.378 | 0.300 | 0.038 | 0.183 |
| PC3809-74 | 734.0 | 26.79 | 5.68 | 2.88 | 0.12 | 3.13 | 2.87 | 1.385 | 0.302 | 0.036 | 0.187 |
| PC3809-75 | 744.0 | 28.81 | 5.46 | 2.85 | 0.11 | 2.82 | 3.31 | 1.379 | 0.275 | 0.038 | 0.151 |
| PC3809-76 | 754.0 | 27.82 | 5.01 | 2.56 | 0.10 | 2.66 | 3.22 | 1.256 | 0.259 | 0.034 | 0.097 |
| PC3809-77 | 764.0 | 26.97 | 5.70 | 2.81 | 0.11 | 3.20 | 2.76 | 1.488 | 0.294 | 0.040 | 0.126 |
| PC3809-78 | 774.0 | 27.32 | 5.84 | 2.98 | 0.11 | 3.01 | 2.65 | 1.444 | 0.317 | 0.040 | 0.132 |
| PC3809-79 | 784.0 | 27.73 | 5.56 | 2.89 | 0.11 | 2.92 | 2.74 | 1.427 | 0.297 | 0.035 | 0.123 |
| PC3809-80 | 794.0 | 27.94 | 5.60 | 2.73 | 0.11 | 2.96 | 2.69 | 1.453 | 0.298 | 0.034 | 0.143 |
| PC3809-81 | 804.0 | 28.48 | 5.35 | 2.62 | 0.10 | 2.62 | 2.77 | 1.341 | 0.291 | 0.033 | 0.177 |
| PC3809-82 | 813.0 | 28.05 | 5.56 | 3.00 | 0.12 | 3.35 | 2.69 | 1.318 | 0.305 | 0.037 | 0.290 |
| PC3809-83 | 823.0 | 28.51 | 5.42 | 2.79 | 0.10 | 2.68 | 2.68 | 1.355 | 0.295 | 0.038 | 0.193 |
| PC3809-84 | 834.0 | 28.01 | 5.62 | 2.74 | 0.10 | 2.63 | 2.65 | 1.383 | 0.305 | 0.035 | 0.157 |
| PC3809-85 | 845.0 | 29.21 | 5.67 | 2.72 | 0.11 | 2.64 | 2.85 | 1.436 | 0.293 | 0.036 | 0.185 |
| PC3809-86 | 854.0 | 28.02 | 6.41 | 3.15 | 0.12 | 2.32 | 2.74 | 1.641 | 0.329 | 0.047 | 0.096 |
| | | | | | | | | | | | |
| PC38-10 | 257m | | | | | | | | | | |
| | | | | | | | | | | | |
| PC3810-01 | 6.0 | 19.93 | 4.82 | 1.84 | 0.10 | 5.89 | 3.41 | 1.155 | 0.240 | 0.017 | 0.432 |
| PC3810-02 | 14.0 | 24.88 | 5.26 | 1.80 | 0.09 | 5.32 | 2.66 | 1.256 | 0.285 | 0.025 | 1.020 |
| PC3810-03 | 24.0 | 28.05 | 5.44 | 1.55 | 0.07 | 6.69 | 2.27 | 1.343 | 0.274 | 0.027 | 1.926 |
| PC3810-04 | 34.0 | 27.97 | 5.41 | 1.45 | 0.07 | 6.37 | 2.32 | 1.306 | 0.272 | 0.021 | 1.004 |
| PC3810-05 | 44.0 | 26.32 | 5.55 | 2.00 | 0.10 | 2.17 | 2.98 | 1.452 | 0.299 | 0.029 | 0.412 |
| PC3810-06 | 54.0 | 26.89 | 5.61 | 2.00 | 0.10 | 1.75 | 3.23 | 1.436 | 0.284 | 0.020 | 0.276 |
| PC3810-07 | 64.0 | 28.05 | 5.83 | 2.29 | 0.09 | 2.25 | 2.96 | 1.526 | 0.305 | 0.024 | 0.440 |
| PC3810-08 | 74.0 | 28.78 | 6.10 | 2.19 | 0.08 | 3.00 | 2.70 | 1.582 | 0.315 | 0.029 | 0.680 |
| PC3810-09 | 84.0 | 31.45 | 5.34 | 1.73 | 0.06 | 4.25 | 2.00 | 1.464 | 0.264 | 0.027 | 1.073 |
| PC3810-10 | 94.0 | 30.06 | 5.67 | 1.78 | 0.06 | 5.68 | 2.14 | 1.420 | 0.262 | 0.027 | 1.486 |
| PC3810-10 | 104.0 | 29.01 | 5.34 | 1.48 | 0.06 | 6.85 | 2.18 | 1.375 | 0.252 | 0.025 | 0.853 |
| PC3810-11 | 113.0 | 29.99 | 5.51 | 1.45 | 0.05 | 6.17 | 2.09 | 1.349 | 0.250 | 0.027 | 0.572 |
| PC3810-12 | 126.0 | 26.17 | 4.52 | 1.82 | 0.09 | 5.89 | 2.85 | 1.153 | 0.230 | 0.019 | 0.493 |
| PC3810-13 | 134.0 | 26.34 | 4.45 | 1.88 | 0.09 | 4.04 | 2.77 | 1.136 | 0.229 | 0.019 | 0.526 |
| PC3810-14 | 146.0 | 27.03 | 5.23 | 2.13 | 0.09 | 3.80 | 2.66 | 1.329 | 0.275 | 0.022 | 0.409 |
| PC3810-15 | 154.0 | 24.62 | 4.82 | 2.01 | 0.09 | 6.26 | 2.55 | 1.205 | 0.249 | 0.024 | 0.411 |
| PC3810-16 | 167.0 | 26.81 | 5.06 | 2.04 | 0.10 | 3.37 | 2.86 | 1.308 | 0.268 | 0.019 | 0.299 |
| PC3810-17 | 174.0 | 28.09 | 5.41 | 2.00 | 0.10 | 2.00 | 2.83 | 1.397 | 0.275 | 0.023 | 0.344 |
| PC3810-18 | 185.0 | 28.71 | 5.41 | 2.13 | 0.10 | 1.46 | 2.61 | 1.424 | 0.283 | 0.026 | 0.284 |
| PC3810-19 | 194.0 | 25.79 | 4.50 | 1.92 | 0.10 | 4.05 | 2.96 | 1.190 | 0.222 | 0.020 | 0.254 |
| PC3810-20 | 203.0 | 27.94 | 5.67 | 2.12 | 0.10 | 2.26 | 2.66 | 1.448 | 0.298 | 0.024 | 0.363 |
| PC3810-21 | 216.0 | 25.50 | 4.26 | 1.79 | 0.09 | 4.22 | 3.02 | 1.113 | 0.219 | 0.017 | 0.318 |
| PC3810-22 | 224.0 | 26.29 | 4.51 | 1.92 | 0.10 | 2.85 | 2.96 | 1.141 | 0.228 | 0.017 | 0.253 |
| PC3810-23 | 233.0 | 25.93 | 5.20 | 2.12 | 0.11 | 2.54 | 2.94 | 1.351 | 0.270 | 0.024 | 0.281 |
| PC3810-24 | 244.0 | 25.43 | 5.31 | 2.17 | 0.10 | 4.31 | 2.73 | 1.333 | 0.276 | 0.022 | 0.354 |
| PC3810-25 | 254.0 | 26.66 | 4.96 | 1.70 | 0.08 | 4.87 | 2.92 | 1.278 | 0.249 | 0.021 | 0.660 |
| PC3810-26 | 263.0 | 25.40 | 4.63 | 1.70 | 0.09 | 5.21 | 3.01 | 1.179 | 0.234 | 0.018 | 0.536 |
| PC3810-27 | 273.0 | 24.60 | 5.26 | 2.18 | 0.10 | 4.49 | 2.65 | 1.345 | 0.273 | 0.025 | 0.305 |
| PC3810-28 | 284.0 | 24.82 | 5.03 | 1.97 | 0.09 | 5.75 | 2.40 | 1.253 | 0.269 | 0.023 | 0.350 |
| PC3810-29 | 295.0 | 20.99 | 3.79 | 1.66 | 0.09 | 8.80 | 2.57 | 0.967 | 0.187 | 0.016 | 0.289 |
| PC3810-30 | 305.0 | 23.96 | 5.18 | 2.24 | 0.10 | 5.78 | 2.48 | 1.246 | 0.275 | 0.025 | 0.263 |
| PC3810-31 | 314.0 | 24.53 | 5.47 | 2.07 | 0.10 | 5.84 | 2.40 | 1.319 | 0.293 | 0.021 | 0.311 |
| PC3810-32 | 324.0 | 22.88 | 4.14 | 1.80 | 0.09 | 6.28 | 2.80 | 1.038 | 0.206 | 0.021 | 0.278 |
| PC3810-33 | 335.0 | 24.05 | 5.18 | 2.05 | 0.10 | 5.05 | 2.55 | 1.304 | 0.268 | 0.023 | 0.294 |
| PC3810-34 | 344.0 | 23.32 | 3.57 | 1.59 | 0.09 | 6.84 | 2.87 | 0.891 | 0.177 | 0.015 | 0.295 |
| PC3810-35 | 354.0 | 26.28 | 3.26 | 1.33 | 0.08 | 4.04 | 3.23 | 0.851 | 0.161 | 0.007 | 0.220 |
| PC3810-36 | 364.0 | 26.12 | 2.87 | 1.21 | 0.08 | 5.12 | 3.18 | 0.763 | 0.141 | 0.010 | 0.240 |
| PC3810-37 | 374.0 | 27.07 | 3.02 | 1.16 | 0.08 | 3.91 | 3.02 | 0.766 | 0.147 | 0.007 | 0.202 |
| PC3810-38 | 383.0 | 24.28 | 5.55 | 2.16 | 0.11 | 4.60 | 2.48 | 1.304 | 0.283 | 0.024 | 0.228 |
| PC3810-39 | 394.0 | 24.59 | 4.45 | 1.63 | 0.09 | 4.07 | 2.73 | 1.084 | 0.229 | 0.016 | 0.279 |
| PC3810-40 | 404.0 | 24.91 | 5.22 | 1.85 | 0.10 | 4.79 | 2.48 | 1.248 | 0.282 | 0.023 | 0.274 |
| PC3810-41 | 417.0 | 22.22 | 4.41 | 1.71 | 0.09 | 7.26 | 2.46 | 1.039 | 0.231 | 0.015 | 0.328 |
| PC3810-42 | 424.0 | 23.52 | 4.60 | 1.71 | 0.09 | 5.53 | 2.66 | 1.128 | 0.234 | 0.024 | 0.296 |
| PC3810-43 | 434.0 | 21.10 | 2.11 | 0.87 | 0.07 | 10.76 | 2.98 | 0.576 | 0.107 | 0.007 | 0.348 |
| PC3810-44 | 445.0 | 22.31 | 3.62 | 1.41 | 0.08 | 8.08 | 2.60 | 0.901 | 0.178 | 0.010 | 0.250 |

| APPENDIX C.6. UNCORRECTED MAJOR ELEMENTS | | | | | | | | | | | |
|---|---|---|---|---|---|---|---|---|---|---|---|
| | | | | | | | | | | | |
| PC38-10 | 257m | . | | | | | | | | | |
| Sample | Depth | Si | Al | Fe | Mg | Ca | Na | K | Ti | Mn | P |
| | (cm) | (wt.%) | (wt.%) | (wt.%) | (wt.%) | (wt.%) | (wt.%) | (wt.%) | (wt.%) | (wt.%) | (wt.%) |
| | | | | | | | | | | | |
| PC3810-45 | 456.0 | 22.80 | 3.29 | 1.30 | 0.08 | 7.17 | 2.79 | 0.808 | 0.163 | 0.011 | 0.256 |
| PC3810-46 | 467.0 | 23.74 | 2.20 | 0.90 | 0.07 | 7.22 | 3.32 | 0.614 | 0.108 | 0.003 | 0.194 |
| PC3810-47 | 476.0 | 20.82 | 4.51 | 1.71 | 0.09 | 8.15 | 2.33 | 1.086 | 0.236 | 0.019 | 0.471 |
| PC3810-48 | 484.0 | 20.41 | 4.26 | 1.66 | 0.09 | 8.77 | 2.15 | 1.019 | 0.221 | 0.014 | 0.443 |
| PC3810-49 | 494.0 | 21.11 | 4.08 | 1.43 | 0.08 | 9.06 | 2.11 | 0.946 | 0.219 | 0.017 | 0.860 |
| PC3810-50 | 504.0 | 26.75 | 5.15 | 1.57 | 0.07 | 7.77 | 2.14 | 1.263 | 0.261 | 0.020 | 2.365 |
| PC3810-51 | 514.0 | 27.91 | 5.28 | 2.61 | 0.11 | 2.42 | 2.78 | 1.254 | 0.292 | 0.029 | 0.111 |
| PC3810-52 | 524.0 | 29.30 | 5.77 | 2.74 | 0.12 | 2.12 | 2.74 | 1.364 | 0.318 | 0.036 | 0.103 |
| PC3810-53 | 534.0 | 20.55 | 4.19 | 1.65 | 0.10 | 4.67 | 2.94 | 1.005 | 0.189 | 0.015 | 0.247 |
| PC3810-54 | 545.0 | 23.37 | 4.23 | 1.63 | 0.10 | 3.62 | 2.98 | 1.069 | 0.195 | 0.016 | 0.191 |
| PC3810-55 | 554.0 | 21.37 | 3.81 | 1.52 | 0.10 | 5.12 | 3.13 | 0.940 | 0.171 | 0.015 | 0.184 |
| PC3810-56 | 564.0 | 22.38 | 3.24 | 1.40 | 0.10 | 7.20 | 3.24 | 0.825 | 0.154 | 0.017 | 0.274 |
| PC3810-57 | 574.0 | 20.44 | 3.76 | 1.58 | 0.11 | 8.19 | 2.74 | 0.903 | 0.179 | 0.017 | 0.235 |
| PC3810-58 | 584.0 | 21.97 | 3.68 | 1.56 | 0.10 | 7.03 | 3.03 | 0.959 | 0.175 | 0.020 | 0.178 |
| PC3810-59 | 596.0 | 22.56 | 3.64 | 1.53 | 0.10 | 6.20 | 3.13 | 0.946 | 0.171 | 0.014 | 0.187 |
| PC3810-60 | 604.0 | 21.47 | 3.71 | 1.60 | 0.10 | 7.57 | 3.08 | 0.974 | 0.173 | 0.018 | 0.191 |
| PC3810-61 | 614.0 | 23.34 | 4.11 | 1.74 | 0.10 | 5.41 | 2.98 | 1.035 | 0.190 | 0.016 | 0.137 |
| PC3810-62 | 624.0 | 22.62 | 4.50 | 1.86 | 0.10 | 6.37 | 2.61 | 1.170 | 0.218 | 0.021 | 0.192 |
| PC3810-63 | 634.0 | 23.00 | 4.41 | 1.79 | 0.10 | 6.38 | 3.34 | 1.138 | 0.206 | 0.020 | 0.204 |
| PC3810-64 | 645.0 | 23.75 | 4.28 | 1.86 | 0.10 | 4.88 | 3.00 | 1.072 | 0.197 | 0.025 | 0.136 |
| PC3810-65 | 655.0 | 22.66 | 4.11 | 1.76 | 0.10 | 5.43 | 3.09 | 1.043 | 0.185 | 0.016 | 0.126 |
| PC3810-66 | 667.0 | 23.38 | 4.56 | 1.92 | 0.10 | 5.23 | 2.91 | 1.186 | 0.206 | 0.020 | 0.165 |
| PC3810-67 | 674.0 | 24.01 | 5.31 | 2.17 | 0.11 | 3.99 | 2.73 | 1.370 | 0.244 | 0.025 | 0.172 |
| PC3810-68 | 683.0 | 23.92 | 4.88 | 1.97 | 0.10 | 4.65 | 2.77 | 1.283 | 0.214 | 0.021 | 0.131 |
| PC3810-69 | 694.0 | 24.98 | 6.45 | 2.60 | 0.12 | 3.20 | 2.55 | 1.683 | 0.299 | 0.027 | 0.196 |
| PC3810-70 | 704.0 | 25.80 | 7.19 | 2.53 | 0.13 | 1.80 | 2.40 | 1.932 | 0.349 | 0.034 | 0.185 |
| PC3810-71 | 714.0 | 24.38 | 6.40 | 2.48 | 0.13 | 3.74 | 2.53 | 1.734 | 0.286 | 0.028 | 0.204 |
| PC3810-72 | 724.0 | 24.57 | 5.63 | 2.21 | 0.12 | 4.45 | 2.48 | 1.474 | 0.245 | 0.029 | 0.183 |
| PC3810-74 | 734.0 | 26.68 | 6.83 | 2.33 | 0.13 | 1.54 | 2.61 | 1.831 | 0.323 | 0.024 | 0.205 |
| PC3810-75 | 745.0 | 27.01 | 7.61 | 2.76 | 0.13 | 1.55 | 2.56 | 2.019 | 0.367 | 0.036 | 0.194 |
| PC3810-76 | 754.0 | 27.22 | 6.10 | 2.31 | 0.12 | 1.81 | 2.73 | 1.616 | 0.296 | 0.028 | 0.241 |
| PC3810-77 | 764.0 | 28.41 | 6.86 | 2.34 | 0.11 | 2.58 | 2.40 | 1.788 | 0.364 | 0.032 | 0.523 |
| | | | | | | | | | | | |
| PC38-02 | 2525m | | | | | | | | | | |
| | | | | | | | | | | | |
| PC3802-01 | 8.0 | 21.89 | 5.46 | 2.89 | 1.39 | 8.34 | 2.75 | 1.428 | 0.268 | 0.026 | 0.111 |
| PC3802-02 | 18.0 | 19.96 | 4.90 | 2.53 | 1.29 | 11.25 | 2.53 | 1.316 | 0.236 | 0.027 | 0.107 |
| PC3802-03 | 28.0 | 19.13 | 4.74 | 2.46 | 1.26 | 12.17 | 2.59 | 1.223 | 0.232 | 0.022 | 0.100 |
| PC3802-04 | 38.0 | 18.93 | 5.16 | 2.56 | 1.33 | 10.25 | 2.75 | 1.404 | 0.242 | 0.023 | 0.090 |
| PC3802-05 | 48.0 | 18.41 | 5.11 | 2.51 | 1.27 | 12.16 | 2.44 | 1.349 | 0.253 | 0.023 | 0.087 |
| PC3802-06 | 57.5 | 18.44 | 4.99 | 2.64 | 1.25 | 11.79 | 2.50 | 1.358 | 0.243 | 0.025 | 0.086 |
| PC3802-07 | 70.0 | 19.09 | 5.37 | 2.60 | 1.30 | 11.92 | 1.94 | 1.360 | 0.271 | 0.026 | 0.093 |
| PC3802-08 | 79.0 | 18.71 | 5.24 | 2.65 | 1.34 | 11.54 | 2.37 | 1.384 | 0.261 | 0.022 | 0.090 |
| PC3802-09 | 89.0 | 17.49 | 4.88 | 2.47 | 1.26 | 13.04 | 2.36 | 1.277 | 0.256 | 0.023 | 0.092 |
| PC3802-10 | 100.0 | 16.59 | 4.54 | 2.30 | 1.19 | 14.16 | 2.37 | 1.191 | 0.242 | 0.022 | 0.091 |
| PC3802-11 | 110.0 | 16.80 | 4.44 | 2.24 | 1.17 | 14.39 | 2.31 | 1.181 | 0.235 | 0.026 | 0.090 |
| PC3802-12 | 120.0 | 16.06 | 4.10 | 2.23 | 1.09 | 15.16 | 2.34 | 1.129 | 0.220 | 0.021 | 0.085 |
| PC3802-13 | 130.0 | 16.76 | 4.51 | 2.46 | 1.16 | 14.19 | 2.29 | 1.158 | 0.230 | 0.023 | 0.087 |
| PC3802-14 | 139.0 | 18.42 | 5.19 | 2.47 | 1.29 | 11.80 | 2.54 | 1.376 | 0.259 | 0.027 | 0.092 |
| PC3802-15 | 150.0 | 18.88 | 5.35 | 2.65 | 1.33 | 11.30 | 2.63 | 1.436 | 0.264 | 0.026 | 0.093 |
| PC3802-16 | 160.0 | 19.99 | 5.86 | 2.85 | 1.39 | 10.46 | 2.29 | 1.570 | 0.294 | 0.029 | 0.099 |
| PC3802-17 | 171.0 | 20.72 | 5.95 | 2.87 | 1.43 | 9.14 | 2.54 | 1.631 | 0.296 | 0.027 | 0.098 |
| PC3802-18 | 181.0 | 22.07 | 5.60 | 3.15 | 1.41 | 7.93 | 2.75 | 1.595 | 0.291 | 0.030 | 0.098 |
| PC3802-19 | 191.0 | 21.46 | 5.53 | 3.00 | 1.40 | 8.59 | 2.63 | 1.528 | 0.284 | 0.029 | 0.098 |
| PC3802-20 | 201.0 | 22.15 | 5.86 | 3.00 | 1.47 | 7.46 | 2.77 | 1.616 | 0.304 | 0.028 | 0.098 |
| PC3802-21 | 211.0 | 21.14 | 5.97 | 3.01 | 1.45 | 8.41 | 2.60 | 1.606 | 0.302 | 0.029 | 0.098 |
| PC3802-22 | 221.0 | 21.07 | 5.91 | 2.99 | 1.46 | 8.94 | 2.60 | 1.597 | 0.297 | 0.029 | 0.098 |
| PC3802-23 | 231.0 | 21.78 | 6.22 | 3.08 | 1.51 | 7.99 | 2.63 | 1.686 | 0.318 | 0.032 | 0.101 |
| PC3802-24 | 241.0 | 24.82 | 6.91 | 3.42 | 1.68 | 4.18 | 2.91 | 1.942 | 0.355 | 0.033 | 0.106 |
| PC3802-25 | 251.0 | 23.44 | 6.27 | 3.23 | 1.56 | 5.76 | 2.77 | 1.716 | 0.331 | 0.030 | 0.112 |
| PC3802-26 | 261.0 | 21.76 | 5.62 | 2.97 | 1.41 | 8.32 | 2.63 | 1.547 | 0.297 | 0.028 | 0.114 |
| PC3802-27 | 271.0 | 24.69 | 6.59 | 3.34 | 1.59 | 4.41 | 2.89 | 1.875 | 0.333 | 0.032 | 0.111 |
| PC3802-28 | 281.0 | 24.30 | 6.63 | 3.33 | 1.55 | 4.92 | 2.77 | 1.907 | 0.327 | 0.028 | 0.108 |
| PC3802-29 | 291.0 | 25.76 | 7.19 | 3.50 | 1.66 | 2.76 | 2.85 | 2.048 | 0.354 | 0.031 | 0.107 |
| PC3802-30 | 301.0 | 25.54 | 6.95 | 3.52 | 1.65 | 3.59 | 2.80 | 1.962 | 0.355 | 0.033 | 0.125 |
| PC3802-31 | 312.0 | 24.40 | 6.20 | 3.21 | 1.54 | 5.92 | 2.73 | 1.705 | 0.321 | 0.029 | 0.124 |
| PC3802-32 | 322.0 | 23.88 | 6.32 | 3.29 | 1.60 | 5.77 | 2.71 | 1.766 | 0.321 | 0.032 | 0.118 |

| APPENDIX C.6. UNCORRECTED MAJOR ELEMENTS | | | | | | | | | | | |
|---|---|---|---|---|---|---|---|---|---|---|---|
| PC38-02 | 2525m | | | | | | | | | | |
| Sample | Depth | Si | Al | Fe | Mg | Ca | Na | K | Ti | Mn | P |
| | (cm) | (wt.%) | (wt.%) | (wt.%) | (wt.%) | (wt.%) | (wt.%) | (wt.%) | (wt.%) | (wt.%) | (wt.%) |
| PC3802-33 | 332.0 | 23.85 | 6.32 | 3.51 | 1.55 | 5.75 | 2.64 | 1.771 | 0.314 | 0.033 | 0.104 |
| PC3802-34 | 342.0 | 23.94 | 6.22 | 3.49 | 1.58 | 5.84 | 2.75 | 1.720 | 0.303 | 0.028 | 0.109 |
| PC3802-35 | 352.0 | 21.62 | 5.38 | 2.71 | 1.33 | 9.24 | 2.59 | 1.492 | 0.249 | 0.027 | 0.096 |
| PC3802-36 | 362.0 | 19.26 | 5.24 | 2.67 | 1.29 | 11.60 | 2.41 | 1.384 | 0.241 | 0.028 | 0.085 |
| PC3802-37 | 372.0 | 18.43 | 5.27 | 2.65 | 1.28 | 12.71 | 2.34 | 1.374 | 0.246 | 0.026 | 0.079 |
| PC3802-38 | 381.0 | 18.01 | 5.08 | 2.62 | 1.27 | 13.38 | 2.18 | 1.406 | 0.251 | 0.025 | 0.079 |
| PC3802-39 | 391.0 | 17.91 | 4.94 | 2.53 | 1.24 | 13.50 | 2.14 | 1.342 | 0.248 | 0.023 | 0.080 |
| PC3802-40 | 400.0 | 17.43 | 4.76 | 2.42 | 1.21 | 14.52 | 2.21 | 1.311 | 0.239 | 0.025 | 0.083 |
| PC3802-41 | 410.0 | 17.57 | 4.88 | 2.40 | 1.18 | 14.25 | 2.26 | 1.344 | 0.240 | 0.026 | 0.083 |
| PC3802-42 | 420.0 | 18.15 | 4.87 | 2.44 | 1.18 | 13.69 | 2.30 | 1.355 | 0.238 | 0.024 | 0.080 |
| PC3802-43 | 430.0 | 16.99 | 4.80 | 2.40 | 1.19 | 14.55 | 2.14 | 1.265 | 0.239 | 0.026 | 0.080 |
| PC3802-44 | 440.0 | 17.98 | 4.99 | 2.46 | 1.23 | 13.69 | 2.21 | 1.392 | 0.254 | 0.024 | 0.084 |
| PC3802-45 | 450.0 | 19.30 | 5.46 | 2.79 | 1.35 | 11.53 | 2.34 | 1.434 | 0.270 | 0.027 | 0.085 |
| PC3802-46 | 460.0 | 19.95 | 5.81 | 2.88 | 1.40 | 10.34 | 2.54 | 1.629 | 0.288 | 0.029 | 0.088 |
| PC3802-47 | 470.0 | 17.05 | 4.97 | 2.53 | 1.22 | 14.73 | 2.13 | 1.232 | 0.243 | 0.024 | 0.088 |
| PC3802-48 | 481.0 | 16.59 | 4.70 | 2.44 | 1.17 | 15.19 | 1.90 | 0.932 | 0.243 | 0.025 | 0.086 |
| PC3802-49 | 491.0 | 17.11 | 4.78 | 2.46 | 1.18 | 14.91 | 2.09 | 1.328 | 0.240 | 0.021 | 0.087 |
| PC3802-50 | 501.0 | 18.07 | 5.06 | 2.72 | 1.24 | 13.95 | 2.26 | 1.396 | 0.246 | 0.029 | 0.094 |
| PC3802-51 | 511.0 | 19.18 | 5.28 | 2.58 | 1.24 | 12.41 | 2.25 | 1.434 | 0.263 | 0.027 | 0.090 |
| PC3802-52 | 521.0 | 20.96 | 5.83 | 2.88 | 1.30 | 10.04 | 2.51 | 1.727 | 0.266 | 0.029 | 0.093 |
| PC3802-53 | 531.0 | 25.00 | 6.53 | 2.48 | 1.11 | 8.02 | 2.82 | 2.248 | 0.251 | 0.029 | 0.085 |
| PC3802-54 | 540.0 | 23.41 | 6.80 | 3.42 | 1.60 | 5.95 | 2.64 | 1.938 | 0.338 | 0.034 | 0.109 |
| PC3802-55 | 550.0 | 23.45 | 6.74 | 3.58 | 1.62 | 5.51 | 2.62 | 1.872 | 0.338 | 0.033 | 0.110 |
| PC3802-56 | 560.0 | 23.26 | 6.40 | 3.98 | 1.60 | 4.33 | 2.63 | 1.829 | 0.333 | 0.032 | 0.110 |
| PC3802-57 | 572.0 | 22.46 | 6.05 | 3.38 | 1.58 | 7.48 | 2.92 | 1.704 | 0.291 | 0.029 | 0.108 |
| PC3802-58 | 582.0 | 21.90 | 6.28 | 3.31 | 1.50 | 7.92 | 2.57 | 1.753 | 0.294 | 0.031 | 0.100 |
| PC3802-59 | 591.0 | 21.31 | 6.34 | 3.35 | 1.51 | 8.57 | 2.47 | 1.720 | 0.294 | 0.030 | 0.096 |
| PC3802-60 | 601.0 | 16.48 | 4.75 | 2.60 | 1.19 | 15.46 | 2.00 | 1.196 | 0.237 | 0.023 | 0.093 |
| PC3802-61 | 611.0 | 16.47 | 4.64 | 2.50 | 1.21 | 16.15 | 2.12 | 1.310 | 0.227 | 0.026 | 0.091 |
| PC3802-62 | 621.0 | 17.99 | 5.12 | 2.74 | 1.30 | 13.80 | 2.14 | 1.424 | 0.264 | 0.028 | 0.091 |
| PC3802-63 | 631.0 | 18.41 | 5.41 | 2.79 | 1.33 | 13.11 | 2.14 | 1.453 | 0.273 | 0.029 | 0.091 |
| PC3802-64 | 641.0 | 20.58 | 6.05 | 3.05 | 1.45 | 11.13 | 2.26 | 1.631 | 0.292 | 0.030 | 0.098 |
| PC3802-65 | 651.0 | 22.17 | 6.40 | 3.14 | 1.53 | 7.83 | 2.45 | 1.836 | 0.303 | 0.029 | 0.098 |
| PC3802-66 | 662.0 | 21.95 | 5.87 | 3.12 | 1.47 | 8.36 | 2.66 | 1.698 | 0.284 | 0.029 | 0.108 |
| PC3802-67 | 671.0 | 17.57 | 4.52 | 2.25 | 1.16 | 14.03 | 2.29 | 1.273 | 0.209 | 0.024 | 0.090 |
| PC3802-68 | 681.0 | 18.03 | 5.15 | 2.49 | 1.24 | 13.24 | 2.21 | 1.466 | 0.242 | 0.026 | 0.082 |
| PC3802-69 | 691.0 | 19.01 | 5.67 | 2.65 | 1.29 | 11.69 | 2.31 | 1.573 | 0.267 | 0.028 | 0.076 |
| PC3802-70 | 701.0 | 18.63 | 5.44 | 2.49 | 1.26 | 12.39 | 2.17 | 1.514 | 0.260 | 0.026 | 0.074 |
| PC3802-71 | 711.0 | 19.54 | 5.49 | 2.74 | 1.41 | 12.64 | 2.35 | 1.503 | 0.256 | 0.026 | 0.076 |
| PC3802-72 | 721.0 | 19.33 | 5.27 | 2.53 | 1.29 | 11.85 | 2.28 | 1.514 | 0.257 | 0.026 | 0.078 |
| PC3802-73 | 731.0 | 19.23 | 5.35 | 2.52 | 1.28 | 11.89 | 2.23 | 1.528 | 0.261 | 0.029 | 0.080 |
| PC3802-74 | 741.0 | 19.39 | 5.38 | 2.56 | 1.31 | 11.28 | 2.26 | 1.505 | 0.270 | 0.029 | 0.084 |
| PC38-11 | 3835m | | | | | | | | | | |
| PC3811-01 | 3.0 | 25.82 | 6.77 | 2.32 | 1.27 | 1.85 | 2.68 | 1.66 | 0.36 | 0.03 | 0.30 |
| PC3811-02 | 13.0 | 23.34 | 5.74 | 2.44 | 1.06 | 5.76 | 2.49 | 1.29 | 0.32 | 0.03 | 0.36 |
| PC3811-03 | 23.0 | 25.78 | 5.87 | 2.37 | 0.98 | 5.00 | 2.38 | 1.39 | 0.35 | 0.03 | 0.35 |
| PC3811-04 | 33.0 | 26.71 | 6.99 | 2.53 | 1.48 | 1.46 | 2.80 | 1.82 | 0.35 | 0.03 | 0.19 |
| PC3811-05 | 43.0 | 25.84 | 6.87 | 2.32 | 1.45 | 2.27 | 2.84 | 1.78 | 0.34 | 0.03 | 0.16 |
| PC3811-06 | 53.0 | 24.50 | 6.72 | 2.74 | 1.34 | 2.83 | 2.66 | 1.74 | 0.33 | 0.03 | 0.13 |
| PC3811-07 | 63.0 | 24.81 | 6.89 | 2.65 | 1.37 | 2.99 | 2.74 | 1.79 | 0.33 | 0.03 | 0.12 |
| PC3811-08 | 73.0 | 24.33 | 6.79 | 2.73 | 1.35 | 3.49 | 2.61 | 1.75 | 0.33 | 0.03 | 0.13 |
| PC3811-09 | 85.0 | 27.78 | 6.97 | 2.62 | 1.15 | 5.14 | 2.67 | 1.77 | 0.31 | 0.04 | 0.26 |
| PC3811-10 | 95.0 | 24.13 | 6.42 | 2.68 | 1.40 | 4.49 | 2.61 | 1.71 | 0.32 | 0.03 | 0.13 |
| PC3811-11 | 105.0 | 23.45 | 6.17 | 2.72 | 1.36 | 4.93 | 2.57 | 1.61 | 0.31 | 0.03 | 0.13 |
| PC3811-12 | 116.0 | 24.40 | 6.32 | 2.82 | 1.37 | 3.97 | 2.59 | 1.64 | 0.31 | 0.03 | 0.13 |
| PC3811-13 | 125.0 | 24.26 | 6.50 | 2.76 | 1.42 | 4.07 | 2.63 | 1.75 | 0.32 | 0.03 | 0.13 |
| PC3811-14 | 135.0 | 24.12 | 6.47 | 2.73 | 1.37 | 4.56 | 2.58 | 1.65 | 0.33 | 0.03 | 0.15 |
| PC3811-15 | 145.0 | 25.42 | 6.86 | 2.72 | 1.53 | 4.03 | 2.83 | 1.75 | 0.33 | 0.03 | 0.14 |
| PC3811-16 | 155.0 | 23.67 | 6.26 | 2.63 | 1.30 | 5.26 | 2.49 | 1.58 | 0.32 | 0.03 | 0.16 |
| PC3811-17 | 165.0 | 25.62 | 6.99 | 2.84 | 1.56 | 4.49 | 2.92 | 1.78 | 0.32 | 0.03 | 0.14 |
| PC3811-18 | 175.0 | 24.96 | 6.47 | 2.70 | 1.25 | 5.31 | 2.53 | 1.71 | 0.32 | 0.03 | 0.22 |
| PC3811-19 | 186.0 | 24.30 | 6.54 | 2.46 | 1.36 | 3.46 | 2.60 | 1.76 | 0.32 | 0.03 | 0.14 |
| PC3811-20 | 197.0 | 24.22 | 6.69 | 2.84 | 1.42 | 3.16 | 2.60 | 1.73 | 0.33 | 0.03 | 0.14 |
| PC3811-21 | 204.0 | 24.64 | 6.78 | 2.79 | 1.40 | 2.41 | 2.70 | 1.83 | 0.32 | 0.03 | 0.13 |
| PC3811-22 | 215.0 | 22.79 | 6.05 | 2.74 | 1.28 | 5.52 | 2.62 | 1.58 | 0.30 | 0.03 | 0.18 |

APPENDIX C.6. UNCORRECTED MAJOR ELEMENTS

| PC38-11 | 3835m | | | | | | | | | | |
|---|---|---|---|---|---|---|---|---|---|---|---|
| Sample | Depth | Si | Al | Fe | Mg | Ca | Na | K | Ti | Mn | P |
| | (cm) | (wt.%) | (wt.%) | (wt.%) | (wt.%) | (wt.%) | (wt.%) | (wt.%) | (wt.%) | (wt.%) | (wt.%) |
| PC3811-23 | 225.0 | 23.05 | 6.20 | 2.83 | 1.37 | 4.89 | 2.73 | 1.61 | 0.30 | 0.03 | 0.14 |
| PC3811-24 | 235.0 | 22.94 | 6.34 | 2.79 | 1.33 | 4.44 | 2.51 | 1.62 | 0.31 | 0.03 | 0.14 |
| PC3811-25 | 245.0 | 23.24 | 6.37 | 2.77 | 1.40 | 4.75 | 2.63 | 1.63 | 0.30 | 0.03 | 0.15 |
| PC3811-26 | 255.0 | 22.39 | 5.57 | 2.78 | 1.18 | 6.36 | 2.42 | 1.42 | 0.27 | 0.02 | 0.14 |
| PC3811-27 | 265.0 | 23.41 | 5.63 | 2.58 | 1.23 | 5.59 | 2.45 | 1.46 | 0.27 | 0.02 | 0.14 |
| PC3811-28 | 275.0 | 24.10 | 5.93 | 2.65 | 1.23 | 4.66 | 2.44 | 1.50 | 0.29 | 0.02 | 0.15 |
| PC3811-29 | 285.0 | 25.41 | 7.17 | 2.64 | 1.34 | 1.88 | 2.60 | 1.97 | 0.35 | 0.03 | 0.15 |
| PC3811-30 | 297.0 | 25.29 | 7.10 | 2.84 | 1.33 | 2.55 | 2.37 | 1.88 | 0.35 | 0.03 | 0.15 |
| PC3811-31 | 305.0 | 26.32 | 7.36 | 2.70 | 1.36 | 1.51 | 2.48 | 2.02 | 0.37 | 0.03 | 0.15 |
| PC3811-32 | 315.0 | 26.88 | 7.66 | 2.64 | 1.40 | 1.60 | 2.53 | 2.02 | 0.37 | 0.03 | 0.19 |
| PC3811-33 | 325.0 | 22.90 | 5.25 | 2.15 | 0.95 | 8.93 | 1.87 | 1.31 | 0.27 | 0.02 | 0.43 |
| PC3811-34 | 335.0 | 26.31 | 6.41 | 2.62 | 1.27 | 1.77 | 2.49 | 1.76 | 0.32 | 0.02 | 0.14 |
| PC3811-35 | 345.0 | 26.01 | 6.37 | 2.63 | 1.28 | 2.02 | 2.56 | 1.72 | 0.31 | 0.02 | 0.14 |
| PC3811-36 | 355.0 | 26.89 | 6.08 | 2.25 | 1.25 | 1.88 | 2.68 | 1.62 | 0.30 | 0.02 | 0.15 |
| PC3811-37 | 365.0 | 26.04 | 6.34 | 2.45 | 1.27 | 1.81 | 2.66 | 1.66 | 0.31 | 0.02 | 0.15 |
| PC3811-38 | 375.0 | 24.82 | 6.52 | 2.98 | 1.28 | 2.21 | 2.47 | 1.71 | 0.32 | 0.02 | 0.13 |
| PC3811-39 | 385.0 | 24.92 | 7.08 | 2.79 | 1.39 | 2.30 | 2.45 | 1.88 | 0.36 | 0.03 | 0.15 |
| PC3811-40 | 395.0 | 25.34 | 7.25 | 3.04 | 1.48 | 2.61 | 2.48 | 1.89 | 0.36 | 0.03 | 0.15 |
| PC3811-41 | 405.0 | 24.00 | 6.95 | 2.97 | 1.44 | 2.59 | 2.42 | 1.84 | 0.35 | 0.03 | 0.15 |
| PC3811-42 | 415.0 | 27.83 | 7.65 | 3.08 | 1.53 | 1.20 | 2.64 | 2.03 | 0.37 | 0.03 | 0.15 |
| PC3811-43 | 425.0 | 24.56 | 6.50 | 2.71 | 1.32 | 1.67 | 2.46 | 1.80 | 0.34 | 0.02 | 0.15 |
| PC3811-44 | 435.0 | 26.89 | 6.44 | 2.65 | 1.42 | 3.50 | 2.59 | 1.61 | 0.30 | 0.03 | 0.19 |
| PC3811-45 | 445.0 | 26.43 | 6.28 | 2.46 | 1.28 | 2.58 | 2.54 | 1.61 | 0.31 | 0.02 | 0.17 |
| PC3811-46 | 455.0 | 26.64 | 7.25 | 2.58 | 1.47 | 1.20 | 2.57 | 1.96 | 0.37 | 0.03 | 0.17 |
| PC3811-47 | 465.0 | 26.00 | 7.47 | 2.84 | 1.47 | 1.14 | 2.60 | 2.01 | 0.37 | 0.02 | 0.16 |
| PC3811-48 | 475.0 | 27.03 | 7.28 | 3.17 | 1.48 | 2.22 | 2.60 | 1.87 | 0.34 | 0.03 | 0.17 |
| PC3811-49 | 485.0 | 26.72 | 7.29 | 3.12 | 1.44 | 1.18 | 2.63 | 1.95 | 0.35 | 0.03 | 0.15 |
| PC3811-50 | 495.0 | 26.94 | 7.00 | 3.08 | 1.41 | 1.14 | 2.58 | 1.87 | 0.34 | 0.03 | 0.16 |
| PC3811-51 | 505.0 | 27.82 | 7.08 | 2.83 | 1.44 | 1.09 | 2.63 | 1.90 | 0.34 | 0.02 | 0.15 |
| PC3811-52 | 515.0 | 27.37 | 6.92 | 3.02 | 1.40 | 1.11 | 2.54 | 1.90 | 0.34 | 0.03 | 0.16 |
| PC3811-53 | 525.0 | 28.61 | 6.95 | 2.84 | 1.44 | 1.04 | 2.66 | 1.90 | 0.34 | 0.03 | 0.14 |
| PC3811-54 | 535.0 | 26.53 | 6.40 | 3.00 | 1.31 | 1.12 | 2.44 | 1.84 | 0.34 | 0.03 | 0.16 |
| PC3811-55 | 545.0 | 28.18 | 6.69 | 3.37 | 1.40 | 1.35 | 2.54 | 1.81 | 0.33 | 0.03 | 0.17 |
| PC3811-56 | 555.0 | 28.66 | 6.67 | 2.70 | 1.41 | 1.14 | 2.64 | 1.79 | 0.33 | 0.02 | 0.17 |
| PC3811-57 | 565.0 | 27.31 | 6.38 | 2.71 | 1.36 | 1.30 | 2.57 | 1.75 | 0.33 | 0.02 | 0.18 |

| APPENDIX C.7. SALT-CORRECTED MAJOR ELEMENTS | | | | | | | | | | |
|---|---|---|---|---|---|---|---|---|---|---|
| | | | | | | | | | | |
| BC38-02 | 2530m | | | | | | | | | |
| Sample | Depth | Al | Si | Fe | Ca | Na | K | P | Mn | Ti |
| | (cm) | (wt.%) | (wt.%) | (wt.%) | (wt.%) | (wt.%) | (wt.%) | (wt.%) | (wt.%) | (wt.%) |
| | | | | | | | | | | |
| BC3802-01 | 0.5 | 6.49 | 25.85 | 4.02 | 6.73 | 0.72 | 1.707 | 0.147 | 0.043 | 0.297 |
| BC3802-02 | 1.5 | 6.58 | 26.12 | 4.05 | 6.45 | 0.49 | 1.741 | 0.140 | 0.042 | 0.299 |
| BC3802-03 | 2.5 | 6.38 | 25.45 | 3.94 | 6.61 | 0.94 | 1.710 | 0.134 | 0.040 | 0.293 |
| BC3802-04 | 3.5 | 6.35 | 25.23 | 3.92 | 6.78 | 0.83 | 1.656 | 0.136 | 0.030 | 0.289 |
| BC3802-05 | 4.5 | 6.35 | 25.33 | 3.91 | 7.05 | 0.79 | 1.747 | 0.135 | 0.028 | 0.291 |
| BC3802-06 | 5.5 | 6.24 | 24.86 | 3.78 | 7.05 | 1.09 | 1.740 | 0.139 | 0.029 | 0.283 |
| BC3802-07 | 6.5 | 6.43 | 24.58 | 3.81 | 7.17 | 1.42 | 1.743 | 0.127 | 0.027 | 0.286 |
| BC3802-08 | 7.5 | 6.21 | 24.52 | 3.82 | 7.01 | 1.39 | 1.716 | 0.130 | 0.026 | 0.281 |
| BC3802-09 | 8.5 | 6.33 | 24.38 | 3.79 | 7.18 | 1.39 | 1.778 | 0.135 | 0.031 | 0.291 |
| BC3802-10 | 9.5 | 6.29 | 24.18 | 3.71 | 7.42 | 1.25 | 1.730 | 0.127 | 0.029 | 0.292 |
| BC3802-11 | 11.0 | 6.61 | 25.17 | 3.80 | 8.39 | 1.21 | 1.788 | 0.130 | 0.031 | 0.294 |
| BC3802-12 | 13.0 | 5.86 | 23.03 | 3.64 | 9.22 | 0.93 | 1.647 | 0.124 | 0.026 | 0.277 |
| BC3802-13 | 15.0 | 5.79 | 22.51 | 3.31 | 9.60 | 1.48 | 1.642 | 0.124 | 0.028 | 0.267 |
| BC3802-13A | 17.0 | 5.51 | 20.84 | 2.91 | 11.80 | 1.29 | 1.507 | 0.116 | 0.025 | 0.248 |
| BC3802-14 | 19.0 | 5.06 | 20.15 | 2.72 | 12.96 | 1.21 | 1.417 | 0.116 | 0.024 | 0.235 |
| BC3802-15 | 21.0 | 4.99 | 19.82 | 2.66 | 13.95 | 0.89 | 1.420 | 0.115 | 0.026 | 0.234 |
| BC3802-16 | 23.0 | 4.84 | 19.29 | 2.62 | 14.21 | 1.18 | 1.338 | 0.114 | 0.021 | 0.228 |
| BC3802-17 | 25.0 | 4.84 | 19.10 | 2.59 | 14.73 | 0.80 | 1.366 | 0.115 | 0.022 | 0.226 |
| BC3802-18 | 27.0 | 4.75 | 18.46 | 2.54 | 14.94 | 1.10 | 1.299 | 0.111 | 0.024 | 0.221 |
| BC3802-19 | 29.0 | 4.69 | 18.29 | 2.49 | 15.77 | 0.72 | 1.304 | 0.112 | 0.021 | 0.220 |
| BC3802-20 | 31.0 | 4.65 | 18.00 | 2.44 | 15.34 | 1.10 | 1.235 | 0.111 | 0.023 | 0.218 |
| BC3802-21 | 33.0 | 4.83 | 18.25 | 2.49 | 15.15 | 0.76 | 1.409 | 0.108 | 0.025 | 0.225 |
| BC3802-21A | 35.0 | 5.04 | 18.33 | 2.53 | 13.87 | 1.08 | 1.402 | 0.092 | 0.019 | 0.237 |
| BC3802-22 | 37.0 | 4.96 | 18.41 | 2.54 | 14.44 | 0.75 | 1.347 | 0.098 | 0.017 | 0.231 |
| BC3802-23 | 39.0 | 4.78 | 18.07 | 2.48 | 14.85 | 1.16 | 1.344 | 0.107 | 0.022 | 0.223 |
| BC3802-24 | 41.0 | 5.05 | 18.30 | 2.58 | 14.40 | 0.96 | 1.394 | 0.093 | 0.024 | 0.235 |
| BC3802-25 | 43.0 | 5.13 | 18.43 | 2.64 | 14.09 | 1.13 | 1.494 | 0.093 | 0.020 | 0.240 |
| BC3802-26 | 45.0 | 5.04 | 18.15 | 2.62 | 13.92 | 0.86 | 1.474 | 0.093 | 0.024 | 0.243 |
| BC3802-27 | 47.0 | 5.17 | 18.40 | 2.58 | 13.89 | 1.15 | 1.487 | 0.095 | 0.019 | 0.243 |
| BC3802-28 | 49.0 | 5.19 | 18.58 | 2.61 | 13.92 | 1.00 | 1.496 | 0.095 | 0.022 | 0.247 |
| BC3802-29 | 51.0 | 5.19 | 18.58 | 2.60 | 13.75 | 1.10 | 1.468 | 0.095 | 0.023 | 0.247 |
| BC3802-30 | 53.0 | 5.24 | 18.59 | 2.58 | 13.61 | 1.06 | 1.450 | 0.101 | 0.025 | 0.247 |
| | | | | | | | | | | |
| BC38-03 | 4289m | | | | | | | | | |
| | | | | | | | | | | |
| BC3803-01 | 0.5 | 7.18 | 31.80 | 4.37 | 1.03 | 0.04 | 1.792 | 0.130 | 0.090 | 0.331 |
| BC3803-02 | 1.5 | 6.96 | 30.93 | 4.42 | 1.00 | 0.49 | 1.781 | 0.127 | 0.071 | 0.325 |
| BC3803-03 | 2.5 | 6.97 | 30.94 | 4.46 | 1.00 | 0.34 | 1.794 | 0.126 | 0.050 | 0.326 |
| BC3803-04 | 3.5 | 6.80 | 30.18 | 4.04 | 1.00 | 1.14 | 1.742 | 0.112 | 0.029 | 0.317 |
| BC3803-05 | 4.5 | 7.20 | 31.20 | 3.64 | 1.02 | 1.10 | 1.870 | 0.102 | 0.025 | 0.330 |
| BC3803-06 | 5.5 | 7.04 | 30.48 | 2.98 | 1.01 | 1.04 | 1.853 | 0.099 | 0.028 | 0.328 |
| BC3803-07 | 6.5 | 6.97 | 30.17 | 2.94 | 1.01 | 1.38 | 1.863 | 0.096 | 0.026 | 0.328 |
| BC3803-08 | 7.5 | 7.09 | 30.29 | 3.08 | 1.02 | 1.41 | 1.876 | 0.094 | 0.023 | 0.331 |
| BC3803-09 | 8.5 | 7.12 | 30.45 | 3.18 | 1.04 | 1.18 | 1.894 | 0.095 | 0.025 | 0.333 |
| BC3803-10 | 9.5 | 7.55 | 31.45 | 3.35 | 1.07 | 1.48 | 1.922 | 0.097 | 0.031 | 0.343 |
| BC3803-11 | 11.0 | 7.33 | 30.41 | 3.26 | 1.06 | 1.56 | 1.919 | 0.098 | 0.029 | 0.342 |
| BC3803-12 | 13.0 | 7.39 | 30.51 | 3.03 | 1.09 | 1.11 | 1.945 | 0.097 | 0.029 | 0.352 |
| BC3803-13 | 15.0 | 7.20 | 29.89 | 3.31 | 1.09 | 1.62 | 1.944 | 0.099 | 0.032 | 0.343 |
| BC3803-14 | 17.0 | 7.36 | 30.67 | 3.14 | 1.13 | 1.15 | 1.968 | 0.103 | 0.029 | 0.356 |
| BC3803-15 | 19.0 | 7.33 | 30.22 | 3.04 | 1.16 | 1.57 | 1.944 | 0.106 | 0.032 | 0.351 |
| BC3803-16 | 21.0 | 7.00 | 30.47 | 2.85 | 1.11 | 1.33 | 1.865 | 0.101 | 0.024 | 0.337 |
| BC3803-17 | 23.0 | 7.03 | 30.40 | 3.16 | 1.11 | 1.53 | 1.881 | 0.103 | 0.027 | 0.335 |
| BC3803-18 | 25.0 | 7.10 | 30.30 | 2.92 | 1.15 | 1.24 | 1.896 | 0.106 | 0.030 | 0.344 |
| BC3803-19 | 27.0 | 6.91 | 29.85 | 3.01 | 1.16 | 1.69 | 1.857 | 0.105 | 0.029 | 0.337 |
| BC3803-20 | 29.0 | 7.20 | 30.46 | 3.14 | 1.20 | 1.29 | 1.934 | 0.109 | 0.034 | 0.349 |
| BC3803-21 | 31.0 | 7.04 | 29.97 | 3.25 | 1.20 | 1.84 | 1.950 | 0.106 | 0.036 | 0.342 |
| BC3803-22 | 33.0 | 7.09 | 30.18 | 3.04 | 1.22 | 1.55 | 1.915 | 0.109 | 0.030 | 0.343 |
| BC3803-23 | 35.0 | 6.99 | 29.96 | 2.97 | 1.23 | 1.67 | 1.919 | 0.107 | 0.030 | 0.340 |
| BC3803-24 | 37.0 | 7.28 | 30.82 | 3.27 | 1.31 | 1.64 | 1.970 | 0.111 | 0.033 | 0.347 |
| BC3803-25 | 39.0 | 7.33 | 31.42 | 3.31 | 1.37 | 1.62 | 1.994 | 0.149 | 0.036 | 0.347 |
| BC3803-26 | 41.0 | 7.03 | 30.31 | 3.22 | 1.30 | 1.29 | 1.962 | 0.107 | 0.033 | 0.345 |
| BC3803-27 | 43.0 | 7.09 | 30.21 | 3.33 | 1.33 | 1.73 | 1.972 | 0.108 | 0.032 | 0.344 |
| BC3803-28 | 45.0 | 6.98 | 30.12 | 3.14 | 1.31 | 1.44 | 1.949 | 0.108 | 0.028 | 0.340 |
| BC3803-29 | 47.0 | 6.95 | 30.01 | 3.30 | 1.31 | 1.61 | 1.971 | 0.108 | 0.033 | 0.340 |
| BC3803-30 | 49.0 | 7.04 | 30.31 | 3.29 | 1.33 | 1.31 | 1.977 | 0.110 | 0.031 | 0.342 |
| BC3803-31 | 51.0 | 7.22 | 30.51 | 3.52 | 1.36 | 1.53 | 2.031 | 0.116 | 0.031 | 0.351 |
| BC3803-32 | 53.0 | 7.09 | 29.79 | 3.29 | 1.38 | 1.64 | 1.984 | 0.112 | 0.032 | 0.347 |

| APPENDIX C.7. SALT-CORRECTED MAJOR ELEMENTS | | | | | | | | | | |
|---|---|---|---|---|---|---|---|---|---|---|
| | | | | | | | | | | |
| PC38-09 | 148m | | | | | | | | | |
| Sample | Depth | Al | Si | Fe | Ca | Na | K | P | Mn | Ti |
| | (cm) | (wt.%) | (wt.%) | (wt.%) | (wt.%) | (wt.%) | (wt.%) | (wt.%) | (wt.%) | (wt.%) |
| | | | | | | | | | | |
| PC3809-01 | 4.0 | 5.88 | 27.14 | 2.60 | 2.10 | 1.37 | 1.299 | 0.240 | 0.023 | 0.322 |
| PC3809-02 | 13.0 | 5.91 | 27.83 | 2.32 | 2.40 | 0.98 | 1.225 | 0.176 | 0.024 | 0.301 |
| PC3809-03 | 23.0 | 7.54 | 26.93 | 2.74 | 1.82 | 1.55 | 1.512 | 0.201 | 0.031 | 0.349 |
| PC3809-04 | 34.0 | 6.94 | 27.32 | 2.54 | 1.51 | 1.63 | 1.439 | 0.199 | 0.027 | 0.345 |
| PC3809-05 | 43.0 | 6.99 | 29.26 | 2.59 | 1.95 | 1.58 | 1.557 | 0.250 | 0.036 | 0.391 |
| PC3809-06 | 53.0 | 6.44 | 27.28 | 2.69 | 1.50 | 1.33 | 1.385 | 0.272 | 0.030 | 0.338 |
| PC3809-07 | 62.0 | 5.90 | 25.61 | 2.34 | 2.29 | 1.53 | 1.162 | 0.231 | 0.020 | 0.286 |
| PC3809-08 | 73.0 | 7.06 | 28.84 | 2.62 | 1.49 | 0.78 | 1.486 | 0.208 | 0.034 | 0.378 |
| PC3809-09 | 84.0 | 8.08 | 26.10 | 3.12 | 1.12 | 1.28 | 1.699 | 0.165 | 0.031 | 0.412 |
| PC3809-10 | 94.0 | 7.52 | 25.64 | 3.37 | 1.41 | 1.22 | 1.596 | 0.174 | 0.032 | 0.366 |
| PC3809-11 | 104.0 | 6.76 | 26.77 | 2.52 | 1.14 | 1.17 | 1.423 | 0.158 | 0.024 | 0.328 |
| PC3809-12 | 113.0 | 8.29 | 27.25 | 3.24 | 1.24 | 1.51 | 1.787 | 0.161 | 0.035 | 0.429 |
| PC3809-13 | 124.0 | 7.33 | 27.04 | 2.60 | 2.04 | 1.29 | 1.566 | 0.239 | 0.032 | 0.405 |
| PC3809-14 | 134.0 | 6.42 | 27.62 | 2.48 | 2.00 | 1.51 | 1.350 | 0.296 | 0.026 | 0.330 |
| PC3809-15 | 144.0 | 5.71 | 28.32 | 2.29 | 1.70 | 1.29 | 1.234 | 0.203 | 0.022 | 0.297 |
| PC3809-16 | 152.0 | 5.67 | 29.65 | 2.40 | 1.71 | 1.20 | 1.252 | 0.147 | 0.021 | 0.295 |
| PC3809-17 | 165.0 | 5.50 | 29.57 | 2.25 | 2.42 | 1.28 | 1.188 | 0.241 | 0.024 | 0.297 |
| PC3809-18 | 174.0 | 6.69 | 30.16 | 2.35 | 1.90 | 1.48 | 1.495 | 0.267 | 0.030 | 0.362 |
| PC3809-19 | 185.0 | 5.96 | 31.31 | 2.11 | 2.47 | 1.60 | 1.341 | 0.427 | 0.029 | 0.329 |
| PC3809-20 | 194.0 | 6.11 | 30.38 | 2.09 | 3.02 | 1.66 | 1.365 | 0.409 | 0.035 | 0.346 |
| PC3809-21 | 205.0 | 6.78 | 29.56 | 3.12 | 2.77 | 1.80 | 1.530 | 0.155 | 0.049 | 0.383 |
| PC3809-22 | 214.0 | 5.65 | 29.34 | 1.97 | 2.36 | 1.45 | 1.259 | 0.398 | 0.024 | 0.308 |
| PC3809-23 | 224.0 | 5.98 | 33.00 | 1.75 | 2.95 | 1.80 | 1.393 | 0.494 | 0.028 | 0.316 |
| PC3809-24 | 234.0 | 5.37 | 32.00 | 2.02 | 2.90 | 1.57 | 1.202 | 0.592 | 0.023 | 0.290 |
| PC3809-25 | 243.0 | 4.35 | 32.27 | 1.93 | 1.69 | 1.34 | 0.983 | 0.347 | 0.023 | 0.225 |
| PC3809-26 | 257.0 | 5.11 | 31.35 | 2.20 | 1.74 | 1.32 | 1.165 | 0.301 | 0.023 | 0.276 |
| PC3809-27 | 267.0 | 5.09 | 31.30 | 1.85 | 3.88 | 1.52 | 1.211 | 1.036 | 0.027 | 0.273 |
| PC3809-28 | 273.0 | 2.58 | 14.24 | 2.93 | 18.46 | 1.07 | 0.665 | 5.797 | 0.018 | 0.140 |
| PC3809-29 | 284.0 | 6.02 | 28.57 | 2.87 | 2.04 | 1.43 | 1.309 | 0.314 | 0.035 | 0.338 |
| PC3809-30 | 294.0 | 4.83 | 29.84 | 2.23 | 1.92 | 1.55 | 1.084 | 0.165 | 0.021 | 0.249 |
| PC3809-31 | 304.0 | 6.19 | 29.12 | 2.92 | 1.39 | 1.48 | 1.334 | 0.168 | 0.037 | 0.346 |
| PC3809-32 | 314.0 | 6.07 | 26.34 | 2.74 | 1.58 | 1.30 | 1.291 | 0.140 | 0.029 | 0.299 |
| PC3809-33 | 324.0 | 6.30 | 27.87 | 3.17 | 1.63 | 1.37 | 1.349 | 0.222 | 0.033 | 0.346 |
| PC3809-34 | 335.0 | 5.43 | 28.84 | 2.66 | 1.44 | 1.30 | 1.160 | 0.160 | 0.030 | 0.285 |
| PC3809-35 | 344.0 | 4.96 | 29.36 | 2.69 | 1.36 | 1.31 | 1.061 | 0.160 | 0.023 | 0.278 |
| PC3809-36 | 355.0 | 4.20 | 30.29 | 1.94 | 2.02 | 1.56 | 0.923 | 0.105 | 0.022 | 0.204 |
| PC3809-37 | 364.0 | 4.11 | 29.56 | 2.05 | 3.23 | 1.17 | 0.893 | 0.102 | 0.020 | 0.198 |
| PC3809-38 | 375.0 | 5.57 | 28.62 | 2.57 | 1.63 | 1.49 | 1.245 | 0.112 | 0.028 | 0.269 |
| PC3809-39 | 384.0 | 5.87 | 28.02 | 2.96 | 2.67 | 1.39 | 1.257 | 0.211 | 0.035 | 0.321 |
| PC3809-40 | 394.0 | 5.06 | 29.63 | 2.29 | 1.90 | 1.35 | 1.126 | 0.159 | 0.027 | 0.258 |
| PC3809-41 | 404.0 | 5.62 | 30.26 | 2.55 | 1.19 | 1.41 | 1.270 | 0.122 | 0.031 | 0.287 |
| PC3809-42 | 416.0 | 4.79 | 28.20 | 2.23 | 3.31 | 1.30 | 1.036 | 0.145 | 0.019 | 0.240 |
| PC3809-43 | 424.0 | 5.24 | 30.06 | 2.29 | 1.19 | 1.37 | 1.197 | 0.101 | 0.027 | 0.257 |
| PC3809-44 | 434.0 | 5.94 | 28.44 | 2.74 | 1.23 | 1.48 | 1.361 | 0.127 | 0.029 | 0.287 |
| PC3809-45 | 444.0 | 4.90 | 30.13 | 2.45 | 2.48 | 1.37 | 1.084 | 0.140 | 0.027 | 0.246 |
| PC3809-46 | 453.0 | 5.97 | 29.08 | 2.79 | 1.65 | 1.38 | 1.293 | 0.167 | 0.029 | 0.327 |
| PC3809-47 | 465.0 | 5.63 | 28.48 | 2.79 | 2.00 | 1.22 | 1.234 | 0.163 | 0.031 | 0.292 |
| PC3809-48 | 474.0 | 5.29 | 28.00 | 2.36 | 2.82 | 1.31 | 1.215 | 0.145 | 0.022 | 0.248 |
| PC3809-49 | 483.0 | 5.78 | 30.05 | 2.78 | 1.45 | 1.45 | 1.320 | 0.176 | 0.029 | 0.313 |
| PC3809-50 | 493.0 | 5.75 | 29.02 | 2.78 | 1.63 | 1.40 | 1.365 | 0.155 | 0.038 | 0.289 |
| PC3809-51 | 504.0 | 6.04 | 29.84 | 2.87 | 1.65 | 1.43 | 1.400 | 0.182 | 0.033 | 0.334 |
| PC3809-52 | 515.0 | 6.04 | 29.37 | 2.83 | 1.46 | 1.60 | 1.438 | 0.145 | 0.032 | 0.320 |
| PC3809-53 | 525.0 | 5.65 | 28.27 | 2.56 | 2.24 | 1.49 | 1.319 | 0.118 | 0.030 | 0.271 |
| PC3809-54 | 536.0 | 5.15 | 29.50 | 2.39 | 2.99 | 1.44 | 1.187 | 0.115 | 0.030 | 0.252 |
| PC3809-55 | 544.0 | 6.10 | 28.92 | 3.00 | 2.12 | 1.47 | 1.404 | 0.155 | 0.034 | 0.329 |
| PC3809-56 | 553.0 | 5.73 | 28.95 | 2.92 | 2.71 | 1.39 | 1.283 | 0.100 | 0.037 | 0.288 |
| PC3809-57 | 564.0 | 5.30 | 29.92 | 2.70 | 2.62 | 1.37 | 1.155 | 0.104 | 0.034 | 0.278 |
| PC3809-58 | 574.0 | 5.28 | 29.28 | 2.74 | 2.85 | 1.46 | 1.245 | 0.120 | 0.035 | 0.274 |
| PC3809-59 | 585.0 | 5.09 | 29.48 | 2.59 | 3.72 | 1.32 | 1.162 | 0.319 | 0.033 | 0.268 |
| PC3809-60 | 594.0 | 5.10 | 30.40 | 2.52 | 2.78 | 1.42 | 1.204 | 0.132 | 0.033 | 0.268 |
| PC3809-61 | 605.0 | 5.72 | 28.62 | 2.96 | 3.20 | 1.33 | 1.326 | 0.188 | 0.038 | 0.304 |
| PC3809-62 | 615.0 | 5.06 | 30.27 | 2.45 | 3.03 | 1.34 | 1.226 | 0.224 | 0.035 | 0.264 |
| PC3809-63 | 625.0 | 5.61 | 29.56 | 2.82 | 2.92 | 1.46 | 1.299 | 0.205 | 0.039 | 0.299 |
| PC3809-64 | 635.0 | 5.72 | 28.91 | 2.91 | 3.18 | 1.38 | 1.313 | 0.203 | 0.040 | 0.308 |
| PC3809-65 | 646.0 | 5.03 | 30.67 | 2.40 | 2.58 | 1.33 | 1.129 | 0.139 | 0.031 | 0.259 |
| PC3809-66 | 654.0 | 4.80 | 31.32 | 2.30 | 2.33 | 1.26 | 1.076 | 0.109 | 0.033 | 0.257 |
| PC3809-67 | 664.0 | 4.83 | 31.49 | 2.30 | 2.51 | 1.33 | 1.100 | 0.094 | 0.027 | 0.246 |

| APPENDIX C.7. SALT-CORRECTED MAJOR ELEMENTS | | | | | | | | | | |
|---|---|---|---|---|---|---|---|---|---|---|
| PC38-09 | 148m | | | | | | | | | |
| Sample | Depth | Al | Si | Fe | Ca | Na | K | P | Mn | Ti |
| | (cm) | (wt.%) | (wt.%) | (wt.%) | (wt.%) | (wt.%) | (wt.%) | (wt.%) | (wt.%) | (wt.%) |
| PC3809-68 | 674.0 | 4.21 | 30.53 | 2.22 | 2.12 | 1.08 | 1.010 | 0.084 | 0.027 | 0.230 |
| PC3809-69 | 684.0 | 5.64 | 29.97 | 2.79 | 2.61 | 1.42 | 1.354 | 0.118 | 0.031 | 0.289 |
| PC3809-70 | 694.0 | 6.04 | 29.55 | 2.97 | 2.68 | 1.41 | 1.351 | 0.119 | 0.041 | 0.311 |
| PC3809-71 | 703.0 | 5.98 | 28.89 | 3.06 | 2.52 | 1.44 | 1.420 | 0.098 | 0.039 | 0.300 |
| PC3809-72 | 714.0 | 5.45 | 29.33 | 2.75 | 2.88 | 1.48 | 1.283 | 0.138 | 0.032 | 0.285 |
| PC3809-73 | 724.0 | 5.95 | 29.45 | 3.08 | 2.95 | 1.47 | 1.397 | 0.194 | 0.040 | 0.317 |
| PC3809-74 | 734.0 | 6.00 | 28.30 | 3.04 | 3.24 | 1.40 | 1.404 | 0.198 | 0.038 | 0.319 |
| PC3809-75 | 744.0 | 5.85 | 30.87 | 3.05 | 2.94 | 1.51 | 1.404 | 0.162 | 0.041 | 0.295 |
| PC3809-76 | 754.0 | 5.38 | 29.89 | 2.75 | 2.78 | 1.34 | 1.273 | 0.104 | 0.036 | 0.278 |
| PC3809-77 | 764.0 | 6.01 | 28.45 | 2.96 | 3.31 | 1.32 | 1.512 | 0.133 | 0.042 | 0.310 |
| PC3809-78 | 774.0 | 6.12 | 28.64 | 3.12 | 3.10 | 1.36 | 1.463 | 0.138 | 0.042 | 0.332 |
| PC3809-79 | 784.0 | 5.87 | 29.26 | 3.05 | 3.02 | 1.29 | 1.448 | 0.130 | 0.037 | 0.313 |
| PC3809-80 | 794.0 | 5.89 | 29.39 | 2.87 | 3.05 | 1.32 | 1.474 | 0.150 | 0.036 | 0.314 |
| PC3809-81 | 804.0 | 5.64 | 30.02 | 2.76 | 2.70 | 1.35 | 1.357 | 0.187 | 0.035 | 0.307 |
| PC3809-82 | 813.0 | 5.82 | 29.38 | 3.14 | 3.45 | 1.43 | 1.331 | 0.304 | 0.039 | 0.320 |
| PC3809-83 | 823.0 | 5.69 | 29.91 | 2.93 | 2.76 | 1.38 | 1.370 | 0.203 | 0.040 | 0.310 |
| PC3809-84 | 834.0 | 5.90 | 29.38 | 2.87 | 2.70 | 1.35 | 1.399 | 0.165 | 0.037 | 0.320 |
| PC3809-85 | 845.0 | 5.97 | 30.74 | 2.86 | 2.72 | 1.47 | 1.457 | 0.195 | 0.038 | 0.308 |
| PC3809-86 | 854.0 | 6.71 | 29.34 | 3.30 | 2.38 | 1.50 | 1.669 | 0.101 | 0.049 | 0.344 |
| PC38-10 | 257m | | | | | | | | | |
| PC3810-01 | 6.0 | 5.23 | 21.63 | 2.00 | 6.30 | 1.30 | 1.167 | 0.469 | 0.018 | 0.260 |
| PC3810-02 | 14.0 | 5.47 | 25.89 | 1.87 | 5.49 | 1.57 | 1.264 | 1.062 | 0.026 | 0.297 |
| PC3810-03 | 24.0 | 5.53 | 28.52 | 1.58 | 6.78 | 1.80 | 1.347 | 1.959 | 0.027 | 0.279 |
| PC3810-04 | 34.0 | 5.53 | 28.61 | 1.48 | 6.49 | 1.69 | 1.311 | 1.027 | 0.021 | 0.278 |
| PC3810-05 | 44.0 | 5.85 | 27.76 | 2.11 | 2.23 | 1.56 | 1.474 | 0.435 | 0.031 | 0.315 |
| PC3810-06 | 54.0 | 5.97 | 28.62 | 2.13 | 1.79 | 1.58 | 1.462 | 0.294 | 0.021 | 0.302 |
| PC3810-07 | 64.0 | 6.12 | 29.46 | 2.40 | 2.31 | 1.64 | 1.550 | 0.462 | 0.025 | 0.320 |
| PC3810-08 | 74.0 | 6.32 | 29.83 | 2.27 | 3.07 | 1.72 | 1.601 | 0.705 | 0.030 | 0.327 |
| PC3810-09 | 84.0 | 5.41 | 31.84 | 1.75 | 4.29 | 1.65 | 1.469 | 1.086 | 0.027 | 0.267 |
| PC3810-10 | 94.0 | 5.74 | 30.44 | 1.80 | 5.74 | 1.78 | 1.424 | 1.505 | 0.027 | 0.265 |
| PC3810-10 | 104.0 | 5.43 | 29.49 | 1.50 | 6.94 | 1.72 | 1.380 | 0.867 | 0.025 | 0.256 |
| PC3810-11 | 113.0 | 5.58 | 30.38 | 1.47 | 6.23 | 1.73 | 1.352 | 0.579 | 0.027 | 0.253 |
| PC3810-12 | 126.0 | 4.80 | 27.82 | 1.94 | 6.19 | 1.21 | 1.160 | 0.524 | 0.020 | 0.245 |
| PC3810-13 | 134.0 | 4.73 | 27.99 | 2.00 | 4.22 | 1.14 | 1.142 | 0.559 | 0.020 | 0.243 |
| PC3810-14 | 146.0 | 5.48 | 28.31 | 2.23 | 3.93 | 1.40 | 1.342 | 0.428 | 0.023 | 0.288 |
| PC3810-15 | 154.0 | 5.07 | 25.91 | 2.11 | 6.53 | 1.16 | 1.213 | 0.433 | 0.025 | 0.262 |
| PC3810-16 | 167.0 | 5.38 | 28.52 | 2.17 | 3.51 | 1.20 | 1.325 | 0.318 | 0.020 | 0.285 |
| PC3810-17 | 174.0 | 5.72 | 29.69 | 2.11 | 2.05 | 1.34 | 1.417 | 0.364 | 0.024 | 0.291 |
| PC3810-18 | 185.0 | 5.70 | 30.25 | 2.24 | 1.48 | 1.19 | 1.444 | 0.299 | 0.027 | 0.298 |
| PC3810-19 | 194.0 | 4.84 | 27.72 | 2.06 | 4.27 | 1.05 | 1.203 | 0.273 | 0.021 | 0.239 |
| PC3810-20 | 203.0 | 5.95 | 29.32 | 2.22 | 2.31 | 1.35 | 1.468 | 0.381 | 0.025 | 0.313 |
| PC3810-21 | 216.0 | 4.57 | 27.38 | 1.92 | 4.45 | 1.15 | 1.119 | 0.341 | 0.018 | 0.235 |
| PC3810-22 | 224.0 | 4.84 | 28.24 | 2.06 | 2.98 | 1.06 | 1.150 | 0.272 | 0.018 | 0.245 |
| PC3810-23 | 233.0 | 5.54 | 27.65 | 2.26 | 2.63 | 1.23 | 1.372 | 0.300 | 0.026 | 0.288 |
| PC3810-24 | 244.0 | 5.61 | 26.86 | 2.29 | 4.49 | 1.26 | 1.349 | 0.374 | 0.023 | 0.292 |
| PC3810-25 | 254.0 | 5.25 | 28.19 | 1.80 | 5.08 | 1.43 | 1.292 | 0.698 | 0.022 | 0.263 |
| PC3810-26 | 263.0 | 4.93 | 27.05 | 1.81 | 5.48 | 1.34 | 1.188 | 0.571 | 0.019 | 0.249 |
| PC3810-27 | 273.0 | 5.55 | 25.93 | 2.30 | 4.67 | 1.22 | 1.361 | 0.322 | 0.026 | 0.288 |
| PC3810-28 | 284.0 | 5.27 | 26.02 | 2.06 | 5.97 | 1.11 | 1.263 | 0.367 | 0.024 | 0.282 |
| PC3810-29 | 295.0 | 4.04 | 22.39 | 1.77 | 9.31 | 0.82 | 0.963 | 0.308 | 0.017 | 0.200 |
| PC3810-30 | 305.0 | 5.46 | 25.25 | 2.36 | 6.03 | 1.05 | 1.257 | 0.277 | 0.026 | 0.290 |
| PC3810-31 | 314.0 | 5.72 | 25.65 | 2.16 | 6.05 | 1.18 | 1.331 | 0.325 | 0.022 | 0.306 |
| PC3810-32 | 324.0 | 4.44 | 24.53 | 1.93 | 6.65 | 0.94 | 1.039 | 0.298 | 0.022 | 0.221 |
| PC3810-33 | 335.0 | 5.45 | 25.29 | 2.16 | 5.25 | 1.18 | 1.317 | 0.309 | 0.024 | 0.282 |
| PC3810-34 | 344.0 | 3.84 | 25.10 | 1.71 | 7.28 | 0.92 | 0.881 | 0.318 | 0.016 | 0.190 |
| PC3810-35 | 354.0 | 3.56 | 28.68 | 1.45 | 4.31 | 0.97 | 0.837 | 0.240 | 0.008 | 0.176 |
| PC3810-36 | 364.0 | 3.13 | 28.50 | 1.32 | 5.49 | 0.91 | 0.741 | 0.262 | 0.011 | 0.154 |
| PC3810-37 | 374.0 | 3.28 | 29.44 | 1.26 | 4.16 | 0.82 | 0.744 | 0.220 | 0.008 | 0.160 |
| PC3810-38 | 383.0 | 5.85 | 25.60 | 2.28 | 4.79 | 1.04 | 1.318 | 0.240 | 0.025 | 0.298 |
| PC3810-39 | 394.0 | 4.75 | 26.22 | 1.74 | 4.27 | 1.01 | 1.088 | 0.297 | 0.017 | 0.244 |
| PC3810-40 | 404.0 | 5.49 | 26.21 | 1.95 | 4.98 | 1.09 | 1.259 | 0.288 | 0.024 | 0.297 |
| PC3810-41 | 417.0 | 4.67 | 23.52 | 1.81 | 7.62 | 0.91 | 1.039 | 0.347 | 0.016 | 0.245 |
| PC3810-42 | 424.0 | 4.89 | 24.99 | 1.82 | 5.81 | 1.03 | 1.134 | 0.314 | 0.025 | 0.249 |
| PC3810-43 | 434.0 | 2.31 | 23.05 | 0.95 | 11.66 | 0.66 | 0.536 | 0.380 | 0.008 | 0.117 |
| PC3810-44 | 445.0 | 3.87 | 23.83 | 1.51 | 8.55 | 0.83 | 0.892 | 0.267 | 0.011 | 0.190 |

| APPENDIX C.7. SALT-CORRECTED MAJOR ELEMENTS | | | | | | | | | | |
|---|---|---|---|---|---|---|---|---|---|---|
| | | | | | | | | | | |
| PC38-10 | 257m | | | | | | | | | |
| Sample | Depth | Al | Si | Fe | Ca | Na | K | P | Mn | Ti |
| | (cm) | (wt.%) | (wt.%) | (wt.%) | (wt.%) | (wt.%) | (wt.%) | (wt.%) | (wt.%) | (wt.%) |
| | | | | | | | | | | |
| PC3810-45 | 456.0 | 3.54 | 24.57 | 1.40 | 7.64 | 0.80 | 0.791 | 0.276 | 0.012 | 0.176 |
| PC3810-46 | 467.0 | 2.44 | 26.27 | 1.00 | 7.88 | 0.72 | 0.573 | 0.215 | 0.003 | 0.120 |
| PC3810-47 | 476.0 | 4.73 | 21.86 | 1.80 | 8.50 | 0.99 | 1.088 | 0.495 | 0.020 | 0.248 |
| PC3810-48 | 484.0 | 4.46 | 21.36 | 1.74 | 9.12 | 0.89 | 1.018 | 0.464 | 0.015 | 0.231 |
| PC3810-49 | 494.0 | 4.23 | 21.91 | 1.48 | 9.36 | 1.08 | 0.942 | 0.892 | 0.018 | 0.227 |
| PC3810-50 | 504.0 | 5.23 | 27.19 | 1.60 | 7.88 | 1.68 | 1.266 | 2.404 | 0.020 | 0.265 |
| PC3810-51 | 514.0 | 5.56 | 29.39 | 2.75 | 2.49 | 1.39 | 1.265 | 0.117 | 0.031 | 0.307 |
| PC3810-52 | 524.0 | 6.04 | 30.65 | 2.87 | 2.17 | 1.51 | 1.378 | 0.108 | 0.038 | 0.333 |
| PC3810-53 | 534.0 | 4.48 | 21.98 | 1.77 | 4.92 | 1.16 | 1.003 | 0.264 | 0.016 | 0.202 |
| PC3810-54 | 545.0 | 4.51 | 24.92 | 1.74 | 3.79 | 1.27 | 1.071 | 0.204 | 0.017 | 0.208 |
| PC3810-55 | 554.0 | 4.12 | 23.08 | 1.64 | 5.44 | 1.11 | 0.934 | 0.199 | 0.016 | 0.185 |
| PC3810-56 | 564.0 | 3.53 | 24.39 | 1.53 | 7.75 | 1.01 | 0.808 | 0.299 | 0.019 | 0.168 |
| PC3810-57 | 574.0 | 4.02 | 21.85 | 1.69 | 8.68 | 0.95 | 0.894 | 0.251 | 0.018 | 0.191 |
| PC3810-58 | 584.0 | 3.96 | 23.65 | 1.68 | 7.48 | 1.09 | 0.954 | 0.192 | 0.021 | 0.188 |
| PC3810-59 | 596.0 | 3.92 | 24.32 | 1.65 | 6.60 | 1.16 | 0.940 | 0.202 | 0.015 | 0.184 |
| PC3810-60 | 604.0 | 3.99 | 23.06 | 1.72 | 8.05 | 1.19 | 0.970 | 0.205 | 0.019 | 0.186 |
| PC3810-61 | 614.0 | 4.42 | 25.10 | 1.87 | 5.73 | 1.06 | 1.036 | 0.147 | 0.017 | 0.204 |
| PC3810-62 | 624.0 | 4.77 | 23.99 | 1.97 | 6.69 | 1.02 | 1.178 | 0.204 | 0.022 | 0.231 |
| PC3810-63 | 634.0 | 4.68 | 24.40 | 1.90 | 6.70 | 1.79 | 1.144 | 0.216 | 0.021 | 0.218 |
| PC3810-64 | 645.0 | 4.59 | 25.49 | 2.00 | 5.16 | 1.13 | 1.075 | 0.146 | 0.027 | 0.211 |
| PC3810-65 | 655.0 | 4.42 | 24.38 | 1.89 | 5.76 | 1.16 | 1.045 | 0.136 | 0.017 | 0.199 |
| PC3810-66 | 667.0 | 4.86 | 24.94 | 2.05 | 5.50 | 1.19 | 1.196 | 0.176 | 0.021 | 0.220 |
| PC3810-67 | 674.0 | 5.65 | 25.52 | 2.31 | 4.17 | 1.09 | 1.391 | 0.183 | 0.027 | 0.259 |
| PC3810-68 | 683.0 | 5.19 | 25.46 | 2.10 | 4.88 | 1.09 | 1.299 | 0.139 | 0.022 | 0.228 |
| PC3810-69 | 694.0 | 6.77 | 26.21 | 2.73 | 3.30 | 1.24 | 1.714 | 0.206 | 0.028 | 0.314 |
| PC3810-70 | 704.0 | 7.50 | 26.93 | 2.64 | 1.83 | 1.22 | 1.970 | 0.193 | 0.035 | 0.364 |
| PC3810-71 | 714.0 | 6.73 | 25.65 | 2.61 | 3.88 | 1.15 | 1.770 | 0.215 | 0.029 | 0.301 |
| PC3810-72 | 724.0 | 5.95 | 25.96 | 2.33 | 4.64 | 0.99 | 1.498 | 0.193 | 0.031 | 0.259 |
| PC3810-74 | 734.0 | 7.17 | 28.03 | 2.45 | 1.56 | 1.27 | 1.871 | 0.215 | 0.025 | 0.339 |
| PC3810-75 | 745.0 | 7.92 | 28.11 | 2.87 | 1.57 | 1.47 | 2.058 | 0.202 | 0.037 | 0.382 |
| PC3810-76 | 754.0 | 6.43 | 28.69 | 2.43 | 1.85 | 1.30 | 1.647 | 0.254 | 0.029 | 0.312 |
| PC3810-77 | 764.0 | 7.07 | 29.30 | 2.41 | 2.62 | 1.55 | 1.811 | 0.539 | 0.033 | 0.375 |
| | | | | | | | | | | |
| PC38-02 | 2525m | | | | | | | | | |
| | (Age) | | | | | | | | | |
| PC3802-01 | 2.76 | 5.75 | 23.04 | 3.04 | 8.72 | 1.28 | 1.45 | 0.117 | 0.028 | 0.282 |
| PC3802-02 | 6.21 | 5.14 | 20.94 | 2.66 | 11.75 | 1.15 | 1.33 | 0.113 | 0.028 | 0.247 |
| PC3802-03 | 9.66 | 4.99 | 20.16 | 2.59 | 12.76 | 1.08 | 1.23 | 0.105 | 0.024 | 0.245 |
| PC3802-04 | 12.77 | 5.46 | 20.04 | 2.71 | 10.78 | 1.12 | 1.42 | 0.096 | 0.025 | 0.256 |
| PC3802-05 | 15.18 | 5.36 | 19.31 | 2.63 | 12.69 | 1.06 | 1.36 | 0.092 | 0.024 | 0.265 |
| PC3802-06 | 17.47 | 5.23 | 19.35 | 2.77 | 12.31 | 1.12 | 1.37 | 0.091 | 0.026 | 0.255 |
| PC3802-07 | 20.48 | 5.63 | 20.04 | 2.73 | 12.45 | 0.52 | 1.37 | 0.097 | 0.027 | 0.284 |
| PC3802-08 | 22.65 | 5.50 | 19.67 | 2.79 | 12.06 | 0.93 | 1.40 | 0.095 | 0.023 | 0.275 |
| PC3802-09 | 25.22 | 5.11 | 18.34 | 2.59 | 13.62 | 0.98 | 1.29 | 0.097 | 0.024 | 0.268 |
| PC3802-10 | 28.29 | 4.76 | 17.39 | 2.41 | 14.79 | 1.01 | 1.20 | 0.095 | 0.024 | 0.253 |
| PC3802-11 | 31.07 | 4.65 | 17.59 | 2.35 | 15.02 | 0.97 | 1.18 | 0.094 | 0.028 | 0.246 |
| PC3802-12 | 33.86 | 4.30 | 16.85 | 2.34 | 15.84 | 0.94 | 1.13 | 0.089 | 0.022 | 0.231 |
| PC3802-13 | 36.64 | 4.72 | 17.58 | 2.58 | 14.83 | 0.91 | 1.16 | 0.092 | 0.024 | 0.241 |
| PC3802-14 | 39.15 | 5.45 | 19.35 | 2.60 | 12.33 | 1.13 | 1.39 | 0.097 | 0.028 | 0.272 |
| PC3802-15 | 42.22 | 5.62 | 19.85 | 2.78 | 11.82 | 1.20 | 1.45 | 0.098 | 0.027 | 0.278 |
| PC3802-16 | 45.00 | 6.12 | 20.89 | 2.98 | 10.87 | 1.02 | 1.59 | 0.103 | 0.030 | 0.308 |
| PC3802-17 | 48.07 | 6.22 | 21.66 | 3.00 | 9.50 | 1.26 | 1.65 | 0.102 | 0.028 | 0.310 |
| PC3802-18 | 50.85 | 5.89 | 23.23 | 3.32 | 8.28 | 1.28 | 1.62 | 0.103 | 0.032 | 0.307 |
| PC3802-19 | 53.64 | 5.80 | 22.53 | 3.15 | 8.95 | 1.23 | 1.55 | 0.103 | 0.030 | 0.298 |
| PC3802-20 | 56.42 | 6.16 | 23.32 | 3.15 | 7.79 | 1.30 | 1.64 | 0.103 | 0.029 | 0.320 |
| PC3802-21 | 59.29 | 6.26 | 22.17 | 3.16 | 8.77 | 1.23 | 1.63 | 0.103 | 0.031 | 0.316 |
| PC3802-22 | 62.61 | 6.18 | 22.05 | 3.13 | 9.30 | 1.29 | 1.62 | 0.103 | 0.030 | 0.311 |
| PC3802-23 | 65.94 | 6.50 | 22.77 | 3.22 | 8.30 | 1.37 | 1.71 | 0.105 | 0.033 | 0.333 |
| PC3802-24 | 69.26 | 7.24 | 25.99 | 3.58 | 4.32 | 1.60 | 1.98 | 0.111 | 0.034 | 0.372 |
| PC3802-25 | 72.58 | 6.56 | 24.54 | 3.39 | 5.98 | 1.47 | 1.75 | 0.117 | 0.032 | 0.347 |
| PC3802-26 | 76.96 | 5.87 | 22.74 | 3.10 | 8.64 | 1.37 | 1.57 | 0.119 | 0.029 | 0.310 |
| PC3802-27 | 82.03 | 6.90 | 25.86 | 3.50 | 4.57 | 1.58 | 1.91 | 0.116 | 0.033 | 0.349 |
| PC3802-28 | 87.11 | 6.94 | 25.42 | 3.48 | 5.09 | 1.49 | 1.94 | 0.113 | 0.029 | 0.342 |
| PC3802-29 | 92.18 | 7.54 | 26.98 | 3.67 | 2.84 | 1.53 | 2.09 | 0.113 | 0.032 | 0.371 |
| PC3802-30 | 97.26 | 7.29 | 26.76 | 3.69 | 3.71 | 1.47 | 2.00 | 0.131 | 0.034 | 0.372 |
| PC3802-31 | 102.84 | 6.50 | 25.59 | 3.37 | 6.15 | 1.37 | 1.73 | 0.130 | 0.031 | 0.336 |
| PC3802-32 | 107.92 | 6.62 | 25.01 | 3.45 | 5.99 | 1.39 | 1.80 | 0.124 | 0.033 | 0.336 |

| APPENDIX C.7. SALT-CORRECTED MAJOR ELEMENTS | | | | | | | | | | |
|---|---|---|---|---|---|---|---|---|---|---|
| | | | | | | | | | | |
| PC38-02 | 2525m | | | | | | | | | |
| Sample | Age | Al | Si | Fe | Ca | Na | K | P | Mn | Ti |
| | (ka) | (wt.%) | (wt.%) | (wt.%) | (wt.%) | (wt.%) | (wt.%) | (wt.%) | (wt.%) | (wt.%) |
| | | | | | | | | | | |
| PC3802-33 | 113.00 | 6.61 | 24.95 | 3.67 | 5.96 | 1.35 | 1.80 | 0.109 | 0.035 | 0.328 |
| PC3802-34 | 118.07 | 6.53 | 25.12 | 3.67 | 6.06 | 1.37 | 1.75 | 0.114 | 0.029 | 0.318 |
| PC3802-35 | 123.15 | 5.65 | 22.67 | 2.84 | 9.63 | 1.23 | 1.51 | 0.101 | 0.028 | 0.261 |
| PC3802-36 | 128.22 | 5.48 | 20.16 | 2.79 | 12.08 | 1.10 | 1.40 | 0.089 | 0.029 | 0.252 |
| PC3802-37 | 132.23 | 5.50 | 19.23 | 2.77 | 13.21 | 1.11 | 1.39 | 0.083 | 0.027 | 0.257 |
| PC3802-38 | 135.30 | 5.28 | 18.72 | 2.72 | 13.86 | 1.05 | 1.42 | 0.082 | 0.026 | 0.261 |
| PC3802-39 | 138.71 | 5.14 | 18.62 | 2.63 | 13.99 | 1.02 | 1.35 | 0.084 | 0.024 | 0.257 |
| PC3802-40 | 141.79 | 4.95 | 18.13 | 2.51 | 15.06 | 1.07 | 1.32 | 0.087 | 0.026 | 0.249 |
| PC3802-41 | 145.20 | 5.08 | 18.27 | 2.50 | 14.77 | 1.13 | 1.35 | 0.086 | 0.027 | 0.249 |
| PC3802-42 | 148.61 | 5.07 | 18.89 | 2.54 | 14.19 | 1.15 | 1.37 | 0.083 | 0.025 | 0.248 |
| PC3802-43 | 152.02 | 4.99 | 17.65 | 2.49 | 15.06 | 1.04 | 1.27 | 0.083 | 0.027 | 0.248 |
| PC3802-44 | 155.44 | 5.18 | 18.66 | 2.55 | 14.16 | 1.14 | 1.40 | 0.087 | 0.025 | 0.263 |
| PC3802-45 | 158.85 | 5.69 | 20.11 | 2.90 | 11.96 | 1.16 | 1.45 | 0.088 | 0.028 | 0.281 |
| PC3802-46 | 162.26 | 6.05 | 20.78 | 3.00 | 10.72 | 1.37 | 1.65 | 0.092 | 0.031 | 0.300 |
| PC3802-47 | 165.68 | 5.16 | 17.71 | 2.62 | 15.25 | 1.03 | 1.24 | 0.091 | 0.025 | 0.253 |
| PC3802-48 | 169.43 | 4.88 | 17.24 | 2.53 | 15.74 | 0.78 | 0.93 | 0.090 | 0.026 | 0.252 |
| PC3802-49 | 172.84 | 4.97 | 17.79 | 2.56 | 15.45 | 0.96 | 1.34 | 0.090 | 0.022 | 0.250 |
| PC3802-50 | 176.26 | 5.27 | 18.81 | 2.84 | 14.47 | 1.09 | 1.41 | 0.098 | 0.031 | 0.257 |
| PC3802-51 | 179.67 | 5.49 | 19.93 | 2.68 | 12.85 | 1.14 | 1.45 | 0.094 | 0.028 | 0.273 |
| PC3802-52 | 183.08 | 6.06 | 21.81 | 2.99 | 10.40 | 1.38 | 1.75 | 0.096 | 0.030 | 0.276 |
| PC3802-53 | 186.50 | 6.75 | 25.84 | 2.56 | 8.25 | 1.89 | 2.29 | 0.088 | 0.030 | 0.260 |
| PC3802-54 | 189.57 | 7.09 | 24.42 | 3.56 | 6.15 | 1.44 | 1.97 | 0.113 | 0.036 | 0.352 |
| PC3802-55 | 193.52 | 7.04 | 24.49 | 3.74 | 5.70 | 1.37 | 1.91 | 0.115 | 0.034 | 0.353 |
| PC3802-56 | 197.42 | 6.71 | 24.39 | 4.18 | 4.48 | 1.28 | 1.86 | 0.115 | 0.033 | 0.349 |
| PC3802-57 | 202.11 | 6.22 | 23.09 | 3.48 | 7.65 | 2.15 | 1.72 | 0.111 | 0.029 | 0.299 |
| PC3802-58 | 206.02 | 6.46 | 22.52 | 3.41 | 8.11 | 1.77 | 1.77 | 0.103 | 0.032 | 0.302 |
| PC3802-59 | 209.53 | 6.58 | 22.10 | 3.48 | 8.85 | 1.42 | 1.74 | 0.100 | 0.031 | 0.305 |
| PC3802-60 | 213.44 | 4.92 | 17.05 | 2.69 | 15.96 | 1.01 | 1.20 | 0.096 | 0.024 | 0.246 |
| PC3802-61 | 217.34 | 4.80 | 17.05 | 2.59 | 16.67 | 1.13 | 1.32 | 0.094 | 0.026 | 0.235 |
| PC3802-62 | 221.25 | 5.31 | 18.63 | 2.84 | 14.25 | 1.13 | 1.44 | 0.094 | 0.029 | 0.274 |
| PC3802-63 | 225.16 | 5.59 | 19.02 | 2.88 | 13.51 | 1.19 | 1.47 | 0.094 | 0.030 | 0.282 |
| PC3802-64 | 229.06 | 6.26 | 21.31 | 3.15 | 11.48 | 1.25 | 1.65 | 0.102 | 0.031 | 0.302 |
| PC3802-65 | 232.97 | 6.65 | 23.05 | 3.26 | 8.09 | 1.33 | 1.87 | 0.102 | 0.030 | 0.315 |
| PC3802-66 | 237.27 | 6.11 | 22.87 | 3.25 | 8.66 | 1.50 | 1.72 | 0.112 | 0.031 | 0.295 |
| PC3802-67 | 240.78 | 4.71 | 18.29 | 2.35 | 14.56 | 1.12 | 1.28 | 0.094 | 0.025 | 0.217 |
| PC3802-68 | 244.50 | 5.34 | 18.73 | 2.59 | 13.71 | 1.12 | 1.48 | 0.085 | 0.027 | 0.252 |
| PC3802-69 | 247.71 | 5.90 | 19.77 | 2.75 | 12.11 | 1.18 | 1.59 | 0.079 | 0.029 | 0.277 |
| PC3802-70 | 250.91 | 5.65 | 19.35 | 2.58 | 12.81 | 1.08 | 1.53 | 0.077 | 0.027 | 0.270 |
| PC3802-71 | 254.12 | 5.71 | 20.33 | 2.85 | 13.10 | 1.22 | 1.52 | 0.079 | 0.027 | 0.266 |
| PC3802-72 | 257.32 | 5.48 | 20.11 | 2.63 | 12.28 | 1.14 | 1.53 | 0.081 | 0.027 | 0.268 |
| PC3802-73 | 260.53 | 5.56 | 19.98 | 2.62 | 12.31 | 1.13 | 1.54 | 0.083 | 0.031 | 0.271 |
| PC3802-74 | 263.73 | 5.59 | 20.16 | 2.66 | 11.68 | 1.12 | 1.52 | 0.088 | 0.030 | 0.281 |
| | | | | | | | | | | |
| PC38-11 | 3835m | | | | | | | | | |
| | | | | | | | | | | |
| PC3811-01 | 0.80 | 7.12 | 27.18 | 2.44 | 1.88 | 1.21 | 1.69 | 0.313 | 0.029 | 0.376 |
| PC3811-02 | 2.00 | 6.01 | 24.44 | 2.55 | 5.98 | 1.16 | 1.30 | 0.378 | 0.033 | 0.338 |
| PC3811-03 | 2.20 | 6.09 | 26.76 | 2.46 | 5.14 | 1.31 | 1.40 | 0.363 | 0.036 | 0.368 |
| PC3811-04 | 3.49 | 7.38 | 28.22 | 2.68 | 1.47 | 1.23 | 1.86 | 0.197 | 0.028 | 0.368 |
| PC3811-05 | 6.17 | 7.27 | 27.36 | 2.45 | 2.33 | 1.21 | 1.82 | 0.169 | 0.030 | 0.359 |
| PC3811-06 | 8.85 | 7.11 | 25.90 | 2.89 | 2.92 | 1.07 | 1.78 | 0.133 | 0.029 | 0.352 |
| PC3811-07 | 11.53 | 7.27 | 26.20 | 2.79 | 3.09 | 1.18 | 1.83 | 0.129 | 0.034 | 0.350 |
| PC3811-08 | 13.80 | 7.15 | 25.60 | 2.87 | 3.61 | 1.16 | 1.78 | 0.140 | 0.032 | 0.348 |
| PC3811-09 | 16.44 | 7.14 | 28.48 | 2.68 | 5.23 | 1.97 | 1.79 | 0.271 | 0.038 | 0.318 |
| PC3811-10 | 18.63 | 6.74 | 25.34 | 2.82 | 4.65 | 1.20 | 1.74 | 0.139 | 0.033 | 0.339 |
| PC3811-11 | 20.82 | 6.49 | 24.65 | 2.86 | 5.12 | 1.12 | 1.63 | 0.135 | 0.032 | 0.329 |
| PC3811-12 | 23.23 | 6.64 | 25.63 | 2.96 | 4.11 | 1.17 | 1.67 | 0.140 | 0.029 | 0.331 |
| PC3811-13 | 25.11 | 6.83 | 25.51 | 2.90 | 4.22 | 1.19 | 1.78 | 0.134 | 0.031 | 0.339 |
| PC3811-14 | 27.10 | 6.79 | 25.30 | 2.86 | 4.72 | 1.21 | 1.68 | 0.153 | 0.031 | 0.341 |
| PC3811-15 | 29.09 | 7.22 | 26.76 | 2.87 | 4.18 | 1.37 | 1.79 | 0.152 | 0.033 | 0.348 |
| PC3811-16 | 31.08 | 6.55 | 24.76 | 2.75 | 5.44 | 1.19 | 1.60 | 0.164 | 0.036 | 0.333 |
| PC3811-17 | 33.07 | 7.38 | 27.02 | 3.00 | 4.67 | 1.40 | 1.82 | 0.152 | 0.034 | 0.341 |
| PC3811-18 | 35.07 | 6.72 | 25.89 | 2.80 | 5.46 | 1.48 | 1.73 | 0.223 | 0.035 | 0.327 |
| PC3811-19 | 37.26 | 6.88 | 25.56 | 2.58 | 3.58 | 1.15 | 1.80 | 0.151 | 0.036 | 0.337 |
| PC3811-20 | 39.45 | 7.05 | 25.53 | 2.99 | 3.26 | 1.09 | 1.77 | 0.145 | 0.029 | 0.346 |
| PC3811-21 | 40.84 | 7.15 | 25.99 | 2.95 | 2.47 | 1.16 | 1.87 | 0.139 | 0.029 | 0.342 |
| PC3811-22 | 43.03 | 6.38 | 24.01 | 2.88 | 5.75 | 1.12 | 1.61 | 0.185 | 0.032 | 0.317 |

| APPENDIX C.7. SALT-CORRECTED MAJOR ELEMENTS | | | | | | | | | | |
|---|---|---|---|---|---|---|---|---|---|---|
| | | | | | | | | | | |
| PC38-11 | 3835m | | | | | | | | | |
| Sample | Age | Al | Si | Fe | Ca | Na | K | P | Mn | Ti |
| | (ka) | (wt.%) | (wt.%) | (wt.%) | (wt.%) | (wt.%) | (wt.%) | (wt.%) | (wt.%) | (wt.%) |
| | | | | | | | | | | |
| PC3811-23 | 45.03 | 6.56 | 24.39 | 2.99 | 5.10 | 1.11 | 1.63 | 0.152 | 0.031 | 0.317 |
| PC3811-24 | 47.02 | 6.69 | 24.20 | 2.95 | 4.61 | 0.96 | 1.65 | 0.152 | 0.029 | 0.325 |
| PC3811-25 | 49.01 | 6.71 | 24.49 | 2.92 | 4.94 | 1.13 | 1.66 | 0.155 | 0.029 | 0.314 |
| PC3811-26 | 51.00 | 5.86 | 23.58 | 2.93 | 6.63 | 0.92 | 1.44 | 0.148 | 0.025 | 0.287 |
| PC3811-27 | 52.99 | 5.94 | 24.68 | 2.72 | 5.83 | 0.93 | 1.48 | 0.150 | 0.024 | 0.289 |
| PC3811-28 | 54.99 | 6.26 | 25.41 | 2.80 | 4.85 | 0.91 | 1.52 | 0.154 | 0.026 | 0.308 |
| PC3811-29 | 56.98 | 7.54 | 26.71 | 2.77 | 1.91 | 1.15 | 2.02 | 0.154 | 0.027 | 0.370 |
| PC3811-30 | 59.62 | 7.39 | 26.34 | 2.95 | 2.61 | 1.20 | 1.91 | 0.160 | 0.029 | 0.368 |
| PC3811-31 | 62.28 | 7.68 | 27.47 | 2.81 | 1.53 | 1.25 | 2.06 | 0.155 | 0.028 | 0.383 |
| PC3811-32 | 65.60 | 7.98 | 28.03 | 2.75 | 1.62 | 1.34 | 2.06 | 0.200 | 0.031 | 0.388 |
| PC3811-33 | 68.93 | 5.39 | 23.51 | 2.21 | 9.13 | 1.11 | 1.32 | 0.439 | 0.025 | 0.281 |
| PC3811-34 | 72.25 | 6.72 | 27.62 | 2.75 | 1.80 | 1.09 | 1.79 | 0.152 | 0.025 | 0.337 |
| PC3811-35 | 74.95 | 6.70 | 27.33 | 2.77 | 2.06 | 1.14 | 1.75 | 0.151 | 0.026 | 0.328 |
| PC3811-36 | 77.04 | 6.39 | 28.30 | 2.37 | 1.91 | 1.22 | 1.65 | 0.154 | 0.024 | 0.313 |
| PC3811-37 | 79.12 | 6.66 | 27.35 | 2.57 | 1.84 | 1.26 | 1.69 | 0.157 | 0.023 | 0.326 |
| PC3811-38 | 81.20 | 6.84 | 26.05 | 3.12 | 2.26 | 1.08 | 1.74 | 0.139 | 0.024 | 0.340 |
| PC3811-39 | 83.29 | 7.41 | 26.07 | 2.92 | 2.35 | 1.15 | 1.92 | 0.153 | 0.032 | 0.373 |
| PC3811-40 | 85.37 | 7.57 | 26.46 | 3.17 | 2.68 | 1.24 | 1.93 | 0.158 | 0.032 | 0.375 |
| PC3811-41 | 87.45 | 7.27 | 25.09 | 3.10 | 2.65 | 1.13 | 1.87 | 0.153 | 0.031 | 0.364 |
| PC3811-42 | 89.54 | 7.99 | 29.07 | 3.22 | 1.20 | 1.40 | 2.07 | 0.161 | 0.028 | 0.381 |
| PC3811-43 | 91.62 | 6.81 | 25.74 | 2.84 | 1.69 | 1.11 | 1.84 | 0.155 | 0.026 | 0.357 |
| PC3811-44 | 93.70 | 6.76 | 28.20 | 2.77 | 3.61 | 1.23 | 1.63 | 0.198 | 0.027 | 0.318 |
| PC3811-45 | 95.79 | 6.60 | 27.78 | 2.59 | 2.65 | 1.11 | 1.64 | 0.183 | 0.024 | 0.328 |
| PC3811-46 | 97.87 | 7.59 | 27.88 | 2.70 | 1.20 | 1.27 | 2.00 | 0.180 | 0.028 | 0.385 |
| PC3811-47 | 99.95 | 7.83 | 27.24 | 2.97 | 1.13 | 1.26 | 2.05 | 0.164 | 0.024 | 0.386 |
| PC3811-48 | 102.04 | 7.62 | 28.30 | 3.32 | 2.27 | 1.29 | 1.91 | 0.176 | 0.031 | 0.358 |
| PC3811-49 | 104.12 | 7.64 | 28.01 | 3.27 | 1.18 | 1.28 | 1.99 | 0.157 | 0.028 | 0.366 |
| PC3811-50 | 106.20 | 7.36 | 28.29 | 3.23 | 1.13 | 1.18 | 1.91 | 0.172 | 0.028 | 0.356 |
| PC3811-51 | 108.29 | 7.43 | 29.22 | 2.97 | 1.09 | 1.22 | 1.94 | 0.160 | 0.025 | 0.362 |
| PC3811-52 | 110.37 | 7.26 | 28.70 | 3.17 | 1.10 | 1.18 | 1.94 | 0.168 | 0.028 | 0.360 |
| PC3811-53 | 112.45 | 7.30 | 30.06 | 2.98 | 1.03 | 1.24 | 1.94 | 0.151 | 0.028 | 0.356 |
| PC3811-54 | 114.54 | 6.70 | 27.78 | 3.14 | 1.12 | 1.12 | 1.87 | 0.171 | 0.027 | 0.351 |
| PC3811-55 | 116.62 | 7.02 | 29.58 | 3.53 | 1.36 | 1.15 | 1.85 | 0.174 | 0.028 | 0.350 |
| PC3811-56 | 118.70 | 7.00 | 30.05 | 2.83 | 1.13 | 1.28 | 1.83 | 0.181 | 0.024 | 0.346 |
| PC3811-57 | 120.79 | 6.68 | 28.60 | 2.84 | 1.30 | 1.25 | 1.78 | 0.187 | 0.022 | 0.346 |

| APPENDIX C.8. SALT-CORRECTED MAJOR ELEMENT/Al RATIOS | | | | | | | | | |
|---|---|---|---|---|---|---|---|---|---|
| | | | | | | | | | |
| BC38-02 | 2530m | | | | | | | | |
| Sample | Depth (cm) | Si terr/Al | Fe/Al | Ca/Al | Na/Al | K/Al | P/Al | Mn/Al | Ti/Al |
| | | | | | | | | | |
| BC3802-01 | 0.5 | 2.68 | 0.62 | 1.04 | 0.11 | 0.263 | 0.023 | 6.6E-03 | 0.0458 |
| BC3802-02 | 1.5 | 2.69 | 0.62 | 0.98 | 0.07 | 0.265 | 0.021 | 6.4E-03 | 0.0454 |
| BC3802-03 | 2.5 | 2.79 | 0.62 | 1.04 | 0.15 | 0.268 | 0.021 | 6.3E-03 | 0.0459 |
| BC3802-04 | 3.5 | 2.69 | 0.62 | 1.07 | 0.13 | 0.261 | 0.021 | 4.7E-03 | 0.0455 |
| BC3802-05 | 4.5 | 2.71 | 0.62 | 1.11 | 0.12 | 0.275 | 0.021 | 4.4E-03 | 0.0458 |
| BC3802-06 | 5.5 | 2.75 | 0.61 | 1.13 | 0.17 | 0.279 | 0.022 | 4.6E-03 | 0.0454 |
| BC3802-07 | 6.5 | 2.58 | 0.59 | 1.12 | 0.22 | 0.271 | 0.020 | 4.2E-03 | 0.0445 |
| BC3802-08 | 7.5 | 2.52 | 0.62 | 1.13 | 0.22 | 0.276 | 0.021 | 4.2E-03 | 0.0452 |
| BC3802-09 | 8.5 | 2.62 | 0.60 | 1.13 | 0.22 | 0.281 | 0.021 | 4.9E-03 | 0.0460 |
| BC3802-10 | 9.5 | 2.52 | 0.59 | 1.18 | 0.20 | 0.275 | 0.020 | 4.6E-03 | 0.0464 |
| BC3802-11 | 11.0 | 2.62 | 0.57 | 1.27 | 0.18 | 0.270 | 0.020 | 4.7E-03 | 0.0445 |
| BC3802-12 | 13.0 | 2.59 | 0.62 | 1.57 | 0.16 | 0.281 | 0.021 | 4.4E-03 | 0.0473 |
| BC3802-13 | 15.0 | 2.55 | 0.57 | 1.66 | 0.26 | 0.284 | 0.021 | 4.8E-03 | 0.0461 |
| BC3802-13A | 17.0 | 2.43 | 0.53 | 2.14 | 0.23 | 0.274 | 0.021 | 4.5E-03 | 0.0450 |
| BC3802-14 | 19.0 | 2.49 | 0.54 | 2.56 | 0.24 | 0.280 | 0.023 | 4.7E-03 | 0.0464 |
| BC3802-15 | 21.0 | 2.56 | 0.53 | 2.80 | 0.18 | 0.285 | 0.023 | 5.2E-03 | 0.0469 |
| BC3802-16 | 23.0 | 2.79 | 0.54 | 2.94 | 0.24 | 0.276 | 0.024 | 4.3E-03 | 0.0471 |
| BC3802-17 | 25.0 | 2.73 | 0.54 | 3.04 | 0.17 | 0.282 | 0.024 | 4.5E-03 | 0.0467 |
| BC3802-18 | 27.0 | 2.73 | 0.53 | 3.15 | 0.23 | 0.273 | 0.023 | 5.1E-03 | 0.0465 |
| BC3802-19 | 29.0 | 2.73 | 0.53 | 3.36 | 0.15 | 0.278 | 0.024 | 4.5E-03 | 0.0469 |
| BC3802-20 | 31.0 | 2.80 | 0.52 | 3.30 | 0.24 | 0.266 | 0.024 | 4.9E-03 | 0.0469 |
| BC3802-21 | 33.0 | 2.71 | 0.52 | 3.14 | 0.16 | 0.292 | 0.022 | 5.2E-03 | 0.0466 |
| BC3802-21A | 35.0 | 2.63 | 0.50 | 2.75 | 0.21 | 0.278 | 0.018 | 3.8E-03 | 0.0470 |
| BC3802-22 | 37.0 | 2.70 | 0.51 | 2.91 | 0.15 | 0.272 | 0.020 | 3.4E-03 | 0.0466 |
| BC3802-23 | 39.0 | 2.82 | 0.52 | 3.11 | 0.24 | 0.281 | 0.022 | 4.6E-03 | 0.0467 |
| BC3802-24 | 41.0 | 2.65 | 0.51 | 2.85 | 0.19 | 0.276 | 0.018 | 4.8E-03 | 0.0465 |
| BC3802-25 | 43.0 | 2.57 | 0.51 | 2.75 | 0.22 | 0.291 | 0.018 | 3.9E-03 | 0.0468 |
| BC3802-26 | 45.0 | 2.57 | 0.52 | 2.76 | 0.17 | 0.292 | 0.018 | 4.8E-03 | 0.0482 |
| BC3802-27 | 47.0 | 2.63 | 0.50 | 2.69 | 0.22 | 0.288 | 0.018 | 3.7E-03 | 0.0470 |
| BC3802-28 | 49.0 | 2.69 | 0.50 | 2.68 | 0.19 | 0.288 | 0.018 | 4.2E-03 | 0.0476 |
| BC3802-29 | 51.0 | 2.64 | 0.50 | 2.65 | 0.21 | 0.283 | 0.018 | 4.4E-03 | 0.0476 |
| BC3802-30 | 53.0 | 2.65 | 0.49 | 2.60 | 0.20 | 0.277 | 0.019 | 4.8E-03 | 0.0471 |
| | | | | | | | | | |
| BC38-03 | 4289m | | | | | | | | |
| | | | | | | | | | |
| BC3803-01 | 0.5 | 1.94 | 0.61 | 0.14 | 0.01 | 0.250 | 0.018 | 1.3E-02 | 0.0461 |
| BC3803-02 | 1.5 | 2.14 | 0.64 | 0.14 | 0.07 | 0.256 | 0.018 | 1.0E-02 | 0.0467 |
| BC3803-03 | 2.5 | 2.06 | 0.64 | 0.14 | 0.05 | 0.257 | 0.018 | 7.2E-03 | 0.0468 |
| BC3803-04 | 3.5 | 2.00 | 0.59 | 0.15 | 0.17 | 0.256 | 0.016 | 4.3E-03 | 0.0466 |
| BC3803-05 | 4.5 | 1.97 | 0.51 | 0.14 | 0.15 | 0.260 | 0.014 | 3.5E-03 | 0.0458 |
| BC3803-06 | 5.5 | 1.89 | 0.42 | 0.14 | 0.15 | 0.263 | 0.014 | 4.0E-03 | 0.0466 |
| BC3803-07 | 6.5 | 1.96 | 0.42 | 0.14 | 0.20 | 0.267 | 0.014 | 3.7E-03 | 0.0471 |
| BC3803-08 | 7.5 | 2.09 | 0.43 | 0.14 | 0.20 | 0.265 | 0.013 | 3.2E-03 | 0.0467 |
| BC3803-09 | 8.5 | 2.06 | 0.45 | 0.15 | 0.17 | 0.266 | 0.013 | 3.5E-03 | 0.0468 |
| BC3803-10 | 9.5 | 2.07 | 0.44 | 0.14 | 0.20 | 0.255 | 0.013 | 4.1E-03 | 0.0454 |
| BC3803-11 | 11.0 | 2.14 | 0.44 | 0.14 | 0.21 | 0.262 | 0.013 | 4.0E-03 | 0.0467 |
| BC3803-12 | 13.0 | 2.11 | 0.41 | 0.15 | 0.15 | 0.263 | 0.013 | 3.9E-03 | 0.0476 |
| BC3803-13 | 15.0 | 2.12 | 0.46 | 0.15 | 0.23 | 0.270 | 0.014 | 4.4E-03 | 0.0476 |
| BC3803-14 | 17.0 | 2.29 | 0.43 | 0.15 | 0.16 | 0.267 | 0.014 | 3.9E-03 | 0.0484 |
| BC3803-15 | 19.0 | 2.25 | 0.41 | 0.16 | 0.21 | 0.265 | 0.014 | 4.4E-03 | 0.0479 |
| BC3803-16 | 21.0 | 2.06 | 0.41 | 0.16 | 0.19 | 0.266 | 0.014 | 3.4E-03 | 0.0481 |
| BC3803-17 | 23.0 | 1.93 | 0.45 | 0.16 | 0.22 | 0.268 | 0.015 | 3.8E-03 | 0.0477 |
| BC3803-18 | 25.0 | 2.02 | 0.41 | 0.16 | 0.17 | 0.267 | 0.015 | 4.2E-03 | 0.0485 |
| BC3803-19 | 27.0 | 2.04 | 0.44 | 0.17 | 0.24 | 0.269 | 0.015 | 4.2E-03 | 0.0488 |
| BC3803-20 | 29.0 | 2.28 | 0.44 | 0.17 | 0.18 | 0.269 | 0.015 | 4.7E-03 | 0.0485 |
| BC3803-21 | 31.0 | 2.33 | 0.46 | 0.17 | 0.26 | 0.277 | 0.015 | 5.1E-03 | 0.0486 |
| BC3803-22 | 33.0 | 2.32 | 0.43 | 0.17 | 0.22 | 0.270 | 0.015 | 4.2E-03 | 0.0484 |
| BC3803-23 | 35.0 | 2.25 | 0.42 | 0.18 | 0.24 | 0.275 | 0.015 | 4.3E-03 | 0.0486 |
| BC3803-24 | 37.0 | 2.38 | 0.45 | 0.18 | 0.23 | 0.271 | 0.015 | 4.5E-03 | 0.0477 |
| BC3803-25 | 39.0 | 2.31 | 0.45 | 0.19 | 0.22 | 0.272 | 0.020 | 4.9E-03 | 0.0473 |
| BC3803-26 | 41.0 | 2.50 | 0.46 | 0.18 | 0.18 | 0.279 | 0.015 | 4.7E-03 | 0.0491 |
| BC3803-27 | 43.0 | 2.46 | 0.47 | 0.19 | 0.24 | 0.278 | 0.015 | 4.5E-03 | 0.0485 |
| BC3803-28 | 45.0 | 2.41 | 0.45 | 0.19 | 0.21 | 0.279 | 0.015 | 4.0E-03 | 0.0487 |
| BC3803-29 | 47.0 | 2.41 | 0.47 | 0.19 | 0.23 | 0.284 | 0.016 | 4.7E-03 | 0.0489 |
| BC3803-30 | 49.0 | 2.54 | 0.47 | 0.19 | 0.19 | 0.281 | 0.016 | 4.4E-03 | 0.0486 |
| BC3803-31 | 51.0 | 2.52 | 0.49 | 0.19 | 0.21 | 0.281 | 0.016 | 4.3E-03 | 0.0486 |
| BC3803-32 | 53.0 | 2.51 | 0.46 | 0.19 | 0.23 | 0.280 | 0.016 | 4.5E-03 | 0.0489 |

| APPENDIX C.8. SALT-CORRECTED MAJOR ELEMENT/Al RATIOS | | | | | | | | | |
|---|---|---|---|---|---|---|---|---|---|
| PC38-09 | 148m | | | | | | | | |
| Sample | Depth (cm) | Si terr/Al | Fe/Al | Ca/Al | Na/Al | K/Al | P/Al | Mn/Al | Ti/Al |
| PC3809-01 | 4.0 | 3.28 | 0.44 | 0.36 | 0.233 | 0.221 | 0.041 | 3.9E-03 | 0.0548 |
| PC3809-02 | 13.0 | 2.98 | 0.39 | 0.41 | 0.166 | 0.207 | 0.030 | 4.1E-03 | 0.0509 |
| PC3809-03 | 23.0 | 2.70 | 0.36 | 0.24 | 0.206 | 0.201 | 0.027 | 4.1E-03 | 0.0463 |
| PC3809-04 | 34.0 | 2.94 | 0.37 | 0.22 | 0.235 | 0.207 | 0.029 | 3.9E-03 | 0.0497 |
| PC3809-05 | 43.0 | 3.71 | 0.37 | 0.28 | 0.226 | 0.223 | 0.036 | 5.2E-03 | 0.0559 |
| PC3809-06 | 53.0 | 2.95 | 0.42 | 0.23 | 0.207 | 0.215 | 0.042 | 4.7E-03 | 0.0525 |
| PC3809-07 | 62.0 | 2.89 | 0.40 | 0.39 | 0.259 | 0.197 | 0.039 | 3.4E-03 | 0.0485 |
| PC3809-08 | 73.0 | 3.08 | 0.37 | 0.21 | 0.110 | 0.210 | 0.029 | 4.8E-03 | 0.0535 |
| PC3809-09 | 84.0 | 2.61 | 0.39 | 0.14 | 0.158 | 0.210 | 0.020 | 3.8E-03 | 0.0510 |
| PC3809-10 | 94.0 | 2.51 | 0.45 | 0.19 | 0.162 | 0.212 | 0.023 | 4.3E-03 | 0.0487 |
| PC3809-11 | 104.0 | 2.69 | 0.37 | 0.17 | 0.173 | 0.211 | 0.023 | 3.6E-03 | 0.0485 |
| PC3809-12 | 113.0 | 2.63 | 0.39 | 0.15 | 0.182 | 0.216 | 0.019 | 4.2E-03 | 0.0517 |
| PC3809-13 | 124.0 | 3.17 | 0.35 | 0.28 | 0.176 | 0.214 | 0.033 | 4.4E-03 | 0.0553 |
| PC3809-14 | 134.0 | 3.26 | 0.39 | 0.31 | 0.235 | 0.210 | 0.046 | 4.0E-03 | 0.0514 |
| PC3809-15 | 144.0 | 3.29 | 0.40 | 0.30 | 0.226 | 0.216 | 0.036 | 3.9E-03 | 0.0520 |
| PC3809-16 | 152.0 | 3.56 | 0.42 | 0.30 | 0.212 | 0.221 | 0.026 | 3.7E-03 | 0.0520 |
| PC3809-17 | 165.0 | 3.68 | 0.41 | 0.44 | 0.233 | 0.216 | 0.044 | 4.4E-03 | 0.0540 |
| PC3809-18 | 174.0 | 3.87 | 0.35 | 0.28 | 0.221 | 0.223 | 0.040 | 4.5E-03 | 0.0541 |
| PC3809-19 | 185.0 | 4.58 | 0.35 | 0.41 | 0.268 | 0.225 | 0.072 | 4.9E-03 | 0.0552 |
| PC3809-20 | 194.0 | 4.50 | 0.34 | 0.49 | 0.272 | 0.223 | 0.067 | 5.7E-03 | 0.0566 |
| PC3809-21 | 205.0 | 3.78 | 0.46 | 0.41 | 0.265 | 0.226 | 0.023 | 7.2E-03 | 0.0565 |
| PC3809-22 | 214.0 | 4.19 | 0.35 | 0.42 | 0.257 | 0.223 | 0.070 | 4.2E-03 | 0.0545 |
| PC3809-23 | 224.0 | 5.28 | 0.29 | 0.49 | 0.301 | 0.233 | 0.083 | 4.7E-03 | 0.0528 |
| PC3809-24 | 234.0 | 4.94 | 0.38 | 0.54 | 0.292 | 0.224 | 0.110 | 4.3E-03 | 0.0540 |
| PC3809-25 | 243.0 | 4.65 | 0.44 | 0.39 | 0.308 | 0.226 | 0.080 | 5.3E-03 | 0.0517 |
| PC3809-26 | 257.0 | 4.62 | 0.43 | 0.34 | 0.258 | 0.228 | 0.059 | 4.5E-03 | 0.0540 |
| PC3809-27 | 267.0 | 5.24 | 0.36 | 0.76 | 0.299 | 0.238 | 0.204 | 5.3E-03 | 0.0536 |
| PC3809-28 | 273.0 | 4.79 | 1.14 | 7.16 | 0.415 | 0.258 | 2.247 | 7.0E-03 | 0.0543 |
| PC3809-29 | 284.0 | 3.69 | 0.48 | 0.34 | 0.238 | 0.217 | 0.052 | 5.8E-03 | 0.0561 |
| PC3809-30 | 294.0 | 4.37 | 0.46 | 0.40 | 0.321 | 0.224 | 0.034 | 4.3E-03 | 0.0516 |
| PC3809-31 | 304.0 | 3.46 | 0.47 | 0.22 | 0.239 | 0.216 | 0.027 | 6.0E-03 | 0.0559 |
| PC3809-32 | 314.0 | 3.24 | 0.45 | 0.26 | 0.214 | 0.213 | 0.023 | 4.8E-03 | 0.0493 |
| PC3809-33 | 324.0 | 3.41 | 0.50 | 0.26 | 0.217 | 0.214 | 0.035 | 5.2E-03 | 0.0549 |
| PC3809-34 | 335.0 | 3.79 | 0.49 | 0.27 | 0.239 | 0.214 | 0.029 | 5.5E-03 | 0.0525 |
| PC3809-35 | 344.0 | 3.94 | 0.54 | 0.27 | 0.264 | 0.214 | 0.032 | 4.6E-03 | 0.0560 |
| PC3809-36 | 355.0 | 4.76 | 0.46 | 0.48 | 0.371 | 0.220 | 0.025 | 5.2E-03 | 0.0486 |
| PC3809-37 | 364.0 | 4.38 | 0.50 | 0.79 | 0.285 | 0.217 | 0.025 | 4.9E-03 | 0.0482 |
| PC3809-38 | 375.0 | 3.81 | 0.46 | 0.29 | 0.268 | 0.224 | 0.020 | 5.0E-03 | 0.0483 |
| PC3809-39 | 384.0 | 3.44 | 0.50 | 0.45 | 0.237 | 0.214 | 0.036 | 6.0E-03 | 0.0547 |
| PC3809-40 | 394.0 | 3.75 | 0.45 | 0.38 | 0.267 | 0.223 | 0.031 | 5.3E-03 | 0.0510 |
| PC3809-41 | 404.0 | 3.66 | 0.45 | 0.21 | 0.251 | 0.226 | 0.022 | 5.5E-03 | 0.0511 |
| PC3809-42 | 416.0 | 3.74 | 0.47 | 0.69 | 0.271 | 0.216 | 0.030 | 4.0E-03 | 0.0501 |
| PC3809-43 | 424.0 | 3.62 | 0.44 | 0.23 | 0.261 | 0.228 | 0.019 | 5.2E-03 | 0.0490 |
| PC3809-44 | 434.0 | 3.45 | 0.46 | 0.21 | 0.249 | 0.229 | 0.021 | 4.9E-03 | 0.0483 |
| PC3809-45 | 444.0 | 3.86 | 0.50 | 0.51 | 0.280 | 0.221 | 0.029 | 5.5E-03 | 0.0502 |
| PC3809-46 | 453.0 | 3.56 | 0.47 | 0.28 | 0.231 | 0.217 | 0.028 | 4.9E-03 | 0.0548 |
| PC3809-47 | 465.0 | 3.48 | 0.50 | 0.36 | 0.217 | 0.219 | 0.029 | 5.5E-03 | 0.0519 |
| PC3809-48 | 474.0 | 3.70 | 0.45 | 0.53 | 0.248 | 0.230 | 0.027 | 4.2E-03 | 0.0469 |
| PC3809-49 | 483.0 | 3.74 | 0.48 | 0.25 | 0.251 | 0.228 | 0.030 | 5.0E-03 | 0.0542 |
| PC3809-50 | 493.0 | 3.59 | 0.48 | 0.28 | 0.243 | 0.237 | 0.027 | 6.6E-03 | 0.0503 |
| PC3809-51 | 504.0 | 4.05 | 0.48 | 0.27 | 0.237 | 0.232 | 0.030 | 5.5E-03 | 0.0553 |
| PC3809-52 | 515.0 | 3.99 | 0.47 | 0.24 | 0.265 | 0.238 | 0.024 | 5.3E-03 | 0.0530 |
| PC3809-53 | 525.0 | 3.86 | 0.45 | 0.40 | 0.264 | 0.233 | 0.021 | 5.3E-03 | 0.0480 |
| PC3809-54 | 536.0 | 4.17 | 0.46 | 0.58 | 0.280 | 0.230 | 0.022 | 5.8E-03 | 0.0489 |
| PC3809-55 | 544.0 | 3.82 | 0.49 | 0.35 | 0.241 | 0.230 | 0.025 | 5.6E-03 | 0.0539 |
| PC3809-56 | 553.0 | 3.97 | 0.51 | 0.47 | 0.243 | 0.224 | 0.017 | 6.5E-03 | 0.0503 |
| PC3809-57 | 564.0 | 4.06 | 0.51 | 0.49 | 0.258 | 0.218 | 0.020 | 6.4E-03 | 0.0525 |
| PC3809-58 | 574.0 | 4.35 | 0.52 | 0.54 | 0.277 | 0.236 | 0.023 | 6.6E-03 | 0.0519 |
| PC3809-59 | 585.0 | 4.31 | 0.51 | 0.73 | 0.259 | 0.228 | 0.063 | 6.5E-03 | 0.0527 |
| PC3809-60 | 594.0 | 4.53 | 0.49 | 0.55 | 0.278 | 0.236 | 0.026 | 6.5E-03 | 0.0525 |
| PC3809-61 | 605.0 | 3.95 | 0.52 | 0.56 | 0.233 | 0.232 | 0.033 | 6.6E-03 | 0.0531 |
| PC3809-62 | 615.0 | 4.31 | 0.48 | 0.60 | 0.265 | 0.242 | 0.044 | 6.9E-03 | 0.0522 |
| PC3809-63 | 625.0 | 4.14 | 0.50 | 0.52 | 0.260 | 0.232 | 0.037 | 7.0E-03 | 0.0533 |
| PC3809-64 | 635.0 | 3.96 | 0.51 | 0.56 | 0.241 | 0.230 | 0.035 | 7.0E-03 | 0.0538 |
| PC3809-65 | 646.0 | 4.34 | 0.48 | 0.51 | 0.264 | 0.224 | 0.028 | 6.2E-03 | 0.0515 |
| PC3809-66 | 654.0 | 4.42 | 0.48 | 0.49 | 0.263 | 0.224 | 0.023 | 6.9E-03 | 0.0535 |
| PC3809-67 | 664.0 | 4.49 | 0.48 | 0.52 | 0.275 | 0.228 | 0.019 | 5.6E-03 | 0.0509 |

| APPENDIX C.8. SALT-CORRECTED MAJOR ELEMENT/Al RATIOS | | | | | | | | | |
|---|---|---|---|---|---|---|---|---|---|
| | | | | | | | | | |
| PC38-09 | 148m | | | | | | | | |
| Sample | Depth (cm) | Si terr/Al | Fe/Al | Ca/Al | Na/Al | K/Al | P/Al | Mn/Al | Ti/Al |
| | | | | | | | | | |
| PC3809-68 | 674.0 | 4.65 | 0.53 | 0.50 | 0.257 | 0.240 | 0.020 | 6.4E-03 | 0.0546 |
| PC3809-69 | 684.0 | 4.04 | 0.49 | 0.46 | 0.252 | 0.240 | 0.021 | 5.5E-03 | 0.0512 |
| PC3809-70 | 694.0 | 3.72 | 0.49 | 0.44 | 0.233 | 0.224 | 0.020 | 6.8E-03 | 0.0515 |
| PC3809-71 | 703.0 | 3.69 | 0.51 | 0.42 | 0.241 | 0.237 | 0.016 | 6.5E-03 | 0.0502 |
| PC3809-72 | 714.0 | 3.86 | 0.50 | 0.53 | 0.272 | 0.235 | 0.025 | 5.9E-03 | 0.0523 |
| PC3809-73 | 724.0 | 3.89 | 0.52 | 0.50 | 0.247 | 0.235 | 0.033 | 6.7E-03 | 0.0533 |
| PC3809-74 | 734.0 | 3.71 | 0.51 | 0.54 | 0.233 | 0.234 | 0.033 | 6.3E-03 | 0.0532 |
| PC3809-75 | 744.0 | 4.05 | 0.52 | 0.50 | 0.258 | 0.240 | 0.028 | 7.0E-03 | 0.0504 |
| PC3809-76 | 754.0 | 4.20 | 0.51 | 0.52 | 0.249 | 0.237 | 0.019 | 6.7E-03 | 0.0517 |
| PC3809-77 | 764.0 | 3.74 | 0.49 | 0.55 | 0.220 | 0.252 | 0.022 | 7.0E-03 | 0.0516 |
| PC3809-78 | 774.0 | 3.80 | 0.51 | 0.51 | 0.222 | 0.239 | 0.023 | 6.9E-03 | 0.0542 |
| PC3809-79 | 784.0 | 3.98 | 0.52 | 0.51 | 0.220 | 0.247 | 0.022 | 6.3E-03 | 0.0533 |
| PC3809-80 | 794.0 | 3.96 | 0.49 | 0.52 | 0.224 | 0.250 | 0.025 | 6.1E-03 | 0.0533 |
| PC3809-81 | 804.0 | 4.30 | 0.49 | 0.48 | 0.239 | 0.241 | 0.033 | 6.2E-03 | 0.0544 |
| PC3809-82 | 813.0 | 3.96 | 0.54 | 0.59 | 0.246 | 0.229 | 0.052 | 6.7E-03 | 0.0550 |
| PC3809-83 | 823.0 | 4.25 | 0.51 | 0.49 | 0.243 | 0.241 | 0.036 | 7.0E-03 | 0.0545 |
| PC3809-84 | 834.0 | 4.00 | 0.49 | 0.46 | 0.229 | 0.237 | 0.028 | 6.3E-03 | 0.0542 |
| PC3809-85 | 845.0 | 4.00 | 0.48 | 0.46 | 0.246 | 0.244 | 0.033 | 6.4E-03 | 0.0516 |
| PC3809-86 | 854.0 | 3.57 | 0.49 | 0.35 | 0.224 | 0.249 | 0.015 | 7.3E-03 | 0.0513 |
| | | | | | | | | | |
| PC38-10 | 257m | | | | | | | | |
| | | | | | | | | | |
| PC3810-01 | 6.0 | 3.30 | 0.38 | 1.20 | 0.249 | 0.223 | 0.090 | 3.4E-03 | 0.0497 |
| PC3810-02 | 14.0 | 4.44 | 0.34 | 1.00 | 0.287 | 0.231 | 0.194 | 4.8E-03 | 0.0543 |
| PC3810-03 | 24.0 | 5.06 | 0.29 | 1.23 | 0.325 | 0.244 | 0.354 | 4.9E-03 | 0.0505 |
| PC3810-04 | 34.0 | 4.99 | 0.27 | 1.17 | 0.306 | 0.237 | 0.186 | 3.8E-03 | 0.0503 |
| PC3810-05 | 44.0 | 4.30 | 0.36 | 0.38 | 0.267 | 0.252 | 0.074 | 5.3E-03 | 0.0538 |
| PC3810-06 | 54.0 | 4.10 | 0.36 | 0.30 | 0.265 | 0.245 | 0.049 | 3.5E-03 | 0.0506 |
| PC3810-07 | 64.0 | 4.14 | 0.39 | 0.38 | 0.268 | 0.253 | 0.075 | 4.1E-03 | 0.0523 |
| PC3810-08 | 74.0 | 4.41 | 0.36 | 0.49 | 0.272 | 0.253 | 0.112 | 4.7E-03 | 0.0517 |
| PC3810-09 | 84.0 | 5.79 | 0.32 | 0.79 | 0.305 | 0.272 | 0.201 | 5.0E-03 | 0.0494 |
| PC3810-10 | 94.0 | 5.26 | 0.31 | 1.00 | 0.310 | 0.248 | 0.262 | 4.7E-03 | 0.0462 |
| PC3810-10 | 104.0 | 5.35 | 0.28 | 1.28 | 0.317 | 0.254 | 0.160 | 4.6E-03 | 0.0471 |
| PC3810-11 | 113.0 | 5.37 | 0.26 | 1.12 | 0.310 | 0.242 | 0.104 | 4.8E-03 | 0.0453 |
| PC3810-12 | 126.0 | 4.24 | 0.40 | 1.29 | 0.252 | 0.242 | 0.109 | 4.2E-03 | 0.0510 |
| PC3810-13 | 134.0 | 4.09 | 0.42 | 0.89 | 0.241 | 0.241 | 0.118 | 4.2E-03 | 0.0514 |
| PC3810-14 | 146.0 | 4.11 | 0.41 | 0.72 | 0.255 | 0.245 | 0.078 | 4.2E-03 | 0.0526 |
| PC3810-15 | 154.0 | 3.86 | 0.42 | 1.29 | 0.229 | 0.239 | 0.085 | 4.9E-03 | 0.0517 |
| PC3810-16 | 167.0 | 3.95 | 0.40 | 0.65 | 0.223 | 0.246 | 0.059 | 3.7E-03 | 0.0530 |
| PC3810-17 | 174.0 | 3.85 | 0.37 | 0.36 | 0.234 | 0.248 | 0.064 | 4.2E-03 | 0.0509 |
| PC3810-18 | 185.0 | 3.90 | 0.39 | 0.26 | 0.209 | 0.253 | 0.052 | 4.7E-03 | 0.0523 |
| PC3810-19 | 194.0 | 3.79 | 0.43 | 0.88 | 0.217 | 0.249 | 0.056 | 4.3E-03 | 0.0494 |
| PC3810-20 | 203.0 | 3.88 | 0.37 | 0.39 | 0.227 | 0.247 | 0.064 | 4.2E-03 | 0.0526 |
| PC3810-21 | 216.0 | 3.96 | 0.42 | 0.97 | 0.252 | 0.245 | 0.075 | 3.9E-03 | 0.0514 |
| PC3810-22 | 224.0 | 4.00 | 0.43 | 0.62 | 0.219 | 0.238 | 0.056 | 3.7E-03 | 0.0506 |
| PC3810-23 | 233.0 | 3.52 | 0.41 | 0.47 | 0.222 | 0.248 | 0.054 | 4.7E-03 | 0.0520 |
| PC3810-24 | 244.0 | 3.71 | 0.41 | 0.80 | 0.225 | 0.240 | 0.067 | 4.1E-03 | 0.0520 |
| PC3810-25 | 254.0 | 4.49 | 0.34 | 0.97 | 0.272 | 0.246 | 0.133 | 4.2E-03 | 0.0501 |
| PC3810-26 | 263.0 | 4.34 | 0.37 | 1.11 | 0.272 | 0.241 | 0.116 | 3.9E-03 | 0.0505 |
| PC3810-27 | 273.0 | 3.70 | 0.41 | 0.84 | 0.220 | 0.245 | 0.058 | 4.7E-03 | 0.0519 |
| PC3810-28 | 284.0 | 3.89 | 0.39 | 1.13 | 0.211 | 0.240 | 0.070 | 4.6E-03 | 0.0535 |
| PC3810-29 | 295.0 | 3.82 | 0.44 | 2.30 | 0.203 | 0.238 | 0.076 | 4.2E-03 | 0.0495 |
| PC3810-30 | 305.0 | 3.54 | 0.43 | 1.10 | 0.192 | 0.230 | 0.051 | 4.8E-03 | 0.0531 |
| PC3810-31 | 314.0 | 3.70 | 0.38 | 1.06 | 0.206 | 0.233 | 0.057 | 3.8E-03 | 0.0535 |
| PC3810-32 | 324.0 | 3.77 | 0.43 | 1.50 | 0.212 | 0.234 | 0.067 | 5.0E-03 | 0.0498 |
| PC3810-33 | 335.0 | 3.77 | 0.40 | 0.96 | 0.217 | 0.242 | 0.057 | 4.4E-03 | 0.0517 |
| PC3810-34 | 344.0 | 4.32 | 0.45 | 1.90 | 0.240 | 0.229 | 0.083 | 4.2E-03 | 0.0495 |
| PC3810-35 | 354.0 | 5.21 | 0.41 | 1.21 | 0.272 | 0.235 | 0.067 | 2.2E-03 | 0.0494 |
| PC3810-36 | 364.0 | 4.84 | 0.42 | 1.75 | 0.291 | 0.237 | 0.084 | 3.5E-03 | 0.0492 |
| PC3810-37 | 374.0 | 5.12 | 0.38 | 1.27 | 0.250 | 0.227 | 0.067 | 2.4E-03 | 0.0488 |
| PC3810-38 | 383.0 | 3.21 | 0.39 | 0.82 | 0.178 | 0.225 | 0.041 | 4.3E-03 | 0.0509 |
| PC3810-39 | 394.0 | 3.76 | 0.37 | 0.90 | 0.213 | 0.229 | 0.063 | 3.6E-03 | 0.0514 |
| PC3810-40 | 404.0 | 3.54 | 0.36 | 0.91 | 0.199 | 0.229 | 0.052 | 4.4E-03 | 0.0541 |
| PC3810-41 | 417.0 | 3.59 | 0.39 | 1.63 | 0.195 | 0.222 | 0.074 | 3.4E-03 | 0.0525 |
| PC3810-42 | 424.0 | 3.40 | 0.37 | 1.19 | 0.211 | 0.232 | 0.064 | 5.1E-03 | 0.0509 |
| PC3810-43 | 434.0 | 5.14 | 0.41 | 5.05 | 0.286 | 0.232 | 0.165 | 3.5E-03 | 0.0506 |
| PC3810-44 | 445.0 | 3.76 | 0.39 | 2.21 | 0.214 | 0.230 | 0.069 | 2.8E-03 | 0.0491 |

| APPENDIX C.8. SALT-CORRECTED MAJOR ELEMENT/Al RATIOS | | | | | | | | | |
|---|---|---|---|---|---|---|---|---|---|
| | | | | | | | | | |
| PC38-10 | 257m | | | | | | | | |
| Sample | Depth | Si terr/Al | Fe/Al | Ca/Al | Na/Al | K/Al | P/Al | Mn/Al | Ti/Al |
| | (cm) | | | | | | | | |
| | | | | | | | | | |
| PC3810-45 | 456.0 | 4.24 | 0.40 | 2.16 | 0.226 | 0.223 | 0.078 | 3.4E-03 | 0.0497 |
| PC3810-46 | 467.0 | 5.33 | 0.41 | 3.23 | 0.295 | 0.235 | 0.088 | 1.2E-03 | 0.0492 |
| PC3810-47 | 476.0 | 3.54 | 0.38 | 1.80 | 0.209 | 0.230 | 0.105 | 4.2E-03 | 0.0524 |
| PC3810-48 | 484.0 | 3.58 | 0.39 | 2.04 | 0.200 | 0.228 | 0.104 | 3.4E-03 | 0.0518 |
| PC3810-49 | 494.0 | 4.20 | 0.35 | 2.21 | 0.255 | 0.223 | 0.211 | 4.3E-03 | 0.0537 |
| PC3810-50 | 504.0 | 5.02 | 0.31 | 1.51 | 0.321 | 0.242 | 0.460 | 3.8E-03 | 0.0507 |
| PC3810-51 | 514.0 | 4.20 | 0.49 | 0.45 | 0.250 | 0.228 | 0.021 | 5.6E-03 | 0.0552 |
| PC3810-52 | 524.0 | 4.17 | 0.48 | 0.36 | 0.250 | 0.228 | 0.018 | 6.3E-03 | 0.0551 |
| PC3810-53 | 534.0 | 3.79 | 0.40 | 1.10 | 0.259 | 0.224 | 0.059 | 3.6E-03 | 0.0451 |
| PC3810-54 | 545.0 | 3.94 | 0.39 | 0.84 | 0.282 | 0.237 | 0.045 | 3.8E-03 | 0.0461 |
| PC3810-55 | 554.0 | 3.95 | 0.40 | 1.32 | 0.269 | 0.227 | 0.048 | 3.9E-03 | 0.0449 |
| PC3810-56 | 564.0 | 4.16 | 0.43 | 2.20 | 0.286 | 0.229 | 0.085 | 5.4E-03 | 0.0476 |
| PC3810-57 | 574.0 | 3.91 | 0.42 | 2.16 | 0.236 | 0.222 | 0.062 | 4.5E-03 | 0.0475 |
| PC3810-58 | 584.0 | 4.03 | 0.42 | 1.89 | 0.275 | 0.241 | 0.048 | 5.3E-03 | 0.0475 |
| PC3810-59 | 596.0 | 4.14 | 0.42 | 1.68 | 0.296 | 0.240 | 0.052 | 3.8E-03 | 0.0469 |
| PC3810-60 | 604.0 | 3.82 | 0.43 | 2.02 | 0.298 | 0.243 | 0.051 | 4.8E-03 | 0.0466 |
| PC3810-61 | 614.0 | 3.84 | 0.42 | 1.30 | 0.240 | 0.234 | 0.033 | 3.8E-03 | 0.0462 |
| PC3810-62 | 624.0 | 3.74 | 0.41 | 1.40 | 0.214 | 0.247 | 0.043 | 4.6E-03 | 0.0484 |
| PC3810-63 | 634.0 | 3.74 | 0.41 | 1.43 | 0.382 | 0.244 | 0.046 | 4.5E-03 | 0.0466 |
| PC3810-64 | 645.0 | 3.77 | 0.44 | 1.12 | 0.246 | 0.234 | 0.032 | 5.9E-03 | 0.0460 |
| PC3810-65 | 655.0 | 3.82 | 0.43 | 1.30 | 0.262 | 0.236 | 0.031 | 3.8E-03 | 0.0450 |
| PC3810-66 | 667.0 | 3.82 | 0.42 | 1.13 | 0.245 | 0.246 | 0.036 | 4.3E-03 | 0.0453 |
| PC3810-67 | 674.0 | 3.42 | 0.41 | 0.74 | 0.193 | 0.246 | 0.032 | 4.8E-03 | 0.0458 |
| PC3810-68 | 683.0 | 3.55 | 0.40 | 0.94 | 0.210 | 0.250 | 0.027 | 4.2E-03 | 0.0439 |
| PC3810-69 | 694.0 | 3.08 | 0.40 | 0.49 | 0.183 | 0.253 | 0.030 | 4.1E-03 | 0.0464 |
| PC3810-70 | 704.0 | 3.05 | 0.35 | 0.24 | 0.163 | 0.263 | 0.026 | 4.7E-03 | 0.0485 |
| PC3810-71 | 714.0 | 2.99 | 0.39 | 0.58 | 0.171 | 0.263 | 0.032 | 4.3E-03 | 0.0447 |
| PC3810-72 | 724.0 | 3.27 | 0.39 | 0.78 | 0.166 | 0.252 | 0.032 | 5.2E-03 | 0.0435 |
| PC3810-74 | 734.0 | 3.09 | 0.34 | 0.22 | 0.177 | 0.261 | 0.030 | 3.5E-03 | 0.0473 |
| PC3810-75 | 745.0 | 3.09 | 0.36 | 0.20 | 0.186 | 0.260 | 0.026 | 4.7E-03 | 0.0482 |
| PC3810-76 | 754.0 | 3.36 | 0.38 | 0.29 | 0.202 | 0.256 | 0.040 | 4.5E-03 | 0.0485 |
| PC3810-77 | 764.0 | 3.71 | 0.34 | 0.37 | 0.219 | 0.256 | 0.076 | 4.7E-03 | 0.0530 |
| | | | | | | | | | |
| PC38-02 | 2525m | | | | | | | | |
| | (Age) | | | | | | | | |
| PC3802-01 | 2.76 | 2.35 | 0.53 | 1.52 | 0.223 | 0.252 | 0.020 | 4.8E-03 | 0.0491 |
| PC3802-02 | 6.21 | 2.43 | 0.52 | 2.29 | 0.223 | 0.258 | 0.022 | 5.5E-03 | 0.0481 |
| PC3802-03 | 9.66 | 2.57 | 0.52 | 2.56 | 0.216 | 0.246 | 0.021 | 4.7E-03 | 0.0490 |
| PC3802-04 | 12.77 | 2.36 | 0.50 | 1.97 | 0.204 | 0.260 | 0.018 | 4.5E-03 | 0.0469 |
| PC3802-05 | 15.18 | 2.49 | 0.49 | 2.37 | 0.198 | 0.254 | 0.017 | 4.5E-03 | 0.0495 |
| PC3802-06 | 17.47 | 2.48 | 0.53 | 2.35 | 0.214 | 0.262 | 0.017 | 5.0E-03 | 0.0488 |
| PC3802-07 | 20.48 | 2.57 | 0.48 | 2.21 | 0.092 | 0.244 | 0.017 | 4.8E-03 | 0.0505 |
| PC3802-08 | 22.65 | 2.61 | 0.51 | 2.19 | 0.168 | 0.254 | 0.017 | 4.1E-03 | 0.0499 |
| PC3802-09 | 25.22 | 2.54 | 0.51 | 2.66 | 0.193 | 0.251 | 0.019 | 4.8E-03 | 0.0525 |
| PC3802-10 | 28.29 | 2.38 | 0.51 | 3.11 | 0.211 | 0.251 | 0.020 | 4.9E-03 | 0.0532 |
| PC3802-11 | 31.07 | 2.22 | 0.50 | 3.23 | 0.209 | 0.255 | 0.020 | 5.9E-03 | 0.0530 |
| PC3802-12 | 33.86 | 2.05 | 0.54 | 3.69 | 0.220 | 0.263 | 0.021 | 5.1E-03 | 0.0537 |
| PC3802-13 | 36.64 | 2.32 | 0.55 | 3.14 | 0.192 | 0.246 | 0.019 | 5.2E-03 | 0.0511 |
| PC3802-14 | 39.15 | 2.48 | 0.48 | 2.26 | 0.206 | 0.255 | 0.018 | 5.2E-03 | 0.0499 |
| PC3802-15 | 42.22 | 2.26 | 0.49 | 2.10 | 0.214 | 0.258 | 0.017 | 4.8E-03 | 0.0494 |
| PC3802-16 | 45.00 | 2.69 | 0.49 | 1.78 | 0.166 | 0.260 | 0.017 | 4.9E-03 | 0.0503 |
| PC3802-17 | 48.07 | 2.55 | 0.48 | 1.53 | 0.203 | 0.266 | 0.016 | 4.6E-03 | 0.0498 |
| PC3802-18 | 50.85 | 2.49 | 0.56 | 1.41 | 0.218 | 0.275 | 0.018 | 5.4E-03 | 0.0521 |
| PC3802-19 | 53.64 | 2.45 | 0.54 | 1.54 | 0.212 | 0.267 | 0.018 | 5.2E-03 | 0.0514 |
| PC3802-20 | 56.42 | 2.55 | 0.51 | 1.26 | 0.212 | 0.267 | 0.017 | 4.8E-03 | 0.0519 |
| PC3802-21 | 59.29 | 2.51 | 0.50 | 1.40 | 0.196 | 0.261 | 0.016 | 4.9E-03 | 0.0505 |
| PC3802-22 | 62.61 | 2.61 | 0.51 | 1.50 | 0.208 | 0.262 | 0.017 | 4.9E-03 | 0.0503 |
| PC3802-23 | 65.94 | 2.59 | 0.50 | 1.28 | 0.211 | 0.263 | 0.016 | 5.1E-03 | 0.0512 |
| PC3802-24 | 69.26 | 2.64 | 0.50 | 0.60 | 0.221 | 0.274 | 0.015 | 4.7E-03 | 0.0514 |
| PC3802-25 | 72.58 | 2.58 | 0.52 | 0.91 | 0.223 | 0.266 | 0.018 | 4.8E-03 | 0.0528 |
| PC3802-26 | 76.96 | 2.53 | 0.53 | 1.47 | 0.233 | 0.267 | 0.020 | 5.0E-03 | 0.0528 |
| PC3802-27 | 82.03 | 2.50 | 0.51 | 0.66 | 0.229 | 0.277 | 0.017 | 4.8E-03 | 0.0506 |
| PC3802-28 | 87.11 | 2.70 | 0.50 | 0.73 | 0.214 | 0.280 | 0.016 | 4.2E-03 | 0.0493 |
| PC3802-29 | 92.18 | 2.54 | 0.49 | 0.38 | 0.203 | 0.278 | 0.015 | 4.3E-03 | 0.0492 |
| PC3802-30 | 97.26 | 2.58 | 0.51 | 0.51 | 0.202 | 0.275 | 0.018 | 4.7E-03 | 0.0511 |
| PC3802-31 | 102.84 | 2.52 | 0.52 | 0.95 | 0.211 | 0.267 | 0.020 | 4.7E-03 | 0.0517 |
| PC3802-32 | 107.92 | 2.48 | 0.52 | 0.90 | 0.210 | 0.272 | 0.019 | 5.0E-03 | 0.0507 |

| APPENDIX C.8. SALT-CORRECTED MAJOR ELEMENT/Al RATIOS | | | | | | | | | |
|---|---|---|---|---|---|---|---|---|---|
| | | | | | | | | | |
| PC38-02 | 2525m | | | | | | | | |
| Sample | Age | Si terr/Al | Fe/Al | Ca/Al | Na/Al | K/Al | P/Al | Mn/Al | Ti/Al |
| | (ka) | | | | | | | | |
| | | | | | | | | | |
| PC3802-33 | 113.00 | 2.38 | 0.56 | 0.90 | 0.204 | 0.273 | 0.017 | 5.3E-03 | 0.0496 |
| PC3802-34 | 118.07 | 2.50 | 0.56 | 0.93 | 0.210 | 0.268 | 0.017 | 4.5E-03 | 0.0487 |
| PC3802-35 | 123.15 | 2.27 | 0.50 | 1.71 | 0.218 | 0.268 | 0.018 | 5.0E-03 | 0.0463 |
| PC3802-36 | 128.22 | 2.17 | 0.51 | 2.21 | 0.200 | 0.255 | 0.016 | 5.3E-03 | 0.0460 |
| PC3802-37 | 132.23 | 2.53 | 0.50 | 2.40 | 0.202 | 0.252 | 0.015 | 5.0E-03 | 0.0467 |
| PC3802-38 | 135.30 | 2.62 | 0.52 | 2.62 | 0.199 | 0.268 | 0.016 | 4.9E-03 | 0.0493 |
| PC3802-39 | 138.71 | 2.37 | 0.51 | 2.72 | 0.198 | 0.263 | 0.016 | 4.7E-03 | 0.0501 |
| PC3802-40 | 141.79 | 2.40 | 0.51 | 3.04 | 0.216 | 0.267 | 0.018 | 5.2E-03 | 0.0503 |
| PC3802-41 | 145.20 | 2.42 | 0.49 | 2.91 | 0.223 | 0.267 | 0.017 | 5.2E-03 | 0.0491 |
| PC3802-42 | 148.61 | 2.35 | 0.50 | 2.80 | 0.227 | 0.269 | 0.016 | 4.9E-03 | 0.0489 |
| PC3802-43 | 152.02 | 2.42 | 0.50 | 3.02 | 0.209 | 0.255 | 0.017 | 5.3E-03 | 0.0498 |
| PC3802-44 | 155.44 | 2.53 | 0.49 | 2.74 | 0.220 | 0.271 | 0.017 | 4.8E-03 | 0.0508 |
| PC3802-45 | 158.85 | 2.67 | 0.51 | 2.10 | 0.203 | 0.255 | 0.016 | 5.0E-03 | 0.0494 |
| PC3802-46 | 162.26 | 2.60 | 0.50 | 1.77 | 0.227 | 0.273 | 0.015 | 5.1E-03 | 0.0497 |
| PC3802-47 | 165.68 | 2.63 | 0.51 | 2.95 | 0.199 | 0.240 | 0.018 | 4.8E-03 | 0.0490 |
| PC3802-48 | 169.43 | 2.59 | 0.52 | 3.23 | 0.160 | 0.190 | 0.018 | 5.3E-03 | 0.0517 |
| PC3802-49 | 172.84 | 2.63 | 0.52 | 3.11 | 0.192 | 0.269 | 0.018 | 4.4E-03 | 0.0503 |
| PC3802-50 | 176.26 | 2.67 | 0.54 | 2.75 | 0.207 | 0.267 | 0.019 | 5.8E-03 | 0.0487 |
| PC3802-51 | 179.67 | 2.62 | 0.49 | 2.34 | 0.207 | 0.264 | 0.017 | 5.1E-03 | 0.0498 |
| PC3802-52 | 183.08 | 2.83 | 0.49 | 1.71 | 0.227 | 0.289 | 0.016 | 4.9E-03 | 0.0456 |
| PC3802-53 | 186.50 | 3.13 | 0.38 | 1.22 | 0.280 | 0.339 | 0.013 | 4.4E-03 | 0.0385 |
| PC3802-54 | 189.57 | 2.67 | 0.50 | 0.87 | 0.203 | 0.278 | 0.016 | 5.0E-03 | 0.0497 |
| PC3802-55 | 193.52 | 2.60 | 0.53 | 0.81 | 0.194 | 0.271 | 0.016 | 4.8E-03 | 0.0502 |
| PC3802-56 | 197.42 | 2.35 | 0.62 | 0.67 | 0.191 | 0.278 | 0.017 | 5.0E-03 | 0.0521 |
| PC3802-57 | 202.11 | 2.50 | 0.56 | 1.23 | 0.345 | 0.277 | 0.018 | 4.7E-03 | 0.0480 |
| PC3802-58 | 206.02 | 2.61 | 0.53 | 1.26 | 0.274 | 0.274 | 0.016 | 4.9E-03 | 0.0467 |
| PC3802-59 | 209.53 | 2.66 | 0.53 | 1.34 | 0.216 | 0.265 | 0.015 | 4.8E-03 | 0.0463 |
| PC3802-60 | 213.44 | 2.63 | 0.55 | 3.24 | 0.204 | 0.244 | 0.019 | 4.9E-03 | 0.0499 |
| PC3802-61 | 217.34 | 2.72 | 0.54 | 3.47 | 0.235 | 0.274 | 0.020 | 5.5E-03 | 0.0489 |
| PC3802-62 | 221.25 | 2.68 | 0.54 | 2.68 | 0.213 | 0.271 | 0.018 | 5.4E-03 | 0.0516 |
| PC3802-63 | 225.16 | 2.77 | 0.51 | 2.42 | 0.213 | 0.262 | 0.017 | 5.3E-03 | 0.0504 |
| PC3802-64 | 229.06 | 2.69 | 0.50 | 1.83 | 0.200 | 0.263 | 0.016 | 5.0E-03 | 0.0483 |
| PC3802-65 | 232.97 | 2.69 | 0.49 | 1.22 | 0.201 | 0.280 | 0.015 | 4.5E-03 | 0.0474 |
| PC3802-66 | 237.27 | 2.62 | 0.53 | 1.42 | 0.245 | 0.282 | 0.018 | 5.0E-03 | 0.0483 |
| PC3802-67 | 240.78 | 2.55 | 0.50 | 3.09 | 0.239 | 0.272 | 0.020 | 5.3E-03 | 0.0461 |
| PC3802-68 | 244.50 | 2.72 | 0.48 | 2.56 | 0.209 | 0.277 | 0.016 | 5.1E-03 | 0.0471 |
| PC3802-69 | 247.71 | 2.71 | 0.47 | 2.05 | 0.200 | 0.270 | 0.013 | 4.9E-03 | 0.0471 |
| PC3802-70 | 250.91 | 2.58 | 0.46 | 2.27 | 0.191 | 0.271 | 0.014 | 4.8E-03 | 0.0477 |
| PC3802-71 | 254.12 | 2.80 | 0.50 | 2.29 | 0.213 | 0.266 | 0.014 | 4.8E-03 | 0.0466 |
| PC3802-72 | 257.32 | 2.63 | 0.48 | 2.24 | 0.208 | 0.279 | 0.015 | 5.0E-03 | 0.0488 |
| PC3802-73 | 260.53 | 2.47 | 0.47 | 2.22 | 0.203 | 0.278 | 0.015 | 5.5E-03 | 0.0488 |
| PC3802-74 | 263.73 | 2.45 | 0.48 | 2.09 | 0.200 | 0.272 | 0.016 | 5.3E-03 | 0.0502 |
| | | | | | | | | | |
| PC38-11 | 3835m | | | | | | | | |
| | | | | | | | | | |
| PC3811-01 | 0.80 | 2.69 | 0.34 | 0.26 | 0.169 | 0.237 | 0.044 | 4.1E-03 | 0.0528 |
| PC3811-02 | 2.00 | 3.26 | 0.42 | 0.99 | 0.192 | 0.217 | 0.063 | 5.5E-03 | 0.0563 |
| PC3811-03 | 2.20 | 3.82 | 0.40 | 0.84 | 0.215 | 0.229 | 0.059 | 5.9E-03 | 0.0603 |
| PC3811-04 | 3.49 | 2.56 | 0.36 | 0.20 | 0.167 | 0.252 | 0.027 | 3.8E-03 | 0.0498 |
| PC3811-05 | 6.17 | 2.48 | 0.34 | 0.32 | 0.167 | 0.251 | 0.023 | 4.2E-03 | 0.0494 |
| PC3811-06 | 8.85 | 2.45 | 0.41 | 0.41 | 0.150 | 0.250 | 0.019 | 4.0E-03 | 0.0495 |
| PC3811-07 | 11.53 | 2.42 | 0.38 | 0.42 | 0.163 | 0.251 | 0.018 | 4.6E-03 | 0.0481 |
| PC3811-08 | 13.80 | 2.56 | 0.40 | 0.51 | 0.162 | 0.249 | 0.020 | 4.4E-03 | 0.0486 |
| PC3811-09 | 16.44 | 3.47 | 0.38 | 0.73 | 0.275 | 0.251 | 0.038 | 5.3E-03 | 0.0445 |
| PC3811-10 | 18.63 | 2.51 | 0.42 | 0.69 | 0.178 | 0.258 | 0.021 | 4.8E-03 | 0.0502 |
| PC3811-11 | 20.82 | 2.46 | 0.44 | 0.79 | 0.173 | 0.252 | 0.021 | 4.9E-03 | 0.0507 |
| PC3811-12 | 23.23 | 2.43 | 0.45 | 0.62 | 0.176 | 0.252 | 0.021 | 4.4E-03 | 0.0498 |
| PC3811-13 | 25.11 | 2.39 | 0.42 | 0.62 | 0.174 | 0.261 | 0.020 | 4.5E-03 | 0.0496 |
| PC3811-14 | 27.10 | 2.58 | 0.42 | 0.70 | 0.178 | 0.247 | 0.023 | 4.5E-03 | 0.0503 |
| PC3811-15 | 29.09 | 2.50 | 0.40 | 0.58 | 0.189 | 0.247 | 0.021 | 4.6E-03 | 0.0482 |
| PC3811-16 | 31.08 | 2.62 | 0.42 | 0.83 | 0.182 | 0.245 | 0.025 | 5.6E-03 | 0.0509 |
| PC3811-17 | 33.07 | 2.50 | 0.41 | 0.63 | 0.190 | 0.247 | 0.021 | 4.7E-03 | 0.0462 |
| PC3811-18 | 35.07 | 2.88 | 0.42 | 0.81 | 0.221 | 0.258 | 0.033 | 5.1E-03 | 0.0487 |
| PC3811-19 | 37.26 | 2.24 | 0.38 | 0.52 | 0.167 | 0.261 | 0.022 | 5.2E-03 | 0.0489 |
| PC3811-20 | 39.45 | 2.13 | 0.42 | 0.46 | 0.155 | 0.251 | 0.021 | 4.2E-03 | 0.0491 |
| PC3811-21 | 40.84 | 2.06 | 0.41 | 0.35 | 0.163 | 0.262 | 0.019 | 4.1E-03 | 0.0478 |
| PC3811-22 | 43.03 | 2.41 | 0.45 | 0.90 | 0.176 | 0.252 | 0.029 | 5.0E-03 | 0.0497 |

| APPENDIX C.8. SALT-CORRECTED MAJOR ELEMENT/Al RATIOS | | | | | | | | | |
|---|---|---|---|---|---|---|---|---|---|
| | | | | | | | | | |
| PC38-11 | 3835m | | | | | | | | |
| Sample | Age | Si terr/Al | Fe/Al | Ca/Al | Na/Al | K/Al | P/Al | Mn/Al | Ti/Al |
| | (ka) | | | | | | | | |
| | | | | | | | | | |
| PC3811-23 | 45.03 | 2.15 | 0.46 | 0.78 | 0.170 | 0.249 | 0.023 | 4.7E-03 | 0.0483 |
| PC3811-24 | 47.02 | 2.05 | 0.44 | 0.69 | 0.143 | 0.247 | 0.023 | 4.3E-03 | 0.0485 |
| PC3811-25 | 49.01 | 2.06 | 0.44 | 0.74 | 0.168 | 0.248 | 0.023 | 4.4E-03 | 0.0468 |
| PC3811-26 | 51.00 | 1.80 | 0.50 | 1.13 | 0.158 | 0.246 | 0.025 | 4.3E-03 | 0.0490 |
| PC3811-27 | 52.99 | 1.84 | 0.46 | 0.98 | 0.156 | 0.248 | 0.025 | 4.1E-03 | 0.0486 |
| PC3811-28 | 54.99 | 1.94 | 0.45 | 0.77 | 0.146 | 0.244 | 0.025 | 4.2E-03 | 0.0493 |
| PC3811-29 | 56.98 | 2.40 | 0.37 | 0.25 | 0.153 | 0.268 | 0.020 | 3.6E-03 | 0.0491 |
| PC3811-30 | 59.62 | 2.42 | 0.40 | 0.35 | 0.163 | 0.258 | 0.022 | 3.9E-03 | 0.0497 |
| PC3811-31 | 62.28 | 2.47 | 0.37 | 0.20 | 0.163 | 0.268 | 0.020 | 3.7E-03 | 0.0499 |
| PC3811-32 | 65.60 | 2.64 | 0.34 | 0.20 | 0.168 | 0.258 | 0.025 | 3.9E-03 | 0.0486 |
| PC3811-33 | 68.93 | 3.72 | 0.41 | 1.69 | 0.206 | 0.245 | 0.081 | 4.7E-03 | 0.0521 |
| PC3811-34 | 72.25 | 2.22 | 0.41 | 0.27 | 0.162 | 0.266 | 0.023 | 3.7E-03 | 0.0502 |
| PC3811-35 | 74.95 | 2.00 | 0.41 | 0.31 | 0.170 | 0.261 | 0.023 | 3.9E-03 | 0.0490 |
| PC3811-36 | 77.04 | 1.80 | 0.37 | 0.30 | 0.191 | 0.258 | 0.024 | 3.7E-03 | 0.0489 |
| PC3811-37 | 79.12 | 2.04 | 0.39 | 0.28 | 0.189 | 0.254 | 0.024 | 3.4E-03 | 0.0489 |
| PC3811-38 | 81.20 | 2.05 | 0.46 | 0.33 | 0.157 | 0.255 | 0.020 | 3.4E-03 | 0.0497 |
| PC3811-39 | 83.29 | 2.30 | 0.39 | 0.32 | 0.155 | 0.259 | 0.021 | 4.3E-03 | 0.0503 |
| PC3811-40 | 85.37 | 2.33 | 0.42 | 0.35 | 0.163 | 0.255 | 0.021 | 4.2E-03 | 0.0495 |
| PC3811-41 | 87.45 | 2.25 | 0.43 | 0.36 | 0.156 | 0.257 | 0.021 | 4.2E-03 | 0.0500 |
| PC3811-42 | 89.54 | 2.35 | 0.40 | 0.15 | 0.175 | 0.259 | 0.020 | 3.4E-03 | 0.0477 |
| PC3811-43 | 91.62 | 2.01 | 0.42 | 0.25 | 0.163 | 0.269 | 0.023 | 3.8E-03 | 0.0524 |
| PC3811-44 | 93.70 | 2.12 | 0.41 | 0.53 | 0.182 | 0.242 | 0.029 | 4.0E-03 | 0.0471 |
| PC3811-45 | 95.79 | 1.94 | 0.39 | 0.40 | 0.167 | 0.248 | 0.028 | 3.7E-03 | 0.0496 |
| PC3811-46 | 97.87 | 2.36 | 0.36 | 0.16 | 0.167 | 0.263 | 0.024 | 3.7E-03 | 0.0507 |
| PC3811-47 | 99.95 | 2.27 | 0.38 | 0.14 | 0.162 | 0.262 | 0.021 | 3.1E-03 | 0.0494 |
| PC3811-48 | 102.04 | 2.14 | 0.44 | 0.30 | 0.169 | 0.251 | 0.023 | 4.0E-03 | 0.0469 |
| PC3811-49 | 104.12 | 2.09 | 0.43 | 0.15 | 0.168 | 0.260 | 0.020 | 3.7E-03 | 0.0479 |
| PC3811-50 | 106.20 | 1.85 | 0.44 | 0.15 | 0.160 | 0.259 | 0.023 | 3.8E-03 | 0.0484 |
| PC3811-51 | 108.29 | 1.97 | 0.40 | 0.15 | 0.164 | 0.262 | 0.022 | 3.4E-03 | 0.0487 |
| PC3811-52 | 110.37 | 2.02 | 0.44 | 0.15 | 0.162 | 0.267 | 0.023 | 3.8E-03 | 0.0496 |
| PC3811-53 | 112.45 | 1.87 | 0.41 | 0.14 | 0.170 | 0.266 | 0.021 | 3.8E-03 | 0.0489 |
| PC3811-54 | 114.54 | 2.00 | 0.47 | 0.17 | 0.167 | 0.279 | 0.025 | 4.0E-03 | 0.0525 |
| PC3811-55 | 116.62 | 1.67 | 0.50 | 0.19 | 0.163 | 0.263 | 0.025 | 4.1E-03 | 0.0499 |
| PC3811-56 | 118.70 | 1.71 | 0.41 | 0.16 | 0.183 | 0.261 | 0.026 | 3.4E-03 | 0.0495 |
| PC3811-57 | 120.79 | 1.72 | 0.42 | 0.20 | 0.186 | 0.266 | 0.028 | 3.3E-03 | 0.0518 |

APPENDIX C.9. UNCORRECTED TRACE ELEMENTS

| BC38-02 | 2530m | | | | | | | | | | | | | | | | | | | |
|---|---|---|---|---|---|---|---|---|---|---|---|---|---|---|---|---|---|---|---|---|
| Sample | Depth | Mo | U | Ba | Ni | Cr | V | Sc | Cu | Zn | Sr | Rb | Zr | Nb | Pb | Th | La | Ce | Nd | Y |
| | (cm) | (ppm) | (ppm) | (ppm) | (ppm) | (ppm) | (ppm) | (ppm) | (ppm) | (ppm) | (ppm) | (ppm) | (ppm) | (ppm) | (ppm) | (ppm) | (ppm) | (ppm) | (ppm) | (ppm) |
| BC3802-01 | 0.5 | 1 | 0 | 2081 | 26 | 82 | 101 | 12 | 50 | 115 | 396 | 76 | 107 | 7 | 12 | 9 | 25 | 39 | 23 | 30 |
| BC3802-02 | 1.5 | 2 | 1 | 2080 | 24 | 80 | 101 | 11 | 51 | 117 | 384 | 76 | 107 | 6 | 13 | 8 | 24 | 40 | 21 | 29 |
| BC3802-03 | 2.5 | 2 | 1 | 2084 | 25 | 85 | 99 | 12 | 52 | 118 | 394 | 77 | 107 | 7 | 12 | 7 | 21 | 37 | 22 | 29 |
| BC3802-04 | 3.5 | 1 | 0 | 2034 | 25 | 84 | 103 | 12 | 51 | 118 | 402 | 76 | 107 | 7 | 12 | 8 | 22 | 39 | 21 | 29 |
| BC3802-05 | 4.5 | 1 | 0 | 2050 | 25 | 82 | 103 | 12 | 53 | 116 | 409 | 76 | 109 | 7 | 12 | 9 | 22 | 38 | 22 | 28 |
| BC3802-06 | 5.5 | 0 | 1 | 2044 | 25 | 85 | 105 | 8 | 53 | 116 | 411 | 76 | 108 | 6 | 14 | 7 | 15 | 39 | 22 | 28 |
| BC3802-07 | 6.5 | 1 | 1 | 2032 | 27 | 86 | 111 | 12 | 57 | 119 | 413 | 77 | 107 | 7 | 13 | 7 | 21 | 39 | 22 | 29 |
| BC3802-08 | 7.5 | 1 | 2 | 2012 | 26 | 87 | 117 | 11 | 58 | 176 | 415 | 77 | 106 | 7 | 11 | 7 | 20 | 39 | 21 | 29 |
| BC3802-09 | 8.5 | 1 | 2 | 2056 | 27 | 85 | 126 | 12 | 60 | 124 | 414 | 79 | 111 | 7 | 13 | 8 | 21 | 41 | 13 | 28 |
| BC3802-10 | 9.5 | 1 | 1 | 2073 | 26 | 86 | 127 | 12 | 60 | 123 | 428 | 79 | 111 | 7 | 13 | 8 | 22 | 37 | 21 | 29 |
| BC3802-11 | 11.0 | 2 | 2 | 2154 | 28 | 91 | 117 | 11 | 61 | 128 | 471 | 82 | 115 | 7 | 12 | 7 | 20 | 42 | 23 | 30 |
| BC3802-12 | 13.0 | 0 | 4 | 2018 | 27 | 84 | 110 | 10 | 54 | 123 | 493 | 75 | 107 | 7 | 12 | 7 | 24 | 38 | 21 | 28 |
| BC3802-13 | 15.0 | 1 | 3 | 1938 | 25 | 78 | 120 | 9 | 61 | 116 | 499 | 72 | 102 | 7 | 10 | 8 | 24 | 36 | 21 | 28 |
| BC3802-13A | 17.0 | 1 | 5 | 1770 | 24 | 72 | 106 | 5 | 53 | 108 | 574 | 67 | 99 | 7 | 8 | 6 | 23 | 36 | 21 | 27 |
| BC3802-14 | 19.0 | 1 | 6 | 1756 | 25 | 70 | 110 | 4 | 58 | 106 | 622 | 64 | 93 | 6 | 8 | 5 | 20 | 34 | 21 | 26 |
| BC3802-15 | 21.0 | 2 | 8 | 1704 | 26 | 68 | 103 | 1 | 56 | 107 | 661 | 64 | 93 | 6 | 8 | 4 | 19 | 35 | 19 | 26 |
| BC3802-16 | 23.0 | 1 | 9 | 1626 | 24 | 66 | 90 | 0 | 49 | 100 | 658 | 61 | 88 | 6 | 9 | 5 | 20 | 31 | 20 | 25 |
| BC3802-17 | 25.0 | 1 | 9 | 1640 | 25 | 66 | 90 | -1 | 50 | 101 | 674 | 62 | 90 | 7 | 8 | 5 | 19 | 32 | 19 | 25 |
| BC3802-18 | 27.0 | 1 | 9 | 1531 | 24 | 64 | 83 | 0 | 46 | 98 | 665 | 61 | 93 | 6 | 7 | 5 | 21 | 37 | 20 | 26 |
| BC3802-19 | 29.0 | 2 | 8 | 1469 | 26 | 63 | 82 | -1 | 44 | 97 | 690 | 61 | 91 | 6 | 7 | 4 | 17 | 34 | 20 | 25 |
| BC3802-20 | 31.0 | 2 | 8 | 1394 | 26 | 64 | 80 | -2 | 43 | 94 | 669 | 60 | 91 | 5 | 8 | 4 | 16 | 33 | 19 | 24 |
| BC3802-21 | 33.0 | 2 | 7 | 1406 | 29 | 66 | 84 | 0 | 46 | 100 | 665 | 63 | 89 | 6 | 7 | 4 | 14 | 32 | 19 | 25 |
| BC3802-21A | 35.0 | 3 | 8 | 1156 | 35 | 61 | 88 | 2 | 46 | 95 | 598 | 67 | 91 | 7 | 11 | 4 | 22 | 34 | 19 | 22 |
| BC3802-22 | 37.0 | 2 | 7 | 1279 | 30 | 63 | 86 | 1 | 45 | 96 | 637 | 66 | 94 | 6 | 9 | 5 | 18 | 32 | 19 | 24 |
| BC3802-23 | 39.0 | 1 | 6 | 1320 | 27 | 63 | 83 | 0 | 43 | 96 | 649 | 63 | 91 | 6 | 8 | 5 | 19 | 33 | 19 | 23 |
| BC3802-24 | 41.0 | 3 | 8 | 1218 | 32 | 62 | 91 | -1 | 48 | 95 | 631 | 66 | 94 | 6 | 8 | 5 | 17 | 34 | 19 | 21 |
| BC3802-25 | 43.0 | 3 | 6 | 1290 | 32 | 63 | 98 | 0 | 50 | 97 | 609 | 68 | 97 | 6 | 10 | 6 | 19 | 31 | 19 | 21 |
| BC3802-26 | 45.0 | 2 | 8 | 1310 | 31 | 62 | 101 | 0 | 50 | 97 | 602 | 69 | 98 | 6 | 10 | 7 | 20 | 37 | 20 | 21 |
| BC3802-27 | 47.0 | 3 | 7 | 1316 | 31 | 61 | 103 | 1 | 50 | 96 | 596 | 69 | 98 | 6 | 10 | 6 | 21 | 35 | 20 | 22 |
| BC3802-28 | 49.0 | 3 | 8 | 1369 | 32 | 63 | 105 | 0 | 51 | 100 | 600 | 69 | 99 | 6 | 12 | 6 | 17 | 36 | 20 | 23 |
| BC3802-29 | 51.0 | 3 | 7 | 1365 | 31 | 62 | 103 | 0 | 52 | 99 | 590 | 69 | 99 | 6 | 9 | 5 | 17 | 32 | 20 | 24 |
| BC3802-30 | 53.0 | 3 | 8 | 1348 | 31 | 61 | 100 | 3 | 50 | 98 | 581 | 69 | 100 | 6 | 11 | 6 | 10 | 31 | 20 | 23 |

APPENDIX C.9. UNCORRECTED TRACE ELEMENTS

| BC38-03 | 4289m | | | | | | | | | | | | | | | | | | | |
|---|---|---|---|---|---|---|---|---|---|---|---|---|---|---|---|---|---|---|---|---|
| Sample | Depth | Mo | U | Ba | Ni | Cr | V | Sc | Cu | Zn | Sr | Rb | Zr | Nb | Pb | Th | La | Ce | Nd | Y |
| | (cm) | (ppm) | (ppm) | (ppm) | (ppm) | (ppm) | (ppm) | (ppm) | (ppm) | (ppm) | (ppm) | (ppm) | (ppm) | (ppm) | (ppm) | (ppm) | (ppm) | (ppm) | (ppm) | (ppm) |
| BC3803-01 | 0.5 | 2 | 1 | 1595 | 20 | 72 | 111 | 12 | 103 | 102 | 205 | 76 | 96 | 6 | 16 | 9 | 11 | 36 | 19 | 17 |
| BC3803-02 | 1.5 | 2 | 1 | 1625 | 19 | 75 | 109 | 11 | 103 | 101 | 208 | 78 | 100 | 7 | 13 | 10 | 19 | 36 | 18 | 18 |
| BC3803-03 | 2.5 | 0 | 1 | 1621 | 19 | 76 | 105 | 12 | 104 | 101 | 205 | 77 | 99 | 7 | 13 | 9 | 20 | 32 | 17 | 17 |
| BC3803-04 | 3.5 | 0 | 2 | 1633 | 21 | 75 | 108 | 10 | 110 | 103 | 204 | 78 | 100 | 7 | 13 | 9 | 18 | 33 | 17 | 18 |
| BC3803-05 | 4.5 | 1 | 2 | 1735 | 24 | 77 | 124 | 12 | 121 | 107 | 207 | 81 | 103 | 7 | 13 | 10 | 18 | 34 | 18 | 19 |
| BC3803-06 | 5.5 | 1 | 3 | 1717 | 22 | 77 | 118 | 12 | 112 | 104 | 200 | 80 | 99 | 7 | 14 | 10 | 18 | 38 | 19 | 18 |
| BC3803-07 | 6.5 | 1 | 3 | 1715 | 23 | 77 | 118 | 11 | 112 | 108 | 202 | 80 | 103 | 7 | 13 | 9 | 19 | 40 | 19 | 18 |
| BC3803-08 | 7.5 | 1 | 4 | 1742 | 22 | 77 | 115 | 11 | 114 | 133 | 206 | 82 | 107 | 7 | 13 | 10 | 16 | 36 | 19 | 19 |
| BC3803-09 | 8.5 | 1 | 5 | 1741 | 26 | 77 | 116 | 11 | 114 | 109 | 207 | 82 | 105 | 7 | 14 | 10 | 17 | 40 | 20 | 19 |
| BC3803-10 | 9.5 | 2 | 6 | 1868 | 27 | 81 | 127 | 11 | 129 | 118 | 217 | 87 | 113 | 7 | 15 | 9 | 17 | 40 | 19 | 22 |
| BC3803-11 | 11.0 | 1 | 6 | 1785 | 27 | 82 | 132 | 11 | 126 | 117 | 210 | 85 | 109 | 8 | 15 | 12 | 17 | 36 | 20 | 21 |
| BC3803-12 | 13.0 | 2 | 7 | 1849 | 33 | 82 | 130 | 12 | 124 | 120 | 211 | 85 | 111 | 8 | 13 | 10 | 16 | 39 | 21 | 21 |
| BC3803-13 | 15.0 | 2 | 8 | 1832 | 27 | 79 | 129 | 12 | 126 | 121 | 216 | 85 | 111 | 7 | 14 | 10 | 19 | 37 | 21 | 21 |
| BC3803-14 | 17.0 | 3 | 8 | 1925 | 35 | 84 | 132 | 13 | 135 | 126 | 219 | 87 | 115 | 8 | 13 | 9 | 19 | 41 | 22 | 22 |
| BC3803-15 | 19.0 | 3 | 8 | 1878 | 37 | 80 | 124 | 14 | 129 | 122 | 218 | 85 | 112 | 8 | 12 | 9 | 19 | 40 | 21 | 21 |
| BC3803-16 | 21.0 | 4 | 6 | 1888 | 27 | 79 | 119 | 11 | 128 | 122 | 214 | 83 | 111 | 8 | 13 | 10 | 23 | 38 | 20 | 21 |
| BC3803-17 | 23.0 | 2 | 5 | 1820 | 31 | 79 | 117 | 13 | 130 | 118 | 215 | 82 | 108 | 8 | 13 | 10 | 20 | 37 | 20 | 20 |
| BC3803-18 | 25.0 | 3 | 8 | 1882 | 31 | 80 | 122 | 12 | 129 | 123 | 217 | 83 | 112 | 8 | 13 | 10 | 19 | 38 | 20 | 21 |
| BC3803-19 | 27.0 | 4 | 8 | 1838 | 29 | 77 | 121 | 13 | 124 | 123 | 215 | 81 | 109 | 8 | 12 | 10 | 22 | 38 | 19 | 21 |
| BC3803-20 | 29.0 | 3 | 9 | 1951 | 30 | 81 | 127 | 13 | 131 | 130 | 225 | 84 | 115 | 8 | 13 | 10 | 15 | 37 | 21 | 21 |
| BC3803-21 | 31.0 | 2 | 8 | 1889 | 28 | 77 | 122 | 13 | 123 | 124 | 223 | 83 | 114 | 8 | 12 | 11 | 16 | 41 | 23 | 21 |
| BC3803-22 | 33.0 | 3 | 8 | 1921 | 28 | 77 | 123 | 14 | 126 | 125 | 223 | 82 | 115 | 8 | 11 | 8 | 13 | 42 | 22 | 21 |
| BC3803-23 | 35.0 | 3 | 9 | 1894 | 29 | 78 | 120 | 13 | 124 | 124 | 220 | 80 | 112 | 8 | 11 | 8 | 22 | 40 | 22 | 21 |
| BC3803-24 | 37.0 | 2 | 9 | 1927 | 32 | 79 | 124 | 13 | 126 | 129 | 230 | 84 | 119 | 8 | 12 | 9 | 16 | 43 | 22 | 23 |
| BC3803-25 | 39.0 | 3 | 10 | 1874 | 33 | 79 | 126 | 12 | 127 | 130 | 231 | 83 | 118 | 8 | 12 | 8 | 21 | 43 | 22 | 23 |
| BC3803-26 | 41.0 | 2 | 9 | 1823 | 30 | 79 | 126 | 14 | 118 | 128 | 225 | 84 | 116 | 8 | 12 | 11 | 21 | 40 | 21 | 22 |
| BC3803-27 | 43.0 | 2 | 9 | 1753 | 37 | 79 | 122 | 12 | 113 | 125 | 226 | 84 | 118 | 8 | 13 | 10 | 15 | 42 | 21 | 22 |
| BC3803-28 | 45.0 | 2 | 9 | 1762 | 30 | 79 | 121 | 12 | 110 | 124 | 223 | 82 | 116 | 8 | 12 | 9 | 20 | 43 | 21 | 22 |
| BC3803-29 | 47.0 | 3 | 9 | 1725 | 32 | 77 | 121 | 12 | 109 | 125 | 223 | 82 | 115 | 8 | 12 | 10 | 21 | 45 | 21 | 22 |
| BC3803-30 | 49.0 | 3 | 8 | 1716 | 31 | 80 | 120 | 13 | 108 | 125 | 226 | 84 | 119 | 8 | 12 | 10 | 22 | 41 | 21 | 22 |
| BC3803-31 | 51.0 | 2 | 9 | 1707 | 31 | 81 | 122 | 13 | 104 | 128 | 229 | 86 | 121 | 8 | 12 | 9 | 30 | 44 | 21 | 23 |
| BC3803-32 | 53.0 | 2 | 11 | 1564 | 31 | 83 | 120 | 13 | 99 | 128 | 223 | 85 | 119 | 8 | 12 | 10 | 23 | 40 | 20 | 22 |

| APPENDIX C.9. UNCORRECTED TRACE ELEMENTS | | | | | | | | | | | | | | | | | | | | |
|---|---|---|---|---|---|---|---|---|---|---|---|---|---|---|---|---|---|---|---|---|
| PC38-09 | 148m | | | | | | | | | | | | | | | | | | | |
| Sample | Depth | Mo | U | Ba | Ni | Cr | V | Sc | Cu | Zn | Sr | Rb | Zr | Nb | Pb | Th | La | Ce | Nd | Y |
| | (cm) | (ppm) | (ppm) | (ppm) | (ppm) | (ppm) | (ppm) | (ppm) | (ppm) | (ppm) | (ppm) | (ppm) | (ppm) | (ppm) | (ppm) | (ppm) | (ppm) | (ppm) | (ppm) | (ppm) |
| PC3809-01 | 4.0 | 63 | 9 | 273 | 61 | 110 | 99 | 9 | 27 | 114 | 184 | 64 | 121 | 8 | 13 | 10 | 18 | 35 | 16 | 16 |
| PC3809-02 | 13.0 | 60 | 9 | 223 | 56 | 99 | 115 | 10 | 22 | 90 | 175 | 60 | 97 | 7 | 14 | 9 | 15 | 29 | 14 | 14 |
| PC3809-03 | 23.0 | 55 | 9 | 274 | 59 | 114 | 115 | 12 | 30 | 102 | 181 | 71 | 128 | 9 | 19 | 11 | 18 | 42 | 18 | 18 |
| PC3809-04 | 34.0 | 53 | 9 | 253 | 60 | 113 | 115 | 9 | 30 | 101 | 167 | 68 | 119 | 8 | 17 | 10 | 19 | 38 | 17 | 17 |
| PC3809-05 | 43.0 | 26 | 8 | 325 | 42 | 95 | 101 | 12 | 22 | 95 | 230 | 71 | 190 | 9 | 16 | 11 | 17 | 43 | 20 | 22 |
| PC3809-06 | 53.0 | 53 | 6 | 249 | 55 | 108 | 109 | 11 | 30 | 107 | 162 | 66 | 104 | 8 | 17 | 10 | 16 | 35 | 15 | 16 |
| PC3809-07 | 62.0 | 91 | 9 | 224 | 69 | 116 | 108 | 8 | 31 | 95 | 179 | 54 | 89 | 7 | 13 | 8 | 19 | 29 | 13 | 14 |
| PC3809-08 | 73.0 | 37 | 8 | 280 | 53 | 117 | 110 | 11 | 25 | 101 | 174 | 70 | 137 | 9 | 17 | 11 | 17 | 44 | 19 | 20 |
| PC3809-09 | 84.0 | 44 | 7 | 296 | 58 | 128 | 128 | 12 | 31 | 115 | 157 | 83 | 127 | 10 | 20 | 12 | 21 | 45 | 21 | 20 |
| PC3809-10 | 94.0 | 63 | 7 | 273 | 64 | 122 | 133 | 11 | 37 | 112 | 158 | 78 | 113 | 8 | 20 | 11 | 21 | 41 | 18 | 17 |
| PC3809-11 | 104.0 | 77 | 9 | 271 | 62 | 111 | 134 | 10 | 31 | 112 | 139 | 68 | 95 | 7 | 19 | 10 | 16 | 37 | 16 | 15 |
| PC3809-12 | 113.0 | 35 | 8 | 305 | 53 | 118 | 135 | 14 | 48 | 139 | 157 | 88 | 124 | 9 | 25 | 13 | 26 | 44 | 21 | 21 |
| PC3809-13 | 124.0 | 38 | 9 | 316 | 49 | 124 | 111 | 11 | 20 | 99 | 204 | 74 | 160 | 10 | 18 | 11 | 22 | 47 | 22 | 21 |
| PC3809-14 | 134.0 | 58 | 8 | 259 | 57 | 111 | 110 | 9 | 25 | 87 | 198 | 62 | 137 | 8 | 14 | 8 | 14 | 39 | 18 | 17 |
| PC3809-15 | 144.0 | 63 | 8 | 241 | 60 | 110 | 100 | 9 | 23 | 86 | 169 | 57 | 107 | 7 | 16 | 9 | 18 | 33 | 15 | 15 |
| PC3809-16 | 152.0 | 42 | 7 | 209 | 49 | 90 | 99 | 9 | 24 | 85 | 166 | 58 | 108 | 8 | 15 | 9 | 9 | 28 | 14 | 14 |
| PC3809-17 | 165.0 | 48 | 9 | 231 | 49 | 83 | 97 | 8 | 22 | 82 | 203 | 53 | 127 | 7 | 13 | 7 | 12 | 31 | 15 | 16 |
| PC3809-18 | 174.0 | 27 | 9 | 327 | 43 | 96 | 95 | 9 | 19 | 89 | 233 | 67 | 196 | 9 | 15 | 9 | 17 | 43 | 21 | 21 |
| PC3809-19 | 185.0 | 31 | 10 | 308 | 41 | 77 | 81 | 10 | 18 | 82 | 276 | 57 | 204 | 7 | 12 | 8 | 13 | 34 | 17 | 20 |
| PC3809-20 | 194.0 | 27 | 8 | 338 | 38 | 75 | 82 | 9 | 19 | 87 | 297 | 59 | 225 | 8 | 11 | 7 | 15 | 39 | 18 | 23 |
| PC3809-21 | 205.0 | 38 | 5 | 424 | 35 | 60 | 110 | 13 | 34 | 118 | 246 | 67 | 147 | 8 | 17 | 9 | 15 | 39 | 18 | 21 |
| PC3809-22 | 214.0 | 52 | 12 | 270 | 69 | 110 | 98 | 8 | 23 | 91 | 242 | 55 | 171 | 7 | 13 | 9 | 15 | 33 | 16 | 18 |
| PC3809-23 | 224.0 | 13 | 11 | 383 | 30 | 56 | 62 | 9 | 9 | 59 | 340 | 54 | 276 | 8 | 10 | 7 | 14 | 46 | 20 | 23 |
| PC3809-24 | 234.0 | 40 | 8 | 305 | 41 | 73 | 76 | 8 | 16 | 69 | 292 | 47 | 192 | 6 | 11 | 7 | 11 | 32 | 15 | 19 |
| PC3809-25 | 243.0 | 68 | 9 | 211 | 59 | 87 | 95 | 7 | 21 | 64 | 170 | 39 | 94 | 6 | 10 | 6 | 2 | 25 | 11 | 12 |
| PC3809-26 | 257.0 | 56 | 10 | 258 | 56 | 100 | 89 | 7 | 19 | 74 | 189 | 47 | 126 | 6 | 12 | 7 | 4 | 30 | 14 | 16 |
| PC3809-27 | 267.0 | 31 | 15 | 323 | 41 | 82 | 75 | 7 | 13 | 83 | 359 | 48 | 183 | 7 | 11 | 6 | 16 | 33 | 18 | 24 |
| PC3809-28 | 273.0 | 51 | 163 | 180 | 42 | 119 | 84 | -1 | 9 | 57 | 1163 | 29 | 106 | 6 | 4 | • | 2 | 26 | 14 | 24 |
| PC3809-29 | 284.0 | 65 | 12 | 232 | 64 | 128 | 115 | 12 | 32 | 99 | 190 | 58 | 102 | 7 | 11 | 8 | 16 | 34 | 16 | 19 |
| PC3809-30 | 294.0 | 73 | 7 | 194 | 63 | 109 | 98 | 7 | 22 | 72 | 158 | 45 | 76 | 5 | 12 | 7 | 10 | 24 | 12 | 14 |
| PC3809-31 | 304.0 | 46 | 7 | 319 | 57 | 120 | 109 | 10 | 33 | 142 | 161 | 59 | 98 | 7 | 12 | 8 | 12 | 30 | 15 | 17 |
| PC3809-32 | 314.0 | 63 | 7 | 246 | 66 | 125 | 114 | 10 | 32 | 94 | 152 | 59 | 85 | 6 | 15 | 8 | 11 | 28 | 12 | 16 |

APPENDIX C.9. UNCORRECTED TRACE ELEMENTS

| PC38-09 | 148m | | | | | | | | | | | | | | | | | | | |
|---|---|---|---|---|---|---|---|---|---|---|---|---|---|---|---|---|---|---|---|---|
| Sample | Depth | Mo | U | Ba | Ni | Cr | V | Sc | Cu | Zn | Sr | Rb | Zr | Nb | Pb | Th | La | Ce | Nd | Y |
| | (cm) | (ppm) | (ppm) | (ppm) | (ppm) | (ppm) | (ppm) | (ppm) | (ppm) | (ppm) | (ppm) | (ppm) | (ppm) | (ppm) | (ppm) | (ppm) | (ppm) | (ppm) | (ppm) | (ppm) |
| PC3809-33 | 324.0 | 47 | 7 | 250 | 71 | 142 | 120 | 12 | 33 | 96 | 177 | 59 | 106 | 7 | 13 | 9 | 15 | 32 | 15 | 20 |
| PC3809-34 | 335.0 | 66 | 8 | 206 | 70 | 128 | 111 | 10 | 27 | 78 | 152 | 48 | 87 | 6 | 13 | 8 | 13 | 27 | 13 | 16 |
| PC3809-35 | 344.0 | 65 | 6 | 189 | 70 | 130 | 107 | 8 | 29 | 82 | 142 | 45 | 79 | 6 | 10 | 7 | 11 | 28 | 13 | 14 |
| PC3809-36 | 355.0 | 71 | 5 | 183 | 59 | 98 | 113 | 7 | 19 | 61 | 142 | 36 | 59 | 4 | 9 | 6 | 9 | 19 | 9 | 10 |
| PC3809-37 | 364.0 | 83 | 5 | 175 | 64 | 97 | 115 | 9 | 21 | 60 | 169 | 36 | 58 | 3 | 10 | 4 | 9 | 18 | 9 | 10 |
| PC3809-38 | 375.0 | 90 | 6 | 236 | 71 | 125 | 134 | 8 | 29 | 78 | 151 | 51 | 82 | 6 | 14 | 7 | 15 | 24 | 12 | 14 |
| PC3809-39 | 384.0 | 55 | 8 | 245 | 62 | 137 | 123 | 12 | 32 | 92 | 203 | 54 | 104 | 7 | 12 | 8 | 20 | 29 | 14 | 18 |
| PC3809-40 | 394.0 | 62 | 7 | 214 | 67 | 120 | 117 | 9 | 27 | 75 | 167 | 47 | 82 | 5 | 11 | 7 | 17 | 28 | 13 | 14 |
| PC3809-41 | 404.0 | 48 | 7 | 247 | 61 | 118 | 117 | 9 | 25 | 83 | 147 | 53 | 91 | 6 | 14 | 8 | 14 | 30 | 13 | 15 |
| PC3809-42 | 416.0 | 79 | 9 | 192 | 64 | 117 | 121 | 9 | 25 | 72 | 188 | 44 | 75 | 5 | 10 | 7 | 9 | 24 | 12 | 13 |
| PC3809-43 | 424.0 | 64 | 8 | 218 | 63 | 113 | 125 | 8 | 23 | 71 | 139 | 49 | 78 | 6 | 13 | 7 | 5 | 25 | 11 | 13 |
| PC3809-44 | 434.0 | 77 | 9 | 249 | 80 | 137 | 148 | 9 | 35 | 87 | 156 | 60 | 91 | 6 | 14 | 9 | 15 | 32 | 14 | 15 |
| PC3809-45 | 444.0 | 60 | 7 | 221 | 52 | 99 | 111 | 9 | 25 | 77 | 173 | 46 | 75 | 5 | 11 | 7 | 11 | 23 | 10 | 13 |
| PC3809-46 | 453.0 | 48 | 8 | 258 | 53 | 122 | 128 | 10 | 29 | 85 | 170 | 57 | 102 | 7 | 13 | 8 | 15 | 29 | 14 | 17 |
| PC3809-47 | 465.0 | 69 | 6 | 230 | 62 | 130 | 122 | 10 | 32 | 87 | 172 | 56 | 87 | 7 | 11 | 7 | 14 | 30 | 14 | 15 |
| PC3809-48 | 474.0 | 92 | 9 | 245 | 63 | 121 | 129 | 8 | 27 | 76 | 188 | 53 | 78 | 6 | 14 | 7 | 14 | 25 | 12 | 13 |
| PC3809-49 | 483.0 | 46 | 8 | 255 | 55 | 124 | 112 | 10 | 28 | 86 | 169 | 58 | 108 | 7 | 12 | 8 | 19 | 29 | 13 | 17 |
| PC3809-50 | 493.0 | 61 | 7 | 1357 | 58 | 124 | 116 | 10 | 27 | 85 | 260 | 59 | 95 | 7 | 14 | 7 | 12 | 28 | 15 | 15 |
| PC3809-51 | 504.0 | 39 | 9 | 298 | 51 | 130 | 108 | 11 | 28 | 88 | 185 | 61 | 122 | 7 | 13 | 9 | 11 | 34 | 16 | 20 |
| PC3809-52 | 515.0 | 46 | 8 | 292 | 55 | 131 | 112 | 11 | 29 | 89 | 175 | 63 | 111 | 7 | 14 | 8 | 15 | 34 | 16 | 17 |
| PC3809-53 | 525.0 | 73 | 7 | 240 | 62 | 125 | 123 | 9 | 29 | 81 | 183 | 56 | 86 | 6 | 14 | 7 | 15 | 31 | 13 | 14 |
| PC3809-54 | 536.0 | 71 | 5 | 227 | 52 | 109 | 107 | 9 | 25 | 75 | 187 | 51 | 78 | 5 | 12 | 7 | 13 | 26 | 12 | 13 |
| PC3809-55 | 544.0 | 46 | 6 | 299 | 48 | 117 | 118 | 12 | 29 | 92 | 192 | 62 | 110 | 7 | 15 | 9 | 15 | 33 | 15 | 17 |
| PC3809-56 | 553.0 | 49 | 4 | 262 | 37 | 98 | 114 | 11 | 30 | 88 | 186 | 57 | 83 | 6 | 15 | 7 | 14 | 28 | 13 | 14 |
| PC3809-57 | 564.0 | 48 | 4 | 257 | 36 | 95 | 114 | 9 | 27 | 80 | 179 | 51 | 76 | 5 | 15 | 7 | 12 | 23 | 11 | 13 |
| PC3809-58 | 574.0 | 47 | 4 | 257 | 38 | 98 | 108 | 8 | 24 | 83 | 195 | 54 | 85 | 6 | 14 | 7 | 15 | 28 | 12 | 14 |
| PC3809-59 | 585.0 | 34 | 5 | 364 | 32 | 89 | 109 | 8 | 19 | 77 | 263 | 51 | 93 | 6 | 14 | 6 | 13 | 27 | 13 | 14 |
| PC3809-60 | 594.0 | 40 | 4 | 250 | 32 | 88 | 105 | 7 | 19 | 75 | 199 | 51 | 90 | 6 | 14 | 7 | 12 | 25 | 13 | 13 |
| PC3809-61 | 605.0 | 37 | 4 | 269 | 33 | 103 | 111 | 11 | 27 | 92 | 225 | 59 | 107 | 8 | 16 | 9 | 11 | 34 | 15 | 17 |
| PC3809-62 | 615.0 | 32 | 5 | 230 | 31 | 92 | 106 | 9 | 18 | 78 | 218 | 54 | 89 | 6 | 16 | 7 | 11 | 26 | 13 | 14 |
| PC3809-63 | 625.0 | 30 | 5 | 260 | 31 | 96 | 111 | 11 | 24 | 91 | 220 | 57 | 102 | 7 | 16 | 8 | 14 | 27 | 14 | 15 |
| PC3809-64 | 635.0 | 34 | 6 | 263 | 34 | 103 | 120 | 11 | 26 | 87 | 229 | 59 | 103 | 7 | 15 | 8 | 13 | 31 | 14 | 16 |

| APPENDIX C.9. UNCORRECTED TRACE ELEMENTS | | | | | | | | | | | | | | | | | | | | |
|---|---|---|---|---|---|---|---|---|---|---|---|---|---|---|---|---|---|---|---|---|
| PC38-09 | 148m | | | | | | | | | | | | | | | | | | | |
| Sample | Depth | Mo | U | Ba | Ni | Cr | V | Sc | Cu | Zn | Sr | Rb | Zr | Nb | Pb | Th | La | Ce | Nd | Y |
| | (cm) | (ppm) | (ppm) | (ppm) | (ppm) | (ppm) | (ppm) | (ppm) | (ppm) | (ppm) | (ppm) | (ppm) | (ppm) | (ppm) | (ppm) | (ppm) | (ppm) | (ppm) | (ppm) | (ppm) |
| PC3809-65 | 646.0 | 44 | 5 | 216 | 35 | 85 | 115 | 8 | 17 | 70 | 185 | 48 | 81 | 5 | 12 | 6 | 11 | 26 | 12 | 12 |
| PC3809-66 | 654.0 | 37 | 7 | 223 | 31 | 87 | 115 | 7 | 17 | 67 | 173 | 46 | 83 | 6 | 12 | 7 | 11 | 24 | 11 | 12 |
| PC3809-67 | 664.0 | 40 | 8 | 233 | 31 | 79 | 117 | 7 | 17 | 68 | 174 | 47 | 76 | 6 | 12 | 6 | 7 | 27 | 12 | 12 |
| PC3809-68 | 674.0 | 34 | 7 | 209 | 26 | 67 | 102 | 6 | 10 | 58 | 157 | 42 | 73 | 5 | 12 | 6 | 13 | 23 | 10 | 11 |
| PC3809-69 | 684.0 | 40 | 6 | 282 | 33 | 90 | 122 | 8 | 20 | 81 | 198 | 59 | 95 | 6 | 15 | 8 | 13 | 32 | 14 | 15 |
| PC3809-70 | 694.0 | 38 | 7 | 268 | 34 | 101 | 129 | 8 | 26 | 85 | 199 | 61 | 98 | 7 | 15 | 7 | 15 | 30 | 14 | 15 |
| PC3809-71 | 703.0 | 50 | 6 | 264 | 36 | 95 | 135 | 9 | 27 | 86 | 189 | 61 | 95 | 6 | 18 | 8 | 17 | 29 | 14 | 15 |
| PC3809-72 | 714.0 | 45 | 7 | 244 | 38 | 96 | 127 | 11 | 23 | 82 | 204 | 54 | 90 | 6 | 14 | 6 | 12 | 30 | 13 | 15 |
| PC3809-73 | 724.0 | 31 | 5 | 286 | 33 | 97 | 118 | 11 | 28 | 87 | 219 | 62 | 100 | 7 | 15 | 7 | 10 | 31 | 15 | 16 |
| PC3809-74 | 734.0 | 31 | 5 | 266 | 34 | 103 | 119 | 11 | 26 | 93 | 225 | 62 | 104 | 7 | 18 | 7 | 16 | 33 | 15 | 16 |
| PC3809-75 | 744.0 | 43 | 7 | 282 | 35 | 91 | 123 | 10 | 26 | 84 | 211 | 61 | 98 | 6 | 17 | 7 | 15 | 35 | 14 | 15 |
| PC3809-76 | 754.0 | 46 | 4 | 238 | 33 | 81 | 113 | 10 | 19 | 78 | 188 | 53 | 92 | 7 | 17 | 6 | 11 | 33 | 13 | 14 |
| PC3809-77 | 764.0 | 38 | 5 | 276 | 33 | 91 | 123 | 10 | 24 | 90 | 206 | 66 | 104 | 8 | 18 | 8 | 15 | 35 | 15 | 17 |
| PC3809-78 | 774.0 | 36 | 4 | 276 | 34 | 97 | 119 | 12 | 25 | 94 | 209 | 66 | 117 | 8 | 18 | 9 | 23 | 37 | 17 | 18 |
| PC3809-79 | 784.0 | 36 | 6 | 262 | 35 | 91 | 116 | 10 | 25 | 90 | 204 | 63 | 108 | 7 | 17 | 8 | 15 | 36 | 17 | 17 |
| PC3809-80 | 794.0 | 32 | 4 | 282 | 32 | 93 | 112 | 11 | 21 | 88 | 211 | 64 | 114 | 7 | 16 | 8 | 20 | 36 | 16 | 17 |
| PC3809-81 | 804.0 | 31 | 5 | 307 | 32 | 94 | 107 | 11 | 22 | 81 | 213 | 58 | 114 | 7 | 13 | 7 | 15 | 34 | 15 | 16 |
| PC3809-82 | 813.0 | 27 | 5 | 297 | 32 | 98 | 108 | 13 | 27 | 86 | 258 | 60 | 116 | 7 | 16 | 7 | 16 | 31 | 15 | 17 |
| PC3809-83 | 823.0 | 28 | 4 | 282 | 33 | 95 | 102 | 10 | 22 | 84 | 219 | 60 | 120 | 8 | 13 | 7 | 18 | 31 | 15 | 18 |
| PC3809-84 | 834.0 | 29 | 4 | 278 | 31 | 99 | 104 | 11 | 23 | 85 | 211 | 61 | 118 | 8 | 16 | 7 | 14 | 32 | 15 | 17 |
| PC3809-85 | 845.0 | 36 | 4 | 284 | 34 | 97 | 109 | 10 | 25 | 80 | 220 | 63 | 113 | 7 | 17 | 7 | 17 | 32 | 16 | 17 |
| PC3809-86 | 854.0 | 29 | 5 | 335 | 29 | 82 | 108 | 11 | 32 | 98 | 196 | 78 | 119 | 9 | 23 | 9 | 20 | 40 | 18 | 19 |
| PC38-10 | 257m | | | | | | | | | | | | | | | | | | | |
| PC3810-01 | 6.0 | 48 | 14 | 251 | 105 | 124 | 137 | 8 | 35 | 107 | 319 | 57 | 106 | 7 | 10 | 9 | 16 | 28 | 15 | 18 |
| PC3810-02 | 14.0 | 24 | 19 | 323 | 74 | 102 | 87 | 8 | 24 | 94 | 418 | 57 | 194 | 8 | 10 | 8 | 30 | 40 | 20 | 27 |
| PC3810-03 | 24.0 | 11 | 20 | 352 | 35 | 62 | 53 | 7 | 11 | 56 | 587 | 53 | 242 | 8 | 8 | 5 | 17 | 39 | 20 | 29 |
| PC3810-04 | 34.0 | 17 | 15 | 328 | 38 | 67 | 56 | 5 | 12 | 59 | 483 | 54 | 220 | 7 | 10 | 6 | 19 | 42 | 20 | 28 |
| PC3810-05 | 44.0 | 35 | 15 | 336 | 98 | 137 | 97 | 10 | 27 | 88 | 250 | 62 | 162 | 8 | 12 | 10 | 15 | 37 | 18 | 22 |
| PC3810-06 | 54.0 | 44 | 14 | 306 | 88 | 128 | 120 | 8 | 28 | 89 | 221 | 63 | 153 | 7 | 13 | 8 | 18 | 35 | 16 | 19 |
| PC3810-07 | 64.0 | 37 | 14 | 329 | 72 | 107 | 111 | 9 | 26 | 90 | 270 | 64 | 197 | 8 | 13 | 9 | 22 | 44 | 19 | 22 |

APPENDIX C.9. UNCORRECTED TRACE ELEMENTS

| PC38-10 | 257m | | | | | | | | | | | | | | | | | | | |
|---|---|---|---|---|---|---|---|---|---|---|---|---|---|---|---|---|---|---|---|---|
| Sample | Depth | Mo | U | Ba | Ni | Cr | V | Sc | Cu | Zn | Sr | Rb | Zr | Nb | Pb | Th | La | Ce | Nd | Y |
| | (cm) | (ppm) | (ppm) | (ppm) | (ppm) | (ppm) | (ppm) | (ppm) | (ppm) | (ppm) | (ppm) | (ppm) | (ppm) | (ppm) | (ppm) | (ppm) | (ppm) | (ppm) | (ppm) | (ppm) |
| PC3810-08 | 74.0 | 29 | 15 | 383 | 56 | 100 | 107 | 9 | 22 | 90 | 328 | 68 | 237 | 7 | 15 | 10 | 22 | 45 | 22 | 25 |
| PC3810-09 | 84.0 | 13 | 15 | 384 | 20 | 60 | 60 | 7 | 8 | 70 | 426 | 56 | 228 | 7 | 14 | 7 | 23 | 43 | 23 | 29 |
| PC3810-10 | 94.0 | 41 | 27 | 374 | 30 | 52 | 52 | 6 | 9 | 60 | 498 | 56 | 261 | 8 | 10 | 6 | 17 | 41 | 20 | 29 |
| PC3810-10 | 104.0 | 31 | 16 | 358 | 31 | 54 | 54 | 4 | 10 | 52 | 466 | 53 | 274 | 7 | 10 | 8 | 18 | 40 | 20 | 28 |
| PC3810-11 | 113.0 | 17 | 10 | 342 | 24 | 45 | 45 | 5 | 7 | 50 | 430 | 53 | 241 | 7 | 10 | 6 | 18 | 39 | 20 | 27 |
| PC3810-12 | 126.0 | 46 | 10 | 201 | 55 | 86 | 86 | 6 | 28 | 79 | 327 | 50 | 124 | 6 | 9 | 6 | 19 | 26 | 14 | 18 |
| PC3810-13 | 134.0 | 58 | 12 | 206 | 70 | 98 | 98 | 7 | 32 | 86 | 266 | 52 | 110 | 6 | 10 | 8 | 13 | 26 | 13 | 17 |
| PC3810-14 | 146.0 | 50 | 12 | 268 | 63 | 91 | 99 | 9 | 33 | 94 | 280 | 60 | 149 | 8 | 11 | 8 | 17 | 37 | 17 | 20 |
| PC3810-15 | 154.0 | 43 | 12 | 251 | 66 | 97 | 107 | 8 | 34 | 92 | 333 | 56 | 127 | 7 | 11 | 7 | 16 | 30 | 15 | 19 |
| PC3810-16 | 167.0 | 46 | 11 | 271 | 60 | 95 | 112 | 8 | 29 | 91 | 239 | 61 | 120 | 7 | 12 | 8 | 17 | 33 | 15 | 19 |
| PC3810-17 | 174.0 | 45 | 12 | 295 | 66 | 102 | 115 | 8 | 34 | 95 | 213 | 63 | 125 | 7 | 13 | 9 | 20 | 34 | 15 | 19 |
| PC3810-18 | 185.0 | 33 | 11 | 280 | 55 | 97 | 111 | 8 | 27 | 92 | 179 | 68 | 115 | 7 | 13 | 9 | 17 | 32 | 15 | 19 |
| PC3810-19 | 194.0 | 57 | 10 | 250 | 67 | 93 | 119 | 7 | 38 | 90 | 239 | 56 | 91 | 6 | 11 | 8 | 23 | 28 | 13 | 16 |
| PC3810-20 | 203.0 | 44 | 15 | 324 | 60 | 95 | 129 | 8 | 29 | 106 | 227 | 67 | 141 | 8 | 14 | 9 | 22 | 36 | 17 | 20 |
| PC3810-21 | 216.0 | 62 | 11 | 257 | 68 | 97 | 124 | 8 | 33 | 86 | 245 | 52 | 91 | 6 | 12 | 8 | 13 | 26 | 13 | 16 |
| PC3810-22 | 224.0 | 56 | 11 | 249 | 75 | 104 | 125 | 8 | 37 | 94 | 198 | 56 | 91 | 6 | 14 | 8 | 16 | 27 | 14 | 16 |
| PC3810-23 | 233.0 | 55 | 13 | 282 | 75 | 113 | 136 | 10 | 41 | 100 | 208 | 63 | 112 | 7 | 14 | 9 | 17 | 32 | 16 | 19 |
| PC3810-24 | 244.0 | 42 | 11 | 243 | 62 | 103 | 114 | 9 | 30 | 95 | 268 | 63 | 129 | 7 | 13 | 9 | 17 | 33 | 16 | 19 |
| PC3810-25 | 254.0 | 43 | 14 | 282 | 53 | 87 | 102 | 8 | 23 | 83 | 336 | 55 | 169 | 7 | 13 | 7 | 9 | 36 | 17 | 21 |
| PC3810-26 | 263.0 | 53 | 12 | 269 | 59 | 88 | 113 | 8 | 28 | 81 | 326 | 52 | 132 | 7 | 12 | 6 | 15 | 30 | 14 | 19 |
| PC3810-27 | 273.0 | 42 | 11 | 269 | 66 | 109 | 125 | 9 | 33 | 106 | 268 | 63 | 123 | 8 | 13 | 8 | 18 | 33 | 15 | 20 |
| PC3810-28 | 284.0 | 36 | 13 | 268 | 59 | 97 | 108 | 9 | 29 | 93 | 314 | 60 | 126 | 7 | 11 | 8 | 16 | 33 | 17 | 21 |
| PC3810-29 | 295.0 | 55 | 10 | 219 | 68 | 101 | 115 | 6 | 33 | 83 | 395 | 48 | 69 | 5 | 10 | 6 | 16 | 22 | 12 | 15 |
| PC3810-30 | 305.0 | 35 | 11 | 265 | 60 | 98 | 125 | 9 | 28 | 99 | 304 | 62 | 114 | 7 | 13 | 8 | 28 | 34 | 16 | 20 |
| PC3810-31 | 314.0 | 34 | 11 | 276 | 62 | 104 | 130 | 10 | 29 | 103 | 328 | 64 | 137 | 8 | 11 | 9 | 21 | 37 | 18 | 20 |
| PC3810-32 | 324.0 | 60 | 11 | 245 | 74 | 100 | 140 | 8 | 36 | 90 | 305 | 51 | 80 | 5 | 12 | 6 | 22 | 26 | 14 | 15 |
| PC3810-33 | 335.0 | 33 | 12 | 256 | 72 | 111 | 136 | 8 | 28 | 97 | 287 | 64 | 112 | 8 | 11 | 7 | 21 | 32 | 16 | 19 |
| PC3810-34 | 344.0 | 58 | 10 | 152 | 73 | 93 | 124 | 7 | 30 | 82 | 306 | 43 | 68 | 6 | 10 | 6 | 10 | 24 | 11 | 13 |
| PC3810-35 | 354.0 | 61 | 9 | 209 | 66 | 79 | 121 | 6 | 27 | 74 | 212 | 39 | 60 | 5 | 11 | 5 | 13 | 20 | 10 | 11 |
| PC3810-36 | 364.0 | 62 | 9 | 165 | 63 | 70 | 121 | 6 | 25 | 70 | 247 | 36 | 49 | 4 | 9 | 5 | 15 | 19 | 10 | 11 |
| PC3810-37 | 374.0 | 58 | 11 | 195 | 63 | 75 | 126 | 7 | 22 | 63 | 197 | 39 | 50 | 5 | 9 | 5 | 9 | 20 | 10 | 10 |
| PC3810-38 | 383.0 | 29 | 12 | 274 | 63 | 104 | 134 | 10 | 32 | 103 | 255 | 67 | 98 | 7 | 15 | 9 | 22 | 36 | 16 | 18 |

| APPENDIX C.9. UNCORRECTED TRACE ELEMENTS | | | | | | | | | | | | | | | | | | | | |
|---|---|---|---|---|---|---|---|---|---|---|---|---|---|---|---|---|---|---|---|---|
| PC38-10 | 257m | | | | | | | | | | | | | | | | | | | |
| Sample | Depth | Mo | U | Ba | Ni | Cr | V | Sc | Cu | Zn | Sr | Rb | Zr | Nb | Pb | Th | La | Ce | Nd | Y |
| | (cm) | (ppm) | (ppm) | (ppm) | (ppm) | (ppm) | (ppm) | (ppm) | (ppm) | (ppm) | (ppm) | (ppm) | (ppm) | (ppm) | (ppm) | (ppm) | (ppm) | (ppm) | (ppm) | (ppm) |
| PC3810-39 | 394.0 | 41 | 13 | 224 | 81 | 112 | 141 | 8 | 27 | 87 | 234 | 54 | 91 | 6 | 12 | 8 | 18 | 29 | 13 | 17 |
| PC3810-40 | 404.0 | 27 | 12 | 241 | 64 | 106 | 114 | 11 | 24 | 93 | 274 | 61 | 122 | 7 | 13 | 8 | 27 | 33 | 16 | 21 |
| PC3810-41 | 417.0 | 49 | 12 | 229 | 72 | 105 | 112 | 9 | 29 | 91 | 363 | 52 | 99 | 6 | 12 | 7 | 21 | 31 | 15 | 18 |
| PC3810-42 | 424.0 | 44 | 14 | 200 | 78 | 107 | 126 | 8 | 30 | 95 | 282 | 54 | 92 | 7 | 13 | 8 | 20 | 29 | 14 | 17 |
| PC3810-43 | 434.0 | 60 | 9 | 157 | 55 | 67 | 98 | 0 | 15 | 62 | 468 | 24 | 45 | 4 | 5 | 2 | 8 | 16 | 9 | 10 |
| PC3810-44 | 445.0 | 42 | 11 | 187 | 66 | 88 | 119 | 6 | 22 | 76 | 363 | 44 | 64 | 6 | 11 | 6 | 14 | 24 | 12 | 13 |
| PC3810-45 | 456.0 | 68 | 13 | 233 | 76 | 87 | 154 | 7 | 25 | 77 | 327 | 40 | 61 | 5 | 10 | 6 | 12 | 17 | 9 | 12 |
| PC3810-46 | 467.0 | 66 | 6 | 170 | 57 | 62 | 104 | 2 | 15 | 57 | 314 | 25 | 37 | 3 | 7 | 3 | 13 | 15 | 9 | 9 |
| PC3810-47 | 476.0 | 34 | 16 | 255 | 84 | 115 | 131 | 7 | 29 | 96 | 415 | 54 | 96 | 7 | 10 | 7 | 19 | 30 | 16 | 19 |
| PC3810-48 | 484.0 | 35 | 14 | 244 | 87 | 113 | 124 | 8 | 30 | 90 | 433 | 51 | 93 | 6 | 11 | 7 | 15 | 30 | 15 | 19 |
| PC3810-49 | 494.0 | 37 | 23 | 261 | 89 | 115 | 106 | 3 | 26 | 80 | 456 | 45 | 130 | 6 | 8 | 6 | 18 | 30 | 16 | 25 |
| PC3810-50 | 504.0 | 14 | 21 | 313 | 43 | 65 | 63 | 7 | 14 | 61 | 632 | 49 | 235 | 8 | 7 | 4 | 20 | 38 | 19 | 32 |
| PC3810-51 | 514.0 | 64 | 6 | 278 | 50 | 89 | 122 | 11 | 25 | 82 | 187 | 53 | 104 | 7 | 14 | 7 | 14 | 30 | 14 | 16 |
| PC3810-52 | 524.0 | 50 | 6 | 333 | 44 | 80 | 129 | 10 | 26 | 85 | 184 | 56 | 114 | 7 | 15 | 7 | 16 | 35 | 15 | 17 |
| PC3810-53 | 534.0 | 121 | 21 | 368 | 154 | 170 | 339 | 8 | 46 | 83 | 256 | 45 | 68 | 5 | 11 | 6 | 9 | 22 | 11 | 14 |
| PC3810-54 | 545.0 | 104 | 16 | 309 | 121 | 139 | 260 | 9 | 34 | 74 | 227 | 47 | 72 | 5 | 11 | 7 | 12 | 22 | 12 | 14 |
| PC3810-55 | 554.0 | 116 | 17 | 314 | 121 | 135 | 281 | 8 | 37 | 75 | 264 | 43 | 61 | 5 | 10 | 6 | 11 | 22 | 10 | 12 |
| PC3810-56 | 564.0 | 87 | 10 | 287 | 66 | 97 | 201 | 6 | 20 | 56 | 379 | 36 | 64 | 4 | 9 | 5 | 10 | 21 | 11 | 11 |
| PC3810-57 | 574.0 | 79 | 10 | 298 | 73 | 112 | 239 | 6 | 24 | 67 | 445 | 42 | 80 | 5 | 9 | 4 | 13 | 23 | 12 | 13 |
| PC3810-58 | 584.0 | 75 | 8 | 321 | 68 | 105 | 193 | 8 | 23 | 67 | 390 | 41 | 73 | 5 | 9 | 4 | 12 | 21 | 11 | 13 |
| PC3810-59 | 596.0 | 81 | 21 | 330 | 70 | 111 | 242 | 7 | 23 | 67 | 381 | 41 | 76 | 5 | 11 | 5 | 10 | 21 | 11 | 13 |
| PC3810-60 | 604.0 | 82 | 16 | 361 | 68 | 113 | 233 | 6 | 25 | 69 | 417 | 42 | 72 | 5 | 10 | 4 | 12 | 24 | 11 | 14 |
| PC3810-61 | 614.0 | 80 | 14 | 320 | 66 | 111 | 234 | 9 | 24 | 70 | 327 | 47 | 81 | 6 | 12 | 5 | 12 | 25 | 12 | 13 |
| PC3810-62 | 624.0 | 73 | 10 | 315 | 68 | 109 | 234 | 7 | 24 | 79 | 400 | 53 | 89 | 6 | 14 | 6 | 14 | 28 | 15 | 16 |
| PC3810-63 | 634.0 | 61 | 9 | 282 | 65 | 115 | 205 | 6 | 26 | 72 | 426 | 49 | 90 | 6 | 11 | 6 | 12 | 26 | 13 | 15 |
| PC3810-64 | 645.0 | 83 | 10 | 357 | 60 | 101 | 199 | 8 | 25 | 68 | 296 | 50 | 76 | 6 | 13 | 7 | 11 | 27 | 13 | 14 |
| PC3810-65 | 655.0 | 108 | 8 | 319 | 71 | 103 | 211 | 7 | 23 | 70 | 305 | 46 | 70 | 5 | 13 | 6 | 13 | 21 | 13 | 13 |
| PC3810-66 | 667.0 | 99 | 11 | 280 | 69 | 107 | 211 | 9 | 25 | 78 | 310 | 52 | 79 | 6 | 15 | 6 | 15 | 25 | 13 | 15 |
| PC3810-67 | 674.0 | 91 | 13 | 264 | 68 | 114 | 209 | 10 | 29 | 96 | 241 | 65 | 90 | 6 | 20 | 8 | 20 | 33 | 15 | 15 |
| PC3810-68 | 683.0 | 87 | 11 | 239 | 66 | 103 | 201 | 9 | 26 | 89 | 255 | 61 | 80 | 6 | 20 | 6 | 13 | 33 | 15 | 13 |
| PC3810-69 | 694.0 | 56 | 9 | 304 | 55 | 114 | 165 | 11 | 26 | 115 | 224 | 82 | 116 | 8 | 23 | 10 | 18 | 42 | 19 | 18 |
| PC3810-70 | 704.0 | 46 | 8 | 332 | 50 | 128 | 162 | 11 | 27 | 117 | 186 | 93 | 131 | 9 | 23 | 11 | 20 | 45 | 20 | 21 |

| APPENDIX C.9. UNCORRECTED TRACE ELEMENTS | | | | | | | | | | | | | | | | | | | | |
|---|---|---|---|---|---|---|---|---|---|---|---|---|---|---|---|---|---|---|---|---|
| PC38-10 | 257m | | | | | | | | | | | | | | | | | | | |
| Sample | Depth | Mo | U | Ba | Ni | Cr | V | Sc | Cu | Zn | Sr | Rb | Zr | Nb | Pb | Th | La | Ce | Nd | Y |
| | (cm) | (ppm) | (ppm) | (ppm) | (ppm) | (ppm) | (ppm) | (ppm) | (ppm) | (ppm) | (ppm) | (ppm) | (ppm) | (ppm) | (ppm) | (ppm) | (ppm) | (ppm) | (ppm) | (ppm) |
| PC3810-71 | 714.0 | 66 | 8 | 309 | 51 | 109 | 154 | 11 | 28 | 112 | 240 | 83 | 107 | 8 | 21 | 9 | 19 | 38 | 17 | 18 |
| PC3810-72 | 724.0 | 74 | 10 | 274 | 49 | 91 | 147 | 9 | 22 | 97 | 245 | 72 | 91 | 6 | 21 | 8 | 16 | 33 | 17 | 15 |
| PC3810-74 | 734.0 | 56 | 11 | 313 | 46 | 104 | 146 | 12 | 24 | 110 | 176 | 84 | 123 | 8 | 25 | 12 | 18 | 44 | 20 | 18 |
| PC3810-75 | 745.0 | 36 | 9 | 355 | 39 | 98 | 139 | 12 | 32 | 130 | 194 | 95 | 156 | 8 | 27 | 12 | 25 | 47 | 22 | 20 |
| PC3810-76 | 754.0 | 50 | 9 | 281 | 48 | 100 | 127 | 9 | 29 | 101 | 185 | 77 | 155 | 8 | 19 | 10 | 18 | 34 | 17 | 16 |
| PC3810-77 | 764.0 | 29 | 11 | 371 | 35 | 94 | 112 | 12 | 20 | 100 | 289 | 80 | 217 | 9 | 19 | 11 | 25 | 48 | 22 | 24 |
| PC38-02 | 2525m | | | | | | | | | | | | | | | | | | | |
| PC3802-01 | 8.0 | -1 | 8 | 2044 | 28 | 84 | 123 | 16 | 70 | 123 | 509 | 79 | 101 | 7 | 10 | 7 | 16 | 33 | 22 | 23 |
| PC3802-02 | 18.0 | 0 | 6 | 1769 | 26 | 73 | 97 | 8 | 66 | 110 | 612 | 70 | 92 | 7 | 10 | 7 | 14 | 40 | 30 | 19 |
| PC3802-03 | 28.0 | 0 | 7 | 1688 | 22 | 69 | 90 | 12 | 56 | 104 | 647 | 69 | 92 | 6 | 9 | 6 | 19 | 26 | 23 | 19 |
| PC3802-04 | 38.0 | 2 | 8 | 1196 | 45 | 80 | 92 | 11 | 62 | 114 | 538 | 80 | 98 | 6 | 9 | 8 | 21 | 34 | 27 | 17 |
| PC3802-05 | 48.0 | 2 | 7 | 1243 | 33 | 72 | 99 | 14 | 62 | 104 | 590 | 77 | 98 | 7 | 11 | 8 | 16 | 41 | 21 | 17 |
| PC3802-06 | 57.5 | 2 | 6 | 1170 | 35 | 67 | 97 | 13 | 59 | 100 | 579 | 76 | 96 | 7 | 12 | 7 | 18 | 30 | 25 | 18 |
| PC3802-07 | 70.0 | 1 | 6 | 1460 | 35 | 81 | 110 | 11 | 69 | 106 | 557 | 79 | 103 | 6 | 12 | 9 | 18 | 45 | 32 | 20 |
| PC3802-08 | 79.0 | 2 | 6 | 1364 | 36 | 74 | 109 | 8 | 67 | 108 | 548 | 79 | 101 | 7 | 10 | 7 | 22 | 41 | 26 | 19 |
| PC3802-09 | 89.0 | 2 | 10 | 1344 | 35 | 68 | 102 | 13 | 67 | 105 | 595 | 75 | 97 | 7 | 9 | 6 | 10 | 40 | 28 | 19 |
| PC3802-10 | 100.0 | 2 | 6 | 1307 | 31 | 60 | 96 | 9 | 64 | 103 | 637 | 70 | 91 | 7 | 9 | 6 | 19 | 29 | 26 | 18 |
| PC3802-11 | 110.0 | 3 | 7 | 1291 | 30 | 63 | 89 | 10 | 61 | 101 | 641 | 69 | 90 | 5 | 9 | 6 | 16 | 39 | 27 | 16 |
| PC3802-12 | 120.0 | 4 | 7 | 1254 | 33 | 59 | 78 | 11 | 58 | 100 | 671 | 65 | 85 | 6 | 8 | 5 | 13 | 36 | 26 | 16 |
| PC3802-13 | 130.0 | 4 | 8 | 1326 | 33 | 57 | 88 | 12 | 61 | 99 | 663 | 70 | 90 | 7 | 7 | 9 | 14 | 36 | 26 | 17 |
| PC3802-14 | 139.0 | 3 | 6 | 1427 | 32 | 66 | 96 | 11 | 68 | 114 | 568 | 79 | 104 | 7 | 10 | 7 | 23 | 37 | 24 | 19 |
| PC3802-15 | 150.0 | 3 | 6 | 1338 | 34 | 64 | 98 | 8 | 64 | 90 | 553 | 79 | 101 | 6 | 10 | 7 | 14 | 39 | 29 | 20 |
| PC3802-16 | 160.0 | 3 | 5 | 1435 | 27 | 70 | 122 | 9 | 67 | 115 | 526 | 86 | 113 | 7 | 12 | 8 | 20 | 43 | 31 | 20 |
| PC3802-17 | 171.0 | 2 | 10 | 1469 | 28 | 74 | 119 | 15 | 77 | 126 | 489 | 88 | 116 | 8 | 13 | 7 | 25 | 42 | 26 | 22 |
| PC3802-18 | 181.0 | 3 | 10 | 1537 | 32 | 71 | 119 | 17 | 68 | 118 | 437 | 86 | 113 | 7 | 11 | 9 | 25 | 43 | 25 | 21 |
| PC3802-19 | 191.0 | 2 | 10 | 1683 | 35 | 79 | 118 | 14 | 73 | 123 | 478 | 83 | 111 | 6 | 11 | 9 | 21 | 50 | 33 | 23 |
| PC3802-20 | 201.0 | 2 | 9 | 1587 | 35 | 84 | 117 | 10 | 76 | 127 | 439 | 87 | 123 | 7 | 11 | 8 | 21 | 38 | 24 | 23 |
| PC3802-21 | 211.0 | 3 | 8 | 1451 | 36 | 76 | 117 | 15 | 79 | 124 | 468 | 88 | 114 | 7 | 13 | 10 | 18 | 42 | 29 | 23 |
| PC3802-22 | 221.0 | 3 | 9 | 1472 | 32 | 72 | 115 | 6 | 77 | 100 | 489 | 87 | 113 | 7 | 13 | 10 | 24 | 41 | 33 | 23 |
| PC3802-23 | 231.0 | 3 | 5 | 1333 | 30 | 72 | 129 | 15 | 77 | 119 | 439 | 91 | 117 | 8 | 13 | 9 | 24 | 37 | 27 | 24 |

APPENDIX C.9. UNCORRECTED TRACE ELEMENTS

| PC38-02 | 2525m | | | | | | | | | | | | | | | | | | | |
|---|---|---|---|---|---|---|---|---|---|---|---|---|---|---|---|---|---|---|---|---|
| Sample | Depth | Mo | U | Ba | Ni | Cr | V | Sc | Cu | Zn | Sr | Rb | Zr | Nb | Pb | Th | La | Ce | Nd | Y |
| | (cm) | (ppm) | (ppm) | (ppm) | (ppm) | (ppm) | (ppm) | (ppm) | (ppm) | (ppm) | (ppm) | (ppm) | (ppm) | (ppm) | (ppm) | (ppm) | (ppm) | (ppm) | (ppm) | (ppm) |
| PC3802-24 | 241.0 | 1 | 7 | 1750 | 27 | 83 | 142 | 13 | 81 | 135 | 345 | 102 | 130 | 8 | 16 | 11 | 26 | 40 | 28 | 25 |
| PC3802-25 | 251.0 | 3 | 9 | 1669 | 34 | 77 | 129 | 14 | 80 | 138 | 382 | 96 | 120 | 7 | 12 | 8 | 24 | 39 | 29 | 25 |
| PC3802-26 | 261.0 | 2 | 9 | 1881 | 31 | 69 | 112 | 13 | 76 | 132 | 471 | 85 | 112 | 7 | 10 | 10 | 21 | 41 | 30 | 24 |
| PC3802-27 | 271.0 | 3 | 6 | 1874 | 36 | 77 | 135 | 14 | 81 | 142 | 346 | 98 | 126 | 8 | 12 | 10 | 23 | 38 | 26 | 25 |
| PC3802-28 | 281.0 | 2 | 8 | 1747 | 35 | 78 | 132 | 14 | 83 | 135 | 360 | 98 | 126 | 8 | 14 | 9 | 29 | 44 | 26 | 25 |
| PC3802-29 | 291.0 | 1 | 7 | 1870 | 33 | 81 | 143 | 16 | 80 | 141 | 297 | 107 | 132 | 9 | 15 | 10 | 30 | 45 | 28 | 25 |
| PC3802-30 | 301.0 | 2 | 8 | 2027 | 28 | 83 | 159 | 20 | 89 | 142 | 320 | 103 | 129 | 11 | 15 | 10 | 26 | 41 | 26 | 27 |
| PC3802-31 | 312.0 | 2 | 10 | 1908 | 33 | 78 | 138 | 16 | 86 | 139 | 384 | 91 | 119 | 7 | 11 | 9 | 20 | 37 | 30 | 26 |
| PC3802-32 | 322.0 | 2 | 10 | 1997 | 33 | 81 | 147 | 14 | 84 | 135 | 380 | 94 | 118 | 7 | 13 | 10 | 28 | 37 | 28 | 26 |
| PC3802-33 | 332.0 | 1 | 6 | 1922 | 33 | 84 | 142 | 14 | 77 | 136 | 385 | 91 | 116 | 8 | 12 | 8 | 25 | 41 | 30 | 27 |
| PC3802-34 | 342.0 | 2 | 8 | 2310 | 26 | 86 | 132 | 14 | 73 | 133 | 415 | 91 | 115 | 7 | 14 | 9 | 26 | 46 | 30 | 26 |
| PC3802-35 | 352.0 | 1 | 8 | 1892 | 26 | 70 | 106 | 12 | 65 | 115 | 534 | 77 | 99 | 6 | 12 | 8 | 20 | 46 | 29 | 21 |
| PC3802-36 | 362.0 | 2 | 7 | 1343 | 27 | 72 | 105 | 12 | 57 | 106 | 593 | 77 | 94 | 6 | 13 | 8 | 19 | 39 | 28 | 17 |
| PC3802-37 | 372.0 | 1 | 8 | 1252 | 25 | 74 | 106 | 10 | 53 | 100 | 624 | 77 | 96 | 7 | 11 | 7 | 17 | 40 | 27 | 18 |
| PC3802-38 | 381.0 | 1 | 7 | 1282 | 23 | 73 | 116 | 11 | 55 | 93 | 642 | 77 | 97 | 6 | 6 | 8 | 21 | 39 | 29 | 18 |
| PC3802-39 | 391.0 | 1 | 9 | 1250 | 24 | 67 | 106 | 7 | 56 | 90 | 626 | 73 | 96 | 7 | 13 | 7 | 18 | 39 | 26 | 19 |
| PC3802-40 | 400.0 | 1 | 8 | 1307 | 23 | 61 | 94 | 10 | 57 | 97 | 656 | 72 | 96 | 6 | 10 | 8 | 20 | 39 | 29 | 19 |
| PC3802-41 | 410.0 | 2 | 5 | 1316 | 22 | 59 | 104 | 12 | 61 | 101 | 658 | 74 | 90 | 6 | 9 | 7 | 17 | 30 | 26 | 18 |
| PC3802-42 | 420.0 | 1 | 6 | 1203 | 22 | 61 | 97 | 13 | 53 | 97 | 648 | 72 | 97 | 7 | 10 | 8 | 17 | 38 | 26 | 18 |
| PC3802-43 | 430.0 | 0 | 7 | 1057 | 21 | 60 | 105 | 13 | 54 | 91 | 667 | 72 | 92 | 6 | 10 | 6 | 19 | 34 | 22 | 18 |
| PC3802-44 | 440.0 | 1 | 11 | 1211 | 19 | 64 | 112 | 12 | 56 | 93 | 637 | 75 | 97 | 7 | 11 | 7 | 25 | 43 | 25 | 18 |
| PC3802-45 | 450.0 | 1 | 7 | 1186 | 24 | 73 | 118 | 11 | 60 | 103 | 555 | 81 | 103 | 7 | 13 | 8 | 30 | 39 | 25 | 19 |
| PC3802-46 | 460.0 | 2 | 7 | 1205 | 26 | 69 | 116 | 9 | 68 | 105 | 510 | 87 | 107 | 6 | 14 | 9 | 29 | 42 | 25 | 21 |
| PC3802-47 | 470.0 | 1 | 8 | 1230 | 26 | 54 | 98 | 13 | 62 | 101 | 654 | 75 | 93 | 6 | 11 | 9 | 22 | 42 | 29 | 18 |
| PC3802-48 | 481.0 | 2 | 9 | 1302 | 24 | 54 | 90 | 12 | 59 | 100 | 680 | 73 | 93 | 7 | 10 | 8 | 15 | 49 | 28 | 18 |
| PC3802-49 | 491.0 | 2 | 6 | 1320 | 23 | 50 | 96 | 8 | 58 | 99 | 672 | 73 | 94 | 7 | 10 | 8 | 14 | 35 | 24 | 19 |
| PC3802-50 | 501.0 | 2 | 8 | 1337 | 30 | 57 | 97 | 5 | 62 | 100 | 642 | 75 | 95 | 7 | 10 | 8 | 19 | 37 | 26 | 20 |
| PC3802-51 | 511.0 | 1 | 9 | 1333 | 20 | 55 | 103 | 14 | 61 | 98 | 617 | 80 | 100 | 7 | 14 | 9 | 24 | 39 | 25 | 20 |
| PC3802-52 | 521.0 | 3 | 6 | 1112 | 23 | 63 | 111 | 13 | 59 | 97 | 533 | 86 | 107 | 7 | 14 | 8 | 22 | 44 | 29 | 20 |
| PC3802-53 | 531.0 | 0 | 2 | 1090 | 15 | 41 | 86 | 10 | 44 | 84 | 488 | 90 | 123 | 7 | 14 | 8 | 18 | 50 | 28 | 17 |
| PC3802-54 | 540.0 | 2 | 6 | 1538 | 29 | 76 | 144 | 15 | 80 | 129 | 382 | 102 | 126 | 8 | 17 | 10 | 29 | 58 | 36 | 26 |
| PC3802-55 | 550.0 | 3 | 5 | 1659 | 33 | 80 | 141 | 12 | 80 | 129 | 365 | 101 | 124 | 8 | 16 | 11 | 31 | 53 | 33 | 27 |

| APPENDIX C.9. UNCORRECTED TRACE ELEMENTS | | | | | | | | | | | | | | | | | | | | |
|---|---|---|---|---|---|---|---|---|---|---|---|---|---|---|---|---|---|---|---|---|
| PC38-02 | 2525m | | | | | | | | | | | | | | | | | | | |
| Sample | Depth | Mo | U | Ba | Ni | Cr | V | Sc | Cu | Zn | Sr | Rb | Zr | Nb | Pb | Th | La | Ce | Nd | Y |
| | (cm) | (ppm) | (ppm) | (ppm) | (ppm) | (ppm) | (ppm) | (ppm) | (ppm) | (ppm) | (ppm) | (ppm) | (ppm) | (ppm) | (ppm) | (ppm) | (ppm) | (ppm) | (ppm) | (ppm) |
| PC3802-56 | 560.0 | 2 | 6 | 2088 | 50 | 83 | 139 | 15 | 90 | 150 | 329 | 101 | 120 | 8 | 12 | 10 | 38 | 54 | 35 | 28 |
| PC3802-57 | 572.0 | 2 | 8 | 2040 | 33 | 77 | 125 | 16 | 79 | 133 | 445 | 89 | 106 | 7 | 10 | 10 | 26 | 45 | 31 | 26 |
| PC3802-58 | 582.0 | 1 | 7 | 1963 | 32 | 84 | 123 | 14 | 80 | 130 | 470 | 91 | 112 | 7 | 14 | 10 | 18 | 42 | 30 | 26 |
| PC3802-59 | 591.0 | 2 | 6 | 1844 | 27 | 79 | 134 | 16 | 79 | 125 | 490 | 93 | 111 | 8 | 17 | 10 | 22 | 47 | 28 | 25 |
| PC3802-60 | 601.0 | 1 | 9 | 1940 | 23 | 66 | 105 | 8 | 67 | 105 | 765 | 71 | 89 | 6 | 11 | 6 | 20 | 38 | 27 | 23 |
| PC3802-61 | 611.0 | 0 | 9 | 1704 | 22 | 61 | 111 | 7 | 67 | 101 | 785 | 68 | 88 | 6 | 10 | 7 | 21 | 40 | 24 | 21 |
| PC3802-62 | 621.0 | 1 | 8 | 1565 | 22 | 59 | 125 | 12 | 65 | 106 | 648 | 77 | 98 | 6 | 17 | 9 | 13 | 34 | 24 | 22 |
| PC3802-63 | 631.0 | 2 | 8 | 1389 | 23 | 60 | 121 | 16 | 63 | 85 | 635 | 81 | 101 | 7 | 13 | 8 | 19 | 46 | 31 | 22 |
| PC3802-64 | 641.0 | 1 | 8 | 1597 | 23 | 69 | 129 | 13 | 67 | 112 | 564 | 87 | 108 | 8 | 11 | 10 | 19 | 40 | 30 | 25 |
| PC3802-65 | 651.0 | 1 | 5 | 1775 | 24 | 79 | 137 | 17 | 76 | 127 | 462 | 95 | 115 | 7 | 12 | 10 | 22 | 43 | 29 | 25 |
| PC3802-66 | 662.0 | 1 | 5 | 2303 | 28 | 85 | 128 | 6 | 82 | 132 | 511 | 89 | 111 | 8 | 12 | 9 | 19 | 49 | 30 | 24 |
| PC3802-67 | 671.0 | 1 | 11 | 1922 | 24 | 65 | 101 | 12 | 65 | 103 | 736 | 70 | 90 | 6 | 12 | 8 | 14 | 39 | 28 | 19 |
| PC3802-68 | 681.0 | 0 | 9 | 1447 | 22 | 63 | 125 | 16 | 59 | 104 | 674 | 79 | 100 | 7 | 13 | 9 | 20 | 41 | 28 | 18 |
| PC3802-69 | 691.0 | 1 | 9 | 1299 | 25 | 65 | 118 | 15 | 57 | 104 | 598 | 85 | 108 | 7 | 16 | 8 | 24 | 38 | 26 | 18 |
| PC3802-70 | 701.0 | 1 | 8 | 1283 | 23 | 64 | 107 | 10 | 59 | 101 | 618 | 83 | 106 | 8 | 14 | 7 | 17 | 45 | 31 | 18 |
| PC3802-71 | 711.0 | 1 | 7 | 1459 | 22 | 70 | 116 | 15 | 56 | 102 | 610 | 83 | 103 | 7 | 10 | 8 | 21 | 42 | 25 | 19 |
| PC3802-72 | 721.0 | 1 | 6 | 1458 | 24 | 68 | 103 | 12 | 62 | 108 | 589 | 83 | 104 | 7 | 10 | 5 | 22 | 44 | 25 | 20 |
| PC3802-73 | 731.0 | 0 | 8 | 1421 | 25 | 64 | 110 | 15 | 63 | 102 | 587 | 84 | 103 | 8 | 12 | 9 | 14 | 50 | 30 | 21 |
| PC3802-74 | 741.0 | 2 | 8 | 1352 | 29 | 61 | 110 | 13 | 69 | 109 | 551 | 84 | 105 | 7 | 10 | 9 | 22 | 40 | 30 | 23 |
| PC38-11 | 3835m | | | | | | | | | | | | | | | | | | | |
| PC3811-01 | 3.0 | 6 | 10 | 1212 | 51 | 116 | 132 | 16 | 122 | 163 | 245 | 94 | 154 | 9 | 15 | 9 | 25 | 49 | 28 | 25 |
| PC3811-02 | 13.0 | 19 | 9 | 404 | 54 | 96 | 100 | 11 | 35 | 111 | 332 | 76 | 163 | 8 | 14 | 8 | 16 | 38 | 25 | 20 |
| PC3811-03 | 23.0 | 13 | 7 | 371 | 46 | 79 | 96 | 12 | 28 | 96 | 318 | 72 | 214 | 9 | 14 | 8 | 21 | 47 | 28 | 23 |
| PC3811-04 | 33.0 | 2 | 13 | 1908 | 47 | 111 | 132 | 15 | 134 | 173 | 247 | 97 | 136 | 9 | 10 | 10 | 21 | 38 | 29 | 28 |
| PC3811-05 | 43.0 | 2 | 11 | 1330 | 53 | 110 | 123 | 17 | 97 | 150 | 242 | 97 | 131 | 9 | 10 | 9 | 28 | 46 | 28 | 24 |
| PC3811-06 | 53.0 | 4 | 10 | 923 | 54 | 102 | 116 | 15 | 77 | 132 | 242 | 97 | 129 | 9 | 12 | 8 | 21 | 50 | 28 | 21 |
| PC3811-07 | 63.0 | 5 | 12 | 790 | 48 | 95 | 123 | 15 | 70 | 128 | 226 | 97 | 133 | 9 | 13 | 9 | 30 | 51 | 30 | 10 |
| PC3811-08 | 73.0 | 7 | 7 | 828 | 44 | 87 | 122 | 12 | 70 | 127 | 265 | 97 | 135 | 9 | 14 | 9 | 22 | 53 | 28 | 20 |
| PC3811-09 | 85.0 | 4 | 5 | 661 | 31 | 66 | 96 | 13 | 34 | 80 | 366 | 82 | 158 | 8 | 14 | 9 | 23 | 47 | 29 | 22 |
| PC3811-10 | 95.0 | 10 | 9 | 798 | 43 | 86 | 118 | 11 | 65 | 120 | 289 | 92 | 127 | 9 | 14 | 9 | 22 | 49 | 25 | 20 |

| APPENDIX C.9. UNCORRECTED TRACE ELEMENTS | | | | | | | | | | | | | | | | | | | | |
|---|---|---|---|---|---|---|---|---|---|---|---|---|---|---|---|---|---|---|---|---|
| PC38-11 | 3835m | | | | | | | | | | | | | | | | | | | |
| Sample | Depth | Mo | U | Ba | Ni | Cr | V | Sc | Cu | Zn | Sr | Rb | Zr | Nb | Pb | Th | La | Ce | Nd | Y |
| | (cm) | (ppm) | (ppm) | (ppm) | (ppm) | (ppm) | (ppm) | (ppm) | (ppm) | (ppm) | (ppm) | (ppm) | (ppm) | (ppm) | (ppm) | (ppm) | (ppm) | (ppm) | (ppm) | (ppm) |
| PC3811-11 | 105.0 | 10 | 5 | 734 | 45 | 89 | 113 | 15 | 65 | 118 | 303 | 90 | 122 | 8 | 12 | 10 | 23 | 49 | 28 | 20 |
| PC3811-12 | 116.0 | 9 | 4 | 816 | 44 | 91 | 116 | 16 | 104 | 153 | 271 | 92 | 123 | 9 | 15 | 9 | 19 | 35 | 26 | 20 |
| PC3811-13 | 125.0 | 10 | 5 | 851 | 43 | 91 | 123 | 10 | 71 | 124 | 277 | 95 | 124 | 9 | 14 | 9 | 22 | 44 | 30 | 20 |
| PC3811-14 | 135.0 | 9 | 5 | 777 | 43 | 89 | 119 | 10 | 59 | 117 | 298 | 92 | 125 | 8 | 12 | 7 | 23 | 53 | 30 | 20 |
| PC3811-15 | 145.0 | 9 | 6 | 859 | 43 | 88 | 120 | 15 | 67 | 122 | 277 | 95 | 126 | 8 | 13 | 8 | 29 | 41 | 27 | 20 |
| PC3811-16 | 155.0 | 8 | 8 | 695 | 38 | 83 | 112 | 14 | 54 | 112 | 326 | 88 | 128 | 8 | 12 | 9 | 23 | 36 | 27 | 20 |
| PC3811-17 | 165.0 | 8 | 8 | 815 | 40 | 83 | 118 | 12 | 62 | 120 | 292 | 94 | 122 | 9 | 14 | 9 | 25 | 41 | 26 | 20 |
| PC3811-18 | 175.0 | 7 | 9 | 800 | 39 | 82 | 107 | 13 | 54 | 105 | 349 | 88 | 138 | 9 | 13 | 8 | 23 | 55 | 31 | 23 |
| PC3811-19 | 186.0 | 11 | 9 | 1014 | 51 | 97 | 120 | 12 | 88 | 138 | 265 | 97 | 125 | 9 | 12 | 10 | 24 | 49 | 29 | 23 |
| PC3811-20 | 197.0 | 10 | 6 | 1002 | 51 | 98 | 122 | 14 | 83 | 138 | 249 | 98 | 120 | 9 | 13 | 8 | 30 | 45 | 28 | 22 |
| PC3811-21 | 204.0 | 6 | 5 | 1046 | 53 | 103 | 125 | 17 | 85 | 137 | 232 | 100 | 121 | 9 | 11 | 9 | 24 | 47 | 29 | 23 |
| PC3811-22 | 215.0 | 8 | 10 | 1053 | 47 | 88 | 111 | 11 | 77 | 122 | 340 | 87 | 124 | 9 | 11 | 7 | 20 | 46 | 29 | 22 |
| PC3811-23 | 225.0 | 9 | 6 | 1309 | 56 | 94 | 117 | 15 | 102 | 141 | 308 | 92 | 115 | 8 | 10 | 9 | 25 | 46 | 26 | 23 |
| PC3811-24 | 235.0 | 10 | 10 | 1308 | 60 | 98 | 114 | 13 | 105 | 145 | 289 | 95 | 117 | 8 | 12 | 8 | 26 | 43 | 31 | 24 |
| PC3811-25 | 245.0 | 11 | 10 | 1367 | 59 | 99 | 122 | 16 | 111 | 146 | 300 | 93 | 115 | 8 | 10 | 9 | 22 | 41 | 29 | 24 |
| PC3811-26 | 255.0 | 11 | 9 | 1343 | 57 | 89 | 100 | 10 | 103 | 135 | 341 | 83 | 107 | 7 | 8 | 8 | 22 | 43 | 28 | 23 |
| PC3811-27 | 265.0 | 10 | 9 | 1392 | 56 | 90 | 105 | 15 | 110 | 137 | 326 | 85 | 109 | 8 | 10 | 8 | 22 | 36 | 24 | 24 |
| PC3811-28 | 275.0 | 9 | 9 | 1410 | 53 | 92 | 109 | 13 | 112 | 137 | 298 | 86 | 112 | 8 | 10 | 8 | 22 | 35 | 23 | 25 |
| PC3811-29 | 285.0 | 8 | 10 | 1270 | 52 | 105 | 128 | 18 | 100 | 146 | 229 | 106 | 137 | 9 | 13 | 9 | 29 | 49 | 31 | 26 |
| PC3811-30 | 297.0 | 6 | 9 | 1147 | 51 | 99 | 129 | 14 | 101 | 144 | 243 | 105 | 137 | 9 | 13 | 10 | 23 | 48 | 31 | 25 |
| PC3811-31 | 305.0 | 8 | 7 | 1349 | 43 | 103 | 138 | 16 | 110 | 143 | 226 | 108 | 144 | 10 | 12 | 15 | 30 | 51 | 34 | 28 |
| PC3811-32 | 315.0 | 7 | 10 | 1069 | 45 | 106 | 135 | 16 | 98 | 143 | 226 | 108 | 154 | 10 | 17 | 11 | 25 | 50 | 30 | 27 |
| PC3811-33 | 325.0 | 16 | 17 | 489 | 56 | 89 | 96 | 5 | 45 | 99 | 412 | 69 | 164 | 8 | 13 | 7 | 20 | 45 | 24 | 23 |
| PC3811-34 | 335.0 | 10 | 10 | 1537 | 52 | 97 | 121 | 15 | 113 | 150 | 231 | 100 | 126 | 9 | 10 | 9 | 23 | 42 | 27 | 25 |
| PC3811-35 | 345.0 | 11 | 9 | 1452 | 57 | 101 | 121 | 13 | 116 | 153 | 235 | 99 | 124 | 9 | 11 | 9 | 25 | 42 | 31 | 25 |
| PC3811-36 | 355.0 | 9 | 8 | 1636 | 54 | 97 | 115 | 16 | 113 | 141 | 236 | 90 | 116 | 8 | 10 | 8 | 20 | 37 | 26 | 26 |
| PC3811-37 | 365.0 | 8 | 4 | 1486 | 61 | 107 | 112 | 15 | 119 | 152 | 230 | 93 | 120 | 9 | 10 | 8 | 23 | 43 | 31 | 28 |
| PC3811-38 | 375.0 | 9 | 8 | 1199 | 71 | 105 | 122 | 14 | 121 | 157 | 235 | 98 | 121 | 9 | 11 | 10 | 26 | 46 | 30 | 26 |
| PC3811-39 | 385.0 | 14 | 9 | 1278 | 58 | 107 | 131 | 14 | 111 | 167 | 245 | 106 | 132 | 10 | 17 | 11 | 30 | 50 | 29 | 29 |
| PC3811-40 | 395.0 | 11 | 7 | 1261 | 51 | 100 | 139 | 19 | 115 | 150 | 249 | 103 | 131 | 10 | 13 | 9 | 29 | 45 | 28 | 30 |
| PC3811-41 | 405.0 | 12 | 8 | 1309 | 53 | 101 | 145 | 16 | 121 | 149 | 247 | 104 | 128 | 9 | 15 | 11 | 32 | 55 | 34 | 30 |
| PC3811-42 | 415.0 | 10 | 8 | 1794 | 47 | 106 | 147 | 15 | 136 | 150 | 223 | 105 | 135 | 10 | 13 | 10 | 28 | 47 | 28 | 32 |

APPENDIX C.9. UNCORRECTED TRACE ELEMENTS

| PC38-11 | 3835m | | | | | | | | | | | | | | | | | | | |
|---|---|---|---|---|---|---|---|---|---|---|---|---|---|---|---|---|---|---|---|---|
| Sample | Depth | Mo | U | Ba | Ni | Cr | V | Sc | Cu | Zn | Sr | Rb | Zr | Nb | Pb | Th | La | Ce | Nd | Y |
| | (cm) | (ppm) | (ppm) | (ppm) | (ppm) | (ppm) | (ppm) | (ppm) | (ppm) | (ppm) | (ppm) | (ppm) | (ppm) | (ppm) | (ppm) | (ppm) | (ppm) | (ppm) | (ppm) | (ppm) |
| PC3811-43 | 425.0 | 9 | 7 | 1986 | 48 | 103 | 142 | 17 | 152 | 147 | 242 | 101 | 131 | 9 | 12 | 10 | 28 | 47 | 31 | 32 |
| PC3811-44 | 435.0 | 8 | 11 | 2379 | 49 | 93 | 130 | 16 | 147 | 158 | 298 | 86 | 118 | 8 | 7 | 8 | 23 | 37 | 27 | 32 |
| PC3811-45 | 445.0 | 7 | 9 | 2149 | 53 | 98 | 136 | 14 | 134 | 155 | 266 | 89 | 118 | 8 | 9 | 9 | 20 | 47 | 28 | 32 |
| PC3811-46 | 455.0 | 6 | 9 | 1900 | 54 | 110 | 139 | 22 | 141 | 164 | 227 | 103 | 137 | 9 | 11 | 9 | 28 | 48 | 30 | 35 |
| PC3811-47 | 465.0 | 8 | 8 | 1676 | 48 | 105 | 148 | 18 | 143 | 157 | 220 | 109 | 135 | 10 | 14 | 10 | 27 | 51 | 34 | 33 |
| PC3811-48 | 475.0 | 8 | 10 | 1802 | 53 | 97 | 139 | 19 | 147 | 154 | 244 | 98 | 124 | 8 | 10 | 9 | 28 | 42 | 35 | 33 |
| PC3811-49 | 485.0 | 8 | 5 | 1760 | 47 | 100 | 137 | 19 | 139 | 148 | 212 | 101 | 127 | 9 | 12 | 10 | 24 | 43 | 33 | 32 |
| PC3811-50 | 495.0 | 6 | 8 | 1810 | 49 | 102 | 142 | 18 | 141 | 154 | 215 | 99 | 125 | 9 | 12 | 10 | 26 | 43 | 33 | 31 |
| PC3811-51 | 505.0 | 4 | 6 | 1845 | 42 | 97 | 140 | 18 | 131 | 148 | 213 | 100 | 124 | 9 | 11 | 8 | 27 | 46 | 31 | 30 |
| PC3811-52 | 515.0 | 4 | 4 | 1875 | 41 | 97 | 137 | 18 | 125 | 144 | 216 | 100 | 123 | 9 | 11 | 7 | 26 | 46 | 33 | 31 |
| PC3811-53 | 525.0 | 3 | 4 | 1960 | 36 | 94 | 134 | 18 | 126 | 140 | 212 | 99 | 122 | 9 | 11 | 10 | 24 | 43 | 32 | 29 |
| PC3811-54 | 535.0 | 4 | 6 | 1974 | 40 | 97 | 141 | 19 | 143 | 138 | 225 | 97 | 129 | 9 | 10 | 10 | 23 | 48 | 33 | 33 |
| PC3811-55 | 545.0 | 3 | 6 | 2002 | 37 | 96 | 134 | 20 | 119 | 144 | 224 | 92 | 124 | 8 | 9 | 9 | 26 | 49 | 33 | 30 |
| PC3811-56 | 555.0 | 4 | 4 | 2213 | 38 | 96 | 140 | 17 | 132 | 145 | 227 | 91 | 124 | 9 | 9 | 9 | 25 | 42 | 31 | 33 |
| PC3811-57 | 565.0 | 1 | 6 | 2061 | 38 | 97 | 140 | 21 | 137 | 143 | 233 | 90 | 129 | 8 | 8 | 8 | 26 | 48 | 31 | 33 |

| APPENDIX C.10. SALT-CORRECTED TRACE ELEMENTS | | | | | | | | | | | | | | | | | | | | |
|---|---|---|---|---|---|---|---|---|---|---|---|---|---|---|---|---|---|---|---|---|
| BC38-02 Sample | 2530m Depth (cm) | Mo (ppm) | U (ppm) | Ba (ppm) | Ni (ppm) | Cr (ppm) | V (ppm) | Sc (ppm) | Cu (ppm) | Zn (ppm) | Sr (ppm) | Rb (ppm) | Zr (ppm) | Nb (ppm) | Pb (ppm) | Th (ppm) | La (ppm) | Ce (ppm) | Nd (ppm) | Y (ppm) |
| BC3802-01 | 0.5 | 2 | 0 | 2289 | 29 | 90 | 111 | 13 | 55 | 126 | 436 | 84 | 118 | 8 | 13 | 10 | 27 | 43 | 25 | 33 |
| BC3802-02 | 1.5 | 2 | 1 | 2298 | 27 | 88 | 112 | 12 | 56 | 129 | 424 | 84 | 118 | 7 | 14 | 9 | 27 | 44 | 23 | 32 |
| BC3802-03 | 2.5 | 2 | 1 | 2247 | 27 | 92 | 107 | 13 | 56 | 127 | 425 | 83 | 115 | 8 | 13 | 8 | 23 | 40 | 24 | 31 |
| BC3802-04 | 3.5 | 2 | 0 | 2193 | 27 | 91 | 111 | 13 | 55 | 127 | 433 | 82 | 115 | 8 | 13 | 9 | 24 | 42 | 23 | 31 |
| BC3802-05 | 4.5 | 1 | 0 | 2219 | 27 | 89 | 111 | 13 | 57 | 126 | 443 | 82 | 118 | 8 | 13 | 10 | 24 | 41 | 24 | 30 |
| BC3802-06 | 5.5 | 0 | 1 | 2185 | 27 | 91 | 112 | 9 | 57 | 124 | 439 | 81 | 115 | 6 | 15 | 7 | 16 | 42 | 24 | 30 |
| BC3802-07 | 6.5 | 1 | 1 | 2153 | 29 | 91 | 118 | 13 | 60 | 126 | 438 | 82 | 113 | 7 | 14 | 7 | 22 | 41 | 23 | 31 |
| BC3802-08 | 7.5 | 1 | 2 | 2122 | 27 | 92 | 123 | 12 | 61 | 186 | 438 | 81 | 112 | 7 | 12 | 7 | 21 | 41 | 22 | 31 |
| BC3802-09 | 8.5 | 1 | 2 | 2168 | 28 | 90 | 133 | 13 | 63 | 131 | 437 | 83 | 117 | 7 | 14 | 8 | 22 | 43 | 14 | 30 |
| BC3802-10 | 9.5 | 1 | 1 | 2185 | 27 | 91 | 134 | 13 | 63 | 130 | 451 | 83 | 117 | 7 | 14 | 8 | 23 | 39 | 22 | 31 |
| BC3802-11 | 11.0 | 2 | 2 | 2272 | 30 | 96 | 123 | 12 | 64 | 135 | 497 | 86 | 121 | 7 | 13 | 7 | 21 | 44 | 24 | 32 |
| BC3802-12 | 13.0 | 0 | 4 | 2128 | 28 | 89 | 116 | 11 | 57 | 130 | 520 | 79 | 113 | 7 | 13 | 7 | 25 | 40 | 22 | 30 |
| BC3802-13 | 15.0 | 1 | 3 | 2040 | 26 | 82 | 126 | 9 | 64 | 122 | 525 | 76 | 107 | 7 | 11 | 8 | 25 | 38 | 22 | 29 |
| BC3802-13A | 17.0 | 1 | 5 | 1857 | 25 | 76 | 111 | 5 | 56 | 113 | 602 | 70 | 104 | 7 | 8 | 6 | 24 | 38 | 22 | 28 |
| BC3802-14 | 19.0 | 1 | 6 | 1835 | 26 | 73 | 115 | 4 | 61 | 111 | 650 | 67 | 97 | 6 | 8 | 5 | 21 | 36 | 22 | 27 |
| BC3802-15 | 21.0 | 2 | 8 | 1779 | 27 | 71 | 108 | 1 | 58 | 112 | 690 | 67 | 97 | 6 | 8 | 4 | 20 | 37 | 20 | 27 |
| BC3802-16 | 23.0 | 1 | 9 | 1698 | 25 | 69 | 94 | 0 | 51 | 104 | 687 | 64 | 92 | 6 | 9 | 5 | 21 | 32 | 21 | 26 |
| BC3802-17 | 25.0 | 1 | 9 | 1712 | 26 | 69 | 94 | 0 | 52 | 105 | 703 | 65 | 94 | 7 | 8 | 5 | 20 | 33 | 20 | 26 |
| BC3802-18 | 27.0 | 1 | 9 | 1597 | 25 | 67 | 87 | 0 | 48 | 102 | 694 | 64 | 97 | 6 | 7 | 5 | 22 | 39 | 21 | 27 |
| BC3802-19 | 29.0 | 2 | 9 | 1536 | 27 | 66 | 86 | 0 | 46 | 101 | 721 | 64 | 95 | 6 | 7 | 4 | 18 | 36 | 21 | 26 |
| BC3802-20 | 31.0 | 2 | 8 | 1457 | 27 | 67 | 84 | 0 | 45 | 98 | 699 | 63 | 95 | 5 | 8 | 4 | 17 | 34 | 20 | 25 |
| BC3802-21 | 33.0 | 2 | 7 | 1471 | 30 | 69 | 88 | 0 | 48 | 105 | 696 | 66 | 93 | 6 | 7 | 4 | 15 | 33 | 20 | 26 |
| BC3802-21A | 35.0 | 3 | 9 | 1211 | 37 | 64 | 92 | 2 | 48 | 100 | 626 | 70 | 95 | 7 | 12 | 4 | 23 | 36 | 20 | 23 |
| BC3802-22 | 37.0 | 2 | 7 | 1339 | 31 | 66 | 90 | 1 | 47 | 101 | 667 | 69 | 98 | 6 | 9 | 5 | 19 | 34 | 20 | 25 |
| BC3802-23 | 39.0 | 1 | 6 | 1383 | 28 | 66 | 87 | 0 | 45 | 101 | 680 | 66 | 95 | 6 | 8 | 5 | 20 | 35 | 20 | 24 |
| BC3802-24 | 41.0 | 3 | 8 | 1275 | 33 | 65 | 95 | 0 | 50 | 99 | 661 | 69 | 98 | 6 | 8 | 5 | 18 | 36 | 20 | 22 |
| BC3802-25 | 43.0 | 3 | 7 | 1351 | 34 | 66 | 103 | 0 | 52 | 102 | 638 | 71 | 102 | 6 | 10 | 6 | 20 | 32 | 20 | 22 |
| BC3802-26 | 45.0 | 2 | 8 | 1373 | 32 | 65 | 106 | 0 | 52 | 102 | 631 | 72 | 103 | 6 | 10 | 7 | 21 | 39 | 21 | 22 |
| BC3802-27 | 47.0 | 3 | 8 | 1379 | 32 | 64 | 108 | 1 | 52 | 101 | 624 | 72 | 103 | 6 | 10 | 6 | 22 | 37 | 21 | 23 |
| BC3802-28 | 49.0 | 3 | 8 | 1433 | 33 | 66 | 110 | 0 | 53 | 105 | 628 | 72 | 104 | 6 | 13 | 6 | 18 | 38 | 21 | 24 |
| BC3802-29 | 51.0 | 3 | 7 | 1428 | 32 | 65 | 108 | 0 | 54 | 104 | 617 | 72 | 104 | 6 | 9 | 5 | 18 | 33 | 21 | 25 |
| BC3802-30 | 53.0 | 3 | 8 | 1412 | 32 | 64 | 105 | 3 | 52 | 103 | 609 | 72 | 105 | 6 | 12 | 6 | 10 | 32 | 21 | 24 |

APPENDIX C.10. SALT-CORRECTED TRACE ELEMENTS

| BC38-03 Sample | 4289m Depth (cm) | Mo (ppm) | U (ppm) | Ba (ppm) | Ni (ppm) | Cr (ppm) | V (ppm) | Sc (ppm) | Cu (ppm) | Zn (ppm) | Sr (ppm) | Rb (ppm) | Zr (ppm) | Nb (ppm) | Pb (ppm) | Th (ppm) | La (ppm) | Ce (ppm) | Nd (ppm) | Y (ppm) |
|---|---|---|---|---|---|---|---|---|---|---|---|---|---|---|---|---|---|---|---|---|
| BC3803-01 | 0.5 | 3 | 1 | 1889 | 24 | 85 | 131 | 14 | 122 | 121 | 243 | 90 | 114 | 7 | 19 | 11 | 13 | 43 | 23 | 20 |
| BC3803-02 | 1.5 | 2 | 1 | 1842 | 22 | 85 | 124 | 12 | 117 | 114 | 236 | 88 | 113 | 8 | 15 | 11 | 22 | 41 | 20 | 20 |
| BC3803-03 | 2.5 | 0 | 1 | 1853 | 22 | 87 | 120 | 14 | 119 | 115 | 234 | 88 | 113 | 8 | 15 | 10 | 23 | 37 | 19 | 19 |
| BC3803-04 | 3.5 | 0 | 2 | 1802 | 23 | 83 | 119 | 11 | 121 | 114 | 225 | 86 | 110 | 8 | 14 | 10 | 20 | 36 | 19 | 20 |
| BC3803-05 | 4.5 | 2 | 2 | 1927 | 27 | 86 | 138 | 13 | 134 | 119 | 230 | 90 | 114 | 8 | 14 | 11 | 20 | 38 | 20 | 21 |
| BC3803-06 | 5.5 | 1 | 3 | 1898 | 24 | 85 | 130 | 13 | 124 | 115 | 221 | 88 | 109 | 8 | 15 | 11 | 20 | 42 | 21 | 20 |
| BC3803-07 | 6.5 | 1 | 3 | 1858 | 25 | 83 | 128 | 12 | 121 | 117 | 219 | 87 | 112 | 8 | 14 | 10 | 21 | 43 | 21 | 20 |
| BC3803-08 | 7.5 | 1 | 4 | 1891 | 24 | 84 | 125 | 12 | 124 | 144 | 224 | 89 | 116 | 8 | 14 | 11 | 17 | 39 | 21 | 21 |
| BC3803-09 | 8.5 | 2 | 6 | 1904 | 28 | 84 | 127 | 12 | 125 | 119 | 226 | 90 | 115 | 8 | 15 | 11 | 19 | 44 | 22 | 21 |
| BC3803-10 | 9.5 | 2 | 7 | 2023 | 29 | 88 | 138 | 12 | 140 | 128 | 235 | 94 | 122 | 8 | 16 | 10 | 18 | 43 | 21 | 24 |
| BC3803-11 | 11.0 | 2 | 7 | 1936 | 29 | 89 | 143 | 12 | 137 | 127 | 228 | 92 | 118 | 9 | 16 | 13 | 18 | 39 | 22 | 23 |
| BC3803-12 | 13.0 | 2 | 8 | 2003 | 36 | 89 | 141 | 13 | 134 | 130 | 229 | 92 | 120 | 9 | 14 | 11 | 17 | 42 | 23 | 23 |
| BC3803-13 | 15.0 | 2 | 8 | 1970 | 29 | 85 | 139 | 13 | 135 | 130 | 232 | 91 | 119 | 8 | 15 | 11 | 20 | 40 | 23 | 23 |
| BC3803-14 | 17.0 | 3 | 9 | 2071 | 38 | 90 | 142 | 14 | 145 | 136 | 236 | 94 | 124 | 9 | 14 | 10 | 20 | 44 | 24 | 24 |
| BC3803-15 | 19.0 | 3 | 8 | 2013 | 40 | 86 | 133 | 15 | 138 | 131 | 234 | 91 | 120 | 9 | 13 | 10 | 20 | 43 | 23 | 23 |
| BC3803-16 | 21.0 | 4 | 7 | 2017 | 29 | 84 | 127 | 12 | 137 | 130 | 229 | 89 | 119 | 9 | 14 | 11 | 25 | 41 | 21 | 22 |
| BC3803-17 | 23.0 | 2 | 6 | 1952 | 33 | 85 | 125 | 14 | 139 | 127 | 231 | 88 | 116 | 9 | 14 | 11 | 21 | 40 | 21 | 21 |
| BC3803-18 | 25.0 | 3 | 8 | 2014 | 33 | 86 | 131 | 13 | 138 | 132 | 232 | 89 | 120 | 9 | 14 | 11 | 20 | 41 | 21 | 22 |
| BC3803-19 | 27.0 | 4 | 9 | 1960 | 31 | 82 | 129 | 14 | 132 | 131 | 229 | 86 | 116 | 9 | 13 | 11 | 23 | 41 | 20 | 22 |
| BC3803-20 | 29.0 | 3 | 9 | 2079 | 32 | 86 | 135 | 14 | 140 | 139 | 240 | 90 | 123 | 9 | 14 | 11 | 16 | 39 | 22 | 22 |
| BC3803-21 | 31.0 | 3 | 9 | 2013 | 30 | 82 | 130 | 14 | 131 | 132 | 238 | 88 | 121 | 9 | 13 | 12 | 17 | 44 | 25 | 22 |
| BC3803-22 | 33.0 | 4 | 9 | 2039 | 30 | 82 | 131 | 15 | 134 | 133 | 237 | 87 | 122 | 8 | 12 | 8 | 14 | 45 | 23 | 22 |
| BC3803-23 | 35.0 | 3 | 9 | 2012 | 31 | 83 | 127 | 14 | 132 | 132 | 234 | 85 | 119 | 8 | 12 | 8 | 23 | 42 | 23 | 22 |
| BC3803-24 | 37.0 | 2 | 9 | 2039 | 34 | 84 | 131 | 14 | 133 | 136 | 243 | 89 | 126 | 8 | 13 | 10 | 17 | 45 | 23 | 24 |
| BC3803-25 | 39.0 | 3 | 10 | 2002 | 35 | 84 | 135 | 13 | 136 | 139 | 247 | 89 | 126 | 9 | 13 | 9 | 22 | 46 | 23 | 25 |
| BC3803-26 | 41.0 | 2 | 10 | 1943 | 32 | 84 | 134 | 15 | 126 | 136 | 240 | 90 | 124 | 9 | 13 | 12 | 22 | 43 | 22 | 23 |
| BC3803-27 | 43.0 | 2 | 9 | 1857 | 39 | 84 | 129 | 13 | 120 | 132 | 239 | 89 | 125 | 8 | 14 | 11 | 16 | 44 | 22 | 23 |
| BC3803-28 | 45.0 | 3 | 10 | 1867 | 32 | 84 | 128 | 13 | 117 | 131 | 236 | 87 | 123 | 8 | 13 | 10 | 21 | 46 | 22 | 23 |
| BC3803-29 | 47.0 | 3 | 10 | 1831 | 34 | 82 | 128 | 13 | 116 | 133 | 237 | 87 | 122 | 8 | 13 | 11 | 22 | 48 | 22 | 23 |
| BC3803-30 | 49.0 | 3 | 9 | 1822 | 33 | 85 | 127 | 14 | 115 | 133 | 240 | 89 | 126 | 8 | 13 | 11 | 23 | 44 | 22 | 23 |
| BC3803-31 | 51.0 | 2 | 10 | 1818 | 33 | 86 | 130 | 14 | 111 | 136 | 244 | 92 | 129 | 9 | 13 | 10 | 32 | 47 | 22 | 24 |
| BC3803-32 | 53.0 | 2 | 11 | 1663 | 33 | 88 | 128 | 14 | 105 | 136 | 237 | 90 | 127 | 9 | 13 | 11 | 24 | 43 | 21 | 23 |

| APPENDIX C.10. SALT-CORRECTED TRACE ELEMENTS | | | | | | | | | | | | | | | | | | | | |
|---|---|---|---|---|---|---|---|---|---|---|---|---|---|---|---|---|---|---|---|---|
| PC38-09 | 148m | | | | | | | | | | | | | | | | | | | |
| Sample | Depth | Mo | U | Ba | Ni | Cr | V | Sc | Cu | Zn | Sr | Rb | Zr | Nb | Pb | Th | La | Ce | Nd | Y |
| | (cm) | (ppm) | (ppm) | (ppm) | (ppm) | (ppm) | (ppm) | (ppm) | (ppm) | (ppm) | (ppm) | (ppm) | (ppm) | (ppm) | (ppm) | (ppm) | (ppm) | (ppm) | (ppm) | (ppm) |
| PC3809-01 | 4.0 | 68 | 10 | 295 | 66 | 119 | 107 | 10 | 29 | 123 | 199 | 69 | 131 | 9 | 14 | 11 | 19 | 38 | 17 | 17 |
| PC3809-02 | 13.0 | 67 | 10 | 249 | 62 | 110 | 128 | 11 | 25 | 100 | 195 | 67 | 108 | 8 | 16 | 10 | 17 | 32 | 16 | 16 |
| PC3809-03 | 23.0 | 58 | 10 | 293 | 63 | 122 | 123 | 13 | 32 | 109 | 194 | 76 | 137 | 10 | 20 | 12 | 19 | 45 | 19 | 19 |
| PC3809-04 | 34.0 | 57 | 9 | 272 | 64 | 121 | 123 | 10 | 32 | 108 | 179 | 73 | 128 | 9 | 18 | 11 | 20 | 41 | 18 | 18 |
| PC3809-05 | 43.0 | 27 | 8 | 339 | 44 | 99 | 105 | 13 | 23 | 99 | 240 | 74 | 198 | 9 | 17 | 11 | 18 | 45 | 21 | 23 |
| PC3809-06 | 53.0 | 57 | 6 | 269 | 60 | 117 | 118 | 12 | 32 | 116 | 175 | 71 | 113 | 9 | 18 | 11 | 17 | 38 | 16 | 17 |
| PC3809-07 | 62.0 | 99 | 10 | 244 | 75 | 126 | 118 | 9 | 34 | 103 | 195 | 59 | 97 | 8 | 14 | 9 | 21 | 32 | 14 | 15 |
| PC3809-08 | 73.0 | 40 | 9 | 303 | 57 | 127 | 119 | 12 | 27 | 109 | 188 | 76 | 148 | 10 | 18 | 12 | 18 | 48 | 21 | 22 |
| PC3809-09 | 84.0 | 47 | 7 | 316 | 62 | 137 | 137 | 13 | 33 | 123 | 168 | 89 | 136 | 11 | 21 | 13 | 22 | 48 | 22 | 21 |
| PC3809-10 | 94.0 | 68 | 8 | 294 | 69 | 131 | 143 | 12 | 40 | 121 | 170 | 84 | 122 | 9 | 22 | 12 | 23 | 44 | 19 | 18 |
| PC3809-11 | 104.0 | 84 | 10 | 295 | 67 | 121 | 146 | 11 | 34 | 122 | 151 | 74 | 103 | 8 | 21 | 11 | 17 | 40 | 17 | 16 |
| PC3809-12 | 113.0 | 37 | 9 | 322 | 56 | 124 | 142 | 15 | 51 | 147 | 166 | 93 | 131 | 9 | 26 | 14 | 27 | 46 | 22 | 22 |
| PC3809-13 | 124.0 | 40 | 10 | 332 | 52 | 130 | 117 | 12 | 21 | 104 | 214 | 78 | 168 | 11 | 19 | 12 | 23 | 49 | 23 | 22 |
| PC3809-14 | 134.0 | 62 | 9 | 278 | 61 | 119 | 118 | 10 | 27 | 93 | 213 | 67 | 147 | 9 | 15 | 9 | 15 | 42 | 19 | 18 |
| PC3809-15 | 144.0 | 68 | 8 | 261 | 65 | 119 | 108 | 10 | 25 | 93 | 183 | 62 | 116 | 8 | 17 | 10 | 20 | 36 | 16 | 16 |
| PC3809-16 | 152.0 | 46 | 7 | 226 | 53 | 97 | 107 | 10 | 26 | 92 | 180 | 63 | 117 | 9 | 16 | 10 | 10 | 30 | 15 | 15 |
| PC3809-17 | 165.0 | 52 | 10 | 250 | 53 | 90 | 105 | 9 | 24 | 89 | 220 | 57 | 138 | 8 | 14 | 8 | 13 | 34 | 16 | 17 |
| PC3809-18 | 174.0 | 28 | 9 | 341 | 45 | 100 | 99 | 9 | 20 | 93 | 243 | 70 | 204 | 9 | 16 | 9 | 18 | 45 | 22 | 22 |
| PC3809-19 | 185.0 | 32 | 11 | 322 | 43 | 81 | 85 | 10 | 19 | 86 | 289 | 60 | 213 | 7 | 13 | 8 | 14 | 36 | 18 | 21 |
| PC3809-20 | 194.0 | 28 | 8 | 349 | 39 | 77 | 85 | 9 | 20 | 90 | 306 | 61 | 232 | 8 | 11 | 7 | 15 | 40 | 19 | 24 |
| PC3809-21 | 205.0 | 39 | 5 | 441 | 36 | 62 | 115 | 14 | 35 | 123 | 256 | 70 | 153 | 8 | 18 | 9 | 16 | 41 | 19 | 22 |
| PC3809-22 | 214.0 | 55 | 13 | 286 | 73 | 116 | 104 | 8 | 24 | 96 | 256 | 58 | 181 | 7 | 14 | 10 | 16 | 35 | 17 | 19 |
| PC3809-23 | 224.0 | 13 | 11 | 391 | 31 | 57 | 63 | 9 | 9 | 60 | 347 | 55 | 282 | 8 | 10 | 7 | 14 | 47 | 20 | 23 |
| PC3809-24 | 234.0 | 42 | 9 | 319 | 43 | 76 | 79 | 8 | 17 | 72 | 305 | 49 | 201 | 6 | 12 | 7 | 12 | 33 | 16 | 20 |
| PC3809-25 | 243.0 | 74 | 10 | 230 | 64 | 95 | 104 | 8 | 23 | 70 | 185 | 43 | 103 | 7 | 11 | 7 | 2 | 27 | 12 | 13 |
| PC3809-26 | 257.0 | 59 | 10 | 275 | 60 | 107 | 95 | 7 | 20 | 79 | 201 | 50 | 134 | 6 | 13 | 7 | 4 | 32 | 15 | 17 |
| PC3809-27 | 267.0 | 32 | 15 | 336 | 43 | 85 | 78 | 7 | 14 | 86 | 374 | 50 | 190 | 7 | 11 | 6 | 17 | 34 | 19 | 25 |
| PC3809-28 | 273.0 | 53 | 167 | 185 | 43 | 122 | 86 | 0 | 9 | 59 | 1195 | 30 | 109 | 6 | 4 | 0 | 2 | 27 | 14 | 25 |
| PC3809-29 | 284.0 | 69 | 13 | 246 | 68 | 136 | 122 | 13 | 34 | 105 | 202 | 62 | 108 | 7 | 12 | 8 | 17 | 36 | 17 | 20 |
| PC3809-30 | 294.0 | 79 | 7 | 209 | 68 | 117 | 105 | 8 | 24 | 78 | 170 | 48 | 82 | 5 | 13 | 8 | 11 | 26 | 13 | 15 |
| PC3809-31 | 304.0 | 49 | 8 | 339 | 61 | 127 | 116 | 11 | 35 | 151 | 171 | 63 | 104 | 7 | 13 | 8 | 13 | 32 | 16 | 18 |
| PC3809-32 | 314.0 | 67 | 7 | 263 | 70 | 133 | 122 | 11 | 34 | 100 | 162 | 63 | 91 | 6 | 16 | 9 | 12 | 30 | 13 | 17 |

| APPENDIX C.10. SALT-CORRECTED TRACE ELEMENTS | | | | | | | | | | | | | | | | | | | | |
|---|---|---|---|---|---|---|---|---|---|---|---|---|---|---|---|---|---|---|---|---|
| PC38-09 | 148m | | | | | | | | | | | | | | | | | | | |
| Sample | Depth | Mo | U | Ba | Ni | Cr | V | Sc | Cu | Zn | Sr | Rb | Zr | Nb | Pb | Th | La | Ce | Nd | Y |
| | (cm) | (ppm) | (ppm) | (ppm) | (ppm) | (ppm) | (ppm) | (ppm) | (ppm) | (ppm) | (ppm) | (ppm) | (ppm) | (ppm) | (ppm) | (ppm) | (ppm) | (ppm) | (ppm) | (ppm) |
| PC3809-33 | 324.0 | 50 | 8 | 264 | 75 | 150 | 127 | 13 | 35 | 101 | 187 | 62 | 112 | 7 | 14 | 9 | 16 | 34 | 16 | 21 |
| PC3809-34 | 335.0 | 71 | 8 | 220 | 75 | 137 | 119 | 11 | 29 | 83 | 163 | 51 | 93 | 6 | 14 | 9 | 14 | 29 | 14 | 17 |
| PC3809-35 | 344.0 | 70 | 7 | 203 | 75 | 140 | 115 | 9 | 31 | 88 | 153 | 48 | 85 | 6 | 11 | 8 | 12 | 30 | 14 | 15 |
| PC3809-36 | 355.0 | 78 | 5 | 201 | 65 | 107 | 124 | 8 | 21 | 67 | 156 | 39 | 65 | 4 | 10 | 7 | 10 | 21 | 10 | 11 |
| PC3809-37 | 364.0 | 91 | 5 | 191 | 70 | 106 | 126 | 10 | 23 | 66 | 185 | 39 | 63 | 3 | 11 | 4 | 10 | 20 | 10 | 11 |
| PC3809-38 | 375.0 | 96 | 7 | 253 | 76 | 134 | 143 | 9 | 31 | 84 | 162 | 55 | 88 | 6 | 15 | 7 | 16 | 26 | 13 | 15 |
| PC3809-39 | 384.0 | 58 | 8 | 258 | 65 | 144 | 129 | 13 | 34 | 97 | 214 | 57 | 109 | 7 | 13 | 8 | 21 | 31 | 15 | 19 |
| PC3809-40 | 394.0 | 66 | 8 | 229 | 72 | 128 | 125 | 10 | 29 | 80 | 179 | 50 | 88 | 5 | 12 | 7 | 18 | 30 | 14 | 15 |
| PC3809-41 | 404.0 | 51 | 8 | 262 | 65 | 125 | 124 | 10 | 26 | 88 | 156 | 56 | 96 | 6 | 15 | 8 | 15 | 32 | 14 | 16 |
| PC3809-42 | 416.0 | 84 | 9 | 206 | 69 | 126 | 130 | 10 | 27 | 77 | 202 | 47 | 80 | 5 | 11 | 8 | 10 | 26 | 13 | 14 |
| PC3809-43 | 424.0 | 68 | 8 | 234 | 68 | 121 | 134 | 9 | 25 | 76 | 149 | 53 | 84 | 6 | 14 | 8 | 5 | 27 | 12 | 14 |
| PC3809-44 | 434.0 | 82 | 10 | 263 | 85 | 145 | 156 | 10 | 37 | 92 | 165 | 63 | 96 | 6 | 15 | 10 | 16 | 34 | 15 | 16 |
| PC3809-45 | 444.0 | 64 | 8 | 237 | 56 | 106 | 119 | 10 | 27 | 83 | 186 | 49 | 80 | 5 | 12 | 8 | 12 | 25 | 11 | 14 |
| PC3809-46 | 453.0 | 50 | 8 | 271 | 56 | 128 | 135 | 11 | 31 | 89 | 179 | 60 | 107 | 7 | 14 | 8 | 16 | 31 | 15 | 18 |
| PC3809-47 | 465.0 | 73 | 7 | 245 | 66 | 138 | 130 | 11 | 34 | 93 | 183 | 60 | 93 | 7 | 12 | 7 | 15 | 32 | 15 | 16 |
| PC3809-48 | 474.0 | 98 | 9 | 262 | 67 | 129 | 138 | 9 | 29 | 81 | 201 | 57 | 83 | 6 | 15 | 7 | 15 | 27 | 13 | 14 |
| PC3809-49 | 483.0 | 48 | 9 | 269 | 58 | 131 | 118 | 11 | 29 | 91 | 178 | 61 | 114 | 7 | 13 | 8 | 20 | 31 | 14 | 18 |
| PC3809-50 | 493.0 | 65 | 8 | 1438 | 61 | 131 | 123 | 11 | 29 | 90 | 276 | 63 | 101 | 7 | 15 | 7 | 13 | 30 | 16 | 16 |
| PC3809-51 | 504.0 | 41 | 9 | 311 | 53 | 136 | 113 | 11 | 29 | 92 | 193 | 64 | 127 | 7 | 14 | 9 | 11 | 35 | 17 | 21 |
| PC3809-52 | 515.0 | 48 | 8 | 304 | 57 | 136 | 117 | 11 | 30 | 93 | 182 | 66 | 116 | 7 | 15 | 8 | 16 | 35 | 17 | 18 |
| PC3809-53 | 525.0 | 78 | 7 | 254 | 66 | 132 | 130 | 10 | 31 | 86 | 194 | 59 | 91 | 6 | 15 | 7 | 16 | 33 | 14 | 15 |
| PC3809-54 | 536.0 | 76 | 5 | 242 | 55 | 116 | 114 | 10 | 27 | 80 | 200 | 54 | 83 | 5 | 13 | 7 | 14 | 28 | 13 | 14 |
| PC3809-55 | 544.0 | 49 | 6 | 313 | 50 | 123 | 124 | 13 | 30 | 96 | 201 | 65 | 115 | 7 | 16 | 9 | 16 | 35 | 16 | 18 |
| PC3809-56 | 553.0 | 52 | 4 | 279 | 39 | 104 | 121 | 12 | 32 | 94 | 198 | 61 | 88 | 6 | 16 | 7 | 15 | 30 | 14 | 15 |
| PC3809-57 | 564.0 | 52 | 4 | 277 | 39 | 102 | 123 | 10 | 29 | 86 | 193 | 55 | 82 | 5 | 16 | 8 | 13 | 25 | 12 | 14 |
| PC3809-58 | 574.0 | 50 | 4 | 275 | 41 | 105 | 115 | 9 | 26 | 89 | 208 | 58 | 91 | 6 | 15 | 7 | 16 | 30 | 13 | 15 |
| PC3809-59 | 585.0 | 37 | 5 | 390 | 34 | 95 | 117 | 9 | 20 | 83 | 282 | 55 | 100 | 6 | 15 | 6 | 14 | 29 | 14 | 15 |
| PC3809-60 | 594.0 | 43 | 5 | 269 | 34 | 95 | 113 | 8 | 20 | 81 | 214 | 55 | 97 | 6 | 15 | 8 | 13 | 27 | 14 | 14 |
| PC3809-61 | 605.0 | 39 | 5 | 284 | 35 | 109 | 117 | 12 | 28 | 97 | 237 | 62 | 113 | 8 | 17 | 9 | 12 | 36 | 16 | 18 |
| PC3809-62 | 615.0 | 35 | 5 | 247 | 33 | 99 | 114 | 10 | 19 | 84 | 234 | 58 | 96 | 6 | 17 | 8 | 12 | 28 | 14 | 15 |
| PC3809-63 | 625.0 | 32 | 5 | 276 | 33 | 102 | 118 | 12 | 25 | 97 | 233 | 60 | 108 | 7 | 17 | 8 | 15 | 29 | 15 | 16 |
| PC3809-64 | 635.0 | 36 | 7 | 278 | 36 | 109 | 127 | 12 | 27 | 92 | 242 | 62 | 109 | 7 | 16 | 8 | 14 | 33 | 15 | 17 |

| APPENDIX C.10. SALT-CORRECTED TRACE ELEMENTS | | | | | | | | | | | | | | | | | | | | |
|---|---|---|---|---|---|---|---|---|---|---|---|---|---|---|---|---|---|---|---|---|
| PC38-09 | 148m | | | | | | | | | | | | | | | | | | | |
| Sample | Depth | Mo | U | Ba | Ni | Cr | V | Sc | Cu | Zn | Sr | Rb | Zr | Nb | Pb | Th | La | Ce | Nd | Y |
| | (cm) | (ppm) | (ppm) | (ppm) | (ppm) | (ppm) | (ppm) | (ppm) | (ppm) | (ppm) | (ppm) | (ppm) | (ppm) | (ppm) | (ppm) | (ppm) | (ppm) | (ppm) | (ppm) | (ppm) |
| PC3809-65 | 646.0 | 47 | 5 | 234 | 38 | 92 | 125 | 9 | 18 | 76 | 201 | 52 | 88 | 5 | 13 | 7 | 12 | 28 | 13 | 13 |
| PC3809-66 | 654.0 | 40 | 7 | 241 | 34 | 94 | 124 | 8 | 18 | 72 | 187 | 50 | 90 | 6 | 13 | 8 | 12 | 26 | 12 | 13 |
| PC3809-67 | 664.0 | 44 | 8 | 253 | 34 | 86 | 127 | 8 | 18 | 74 | 189 | 51 | 82 | 7 | 13 | 7 | 8 | 29 | 13 | 13 |
| PC3809-68 | 674.0 | 37 | 8 | 227 | 28 | 73 | 111 | 7 | 11 | 63 | 171 | 46 | 79 | 5 | 13 | 7 | 14 | 25 | 11 | 12 |
| PC3809-69 | 684.0 | 43 | 7 | 301 | 35 | 96 | 130 | 9 | 21 | 86 | 211 | 63 | 101 | 6 | 16 | 9 | 14 | 34 | 15 | 16 |
| PC3809-70 | 694.0 | 40 | 7 | 285 | 36 | 107 | 137 | 9 | 28 | 90 | 212 | 65 | 104 | 7 | 16 | 7 | 16 | 32 | 15 | 16 |
| PC3809-71 | 703.0 | 53 | 7 | 281 | 38 | 101 | 144 | 10 | 29 | 92 | 201 | 65 | 101 | 6 | 19 | 9 | 18 | 31 | 15 | 16 |
| PC3809-72 | 714.0 | 48 | 7 | 261 | 41 | 103 | 136 | 12 | 25 | 88 | 218 | 58 | 96 | 6 | 15 | 6 | 13 | 32 | 14 | 16 |
| PC3809-73 | 724.0 | 32 | 5 | 302 | 35 | 103 | 125 | 12 | 30 | 92 | 232 | 66 | 106 | 7 | 16 | 7 | 11 | 33 | 16 | 17 |
| PC3809-74 | 734.0 | 33 | 5 | 281 | 36 | 109 | 126 | 12 | 27 | 98 | 238 | 65 | 110 | 7 | 19 | 7 | 17 | 35 | 16 | 17 |
| PC3809-75 | 744.0 | 46 | 7 | 302 | 38 | 98 | 132 | 11 | 28 | 90 | 226 | 65 | 105 | 6 | 18 | 8 | 16 | 38 | 15 | 16 |
| PC3809-76 | 754.0 | 50 | 4 | 256 | 35 | 87 | 121 | 11 | 20 | 84 | 202 | 57 | 99 | 8 | 18 | 6 | 12 | 35 | 14 | 15 |
| PC3809-77 | 764.0 | 40 | 5 | 291 | 35 | 96 | 130 | 11 | 25 | 95 | 217 | 70 | 110 | 8 | 19 | 8 | 16 | 37 | 16 | 18 |
| PC3809-78 | 774.0 | 38 | 4 | 289 | 36 | 102 | 125 | 13 | 26 | 99 | 219 | 69 | 123 | 8 | 19 | 9 | 24 | 39 | 18 | 19 |
| PC3809-79 | 784.0 | 38 | 6 | 276 | 37 | 96 | 122 | 11 | 26 | 95 | 215 | 66 | 114 | 7 | 18 | 8 | 16 | 38 | 18 | 18 |
| PC3809-80 | 794.0 | 33 | 5 | 297 | 34 | 98 | 118 | 12 | 22 | 93 | 222 | 67 | 120 | 7 | 17 | 8 | 21 | 38 | 17 | 18 |
| PC3809-81 | 804.0 | 33 | 5 | 324 | 34 | 99 | 113 | 12 | 23 | 85 | 224 | 61 | 120 | 7 | 14 | 7 | 16 | 36 | 16 | 17 |
| PC3809-82 | 813.0 | 29 | 6 | 311 | 34 | 103 | 113 | 14 | 28 | 90 | 270 | 63 | 122 | 7 | 17 | 7 | 17 | 32 | 16 | 18 |
| PC3809-83 | 823.0 | 29 | 5 | 296 | 35 | 100 | 107 | 10 | 23 | 88 | 230 | 63 | 126 | 8 | 14 | 7 | 19 | 33 | 16 | 19 |
| PC3809-84 | 834.0 | 31 | 5 | 292 | 33 | 104 | 109 | 12 | 24 | 89 | 221 | 64 | 124 | 8 | 17 | 7 | 15 | 34 | 16 | 18 |
| PC3809-85 | 845.0 | 38 | 4 | 299 | 36 | 102 | 115 | 11 | 26 | 84 | 232 | 66 | 119 | 7 | 18 | 7 | 18 | 34 | 17 | 18 |
| PC3809-86 | 854.0 | 31 | 5 | 351 | 30 | 86 | 113 | 12 | 34 | 103 | 205 | 82 | 125 | 9 | 24 | 9 | 21 | 42 | 19 | 20 |
| PC38-10 | 257m | | | | | | | | | | | | | | | | | | | |
| PC3810-01 | 6.0 | 52 | 15 | 272 | 114 | 135 | 149 | 9 | 38 | 116 | 346 | 62 | 115 | 8 | 11 | 10 | 17 | 30 | 16 | 20 |
| PC3810-02 | 14.0 | 24 | 20 | 336 | 77 | 106 | 91 | 8 | 25 | 98 | 435 | 59 | 202 | 8 | 10 | 8 | 31 | 42 | 21 | 28 |
| PC3810-03 | 24.0 | 11 | 20 | 358 | 36 | 63 | 54 | 7 | 11 | 57 | 597 | 54 | 246 | 8 | 8 | 5 | 17 | 40 | 20 | 29 |
| PC3810-04 | 34.0 | 18 | 16 | 336 | 39 | 69 | 57 | 5 | 12 | 60 | 494 | 55 | 225 | 7 | 10 | 6 | 19 | 43 | 20 | 29 |
| PC3810-05 | 44.0 | 37 | 15 | 354 | 103 | 144 | 102 | 11 | 28 | 93 | 264 | 65 | 171 | 8 | 13 | 11 | 16 | 39 | 19 | 23 |
| PC3810-06 | 54.0 | 47 | 15 | 326 | 94 | 136 | 128 | 9 | 30 | 95 | 235 | 67 | 163 | 7 | 14 | 9 | 19 | 37 | 17 | 20 |
| PC3810-07 | 64.0 | 39 | 15 | 346 | 76 | 112 | 117 | 9 | 27 | 95 | 284 | 67 | 207 | 8 | 14 | 9 | 23 | 46 | 20 | 23 |

| APPENDIX C.10. SALT-CORRECTED TRACE ELEMENTS | | | | | | | | | | | | | | | | | | | | |
|---|---|---|---|---|---|---|---|---|---|---|---|---|---|---|---|---|---|---|---|---|
| PC38-10 | 257m | | | | | | | | | | | | | | | | | | | |
| Sample | Depth | Mo | U | Ba | Ni | Cr | V | Sc | Cu | Zn | Sr | Rb | Zr | Nb | Pb | Th | La | Ce | Nd | Y |
| | (cm) | (ppm) | (ppm) | (ppm) | (ppm) | (ppm) | (ppm) | (ppm) | (ppm) | (ppm) | (ppm) | (ppm) | (ppm) | (ppm) | (ppm) | (ppm) | (ppm) | (ppm) | (ppm) | (ppm) |
| PC3810-08 | 74.0 | 30 | 16 | 397 | 58 | 104 | 111 | 9 | 23 | 93 | 340 | 70 | 246 | 7 | 16 | 10 | 23 | 47 | 23 | 26 |
| PC3810-09 | 84.0 | 13 | 15 | 389 | 20 | 61 | 61 | 7 | 8 | 71 | 431 | 57 | 231 | 7 | 14 | 7 | 23 | 44 | 23 | 29 |
| PC3810-10 | 94.0 | 41 | 27 | 379 | 30 | 53 | 53 | 6 | 9 | 61 | 504 | 57 | 264 | 8 | 10 | 6 | 17 | 42 | 20 | 29 |
| PC3810-10 | 104.0 | 32 | 16 | 364 | 32 | 55 | 55 | 4 | 10 | 53 | 474 | 54 | 279 | 7 | 10 | 8 | 18 | 41 | 20 | 28 |
| PC3810-11 | 113.0 | 17 | 10 | 346 | 24 | 46 | 46 | 5 | 7 | 51 | 436 | 54 | 244 | 7 | 10 | 6 | 18 | 40 | 20 | 27 |
| PC3810-12 | 126.0 | 49 | 11 | 214 | 58 | 91 | 91 | 6 | 30 | 84 | 348 | 53 | 132 | 6 | 10 | 6 | 20 | 28 | 15 | 19 |
| PC3810-13 | 134.0 | 62 | 13 | 219 | 74 | 104 | 104 | 7 | 34 | 91 | 283 | 55 | 117 | 6 | 11 | 9 | 14 | 28 | 14 | 18 |
| PC3810-14 | 146.0 | 53 | 12 | 281 | 66 | 95 | 104 | 9 | 35 | 98 | 293 | 63 | 156 | 8 | 12 | 8 | 18 | 39 | 18 | 21 |
| PC3810-15 | 154.0 | 46 | 12 | 264 | 69 | 102 | 113 | 8 | 36 | 97 | 350 | 59 | 134 | 7 | 12 | 7 | 17 | 32 | 16 | 20 |
| PC3810-16 | 167.0 | 49 | 12 | 288 | 64 | 101 | 119 | 9 | 31 | 97 | 254 | 65 | 128 | 7 | 13 | 9 | 18 | 35 | 16 | 20 |
| PC3810-17 | 174.0 | 48 | 13 | 312 | 70 | 108 | 122 | 8 | 36 | 100 | 225 | 67 | 132 | 7 | 14 | 10 | 21 | 36 | 16 | 20 |
| PC3810-18 | 185.0 | 35 | 12 | 295 | 58 | 102 | 117 | 8 | 28 | 97 | 189 | 72 | 121 | 7 | 14 | 9 | 18 | 34 | 16 | 20 |
| PC3810-19 | 194.0 | 61 | 11 | 269 | 72 | 100 | 128 | 8 | 41 | 97 | 257 | 60 | 98 | 6 | 12 | 9 | 25 | 30 | 14 | 17 |
| PC3810-20 | 203.0 | 47 | 15 | 340 | 63 | 100 | 135 | 8 | 30 | 111 | 238 | 70 | 148 | 8 | 15 | 9 | 23 | 38 | 18 | 21 |
| PC3810-21 | 216.0 | 66 | 12 | 276 | 73 | 104 | 133 | 9 | 35 | 92 | 263 | 56 | 98 | 6 | 13 | 9 | 14 | 28 | 14 | 17 |
| PC3810-22 | 224.0 | 60 | 12 | 267 | 81 | 112 | 134 | 9 | 40 | 101 | 213 | 60 | 98 | 6 | 15 | 9 | 17 | 29 | 15 | 17 |
| PC3810-23 | 233.0 | 59 | 13 | 301 | 80 | 120 | 145 | 11 | 44 | 107 | 222 | 67 | 119 | 7 | 15 | 10 | 18 | 34 | 17 | 20 |
| PC3810-24 | 244.0 | 45 | 11 | 257 | 65 | 109 | 120 | 10 | 32 | 100 | 283 | 67 | 136 | 7 | 14 | 10 | 18 | 35 | 17 | 20 |
| PC3810-25 | 254.0 | 45 | 15 | 298 | 56 | 92 | 108 | 8 | 24 | 88 | 355 | 58 | 179 | 7 | 14 | 7 | 10 | 38 | 18 | 22 |
| PC3810-26 | 263.0 | 57 | 13 | 287 | 63 | 94 | 120 | 9 | 30 | 86 | 347 | 55 | 141 | 7 | 13 | 6 | 16 | 32 | 15 | 20 |
| PC3810-27 | 273.0 | 44 | 12 | 284 | 70 | 115 | 132 | 9 | 35 | 112 | 283 | 66 | 130 | 8 | 14 | 8 | 19 | 35 | 16 | 21 |
| PC3810-28 | 284.0 | 38 | 13 | 281 | 62 | 102 | 113 | 9 | 30 | 97 | 329 | 63 | 132 | 7 | 12 | 8 | 17 | 35 | 18 | 22 |
| PC3810-29 | 295.0 | 59 | 11 | 234 | 73 | 108 | 123 | 6 | 35 | 89 | 421 | 51 | 74 | 5 | 11 | 6 | 17 | 23 | 13 | 16 |
| PC3810-30 | 305.0 | 37 | 12 | 279 | 63 | 103 | 132 | 9 | 30 | 104 | 320 | 65 | 120 | 7 | 14 | 8 | 30 | 36 | 17 | 21 |
| PC3810-31 | 314.0 | 36 | 12 | 289 | 65 | 109 | 136 | 10 | 30 | 108 | 343 | 67 | 143 | 8 | 12 | 9 | 22 | 39 | 19 | 21 |
| PC3810-32 | 324.0 | 64 | 12 | 263 | 79 | 107 | 150 | 9 | 39 | 96 | 327 | 55 | 86 | 5 | 13 | 6 | 24 | 28 | 15 | 16 |
| PC3810-33 | 335.0 | 35 | 12 | 269 | 76 | 117 | 143 | 8 | 29 | 102 | 302 | 67 | 118 | 8 | 12 | 7 | 22 | 34 | 17 | 20 |
| PC3810-34 | 344.0 | 62 | 11 | 164 | 79 | 100 | 133 | 8 | 32 | 88 | 329 | 46 | 73 | 6 | 11 | 6 | 11 | 26 | 12 | 14 |
| PC3810-35 | 354.0 | 67 | 10 | 228 | 72 | 86 | 132 | 7 | 29 | 81 | 231 | 43 | 65 | 5 | 12 | 5 | 14 | 22 | 11 | 12 |
| PC3810-36 | 364.0 | 68 | 10 | 180 | 69 | 76 | 132 | 7 | 27 | 76 | 270 | 39 | 53 | 4 | 10 | 5 | 16 | 21 | 11 | 12 |
| PC3810-37 | 374.0 | 63 | 12 | 212 | 69 | 82 | 137 | 8 | 24 | 69 | 214 | 42 | 54 | 5 | 10 | 5 | 10 | 22 | 11 | 11 |
| PC3810-38 | 383.0 | 30 | 13 | 289 | 66 | 110 | 141 | 11 | 34 | 109 | 269 | 71 | 103 | 7 | 16 | 9 | 23 | 38 | 17 | 19 |

| APPENDIX C.10. SALT-CORRECTED TRACE ELEMENTS | | | | | | | | | | | | | | | | | | | | |
|---|---|---|---|---|---|---|---|---|---|---|---|---|---|---|---|---|---|---|---|---|
| PC38-10 | 257m | | | | | | | | | | | | | | | | | | | |
| Sample | Depth | Mo | U | Ba | Ni | Cr | V | Sc | Cu | Zn | Sr | Rb | Zr | Nb | Pb | Th | La | Ce | Nd | Y |
| | (cm) | (ppm) | (ppm) | (ppm) | (ppm) | (ppm) | (ppm) | (ppm) | (ppm) | (ppm) | (ppm) | (ppm) | (ppm) | (ppm) | (ppm) | (ppm) | (ppm) | (ppm) | (ppm) | (ppm) |
| PC3810-39 | 394.0 | 44 | 14 | 239 | 86 | 119 | 150 | 9 | 29 | 93 | 250 | 58 | 97 | 6 | 13 | 9 | 19 | 31 | 14 | 18 |
| PC3810-40 | 404.0 | 28 | 13 | 254 | 67 | 112 | 120 | 12 | 25 | 98 | 288 | 64 | 128 | 7 | 14 | 8 | 28 | 35 | 17 | 22 |
| PC3810-41 | 417.0 | 51 | 12 | 242 | 76 | 111 | 119 | 10 | 31 | 96 | 384 | 55 | 105 | 6 | 13 | 7 | 22 | 33 | 16 | 19 |
| PC3810-42 | 424.0 | 47 | 15 | 212 | 83 | 114 | 134 | 8 | 32 | 101 | 300 | 57 | 98 | 7 | 14 | 8 | 21 | 31 | 15 | 18 |
| PC3810-43 | 434.0 | 65 | 10 | 172 | 60 | 73 | 107 | 0 | 16 | 68 | 511 | 26 | 49 | 4 | 5 | 2 | 9 | 17 | 10 | 11 |
| PC3810-44 | 445.0 | 44 | 12 | 200 | 70 | 94 | 127 | 6 | 23 | 81 | 388 | 47 | 68 | 6 | 12 | 6 | 15 | 26 | 13 | 14 |
| PC3810-45 | 456.0 | 74 | 13 | 251 | 82 | 94 | 166 | 8 | 27 | 83 | 352 | 43 | 66 | 5 | 11 | 6 | 13 | 18 | 10 | 13 |
| PC3810-46 | 467.0 | 73 | 6 | 188 | 63 | 69 | 115 | 2 | 17 | 63 | 347 | 28 | 41 | 3 | 8 | 3 | 14 | 17 | 10 | 10 |
| PC3810-47 | 476.0 | 36 | 17 | 268 | 88 | 121 | 138 | 7 | 30 | 101 | 436 | 57 | 101 | 7 | 10 | 7 | 20 | 31 | 17 | 20 |
| PC3810-48 | 484.0 | 36 | 15 | 255 | 91 | 118 | 130 | 8 | 31 | 94 | 453 | 53 | 97 | 6 | 12 | 7 | 16 | 31 | 16 | 20 |
| PC3810-49 | 494.0 | 39 | 24 | 271 | 92 | 119 | 110 | 3 | 27 | 83 | 473 | 47 | 135 | 6 | 8 | 6 | 19 | 31 | 17 | 26 |
| PC3810-50 | 504.0 | 15 | 22 | 318 | 44 | 66 | 64 | 7 | 14 | 62 | 642 | 50 | 239 | 8 | 7 | 4 | 20 | 39 | 19 | 33 |
| PC3810-51 | 514.0 | 67 | 6 | 293 | 53 | 94 | 128 | 12 | 26 | 86 | 197 | 56 | 110 | 7 | 15 | 7 | 15 | 32 | 15 | 17 |
| PC3810-52 | 524.0 | 53 | 6 | 348 | 46 | 84 | 135 | 10 | 27 | 89 | 193 | 59 | 119 | 7 | 16 | 7 | 17 | 37 | 16 | 18 |
| PC3810-53 | 534.0 | 129 | 23 | 394 | 165 | 182 | 363 | 9 | 49 | 89 | 274 | 48 | 73 | 5 | 12 | 6 | 10 | 24 | 12 | 15 |
| PC3810-54 | 545.0 | 111 | 17 | 329 | 129 | 148 | 277 | 10 | 36 | 79 | 242 | 50 | 77 | 5 | 12 | 7 | 13 | 23 | 13 | 15 |
| PC3810-55 | 554.0 | 125 | 18 | 339 | 131 | 146 | 304 | 9 | 40 | 81 | 285 | 46 | 66 | 5 | 11 | 6 | 12 | 24 | 11 | 13 |
| PC3810-56 | 564.0 | 95 | 10 | 313 | 72 | 106 | 219 | 7 | 22 | 61 | 413 | 39 | 70 | 4 | 10 | 5 | 11 | 23 | 12 | 12 |
| PC3810-57 | 574.0 | 85 | 11 | 319 | 78 | 120 | 256 | 6 | 26 | 72 | 476 | 45 | 86 | 5 | 10 | 4 | 14 | 25 | 13 | 14 |
| PC3810-58 | 584.0 | 80 | 9 | 346 | 73 | 113 | 208 | 9 | 25 | 72 | 420 | 44 | 79 | 5 | 10 | 4 | 13 | 23 | 12 | 14 |
| PC3810-59 | 596.0 | 87 | 23 | 356 | 75 | 120 | 261 | 8 | 25 | 72 | 411 | 44 | 82 | 5 | 12 | 5 | 11 | 23 | 12 | 14 |
| PC3810-60 | 604.0 | 88 | 17 | 388 | 73 | 121 | 250 | 6 | 27 | 74 | 448 | 45 | 77 | 5 | 11 | 4 | 13 | 26 | 12 | 15 |
| PC3810-61 | 614.0 | 86 | 15 | 344 | 71 | 119 | 252 | 10 | 26 | 75 | 352 | 51 | 87 | 6 | 13 | 5 | 13 | 27 | 13 | 14 |
| PC3810-62 | 624.0 | 78 | 10 | 334 | 72 | 116 | 248 | 7 | 25 | 84 | 424 | 56 | 94 | 6 | 15 | 6 | 15 | 30 | 16 | 17 |
| PC3810-63 | 634.0 | 64 | 9 | 299 | 69 | 122 | 217 | 6 | 28 | 76 | 452 | 52 | 95 | 6 | 12 | 6 | 13 | 28 | 14 | 16 |
| PC3810-64 | 645.0 | 89 | 11 | 383 | 64 | 108 | 214 | 9 | 27 | 73 | 318 | 54 | 82 | 6 | 14 | 8 | 12 | 29 | 14 | 15 |
| PC3810-65 | 655.0 | 116 | 9 | 343 | 76 | 111 | 227 | 8 | 25 | 75 | 328 | 49 | 75 | 5 | 14 | 6 | 14 | 23 | 14 | 14 |
| PC3810-66 | 667.0 | 106 | 11 | 299 | 74 | 114 | 225 | 10 | 27 | 83 | 331 | 55 | 84 | 6 | 16 | 6 | 16 | 27 | 14 | 16 |
| PC3810-67 | 674.0 | 97 | 14 | 281 | 72 | 121 | 222 | 11 | 31 | 102 | 256 | 69 | 96 | 6 | 21 | 9 | 21 | 35 | 16 | 16 |
| PC3810-68 | 683.0 | 92 | 11 | 254 | 70 | 110 | 214 | 10 | 28 | 95 | 271 | 65 | 85 | 6 | 21 | 6 | 14 | 35 | 16 | 14 |
| PC3810-69 | 694.0 | 59 | 10 | 319 | 58 | 120 | 173 | 12 | 27 | 121 | 235 | 86 | 122 | 8 | 24 | 10 | 19 | 44 | 20 | 19 |
| PC3810-70 | 704.0 | 48 | 8 | 347 | 52 | 134 | 169 | 11 | 28 | 122 | 194 | 97 | 137 | 9 | 24 | 11 | 21 | 47 | 21 | 22 |

| APPENDIX C.10. SALT-CORRECTED TRACE ELEMENTS | | | | | | | | | | | | | | | | | | | | |
|---|---|---|---|---|---|---|---|---|---|---|---|---|---|---|---|---|---|---|---|---|
| PC38-10 | 257m | | | | | | | | | | | | | | | | | | | |
| Sample | Depth | Mo | U | Ba | Ni | Cr | V | Sc | Cu | Zn | Sr | Rb | Zr | Nb | Pb | Th | La | Ce | Nd | Y |
| | (cm) | (ppm) | (ppm) | (ppm) | (ppm) | (ppm) | (ppm) | (ppm) | (ppm) | (ppm) | (ppm) | (ppm) | (ppm) | (ppm) | (ppm) | (ppm) | (ppm) | (ppm) | (ppm) | (ppm) |
| PC3810-71 | 714.0 | 69 | 8 | 325 | 54 | 115 | 162 | 12 | 29 | 118 | 252 | 87 | 113 | 8 | 22 | 9 | 20 | 40 | 18 | 19 |
| PC3810-72 | 724.0 | 78 | 10 | 289 | 52 | 96 | 155 | 10 | 23 | 102 | 259 | 76 | 96 | 6 | 22 | 8 | 17 | 35 | 18 | 16 |
| PC3810-74 | 734.0 | 59 | 11 | 329 | 48 | 109 | 153 | 13 | 25 | 116 | 185 | 88 | 129 | 8 | 26 | 13 | 19 | 46 | 21 | 19 |
| PC3810-75 | 745.0 | 37 | 10 | 369 | 41 | 102 | 145 | 12 | 33 | 135 | 202 | 99 | 162 | 8 | 28 | 12 | 26 | 49 | 23 | 21 |
| PC3810-76 | 754.0 | 52 | 10 | 296 | 51 | 105 | 134 | 9 | 31 | 106 | 195 | 81 | 163 | 8 | 20 | 11 | 19 | 36 | 18 | 17 |
| PC3810-77 | 764.0 | 30 | 11 | 383 | 36 | 97 | 116 | 12 | 21 | 103 | 298 | 83 | 224 | 9 | 20 | 11 | 26 | 50 | 23 | 25 |
| PC38-02 | 2525m | | | | | | | | | | | | | | | | | | | |
| | (Age) | | | | | | | | | | | | | | | | | | | |
| PC3802-01 | 2.76 | 0 | 9 | 2151 | 29 | 88 | 129 | 17 | 74 | 130 | 535 | 83 | 107 | 7 | 10 | 7 | 17 | 35 | 23 | 24 |
| PC3802-02 | 6.21 | 0 | 6 | 1856 | 27 | 77 | 102 | 8 | 70 | 115 | 642 | 73 | 97 | 7 | 11 | 7 | 15 | 42 | 31 | 20 |
| PC3802-03 | 9.66 | 0 | 8 | 1779 | 23 | 73 | 95 | 13 | 59 | 109 | 682 | 73 | 97 | 7 | 9 | 7 | 20 | 28 | 24 | 20 |
| PC3802-04 | 12.77 | 2 | 8 | 1265 | 47 | 84 | 97 | 12 | 66 | 120 | 569 | 85 | 104 | 6 | 10 | 9 | 22 | 35 | 28 | 18 |
| PC3802-05 | 15.18 | 2 | 8 | 1304 | 35 | 75 | 104 | 14 | 65 | 109 | 619 | 81 | 103 | 7 | 12 | 8 | 17 | 43 | 22 | 18 |
| PC3802-06 | 17.47 | 3 | 6 | 1228 | 37 | 71 | 102 | 13 | 62 | 105 | 608 | 80 | 101 | 7 | 13 | 7 | 19 | 31 | 26 | 19 |
| PC3802-07 | 20.48 | 1 | 6 | 1532 | 36 | 85 | 115 | 12 | 73 | 111 | 584 | 82 | 108 | 6 | 12 | 9 | 19 | 48 | 33 | 21 |
| PC3802-08 | 22.65 | 3 | 7 | 1434 | 38 | 78 | 115 | 8 | 70 | 114 | 576 | 83 | 106 | 7 | 11 | 7 | 24 | 43 | 28 | 20 |
| PC3802-09 | 25.22 | 2 | 10 | 1409 | 36 | 72 | 107 | 14 | 71 | 110 | 624 | 79 | 102 | 7 | 9 | 7 | 10 | 42 | 29 | 19 |
| PC3802-10 | 28.29 | 2 | 6 | 1370 | 33 | 62 | 101 | 9 | 67 | 108 | 668 | 74 | 96 | 7 | 9 | 6 | 20 | 31 | 27 | 19 |
| PC3802-11 | 31.07 | 3 | 7 | 1352 | 31 | 66 | 93 | 11 | 64 | 106 | 671 | 72 | 94 | 6 | 9 | 6 | 16 | 41 | 28 | 17 |
| PC3802-12 | 33.86 | 4 | 7 | 1316 | 34 | 61 | 82 | 11 | 61 | 105 | 704 | 68 | 89 | 7 | 8 | 6 | 14 | 38 | 27 | 17 |
| PC3802-13 | 36.64 | 4 | 8 | 1391 | 35 | 59 | 92 | 12 | 63 | 104 | 695 | 74 | 95 | 7 | 7 | 10 | 15 | 38 | 27 | 18 |
| PC3802-14 | 39.15 | 3 | 7 | 1499 | 33 | 70 | 101 | 12 | 72 | 120 | 596 | 83 | 109 | 7 | 11 | 8 | 24 | 39 | 25 | 20 |
| PC3802-15 | 42.22 | 4 | 6 | 1406 | 36 | 67 | 103 | 8 | 67 | 94 | 582 | 83 | 106 | 6 | 10 | 7 | 15 | 41 | 31 | 20 |
| PC3802-16 | 45.00 | 3 | 5 | 1499 | 28 | 73 | 127 | 10 | 70 | 120 | 549 | 90 | 119 | 7 | 13 | 9 | 21 | 45 | 32 | 21 |
| PC3802-17 | 48.07 | 3 | 10 | 1536 | 29 | 77 | 125 | 16 | 81 | 132 | 511 | 92 | 121 | 8 | 14 | 7 | 26 | 44 | 27 | 23 |
| PC3802-18 | 50.85 | 3 | 10 | 1618 | 34 | 75 | 125 | 18 | 72 | 124 | 460 | 90 | 118 | 8 | 11 | 9 | 26 | 45 | 26 | 22 |
| PC3802-19 | 53.64 | 2 | 11 | 1767 | 36 | 83 | 124 | 12 | 77 | 129 | 502 | 87 | 117 | 7 | 11 | 9 | 22 | 53 | 34 | 24 |
| PC3802-20 | 56.42 | 2 | 9 | 1670 | 37 | 88 | 123 | 11 | 80 | 134 | 462 | 92 | 129 | 7 | 12 | 9 | 22 | 40 | 26 | 24 |
| PC3802-21 | 59.29 | 3 | 9 | 1522 | 38 | 80 | 123 | 15 | 83 | 130 | 491 | 93 | 120 | 7 | 13 | 11 | 19 | 44 | 31 | 24 |
| PC3802-22 | 62.61 | 3 | 10 | 1541 | 33 | 76 | 121 | 6 | 80 | 104 | 512 | 91 | 119 | 8 | 14 | 10 | 25 | 43 | 35 | 24 |
| PC3802-23 | 65.94 | 3 | 5 | 1393 | 31 | 75 | 135 | 16 | 81 | 124 | 459 | 95 | 122 | 8 | 14 | 10 | 25 | 39 | 28 | 25 |

APPENDIX C.10. SALT-CORRECTED TRACE ELEMENTS

| PC38-02 | (2525m) | | | | | | | | | | | | | | | | | | | |
|---|---|---|---|---|---|---|---|---|---|---|---|---|---|---|---|---|---|---|---|---|
| Sample | Age | Mo | U | Ba | Ni | Cr | V | Sc | Cu | Zn | Sr | Rb | Zr | Nb | Pb | Th | La | Ce | Nd | Y |
| | (ka) | (ppm) | (ppm) | (ppm) | (ppm) | (ppm) | (ppm) | (ppm) | (ppm) | (ppm) | (ppm) | (ppm) | (ppm) | (ppm) | (ppm) | (ppm) | (ppm) | (ppm) | (ppm) | (ppm) |
| PC3802-24 | 69.26 | 1 | 7 | 1833 | 28 | 87 | 149 | 13 | 84 | 141 | 362 | 106 | 137 | 8 | 17 | 12 | 27 | 42 | 29 | 26 |
| PC3802-25 | 72.58 | 3 | 9 | 1748 | 36 | 81 | 135 | 15 | 84 | 145 | 399 | 100 | 126 | 8 | 12 | 9 | 25 | 40 | 30 | 26 |
| PC3802-26 | 76.96 | 2 | 9 | 1966 | 33 | 72 | 117 | 13 | 79 | 138 | 492 | 89 | 117 | 8 | 11 | 10 | 22 | 43 | 31 | 25 |
| PC3802-27 | 82.03 | 3 | 7 | 1963 | 38 | 81 | 141 | 14 | 85 | 149 | 363 | 102 | 132 | 8 | 12 | 11 | 24 | 40 | 27 | 26 |
| PC3802-28 | 87.11 | 2 | 8 | 1828 | 36 | 81 | 138 | 15 | 87 | 141 | 376 | 103 | 131 | 9 | 14 | 10 | 31 | 46 | 28 | 26 |
| PC3802-29 | 92.18 | 1 | 8 | 1959 | 34 | 85 | 150 | 17 | 84 | 148 | 311 | 112 | 138 | 9 | 16 | 11 | 31 | 47 | 30 | 26 |
| PC3802-30 | 97.26 | 2 | 9 | 2124 | 29 | 87 | 167 | 21 | 93 | 149 | 336 | 108 | 135 | 11 | 15 | 11 | 28 | 43 | 28 | 28 |
| PC3802-31 | 102.84 | 2 | 11 | 2001 | 35 | 82 | 144 | 16 | 91 | 145 | 403 | 96 | 124 | 7 | 11 | 10 | 21 | 39 | 32 | 28 |
| PC3802-32 | 107.92 | 2 | 10 | 2091 | 34 | 85 | 154 | 15 | 88 | 141 | 398 | 98 | 123 | 7 | 13 | 10 | 29 | 39 | 29 | 27 |
| PC3802-33 | 113.00 | 1 | 6 | 2010 | 35 | 88 | 149 | 15 | 80 | 142 | 403 | 95 | 121 | 8 | 13 | 8 | 26 | 42 | 31 | 28 |
| PC3802-34 | 118.07 | 2 | 8 | 2424 | 28 | 90 | 139 | 14 | 77 | 139 | 435 | 95 | 121 | 8 | 15 | 10 | 27 | 48 | 32 | 28 |
| PC3802-35 | 123.15 | 1 | 9 | 1984 | 27 | 74 | 111 | 12 | 68 | 120 | 560 | 81 | 104 | 6 | 12 | 8 | 21 | 48 | 30 | 22 |
| PC3802-36 | 128.22 | 2 | 7 | 1405 | 28 | 76 | 110 | 13 | 59 | 111 | 621 | 80 | 99 | 7 | 13 | 8 | 20 | 41 | 29 | 18 |
| PC3802-37 | 132.23 | 1 | 8 | 1306 | 26 | 77 | 110 | 10 | 56 | 104 | 651 | 81 | 100 | 7 | 11 | 7 | 17 | 42 | 28 | 19 |
| PC3802-38 | 135.30 | 1 | 7 | 1333 | 23 | 76 | 121 | 11 | 58 | 97 | 667 | 80 | 101 | 7 | 6 | 8 | 22 | 40 | 30 | 19 |
| PC3802-39 | 138.71 | 1 | 9 | 1299 | 25 | 69 | 110 | 7 | 58 | 93 | 651 | 76 | 100 | 7 | 13 | 7 | 19 | 40 | 27 | 20 |
| PC3802-40 | 141.79 | 1 | 8 | 1360 | 23 | 63 | 97 | 11 | 59 | 101 | 683 | 75 | 100 | 7 | 11 | 8 | 20 | 40 | 30 | 19 |
| PC3802-41 | 145.20 | 2 | 5 | 1368 | 23 | 62 | 108 | 12 | 63 | 105 | 684 | 77 | 94 | 6 | 9 | 7 | 18 | 31 | 27 | 19 |
| PC3802-42 | 148.61 | 1 | 6 | 1252 | 23 | 63 | 101 | 14 | 55 | 101 | 674 | 75 | 101 | 7 | 10 | 8 | 17 | 40 | 27 | 19 |
| PC3802-43 | 152.02 | 0 | 7 | 1098 | 22 | 62 | 109 | 14 | 56 | 94 | 692 | 74 | 95 | 6 | 10 | 7 | 20 | 35 | 23 | 19 |
| PC3802-44 | 155.44 | 1 | 12 | 1257 | 20 | 66 | 116 | 12 | 58 | 96 | 661 | 78 | 100 | 7 | 11 | 7 | 26 | 45 | 26 | 19 |
| PC3802-45 | 158.85 | 1 | 8 | 1236 | 25 | 76 | 123 | 11 | 63 | 107 | 578 | 85 | 107 | 7 | 13 | 8 | 31 | 40 | 26 | 20 |
| PC3802-46 | 162.26 | 2 | 7 | 1255 | 27 | 72 | 121 | 9 | 71 | 110 | 531 | 90 | 111 | 7 | 15 | 9 | 30 | 44 | 26 | 22 |
| PC3802-47 | 165.68 | 1 | 9 | 1277 | 26 | 56 | 101 | 13 | 64 | 105 | 680 | 77 | 97 | 6 | 12 | 9 | 23 | 43 | 30 | 19 |
| PC3802-48 | 169.43 | 2 | 10 | 1353 | 25 | 56 | 93 | 12 | 61 | 104 | 706 | 76 | 97 | 7 | 10 | 8 | 16 | 50 | 29 | 19 |
| PC3802-49 | 172.84 | 2 | 6 | 1372 | 24 | 52 | 99 | 8 | 61 | 103 | 699 | 76 | 98 | 7 | 10 | 8 | 15 | 36 | 25 | 20 |
| PC3802-50 | 176.26 | 2 | 8 | 1392 | 32 | 59 | 101 | 6 | 65 | 104 | 668 | 78 | 99 | 7 | 10 | 8 | 20 | 39 | 27 | 20 |
| PC3802-51 | 179.67 | 1 | 10 | 1385 | 21 | 57 | 107 | 14 | 63 | 102 | 641 | 83 | 104 | 7 | 14 | 9 | 25 | 40 | 26 | 21 |
| PC3802-52 | 183.08 | 3 | 6 | 1156 | 23 | 66 | 115 | 13 | 61 | 101 | 555 | 90 | 112 | 7 | 15 | 8 | 23 | 46 | 30 | 20 |
| PC3802-53 | 186.50 | 0 | 2 | 1126 | 16 | 43 | 89 | 11 | 45 | 87 | 505 | 93 | 127 | 8 | 14 | 8 | 18 | 51 | 29 | 17 |
| PC3802-54 | 189.57 | 2 | 6 | 1604 | 30 | 79 | 150 | 15 | 83 | 135 | 398 | 106 | 131 | 9 | 17 | 11 | 30 | 60 | 38 | 27 |
| PC3802-55 | 193.52 | 3 | 6 | 1733 | 34 | 83 | 147 | 12 | 84 | 134 | 382 | 106 | 130 | 8 | 17 | 11 | 33 | 55 | 34 | 29 |

| APPENDIX C.10. SALT-CORRECTED TRACE ELEMENTS | | | | | | | | | | | | | | | | | | | | |
|---|---|---|---|---|---|---|---|---|---|---|---|---|---|---|---|---|---|---|---|---|
| PC38-02 | (2525m) | | | | | | | | | | | | | | | | | | | |
| Sample | Age | Mo | U | Ba | Ni | Cr | V | Sc | Cu | Zn | Sr | Rb | Zr | Nb | Pb | Th | La | Ce | Nd | Y |
| | (ka) | (ppm) | (ppm) | (ppm) | (ppm) | (ppm) | (ppm) | (ppm) | (ppm) | (ppm) | (ppm) | (ppm) | (ppm) | (ppm) | (ppm) | (ppm) | (ppm) | (ppm) | (ppm) | (ppm) |
| PC3802-56 | 197.42 | 3 | 7 | 2189 | 53 | 87 | 146 | 16 | 94 | 157 | 345 | 105 | 125 | 9 | 12 | 11 | 40 | 56 | 37 | 29 |
| PC3802-57 | 202.11 | 2 | 9 | 2097 | 34 | 79 | 128 | 16 | 81 | 137 | 457 | 91 | 109 | 8 | 10 | 10 | 27 | 46 | 31 | 27 |
| PC3802-58 | 206.02 | 1 | 7 | 2019 | 32 | 86 | 126 | 14 | 82 | 134 | 483 | 93 | 116 | 7 | 14 | 10 | 18 | 43 | 31 | 27 |
| PC3802-59 | 209.53 | 2 | 7 | 1912 | 28 | 82 | 139 | 16 | 82 | 129 | 509 | 96 | 115 | 8 | 17 | 10 | 23 | 48 | 29 | 26 |
| PC3802-60 | 213.44 | 1 | 9 | 2007 | 24 | 68 | 108 | 8 | 70 | 109 | 791 | 74 | 92 | 6 | 12 | 6 | 20 | 39 | 28 | 24 |
| PC3802-61 | 217.34 | 0 | 9 | 1763 | 23 | 63 | 115 | 7 | 69 | 105 | 812 | 70 | 91 | 6 | 11 | 7 | 22 | 42 | 25 | 22 |
| PC3802-62 | 221.25 | 1 | 8 | 1621 | 23 | 61 | 129 | 13 | 68 | 109 | 671 | 80 | 102 | 6 | 17 | 9 | 14 | 36 | 25 | 23 |
| PC3802-63 | 225.16 | 2 | 8 | 1435 | 23 | 62 | 125 | 16 | 65 | 88 | 656 | 83 | 104 | 7 | 13 | 8 | 19 | 47 | 32 | 22 |
| PC3802-64 | 229.06 | 1 | 8 | 1653 | 24 | 72 | 133 | 14 | 70 | 116 | 584 | 90 | 112 | 8 | 11 | 10 | 20 | 41 | 31 | 25 |
| PC3802-65 | 232.97 | 1 | 5 | 1845 | 24 | 82 | 142 | 17 | 79 | 132 | 480 | 99 | 120 | 8 | 13 | 10 | 23 | 44 | 31 | 26 |
| PC3802-66 | 237.27 | 1 | 5 | 2399 | 29 | 89 | 133 | 6 | 85 | 137 | 532 | 93 | 116 | 8 | 13 | 9 | 20 | 51 | 32 | 25 |
| PC3802-67 | 240.78 | 1 | 12 | 2001 | 25 | 68 | 105 | 12 | 68 | 107 | 766 | 73 | 93 | 6 | 13 | 8 | 15 | 40 | 29 | 20 |
| PC3802-68 | 244.50 | 0 | 9 | 1503 | 23 | 66 | 129 | 17 | 62 | 108 | 700 | 82 | 104 | 7 | 14 | 9 | 21 | 43 | 29 | 18 |
| PC3802-69 | 247.71 | 1 | 9 | 1351 | 26 | 67 | 122 | 15 | 60 | 108 | 622 | 88 | 112 | 7 | 16 | 9 | 25 | 39 | 27 | 19 |
| PC3802-70 | 250.91 | 1 | 9 | 1332 | 24 | 66 | 111 | 11 | 61 | 105 | 641 | 86 | 110 | 8 | 14 | 7 | 17 | 47 | 32 | 19 |
| PC3802-71 | 254.12 | 1 | 8 | 1518 | 23 | 72 | 121 | 15 | 58 | 106 | 635 | 86 | 107 | 7 | 11 | 8 | 22 | 43 | 26 | 20 |
| PC3802-72 | 257.32 | 1 | 6 | 1517 | 25 | 71 | 107 | 13 | 65 | 112 | 613 | 86 | 108 | 7 | 10 | 5 | 23 | 46 | 26 | 20 |
| PC3802-73 | 260.53 | 0 | 8 | 1477 | 26 | 67 | 114 | 15 | 65 | 106 | 610 | 87 | 107 | 8 | 13 | 10 | 14 | 51 | 31 | 22 |
| PC3802-74 | 263.73 | 2 | 8 | 1406 | 30 | 63 | 114 | 13 | 72 | 114 | 573 | 87 | 109 | 7 | 10 | 9 | 23 | 41 | 31 | 24 |
| PC38-11 | (3835m) | | | | | | | | | | | | | | | | | | | |
| PC3811-01 | 0.80 | 6 | 11 | 1276 | 54 | 122 | 139 | 17 | 128 | 172 | 258 | 99 | 162 | 9 | 16 | 9 | 26 | 52 | 30 | 27 |
| PC3811-02 | 2.00 | 19 | 9 | 423 | 56 | 100 | 105 | 11 | 37 | 116 | 348 | 79 | 171 | 9 | 15 | 8 | 16 | 40 | 26 | 21 |
| PC3811-03 | 2.20 | 13 | 8 | 385 | 47 | 82 | 100 | 12 | 29 | 99 | 330 | 75 | 222 | 10 | 14 | 8 | 21 | 48 | 29 | 24 |
| PC3811-04 | 3.49 | 3 | 14 | 2015 | 49 | 117 | 140 | 16 | 141 | 182 | 261 | 102 | 144 | 9 | 11 | 10 | 22 | 40 | 31 | 30 |
| PC3811-05 | 6.17 | 2 | 11 | 1409 | 56 | 116 | 130 | 18 | 102 | 159 | 256 | 102 | 138 | 9 | 11 | 10 | 30 | 49 | 30 | 26 |
| PC3811-06 | 8.85 | 4 | 11 | 975 | 57 | 108 | 122 | 16 | 82 | 140 | 255 | 103 | 137 | 10 | 13 | 9 | 22 | 53 | 30 | 22 |
| PC3811-07 | 11.53 | 5 | 12 | 834 | 51 | 100 | 130 | 16 | 74 | 136 | 239 | 103 | 140 | 10 | 14 | 9 | 32 | 54 | 32 | 10 |
| PC3811-08 | 13.80 | 7 | 8 | 871 | 46 | 92 | 128 | 12 | 73 | 133 | 279 | 102 | 142 | 9 | 14 | 9 | 23 | 56 | 30 | 21 |
| PC3811-09 | 16.44 | 4 | 5 | 677 | 31 | 67 | 98 | 13 | 35 | 82 | 376 | 84 | 162 | 9 | 14 | 9 | 23 | 48 | 29 | 23 |
| PC3811-10 | 18.63 | 10 | 9 | 838 | 45 | 91 | 124 | 11 | 69 | 126 | 303 | 97 | 133 | 9 | 14 | 9 | 23 | 52 | 26 | 21 |

| APPENDIX C.10. SALT-CORRECTED TRACE ELEMENTS | | | | | | | | | | | | | | | | | | | | |
|---|---|---|---|---|---|---|---|---|---|---|---|---|---|---|---|---|---|---|---|---|
| PC38-11 | (3835m) | | | | | | | | | | | | | | | | | | | |
| Sample | Depth | Mo | U | Ba | Ni | Cr | V | Sc | Cu | Zn | Sr | Rb | Zr | Nb | Pb | Th | La | Ce | Nd | Y |
| | (cm) | (ppm) | (ppm) | (ppm) | (ppm) | (ppm) | (ppm) | (ppm) | (ppm) | (ppm) | (ppm) | (ppm) | (ppm) | (ppm) | (ppm) | (ppm) | (ppm) | (ppm) | (ppm) | (ppm) |
| PC3811-11 | 20.82 | 10 | 6 | 771 | 47 | 93 | 118 | 16 | 69 | 124 | 318 | 95 | 128 | 8 | 12 | 10 | 24 | 52 | 29 | 21 |
| PC3811-12 | 23.23 | 9 | 5 | 857 | 46 | 95 | 122 | 16 | 109 | 161 | 285 | 97 | 129 | 9 | 16 | 9 | 20 | 36 | 27 | 20 |
| PC3811-13 | 25.11 | 10 | 5 | 895 | 45 | 95 | 130 | 11 | 74 | 130 | 291 | 100 | 130 | 10 | 15 | 10 | 23 | 46 | 32 | 21 |
| PC3811-14 | 27.10 | 10 | 6 | 815 | 45 | 93 | 125 | 11 | 62 | 123 | 313 | 96 | 131 | 9 | 12 | 8 | 24 | 56 | 31 | 21 |
| PC3811-15 | 29.09 | 10 | 6 | 904 | 45 | 93 | 126 | 16 | 71 | 128 | 291 | 99 | 133 | 9 | 14 | 8 | 31 | 43 | 29 | 21 |
| PC3811-16 | 31.08 | 8 | 9 | 727 | 40 | 87 | 117 | 15 | 56 | 117 | 341 | 92 | 133 | 9 | 13 | 9 | 24 | 38 | 28 | 21 |
| PC3811-17 | 33.07 | 9 | 8 | 860 | 42 | 88 | 124 | 12 | 66 | 126 | 308 | 99 | 129 | 9 | 15 | 9 | 26 | 44 | 27 | 21 |
| PC3811-18 | 35.07 | 7 | 9 | 829 | 40 | 85 | 111 | 14 | 56 | 109 | 362 | 91 | 143 | 9 | 13 | 9 | 24 | 57 | 32 | 24 |
| PC3811-19 | 37.26 | 11 | 9 | 1067 | 53 | 102 | 126 | 12 | 93 | 145 | 279 | 102 | 131 | 9 | 12 | 11 | 26 | 52 | 31 | 24 |
| PC3811-20 | 39.45 | 10 | 6 | 1056 | 54 | 104 | 128 | 15 | 87 | 146 | 262 | 104 | 127 | 10 | 13 | 8 | 31 | 47 | 29 | 23 |
| PC3811-21 | 40.84 | 6 | 6 | 1103 | 55 | 108 | 132 | 18 | 90 | 144 | 245 | 106 | 127 | 9 | 12 | 9 | 25 | 49 | 31 | 24 |
| PC3811-22 | 43.03 | 9 | 11 | 1109 | 49 | 93 | 117 | 12 | 81 | 128 | 358 | 92 | 130 | 9 | 12 | 7 | 21 | 48 | 30 | 24 |
| PC3811-23 | 45.03 | 9 | 7 | 1385 | 59 | 99 | 123 | 16 | 107 | 149 | 325 | 97 | 122 | 8 | 11 | 10 | 27 | 48 | 28 | 25 |
| PC3811-24 | 47.02 | 11 | 10 | 1380 | 63 | 104 | 120 | 13 | 110 | 153 | 305 | 100 | 123 | 9 | 13 | 8 | 27 | 45 | 33 | 26 |
| PC3811-25 | 49.01 | 11 | 10 | 1441 | 62 | 104 | 129 | 17 | 117 | 154 | 316 | 98 | 121 | 8 | 10 | 9 | 23 | 44 | 31 | 25 |
| PC3811-26 | 51.00 | 11 | 10 | 1414 | 59 | 93 | 106 | 11 | 109 | 142 | 359 | 88 | 112 | 8 | 8 | 8 | 23 | 46 | 30 | 25 |
| PC3811-27 | 52.99 | 11 | 10 | 1467 | 59 | 95 | 111 | 15 | 116 | 145 | 343 | 89 | 114 | 8 | 11 | 9 | 23 | 38 | 25 | 25 |
| PC3811-28 | 54.99 | 9 | 10 | 1486 | 55 | 97 | 115 | 13 | 118 | 144 | 314 | 91 | 119 | 8 | 10 | 8 | 23 | 37 | 24 | 26 |
| PC3811-29 | 56.98 | 8 | 10 | 1335 | 54 | 110 | 134 | 19 | 105 | 154 | 241 | 112 | 144 | 10 | 14 | 10 | 30 | 51 | 32 | 27 |
| PC3811-30 | 59.62 | 6 | 9 | 1194 | 54 | 103 | 134 | 15 | 105 | 150 | 253 | 109 | 143 | 9 | 14 | 10 | 24 | 50 | 33 | 26 |
| PC3811-31 | 62.28 | 8 | 7 | 1408 | 45 | 107 | 144 | 17 | 115 | 149 | 236 | 112 | 150 | 10 | 12 | 16 | 31 | 53 | 35 | 29 |
| PC3811-32 | 65.60 | 7 | 10 | 1114 | 47 | 111 | 141 | 17 | 102 | 149 | 235 | 113 | 160 | 11 | 18 | 11 | 26 | 53 | 32 | 28 |
| PC3811-33 | 68.93 | 16 | 17 | 501 | 57 | 91 | 98 | 5 | 46 | 102 | 423 | 71 | 168 | 8 | 13 | 7 | 21 | 46 | 24 | 24 |
| PC3811-34 | 72.25 | 10 | 10 | 1613 | 54 | 102 | 127 | 16 | 119 | 157 | 243 | 104 | 133 | 10 | 11 | 9 | 24 | 44 | 28 | 26 |
| PC3811-35 | 74.95 | 11 | 9 | 1525 | 59 | 106 | 127 | 14 | 122 | 160 | 247 | 104 | 130 | 9 | 12 | 9 | 27 | 44 | 32 | 26 |
| PC3811-36 | 77.04 | 10 | 9 | 1721 | 57 | 102 | 121 | 17 | 119 | 148 | 248 | 95 | 122 | 9 | 10 | 9 | 21 | 39 | 27 | 27 |
| PC3811-37 | 79.12 | 9 | 4 | 1561 | 64 | 112 | 117 | 16 | 125 | 159 | 241 | 97 | 126 | 9 | 10 | 9 | 24 | 45 | 33 | 29 |
| PC3811-38 | 81.20 | 10 | 9 | 1258 | 74 | 111 | 128 | 15 | 127 | 165 | 247 | 103 | 127 | 9 | 11 | 11 | 27 | 49 | 31 | 27 |
| PC3811-39 | 83.29 | 14 | 9 | 1337 | 61 | 112 | 137 | 15 | 116 | 175 | 256 | 110 | 138 | 10 | 18 | 11 | 31 | 52 | 30 | 30 |
| PC3811-40 | 85.37 | 11 | 7 | 1316 | 53 | 105 | 146 | 20 | 120 | 156 | 260 | 107 | 137 | 10 | 13 | 9 | 30 | 47 | 29 | 31 |
| PC3811-41 | 87.45 | 12 | 8 | 1368 | 56 | 106 | 151 | 16 | 127 | 155 | 258 | 108 | 134 | 10 | 15 | 12 | 33 | 57 | 35 | 31 |
| PC3811-42 | 89.54 | 10 | 8 | 1874 | 49 | 111 | 154 | 16 | 142 | 157 | 233 | 110 | 141 | 10 | 13 | 10 | 29 | 49 | 29 | 33 |

APPENDIX C.10. SALT-CORRECTED TRACE ELEMENTS

| PC38-11 | (3835m) | | | | | | | | | | | | | | | | | | | |
|---|---|---|---|---|---|---|---|---|---|---|---|---|---|---|---|---|---|---|---|---|
| Sample | Depth | Mo | U | Ba | Ni | Cr | V | Sc | Cu | Zn | Sr | Rb | Zr | Nb | Pb | Th | La | Ce | Nd | Y |
| | (cm) | (ppm) | (ppm) | (ppm) | (ppm) | (ppm) | (ppm) | (ppm) | (ppm) | (ppm) | (ppm) | (ppm) | (ppm) | (ppm) | (ppm) | (ppm) | (ppm) | (ppm) | (ppm) | (ppm) |
| PC3811-43 | 91.62 | 9 | 7 | 2081 | 50 | 108 | 149 | 17 | 159 | 154 | 253 | 105 | 137 | 10 | 13 | 11 | 29 | 49 | 33 | 33 |
| PC3811-44 | 93.70 | 8 | 12 | 2495 | 51 | 98 | 136 | 16 | 155 | 166 | 313 | 90 | 124 | 8 | 8 | 9 | 25 | 38 | 29 | 34 |
| PC3811-45 | 95.79 | 7 | 9 | 2259 | 55 | 103 | 143 | 15 | 140 | 163 | 279 | 94 | 124 | 8 | 10 | 10 | 21 | 49 | 29 | 33 |
| PC3811-46 | 97.87 | 6 | 9 | 1989 | 56 | 116 | 146 | 23 | 148 | 171 | 238 | 107 | 144 | 9 | 12 | 9 | 29 | 50 | 32 | 37 |
| PC3811-47 | 99.95 | 8 | 8 | 1756 | 50 | 110 | 155 | 19 | 150 | 164 | 230 | 114 | 141 | 10 | 14 | 10 | 28 | 54 | 36 | 34 |
| PC3811-48 | 102.04 | 8 | 11 | 1887 | 55 | 102 | 146 | 20 | 154 | 161 | 255 | 103 | 130 | 9 | 10 | 10 | 30 | 44 | 36 | 34 |
| PC3811-49 | 104.12 | 8 | 5 | 1844 | 49 | 104 | 144 | 20 | 145 | 155 | 222 | 106 | 133 | 9 | 12 | 10 | 25 | 45 | 35 | 33 |
| PC3811-50 | 106.20 | 6 | 8 | 1901 | 51 | 107 | 149 | 18 | 148 | 161 | 226 | 104 | 131 | 10 | 13 | 11 | 28 | 46 | 35 | 32 |
| PC3811-51 | 108.29 | 5 | 6 | 1937 | 44 | 102 | 147 | 18 | 138 | 156 | 223 | 105 | 130 | 9 | 12 | 9 | 29 | 48 | 32 | 32 |
| PC3811-52 | 110.37 | 4 | 4 | 1966 | 43 | 102 | 144 | 18 | 131 | 151 | 226 | 105 | 129 | 10 | 11 | 7 | 27 | 48 | 35 | 32 |
| PC3811-53 | 112.45 | 3 | 5 | 2059 | 38 | 99 | 141 | 19 | 132 | 147 | 223 | 103 | 128 | 9 | 12 | 10 | 25 | 45 | 33 | 31 |
| PC3811-54 | 114.54 | 4 | 6 | 2067 | 42 | 102 | 148 | 20 | 150 | 144 | 235 | 101 | 135 | 10 | 11 | 10 | 24 | 50 | 34 | 34 |
| PC3811-55 | 116.62 | 3 | 6 | 2101 | 39 | 101 | 140 | 21 | 125 | 151 | 235 | 97 | 130 | 9 | 10 | 10 | 27 | 52 | 35 | 31 |
| PC3811-56 | 118.70 | 4 | 4 | 2320 | 40 | 101 | 147 | 18 | 138 | 152 | 238 | 96 | 130 | 9 | 9 | 9 | 26 | 44 | 32 | 35 |
| PC3811-57 | 120.79 | 1 | 6 | 2158 | 39 | 102 | 146 | 21 | 144 | 150 | 243 | 95 | 135 | 8 | 9 | 8 | 27 | 50 | 33 | 35 |

| APPENDIX C.11. TRACE ELEMENT RATIOS | | | | | | | | | |
|---|---|---|---|---|---|---|---|---|---|
| | | | | | | | | | |
| CD38-02 | Box | (2530m) | | | | | | | |
| Sample | Depth | I/Org.C | Br/Org.C | I/Br | Ba/Al | Zr/Rb | K/Rb | Mo/U | |
| | (cm.) | (x10-4) | (x10-4) | | (xE-4) | | (xE-3) | | |
| | | | | | | | | | |
| BC3802-01 | 0.5 | 343.1 | 101.4 | 3.38 | 352.70 | 1.41 | 20.42 | 3.50 | |
| BC3802-02 | 1.5 | 312.5 | 83.5 | 3.74 | 349.24 | 1.41 | 20.73 | 2.83 | |
| BC3802-03 | 2.5 | 357.3 | 127.2 | 2.81 | 352.19 | 1.39 | 20.60 | 2.86 | |
| BC3802-04 | 3.5 | 298.9 | 119.5 | 2.50 | 345.35 | 1.41 | 20.21 | 3.50 | |
| BC3802-05 | 4.5 | 271.0 | 107.4 | 2.52 | 349.45 | 1.43 | 21.24 | 0.00 | |
| BC3802-06 | 5.5 | 260.9 | 127.0 | 2.05 | 350.16 | 1.42 | 21.42 | 0.31 | |
| BC3802-07 | 6.5 | 235.9 | 131.2 | 1.80 | 334.84 | 1.39 | 21.37 | 1.20 | |
| BC3802-08 | 7.5 | 212.0 | 117.5 | 1.80 | 341.71 | 1.38 | 21.13 | 0.74 | |
| BC3802-09 | 8.5 | 214.8 | 110.4 | 1.95 | 342.50 | 1.41 | 21.34 | 0.72 | |
| BC3802-10 | 9.5 | 208.2 | 95.4 | 2.18 | 347.38 | 1.41 | 20.77 | 1.00 | |
| BC3802-11 | 11.0 | 223.3 | 70.4 | 3.17 | 343.72 | 1.40 | 20.67 | 0.94 | |
| BC3802-12 | 13.0 | 180.9 | 60.4 | 2.99 | 363.14 | 1.43 | 20.83 | 0.00 | |
| BC3802-13 | 15.0 | 175.9 | 95.0 | 1.85 | 352.33 | 1.42 | 21.66 | 0.32 | |
| BC3802-13 | 17.0 | 127.6 | 66.0 | 1.93 | 337.02 | 1.48 | 21.44 | 0.30 | |
| BC3802-14 | 19.0 | 154.6 | 75.1 | 2.06 | 362.65 | 1.45 | 21.19 | 0.14 | |
| BC3802-15 | 21.0 | 165.6 | 57.1 | 2.90 | 356.51 | 1.45 | 21.25 | 0.27 | |
| BC3802-16 | 23.0 | 157.1 | 74.5 | 2.11 | 350.83 | 1.44 | 21.00 | 0.16 | |
| BC3802-17 | 25.0 | 153.1 | 49.1 | 3.12 | 353.72 | 1.45 | 21.11 | 0.13 | |
| BC3802-18 | 27.0 | 161.7 | 76.1 | 2.12 | 336.21 | 1.52 | 20.41 | 0.16 | |
| BC3802-19 | 29.0 | 154.8 | 46.8 | 3.31 | 327.51 | 1.49 | 20.45 | 0.25 | |
| BC3802-20 | 31.0 | 168.7 | 78.6 | 2.15 | 313.33 | 1.52 | 19.70 | 0.29 | |
| BC3802-21 | 33.0 | 156.9 | 50.6 | 3.10 | 304.55 | 1.41 | 21.37 | 0.25 | |
| BC3802-21 | 35.0 | 137.4 | 52.7 | 2.61 | 240.28 | 1.36 | 19.98 | 0.32 | |
| BC3802-22 | 37.0 | 147.1 | 49.0 | 3.00 | 269.96 | 1.42 | 19.49 | 0.30 | |
| BC3802-23 | 39.0 | 167.2 | 71.5 | 2.34 | 289.33 | 1.44 | 20.36 | 0.19 | |
| BC3802-24 | 41.0 | 167.6 | 55.7 | 3.01 | 252.48 | 1.42 | 20.18 | 0.37 | |
| BC3802-25 | 43.0 | 182.0 | 59.4 | 3.06 | 263.35 | 1.43 | 20.98 | 0.47 | |
| BC3802-26 | 45.0 | 163.8 | 49.0 | 3.34 | 272.42 | 1.42 | 20.38 | 0.27 | |
| BC3802-27 | 47.0 | 147.3 | 54.4 | 2.71 | 266.73 | 1.42 | 20.57 | 0.38 | |
| BC3802-28 | 49.0 | 154.4 | 52.6 | 2.94 | 276.11 | 1.43 | 20.71 | 0.39 | |
| BC3802-29 | 51.0 | 163.7 | 59.9 | 2.73 | 275.14 | 1.43 | 20.33 | 0.48 | |
| BC3802-30 | 53.0 | 140.3 | 53.5 | 2.62 | 269.47 | 1.45 | 20.06 | 0.32 | |
| | | | | | | | | | |
| CD38-03 | (4289m) | | | | | | | | |
| Sample | Depth | I/Org.C | Br/Org.C | I/Br | Ba/Al | Zr/Rb | K/Rb | Mo/U | |
| | (cm.) | (x10-4) | (x10-4) | | (xE-4) | | (xE-3) | | |
| | | | | | | | | | |
| BC3803-01 | 0.5 | 314.2 | 109.6 | 2.87 | 263.09 | 1.26 | 19.91 | 2.09 | |
| BC3803-02 | 1.5 | 330.0 | 109.3 | 3.02 | 264.66 | 1.28 | 20.15 | 3.60 | |
| BC3803-03 | 2.5 | 286.2 | 102.8 | 2.79 | 265.85 | 1.29 | 20.38 | 0.00 | |
| BC3803-04 | 3.5 | 255.2 | 135.1 | 1.89 | 265.00 | 1.28 | 20.24 | 0.24 | |
| BC3803-05 | 4.5 | 218.5 | 122.4 | 1.79 | 267.64 | 1.27 | 20.79 | 0.67 | |
| BC3803-06 | 5.5 | 161.0 | 95.4 | 1.69 | 269.60 | 1.24 | 20.95 | 0.39 | |
| BC3803-07 | 6.5 | 195.0 | 124.1 | 1.57 | 266.57 | 1.29 | 21.49 | 0.32 | |
| BC3803-08 | 7.5 | 210.4 | 125.5 | 1.68 | 266.71 | 1.30 | 21.08 | 0.24 | |
| BC3803-09 | 8.5 | 189.6 | 106.3 | 1.78 | 267.42 | 1.28 | 21.12 | 0.26 | |
| BC3803-10 | 9.5 | 181.3 | 92.1 | 1.97 | 267.95 | 1.30 | 20.40 | 0.24 | |
| BC3803-11 | 11.0 | 189.2 | 98.1 | 1.93 | 264.12 | 1.28 | 20.82 | 0.22 | |
| BC3803-12 | 13.0 | 151.2 | 58.1 | 2.60 | 271.04 | 1.31 | 21.13 | 0.26 | |
| BC3803-13 | 15.0 | 156.1 | 75.4 | 2.07 | 273.61 | 1.31 | 21.27 | 0.23 | |
| BC3803-14 | 17.0 | 145.6 | 55.7 | 2.61 | 281.39 | 1.32 | 21.02 | 0.36 | |
| BC3803-15 | 19.0 | 136.6 | 67.7 | 2.02 | 274.62 | 1.32 | 21.34 | 0.36 | |
| BC3803-16 | 21.0 | 147.8 | 79.4 | 1.86 | 288.14 | 1.34 | 21.04 | 0.58 | |
| BC3803-17 | 23.0 | 140.4 | 86.5 | 1.62 | 277.67 | 1.32 | 21.39 | 0.28 | |
| BC3803-18 | 25.0 | 120.8 | 64.4 | 1.88 | 283.66 | 1.35 | 21.35 | 0.43 | |
| BC3803-19 | 27.0 | 122.8 | 66.8 | 1.84 | 283.65 | 1.35 | 21.50 | 0.49 | |
| BC3803-20 | 29.0 | 126.9 | 52.4 | 2.42 | 288.75 | 1.37 | 21.61 | 0.30 | |
| BC3803-21 | 31.0 | 132.8 | 64.4 | 2.06 | 285.94 | 1.37 | 22.05 | 0.29 | |
| BC3803-22 | 33.0 | 126.7 | 59.4 | 2.13 | 287.59 | 1.40 | 22.00 | 0.40 | |
| BC3803-23 | 35.0 | 124.9 | 61.6 | 2.03 | 287.84 | 1.40 | 22.58 | 0.37 | |
| BC3803-24 | 37.0 | 110.8 | 54.5 | 2.03 | 280.08 | 1.42 | 22.17 | 0.23 | |
| BC3803-25 | 39.0 | 119.5 | 54.3 | 2.20 | 273.12 | 1.42 | 22.49 | 0.31 | |
| BC3803-26 | 41.0 | 121.8 | 50.3 | 2.42 | 276.39 | 1.38 | 21.92 | 0.19 | |
| BC3803-27 | 43.0 | 122.8 | 60.8 | 2.02 | 261.92 | 1.40 | 22.16 | 0.25 | |
| BC3803-28 | 45.0 | 119.7 | 54.3 | 2.21 | 267.48 | 1.41 | 22.43 | 0.27 | |
| BC3803-29 | 47.0 | 110.2 | 52.3 | 2.11 | 263.45 | 1.40 | 22.64 | 0.30 | |
| BC3803-30 | 49.0 | 118.7 | 46.3 | 2.56 | 258.81 | 1.42 | 22.17 | 0.37 | |
| BC3803-31 | 51.0 | 114.7 | 51.2 | 2.24 | 251.80 | 1.41 | 22.17 | 0.20 | |
| BC3803-32 | 53.0 | 110.1 | 59.2 | 1.86 | 234.56 | 1.40 | 21.95 | 0.22 | |

| APPENDIX C.11. TRACE ELEMENT RATIOS | | | | | | | | | |
|---|---|---|---|---|---|---|---|---|---|
| CD38-09 | (148m) | | | | | | | | |
| Sample | Depth | I/Org.C | Br/Org.C | I/Br | Ba/Al | Zr/Rb | K/Rb | Mo/U | Mo/Uorg |
| | (cm.) | (x10-4) | (x10-4) | | (xE-4) | | (xE-3) | | |
| PC3809-01 | 4.0 | 14.0 | 68.0 | 0.21 | 50.17 | 1.89 | 18.80 | 6.66 | 12.82 |
| PC3809-02 | 13.0 | 12.0 | 59.9 | 0.20 | 42.13 | 1.62 | 18.30 | 6.75 | 11.29 |
| PC3809-03 | 23.0 | 13.4 | 46.3 | 0.29 | 38.86 | 1.80 | 19.89 | 6.07 | 12.45 |
| PC3809-04 | 34.0 | 13.6 | 40.9 | 0.33 | 39.19 | 1.75 | 19.71 | 6.13 | 12.33 |
| PC3809-05 | 43.0 | 13.5 | 49.3 | 0.27 | 48.50 | 2.68 | 21.02 | 3.21 | 9.59 |
| PC3809-06 | 53.0 | 11.0 | 40.8 | 0.27 | 41.77 | 1.58 | 19.39 | 9.38 | 117.25 |
| PC3809-07 | 62.0 | 8.6 | 38.6 | 0.22 | 41.36 | 1.65 | 19.77 | 10.39 | 20.15 |
| PC3809-08 | 73.0 | 13.6 | 46.2 | 0.29 | 42.92 | 1.96 | 19.62 | 4.43 | 9.66 |
| PC3809-09 | 84.0 | 13.7 | 38.0 | 0.36 | 39.11 | 1.53 | 19.18 | 6.53 | 18.08 |
| PC3809-10 | 94.0 | 12.2 | 35.0 | 0.35 | 39.10 | 1.45 | 19.01 | 8.99 | 22.39 |
| PC3809-11 | 104.0 | 8.8 | 32.5 | 0.27 | 43.64 | 1.40 | 19.24 | 8.57 | 14.49 |
| PC3809-12 | 113.0 | 10.3 | 39.1 | 0.26 | 38.84 | 1.41 | 19.26 | 4.35 | 9.71 |
| PC3809-13 | 124.0 | 11.1 | 39.1 | 0.28 | 45.29 | 2.16 | 20.13 | 4.14 | 9.55 |
| PC3809-14 | 134.0 | 9.5 | 33.7 | 0.28 | 43.30 | 2.21 | 20.27 | 6.94 | 20.50 |
| PC3809-15 | 144.0 | 8.8 | 34.4 | 0.26 | 45.71 | 1.88 | 19.98 | 8.21 | 17.04 |
| PC3809-16 | 152.0 | 10.3 | 35.0 | 0.29 | 39.86 | 1.86 | 19.96 | 6.42 | 13.03 |
| PC3809-17 | 165.0 | 9.7 | 28.6 | 0.34 | 45.45 | 2.40 | 20.68 | 5.07 | 9.76 |
| PC3809-18 | 174.0 | 12.6 | 37.2 | 0.34 | 50.97 | 2.93 | 21.40 | 3.00 | 7.96 |
| PC3809-19 | 185.0 | 8.7 | 35.6 | 0.24 | 54.03 | 3.58 | 22.50 | 3.04 | 11.64 |
| PC3809-20 | 194.0 | 13.7 | 31.8 | 0.43 | 57.12 | 3.81 | 22.42 | 3.51 | 85.00 |
| PC3809-21 | 205.0 | 9.6 | 33.9 | 0.28 | 65.04 | 2.19 | 21.93 | 7.88 | 58.35 |
| PC3809-22 | 214.0 | 10.8 | 35.0 | 0.31 | 50.62 | 3.11 | 21.64 | 4.27 | 9.51 |
| PC3809-23 | 224.0 | 14.4 | 33.0 | 0.44 | 65.38 | 5.11 | 25.27 | 1.22 | 6.26 |
| PC3809-24 | 234.0 | 8.6 | 28.1 | 0.30 | 59.40 | 4.09 | 24.45 | 4.81 | |
| PC3809-25 | 243.0 | 5.5 | 23.0 | 0.24 | 52.87 | 2.41 | 23.11 | 7.51 | 19.06 |
| PC3809-26 | 257.0 | 4.4 | 24.0 | 0.19 | 53.82 | 2.68 | 23.25 | 5.80 | 13.00 |
| PC3809-27 | 267.0 | 5.5 | 20.8 | 0.26 | 66.01 | 3.81 | 24.24 | 2.11 | |
| PC3809-28 | 273.0 | 6.6 | 24.7 | 0.27 | 71.71 | 3.66 | 22.32 | 0.36 | 0.81 |
| PC3809-29 | 284.0 | 3.1 | 15.4 | 0.20 | 40.86 | 1.76 | 21.25 | 5.39 | 10.32 |
| PC3809-30 | 294.0 | 3.7 | 17.6 | 0.21 | 43.27 | 1.69 | 22.38 | 10.96 | 21.65 |
| PC3809-31 | 304.0 | 3.2 | 15.8 | 0.20 | 54.77 | 1.66 | 21.29 | 6.34 | 13.54 |
| PC3809-32 | 314.0 | 2.3 | 16.9 | 0.13 | 43.33 | 1.44 | 20.49 | 9.16 | 17.92 |
| PC3809-33 | 324.0 | 3.7 | 15.7 | 0.24 | 41.90 | 1.80 | 21.67 | 6.41 | 16.85 |
| PC3809-34 | 335.0 | 3.4 | 16.3 | 0.21 | 40.52 | 1.81 | 22.59 | 8.38 | 14.73 |
| PC3809-35 | 344.0 | 2.9 | 16.6 | 0.18 | 40.93 | 1.76 | 21.90 | 10.16 | 20.39 |
| PC3809-36 | 355.0 | 2.4 | 17.1 | 0.14 | 47.86 | 1.64 | 23.38 | 14.16 | 25.75 |
| PC3809-37 | 364.0 | 3.1 | 15.6 | 0.20 | 46.47 | 1.61 | 22.67 | 17.29 | 31.94 |
| PC3809-38 | 375.0 | 2.5 | 18.2 | 0.14 | 45.42 | 1.61 | 22.80 | 14.27 | 25.74 |
| PC3809-39 | 384.0 | 1.9 | 16.1 | 0.12 | 43.95 | 1.93 | 22.13 | 6.95 | 15.51 |
| PC3809-40 | 394.0 | 3.0 | 14.4 | 0.21 | 45.26 | 1.74 | 22.40 | 8.66 | 16.18 |
| PC3809-41 | 404.0 | 4.5 | 17.5 | 0.26 | 46.62 | 1.72 | 22.63 | 6.80 | 12.06 |
| PC3809-42 | 416.0 | 2.2 | 17.4 | 0.13 | 43.01 | 1.70 | 21.94 | 9.15 | 14.08 |
| PC3809-43 | 424.0 | 2.8 | 17.5 | 0.16 | 44.66 | 1.59 | 22.75 | 8.49 | 12.99 |
| PC3809-44 | 434.0 | 3.2 | 18.2 | 0.18 | 44.28 | 1.52 | 21.46 | 8.49 | 12.96 |
| PC3809-45 | 444.0 | 3.3 | 18.5 | 0.18 | 48.37 | 1.63 | 21.96 | 8.28 | 14.41 |
| PC3809-46 | 453.0 | 2.5 | 19.0 | 0.13 | 45.39 | 1.79 | 21.56 | 6.30 | 12.70 |
| PC3809-47 | 465.0 | 3.6 | 18.8 | 0.19 | 43.52 | 1.55 | 20.69 | 11.13 | 26.18 |
| PC3809-48 | 474.0 | 1.8 | 17.9 | 0.10 | 49.53 | 1.47 | 21.45 | 10.53 | 16.59 |
| PC3809-49 | 483.0 | 3.1 | 23.3 | 0.13 | 46.54 | 1.86 | 21.61 | 5.68 | 10.94 |
| PC3809-50 | 493.0 | 2.9 | 21.9 | 0.13 | 250.09 | 1.61 | 21.83 | 8.38 | 16.30 |
| PC3809-51 | 504.0 | 2.9 | 21.7 | 0.14 | 51.49 | 2.00 | 21.99 | 4.34 | 8.02 |
| PC3809-52 | 515.0 | 2.7 | 24.8 | 0.11 | 50.33 | 1.76 | 21.93 | 5.94 | 11.12 |
| PC3809-53 | 525.0 | 2.3 | 19.5 | 0.12 | 44.96 | 1.54 | 22.22 | 10.93 | 19.54 |
| PC3809-54 | 536.0 | 3.9 | 22.2 | 0.18 | 46.99 | 1.53 | 21.82 | 14.45 | 33.57 |
| PC3809-55 | 544.0 | 1.6 | 21.2 | 0.08 | 51.31 | 1.77 | 21.62 | 8.44 | 26.84 |
| PC3809-56 | 553.0 | 3.4 | 17.5 | 0.19 | 48.69 | 1.46 | 21.16 | 11.88 | 40.53 |
| PC3809-57 | 564.0 | 0.9 | 18.2 | 0.05 | 52.26 | 1.49 | 21.01 | 13.00 | 52.94 |
| PC3809-58 | 574.0 | 1.3 | 18.3 | 0.07 | 52.08 | 1.57 | 21.58 | 11.39 | 43.20 |
| PC3809-59 | 585.0 | 3.0 | 20.1 | 0.15 | 76.62 | 1.82 | 21.26 | 7.00 | |
| PC3809-60 | 594.0 | 2.5 | 18.8 | 0.13 | 52.75 | 1.76 | 21.92 | 9.02 | 30.87 |
| PC3809-61 | 605.0 | 1.2 | 18.7 | 0.06 | 49.65 | 1.81 | 21.32 | 8.39 | 132.19 |
| PC3809-62 | 615.0 | 1.6 | 20.3 | 0.08 | 48.81 | 1.65 | 21.12 | 7.02 | 106.31 |
| PC3809-63 | 625.0 | 3.4 | 18.8 | 0.18 | 49.20 | 1.79 | 21.49 | 6.14 | 50.60 |
| PC3809-64 | 635.0 | 2.1 | 18.4 | 0.11 | 48.60 | 1.75 | 21.08 | 5.44 | 17.79 |
| PC3809-65 | 646.0 | 2.8 | 22.3 | 0.13 | 46.52 | 1.69 | 21.70 | 8.70 | 23.42 |
| PC3809-66 | 654.0 | 2.0 | 23.3 | 0.09 | 50.21 | 1.80 | 21.63 | 5.64 | 9.60 |
| PC3809-67 | 664.0 | 1.9 | 21.4 | 0.09 | 52.38 | 1.62 | 21.58 | 5.39 | 8.11 |
| PC3809-68 | 674.0 | 3.7 | 23.2 | 0.16 | 53.92 | 1.74 | 22.14 | 4.81 | 7.07 |
| PC3809-69 | 684.0 | 4.3 | 22.6 | 0.19 | 53.37 | 1.61 | 21.53 | 6.57 | 13.46 |

| APPENDIX C.11. TRACE ELEMENT RATIOS | | | | | | | | | |
|---|---|---|---|---|---|---|---|---|---|
| | | | | | | | | | |
| CD38-09 | (148m) | | | | | | | | |
| Sample | Depth | I/Org.C | Br/Org.C | I/Br | Ba/Al | Zr/Rb | K/Rb | Mo/U | Mo/Uorg |
| | (cm.) | (x10-4) | (x10-4) | | (xE-4) | | (xE-3) | | |
| PC3809-70 | 694.0 | 3.9 | 19.3 | 0.20 | 47.19 | 1.61 | 20.83 | 5.56 | 10.69 |
| PC3809-71 | 703.0 | 2.4 | 18.2 | 0.13 | 46.99 | 1.56 | 21.84 | 7.87 | 14.85 |
| PC3809-72 | 714.0 | 4.5 | 19.3 | 0.23 | 47.89 | 1.67 | 22.25 | 6.47 | 12.16 |
| PC3809-73 | 724.0 | 2.0 | 18.2 | 0.11 | 50.76 | 1.61 | 21.31 | 6.12 | 42.22 |
| PC3809-74 | 734.0 | 2.0 | 18.0 | 0.11 | 46.83 | 1.68 | 21.44 | 6.64 | 83.62 |
| PC3809-75 | 744.0 | 3.0 | 18.9 | 0.16 | 51.62 | 1.61 | 21.48 | 6.62 | 15.65 |
| PC3809-76 | 754.0 | 1.9 | 20.8 | 0.09 | 47.58 | 1.74 | 22.35 | 12.49 | 53.37 |
| PC3809-77 | 764.0 | 3.5 | 19.5 | 0.18 | 48.42 | 1.58 | 21.72 | 8.26 | 34.84 |
| PC3809-78 | 774.0 | 4.9 | 17.8 | 0.28 | 47.22 | 1.77 | 21.14 | 9.53 | 206.25 |
| PC3809-79 | 784.0 | 4.0 | 17.0 | 0.24 | 47.02 | 1.71 | 21.78 | 6.62 | 17.60 |
| PC3809-80 | 794.0 | 3.0 | 18.2 | 0.16 | 50.42 | 1.78 | 21.89 | 7.33 | 53.01 |
| PC3809-81 | 804.0 | 4.9 | 17.7 | 0.27 | 57.45 | 1.97 | 22.20 | 6.35 | 38.75 |
| PC3809-82 | 813.0 | 4.2 | 18.0 | 0.24 | 53.44 | 1.93 | 21.18 | 5.07 | |
| PC3809-83 | 823.0 | 4.1 | 18.2 | 0.23 | 52.02 | 2.00 | 21.76 | 6.36 | 617.74 |
| PC3809-84 | 834.0 | 1.7 | 15.9 | 0.11 | 49.49 | 1.93 | 21.86 | 6.84 | 74.51 |
| PC3809-85 | 845.0 | 5.3 | 20.1 | 0.26 | 50.08 | 1.79 | 21.97 | 8.62 | |
| PC3809-86 | 854.0 | 3.7 | 17.2 | 0.21 | 52.31 | 1.53 | 20.44 | 5.88 | 18.01 |
| | | | | | | | | | |
| CD38-10 | (257m) | | | | | | | | |
| | | | | | | | | | |
| PC3810-01 | 6.0 | 14.6 | 50.0 | 0.29 | 52.01 | 1.86 | 18.86 | 3.40 | 6.84 |
| PC3810-02 | 14.0 | 16.8 | 53.4 | 0.32 | 61.43 | 3.40 | 21.31 | 1.23 | 7.14 |
| PC3810-03 | 24.0 | 10.6 | 44.7 | 0.24 | 64.74 | 4.57 | 24.99 | 0.56 | |
| PC3810-04 | 34.0 | 14.6 | 41.6 | 0.35 | 60.76 | 4.07 | 23.73 | 1.13 | |
| PC3810-05 | 44.0 | 6.3 | 33.8 | 0.19 | 60.51 | 2.61 | 22.54 | 2.43 | 4.83 |
| PC3810-06 | 54.0 | 4.6 | 35.4 | 0.13 | 54.61 | 2.43 | 21.80 | 3.20 | 5.20 |
| PC3810-07 | 64.0 | 9.9 | 37.9 | 0.26 | 56.54 | 3.08 | 23.06 | 2.57 | 5.68 |
| PC3810-08 | 74.0 | 6.0 | 35.4 | 0.17 | 62.82 | 3.49 | 22.71 | 1.94 | 8.17 |
| PC3810-09 | 84.0 | 14.7 | 30.0 | 0.49 | 71.90 | 4.07 | 25.91 | 0.86 | |
| PC3810-10 | 94.0 | 6.2 | 32.9 | 0.19 | 66.03 | 4.66 | 25.11 | 1.52 | 10.01 |
| PC3810-10 | 104.0 | 6.6 | 30.7 | 0.21 | 67.03 | 5.17 | 25.62 | 2.00 | 17.83 |
| PC3810-11 | 113.0 | 12.7 | 27.8 | 0.46 | 62.01 | 4.55 | 25.19 | 1.65 | 50.94 |
| PC3810-12 | 126.0 | 6.5 | 26.2 | 0.25 | 44.58 | 2.48 | 21.82 | 4.45 | 21.89 |
| PC3810-13 | 134.0 | 3.8 | 22.4 | 0.17 | 46.30 | 2.12 | 20.66 | 4.92 | 17.86 |
| PC3810-14 | 146.0 | 4.4 | 22.9 | 0.19 | 51.28 | 2.48 | 21.35 | 4.27 | 11.03 |
| PC3810-15 | 154.0 | 5.3 | 21.2 | 0.25 | 52.07 | 2.27 | 20.58 | 3.67 | 9.20 |
| PC3810-16 | 167.0 | 4.6 | 23.6 | 0.20 | 53.53 | 1.97 | 20.42 | 4.07 | 8.07 |
| PC3810-17 | 174.0 | 3.8 | 22.8 | 0.17 | 54.55 | 1.98 | 21.28 | 3.66 | 7.52 |
| PC3810-18 | 185.0 | 4.0 | 26.3 | 0.15 | 51.75 | 1.69 | 20.16 | 2.95 | 5.80 |
| PC3810-19 | 194.0 | 4.7 | 30.4 | 0.15 | 55.58 | 1.63 | 19.98 | 5.65 | 10.63 |
| PC3810-20 | 203.0 | 4.4 | 24.1 | 0.18 | 57.14 | 2.10 | 20.88 | 3.06 | 5.72 |
| PC3810-21 | 216.0 | 4.5 | 26.8 | 0.17 | 60.39 | 1.75 | 20.05 | 5.50 | 10.85 |
| PC3810-22 | 224.0 | 4.3 | 25.2 | 0.17 | 55.17 | 1.63 | 19.12 | 5.07 | 8.80 |
| PC3810-23 | 233.0 | 4.1 | 22.4 | 0.19 | 54.33 | 1.78 | 20.42 | 4.40 | 7.63 |
| PC3810-24 | 244.0 | 5.3 | 22.2 | 0.24 | 45.81 | 2.05 | 20.28 | 3.92 | 9.69 |
| PC3810-25 | 254.0 | 8.6 | 33.7 | 0.26 | 56.76 | 3.07 | 22.22 | 3.09 | 13.46 |
| PC3810-26 | 263.0 | 7.1 | 29.2 | 0.24 | 58.22 | 2.54 | 21.45 | 4.30 | 14.84 |
| PC3810-27 | 273.0 | 4.6 | 19.1 | 0.24 | 51.17 | 1.95 | 20.49 | 3.73 | 7.55 |
| PC3810-28 | 284.0 | 5.5 | 20.4 | 0.27 | 53.32 | 2.10 | 20.08 | 2.90 | 5.86 |
| PC3810-29 | 295.0 | 4.7 | 19.7 | 0.24 | 57.92 | 1.44 | 18.80 | 5.44 | 10.64 |
| PC3810-30 | 305.0 | 4.6 | 20.5 | 0.22 | 51.10 | 1.84 | 19.24 | 3.20 | 5.97 |
| PC3810-31 | 314.0 | 4.5 | 21.1 | 0.21 | 50.52 | 2.14 | 19.89 | 2.98 | 6.19 |
| PC3810-32 | 324.0 | 3.9 | 18.7 | 0.21 | 59.23 | 1.57 | 19.00 | 5.25 | 9.17 |
| PC3810-33 | 335.0 | 5.2 | 24.1 | 0.22 | 49.36 | 1.75 | 19.57 | 2.81 | 5.25 |
| PC3810-34 | 344.0 | 4.0 | 22.6 | 0.18 | 42.71 | 1.58 | 19.03 | 5.72 | 11.18 |
| PC3810-35 | 354.0 | 4.1 | 19.7 | 0.21 | 64.04 | 1.54 | 19.67 | 6.67 | 11.33 |
| PC3810-36 | 364.0 | 3.9 | 24.4 | 0.16 | 57.51 | 1.36 | 18.86 | 6.60 | 11.40 |
| PC3810-37 | 374.0 | 5.5 | 48.6 | 0.11 | 64.63 | 1.28 | 17.54 | 5.34 | 7.86 |
| PC3810-38 | 383.0 | 4.0 | 24.1 | 0.17 | 49.40 | 1.46 | 18.66 | 2.34 | 3.82 |
| PC3810-39 | 394.0 | 3.1 | 30.3 | 0.10 | 50.32 | 1.69 | 18.89 | 3.09 | 4.92 |
| PC3810-40 | 404.0 | 4.3 | 25.5 | 0.17 | 46.27 | 2.00 | 19.62 | 2.15 | 3.76 |
| PC3810-41 | 417.0 | 4.7 | 17.7 | 0.26 | 51.82 | 1.90 | 18.88 | 4.19 | 8.24 |
| PC3810-42 | 424.0 | 4.5 | 17.1 | 0.26 | 43.35 | 1.70 | 19.77 | 3.22 | 5.21 |
| PC3810-43 | 434.0 | 3.9 | 17.6 | 0.22 | 74.46 | 1.88 | 20.44 | 6.36 | 14.53 |
| PC3810-44 | 445.0 | 4.5 | 16.3 | 0.27 | 51.68 | 1.45 | 18.98 | 3.71 | 6.07 |
| PC3810-45 | 456.0 | 4.4 | 18.2 | 0.24 | 70.90 | 1.53 | 18.35 | 5.47 | 8.33 |
| PC3810-46 | 467.0 | 3.6 | 18.8 | 0.19 | 77.05 | 1.48 | 20.71 | 11.80 | 26.28 |
| PC3810-47 | 476.0 | 4.0 | 18.6 | 0.21 | 56.66 | 1.78 | 19.19 | 2.12 | 4.06 |
| PC3810-48 | 484.0 | 4.2 | 18.0 | 0.23 | 57.17 | 1.82 | 19.07 | 2.46 | 5.04 |

| APPENDIX C.11. TRACE ELEMENT RATIOS | | | | | | | | | |
|---|---|---|---|---|---|---|---|---|---|
| CD38-10 | (257m) | | | | | | | | |
| Sample | Depth (cm.) | I/Org.C (x10-4) | Br/Org.C (x10-4) | I/Br | Ba/Al (xE-4) | Zr/Rb | K/Rb (xE-3) | Mo/U | Mo/Uorg |
| PC3810-49 | 494.0 | 4.7 | 17.8 | 0.26 | 64.07 | 2.89 | 20.17 | 1.63 | 3.81 |
| PC3810-50 | 504.0 | 7.4 | 23.2 | 0.32 | 60.80 | 4.80 | 25.42 | 0.67 | |
| PC3810-51 | 514.0 | 3.3 | 18.0 | 0.18 | 52.70 | 1.96 | 22.67 | 11.34 | 25.18 |
| PC3810-52 | 524.0 | 2.5 | 18.4 | 0.14 | 57.62 | 2.04 | 23.52 | 8.26 | 17.31 |
| PC3810-53 | 534.0 | 3.2 | 20.7 | 0.15 | 87.95 | 1.51 | 20.84 | 5.64 | 6.97 |
| PC3810-54 | 545.0 | 2.2 | 28.3 | 0.08 | 72.95 | 1.53 | 21.37 | 6.45 | 8.21 |
| PC3810-55 | 554.0 | 2.8 | 33.2 | 0.08 | 82.28 | 1.42 | 20.11 | 6.86 | 8.44 |
| PC3810-56 | 564.0 | 2.6 | 21.4 | 0.12 | 88.67 | 1.78 | 20.60 | 9.09 | 17.24 |
| PC3810-57 | 574.0 | 2.6 | 21.0 | 0.12 | 79.35 | 1.90 | 19.91 | 7.62 | 12.58 |
| PC3810-58 | 584.0 | 2.7 | 22.4 | 0.12 | 87.37 | 1.78 | 21.62 | 8.89 | 14.59 |
| PC3810-59 | 596.0 | 3.0 | 22.2 | 0.14 | 90.82 | 1.85 | 21.27 | 3.83 | 4.56 |
| PC3810-60 | 604.0 | 2.1 | 20.6 | 0.10 | 97.24 | 1.71 | 21.50 | 5.27 | 6.77 |
| PC3810-61 | 614.0 | 3.2 | 22.4 | 0.14 | 77.83 | 1.72 | 20.50 | 5.70 | 7.13 |
| PC3810-62 | 624.0 | 3.4 | 20.0 | 0.17 | 70.02 | 1.68 | 20.95 | 7.55 | 12.39 |
| PC3810-63 | 634.0 | 3.1 | 19.9 | 0.16 | 63.89 | 1.84 | 22.01 | 6.82 | 12.19 |
| PC3810-64 | 645.0 | 2.9 | 23.5 | 0.12 | 83.44 | 1.52 | 20.03 | 8.38 | 11.89 |
| PC3810-65 | 655.0 | 2.3 | 24.3 | 0.09 | 77.60 | 1.52 | 21.11 | 13.12 | 19.41 |
| PC3810-66 | 667.0 | 2.7 | 19.5 | 0.14 | 61.52 | 1.52 | 21.56 | 9.27 | 13.61 |
| PC3810-67 | 674.0 | 2.8 | 18.0 | 0.16 | 49.73 | 1.38 | 20.13 | 6.83 | 9.54 |
| PC3810-68 | 683.0 | 2.0 | 18.5 | 0.11 | 48.94 | 1.31 | 20.00 | 8.16 | 11.46 |
| PC3810-69 | 694.0 | 3.9 | 19.0 | 0.21 | 47.12 | 1.41 | 19.92 | 6.04 | 12.03 |
| PC3810-70 | 704.0 | 3.9 | 16.8 | 0.23 | 46.27 | 1.41 | 20.30 | 6.03 | 15.59 |
| PC3810-71 | 714.0 | 3.1 | 17.7 | 0.18 | 48.29 | 1.29 | 20.27 | 8.53 | 21.95 |
| PC3810-72 | 724.0 | 3.3 | 18.5 | 0.18 | 48.57 | 1.26 | 19.69 | 7.73 | 13.57 |
| PC3810-74 | 734.0 | 3.6 | 21.9 | 0.17 | 45.89 | 1.46 | 21.20 | 5.33 | 10.03 |
| PC3810-75 | 745.0 | 2.1 | 24.9 | 0.09 | 46.59 | 1.64 | 20.82 | 3.89 | 8.74 |
| PC3810-76 | 754.0 | 2.7 | 35.9 | 0.08 | 46.03 | 2.01 | 20.29 | 5.45 | 12.64 |
| PC3810-77 | 764.0 | 1.4 | 27.0 | 0.05 | 54.17 | 2.71 | 21.95 | 2.71 | 22.81 |
| CD38-02 | (2525m) | | | | | | | | |
| PC3802-01 | 8.0 | 148.7 | 88.4 | 1.68 | 374.44 | 1.29 | 17.49 | 0.00 | 0.00 |
| PC3802-02 | 18.0 | 150.1 | 90.1 | 1.67 | 361.24 | 1.33 | 18.19 | 0.03 | 0.06 |
| PC3802-03 | 28.0 | 156.9 | 87.0 | 1.80 | 356.27 | 1.33 | 16.95 | 0.00 | 0.00 |
| PC3802-04 | 38.0 | 133.2 | 79.7 | 1.67 | 231.61 | 1.22 | 16.73 | 0.24 | 0.34 |
| PC3802-05 | 48.0 | 170.0 | 72.6 | 2.34 | 243.09 | 1.27 | 16.80 | 0.26 | 0.38 |
| PC3802-06 | 57.5 | 152.0 | 69.0 | 2.20 | 234.67 | 1.27 | 17.24 | 0.39 | 0.63 |
| PC3802-07 | 70.0 | 151.9 | 47.2 | 3.22 | 271.99 | 1.31 | 16.64 | 0.10 | 0.18 |
| PC3802-08 | 79.0 | 159.3 | 65.9 | 2.42 | 260.57 | 1.28 | 16.85 | 0.38 | 0.62 |
| PC3802-09 | 89.0 | 131.1 | 62.8 | 2.09 | 275.58 | 1.29 | 16.35 | 0.20 | 0.27 |
| PC3802-10 | 100.0 | 121.2 | 62.6 | 1.94 | 287.76 | 1.30 | 16.24 | 0.35 | 0.56 |
| PC3802-11 | 110.0 | 164.4 | 84.6 | 1.94 | 291.04 | 1.30 | 16.40 | 0.47 | 0.70 |
| PC3802-12 | 120.0 | 127.3 | 76.6 | 1.66 | 306.08 | 1.30 | 16.58 | 0.52 | 0.72 |
| PC3802-13 | 130.0 | 121.7 | 63.8 | 1.91 | 294.36 | 1.29 | 15.74 | 0.47 | 0.65 |
| PC3802-14 | 139.0 | 150.9 | 75.0 | 2.01 | 274.78 | 1.31 | 16.71 | 0.48 | 0.80 |
| PC3802-15 | 150.0 | 111.8 | 57.0 | 1.96 | 250.19 | 1.28 | 17.56 | 0.62 | 1.12 |
| PC3802-16 | 160.0 | 116.6 | 46.8 | 2.49 | 245.01 | 1.32 | 17.72 | 0.56 | 1.38 |
| PC3802-17 | 171.0 | 103.9 | 60.1 | 1.73 | 247.09 | 1.32 | 18.02 | 0.25 | 0.35 |
| PC3802-18 | 181.0 | 127.1 | 66.7 | 1.90 | 274.65 | 1.31 | 17.95 | 0.34 | 0.48 |
| PC3802-19 | 191.0 | 113.6 | 61.8 | 1.84 | 304.52 | 1.33 | 17.72 | 0.15 | 0.20 |
| PC3802-20 | 201.0 | 114.3 | 62.1 | 1.84 | 270.97 | 1.41 | 17.92 | 0.26 | 0.37 |
| PC3802-21 | 211.0 | 109.7 | 54.7 | 2.00 | 243.26 | 1.29 | 17.59 | 0.38 | 0.57 |
| PC3802-22 | 221.0 | 116.8 | 55.5 | 2.10 | 249.14 | 1.30 | 17.71 | 0.30 | 0.44 |
| PC3802-23 | 231.0 | 118.4 | 57.4 | 2.06 | 214.24 | 1.28 | 18.01 | 0.53 | 1.30 |
| PC3802-24 | 241.0 | 105.4 | 53.7 | 1.96 | 253.27 | 1.28 | 18.63 | 0.20 | 0.39 |
| PC3802-25 | 251.0 | 92.5 | 56.9 | 1.62 | 266.33 | 1.26 | 17.45 | 0.31 | 0.47 |
| PC3802-26 | 261.0 | 117.0 | 65.2 | 1.80 | 334.91 | 1.32 | 17.60 | 0.19 | 0.28 |
| PC3802-27 | 271.0 | 82.0 | 54.7 | 1.50 | 284.32 | 1.29 | 18.70 | 0.42 | 0.81 |
| PC3802-28 | 281.0 | 101.9 | 63.8 | 1.60 | 263.42 | 1.28 | 18.91 | 0.24 | 0.40 |
| PC3802-29 | 291.0 | 83.9 | 54.3 | 1.54 | 259.93 | 1.23 | 18.68 | 0.18 | 0.34 |
| PC3802-30 | 301.0 | 89.5 | 61.7 | 1.45 | 291.55 | 1.25 | 18.52 | 0.22 | 0.40 |
| PC3802-31 | 312.0 | 99.5 | 53.4 | 1.86 | 307.82 | 1.30 | 18.10 | 0.17 | 0.24 |
| PC3802-32 | 322.0 | 109.4 | 56.6 | 1.93 | 315.92 | 1.26 | 18.34 | 0.19 | 0.28 |
| PC3802-33 | 332.0 | 113.5 | 58.8 | 1.93 | 304.26 | 1.27 | 18.95 | 0.23 | 0.49 |
| PC3802-34 | 342.0 | 99.0 | 72.2 | 1.37 | 371.40 | 1.27 | 18.37 | 0.23 | 0.38 |
| PC3802-35 | 352.0 | 92.0 | 70.3 | 1.31 | 351.48 | 1.29 | 18.72 | 0.06 | 0.09 |
| PC3802-36 | 362.0 | 109.5 | 66.3 | 1.65 | 256.44 | 1.22 | 17.35 | 0.25 | 0.40 |
| PC3802-37 | 372.0 | 102.3 | 67.3 | 1.52 | 237.40 | 1.24 | 17.18 | 0.12 | 0.17 |
| PC3802-38 | 381.0 | 120.3 | 56.5 | 2.13 | 252.19 | 1.26 | 17.72 | 0.12 | 0.19 |

| APPENDIX C.11. TRACE ELEMENT RATIOS | | | | | | | | | |
|---|---|---|---|---|---|---|---|---|---|
| CD38-02 | (2525m) | | | | | | | | |
| Sample | Depth (cm.) | I/Org.C (x10-4) | Br/Org.C (x10-4) | I/Br | Ba/Al (xE-4) | Zr/Rb | K/Rb (xE-3) | Mo/U | Mo/Uorg |
| PC3802-39 | 391.0 | 116.8 | 56.3 | 2.07 | 252.78 | 1.32 | 17.79 | 0.16 | 0.22 |
| PC3802-40 | 400.0 | 110.6 | 56.7 | 1.95 | 274.70 | 1.34 | 17.69 | 0.14 | 0.21 |
| PC3802-41 | 410.0 | 113.1 | 54.8 | 2.06 | 269.55 | 1.23 | 17.68 | 0.31 | 0.58 |
| PC3802-42 | 420.0 | 127.9 | 57.5 | 2.23 | 246.99 | 1.34 | 18.12 | 0.10 | 0.16 |
| PC3802-43 | 430.0 | 123.4 | 53.8 | 2.30 | 220.21 | 1.29 | 17.12 | 0.04 | 0.06 |
| PC3802-44 | 440.0 | 99.6 | 54.2 | 1.84 | 242.91 | 1.29 | 18.02 | 0.11 | 0.13 |
| PC3802-45 | 450.0 | 118.8 | 64.6 | 1.84 | 217.30 | 1.27 | 17.09 | 0.07 | 0.11 |
| PC3802-46 | 460.0 | 113.6 | 67.2 | 1.69 | 207.47 | 1.23 | 18.33 | 0.29 | 0.51 |
| PC3802-47 | 470.0 | 102.5 | 50.8 | 2.02 | 247.37 | 1.25 | 15.99 | 0.09 | 0.12 |
| PC3802-48 | 481.0 | 90.7 | 47.6 | 1.91 | 277.33 | 1.27 | 12.14 | 0.20 | 0.26 |
| PC3802-49 | 491.0 | 67.3 | 39.0 | 1.73 | 276.05 | 1.29 | 17.64 | 0.41 | 0.67 |
| PC3802-50 | 501.0 | 76.4 | 39.6 | 1.93 | 264.09 | 1.27 | 18.01 | 0.23 | 0.34 |
| PC3802-51 | 511.0 | 67.4 | 45.7 | 1.47 | 252.27 | 1.25 | 17.45 | 0.14 | 0.20 |
| PC3802-52 | 521.0 | 93.1 | 78.7 | 1.18 | 190.72 | 1.24 | 19.54 | 0.49 | 1.01 |
| PC3802-53 | 531.0 | 91.0 | 57.4 | 1.58 | 166.98 | 1.36 | 24.59 | 0.22 | 0.00 |
| PC3802-54 | 540.0 | 91.0 | 60.5 | 1.50 | 226.24 | 1.24 | 18.63 | 0.36 | 0.83 |
| PC3802-55 | 550.0 | 74.7 | 60.3 | 1.24 | 246.10 | 1.22 | 18.00 | 0.60 | 1.63 |
| PC3802-56 | 560.0 | 79.2 | 50.7 | 1.56 | 326.16 | 1.19 | 17.69 | 0.38 | 0.73 |
| PC3802-57 | 572.0 | 98.5 | 94.2 | 1.05 | 337.12 | 1.19 | 18.89 | 0.27 | 0.43 |
| PC3802-58 | 582.0 | 77.6 | 74.1 | 1.05 | 312.42 | 1.24 | 19.04 | 0.11 | 0.20 |
| PC3802-59 | 591.0 | 89.9 | 69.7 | 1.29 | 290.68 | 1.19 | 18.07 | 0.25 | 0.50 |
| PC3802-60 | 601.0 | 74.3 | 61.2 | 1.21 | 408.00 | 1.25 | 16.25 | 0.10 | 0.14 |
| PC3802-61 | 611.0 | 90.9 | 82.1 | 1.11 | 367.34 | 1.30 | 18.77 | 0.05 | 0.06 |
| PC3802-62 | 621.0 | 103.8 | 62.8 | 1.65 | 305.40 | 1.28 | 18.03 | 0.06 | 0.10 |
| PC3802-63 | 631.0 | 81.3 | 48.8 | 1.67 | 256.72 | 1.25 | 17.57 | 0.27 | 0.41 |
| PC3802-64 | 641.0 | 84.0 | 53.8 | 1.56 | 264.08 | 1.24 | 18.31 | 0.09 | 0.15 |
| PC3802-65 | 651.0 | 85.4 | 59.8 | 1.43 | 277.32 | 1.21 | 18.83 | 0.10 | 0.26 |
| PC3802-66 | 662.0 | 90.8 | 90.4 | 1.00 | 392.56 | 1.25 | 18.56 | 0.15 | 0.47 |
| PC3802-67 | 671.0 | 78.6 | 100.9 | 0.78 | 425.09 | 1.28 | 17.61 | 0.08 | 0.10 |
| PC3802-68 | 681.0 | 80.6 | 56.3 | 1.43 | 281.18 | 1.26 | 17.99 | 0.01 | 0.02 |
| PC3802-69 | 691.0 | 88.0 | 42.6 | 2.07 | 229.12 | 1.27 | 18.01 | 0.11 | 0.16 |
| PC3802-70 | 701.0 | 80.4 | 39.7 | 2.03 | 235.82 | 1.28 | 17.83 | 0.13 | 0.19 |
| PC3802-71 | 711.0 | 101.6 | 62.1 | 1.64 | 265.81 | 1.23 | 17.60 | 0.14 | 0.21 |
| PC3802-72 | 721.0 | 88.0 | 47.1 | 1.87 | 276.80 | 1.25 | 17.78 | 0.19 | 0.33 |
| PC3802-73 | 731.0 | 87.6 | 46.2 | 1.90 | 265.79 | 1.23 | 17.68 | 0.05 | 0.07 |
| PC3802-74 | 741.0 | 96.4 | 43.1 | 2.24 | 251.30 | 1.26 | 17.46 | 0.19 | 0.27 |
| CD38-11 | (3835m) | | | | | | | | |
| PC3811-01 | 3.0 | 121.0 | 77.6 | 1.56 | 179.12 | 1.64 | 17.13 | 0.56 | 1.10 |
| PC3811-02 | 13.0 | 51.8 | 64.3 | 0.81 | 70.40 | 2.16 | 16.47 | 2.08 | 5.40 |
| PC3811-03 | 23.0 | 43.8 | 62.1 | 0.71 | 63.14 | 2.98 | 18.73 | 1.74 | 7.71 |
| PC3811-04 | 33.0 | 134.7 | 70.8 | 1.90 | 272.99 | 1.41 | 18.22 | 0.18 | 0.27 |
| PC3811-05 | 43.0 | 117.6 | 69.8 | 1.68 | 193.75 | 1.35 | 17.86 | 0.21 | 0.31 |
| PC3811-06 | 53.0 | 102.0 | 64.6 | 1.58 | 137.20 | 1.33 | 17.33 | 0.38 | 0.55 |
| PC3811-07 | 63.0 | 97.5 | 59.7 | 1.63 | 114.74 | 1.36 | 17.78 | 0.42 | 0.58 |
| PC3811-08 | 73.0 | 101.4 | 58.9 | 1.72 | 121.87 | 1.38 | 17.38 | 0.93 | 1.62 |
| PC3811-09 | 85.0 | 93.3 | 53.0 | 1.76 | 94.83 | 1.93 | 21.38 | 0.78 | |
| PC3811-10 | 95.0 | 90.9 | 59.6 | 1.53 | 124.22 | 1.37 | 17.92 | 1.14 | 1.74 |
| PC3811-11 | 105.0 | 78.9 | 58.6 | 1.35 | 118.96 | 1.35 | 17.28 | 1.83 | 3.89 |
| PC3811-12 | 116.0 | 78.6 | 59.4 | 1.32 | 129.06 | 1.34 | 17.31 | 2.05 | 6.39 |
| PC3811-13 | 125.0 | 89.5 | 58.7 | 1.52 | 131.05 | 1.30 | 17.75 | 1.85 | 4.37 |
| PC3811-14 | 135.0 | 81.5 | 59.6 | 1.37 | 120.02 | 1.36 | 17.45 | 1.72 | 4.28 |
| PC3811-15 | 145.0 | 87.8 | 61.0 | 1.44 | 125.17 | 1.34 | 17.95 | 1.63 | 3.86 |
| PC3811-16 | 155.0 | 79.8 | 58.4 | 1.36 | 111.00 | 1.44 | 17.33 | 0.93 | 1.54 |
| PC3811-17 | 165.0 | 81.6 | 58.7 | 1.39 | 116.52 | 1.30 | 18.35 | 1.11 | 2.01 |
| PC3811-18 | 175.0 | 86.4 | 56.2 | 1.54 | 123.50 | 1.56 | 18.96 | 0.79 | 1.60 |
| PC3811-19 | 186.0 | 94.9 | 62.1 | 1.53 | 155.02 | 1.28 | 17.57 | 1.22 | 1.87 |
| PC3811-20 | 197.0 | 88.1 | 62.5 | 1.41 | 149.78 | 1.22 | 17.07 | 1.58 | 3.27 |
| PC3811-21 | 204.0 | 85.4 | 61.1 | 1.40 | 154.31 | 1.20 | 17.71 | 1.13 | 2.69 |
| PC3811-22 | 215.0 | 77.0 | 53.8 | 1.43 | 174.00 | 1.42 | 17.52 | 0.82 | 1.20 |
| PC3811-23 | 225.0 | 86.9 | 53.3 | 1.63 | 211.10 | 1.25 | 16.87 | 1.44 | 2.67 |
| PC3811-24 | 235.0 | 84.8 | 51.9 | 1.64 | 206.42 | 1.23 | 16.50 | 1.04 | 1.49 |
| PC3811-25 | 245.0 | 86.9 | 52.5 | 1.66 | 214.61 | 1.24 | 17.05 | 1.11 | 1.61 |
| PC3811-26 | 255.0 | 86.6 | 53.3 | 1.62 | 241.10 | 1.28 | 16.44 | 1.18 | 1.65 |
| PC3811-27 | 265.0 | 89.3 | 54.9 | 1.63 | 247.15 | 1.28 | 16.52 | 1.11 | 1.53 |
| PC3811-28 | 275.0 | 83.2 | 52.6 | 1.58 | 237.52 | 1.30 | 16.77 | 0.93 | 1.36 |
| PC3811-29 | 285.0 | 79.5 | 51.0 | 1.56 | 177.17 | 1.29 | 18.04 | 0.80 | 1.20 |
| PC3811-30 | 297.0 | 82.5 | 53.1 | 1.56 | 161.56 | 1.31 | 17.53 | 0.66 | 1.07 |

APPENDIX C.11. TRACE ELEMENT RATIOS

| CD38-11 | (3835m) | | | | | | | | |
|---|---|---|---|---|---|---|---|---|---|
| Sample | Depth (cm.) | I/Org.C (x10-4) | Br/Org.C (x10-4) | I/Br | Ba/Al (xE-4) | Zr/Rb | K/Rb (xE-3) | Mo/U | Mo/Uorg |
| PC3811-31 | 305.0 | 85.7 | 52.4 | 1.64 | 183.36 | 1.33 | 18.36 | 1.09 | 2.26 |
| PC3811-32 | 315.0 | 89.2 | 56.7 | 1.57 | 139.60 | 1.42 | 18.30 | 0.75 | 1.35 |
| PC3811-33 | 325.0 | 42.9 | 43.9 | 0.98 | 93.04 | 2.39 | 18.68 | 0.96 | 1.58 |
| PC3811-34 | 335.0 | 81.2 | 72.3 | 1.12 | 239.87 | 1.27 | 17.12 | 1.02 | 1.49 |
| PC3811-35 | 345.0 | 81.9 | 65.9 | 1.24 | 227.73 | 1.25 | 16.88 | 1.17 | 1.74 |
| PC3811-36 | 355.0 | 85.4 | 58.6 | 1.46 | 269.17 | 1.29 | 17.34 | 1.14 | 1.79 |
| PC3811-37 | 365.0 | 69.2 | 60.9 | 1.14 | 234.53 | 1.30 | 17.36 | 2.10 | 8.46 |
| PC3811-38 | 375.0 | 73.8 | 53.9 | 1.37 | 183.93 | 1.23 | 16.88 | 1.16 | 1.85 |
| PC3811-39 | 385.0 | 79.5 | 49.8 | 1.59 | 180.61 | 1.25 | 17.40 | 1.52 | 2.39 |
| PC3811-40 | 395.0 | 83.9 | 45.9 | 1.83 | 173.79 | 1.27 | 17.96 | 1.59 | 3.20 |
| PC3811-41 | 405.0 | 80.9 | 43.4 | 1.86 | 188.28 | 1.23 | 17.25 | 1.59 | 2.78 |
| PC3811-42 | 415.0 | 88.3 | 45.4 | 1.94 | 234.47 | 1.29 | 18.89 | 1.23 | 2.32 |
| PC3811-43 | 425.0 | 84.7 | 45.5 | 1.86 | 305.47 | 1.30 | 17.41 | 1.23 | 2.31 |
| PC3811-44 | 435.0 | 82.8 | 50.8 | 1.63 | 369.26 | 1.37 | 18.08 | 0.68 | 1.03 |
| PC3811-45 | 445.0 | 77.6 | 51.7 | 1.50 | 342.23 | 1.32 | 17.41 | 0.80 | 1.35 |
| PC3811-46 | 455.0 | 87.5 | 54.1 | 1.62 | 261.94 | 1.34 | 18.62 | 0.62 | 1.08 |
| PC3811-47 | 465.0 | 88.3 | 56.3 | 1.57 | 224.38 | 1.24 | 18.05 | 0.99 | 1.92 |
| PC3811-48 | 475.0 | 84.9 | 56.1 | 1.51 | 247.57 | 1.27 | 18.61 | 0.77 | 1.23 |
| PC3811-49 | 485.0 | 99.1 | 62.2 | 1.59 | 241.36 | 1.25 | 18.79 | 1.58 | 6.80 |
| PC3811-50 | 495.0 | 121.3 | 74.4 | 1.63 | 258.43 | 1.27 | 18.37 | 0.76 | 1.49 |
| PC3811-51 | 505.0 | 86.6 | 61.7 | 1.40 | 260.60 | 1.24 | 18.44 | 0.73 | 1.88 |
| PC3811-52 | 515.0 | 86.7 | 65.5 | 1.32 | 270.95 | 1.23 | 18.52 | 1.05 | 16.94 |
| PC3811-53 | 525.0 | 89.1 | 77.3 | 1.15 | 282.12 | 1.24 | 18.72 | 0.70 | 4.34 |
| PC3811-54 | 535.0 | 86.9 | 54.9 | 1.58 | 308.44 | 1.34 | 18.50 | 0.66 | 1.63 |
| PC3811-55 | 545.0 | 78.6 | 52.0 | 1.51 | 299.34 | 1.34 | 19.08 | 0.48 | 1.26 |
| PC3811-56 | 555.0 | 90.4 | 52.7 | 1.72 | 331.71 | 1.35 | 19.08 | 0.95 | |
| PC3811-57 | 565.0 | 80.3 | 47.6 | 1.68 | 323.07 | 1.43 | 18.78 | 0.25 | 0.81 |

APPENDIX C.12. BIOGENIC COMPONENTS

| BC38-02 Sample | 2530m Depth (cm) | Corg (wt.%) | CaCO3 (wt.%) | Bio.SiO2 (wt.%) | PC38-09 Sample | 148m Depth (cm) | Corg (wt.%) | CaCO3 (wt.%) | Bio.SiO2 (wt.%) |
|---|---|---|---|---|---|---|---|---|---|
| BC3802-01 | 0.5 | 1.02 | 12.34 | 8.48 | PC3809-01 | 4.0 | 6.70 | 2.16 | 16.85 |
| BC3802-02 | 1.5 | 1.20 | 11.58 | 8.45 | PC3809-02 | 13.0 | 6.65 | 3.34 | 21.87 |
| BC3802-03 | 2.5 | 1.06 | 12.11 | 7.68 | PC3809-03 | 23.0 | 6.03 | 1.23 | 14.02 |
| BC3802-04 | 3.5 | 1.14 | 12.54 | 8.15 | PC3809-04 | 34.0 | 6.14 | 0.64 | 14.89 |
| BC3802-05 | 4.5 | 1.13 | 13.23 | 8.09 | PC3809-05 | 43.0 | 3.66 | 1.29 | 7.07 |
| BC3802-06 | 5.5 | 1.08 | 13.31 | 7.73 | PC3809-06 | 53.0 | 5.93 | 0.25 | 17.81 |
| BC3802-07 | 6.5 | 1.13 | 13.46 | 7.97 | PC3809-07 | 62.0 | 8.26 | 2.75 | 18.39 |
| BC3802-08 | 7.5 | 1.12 | 13.23 | 8.90 | PC3809-08 | 73.0 | 5.44 | 0.47 | 15.17 |
| BC3802-09 | 8.5 | 1.02 | 13.57 | 7.78 | PC3809-09 | 84.0 | 5.76 | 0.00 | 10.77 |
| BC3802-10 | 9.5 | 1.00 | 14.20 | 8.32 | PC3809-10 | 94.0 | 6.60 | 0.42 | 14.48 |
| BC3802-11 | 11.0 | 0.88 | 16.40 | 7.82 | PC3809-11 | 104.0 | 6.93 | 0.08 | 18.47 |
| BC3802-12 | 13.0 | 0.89 | 18.99 | 7.83 | PC3809-12 | 113.0 | 4.87 | 0.00 | 11.67 |
| BC3802-13 | 15.0 | 0.87 | 19.97 | 7.74 | PC3809-13 | 124.0 | 5.09 | 1.54 | 8.18 |
| BC3802-13A | 17.0 | 1.09 | 25.67 | 7.44 | PC3809-14 | 134.0 | 6.06 | 1.35 | 14.35 |
| BC3802-14 | 19.0 | 0.93 | 28.88 | 7.57 | PC3809-15 | 144.0 | 6.33 | 1.45 | 20.44 |
| BC3802-15 | 21.0 | 0.86 | 31.38 | 7.07 | PC3809-16 | 152.0 | 5.05 | 1.82 | 20.27 |
| BC3802-16 | 23.0 | 0.89 | 32.14 | 5.81 | PC3809-17 | 165.0 | 4.96 | 3.00 | 20.04 |
| BC3802-17 | 25.0 | 0.96 | 33.43 | 5.91 | PC3809-18 | 174.0 | 3.35 | 1.12 | 9.13 |
| BC3802-18 | 27.0 | 0.94 | 34.02 | 5.49 | PC3809-19 | 185.0 | 3.21 | 1.65 | 8.61 |
| BC3802-19 | 29.0 | 1.09 | 36.15 | 5.47 | PC3809-20 | 194.0 | 2.96 | 3.10 | 6.14 |
| BC3802-20 | 31.0 | 1.09 | 35.10 | 4.98 | PC3809-21 | 205.0 | 2.16 | 4.00 | 8.36 |
| BC3802-21 | 33.0 | 1.28 | 34.50 | 5.15 | PC3809-22 | 214.0 | 5.59 | 1.75 | 12.11 |
| BC3802-21A | 35.0 | 1.83 | 30.66 | 5.06 | PC3809-23 | 224.0 | 1.59 | 2.32 | 3.10 |
| BC3802-22 | 37.0 | 1.51 | 32.64 | 5.04 | PC3809-24 | 234.0 | 2.43 | 1.73 | 11.78 |
| BC3802-23 | 39.0 | 1.19 | 33.78 | 4.58 | PC3809-25 | 243.0 | 4.69 | 0.76 | 25.82 |
| BC3802-24 | 41.0 | 1.43 | 32.47 | 4.91 | PC3809-26 | 257.0 | 4.17 | 0.97 | 16.56 |
| BC3802-25 | 43.0 | 1.45 | 31.64 | 5.23 | PC3809-27 | 267.0 | 2.34 | 1.21 | 9.91 |
| BC3802-26 | 45.0 | 1.57 | 31.28 | 5.21 | PC3809-28 | 273.0 | 1.62 | 5.62 | 4.02 |
| BC3802-27 | 47.0 | 1.70 | 31.10 | 4.82 | PC3809-29 | 284.0 | 5.16 | 1.41 | 13.58 |
| BC3802-28 | 49.0 | 1.69 | 31.18 | 4.63 | PC3809-30 | 294.0 | 5.37 | 2.48 | 18.74 |
| BC3802-29 | 51.0 | 1.54 | 30.75 | 4.86 | PC3809-31 | 304.0 | 4.63 | 0.72 | 16.56 |
| BC3802-30 | 53.0 | 1.76 | 30.37 | 4.71 | PC3809-32 | 314.0 | 5.75 | 1.46 | 14.31 |
| | | | | | PC3809-33 | 324.0 | 5.71 | 0.95 | 13.66 |
| BC38-03 | 4289m | | | | PC3809-34 | 335.0 | 6.08 | 1.17 | 17.70 |
| | | | | | PC3809-35 | 344.0 | 6.43 | 1.11 | 21.08 |
| BC3803-01 | 0.5 | 1.72 | 0.04 | 17.86 | PC3809-36 | 355.0 | 5.85 | 3.34 | 22.09 |
| BC3803-02 | 1.5 | 1.89 | 0.04 | 16.05 | PC3809-37 | 364.0 | 5.67 | 6.40 | 24.81 |
| BC3803-03 | 2.5 | 2.10 | 0.04 | 16.60 | PC3809-38 | 375.0 | 6.19 | 1.94 | 15.87 |
| BC3803-04 | 3.5 | 1.97 | 0.09 | 16.59 | PC3809-39 | 384.0 | 5.07 | 3.73 | 16.74 |
| BC3803-05 | 4.5 | 1.98 | 0.01 | 16.99 | PC3809-40 | 394.0 | 5.74 | 2.42 | 22.87 |
| BC3803-06 | 5.5 | 2.48 | 0.03 | 17.18 | PC3809-41 | 404.0 | 4.68 | 0.70 | 20.73 |
| BC3803-07 | 6.5 | 2.03 | 0.07 | 16.50 | PC3809-42 | 416.0 | 5.89 | 6.12 | 22.02 |
| BC3803-08 | 7.5 | 1.76 | 0.05 | 15.48 | PC3809-43 | 424.0 | 5.54 | 0.98 | 23.72 |
| BC3803-09 | 8.5 | 1.85 | 0.08 | 15.76 | PC3809-44 | 434.0 | 6.55 | 0.74 | 16.99 |
| BC3803-10 | 9.5 | 1.74 | 0.00 | 15.79 | PC3809-45 | 444.0 | 4.66 | 4.00 | 24.07 |
| BC3803-11 | 11.0 | 1.52 | 0.06 | 14.76 | PC3809-46 | 453.0 | 4.71 | 1.44 | 16.83 |
| BC3803-12 | 13.0 | 1.66 | 0.12 | 14.89 | PC3809-47 | 465.0 | 5.52 | 2.47 | 19.07 |
| BC3803-13 | 15.0 | 1.46 | 0.18 | 14.65 | PC3809-48 | 474.0 | 5.89 | 4.75 | 18.07 |
| BC3803-14 | 17.0 | 1.62 | 0.22 | 13.84 | PC3809-49 | 483.0 | 4.56 | 0.93 | 18.07 |
| BC3803-15 | 19.0 | 1.81 | 0.31 | 13.70 | PC3809-50 | 493.0 | 5.07 | 1.55 | 17.96 |
| BC3803-16 | 21.0 | 1.82 | 0.31 | 16.08 | PC3809-51 | 504.0 | 4.18 | 1.30 | 11.53 |
| BC3803-17 | 23.0 | 1.99 | 0.30 | 16.83 | PC3809-52 | 515.0 | 4.78 | 1.10 | 11.24 |
| BC3803-18 | 25.0 | 1.93 | 0.37 | 15.97 | PC3809-53 | 525.0 | 6.00 | 3.39 | 13.81 |
| BC3803-19 | 27.0 | 1.89 | 0.45 | 15.74 | PC3809-54 | 536.0 | 5.22 | 5.40 | 17.24 |
| BC3803-20 | 29.0 | 1.80 | 0.47 | 14.06 | PC3809-55 | 544.0 | 4.08 | 2.64 | 11.98 |
| BC3803-21 | 31.0 | 1.67 | 0.52 | 13.58 | PC3809-56 | 553.0 | 3.62 | 4.58 | 13.28 |
| BC3803-22 | 33.0 | 1.71 | 0.54 | 13.74 | PC3809-57 | 564.0 | 3.41 | 4.44 | 18.01 |
| BC3803-23 | 35.0 | 1.75 | 0.62 | 14.22 | PC3809-58 | 574.0 | 3.45 | 4.91 | 13.57 |
| BC3803-24 | 37.0 | 1.79 | 0.70 | 13.46 | PC3809-59 | 585.0 | 2.88 | 5.75 | 16.18 |
| BC3803-25 | 39.0 | 1.54 | 0.84 | 14.47 | PC3809-60 | 594.0 | 3.18 | 4.70 | 15.64 |
| BC3803-26 | 41.0 | 1.46 | 0.77 | 12.72 | PC3809-61 | 605.0 | 3.31 | 5.19 | 12.94 |
| BC3803-27 | 43.0 | 1.55 | 0.81 | 12.80 | PC3809-62 | 615.0 | 3.43 | 4.71 | 18.09 |
| BC3803-28 | 45.0 | 1.49 | 0.81 | 13.29 | PC3809-63 | 625.0 | 3.04 | 4.39 | 13.61 |
| BC3803-29 | 47.0 | 1.63 | 0.82 | 13.28 | PC3809-64 | 635.0 | 3.44 | 5.04 | 13.44 |
| BC3803-30 | 49.0 | 1.48 | 0.82 | 12.43 | PC3809-65 | 646.0 | 3.47 | 4.18 | 18.91 |
| BC3803-31 | 51.0 | 1.52 | 0.86 | 12.34 | PC3809-66 | 654.0 | 2.91 | 3.81 | 21.65 |
| BC3803-32 | 53.0 | 1.65 | 0.94 | 11.97 | PC3809-67 | 664.0 | 3.14 | 4.36 | 20.96 |

APPENDIX C.12. BIOGENIC COMPONENTS

| PC38-09 Sample | 148m Depth (cm) | Corg (wt.%) | CaCO3 (wt.%) | Bio.SiO2 (wt.%) |
|---|---|---|---|---|
| PC3809-68 | 674.0 | 2.47 | 3.61 | 23.48 |
| PC3809-69 | 684.0 | 3.33 | 4.22 | 15.36 |
| PC3809-70 | 694.0 | 3.42 | 4.28 | 15.20 |
| PC3809-71 | 703.0 | 3.39 | 4.04 | 14.59 |
| PC3809-72 | 714.0 | 3.97 | 4.84 | 17.77 |
| PC3809-73 | 724.0 | 3.11 | 4.45 | 13.49 |
| PC3809-74 | 734.0 | 3.42 | 5.15 | 12.90 |
| PC3809-75 | 744.0 | 3.32 | 4.68 | 15.32 |
| PC3809-76 | 754.0 | 3.28 | 4.81 | 15.64 |
| PC3809-77 | 764.0 | 2.83 | 5.74 | 12.74 |
| PC3809-78 | 774.0 | 2.96 | 5.16 | 11.52 |
| PC3809-79 | 784.0 | 2.71 | 5.07 | 12.59 |
| PC3809-80 | 794.0 | 2.86 | 5.01 | 12.99 |
| PC3809-81 | 804.0 | 3.09 | 3.96 | 12.36 |
| PC3809-82 | 813.0 | 2.64 | 4.96 | 13.56 |
| PC3809-83 | 823.0 | 2.99 | 3.98 | 12.22 |
| PC3809-84 | 834.0 | 3.08 | 4.04 | 12.33 |
| PC3809-85 | 845.0 | 3.05 | 3.86 | 14.75 |
| PC3809-86 | 854.0 | 2.32 | 3.42 | 11.60 |
| | | | | |
| PC38-10 | 257m | | | |
| | | | | |
| PC3810-01 | 6.0 | 9.21 | 10.58 | 9.38 |
| PC3810-02 | 14.0 | 5.04 | 4.23 | 3.47 |
| PC3810-03 | 24.0 | 1.75 | 1.14 | 1.14 |
| PC3810-04 | 34.0 | 2.04 | 6.83 | 2.23 |
| PC3810-05 | 44.0 | 6.84 | 0.29 | 5.56 |
| PC3810-06 | 54.0 | 6.90 | 0.11 | 8.84 |
| PC3810-07 | 64.0 | 4.08 | 0.08 | 8.86 |
| PC3810-08 | 74.0 | 3.04 | 0.19 | 4.26 |
| PC3810-09 | 84.0 | 0.88 | 0.94 | 1.11 |
| PC3810-10 | 94.0 | 0.87 | 1.54 | 0.48 |
| PC3810-10 | 104.0 | 1.05 | 9.06 | 0.99 |
| PC3810-11 | 113.0 | 0.79 | 9.19 | 0.84 |
| PC3810-12 | 126.0 | 3.90 | 9.92 | 16.01 |
| PC3810-13 | 134.0 | 5.39 | 4.84 | 18.54 |
| PC3810-14 | 146.0 | 4.26 | 4.65 | 12.42 |
| PC3810-15 | 154.0 | 4.80 | 11.32 | 13.56 |
| PC3810-16 | 167.0 | 4.70 | 4.42 | 15.60 |
| PC3810-17 | 174.0 | 5.32 | 0.33 | 16.45 |
| PC3810-18 | 185.0 | 4.59 | 0.00 | 17.23 |
| PC3810-19 | 194.0 | 5.47 | 6.89 | 20.10 |
| PC3810-20 | 203.0 | 4.21 | 0.72 | 13.41 |
| PC3810-21 | 216.0 | 5.75 | 7.00 | 19.94 |
| PC3810-22 | 224.0 | 6.30 | 3.70 | 19.04 |
| PC3810-23 | 233.0 | 6.23 | 2.33 | 17.41 |
| PC3810-24 | 244.0 | 5.09 | 6.40 | 13.00 |
| PC3810-25 | 254.0 | 3.95 | 5.76 | 9.92 |
| PC3810-26 | 263.0 | 4.56 | 7.79 | 12.12 |
| PC3810-27 | 273.0 | 5.38 | 7.24 | 11.56 |
| PC3810-28 | 284.0 | 4.52 | 10.27 | 11.79 |
| PC3810-29 | 295.0 | 5.89 | 19.61 | 14.90 |
| PC3810-30 | 305.0 | 5.11 | 10.98 | 12.68 |
| PC3810-31 | 314.0 | 4.64 | 10.57 | 9.59 |
| PC3810-32 | 324.0 | 6.57 | 12.88 | 16.70 |
| PC3810-33 | 335.0 | 5.90 | 8.84 | 10.22 |
| PC3810-34 | 344.0 | 6.42 | 14.58 | 18.27 |
| PC3810-35 | 354.0 | 6.22 | 7.80 | 21.73 |
| PC3810-36 | 364.0 | 5.78 | 10.77 | 28.61 |
| PC3810-37 | 374.0 | 6.05 | 7.68 | 27.10 |
| PC3810-38 | 383.0 | 4.95 | 7.96 | 14.65 |
| PC3810-39 | 394.0 | 7.06 | 6.82 | 17.96 |
| PC3810-40 | 404.0 | 5.22 | 8.27 | 14.48 |
| PC3810-41 | 417.0 | 5.94 | 14.85 | 14.50 |
| PC3810-42 | 424.0 | 6.39 | 10.47 | 17.92 |
| PC3810-43 | 434.0 | 4.93 | 25.71 | 23.97 |
| PC3810-44 | 445.0 | 5.75 | 18.06 | 19.90 |

| PC38-10 Sample | 257m Depth (cm) | Corg (wt.%) | CaCO3 (wt.%) | Bio.SiO2 (wt.%) |
|---|---|---|---|---|
| PC3810-45 | 456.0 | 6.30 | 15.89 | 20.51 |
| PC3810-46 | 467.0 | 5.95 | 17.38 | 28.42 |
| PC3810-47 | 476.0 | 6.55 | 16.03 | 10.94 |
| PC3810-48 | 484.0 | 6.80 | 17.92 | 11.57 |
| PC3810-49 | 494.0 | 6.47 | 15.66 | 8.85 |
| PC3810-50 | 504.0 | 2.01 | 0.97 | 1.99 |
| PC3810-51 | 514.0 | 3.94 | 3.14 | 12.98 |
| PC3810-52 | 524.0 | 3.16 | 2.17 | 11.68 |
| PC3810-53 | 534.0 | 11.92 | 8.97 | 10.70 |
| PC3810-54 | 545.0 | 9.85 | 6.47 | 15.28 |
| PC3810-55 | 554.0 | 10.65 | 10.83 | 14.56 |
| PC3810-56 | 564.0 | 6.27 | 16.01 | 20.77 |
| PC3810-57 | 574.0 | 6.85 | 18.47 | 13.13 |
| PC3810-58 | 584.0 | 6.96 | 15.91 | 16.47 |
| PC3810-59 | 596.0 | 7.37 | 13.67 | 17.34 |
| PC3810-60 | 604.0 | 7.38 | 17.25 | 16.77 |
| PC3810-61 | 614.0 | 7.10 | 11.65 | 17.42 |
| PC3810-62 | 624.0 | 6.28 | 13.47 | 13.21 |
| PC3810-63 | 634.0 | 6.34 | 13.46 | 14.76 |
| PC3810-64 | 645.0 | 6.47 | 10.13 | 17.54 |
| PC3810-65 | 655.0 | 7.46 | 11.81 | 16.04 |
| PC3810-66 | 667.0 | 6.58 | 10.66 | 13.61 |
| PC3810-67 | 674.0 | 6.39 | 6.94 | 13.32 |
| PC3810-68 | 683.0 | 6.29 | 9.21 | 15.09 |
| PC3810-69 | 694.0 | 4.63 | 4.05 | 11.44 |
| PC3810-70 | 704.0 | 4.48 | 0.15 | 8.73 |
| PC3810-71 | 714.0 | 4.85 | 5.47 | 11.85 |
| PC3810-72 | 724.0 | 5.03 | 7.87 | 13.95 |
| PC3810-74 | 734.0 | 3.98 | 0.00 | 12.61 |
| PC3810-75 | 745.0 | 2.97 | 0.00 | 7.74 |
| PC3810-76 | 754.0 | 4.10 | 0.23 | 15.25 |
| PC3810-77 | 764.0 | 2.46 | 0.00 | 6.62 |
| | | | | |
| PC38-02 | 2525m (Age) | | | |
| PC3802-01 | 2.76 | 1.49 | 16.84 | 9.54 |
| PC3802-02 | 6.21 | 1.33 | 24.93 | 8.44 |
| PC3802-03 | 9.66 | 1.31 | 27.60 | 7.30 |
| PC3802-04 | 12.77 | 2.67 | 22.24 | 7.12 |
| PC3802-05 | 15.18 | 1.86 | 27.11 | 5.96 |
| PC3802-06 | 17.47 | 1.95 | 26.27 | 6.36 |
| PC3802-07 | 20.48 | 1.92 | 26.27 | 5.54 |
| PC3802-08 | 22.65 | 1.86 | 25.41 | 5.30 |
| PC3802-09 | 25.22 | 2.04 | 29.64 | 5.35 |
| PC3802-10 | 28.29 | 2.08 | 32.87 | 6.05 |
| PC3802-11 | 31.07 | 1.60 | 33.53 | 7.26 |
| PC3802-12 | 33.86 | 1.89 | 35.90 | 8.03 |
| PC3802-13 | 36.64 | 1.94 | 32.99 | 6.60 |
| PC3802-14 | 39.15 | 1.79 | 26.13 | 5.84 |
| PC3802-15 | 42.22 | 2.32 | 24.69 | 7.13 |
| PC3802-16 | 45.00 | 1.59 | 21.91 | 4.41 |
| PC3802-17 | 48.07 | 1.81 | 18.38 | 5.78 |
| PC3802-18 | 50.85 | 1.62 | 15.62 | 8.56 |
| PC3802-19 | 53.64 | 1.82 | 17.38 | 8.29 |
| PC3802-20 | 56.42 | 2.04 | 14.17 | 7.59 |
| PC3802-21 | 59.29 | 2.14 | 16.52 | 6.48 |
| PC3802-22 | 62.61 | 1.78 | 17.93 | 5.92 |
| PC3802-23 | 65.94 | 1.49 | 15.14 | 5.93 |
| PC3802-24 | 69.26 | 1.63 | 4.56 | 6.90 |
| PC3802-25 | 72.58 | 1.96 | 9.29 | 7.61 |
| PC3802-26 | 76.96 | 1.55 | 16.55 | 7.89 |
| PC3802-27 | 82.03 | 2.17 | 5.46 | 8.61 |
| PC3802-28 | 87.11 | 1.69 | 6.75 | 6.66 |
| PC3802-29 | 92.18 | 1.71 | 0.60 | 7.82 |
| PC3802-30 | 97.26 | 1.29 | 2.99 | 7.97 |
| PC3802-31 | 102.84 | 1.59 | 9.77 | 9.22 |
| PC3802-32 | 107.92 | 1.46 | 9.26 | 8.63 |

APPENDIX C.12. BIOGENIC COMPONENTS

| PC38-02 Sample | 2525m Age (ka) | Corg (wt.%) | CaCO3 (wt.%) | Bio.SiO2 (wt.%) | PC38-11 Sample | 3835m Age (ka) | Corg (wt.%) | CaCO3 (wt.%) | Bio.SiO2 (wt.%) |
|---|---|---|---|---|---|---|---|---|---|
| PC3802-33 | 113.00 | 1.36 | 9.20 | 9.26 | PC3811-23 | 45.03 | 4.22 | 10.42 | 10.28 |
| PC3802-34 | 118.07 | 1.04 | 9.53 | 8.80 | PC3811-24 | 47.02 | 4.55 | 9.16 | 10.52 |
| PC3802-35 | 123.15 | 1.29 | 19.21 | 9.83 | PC3811-25 | 49.01 | 4.34 | 9.97 | 10.66 |
| PC3802-36 | 128.22 | 1.40 | 25.48 | 8.24 | PC3811-26 | 51.00 | 3.90 | 14.50 | 13.04 |
| PC3802-37 | 132.23 | 1.25 | 28.29 | 5.34 | PC3811-27 | 52.99 | 3.94 | 12.47 | 13.74 |
| PC3802-38 | 135.30 | 1.04 | 30.10 | 4.90 | PC3811-28 | 54.99 | 3.60 | 9.89 | 13.25 |
| PC3802-39 | 138.71 | 1.15 | 30.53 | 6.43 | PC3811-29 | 56.98 | 3.76 | 2.11 | 8.62 |
| PC3802-40 | 141.79 | 1.20 | 33.37 | 6.23 | PC3811-30 | 59.62 | 3.24 | 3.89 | 8.43 |
| PC3802-41 | 145.20 | 1.16 | 32.55 | 6.01 | PC3811-31 | 62.28 | 2.87 | 1.10 | 8.47 |
| PC3802-42 | 148.61 | 1.03 | 31.11 | 6.96 | PC3811-32 | 65.60 | 3.04 | 1.21 | 6.99 |
| PC3802-43 | 152.02 | 1.11 | 33.36 | 5.56 | PC3811-33 | 68.93 | 3.16 | 20.92 | 3.47 |
| PC3802-44 | 155.44 | 1.09 | 30.93 | 5.56 | PC3811-34 | 72.25 | 3.58 | 2.12 | 12.67 |
| PC3802-45 | 158.85 | 1.17 | 25.00 | 4.91 | PC3811-35 | 74.95 | 3.79 | 2.78 | 13.92 |
| PC3802-46 | 162.26 | 1.28 | 21.59 | 5.05 | PC3811-36 | 77.04 | 3.51 | 2.52 | 16.76 |
| PC3802-47 | 165.68 | 1.45 | 33.68 | 4.15 | PC3811-37 | 79.12 | 4.09 | 2.23 | 13.78 |
| PC3802-48 | 169.43 | 1.41 | 35.14 | 4.58 | PC3811-38 | 81.20 | 4.25 | 3.24 | 12.02 |
| PC3802-49 | 172.84 | 1.61 | 34.35 | 4.72 | PC3811-39 | 83.29 | 3.94 | 3.25 | 9.07 |
| PC3802-50 | 176.26 | 1.69 | 31.64 | 4.72 | PC3811-40 | 85.37 | 3.41 | 4.01 | 8.84 |
| PC3802-51 | 179.67 | 1.41 | 27.40 | 5.54 | PC3811-41 | 87.45 | 3.66 | 4.05 | 8.75 |
| PC3802-52 | 183.08 | 1.33 | 20.77 | 4.66 | PC3811-42 | 89.54 | 2.96 | 0.17 | 10.29 |
| PC3802-53 | 186.50 | 0.82 | 14.81 | 4.72 | PC3811-43 | 91.62 | 3.05 | 1.82 | 12.07 |
| PC3802-54 | 189.57 | 1.40 | 9.27 | 5.47 | PC3811-44 | 93.70 | 3.06 | 6.63 | 13.85 |
| PC3802-55 | 193.52 | 1.50 | 8.18 | 6.16 | PC3811-45 | 95.79 | 3.16 | 4.28 | 15.01 |
| PC3802-56 | 197.42 | 1.79 | 5.41 | 8.62 | PC3811-46 | 97.87 | 3.22 | 0.31 | 10.00 |
| PC3802-57 | 202.11 | 1.26 | 13.77 | 7.52 | PC3811-47 | 99.95 | 3.14 | 0.06 | 9.44 |
| PC3802-58 | 206.02 | 1.41 | 14.71 | 5.62 | PC3811-48 | 102.04 | 3.17 | 2.97 | 11.99 |
| PC3802-59 | 209.53 | 1.15 | 16.44 | 4.62 | PC3811-49 | 104.12 | 2.67 | 0.23 | 12.03 |
| PC3802-60 | 213.44 | 1.11 | 35.65 | 4.14 | PC3811-50 | 106.20 | 2.28 | 0.22 | 14.66 |
| PC3802-61 | 217.34 | 0.96 | 37.54 | 4.01 | PC3811-51 | 108.29 | 2.66 | 0.08 | 14.56 |
| PC3802-62 | 221.25 | 1.06 | 31.04 | 4.44 | PC3811-52 | 110.37 | 2.51 | 0.18 | 14.03 |
| PC3802-63 | 225.16 | 1.15 | 28.95 | 3.52 | PC3811-53 | 112.45 | 2.29 | 0.00 | 16.43 |
| PC3802-64 | 229.06 | 1.16 | 23.30 | 4.50 | PC3811-54 | 114.54 | 2.37 | 0.42 | 14.39 |
| PC3802-65 | 232.97 | 1.14 | 14.49 | 5.17 | PC3811-55 | 116.62 | 2.33 | 0.90 | 17.83 |
| PC3802-66 | 237.27 | 1.18 | 16.37 | 6.87 | PC3811-56 | 118.70 | 2.08 | 0.35 | 18.09 |
| PC3802-67 | 240.78 | 1.26 | 32.34 | 6.29 | PC3811-57 | 120.79 | 2.31 | 0.89 | 17.09 |
| PC3802-68 | 244.50 | 1.16 | 29.66 | 4.18 | | | | | |
| PC3802-69 | 247.71 | 1.27 | 25.19 | 3.78 | | | | | |
| PC3802-70 | 250.91 | 1.28 | 27.16 | 4.79 | | | | | |
| PC3802-71 | 254.12 | 0.82 | 27.81 | 4.33 | | | | | |
| PC3802-72 | 257.32 | 1.23 | 25.97 | 5.72 | | | | | |
| PC3802-73 | 260.53 | 1.24 | 25.98 | 6.27 | | | | | |
| PC3802-74 | 263.73 | 1.55 | 24.38 | 6.44 | | | | | |
| | | | | | | | | | |
| PC38-11 | 3835m | | | | | | | | |
| | | | | | | | | | |
| PC3811-01 | 0.80 | 3.87 | 2.19 | 7.99 | | | | | |
| PC3811-02 | 2.00 | 4.27 | 12.82 | 4.85 | | | | | |
| PC3811-03 | 2.20 | 3.30 | 10.70 | 3.46 | | | | | |
| PC3811-04 | 3.49 | 2.97 | 1.06 | 9.34 | | | | | |
| PC3811-05 | 6.17 | 3.28 | 3.26 | 9.32 | | | | | |
| PC3811-06 | 8.85 | 3.59 | 4.78 | 8.48 | | | | | |
| PC3811-07 | 11.53 | 3.63 | 5.14 | 8.57 | | | | | |
| PC3811-08 | 13.80 | 3.30 | 6.50 | 7.30 | | | | | |
| PC3811-09 | 16.44 | 1.62 | 10.55 | 3.69 | | | | | |
| PC3811-10 | 18.63 | 3.33 | 9.24 | 8.43 | | | | | |
| PC3811-11 | 20.82 | 3.39 | 10.50 | 8.68 | | | | | |
| PC3811-12 | 23.23 | 3.56 | 7.93 | 9.52 | | | | | |
| PC3811-13 | 25.11 | 3.44 | 8.13 | 9.20 | | | | | |
| PC3811-14 | 27.10 | 3.26 | 9.40 | 7.76 | | | | | |
| PC3811-15 | 29.09 | 3.40 | 7.88 | 8.67 | | | | | |
| PC3811-16 | 31.08 | 2.97 | 11.29 | 7.60 | | | | | |
| PC3811-17 | 33.07 | 3.15 | 9.05 | 8.55 | | | | | |
| PC3811-18 | 35.07 | 2.55 | 11.27 | 6.54 | | | | | |
| PC3811-19 | 37.26 | 3.77 | 6.51 | 10.12 | | | | | |
| PC3811-20 | 39.45 | 4.04 | 5.66 | 10.50 | | | | | |
| PC3811-21 | 40.84 | 4.03 | 3.65 | 11.25 | | | | | |
| PC3811-22 | 43.03 | 3.70 | 12.12 | 8.67 | | | | | |

APPENDIX C.13. PARTITIONED P, U, Y and Sr CONCENTRATIONS

| CD38-09 | (148m) | | | | | | | | | | | | | | | | |
|---|---|---|---|---|---|---|---|---|---|---|---|---|---|---|---|---|---|
| Sample | Depth | P | Pterr | Porg | Pphos | Phos | U | Uterr | Uphos | Uorg | Y | Yphos | Yterr | Sr | Srphos | Srterr | Srcal |
| | (cm) | (wt.%) | (wt.%) | (wt.%) | (wt.%) | (wt.%) | (ppm) | (ppm) | (ppm) | (ppm) | (ppm) | (ppm) | (ppm) | (ppm) | (ppm) | (ppm) | (ppm) |
| | | | | | (non -ve) | | | | (non -ve) | | | | | | | | |
| PC3809-01 | 4.0 | 0.240 | 0.051 | 0.036 | 0.153 | 1.85 | 10 | 3 | 2 | 5 | 17 | 2 | 15 | 199 | 28 | 126 | 44 |
| PC3809-02 | 13.0 | 0.176 | 0.052 | 0.035 | 0.089 | 1.07 | 10 | 3 | 1 | 6 | 16 | 1 | 15 | 195 | 17 | 127 | 52 |
| PC3809-03 | 23.0 | 0.201 | 0.066 | 0.032 | 0.103 | 1.24 | 10 | 3 | 1 | 5 | 19 | 1 | 18 | 194 | 19 | 162 | 13 |
| PC3809-04 | 34.0 | 0.199 | 0.061 | 0.033 | 0.106 | 1.28 | 9 | 3 | 1 | 5 | 18 | 1 | 17 | 179 | 20 | 149 | 11 |
| PC3809-05 | 43.0 | 0.250 | 0.061 | 0.019 | 0.169 | 2.04 | 8 | 3 | 2 | 3 | 23 | 2 | 21 | 240 | 32 | 150 | 59 |
| PC3809-06 | 53.0 | 0.272 | 0.056 | 0.031 | 0.184 | 2.22 | 6 | 3 | 3 | 0 | 17 | 2 | 15 | 175 | 34 | 138 | 3 |
| PC3809-07 | 62.0 | 0.231 | 0.052 | 0.044 | 0.136 | 1.64 | 10 | 3 | 2 | 5 | 15 | 2 | 14 | 195 | 25 | 126 | 43 |
| PC3809-08 | 73.0 | 0.208 | 0.062 | 0.029 | 0.117 | 1.42 | 9 | 3 | 2 | 4 | 22 | 1 | 20 | 188 | 22 | 151 | 15 |
| PC3809-09 | 84.0 | 0.165 | 0.071 | 0.031 | 0.064 | 0.77 | 7 | 4 | 1 | 3 | 21 | 1 | 21 | 168 | 12 | 173 | 0 |
| PC3809-10 | 94.0 | 0.174 | 0.066 | 0.035 | 0.073 | 0.88 | 8 | 3 | 1 | 3 | 18 | 1 | 17 | 170 | 14 | 161 | 0 |
| PC3809-11 | 104.0 | 0.158 | 0.059 | 0.037 | 0.062 | 0.75 | 10 | 3 | 1 | 6 | 16 | 1 | 16 | 151 | 12 | 145 | 0 |
| PC3809-12 | 113.0 | 0.161 | 0.073 | 0.026 | 0.063 | 0.76 | 9 | 4 | 1 | 4 | 22 | 1 | 21 | 166 | 12 | 178 | 0 |
| PC3809-13 | 124.0 | 0.239 | 0.064 | 0.027 | 0.148 | 1.78 | 10 | 3 | 2 | 4 | 22 | 2 | 20 | 214 | 28 | 157 | 30 |
| PC3809-14 | 134.0 | 0.296 | 0.056 | 0.032 | 0.208 | 2.51 | 9 | 3 | 3 | 3 | 18 | 3 | 16 | 213 | 39 | 138 | 36 |
| PC3809-15 | 144.0 | 0.203 | 0.050 | 0.034 | 0.119 | 1.44 | 8 | 3 | 2 | 4 | 16 | 1 | 15 | 183 | 22 | 122 | 39 |
| PC3809-16 | 152.0 | 0.147 | 0.050 | 0.027 | 0.071 | 0.85 | 7 | 3 | 1 | 4 | 15 | 1 | 14 | 180 | 13 | 122 | 45 |
| PC3809-17 | 165.0 | 0.241 | 0.048 | 0.026 | 0.167 | 2.01 | 10 | 3 | 2 | 5 | 17 | 2 | 15 | 220 | 31 | 118 | 71 |
| PC3809-18 | 174.0 | 0.267 | 0.059 | 0.018 | 0.191 | 2.30 | 9 | 3 | 3 | 3 | 22 | 2 | 20 | 243 | 35 | 143 | 64 |
| PC3809-19 | 185.0 | 0.427 | 0.052 | 0.017 | 0.358 | 4.32 | 11 | 3 | 5 | 3 | 21 | 4 | 17 | 289 | 67 | 128 | 94 |
| PC3809-20 | 194.0 | 0.409 | 0.053 | 0.016 | 0.340 | 4.10 | 8 | 3 | 5 | 0 | 24 | 4 | 20 | 306 | 63 | 131 | 112 |
| PC3809-21 | 205.0 | 0.155 | 0.059 | 0.011 | 0.084 | 1.02 | 5 | 3 | 1 | 1 | 22 | 1 | 21 | 256 | 16 | 145 | 95 |
| PC3809-22 | 214.0 | 0.398 | 0.049 | 0.030 | 0.319 | 3.85 | 13 | 3 | 4 | 6 | 19 | 4 | 15 | 256 | 59 | 121 | 76 |
| PC3809-23 | 224.0 | 0.494 | 0.052 | 0.008 | 0.433 | 5.23 | 11 | 3 | 6 | 2 | 23 | 5 | 18 | 347 | 81 | 128 | 138 |
| PC3809-24 | 234.0 | 0.592 | 0.047 | 0.013 | 0.532 | 6.42 | 9 | 2 | 8 | 0 | 20 | 6 | 13 | 305 | 99 | 115 | 91 |
| PC3809-25 | 243.0 | 0.347 | 0.038 | 0.025 | 0.284 | 3.43 | 10 | 2 | 4 | 4 | 13 | 3 | 10 | 185 | 53 | 93 | 39 |
| PC3809-26 | 257.0 | 0.301 | 0.045 | 0.022 | 0.234 | 2.82 | 10 | 2 | 3 | 5 | 17 | 3 | 14 | 201 | 44 | 110 | 48 |
| PC3809-27 | 267.0 | 1.036 | 0.045 | 0.012 | 0.979 | 11.81 | 15 | 2 | 14 | 0 | 25 | 12 | 13 | 374 | 182 | 109 | 82 |
| PC3809-28 | 273.0 | 5.797 | 0.023 | 0.009 | 5.766 | 69.55 | 148 | 1 | 81 | 65 | 25 | 70 | -45 | 1195 | 1072 | 55 | 67 |
| PC3809-29 | 284.0 | 0.314 | 0.053 | 0.027 | 0.234 | 2.82 | 13 | 3 | 3 | 7 | 20 | 3 | 17 | 202 | 44 | 129 | 29 |
| PC3809-30 | 294.0 | 0.165 | 0.042 | 0.028 | 0.094 | 1.14 | 7 | 2 | 1 | 4 | 15 | 1 | 14 | 170 | 18 | 104 | 49 |
| PC3809-31 | 304.0 | 0.168 | 0.054 | 0.025 | 0.089 | 1.08 | 8 | 3 | 1 | 4 | 18 | 1 | 17 | 171 | 17 | 133 | 22 |
| PC3809-32 | 314.0 | 0.140 | 0.053 | 0.030 | 0.056 | 0.68 | 7 | 3 | 1 | 4 | 17 | 1 | 16 | 162 | 10 | 130 | 22 |

APPENDIX C.13. PARTITIONED P, U, Y and Sr CONCENTRATIONS

| CD38-09 Sample | (148m) Depth (cm) | P (wt.%) | Pterr (wt.%) | Porg (wt.%) | Pphos (wt.%) | Phos (wt.%) | U (ppm) | Uterr (ppm) | Uphos (ppm) | Uorg (ppm) | Y (ppm) | Yphos (ppm) | Yterr (ppm) | Sr (ppm) | Srphos (ppm) | Srterr (ppm) | Srcal (ppm) |
|---|---|---|---|---|---|---|---|---|---|---|---|---|---|---|---|---|---|
| | | | | (non -ve) | | | | | (non -ve) | | | | | | | | |
| PC3809-33 | 324.0 | 0.222 | 0.055 | 0.030 | 0.137 | 1.65 | 8 | 3 | 2 | 3 | 21 | 2 | 19 | 187 | 25 | 135 | 26 |
| PC3809-34 | 335.0 | 0.160 | 0.048 | 0.032 | 0.080 | 0.97 | 8 | 3 | 1 | 5 | 17 | 1 | 16 | 163 | 15 | 116 | 31 |
| PC3809-35 | 344.0 | 0.160 | 0.043 | 0.034 | 0.083 | 1.00 | 7 | 2 | 1 | 3 | 15 | 1 | 14 | 153 | 15 | 106 | 31 |
| PC3809-36 | 355.0 | 0.105 | 0.037 | 0.031 | 0.037 | 0.45 | 5 | 2 | 1 | 3 | 11 | 0 | 11 | 156 | 7 | 90 | 59 |
| PC3809-37 | 364.0 | 0.102 | 0.036 | 0.030 | 0.036 | 0.43 | 5 | 2 | 1 | 3 | 11 | 0 | 11 | 185 | 7 | 88 | 90 |
| PC3809-38 | 375.0 | 0.112 | 0.049 | 0.033 | 0.030 | 0.37 | 7 | 3 | 0 | 4 | 15 | 0 | 15 | 162 | 6 | 119 | 37 |
| PC3809-39 | 384.0 | 0.211 | 0.051 | 0.027 | 0.133 | 1.60 | 8 | 3 | 2 | 4 | 19 | 2 | 17 | 214 | 25 | 126 | 63 |
| PC3809-40 | 394.0 | 0.159 | 0.044 | 0.030 | 0.084 | 1.02 | 8 | 2 | 1 | 4 | 15 | 1 | 14 | 179 | 16 | 108 | 54 |
| PC3809-41 | 404.0 | 0.122 | 0.049 | 0.025 | 0.048 | 0.58 | 8 | 3 | 1 | 4 | 16 | 1 | 15 | 156 | 9 | 120 | 26 |
| PC3809-42 | 416.0 | 0.145 | 0.042 | 0.031 | 0.072 | 0.87 | 9 | 2 | 1 | 6 | 14 | 1 | 13 | 202 | 13 | 103 | 86 |
| PC3809-43 | 424.0 | 0.101 | 0.046 | 0.029 | 0.026 | 0.31 | 8 | 2 | 0 | 5 | 14 | 0 | 14 | 149 | 5 | 112 | 32 |
| PC3809-44 | 434.0 | 0.127 | 0.052 | 0.035 | 0.040 | 0.49 | 10 | 3 | 1 | 6 | 16 | 0 | 15 | 165 | 7 | 127 | 30 |
| PC3809-45 | 444.0 | 0.140 | 0.043 | 0.025 | 0.072 | 0.87 | 8 | 2 | 1 | 4 | 14 | 1 | 13 | 186 | 13 | 105 | 67 |
| PC3809-46 | 453.0 | 0.167 | 0.052 | 0.025 | 0.090 | 1.08 | 8 | 3 | 1 | 4 | 18 | 1 | 17 | 179 | 17 | 128 | 34 |
| PC3809-47 | 465.0 | 0.163 | 0.049 | 0.029 | 0.084 | 1.02 | 7 | 3 | 1 | 3 | 16 | 1 | 15 | 183 | 16 | 121 | 47 |
| PC3809-48 | 474.0 | 0.145 | 0.046 | 0.031 | 0.067 | 0.81 | 9 | 2 | 1 | 6 | 14 | 1 | 13 | 201 | 13 | 113 | 75 |
| PC3809-49 | 483.0 | 0.176 | 0.051 | 0.024 | 0.101 | 1.22 | 9 | 3 | 1 | 4 | 18 | 1 | 17 | 178 | 19 | 124 | 35 |
| PC3809-50 | 493.0 | 0.155 | 0.050 | 0.027 | 0.078 | 0.94 | 8 | 3 | 1 | 4 | 16 | 1 | 15 | 276 | 14 | 123 | 138 |
| PC3809-51 | 504.0 | 0.182 | 0.053 | 0.022 | 0.107 | 1.29 | 9 | 3 | 2 | 5 | 21 | 1 | 20 | 193 | 20 | 129 | 44 |
| PC3809-52 | 515.0 | 0.145 | 0.053 | 0.025 | 0.067 | 0.81 | 8 | 3 | 1 | 4 | 18 | 1 | 17 | 182 | 12 | 129 | 40 |
| PC3809-53 | 525.0 | 0.118 | 0.049 | 0.032 | 0.037 | 0.44 | 7 | 3 | 1 | 4 | 15 | 0 | 14 | 194 | 7 | 121 | 66 |
| PC3809-54 | 536.0 | 0.115 | 0.045 | 0.028 | 0.042 | 0.51 | 5 | 2 | 1 | 2 | 14 | 1 | 13 | 200 | 8 | 110 | 81 |
| PC3809-55 | 544.0 | 0.155 | 0.053 | 0.022 | 0.080 | 0.97 | 6 | 3 | 1 | 2 | 18 | 1 | 17 | 201 | 15 | 131 | 55 |
| PC3809-56 | 553.0 | 0.100 | 0.050 | 0.019 | 0.031 | 0.37 | 4 | 3 | 0 | 1 | 15 | 0 | 15 | 198 | 6 | 123 | 69 |
| PC3809-57 | 564.0 | 0.104 | 0.046 | 0.018 | 0.040 | 0.48 | 4 | 2 | 1 | 1 | 14 | 0 | 14 | 193 | 7 | 114 | 72 |
| PC3809-58 | 574.0 | 0.120 | 0.046 | 0.018 | 0.056 | 0.67 | 4 | 2 | 1 | 1 | 15 | 1 | 14 | 208 | 10 | 113 | 85 |
| PC3809-59 | 585.0 | 0.319 | 0.045 | 0.015 | 0.259 | 3.13 | 5 | 2 | 4 | 0 | 15 | 3 | 12 | 282 | 48 | 109 | 125 |
| PC3809-60 | 594.0 | 0.132 | 0.045 | 0.017 | 0.071 | 0.85 | 5 | 2 | 1 | 1 | 14 | 1 | 13 | 214 | 13 | 109 | 92 |
| PC3809-61 | 605.0 | 0.188 | 0.050 | 0.018 | 0.120 | 1.45 | 5 | 3 | 2 | 0 | 18 | 1 | 16 | 237 | 22 | 123 | 92 |
| PC3809-62 | 615.0 | 0.224 | 0.044 | 0.018 | 0.162 | 1.95 | 5 | 2 | 2 | 0 | 15 | 2 | 13 | 234 | 30 | 108 | 96 |
| PC3809-63 | 625.0 | 0.205 | 0.049 | 0.016 | 0.140 | 1.69 | 5 | 3 | 2 | 1 | 16 | 2 | 14 | 233 | 26 | 120 | 87 |
| PC3809-64 | 635.0 | 0.203 | 0.050 | 0.018 | 0.135 | 1.63 | 7 | 3 | 2 | 2 | 17 | 2 | 15 | 242 | 25 | 123 | 94 |

| APPENDIX C.13. PARTITIONED P, U, Y and Sr CONCENTRATIONS | | | | | | | | | | | | | | | | | |
|---|---|---|---|---|---|---|---|---|---|---|---|---|---|---|---|---|---|
| CD38-09 | (148m) | | | | | | | | | | | | | | | | |
| Sample | Depth | P | Pterr | Porg | Pphos | Phos | U | Uterr | Uphos | Uorg | Y | Yphos | Yterr | Sr | Srphos | Srterr | Srcal |
| | (cm) | (wt.%) | (wt.%) | (wt.%) | (wt.%) | (wt.%) | (ppm) | (ppm) | (ppm) | (ppm) | (ppm) | (ppm) | (ppm) | (ppm) | (ppm) | (ppm) | (ppm) |
| | | | | | (non -ve) | | | | (non -ve) | | | | | | | | |
| PC3809-65 | 646.0 | 0.139 | 0.044 | 0.018 | 0.077 | 0.92 | 5 | 2 | 1 | 2 | 13 | 1 | 12 | 201 | 14 | 108 | 79 |
| PC3809-66 | 654.0 | 0.109 | 0.042 | 0.015 | 0.052 | 0.62 | 7 | 2 | 1 | 4 | 13 | 1 | 12 | 187 | 10 | 103 | 75 |
| PC3809-67 | 664.0 | 0.094 | 0.042 | 0.017 | 0.035 | 0.42 | 8 | 2 | 0 | 5 | 13 | 0 | 13 | 189 | 7 | 104 | 79 |
| PC3809-68 | 674.0 | 0.084 | 0.037 | 0.013 | 0.034 | 0.41 | 8 | 2 | 0 | 5 | 12 | 0 | 12 | 171 | 6 | 90 | 74 |
| PC3809-69 | 684.0 | 0.118 | 0.049 | 0.018 | 0.051 | 0.62 | 7 | 3 | 1 | 3 | 16 | 1 | 15 | 211 | 9 | 121 | 81 |
| PC3809-70 | 694.0 | 0.119 | 0.053 | 0.018 | 0.048 | 0.58 | 7 | 3 | 1 | 4 | 16 | 1 | 15 | 212 | 9 | 129 | 73 |
| PC3809-71 | 703.0 | 0.098 | 0.052 | 0.018 | 0.028 | 0.33 | 7 | 3 | 0 | 4 | 16 | 0 | 16 | 201 | 5 | 128 | 68 |
| PC3809-72 | 714.0 | 0.138 | 0.048 | 0.021 | 0.069 | 0.84 | 7 | 3 | 1 | 4 | 16 | 1 | 15 | 218 | 13 | 117 | 88 |
| PC3809-73 | 724.0 | 0.194 | 0.052 | 0.016 | 0.125 | 1.51 | 5 | 3 | 2 | 1 | 17 | 2 | 15 | 232 | 23 | 128 | 81 |
| PC3809-74 | 734.0 | 0.198 | 0.053 | 0.018 | 0.127 | 1.54 | 5 | 3 | 2 | 0 | 17 | 2 | 15 | 238 | 24 | 129 | 85 |
| PC3809-75 | 744.0 | 0.162 | 0.051 | 0.018 | 0.093 | 1.12 | 7 | 3 | 1 | 3 | 16 | 1 | 15 | 226 | 17 | 125 | 83 |
| PC3809-76 | 754.0 | 0.104 | 0.047 | 0.017 | 0.040 | 0.48 | 4 | 2 | 1 | 1 | 15 | 0 | 15 | 202 | 7 | 115 | 79 |
| PC3809-77 | 764.0 | 0.133 | 0.053 | 0.015 | 0.065 | 0.79 | 5 | 3 | 1 | 1 | 18 | 1 | 17 | 217 | 12 | 129 | 76 |
| PC3809-78 | 774.0 | 0.138 | 0.054 | 0.016 | 0.069 | 0.83 | 4 | 3 | 1 | 0 | 19 | 1 | 18 | 219 | 13 | 131 | 75 |
| PC3809-79 | 784.0 | 0.130 | 0.051 | 0.014 | 0.064 | 0.78 | 6 | 3 | 1 | 2 | 18 | 1 | 17 | 215 | 12 | 126 | 78 |
| PC3809-80 | 794.0 | 0.150 | 0.052 | 0.015 | 0.083 | 1.00 | 5 | 3 | 1 | 1 | 18 | 1 | 17 | 222 | 15 | 126 | 80 |
| PC3809-81 | 804.0 | 0.187 | 0.049 | 0.016 | 0.121 | 1.46 | 5 | 3 | 2 | 1 | 17 | 1 | 15 | 224 | 23 | 121 | 81 |
| PC3809-82 | 813.0 | 0.304 | 0.051 | 0.014 | 0.239 | 2.88 | 6 | 3 | 3 | 0 | 18 | 3 | 15 | 270 | 44 | 125 | 101 |
| PC3809-83 | 823.0 | 0.203 | 0.050 | 0.016 | 0.137 | 1.66 | 5 | 3 | 2 | 0 | 19 | 2 | 17 | 230 | 26 | 122 | 82 |
| PC3809-84 | 834.0 | 0.165 | 0.052 | 0.016 | 0.097 | 1.17 | 5 | 3 | 1 | 0 | 18 | 1 | 17 | 221 | 18 | 126 | 77 |
| PC3809-85 | 845.0 | 0.195 | 0.052 | 0.016 | 0.127 | 1.53 | 4 | 3 | 2 | 0 | 18 | 2 | 16 | 232 | 24 | 128 | 80 |
| PC3809-86 | 854.0 | 0.101 | 0.059 | 0.012 | 0.030 | 0.36 | 5 | 3 | 0 | 2 | 20 | 0 | 20 | 205 | 6 | 144 | 56 |
| | | | | | | | | | | | | | | | | | |
| PC38-10 | (257m) | | | | | | | | | | | | | | | | |
| | | | | | | | | | | | | | | | | | |
| PC3810-01 | 6.0 | 0.469 | 0.046 | 0.049 | 0.374 | 4.52 | 15.3 | 2.4 | 5.3 | 7.6 | 20 | 4.5 | 15.0 | 346 | 70 | 112 | 164 |
| PC3810-02 | 14.0 | 1.062 | 0.048 | 0.027 | 0.987 | 11.91 | 19.9 | 2.5 | 13.9 | 3.4 | 28 | 11.9 | 16.2 | 435 | 184 | 117 | 134 |
| PC3810-03 | 24.0 | 1.959 | 0.048 | 0.009 | 1.901 | 22.94 | 19.9 | 2.6 | 26.8 | 0.0 | 29 | 23.0 | 6.5 | 597 | 354 | 119 | 125 |
| PC3810-04 | 34.0 | 1.027 | 0.048 | 0.011 | 0.968 | 11.67 | 15.7 | 2.6 | 13.6 | 0.0 | 29 | 11.7 | 16.9 | 494 | 180 | 119 | 196 |
| PC3810-05 | 44.0 | 0.435 | 0.051 | 0.036 | 0.348 | 4.19 | 15.3 | 2.7 | 4.9 | 7.7 | 23 | 4.2 | 19.0 | 264 | 65 | 125 | 74 |
| PC3810-06 | 54.0 | 0.294 | 0.052 | 0.037 | 0.205 | 2.48 | 14.7 | 2.8 | 2.9 | 9.0 | 20 | 2.5 | 17.7 | 235 | 38 | 128 | 69 |
| PC3810-07 | 64.0 | 0.462 | 0.054 | 0.022 | 0.387 | 4.67 | 15.1 | 2.8 | 5.5 | 6.8 | 23 | 4.7 | 18.4 | 284 | 72 | 131 | 80 |

| APPENDIX C.13. PARTITIONED P, U, Y and Sr CONCENTRATIONS | | | | | | | | | | | | | | | | | |
|---|---|---|---|---|---|---|---|---|---|---|---|---|---|---|---|---|---|
| CD38-10 | (257m) | | | | | | | | | | | | | | | | |
| Sample | Depth | P | Pterr | Porg | Pphos | Phos | U | Uterr | Uphos | Uorg | Y | Yphos | Yterr | Sr | Srphos | Srterr | Srcal |
| | (cm) | (wt.%) | (wt.%) | (wt.%) | (wt.%) | (wt.%) | (ppm) | (ppm) | (ppm) | (ppm) | (ppm) | (ppm) | (ppm) | (ppm) | (ppm) | (ppm) | (ppm) |
| | | | | (non -ve) | | | | | (non -ve) | | | | | | | | |
| PC3810-08 | 74.0 | 0.705 | 0.055 | 0.016 | 0.634 | 7.64 | 15.5 | 2.9 | 8.9 | 3.7 | 26 | 7.7 | 18.2 | 340 | 118 | 135 | 87 |
| PC3810-09 | 84.0 | 1.086 | 0.047 | 0.005 | 1.034 | 12.47 | 15.4 | 2.5 | 14.6 | 0.0 | 29 | 12.5 | 16.8 | 431 | 192 | 116 | 123 |
| PC3810-10 | 94.0 | 1.505 | 0.050 | 0.005 | 1.450 | 17.49 | 27.2 | 2.7 | 20.4 | 4.1 | 29 | 17.5 | 11.8 | 504 | 270 | 123 | 112 |
| PC3810-10 | 104.0 | 0.867 | 0.048 | 0.006 | 0.814 | 9.82 | 15.8 | 2.5 | 11.5 | 1.8 | 28 | 9.8 | 18.6 | 474 | 151 | 116 | 206 |
| PC3810-11 | 113.0 | 0.579 | 0.049 | 0.004 | 0.526 | 6.34 | 10.3 | 2.6 | 7.4 | 0.3 | 27 | 6.4 | 21.0 | 436 | 98 | 120 | 218 |
| PC3810-12 | 126.0 | 0.524 | 0.042 | 0.021 | 0.461 | 5.56 | 10.9 | 2.2 | 6.5 | 2.2 | 19 | 5.6 | 13.6 | 348 | 86 | 103 | 159 |
| PC3810-13 | 134.0 | 0.559 | 0.041 | 0.029 | 0.489 | 5.90 | 12.5 | 2.2 | 6.9 | 3.5 | 18 | 5.9 | 12.2 | 283 | 91 | 101 | 90 |
| PC3810-14 | 146.0 | 0.428 | 0.048 | 0.023 | 0.357 | 4.31 | 12.4 | 2.5 | 5.0 | 4.8 | 21 | 4.3 | 16.6 | 293 | 66 | 117 | 109 |
| PC3810-15 | 154.0 | 0.433 | 0.044 | 0.025 | 0.363 | 4.38 | 12.4 | 2.3 | 5.1 | 5.0 | 20 | 4.4 | 15.6 | 350 | 68 | 109 | 174 |
| PC3810-16 | 167.0 | 0.318 | 0.047 | 0.025 | 0.246 | 2.97 | 12.0 | 2.5 | 3.5 | 6.1 | 20 | 3.0 | 17.2 | 254 | 46 | 115 | 93 |
| PC3810-17 | 174.0 | 0.364 | 0.050 | 0.028 | 0.286 | 3.45 | 13.0 | 2.6 | 4.0 | 6.3 | 20 | 3.5 | 16.6 | 225 | 53 | 123 | 49 |
| PC3810-18 | 185.0 | 0.299 | 0.050 | 0.024 | 0.225 | 2.71 | 11.8 | 2.6 | 3.2 | 6.0 | 20 | 2.7 | 17.3 | 189 | 42 | 122 | 25 |
| PC3810-19 | 194.0 | 0.273 | 0.042 | 0.029 | 0.202 | 2.43 | 10.9 | 2.2 | 2.8 | 5.8 | 17 | 2.4 | 14.8 | 257 | 38 | 104 | 116 |
| PC3810-20 | 203.0 | 0.381 | 0.052 | 0.022 | 0.307 | 3.70 | 15.2 | 2.8 | 4.3 | 8.1 | 21 | 3.7 | 17.3 | 238 | 57 | 128 | 54 |
| PC3810-21 | 216.0 | 0.341 | 0.040 | 0.030 | 0.271 | 3.26 | 12.0 | 2.1 | 3.8 | 6.1 | 17 | 3.3 | 13.9 | 263 | 50 | 98 | 115 |
| PC3810-22 | 224.0 | 0.272 | 0.042 | 0.033 | 0.196 | 2.37 | 11.8 | 2.2 | 2.8 | 6.8 | 17 | 2.4 | 14.8 | 213 | 37 | 104 | 72 |
| PC3810-23 | 233.0 | 0.300 | 0.048 | 0.033 | 0.219 | 2.64 | 13.3 | 2.6 | 3.1 | 7.7 | 20 | 2.6 | 17.6 | 222 | 41 | 119 | 62 |
| PC3810-24 | 244.0 | 0.374 | 0.049 | 0.027 | 0.298 | 3.59 | 11.4 | 2.6 | 4.2 | 4.6 | 20 | 3.6 | 16.5 | 283 | 55 | 120 | 107 |
| PC3810-25 | 254.0 | 0.698 | 0.046 | 0.021 | 0.631 | 7.61 | 14.7 | 2.4 | 8.9 | 3.4 | 22 | 7.6 | 14.6 | 355 | 117 | 113 | 125 |
| PC3810-26 | 263.0 | 0.571 | 0.043 | 0.024 | 0.504 | 6.08 | 13.2 | 2.3 | 7.1 | 3.8 | 20 | 6.1 | 14.1 | 347 | 94 | 106 | 148 |
| PC3810-27 | 273.0 | 0.322 | 0.049 | 0.029 | 0.245 | 2.95 | 11.9 | 2.6 | 3.5 | 5.9 | 21 | 3.0 | 18.1 | 283 | 46 | 119 | 118 |
| PC3810-28 | 284.0 | 0.367 | 0.046 | 0.024 | 0.297 | 3.58 | 13.1 | 2.4 | 4.2 | 6.5 | 22 | 3.6 | 18.4 | 329 | 55 | 113 | 161 |
| PC3810-29 | 295.0 | 0.308 | 0.035 | 0.031 | 0.241 | 2.91 | 10.8 | 1.9 | 3.4 | 5.5 | 16 | 2.9 | 13.1 | 421 | 45 | 87 | 290 |
| PC3810-30 | 305.0 | 0.277 | 0.048 | 0.027 | 0.202 | 2.44 | 11.6 | 2.5 | 2.9 | 6.2 | 21 | 2.4 | 18.6 | 320 | 38 | 117 | 166 |
| PC3810-31 | 314.0 | 0.325 | 0.050 | 0.025 | 0.250 | 3.02 | 11.9 | 2.6 | 3.5 | 5.7 | 21 | 3.0 | 17.9 | 343 | 47 | 123 | 174 |
| PC3810-32 | 324.0 | 0.298 | 0.039 | 0.035 | 0.224 | 2.71 | 12.2 | 2.1 | 3.2 | 7.0 | 16 | 2.7 | 13.4 | 327 | 42 | 95 | 190 |
| PC3810-33 | 335.0 | 0.309 | 0.048 | 0.031 | 0.230 | 2.77 | 12.4 | 2.5 | 3.2 | 6.6 | 20 | 2.8 | 17.2 | 302 | 43 | 117 | 142 |
| PC3810-34 | 344.0 | 0.318 | 0.034 | 0.034 | 0.250 | 3.02 | 10.9 | 1.8 | 3.5 | 5.6 | 14 | 3.0 | 11.0 | 329 | 47 | 82 | 201 |
| PC3810-35 | 354.0 | 0.240 | 0.031 | 0.033 | 0.176 | 2.12 | 10.0 | 1.6 | 2.5 | 5.9 | 12 | 2.1 | 9.9 | 231 | 33 | 76 | 122 |
| PC3810-36 | 364.0 | 0.262 | 0.027 | 0.031 | 0.204 | 2.46 | 10.3 | 1.4 | 2.9 | 5.9 | 12 | 2.5 | 9.5 | 270 | 38 | 67 | 165 |
| PC3810-37 | 374.0 | 0.220 | 0.029 | 0.032 | 0.159 | 1.92 | 11.7 | 1.5 | 2.2 | 8.0 | 11 | 1.9 | 8.9 | 214 | 30 | 70 | 114 |
| PC3810-38 | 383.0 | 0.240 | 0.051 | 0.026 | 0.163 | 1.96 | 12.9 | 2.7 | 2.3 | 7.9 | 19 | 2.0 | 17.0 | 269 | 30 | 125 | 113 |

| APPENDIX C.13. PARTITIONED P, U, Y and Sr CONCENTRATIONS | | | | | | | | | | | | | | | | | |
|---|---|---|---|---|---|---|---|---|---|---|---|---|---|---|---|---|---|
| CD38-10 | (257m) | | | | | | | | | | | | | | | | |
| Sample | Depth | P | Pterr | Porg | Pphos | Phos | U | Uterr | Uphos | Uorg | Y | Yphos | Yterr | Sr | Srphos | Srterr | Srcal |
| | (cm) | (wt.%) | (wt.%) | (wt.%) | (wt.%) | (wt.%) | (ppm) | (ppm) | (ppm) | (ppm) | (ppm) | (ppm) | (ppm) | (ppm) | (ppm) | (ppm) | (ppm) |
| | | | | (non -ve) | | | | | | (non -ve) | | | | | | | |
| PC3810-39 | 394.0 | 0.297 | 0.042 | 0.037 | 0.218 | 2.63 | 14.2 | 2.2 | 3.1 | 8.9 | 18 | 2.6 | 15.5 | 250 | 41 | 102 | 107 |
| PC3810-40 | 404.0 | 0.288 | 0.048 | 0.028 | 0.212 | 2.56 | 12.9 | 2.5 | 3.0 | 7.4 | 22 | 2.6 | 19.5 | 288 | 39 | 118 | 131 |
| PC3810-41 | 417.0 | 0.347 | 0.041 | 0.031 | 0.275 | 3.31 | 12.3 | 2.2 | 3.9 | 6.2 | 19 | 3.3 | 15.7 | 384 | 51 | 100 | 233 |
| PC3810-42 | 424.0 | 0.314 | 0.043 | 0.034 | 0.237 | 2.86 | 14.7 | 2.3 | 3.3 | 9.1 | 18 | 2.9 | 15.2 | 300 | 44 | 105 | 151 |
| PC3810-43 | 434.0 | 0.380 | 0.020 | 0.026 | 0.334 | 4.02 | 10.3 | 1.1 | 4.7 | 4.5 | 11 | 4.0 | 6.9 | 511 | 62 | 50 | 400 |
| PC3810-44 | 445.0 | 0.267 | 0.034 | 0.030 | 0.203 | 2.44 | 12.0 | 1.8 | 2.9 | 7.3 | 14 | 2.5 | 11.4 | 388 | 38 | 83 | 267 |
| PC3810-45 | 456.0 | 0.276 | 0.031 | 0.033 | 0.212 | 2.55 | 13.5 | 1.6 | 3.0 | 8.8 | 13 | 2.6 | 10.4 | 352 | 39 | 76 | 237 |
| PC3810-46 | 467.0 | 0.215 | 0.021 | 0.032 | 0.162 | 1.96 | 6.2 | 1.1 | 2.3 | 2.8 | 10 | 2.0 | 8.0 | 347 | 30 | 52 | 265 |
| PC3810-47 | 476.0 | 0.495 | 0.041 | 0.035 | 0.419 | 5.05 | 16.9 | 2.2 | 5.9 | 8.8 | 20 | 5.1 | 14.9 | 436 | 78 | 101 | 256 |
| PC3810-48 | 484.0 | 0.464 | 0.039 | 0.036 | 0.389 | 4.69 | 14.8 | 2.1 | 5.5 | 7.2 | 20 | 4.7 | 15.2 | 453 | 72 | 96 | 285 |
| PC3810-49 | 494.0 | 0.892 | 0.037 | 0.034 | 0.821 | 9.90 | 23.7 | 2.0 | 11.6 | 10.1 | 26 | 9.9 | 16.0 | 473 | 153 | 91 | 230 |
| PC3810-50 | 504.0 | 2.404 | 0.046 | 0.011 | 2.348 | 28.32 | 21.8 | 2.4 | 33.1 | 0.0 | 33 | 28.4 | 4.1 | 642 | 437 | 112 | 94 |
| PC3810-51 | 514.0 | 0.117 | 0.049 | 0.021 | 0.047 | 0.57 | 5.9 | 2.6 | 0.7 | 2.7 | 17 | 0.6 | 16.3 | 197 | 9 | 119 | 69 |
| PC3810-52 | 524.0 | 0.108 | 0.053 | 0.017 | 0.038 | 0.46 | 6.4 | 2.8 | 0.5 | 3.0 | 18 | 0.5 | 17.3 | 193 | 7 | 129 | 56 |
| PC3810-53 | 534.0 | 0.264 | 0.039 | 0.063 | 0.162 | 1.95 | 22.9 | 2.1 | 2.3 | 18.5 | 15 | 2.0 | 13.0 | 274 | 30 | 96 | 148 |
| PC3810-54 | 545.0 | 0.204 | 0.039 | 0.052 | 0.112 | 1.36 | 17.2 | 2.1 | 1.6 | 13.5 | 15 | 1.4 | 13.6 | 242 | 21 | 97 | 125 |
| PC3810-55 | 554.0 | 0.199 | 0.036 | 0.056 | 0.107 | 1.28 | 18.3 | 1.9 | 1.5 | 14.8 | 13 | 1.3 | 11.7 | 285 | 20 | 88 | 177 |
| PC3810-56 | 564.0 | 0.299 | 0.031 | 0.033 | 0.235 | 2.83 | 10.5 | 1.6 | 3.3 | 5.5 | 12 | 2.8 | 9.1 | 413 | 44 | 76 | 294 |
| PC3810-57 | 574.0 | 0.251 | 0.035 | 0.036 | 0.180 | 2.17 | 11.1 | 1.9 | 2.5 | 6.7 | 14 | 2.2 | 11.7 | 476 | 33 | 86 | 356 |
| PC3810-58 | 584.0 | 0.192 | 0.035 | 0.037 | 0.120 | 1.45 | 9.0 | 1.8 | 1.7 | 5.5 | 14 | 1.5 | 12.5 | 420 | 22 | 85 | 313 |
| PC3810-59 | 596.0 | 0.202 | 0.034 | 0.039 | 0.129 | 1.55 | 22.7 | 1.8 | 1.8 | 19.1 | 14 | 1.6 | 12.5 | 411 | 24 | 84 | 303 |
| PC3810-60 | 604.0 | 0.205 | 0.035 | 0.039 | 0.131 | 1.58 | 16.7 | 1.8 | 1.8 | 13.0 | 15 | 1.6 | 13.5 | 448 | 24 | 86 | 338 |
| PC3810-61 | 614.0 | 0.147 | 0.039 | 0.038 | 0.071 | 0.85 | 15.2 | 2.0 | 1.0 | 12.1 | 14 | 0.9 | 13.1 | 352 | 13 | 95 | 244 |
| PC3810-62 | 624.0 | 0.204 | 0.042 | 0.033 | 0.129 | 1.56 | 10.3 | 2.2 | 1.8 | 6.3 | 17 | 1.6 | 15.4 | 424 | 24 | 102 | 298 |
| PC3810-63 | 634.0 | 0.216 | 0.041 | 0.034 | 0.141 | 1.71 | 9.4 | 2.2 | 2.0 | 5.3 | 16 | 1.7 | 14.2 | 452 | 26 | 100 | 325 |
| PC3810-64 | 645.0 | 0.146 | 0.040 | 0.034 | 0.072 | 0.86 | 10.6 | 2.1 | 1.0 | 7.5 | 15 | 0.9 | 14.2 | 318 | 13 | 98 | 206 |
| PC3810-65 | 655.0 | 0.136 | 0.039 | 0.040 | 0.058 | 0.70 | 8.8 | 2.0 | 0.8 | 6.0 | 14 | 0.7 | 13.3 | 328 | 11 | 95 | 223 |
| PC3810-66 | 667.0 | 0.176 | 0.043 | 0.035 | 0.099 | 1.19 | 11.4 | 2.2 | 1.4 | 7.8 | 16 | 1.2 | 14.8 | 331 | 18 | 104 | 208 |
| PC3810-67 | 674.0 | 0.183 | 0.049 | 0.034 | 0.100 | 1.20 | 14.1 | 2.6 | 1.4 | 10.1 | 16 | 1.2 | 14.7 | 256 | 19 | 121 | 117 |
| PC3810-68 | 683.0 | 0.139 | 0.045 | 0.033 | 0.060 | 0.73 | 11.3 | 2.4 | 0.8 | 8.0 | 14 | 0.7 | 13.1 | 271 | 11 | 111 | 149 |
| PC3810-69 | 694.0 | 0.206 | 0.059 | 0.025 | 0.122 | 1.47 | 9.8 | 3.1 | 1.7 | 4.9 | 19 | 1.5 | 17.4 | 235 | 23 | 145 | 67 |
| PC3810-70 | 704.0 | 0.193 | 0.066 | 0.024 | 0.104 | 1.25 | 8.0 | 3.5 | 1.5 | 3.1 | 22 | 1.3 | 20.7 | 194 | 19 | 161 | 14 |

| APPENDIX C.13. PARTITIONED P, U, Y and Sr CONCENTRATIONS | | | | | | | | | | | | | | | | | |
|---|---|---|---|---|---|---|---|---|---|---|---|---|---|---|---|---|---|
| | | | | | | | | | | | | | | | | | |
| CD38-10 | (257m) | | | | | | | | | | | | | | | | |
| Sample | Depth | P | Pterr | Porg | Pphos | Phos | U | Uterr | Uphos | Uorg | Y | Yphos | Yterr | Sr | Srphos | Srterr | Srcal |
| | (cm) | (wt.%) | (wt.%) | (wt.%) | (wt.%) | (wt.%) | (ppm) | (ppm) | (ppm) | (ppm) | (ppm) | (ppm) | (ppm) | (ppm) | (ppm) | (ppm) | (ppm) |
| | | | | (non -ve) | | | | | (non -ve) | | | | | | | | |
| PC3810-71 | 714.0 | 0.215 | 0.059 | 0.026 | 0.130 | 1.57 | 8.1 | 3.1 | 1.8 | 3.1 | 19 | 1.6 | 17.4 | 252 | 24 | 144 | 84 |
| PC3810-72 | 724.0 | 0.193 | 0.052 | 0.027 | 0.114 | 1.38 | 10.1 | 2.8 | 1.6 | 5.8 | 16 | 1.4 | 14.5 | 259 | 21 | 128 | 110 |
| PC3810-74 | 734.0 | 0.215 | 0.063 | 0.021 | 0.131 | 1.58 | 11.0 | 3.3 | 1.8 | 5.9 | 19 | 1.6 | 17.3 | 185 | 24 | 154 | 7 |
| PC3810-75 | 745.0 | 0.202 | 0.069 | 0.016 | 0.117 | 1.41 | 9.6 | 3.7 | 1.6 | 4.3 | 21 | 1.4 | 19.4 | 202 | 22 | 170 | 10 |
| PC3810-76 | 754.0 | 0.254 | 0.056 | 0.022 | 0.176 | 2.12 | 9.6 | 3.0 | 2.5 | 4.1 | 17 | 2.1 | 14.7 | 195 | 33 | 138 | 24 |
| PC3810-77 | 764.0 | 0.539 | 0.062 | 0.013 | 0.464 | 5.60 | 11.1 | 3.3 | 6.5 | 1.3 | 25 | 5.6 | 19.1 | 298 | 86 | 152 | 60 |
| | | | | | | | | | | | | | | | | | |
| PC38-02 | (2525m) | | | | | | | | | | | | | | | | |
| | (Age) | | | | | | | | | | | | | | | | |
| PC3802-01 | 2.76 | 0.117 | 0.050 | 0.008 | 0.059 | 0.71 | 9 | 2.7 | 0.8 | 5.1 | 24 | 1 | 24 | 535 | 11 | 123 | 401 |
| PC3802-02 | 6.21 | 0.113 | 0.045 | 0.007 | 0.061 | 0.73 | 6 | 2.4 | 0.9 | 3.1 | 20 | 1 | 19 | 642 | 11 | 110 | 521 |
| PC3802-03 | 9.66 | 0.105 | 0.044 | 0.007 | 0.054 | 0.65 | 8 | 2.3 | 0.8 | 4.7 | 20 | 1 | 19 | 682 | 10 | 107 | 565 |
| PC3802-04 | 12.77 | 0.096 | 0.048 | 0.014 | 0.034 | 0.41 | 8 | 2.5 | 0.5 | 5.5 | 18 | 0 | 18 | 569 | 6 | 117 | 446 |
| PC3802-05 | 15.18 | 0.092 | 0.047 | 0.010 | 0.035 | 0.42 | 8 | 2.5 | 0.5 | 4.8 | 18 | 0 | 18 | 619 | 6 | 115 | 497 |
| PC3802-06 | 17.47 | 0.091 | 0.046 | 0.010 | 0.035 | 0.42 | 6 | 2.4 | 0.5 | 3.5 | 19 | 0 | 18 | 608 | 6 | 112 | 489 |
| PC3802-07 | 20.48 | 0.097 | 0.049 | 0.010 | 0.038 | 0.45 | 6 | 2.6 | 0.5 | 3.0 | 21 | 0 | 21 | 584 | 7 | 121 | 456 |
| PC3802-08 | 22.65 | 0.095 | 0.048 | 0.010 | 0.037 | 0.45 | 7 | 2.5 | 0.5 | 3.6 | 20 | 0 | 20 | 576 | 7 | 118 | 451 |
| PC3802-09 | 25.22 | 0.097 | 0.045 | 0.011 | 0.041 | 0.49 | 10 | 2.4 | 0.6 | 7.3 | 19 | 0 | 19 | 624 | 8 | 110 | 507 |
| PC3802-10 | 28.29 | 0.095 | 0.042 | 0.011 | 0.043 | 0.51 | 6 | 2.2 | 0.6 | 3.2 | 19 | 1 | 19 | 668 | 8 | 102 | 558 |
| PC3802-11 | 31.07 | 0.094 | 0.041 | 0.008 | 0.045 | 0.54 | 7 | 2.1 | 0.6 | 4.3 | 17 | 1 | 17 | 671 | 8 | 100 | 564 |
| PC3802-12 | 33.86 | 0.089 | 0.038 | 0.010 | 0.042 | 0.50 | 7 | 2.0 | 0.6 | 4.9 | 17 | 1 | 16 | 704 | 8 | 92 | 604 |
| PC3802-13 | 36.64 | 0.092 | 0.041 | 0.010 | 0.040 | 0.48 | 8 | 2.2 | 0.6 | 5.1 | 18 | 0 | 17 | 695 | 7 | 101 | 586 |
| PC3802-14 | 39.15 | 0.097 | 0.048 | 0.009 | 0.040 | 0.48 | 7 | 2.5 | 0.6 | 3.4 | 20 | 0 | 20 | 596 | 7 | 117 | 472 |
| PC3802-15 | 42.22 | 0.098 | 0.049 | 0.012 | 0.037 | 0.44 | 6 | 2.6 | 0.5 | 2.7 | 20 | 0 | 20 | 582 | 7 | 120 | 454 |
| PC3802-16 | 45.00 | 0.103 | 0.054 | 0.008 | 0.041 | 0.50 | 5 | 2.8 | 0.6 | 1.6 | 21 | 0 | 21 | 549 | 8 | 131 | 410 |
| PC3802-17 | 48.07 | 0.102 | 0.054 | 0.010 | 0.038 | 0.46 | 10 | 2.9 | 0.5 | 6.6 | 23 | 0 | 22 | 511 | 7 | 133 | 371 |
| PC3802-18 | 50.85 | 0.103 | 0.052 | 0.009 | 0.043 | 0.52 | 10 | 2.7 | 0.6 | 6.8 | 22 | 1 | 21 | 460 | 8 | 126 | 326 |
| PC3802-19 | 53.64 | 0.103 | 0.051 | 0.010 | 0.042 | 0.51 | 11 | 2.7 | 0.6 | 7.3 | 24 | 1 | 24 | 502 | 8 | 124 | 370 |
| PC3802-20 | 56.42 | 0.103 | 0.054 | 0.011 | 0.039 | 0.47 | 9 | 2.9 | 0.5 | 6.0 | 24 | 0 | 24 | 462 | 7 | 132 | 323 |
| PC3802-21 | 59.29 | 0.103 | 0.055 | 0.011 | 0.037 | 0.45 | 9 | 2.9 | 0.5 | 5.4 | 24 | 0 | 24 | 491 | 7 | 134 | 350 |
| PC3802-22 | 62.61 | 0.103 | 0.054 | 0.009 | 0.039 | 0.47 | 10 | 2.9 | 0.6 | 6.2 | 24 | 0 | 23 | 512 | 7 | 133 | 372 |
| PC3802-23 | 65.94 | 0.105 | 0.057 | 0.008 | 0.041 | 0.49 | 5 | 3.0 | 0.6 | 1.8 | 25 | 0 | 24 | 459 | 8 | 139 | 312 |

| APPENDIX C.13. PARTITIONED P, U, Y and Sr CONCENTRATIONS | | | | | | | | | | | | | | | | | | |
|---|---|---|---|---|---|---|---|---|---|---|---|---|---|---|---|---|---|---|
| CD38-02 | (2525m) | | | | | | | | | | | | | | | | | |
| Sample | Age | P | Pterr | Porg | Pphos | Phos | U | Uterr | Uphos | Uorg | Y | Yphos | Yterr | Sr | Srphos | Srterr | Srcal | |
| | (ka) | (wt.%) | (wt.%) | (wt.%) | (wt.%) | (wt.%) | (ppm) | (ppm) | (ppm) | (ppm) | (ppm) | (ppm) | (ppm) | (ppm) | (ppm) | (ppm) | (ppm) | |
| | | | | (non -ve) | | | | | (non -ve) | | | | | | | | | |
| PC3802-24 | 69.26 | 0.111 | 0.063 | 0.009 | 0.039 | 0.47 | 7 | 3.3 | 0.6 | 3.0 | 26 | 0 | 25 | 362 | 7 | 155 | 199 | |
| PC3802-25 | 72.58 | 0.117 | 0.057 | 0.010 | 0.050 | 0.60 | 9 | 3.0 | 0.7 | 5.5 | 26 | 1 | 25 | 399 | 9 | 141 | 250 | |
| PC3802-26 | 76.96 | 0.119 | 0.051 | 0.008 | 0.060 | 0.72 | 9 | 2.7 | 0.8 | 5.4 | 25 | 1 | 24 | 492 | 11 | 126 | 356 | |
| PC3802-27 | 82.03 | 0.116 | 0.060 | 0.011 | 0.044 | 0.53 | 7 | 3.2 | 0.6 | 2.9 | 26 | 1 | 26 | 363 | 8 | 148 | 206 | |
| PC3802-28 | 87.11 | 0.113 | 0.061 | 0.009 | 0.043 | 0.52 | 8 | 3.2 | 0.6 | 4.4 | 26 | 1 | 25 | 376 | 8 | 149 | 219 | |
| PC3802-29 | 92.18 | 0.113 | 0.066 | 0.009 | 0.038 | 0.45 | 8 | 3.5 | 0.5 | 3.5 | 26 | 0 | 26 | 311 | 7 | 162 | 143 | |
| PC3802-30 | 97.26 | 0.131 | 0.064 | 0.007 | 0.060 | 0.73 | 9 | 3.4 | 0.9 | 4.4 | 28 | 1 | 27 | 336 | 11 | 156 | 168 | |
| PC3802-31 | 102.84 | 0.130 | 0.057 | 0.008 | 0.064 | 0.78 | 11 | 3.0 | 0.9 | 6.9 | 28 | 1 | 27 | 403 | 12 | 139 | 252 | |
| PC3802-32 | 107.92 | 0.124 | 0.058 | 0.008 | 0.058 | 0.70 | 10 | 3.1 | 0.8 | 6.3 | 27 | 1 | 26 | 398 | 11 | 142 | 246 | |
| PC3802-33 | 113.00 | 0.109 | 0.058 | 0.007 | 0.044 | 0.53 | 6 | 3.1 | 0.6 | 2.6 | 28 | 1 | 28 | 403 | 8 | 142 | 253 | |
| PC3802-34 | 118.07 | 0.114 | 0.057 | 0.006 | 0.051 | 0.62 | 8 | 3.0 | 0.7 | 4.6 | 28 | 1 | 27 | 435 | 10 | 140 | 286 | |
| PC3802-35 | 123.15 | 0.101 | 0.049 | 0.007 | 0.045 | 0.54 | 9 | 2.6 | 0.6 | 5.4 | 22 | 1 | 22 | 560 | 8 | 121 | 431 | |
| PC3802-36 | 128.22 | 0.089 | 0.048 | 0.007 | 0.034 | 0.41 | 7 | 2.5 | 0.5 | 3.8 | 18 | 0 | 17 | 621 | 6 | 117 | 497 | |
| PC3802-37 | 132.23 | 0.083 | 0.048 | 0.007 | 0.028 | 0.34 | 8 | 2.5 | 0.4 | 5.1 | 19 | 0 | 18 | 651 | 5 | 118 | 528 | |
| PC3802-38 | 135.30 | 0.082 | 0.046 | 0.006 | 0.030 | 0.37 | 7 | 2.4 | 0.4 | 4.2 | 19 | 0 | 19 | 667 | 6 | 113 | 548 | |
| PC3802-39 | 138.71 | 0.084 | 0.045 | 0.006 | 0.032 | 0.39 | 9 | 2.4 | 0.5 | 6.4 | 20 | 0 | 19 | 651 | 6 | 110 | 535 | |
| PC3802-40 | 141.79 | 0.087 | 0.043 | 0.006 | 0.037 | 0.45 | 8 | 2.3 | 0.5 | 5.1 | 19 | 0 | 19 | 683 | 7 | 106 | 570 | |
| PC3802-41 | 145.20 | 0.086 | 0.044 | 0.006 | 0.035 | 0.42 | 5 | 2.3 | 0.5 | 2.6 | 19 | 0 | 19 | 684 | 7 | 109 | 569 | |
| PC3802-42 | 148.61 | 0.083 | 0.044 | 0.005 | 0.033 | 0.40 | 6 | 2.3 | 0.5 | 3.6 | 19 | 0 | 19 | 674 | 6 | 109 | 560 | |
| PC3802-43 | 152.02 | 0.083 | 0.044 | 0.006 | 0.033 | 0.40 | 7 | 2.3 | 0.5 | 4.5 | 19 | 0 | 18 | 692 | 6 | 107 | 579 | |
| PC3802-44 | 155.44 | 0.087 | 0.045 | 0.006 | 0.036 | 0.43 | 12 | 2.4 | 0.5 | 8.9 | 19 | 0 | 18 | 661 | 7 | 111 | 544 | |
| PC3802-45 | 158.85 | 0.088 | 0.050 | 0.006 | 0.032 | 0.39 | 8 | 2.6 | 0.5 | 4.6 | 20 | 0 | 19 | 578 | 6 | 122 | 451 | |
| PC3802-46 | 162.26 | 0.092 | 0.053 | 0.007 | 0.032 | 0.39 | 7 | 2.8 | 0.5 | 3.5 | 22 | 0 | 21 | 531 | 6 | 130 | 395 | |
| PC3802-47 | 165.68 | 0.091 | 0.045 | 0.008 | 0.038 | 0.46 | 9 | 2.4 | 0.5 | 5.6 | 19 | 0 | 18 | 680 | 7 | 111 | 562 | |
| PC3802-48 | 169.43 | 0.090 | 0.043 | 0.007 | 0.040 | 0.48 | 10 | 2.3 | 0.6 | 6.7 | 19 | 0 | 18 | 706 | 7 | 105 | 594 | |
| PC3802-49 | 172.84 | 0.090 | 0.043 | 0.009 | 0.038 | 0.46 | 6 | 2.3 | 0.5 | 3.3 | 20 | 0 | 20 | 699 | 7 | 107 | 585 | |
| PC3802-50 | 176.26 | 0.098 | 0.046 | 0.009 | 0.043 | 0.51 | 8 | 2.4 | 0.6 | 5.4 | 20 | 1 | 20 | 668 | 8 | 113 | 547 | |
| PC3802-51 | 179.67 | 0.094 | 0.048 | 0.007 | 0.038 | 0.46 | 10 | 2.5 | 0.5 | 6.5 | 21 | 0 | 20 | 641 | 7 | 118 | 516 | |
| PC3802-52 | 183.08 | 0.096 | 0.053 | 0.007 | 0.036 | 0.44 | 6 | 2.8 | 0.5 | 2.4 | 20 | 0 | 20 | 555 | 7 | 130 | 418 | |
| PC3802-53 | 186.50 | 0.088 | 0.059 | 0.004 | 0.025 | 0.30 | 2 | 3.1 | 0.3 | 0.0 | 17 | 0 | 17 | 505 | 5 | 145 | 356 | |
| PC3802-54 | 189.57 | 0.113 | 0.062 | 0.007 | 0.044 | 0.53 | 6 | 3.3 | 0.6 | 2.3 | 27 | 1 | 26 | 398 | 8 | 152 | 238 | |
| PC3802-55 | 193.52 | 0.115 | 0.062 | 0.008 | 0.046 | 0.55 | 6 | 3.3 | 0.6 | 1.6 | 29 | 1 | 28 | 382 | 9 | 151 | 222 | |

| APPENDIX C.13. PARTITIONED P, U, Y and Sr CONCENTRATIONS | | | | | | | | | | | | | | | | | |
|---|---|---|---|---|---|---|---|---|---|---|---|---|---|---|---|---|---|
| | | | | | | | | | | | | | | | | | |
| CD38-02 | (2525m) | | | | | | | | | | | | | | | | |
| Sample | Age | P | Pterr | Porg | Pphos | Phos | U | Uterr | Uphos | Uorg | Y | Yphos | Yterr | Sr | Srphos | Srterr | Srcal |
| | (ka) | (wt.%) | (wt.%) | (wt.%) | (wt.%) | (wt.%) | (ppm) | (ppm) | (ppm) | (ppm) | (ppm) | (ppm) | (ppm) | (ppm) | (ppm) | (ppm) | (ppm) |
| | | | | (non -ve) | | | | | (non -ve) | | | | | | | | |
| PC3802-56 | 197.42 | 0.115 | 0.059 | 0.010 | 0.047 | 0.57 | 7 | 3.1 | 0.7 | 2.9 | 29 | 1 | 28 | 345 | 9 | 144 | 192 |
| PC3802-57 | 202.11 | 0.111 | 0.054 | 0.007 | 0.050 | 0.60 | 9 | 2.9 | 0.7 | 5.0 | 27 | 1 | 26 | 457 | 9 | 133 | 314 |
| PC3802-58 | 206.02 | 0.103 | 0.057 | 0.007 | 0.039 | 0.47 | 7 | 3.0 | 0.6 | 3.2 | 27 | 0 | 26 | 483 | 7 | 138 | 337 |
| PC3802-59 | 209.53 | 0.100 | 0.058 | 0.006 | 0.036 | 0.44 | 7 | 3.0 | 0.5 | 3.0 | 26 | 0 | 26 | 509 | 7 | 141 | 361 |
| PC3802-60 | 213.44 | 0.096 | 0.043 | 0.006 | 0.047 | 0.57 | 9 | 2.3 | 0.7 | 6.2 | 24 | 1 | 23 | 791 | 9 | 105 | 677 |
| PC3802-61 | 217.34 | 0.094 | 0.042 | 0.005 | 0.047 | 0.57 | 9 | 2.2 | 0.7 | 6.2 | 22 | 1 | 21 | 812 | 9 | 103 | 701 |
| PC3802-62 | 221.25 | 0.094 | 0.046 | 0.006 | 0.042 | 0.51 | 8 | 2.5 | 0.6 | 5.0 | 23 | 1 | 22 | 671 | 8 | 114 | 550 |
| PC3802-63 | 225.16 | 0.094 | 0.049 | 0.006 | 0.039 | 0.47 | 8 | 2.6 | 0.5 | 5.2 | 22 | 0 | 22 | 656 | 7 | 120 | 529 |
| PC3802-64 | 229.06 | 0.102 | 0.055 | 0.006 | 0.041 | 0.49 | 8 | 2.9 | 0.6 | 4.6 | 25 | 0 | 25 | 584 | 8 | 134 | 442 |
| PC3802-65 | 232.97 | 0.102 | 0.058 | 0.006 | 0.038 | 0.46 | 5 | 3.1 | 0.5 | 1.7 | 26 | 0 | 26 | 480 | 7 | 143 | 330 |
| PC3802-66 | 237.27 | 0.112 | 0.053 | 0.006 | 0.053 | 0.64 | 5 | 2.8 | 0.7 | 1.2 | 25 | 1 | 24 | 532 | 10 | 131 | 391 |
| PC3802-67 | 240.78 | 0.094 | 0.041 | 0.007 | 0.046 | 0.55 | 12 | 2.2 | 0.6 | 8.7 | 20 | 1 | 19 | 766 | 9 | 101 | 657 |
| PC3802-68 | 244.50 | 0.085 | 0.047 | 0.006 | 0.032 | 0.38 | 9 | 2.5 | 0.4 | 6.1 | 18 | 0 | 18 | 700 | 6 | 115 | 579 |
| PC3802-69 | 247.71 | 0.079 | 0.052 | 0.007 | 0.020 | 0.24 | 9 | 2.7 | 0.3 | 6.2 | 19 | 0 | 19 | 622 | 4 | 126 | 492 |
| PC3802-70 | 250.91 | 0.077 | 0.049 | 0.007 | 0.021 | 0.25 | 9 | 2.6 | 0.3 | 5.7 | 19 | 0 | 19 | 641 | 4 | 121 | 516 |
| PC3802-71 | 254.12 | 0.079 | 0.050 | 0.004 | 0.025 | 0.30 | 8 | 2.6 | 0.3 | 4.7 | 20 | 0 | 20 | 635 | 5 | 122 | 508 |
| PC3802-72 | 257.32 | 0.081 | 0.048 | 0.007 | 0.026 | 0.32 | 6 | 2.5 | 0.4 | 3.1 | 20 | 0 | 20 | 613 | 5 | 117 | 491 |
| PC3802-73 | 260.53 | 0.083 | 0.049 | 0.007 | 0.028 | 0.34 | 8 | 2.6 | 0.4 | 5.3 | 22 | 0 | 21 | 610 | 5 | 119 | 486 |
| PC3802-74 | 263.73 | 0.088 | 0.049 | 0.008 | 0.030 | 0.37 | 8 | 2.6 | 0.4 | 5.4 | 24 | 0 | 23 | 573 | 6 | 120 | 447 |
| | | | | | | | | | | | | | | | | | |
| PC38-11 | (3835m) | | | | | | | | | | | | | | | | |
| | | | | | | | | | | | | | | | | | |
| PC3811-01 | 0.80 | 0.31 | 0.062 | 0.021 | 0.231 | 2.78 | 11 | 3.3 | 3.3 | 4.4 | 27 | 3 | 24 | 258 | 43 | 153 | 62 |
| PC3811-02 | 2.00 | 0.38 | 0.053 | 0.023 | 0.303 | 3.65 | 9 | 2.8 | 4.3 | 2.3 | 21 | 4 | 17 | 348 | 56 | 129 | 162 |
| PC3811-03 | 2.20 | 0.36 | 0.053 | 0.017 | 0.292 | 3.52 | 8 | 2.8 | 4.1 | 0.6 | 24 | 4 | 20 | 330 | 54 | 131 | 145 |
| PC3811-04 | 3.49 | 0.20 | 0.065 | 0.016 | 0.117 | 1.41 | 14 | 3.4 | 1.7 | 8.7 | 30 | 1 | 28 | 261 | 22 | 158 | 81 |
| PC3811-05 | 6.17 | 0.17 | 0.064 | 0.017 | 0.088 | 1.06 | 11 | 3.4 | 1.2 | 6.8 | 26 | 1 | 25 | 256 | 16 | 156 | 84 |
| PC3811-06 | 8.85 | 0.13 | 0.062 | 0.019 | 0.052 | 0.63 | 11 | 3.3 | 0.7 | 6.5 | 22 | 1 | 22 | 255 | 10 | 152 | 93 |
| PC3811-07 | 11.53 | 0.13 | 0.064 | 0.019 | 0.046 | 0.56 | 12 | 3.4 | 0.7 | 8.1 | 10 | 1 | 10 | 239 | 9 | 156 | 74 |
| PC3811-08 | 13.80 | 0.14 | 0.063 | 0.018 | 0.060 | 0.72 | 8 | 3.3 | 0.8 | 3.6 | 21 | 1 | 20 | 279 | 11 | 153 | 115 |
| PC3811-09 | 16.44 | 0.27 | 0.062 | 0.009 | 0.200 | 2.41 | 5 | 3.3 | 2.8 | 0.0 | 23 | 2 | 20 | 376 | 37 | 153 | 185 |
| PC3811-10 | 18.63 | 0.14 | 0.059 | 0.018 | 0.063 | 0.76 | 9 | 3.1 | 0.9 | 5.0 | 21 | 1 | 20 | 303 | 12 | 145 | 147 |

| APPENDIX C.13. PARTITIONED P, U, Y and Sr CONCENTRATIONS | | | | | | | | | | | | | | | | | |
|---|---|---|---|---|---|---|---|---|---|---|---|---|---|---|---|---|---|
| | | | | | | | | | | | | | | | | | |
| CD38-11 | (3835m) | | | | | | | | | | | | | | | | |
| Sample | Depth | P | Pterr | Porg | Pphos | Phos | U | Uterr | Uphos | Uorg | Y | Yphos | Yterr | Sr | Srphos | Srterr | Srcal |
| | (cm) | (wt.%) | (wt.%) | (wt.%) | (wt.%) | (wt.%) | (ppm) | (ppm) | (ppm) | (ppm) | (ppm) | (ppm) | (ppm) | (ppm) | (ppm) | (ppm) | (ppm) |
| | | | | (non -ve) | | | | | (non -ve) | | | | | | | | |
| PC3811-11 | 20.82 | 0.13 | 0.057 | 0.018 | 0.060 | 0.72 | 6 | 3.0 | 0.8 | 1.8 | 21 | 1 | 20 | 318 | 11 | 139 | 168 |
| PC3811-12 | 23.23 | 0.14 | 0.058 | 0.019 | 0.063 | 0.76 | 5 | 3.1 | 0.9 | 0.6 | 20 | 1 | 20 | 285 | 12 | 142 | 131 |
| PC3811-13 | 25.11 | 0.13 | 0.060 | 0.018 | 0.056 | 0.67 | 5 | 3.2 | 0.8 | 1.5 | 21 | 1 | 20 | 291 | 10 | 146 | 134 |
| PC3811-14 | 27.10 | 0.15 | 0.059 | 0.017 | 0.076 | 0.92 | 6 | 3.1 | 1.1 | 1.3 | 21 | 1 | 20 | 313 | 14 | 146 | 153 |
| PC3811-15 | 29.09 | 0.15 | 0.063 | 0.018 | 0.070 | 0.85 | 6 | 3.3 | 1.0 | 1.6 | 21 | 1 | 20 | 291 | 13 | 155 | 123 |
| PC3811-16 | 31.08 | 0.16 | 0.057 | 0.016 | 0.091 | 1.10 | 9 | 3.0 | 1.3 | 4.5 | 21 | 1 | 20 | 341 | 17 | 140 | 184 |
| PC3811-17 | 33.07 | 0.15 | 0.065 | 0.017 | 0.070 | 0.85 | 8 | 3.4 | 1.0 | 3.5 | 21 | 1 | 20 | 308 | 13 | 158 | 137 |
| PC3811-18 | 35.07 | 0.22 | 0.059 | 0.014 | 0.151 | 1.82 | 9 | 3.1 | 2.1 | 3.6 | 24 | 2 | 22 | 362 | 28 | 144 | 189 |
| PC3811-19 | 37.26 | 0.15 | 0.060 | 0.020 | 0.070 | 0.85 | 9 | 3.2 | 1.0 | 5.0 | 24 | 1 | 23 | 279 | 13 | 147 | 118 |
| PC3811-20 | 39.45 | 0.15 | 0.062 | 0.021 | 0.062 | 0.75 | 6 | 3.3 | 0.9 | 2.2 | 23 | 1 | 23 | 262 | 12 | 151 | 99 |
| PC3811-21 | 40.84 | 0.14 | 0.063 | 0.021 | 0.055 | 0.66 | 6 | 3.3 | 0.8 | 1.6 | 24 | 1 | 23 | 245 | 10 | 153 | 81 |
| PC3811-22 | 43.03 | 0.18 | 0.056 | 0.020 | 0.110 | 1.32 | 11 | 2.9 | 1.5 | 6.4 | 24 | 1 | 22 | 358 | 20 | 137 | 201 |
| PC3811-23 | 45.03 | 0.15 | 0.057 | 0.022 | 0.072 | 0.87 | 7 | 3.0 | 1.0 | 2.5 | 25 | 1 | 24 | 325 | 13 | 141 | 172 |
| PC3811-24 | 47.02 | 0.15 | 0.059 | 0.024 | 0.069 | 0.83 | 10 | 3.1 | 1.0 | 6.2 | 26 | 1 | 25 | 305 | 13 | 143 | 149 |
| PC3811-25 | 49.01 | 0.16 | 0.059 | 0.023 | 0.073 | 0.88 | 10 | 3.1 | 1.0 | 6.0 | 25 | 1 | 24 | 316 | 14 | 144 | 158 |
| PC3811-26 | 51.00 | 0.15 | 0.051 | 0.021 | 0.076 | 0.92 | 10 | 2.7 | 1.1 | 5.8 | 25 | 1 | 24 | 359 | 14 | 126 | 219 |
| PC3811-27 | 52.99 | 0.15 | 0.052 | 0.021 | 0.077 | 0.93 | 10 | 2.7 | 1.1 | 6.1 | 25 | 1 | 24 | 343 | 14 | 127 | 202 |
| PC3811-28 | 54.99 | 0.15 | 0.055 | 0.019 | 0.080 | 0.96 | 10 | 2.9 | 1.1 | 5.7 | 26 | 1 | 25 | 314 | 15 | 134 | 165 |
| PC3811-29 | 56.98 | 0.15 | 0.066 | 0.020 | 0.068 | 0.82 | 10 | 3.5 | 1.0 | 5.9 | 27 | 1 | 27 | 241 | 13 | 162 | 67 |
| PC3811-30 | 59.62 | 0.16 | 0.065 | 0.017 | 0.078 | 0.94 | 9 | 3.4 | 1.1 | 5.0 | 26 | 1 | 25 | 253 | 15 | 158 | 80 |
| PC3811-31 | 62.28 | 0.16 | 0.067 | 0.015 | 0.073 | 0.88 | 7 | 3.6 | 1.0 | 2.7 | 29 | 1 | 28 | 236 | 14 | 165 | 58 |
| PC3811-32 | 65.60 | 0.20 | 0.070 | 0.016 | 0.114 | 1.38 | 10 | 3.7 | 1.6 | 4.6 | 28 | 1 | 26 | 235 | 21 | 171 | 43 |
| PC3811-33 | 68.93 | 0.44 | 0.047 | 0.017 | 0.375 | 4.53 | 17 | 2.5 | 5.3 | 9.3 | 24 | 5 | 19 | 423 | 70 | 116 | 238 |
| PC3811-34 | 72.25 | 0.15 | 0.059 | 0.019 | 0.074 | 0.90 | 10 | 3.1 | 1.0 | 6.0 | 26 | 1 | 25 | 243 | 14 | 144 | 85 |
| PC3811-35 | 74.95 | 0.15 | 0.059 | 0.020 | 0.073 | 0.88 | 9 | 3.1 | 1.0 | 5.3 | 26 | 1 | 25 | 247 | 14 | 144 | 90 |
| PC3811-36 | 77.04 | 0.15 | 0.056 | 0.019 | 0.079 | 0.96 | 9 | 3.0 | 1.1 | 4.4 | 27 | 1 | 26 | 248 | 15 | 137 | 96 |
| PC3811-37 | 79.12 | 0.16 | 0.058 | 0.022 | 0.077 | 0.93 | 4 | 3.1 | 1.1 | 0.0 | 29 | 1 | 28 | 241 | 14 | 143 | 85 |
| PC3811-38 | 81.20 | 0.14 | 0.060 | 0.023 | 0.056 | 0.68 | 9 | 3.2 | 0.8 | 4.5 | 27 | 1 | 26 | 247 | 11 | 147 | 90 |
| PC3811-39 | 83.29 | 0.15 | 0.065 | 0.021 | 0.067 | 0.81 | 9 | 3.4 | 0.9 | 5.0 | 30 | 1 | 29 | 256 | 13 | 159 | 85 |
| PC3811-40 | 85.37 | 0.16 | 0.066 | 0.018 | 0.073 | 0.89 | 7 | 3.5 | 1.0 | 2.7 | 31 | 1 | 30 | 260 | 14 | 162 | 84 |
| PC3811-41 | 87.45 | 0.15 | 0.064 | 0.019 | 0.070 | 0.84 | 8 | 3.4 | 1.0 | 3.5 | 31 | 1 | 30 | 258 | 13 | 156 | 90 |
| PC3811-42 | 89.54 | 0.16 | 0.070 | 0.016 | 0.075 | 0.91 | 8 | 3.7 | 1.1 | 3.6 | 33 | 1 | 32 | 233 | 14 | 171 | 48 |

APPENDIX C.13. PARTITIONED P, U, Y and Sr CONCENTRATIONS

| CD38-11 Sample | (3835m) Depth | P | Pterr | Porg | Pphos | Phos | U | Uterr | Uphos | Uorg | Y | Yphos | Yterr | Sr | Srphos | Srterr | Srcal |
|---|---|---|---|---|---|---|---|---|---|---|---|---|---|---|---|---|---|
| | (cm) | (wt.%) | (wt.%) | (wt.%) | (wt.%) | (wt.%) | (ppm) | (ppm) | (ppm) | (ppm) | (ppm) | (ppm) | (ppm) | (ppm) | (ppm) | (ppm) | (ppm) |
| | | | | (non -ve) | | | | | (non -ve) | | | | | | | | |
| PC3811-43 | 91.62 | 0.15 | 0.060 | 0.016 | 0.079 | 0.95 | 7 | 3.2 | 1.1 | 3.1 | 33 | 1 | 32 | 253 | 15 | 146 | 93 |
| PC3811-44 | 93.70 | 0.20 | 0.059 | 0.016 | 0.122 | 1.48 | 12 | 3.1 | 1.7 | 6.8 | 34 | 1 | 32 | 313 | 23 | 145 | 145 |
| PC3811-45 | 95.79 | 0.18 | 0.058 | 0.017 | 0.109 | 1.31 | 9 | 3.1 | 1.5 | 4.6 | 33 | 1 | 32 | 279 | 20 | 141 | 118 |
| PC3811-46 | 97.87 | 0.18 | 0.066 | 0.017 | 0.097 | 1.16 | 9 | 3.5 | 1.4 | 4.4 | 37 | 1 | 36 | 238 | 18 | 163 | 57 |
| PC3811-47 | 99.95 | 0.16 | 0.068 | 0.017 | 0.079 | 0.95 | 8 | 3.6 | 1.1 | 3.2 | 34 | 1 | 34 | 230 | 15 | 168 | 48 |
| PC3811-48 | 102.04 | 0.18 | 0.067 | 0.017 | 0.093 | 1.12 | 11 | 3.5 | 1.3 | 5.8 | 34 | 1 | 33 | 255 | 17 | 163 | 75 |
| PC3811-49 | 104.12 | 0.16 | 0.067 | 0.014 | 0.075 | 0.91 | 5 | 3.5 | 1.1 | 0.4 | 33 | 1 | 32 | 222 | 14 | 164 | 44 |
| PC3811-50 | 106.20 | 0.17 | 0.064 | 0.012 | 0.096 | 1.15 | 8 | 3.4 | 1.3 | 3.7 | 32 | 1 | 31 | 226 | 18 | 158 | 50 |
| PC3811-51 | 108.29 | 0.16 | 0.065 | 0.014 | 0.081 | 0.98 | 6 | 3.4 | 1.1 | 1.7 | 32 | 1 | 31 | 223 | 15 | 159 | 49 |
| PC3811-52 | 110.37 | 0.17 | 0.063 | 0.013 | 0.091 | 1.10 | 4 | 3.4 | 1.3 | 0.0 | 32 | 1 | 31 | 226 | 17 | 155 | 54 |
| PC3811-53 | 112.45 | 0.15 | 0.064 | 0.012 | 0.075 | 0.90 | 5 | 3.4 | 1.1 | 0.1 | 31 | 1 | 30 | 223 | 14 | 156 | 52 |
| PC3811-54 | 114.54 | 0.17 | 0.059 | 0.013 | 0.099 | 1.20 | 6 | 3.1 | 1.4 | 1.9 | 34 | 1 | 33 | 235 | 18 | 144 | 73 |
| PC3811-55 | 116.62 | 0.17 | 0.061 | 0.012 | 0.100 | 1.21 | 6 | 3.2 | 1.4 | 1.7 | 31 | 1 | 30 | 235 | 19 | 150 | 66 |
| PC3811-56 | 118.70 | 0.18 | 0.061 | 0.011 | 0.109 | 1.31 | 4 | 3.2 | 1.5 | 0.0 | 35 | 1 | 33 | 238 | 20 | 150 | 68 |
| PC3811-57 | 120.79 | 0.19 | 0.058 | 0.012 | 0.116 | 1.40 | 6 | 3.1 | 1.6 | 1.1 | 35 | 1 | 33 | 243 | 22 | 143 | 79 |

APPENDIX C.14. NEW PRODUCTION DATA (after DYMOND et al., 1992)

CD38-02 (2525m)

| Age (ka) | Babio (ppm) | F Babio (ug/cm2/kyr) | Pnew (gC/m2/yr) | Age (ka) | Babio (ppm) | F Babio (ug/cm2/kyr) | Pnew (gC/m2/yr) | Age (ka) | Babio (ppm) | F Babio (ug/cm2/kyr) | Pnew (gC/m2/yr) |
|---|---|---|---|---|---|---|---|---|---|---|---|
| 2.76 | 1720 | 6.26 | 22.08 | 76.96 | 1526 | 4.44 | 13.17 | 179.67 | 973 | 4.24 | 12.26 |
| 6.21 | 1471 | 5.56 | 18.49 | 82.03 | 1445 | 4.10 | 11.66 | 183.08 | 702 | 3.00 | 7.32 |
| 9.66 | 1405 | 5.04 | 15.92 | 87.11 | 1307 | 3.77 | 10.29 | 186.50 | 621 | 2.95 | 7.11 |
| 12.77 | 856 | 3.89 | 10.80 | 92.18 | 1394 | 3.95 | 11.03 | 189.57 | 1072 | 4.43 | 13.11 |
| 15.18 | 902 | 4.57 | 13.75 | 97.26 | 1578 | 4.44 | 13.15 | 193.52 | 1205 | 4.37 | 12.84 |
| 17.47 | 835 | 4.22 | 12.20 | 102.84 | 1514 | 4.22 | 12.20 | 197.42 | 1685 | 5.83 | 19.84 |
| 20.48 | 1110 | 5.59 | 18.61 | 107.92 | 1595 | 4.53 | 13.59 | 202.11 | 1630 | 7.68 | 30.02 |
| 22.65 | 1021 | 5.05 | 15.97 | 113.00 | 1515 | 4.36 | 12.81 | 206.02 | 1534 | 7.15 | 26.97 |
| 25.22 | 1026 | 4.63 | 14.04 | 118.07 | 1935 | 5.36 | 17.49 | 209.53 | 1419 | 5.70 | 19.19 |
| 28.29 | 1013 | 4.60 | 13.90 | 123.15 | 1561 | 4.37 | 12.85 | 213.44 | 1638 | 6.86 | 25.33 |
| 31.07 | 1004 | 4.62 | 13.97 | 128.22 | 994 | 2.85 | 6.75 | 217.34 | 1403 | 5.85 | 19.95 |
| 33.86 | 994 | 4.46 | 13.24 | 132.23 | 893 | 3.66 | 9.87 | 221.25 | 1223 | 5.05 | 15.97 |
| 36.64 | 1036 | 4.68 | 14.27 | 135.30 | 936 | 4.04 | 11.42 | 225.16 | 1016 | 4.35 | 12.78 |
| 39.15 | 1090 | 4.83 | 14.94 | 138.71 | 914 | 3.95 | 11.06 | 229.06 | 1184 | 4.89 | 15.24 |
| 42.22 | 985 | 4.32 | 12.64 | 141.79 | 989 | 4.23 | 12.25 | 232.97 | 1346 | 5.23 | 16.86 |
| 45.00 | 1040 | 4.92 | 15.38 | 145.20 | 987 | 4.25 | 12.35 | 237.27 | 1941 | 7.31 | 27.87 |
| 48.07 | 1070 | 5.02 | 15.82 | 148.61 | 872 | 3.72 | 10.07 | 240.78 | 1648 | 6.25 | 22.03 |
| 50.85 | 1176 | 5.08 | 16.12 | 152.02 | 724 | 3.18 | 7.98 | 244.50 | 1102 | 5.09 | 16.19 |
| 53.64 | 1332 | 5.93 | 20.34 | 155.44 | 869 | 3.85 | 10.64 | 247.71 | 909 | 4.11 | 11.74 |
| 56.42 | 1208 | 5.21 | 16.76 | 158.85 | 809 | 3.38 | 8.74 | 250.91 | 909 | 4.22 | 12.18 |
| 59.29 | 1053 | 4.12 | 11.76 | 162.26 | 801 | 3.37 | 8.69 | 254.12 | 1090 | 4.91 | 15.33 |
| 62.61 | 1077 | 4.33 | 12.67 | 165.68 | 890 | 3.90 | 10.81 | 257.32 | 1106 | 4.98 | 15.65 |
| 65.94 | 905 | 3.71 | 10.06 | 169.43 | 987 | 4.31 | 12.58 | 260.53 | 1060 | 4.86 | 15.08 |
| 69.26 | 1290 | 5.15 | 16.44 | 172.84 | 999 | 4.30 | 12.57 | 263.73 | 986 | 4.45 | 13.21 |
| 72.58 | 1256 | 5.02 | 15.84 | 176.26 | 996 | 4.21 | 12.17 | | | | |

APPENDIX C.15. URANIUM/THORIUM RADIOGENIC ISOTOPE RESULTS

Two duplicate samples from base of phosphorite nodule at 273cm in CD38-09

| | Sample H | | | | Sample I | | | |
|---|---|---|---|---|---|---|---|---|
| | U-238 | U-234 | Th-232 | Th-230 | U-238 | U-234 | Th-232 | Th-230 |
| Isotope corrected counts | 8373.145 | 9264.984 | 81.4551 | 7840.986 | 9178.314 | 10294.25 | 23.3521 | 934.7183 |
| Spike counts (U-232/Th-228) | 17444.58 | 17444.58 | 25037.17 | 25037.17 | 22791.39 | 22791.39 | 3352.682 | 3352.682 |
| Spike activity (dpm/0.1ml) | 62.92 | 62.92 | 68.87 | 68.87 | 62.92 | 62.92 | 68.87 | 68.87 |
| Spike volume (ml) | 0.1 | 0.1 | 0.1 | 0.1 | 0.1 | 0.1 | 0.1 | 0.1 |
| Error on spike added | 0.88088 | 0.88088 | 0.96418 | 0.96418 | 0.88088 | 0.88088 | 0.96418 | 0.96418 |
| Sample weight (g) | 0.36851 | 0.36851 | 0.36851 | 0.36851 | 0.30708 | 0.30708 | 0.30708 | 0.30708 |
| Activity of isotope (dpm/g) | 81.953 | 90.683 | 0.606 | 58.528 | 82.514 | 92.547 | 1.562 | 62.527 |
| Error | ±0.583 | ±0.635 | ±0.025 | ±0.411 | ±0.473 | ±0.522 | ±0.100 | ±0.759 |
| Element concentration (ppm) | 109.9 | (Uranium) | 2.5 | (Thorium) | 110.61 | (Uranium) | 6.34 | (Thorium) |
| Chemical yield (%) | 26.8 | | 35.1 | | 35.0 | | 5.6 | |

| | Sample H | Sample I |
|---|---|---|
| U-234/U-238 | 1.10652 | 1.12159 |
| (Error) | (±0.011) | (±0.009) |
| Th-230/U-234 | 0.64541 | 0.67562 |
| (Error) | (±0.006) | (±0.009) |
| Age (kyr) | 109.895 | 118.595 |
| (Error) | (±1.5) | (±2.6) |
| Average age of phosphorite (kyr) | 114.2 | |
| (Error) | (±6.4) | |

| APPENDIX C.16. CORRELATION MATRICES | | | | | | | | | | | | | | | | | | | |
|---|---|---|---|---|---|---|---|---|---|---|---|---|---|---|---|---|---|---|---|
| CD38-09 | 148m | | | | | | | | | | | | | | | | | | |
| Bio.Silica | 0.473 | | | | | | | | | | | | | | | | | | |
| CaCO3 | -0.468 | 0.033 | | | | | | | | | | | | | | | | | |
| Phos. | -0.279 | -0.344 | 0.121 | | | | | | | | | | | | | | | | |
| Terr. | -0.093 | -0.353 | -0.269 | -0.739 | | | | | | | | | | | | | | | |
| Al | 0.205 | -0.419 | -0.476 | -0.417 | 0.717 | | | | | | | | | | | | | | |
| K | -0.060 | -0.536 | -0.308 | -0.388 | 0.771 | 0.931 | | | | | | | | | | | | | |
| Ti | 0.055 | -0.515 | -0.451 | -0.366 | 0.747 | 0.952 | 0.910 | | | | | | | | | | | | |
| I | 0.587 | -0.028 | -0.521 | -0.073 | 0.092 | 0.544 | 0.310 | 0.465 | | | | | | | | | | | |
| Br | 0.702 | 0.131 | -0.440 | -0.130 | 0.015 | 0.424 | 0.189 | 0.333 | 0.923 | | | | | | | | | | |
| Mo | 0.808 | 0.583 | -0.145 | -0.067 | -0.398 | -0.233 | -0.421 | -0.404 | 0.205 | 0.368 | | | | | | | | | |
| U | -0.159 | -0.272 | 0.077 | 0.982 | -0.777 | -0.389 | -0.389 | -0.357 | -0.008 | -0.045 | 0.032 | | | | | | | | |
| Ni | 0.911 | 0.394 | -0.562 | -0.101 | -0.181 | 0.074 | -0.170 | -0.038 | 0.435 | 0.515 | 0.816 | 0.003 | | | | | | | |
| Cr | 0.738 | 0.198 | -0.399 | -0.025 | -0.143 | 0.197 | 0.036 | 0.114 | 0.216 | 0.327 | 0.575 | 0.089 | 0.770 | | | | | | |
| V | 0.432 | 0.396 | 0.039 | -0.363 | 0.028 | 0.250 | 0.206 | 0.087 | -0.008 | 0.103 | 0.419 | -0.257 | 0.282 | 0.513 | | | | | |
| Cu | 0.536 | 0.081 | -0.326 | -0.374 | 0.286 | 0.599 | 0.488 | 0.497 | 0.250 | 0.296 | 0.341 | -0.291 | 0.477 | 0.613 | 0.637 | | | | |
| Sr | -0.412 | -0.460 | 0.234 | 0.971 | -0.644 | -0.385 | -0.317 | -0.313 | -0.119 | -0.190 | -0.202 | 0.931 | -0.248 | -0.154 | -0.442 | -0.441 | | | |
| Ba | -0.094 | -0.171 | -0.123 | -0.069 | 0.213 | 0.198 | 0.269 | 0.199 | -0.010 | -0.013 | -0.133 | -0.084 | -0.074 | -0.017 | -0.059 | 0.053 | 0.048 | | |
| Zn | 0.314 | -0.229 | -0.402 | -0.260 | 0.417 | 0.795 | 0.694 | 0.780 | 0.517 | 0.482 | -0.045 | -0.213 | 0.200 | 0.323 | 0.310 | 0.733 | -0.279 | 0.132 | |
| Rb | 0.120 | -0.406 | -0.333 | -0.356 | 0.636 | 0.951 | 0.948 | 0.901 | 0.501 | 0.407 | -0.289 | -0.326 | -0.057 | 0.149 | 0.309 | 0.580 | -0.320 | 0.206 | 0.801 |
| Zr | -0.305 | -0.708 | -0.320 | 0.114 | 0.435 | 0.406 | 0.419 | 0.518 | 0.330 | 0.131 | -0.536 | 0.033 | -0.221 | -0.386 | -0.664 | -0.283 | 0.229 | 0.179 | 0.121 |
| Zr/Rb | 0.525 | 0.112 | -0.533 | -0.476 | 0.414 | 0.743 | 0.632 | 0.616 | 0.492 | 0.482 | 0.178 | -0.378 | 0.364 | 0.473 | 0.609 | 0.746 | -0.581 | -0.065 | 0.721 |
| Nb | 0.003 | -0.546 | -0.389 | -0.075 | 0.480 | 0.807 | 0.781 | 0.841 | 0.565 | 0.426 | -0.419 | -0.069 | -0.112 | 0.041 | -0.081 | 0.265 | -0.026 | 0.205 | 0.645 |
| Pb | 0.035 | -0.188 | -0.119 | -0.413 | 0.530 | 0.765 | 0.804 | 0.661 | 0.305 | 0.237 | -0.226 | -0.394 | -0.179 | 0.005 | 0.440 | 0.515 | -0.389 | 0.123 | 0.634 |
| Th | 0.410 | -0.138 | -0.543 | -0.516 | 0.623 | 0.879 | 0.757 | 0.827 | 0.652 | 0.604 | -0.052 | -0.458 | 0.254 | 0.286 | 0.291 | 0.591 | -0.534 | 0.075 | 0.763 |
| La | 0.172 | -0.319 | -0.195 | -0.329 | 0.518 | 0.743 | 0.721 | 0.708 | 0.416 | 0.352 | -0.157 | -0.314 | 0.026 | 0.196 | 0.258 | 0.474 | -0.292 | 0.085 | 0.617 |
| Ce | -0.021 | -0.630 | -0.411 | -0.086 | 0.549 | 0.835 | 0.822 | 0.848 | 0.563 | 0.378 | -0.410 | -0.087 | -0.094 | -0.028 | -0.102 | 0.224 | -0.030 | 0.157 | 0.593 |
| Nd | -0.065 | -0.693 | -0.420 | 0.009 | 0.505 | 0.797 | 0.785 | 0.844 | 0.541 | 0.347 | -0.449 | -0.008 | -0.098 | -0.018 | -0.197 | 0.182 | 0.077 | 0.237 | 0.589 |
| Y | -0.256 | -0.830 | -0.355 | 0.362 | 0.266 | 0.511 | 0.528 | 0.630 | 0.281 | 0.089 | -0.499 | 0.313 | -0.123 | -0.032 | -0.439 | 0.020 | 0.425 | 0.161 | 0.380 |
| Sc | 0.108 | -0.203 | -0.137 | -0.571 | 0.683 | 0.753 | 0.744 | 0.760 | 0.172 | 0.148 | -0.223 | -0.563 | -0.014 | 0.179 | 0.332 | 0.629 | -0.515 | 0.165 | 0.638 |
| | Corg | Bio.Silica | CaCO3 | Phos. | Terr. | Al | K | Ti | I | Br | Mo | U | Ni | Cr | V | Cu | Sr | Ba | Zn |
| Zr | 0.296 | | | | | | | | | | | | | | | | | | |
| Zr/Rb | 0.758 | -0.167 | | | | | | | | | | | | | | | | | |
| Nb | 0.818 | 0.562 | 0.472 | | | | | | | | | | | | | | | | |
| Pb | 0.858 | 0.025 | 0.714 | 0.586 | | | | | | | | | | | | | | | |
| Th | 0.844 | 0.252 | 0.811 | 0.695 | 0.705 | | | | | | | | | | | | | | |
| La | 0.755 | 0.240 | 0.564 | 0.582 | 0.630 | 0.671 | | | | | | | | | | | | | |
| Ce | 0.811 | 0.672 | 0.458 | 0.871 | 0.576 | 0.688 | 0.616 | | | | | | | | | | | | |
| Nd | 0.770 | 0.732 | 0.358 | 0.877 | 0.503 | 0.638 | 0.599 | 0.946 | | | | | | | | | | | |
| Y | 0.449 | 0.787 | 0.018 | 0.681 | 0.142 | 0.305 | 0.372 | 0.733 | 0.822 | | | | | | | | | | |
| Sc | 0.724 | 0.118 | 0.559 | 0.501 | 0.632 | 0.668 | 0.596 | 0.504 | 0.453 | 0.244 | | | | | | | | | |
| | Rb | Zr | Zr/Rb | Nb | Pb | Th | La | Ce | Nd | Y | | | | | | | | | |

| APPENDIX C.16. CORRELATION MATRICES | | | | | | | | | | | | | | | | | | | |
|---|---|---|---|---|---|---|---|---|---|---|---|---|---|---|---|---|---|---|---|
| | | | | | | | | | | | | | | | | | | | |
| CD38-10 | 257m | | | | | | | | | | | | | | | | | | |
| | | | | | | | | | | | | | | | | | | | |
| Bio.Silica | 0.513 | | | | | | | | | | | | | | | | | | |
| CaCO3 | 0.456 | 0.455 | | | | | | | | | | | | | | | | | |
| Phos. | -0.594 | -0.631 | -0.296 | | | | | | | | | | | | | | | | |
| Terr. | -0.523 | -0.710 | -0.864 | 0.206 | | | | | | | | | | | | | | | |
| Al | -0.468 | -0.631 | -0.781 | 0.133 | 0.923 | | | | | | | | | | | | | | |
| K | -0.499 | -0.606 | -0.792 | 0.137 | 0.918 | 0.986 | | | | | | | | | | | | | |
| Ti | -0.493 | -0.613 | -0.781 | 0.164 | 0.901 | 0.961 | 0.929 | | | | | | | | | | | | |
| I | 0.390 | -0.037 | 0.107 | -0.008 | -0.122 | -0.121 | -0.178 | -0.059 | | | | | | | | | | | |
| Br | 0.745 | 0.237 | 0.111 | -0.299 | -0.226 | -0.260 | -0.299 | -0.257 | 0.732 | | | | | | | | | | |
| Mo | 0.728 | 0.521 | 0.370 | -0.565 | -0.431 | -0.425 | -0.403 | -0.557 | -0.051 | 0.402 | | | | | | | | | |
| U | 0.071 | -0.442 | -0.083 | 0.571 | 0.029 | -0.043 | -0.068 | -0.038 | 0.229 | 0.200 | -0.116 | | | | | | | | |
| Ni | 0.927 | 0.310 | 0.317 | -0.414 | -0.382 | -0.369 | -0.419 | -0.353 | 0.482 | 0.763 | 0.556 | 0.265 | | | | | | | |
| Cr | 0.810 | 0.143 | 0.082 | -0.552 | -0.034 | 0.073 | 0.034 | 0.051 | 0.317 | 0.601 | 0.494 | 0.097 | 0.814 | | | | | | |
| V | 0.782 | 0.347 | 0.323 | -0.578 | -0.296 | -0.244 | -0.247 | -0.363 | -0.004 | 0.449 | 0.869 | 0.000 | 0.627 | 0.714 | | | | | |
| Cu | 0.668 | 0.393 | 0.033 | -0.572 | -0.121 | 0.006 | -0.039 | 0.042 | 0.298 | 0.480 | 0.380 | -0.099 | 0.698 | 0.736 | 0.436 | | | | |
| Sr | -0.225 | -0.367 | 0.451 | 0.659 | -0.336 | -0.359 | -0.357 | -0.355 | 0.036 | -0.209 | -0.223 | 0.459 | -0.187 | -0.377 | -0.188 | -0.572 | | | |
| Ba | -0.191 | -0.648 | -0.464 | 0.235 | 0.625 | 0.518 | 0.527 | 0.434 | -0.152 | -0.049 | 0.011 | 0.326 | -0.140 | 0.128 | 0.211 | -0.221 | 0.096 | | |
| Zn | 0.119 | 0.005 | -0.344 | -0.404 | 0.392 | 0.612 | 0.584 | 0.629 | 0.186 | 0.092 | -0.118 | -0.250 | 0.139 | 0.484 | 0.038 | 0.619 | -0.650 | -0.061 | |
| Rb | -0.309 | -0.400 | -0.680 | -0.088 | 0.790 | 0.941 | 0.942 | 0.887 | -0.099 | -0.184 | -0.315 | -0.178 | -0.274 | 0.205 | -0.136 | 0.185 | -0.517 | 0.346 | 0.789 |
| Zr | -0.762 | -0.864 | -0.617 | 0.739 | 0.723 | 0.607 | 0.610 | 0.627 | -0.073 | -0.362 | -0.699 | 0.377 | -0.545 | -0.442 | -0.627 | -0.516 | 0.300 | 0.527 | -0.093 |
| Zr/Rb | -0.691 | -0.763 | -0.338 | 0.864 | 0.406 | 0.229 | 0.232 | 0.259 | -0.050 | -0.338 | -0.606 | 0.493 | -0.483 | -0.584 | -0.612 | -0.659 | 0.591 | 0.403 | -0.470 |
| Nb | -0.505 | -0.647 | -0.711 | 0.299 | 0.813 | 0.876 | 0.850 | 0.909 | 0.036 | -0.230 | -0.611 | 0.083 | -0.360 | -0.011 | -0.422 | -0.032 | -0.194 | 0.365 | 0.547 |
| Pb | -0.129 | -0.120 | -0.489 | -0.337 | 0.581 | 0.730 | 0.756 | 0.602 | -0.247 | -0.187 | 0.070 | -0.349 | -0.223 | 0.235 | 0.163 | 0.170 | -0.606 | 0.275 | 0.688 |
| Th | -0.170 | -0.275 | -0.658 | -0.191 | 0.721 | 0.826 | 0.811 | 0.829 | 0.070 | 0.005 | -0.302 | -0.148 | -0.078 | 0.293 | -0.160 | 0.338 | -0.630 | 0.243 | 0.802 |
| La | -0.410 | -0.416 | -0.427 | 0.209 | 0.513 | 0.598 | 0.562 | 0.669 | 0.062 | -0.218 | -0.603 | 0.028 | -0.296 | -0.090 | -0.440 | 0.000 | -0.117 | 0.131 | 0.489 |
| Ce | -0.648 | -0.757 | -0.739 | 0.377 | 0.891 | 0.914 | 0.908 | 0.908 | -0.107 | -0.361 | -0.631 | 0.106 | -0.500 | -0.148 | -0.456 | -0.233 | -0.110 | 0.511 | 0.420 |
| Nd | -0.682 | -0.821 | -0.678 | 0.479 | 0.849 | 0.854 | 0.854 | 0.846 | -0.068 | -0.372 | -0.669 | 0.161 | -0.526 | -0.218 | -0.509 | -0.325 | 0.032 | 0.520 | 0.323 |
| Y | -0.676 | -0.877 | -0.547 | 0.772 | 0.653 | 0.590 | 0.571 | 0.642 | 0.028 | -0.341 | -0.770 | 0.457 | -0.444 | -0.341 | -0.643 | -0.408 | 0.349 | 0.445 | 0.005 |
| Sc | 0.040 | -0.160 | -0.552 | -0.289 | 0.586 | 0.699 | 0.661 | 0.682 | -0.029 | 0.067 | 0.012 | -0.201 | 0.036 | 0.433 | 0.190 | 0.409 | -0.627 | 0.296 | 0.715 |
| | Corg | Bio.Silica | CaCO3 | Phos. | Terr. | Al | K | Ti | I | Br | Mo | U | Ni | Cr | V | Cu | Sr | Ba | Zn |
| | | | | | | | | | | | | | | | | | | | |
| | | | | | | | | | | | | | | | | | | | |
| Zr | 0.371 | | | | | | | | | | | | | | | | | | |
| Zr/Rb | -0.052 | 0.900 | | | | | | | | | | | | | | | | | |
| Nb | 0.800 | 0.662 | 0.348 | | | | | | | | | | | | | | | | |
| Pb | 0.842 | 0.046 | -0.323 | 0.459 | | | | | | | | | | | | | | | |
| Th | 0.891 | 0.307 | -0.099 | 0.715 | 0.711 | | | | | | | | | | | | | | |
| La | 0.574 | 0.471 | 0.232 | 0.582 | 0.304 | 0.543 | | | | | | | | | | | | | |
| Ce | 0.800 | 0.795 | 0.489 | 0.869 | 0.544 | 0.694 | 0.649 | | | | | | | | | | | | |
| Nd | 0.722 | 0.850 | 0.586 | 0.811 | 0.455 | 0.621 | 0.652 | 0.961 | | | | | | | | | | | |
| Y | 0.377 | 0.929 | 0.841 | 0.693 | -0.006 | 0.313 | 0.570 | 0.780 | 0.844 | | | | | | | | | | |
| Sc | 0.757 | 0.056 | -0.302 | 0.579 | 0.732 | 0.733 | 0.363 | 0.499 | 0.386 | 0.075 | | | | | | | | | |
| | Rb | Zr | Zr/Rb | Nb | Pb | Th | La | Ce | Nd | Y | | | | | | | | | |

| APPENDIX C.16. CORRELATION MATRICES | | | | | | | | | | | | | | | | | | | |
|---|---|---|---|---|---|---|---|---|---|---|---|---|---|---|---|---|---|---|---|
| | | | | | | | | | | | | | | | | | | | |
| CD38-02 | 2525m | | | | | | | | | | | | | | | | | | |
| | | | | | | | | | | | | | | | | | | | |
| Bio.Silica | 0.326 | | | | | | | | | | | | | | | | | | |
| CaCO3 | -0.181 | -0.522 | | | | | | | | | | | | | | | | | |
| Phos. | -0.493 | 0.301 | -0.202 | | | | | | | | | | | | | | | | |
| Terr. | 0.102 | 0.370 | -0.985 | 0.173 | | | | | | | | | | | | | | | |
| Al | 0.049 | 0.254 | -0.948 | 0.125 | 0.984 | | | | | | | | | | | | | | |
| K | -0.058 | 0.217 | -0.893 | 0.121 | 0.934 | 0.948 | | | | | | | | | | | | | |
| Ti | 0.206 | 0.343 | -0.925 | 0.130 | 0.935 | 0.932 | 0.823 | | | | | | | | | | | | |
| I | 0.825 | 0.307 | 0.030 | -0.398 | -0.118 | -0.184 | -0.276 | -0.044 | | | | | | | | | | | |
| Br | 0.766 | 0.441 | -0.124 | -0.150 | 0.025 | -0.081 | -0.136 | 0.001 | 0.810 | | | | | | | | | | |
| Mo | 0.629 | 0.176 | -0.179 | -0.337 | 0.141 | 0.118 | 0.056 | 0.273 | 0.465 | 0.453 | | | | | | | | | |
| U | 0.079 | 0.134 | 0.103 | 0.136 | -0.142 | -0.186 | -0.269 | -0.041 | -0.005 | 0.063 | -0.031 | | | | | | | | |
| Ni | 0.816 | 0.506 | -0.446 | -0.231 | 0.363 | 0.281 | 0.170 | 0.427 | 0.665 | 0.692 | 0.563 | 0.062 | | | | | | | |
| Cr | 0.244 | 0.530 | -0.733 | 0.210 | 0.690 | 0.629 | 0.488 | 0.683 | 0.209 | 0.343 | 0.051 | 0.072 | 0.553 | | | | | | |
| V | -0.092 | 0.244 | -0.811 | 0.338 | 0.839 | 0.844 | 0.753 | 0.879 | -0.281 | -0.176 | 0.004 | 0.053 | 0.225 | 0.709 | | | | | |
| Cu | 0.320 | 0.448 | -0.799 | 0.292 | 0.772 | 0.725 | 0.597 | 0.846 | 0.078 | 0.242 | 0.283 | 0.109 | 0.599 | 0.750 | 0.787 | | | | |
| Sr | -0.263 | -0.511 | 0.980 | -0.102 | -0.963 | -0.932 | -0.862 | -0.944 | -0.055 | -0.140 | -0.283 | 0.120 | -0.513 | -0.707 | -0.785 | -0.795 | | | |
| Ba | -0.066 | 0.540 | -0.619 | 0.652 | 0.571 | 0.495 | 0.432 | 0.520 | -0.198 | 0.111 | -0.123 | 0.139 | 0.282 | 0.671 | 0.627 | 0.741 | -0.520 | | |
| Zn | 0.267 | 0.583 | -0.861 | 0.308 | 0.817 | 0.751 | 0.642 | 0.831 | 0.049 | 0.249 | 0.175 | 0.061 | 0.575 | 0.795 | 0.772 | 0.909 | -0.843 | 0.779 | |
| Rb | 0.114 | 0.252 | -0.940 | 0.062 | 0.973 | 0.980 | 0.921 | 0.949 | -0.154 | -0.051 | 0.192 | -0.144 | 0.357 | 0.632 | 0.849 | 0.758 | -0.938 | 0.482 | 0.781 |
| Zr | 0.165 | 0.305 | -0.939 | 0.045 | 0.961 | 0.959 | 0.914 | 0.943 | -0.074 | -0.020 | 0.209 | -0.117 | 0.345 | 0.604 | 0.792 | 0.734 | -0.940 | 0.451 | 0.762 |
| Zr/Rb | 0.152 | 0.156 | 0.173 | -0.044 | -0.222 | -0.258 | -0.200 | -0.197 | 0.308 | 0.126 | 0.020 | 0.107 | -0.096 | -0.203 | -0.353 | -0.212 | 0.165 | -0.178 | -0.196 |
| Nb | 0.025 | 0.227 | -0.761 | 0.148 | 0.785 | 0.783 | 0.739 | 0.787 | -0.168 | -0.098 | 0.177 | -0.132 | 0.223 | 0.476 | 0.704 | 0.626 | -0.756 | 0.408 | 0.651 |
| Pb | -0.184 | -0.114 | -0.546 | 0.068 | 0.622 | 0.671 | 0.648 | 0.571 | -0.347 | -0.242 | -0.049 | -0.083 | -0.066 | 0.291 | 0.604 | 0.394 | -0.505 | 0.237 | 0.353 |
| Th | 0.083 | 0.175 | -0.710 | 0.112 | 0.737 | 0.752 | 0.687 | 0.736 | -0.174 | -0.067 | 0.116 | 0.011 | 0.293 | 0.452 | 0.690 | 0.645 | -0.702 | 0.424 | 0.612 |
| La | -0.016 | 0.170 | -0.649 | 0.109 | 0.676 | 0.663 | 0.611 | 0.682 | -0.175 | -0.103 | 0.145 | -0.007 | 0.280 | 0.470 | 0.649 | 0.538 | -0.662 | 0.310 | 0.567 |
| Ce | -0.158 | -0.020 | -0.420 | 0.031 | 0.468 | 0.487 | 0.487 | 0.411 | -0.309 | -0.223 | 0.056 | -0.096 | 0.097 | 0.244 | 0.372 | 0.321 | -0.416 | 0.245 | 0.288 |
| Nd | 0.072 | 0.138 | -0.408 | 0.094 | 0.415 | 0.422 | 0.378 | 0.418 | -0.130 | -0.073 | 0.149 | -0.089 | 0.311 | 0.313 | 0.370 | 0.439 | -0.414 | 0.314 | 0.344 |
| Y | 0.019 | 0.380 | -0.823 | 0.432 | 0.821 | 0.800 | 0.704 | 0.855 | -0.234 | -0.044 | 0.094 | 0.044 | 0.358 | 0.690 | 0.864 | 0.893 | -0.793 | 0.786 | 0.848 |
| Sc | -0.046 | 0.234 | -0.480 | 0.123 | 0.481 | 0.465 | 0.405 | 0.466 | -0.109 | -0.053 | -0.016 | 0.176 | 0.116 | 0.314 | 0.522 | 0.355 | -0.476 | 0.260 | 0.467 |
| | Corg | Bio.Silica | CaCO3 | Phos. | Terr. | Al | K | Ti | I | Br | Mo | U | Ni | Cr | V | Cu | Sr | Ba | Zn |
| | | | | | | | | | | | | | | | | | | | |
| | | | | | | | | | | | | | | | | | | | |
| Zr | 0.962 | | | | | | | | | | | | | | | | | | |
| Zr/Rb | -0.321 | -0.051 | | | | | | | | | | | | | | | | | |
| Nb | 0.800 | 0.796 | -0.148 | | | | | | | | | | | | | | | | |
| Pb | 0.646 | 0.607 | -0.261 | 0.470 | | | | | | | | | | | | | | | |
| Th | 0.766 | 0.723 | -0.291 | 0.556 | 0.556 | | | | | | | | | | | | | | |
| La | 0.697 | 0.638 | -0.318 | 0.503 | 0.449 | 0.504 | | | | | | | | | | | | | |
| Ce | 0.516 | 0.470 | -0.243 | 0.387 | 0.440 | 0.437 | 0.383 | | | | | | | | | | | | |
| Nd | 0.447 | 0.394 | -0.248 | 0.299 | 0.266 | 0.476 | 0.264 | 0.670 | | | | | | | | | | | |
| Y | 0.798 | 0.755 | -0.284 | 0.658 | 0.474 | 0.674 | 0.581 | 0.389 | 0.467 | | | | | | | | | | |
| Sc | 0.497 | 0.436 | -0.304 | 0.445 | 0.301 | 0.418 | 0.301 | 0.150 | 0.052 | 0.392 | | | | | | | | | |
| | Rb | Zr | Zr/Rb | Nb | Pb | Th | La | Ce | Nd | Y | | | | | | | | | |

APPENDIX C.16. CORRELATION MATRICES

| CD38-11 | 3835m | | | | | | | | | | | | | | | | | | |
|---|---|---|---|---|---|---|---|---|---|---|---|---|---|---|---|---|---|---|---|
| Bio.Silica | -0.212 | | | | | | | | | | | | | | | | | | |
| CaCO3 | 0.369 | -0.503 | | | | | | | | | | | | | | | | | |
| Phos. | -0.271 | -0.399 | 0.273 | | | | | | | | | | | | | | | | |
| Terr. | -0.316 | -0.172 | -0.754 | -0.105 | | | | | | | | | | | | | | | |
| Al | -0.298 | 0.019 | -0.727 | -0.370 | 0.862 | | | | | | | | | | | | | | |
| K | -0.386 | 0.190 | -0.795 | -0.444 | 0.822 | 0.940 | | | | | | | | | | | | | |
| Ti | -0.257 | -0.100 | -0.747 | -0.111 | 0.927 | 0.838 | 0.777 | | | | | | | | | | | | |
| I | 0.673 | -0.038 | -0.002 | -0.510 | 0.025 | 0.127 | 0.034 | 0.011 | | | | | | | | | | | |
| Br | 0.815 | -0.158 | 0.176 | -0.187 | -0.144 | -0.206 | -0.322 | -0.125 | 0.724 | | | | | | | | | | |
| Mo | 0.604 | -0.411 | 0.566 | 0.192 | -0.389 | -0.445 | -0.511 | -0.305 | 0.022 | 0.348 | | | | | | | | | |
| U | 0.305 | -0.317 | 0.290 | 0.283 | -0.146 | -0.195 | -0.270 | -0.171 | 0.304 | 0.220 | 0.229 | | | | | | | | |
| Ni | 0.810 | 0.026 | 0.111 | -0.197 | -0.222 | -0.210 | -0.248 | -0.204 | 0.560 | 0.606 | 0.466 | 0.427 | | | | | | | |
| Cr | 0.278 | 0.300 | -0.657 | -0.290 | 0.464 | 0.449 | 0.455 | 0.521 | 0.505 | 0.315 | -0.158 | 0.185 | 0.506 | | | | | | |
| V | -0.326 | 0.464 | -0.838 | -0.371 | 0.625 | 0.737 | 0.798 | 0.707 | 0.049 | -0.314 | -0.436 | -0.204 | -0.118 | 0.634 | | | | | |
| Cu | -0.155 | 0.730 | -0.712 | -0.367 | 0.252 | 0.384 | 0.492 | 0.305 | 0.136 | -0.187 | -0.364 | -0.075 | 0.202 | 0.661 | 0.782 | | | | |
| Sr | 0.187 | -0.520 | 0.948 | 0.460 | -0.691 | -0.714 | -0.785 | -0.714 | -0.139 | 0.022 | 0.481 | 0.312 | -0.009 | -0.695 | -0.820 | -0.671 | | | |
| Ba | -0.357 | 0.822 | -0.678 | -0.252 | 0.151 | 0.295 | 0.421 | 0.203 | -0.061 | -0.349 | -0.489 | -0.120 | -0.003 | 0.484 | 0.712 | 0.921 | -0.583 | | |
| Zn | 0.178 | 0.553 | -0.671 | -0.485 | 0.324 | 0.442 | 0.472 | 0.390 | 0.466 | 0.181 | -0.241 | 0.070 | 0.430 | 0.852 | 0.709 | 0.869 | -0.701 | 0.713 | |
| Rb | 0.004 | 0.221 | -0.723 | -0.686 | 0.707 | 0.839 | 0.890 | 0.700 | 0.362 | 0.015 | -0.322 | -0.183 | 0.079 | 0.641 | 0.773 | 0.538 | -0.809 | 0.368 | 0.653 |
| Zr | -0.158 | -0.641 | 0.046 | 0.752 | 0.357 | -0.003 | -0.119 | 0.358 | -0.356 | -0.055 | 0.183 | 0.184 | -0.197 | -0.148 | -0.225 | -0.439 | 0.170 | -0.426 | -0.415 |
| Zr/Rb | -0.096 | -0.562 | 0.404 | 0.886 | -0.118 | -0.439 | -0.540 | -0.106 | -0.456 | -0.046 | 0.331 | 0.225 | -0.147 | -0.427 | -0.550 | -0.579 | 0.526 | -0.487 | -0.623 |
| Nb | -0.151 | -0.110 | -0.642 | -0.173 | 0.819 | 0.699 | 0.707 | 0.814 | 0.042 | -0.021 | -0.162 | -0.125 | -0.124 | 0.428 | 0.551 | 0.187 | -0.656 | 0.070 | 0.289 |
| Pb | 0.125 | -0.669 | 0.066 | 0.122 | 0.429 | 0.308 | 0.188 | 0.417 | 0.069 | 0.134 | 0.317 | 0.010 | -0.112 | -0.033 | -0.048 | -0.420 | 0.022 | -0.598 | -0.213 |
| Th | -0.140 | -0.003 | -0.456 | -0.264 | 0.552 | 0.539 | 0.570 | 0.524 | 0.070 | -0.179 | -0.103 | -0.106 | -0.018 | 0.360 | 0.488 | 0.307 | -0.449 | 0.179 | 0.337 |
| La | -0.062 | 0.118 | -0.475 | -0.383 | 0.484 | 0.640 | 0.655 | 0.539 | 0.152 | -0.171 | -0.195 | -0.121 | 0.029 | 0.383 | 0.588 | 0.359 | -0.528 | 0.257 | 0.381 |
| Ce | -0.104 | -0.263 | -0.217 | -0.058 | 0.466 | 0.371 | 0.409 | 0.448 | 0.012 | -0.161 | -0.169 | -0.067 | -0.115 | 0.139 | 0.276 | -0.096 | -0.223 | -0.133 | -0.070 |
| Nd | -0.339 | 0.295 | -0.653 | -0.232 | 0.543 | 0.575 | 0.661 | 0.553 | -0.101 | -0.281 | -0.443 | -0.313 | -0.158 | 0.347 | 0.646 | 0.482 | -0.625 | 0.449 | 0.357 |
| Y | -0.403 | 0.555 | -0.661 | -0.002 | 0.310 | 0.356 | 0.455 | 0.385 | -0.266 | -0.466 | -0.292 | -0.147 | -0.002 | 0.468 | 0.697 | 0.825 | -0.506 | 0.851 | 0.595 |
| Sc | -0.319 | 0.542 | -0.788 | -0.323 | 0.500 | 0.587 | 0.650 | 0.551 | 0.015 | -0.229 | -0.595 | -0.323 | -0.124 | 0.514 | 0.731 | 0.707 | -0.745 | 0.682 | 0.608 |
| | Corg | Bio.Silica | CaCO3 | Phos. | Terr. | Al | K | Ti | I | Br | Mo | U | Ni | Cr | V | Cu | Sr | Ba | Zn |

| Zr | -0.309 | | | | | | | | | | | | | | | | | | |
|---|---|---|---|---|---|---|---|---|---|---|---|---|---|---|---|---|---|---|---|
| Zr/Rb | -0.726 | 0.872 | | | | | | | | | | | | | | | | | |
| Nb | 0.684 | 0.300 | -0.129 | | | | | | | | | | | | | | | | |
| Pb | 0.207 | 0.470 | 0.223 | 0.523 | | | | | | | | | | | | | | | |
| Th | 0.573 | 0.051 | -0.261 | 0.470 | 0.206 | | | | | | | | | | | | | | |
| La | 0.658 | -0.134 | -0.415 | 0.443 | 0.130 | 0.424 | | | | | | | | | | | | | |
| Ce | 0.368 | 0.228 | -0.030 | 0.401 | 0.305 | 0.303 | 0.384 | | | | | | | | | | | | |
| Nd | 0.576 | -0.054 | -0.325 | 0.443 | -0.083 | 0.405 | 0.489 | 0.458 | | | | | | | | | | | |
| Y | 0.335 | -0.107 | -0.232 | 0.194 | -0.361 | 0.254 | 0.279 | 0.007 | 0.485 | | | | | | | | | | |
| Sc | 0.575 | -0.208 | -0.450 | 0.325 | -0.249 | 0.300 | 0.472 | 0.045 | 0.559 | 0.646 | | | | | | | | | |
| | Rb | Zr | Zr/Rb | Nb | Pb | Th | La | Ce | Nd | Y | | | | | | | | | |

| APPENDIX C.17. PRINCIPAL COMPONENT ANALYSIS RESULTS | | | | | | | | |
|---|---|---|---|---|---|---|---|---|
| CD38-09 | 148m | | | | | | | |
| Eigenvalue | 12.567 | 6.467 | 3.869 | 1.970 | 1.272 | 0.928 | 0.658 | 0.467 |
| Proportion | 0.419 | 0.216 | 0.129 | 0.066 | 0.042 | 0.031 | 0.022 | 0.016 |
| Cumulative | 0.419 | 0.634 | 0.763 | 0.829 | 0.872 | 0.902 | 0.924 | 0.940 |
| Variable | PCF 1 | PCF 2 | PCF 3 | PCF 4 | PCF 5 | PCF 6 | PCF 7 | PCF 8 |
| Corg | -0.068 | 0.320 | 0.230 | 0.127 | -0.026 | 0.018 | 0.164 | -0.066 |
| Bio.Silica | 0.107 | 0.308 | -0.073 | 0.128 | 0.174 | 0.132 | -0.207 | 0.162 |
| CaCO3 | 0.139 | -0.071 | -0.228 | -0.256 | 0.287 | 0.099 | 0.592 | 0.058 |
| Phos. | 0.127 | -0.185 | 0.329 | -0.270 | 0.036 | -0.007 | -0.084 | 0.016 |
| Terr. | -0.204 | -0.047 | -0.268 | 0.218 | -0.195 | -0.097 | 0.043 | -0.112 |
| Al | -0.278 | -0.012 | -0.003 | -0.029 | -0.023 | -0.006 | -0.016 | -0.045 |
| K | -0.260 | -0.082 | -0.099 | -0.106 | -0.051 | 0.029 | -0.047 | -0.160 |
| Tl | -0.269 | -0.076 | -0.016 | 0.002 | -0.081 | -0.072 | 0.006 | 0.138 |
| I | -0.162 | 0.065 | 0.293 | 0.230 | 0.347 | 0.139 | 0.075 | 0.060 |
| Br | -0.134 | 0.137 | 0.278 | 0.211 | 0.347 | 0.202 | 0.174 | 0.129 |
| Mo | 0.063 | 0.317 | 0.187 | 0.026 | -0.061 | 0.059 | 0.212 | -0.179 |
| U | 0.118 | -0.140 | 0.360 | -0.296 | 0.051 | 0.005 | -0.109 | -0.003 |
| Ni | -0.028 | 0.281 | 0.286 | 0.130 | -0.263 | -0.088 | 0.084 | -0.064 |
| Cr | -0.059 | 0.245 | 0.225 | -0.204 | -0.340 | -0.117 | 0.081 | -0.138 |
| V | -0.065 | 0.272 | -0.102 | -0.374 | 0.052 | 0.045 | -0.062 | -0.295 |
| Cu | -0.170 | 0.217 | 0.015 | -0.272 | -0.204 | -0.066 | 0.069 | 0.307 |
| Sr | 0.120 | -0.242 | 0.278 | -0.254 | 0.020 | 0.088 | 0.052 | 0.019 |
| Ba | -0.054 | -0.068 | -0.029 | 0.011 | -0.401 | 0.881 | -0.023 | -0.037 |
| Zn | -0.232 | 0.057 | 0.071 | -0.163 | 0.013 | 0.029 | -0.002 | 0.527 |
| Rb | -0.270 | -0.023 | -0.027 | -0.141 | 0.108 | 0.084 | -0.051 | -0.053 |
| Zr | -0.111 | -0.284 | 0.103 | 0.328 | -0.093 | -0.072 | 0.109 | -0.068 |
| Zr/Rb | -0.215 | 0.196 | 0.010 | -0.116 | 0.103 | -0.101 | -0.357 | -0.087 |
| Nb | -0.232 | -0.137 | 0.102 | -0.009 | 0.108 | 0.075 | -0.080 | 0.060 |
| Pb | -0.216 | 0.023 | -0.145 | -0.217 | 0.266 | 0.137 | -0.180 | -0.150 |
| Th | -0.259 | 0.083 | 0.022 | 0.084 | 0.095 | -0.027 | -0.083 | 0.043 |
| La | -0.218 | 0.002 | -0.019 | -0.105 | 0.092 | -0.042 | 0.427 | -0.373 |
| Ce | -0.236 | -0.157 | 0.097 | 0.035 | 0.076 | -0.029 | -0.019 | -0.178 |
| Nd | -0.226 | -0.189 | 0.131 | 0.033 | -0.002 | 0.020 | 0.017 | -0.114 |
| Y | -0.140 | -0.268 | 0.205 | -0.028 | -0.210 | -0.164 | 0.066 | 0.061 |
| Sc | -0.215 | 0.039 | -0.179 | -0.101 | -0.142 | -0.051 | 0.275 | 0.374 |
| CD38-10 | 257m | | | | | | | |
| Eigenvalue | 13.434 | 7.480 | 3.128 | 2.013 | 0.888 | 0.677 | 0.434 | 0.408 |
| Proportion | 0.448 | 0.249 | 0.104 | 0.067 | 0.030 | 0.023 | 0.014 | 0.014 |
| Cumulative | 0.448 | 0.697 | 0.801 | 0.869 | 0.898 | 0.921 | 0.935 | 0.949 |
| Variable | PCF 1 | PCF 2 | PCF 3 | PCF 4 | PCF 5 | PCF 6 | PCF 7 | PCF 8 |
| Corg | 0.198 | 0.192 | -0.235 | 0.021 | -0.067 | 0.013 | -0.023 | -0.009 |
| Bio.Silica | 0.209 | 0.108 | 0.243 | -0.131 | 0.159 | 0.164 | -0.037 | 0.213 |
| CaCO3 | 0.215 | -0.077 | 0.032 | -0.059 | -0.502 | -0.294 | 0.040 | -0.176 |
| Phos. | -0.120 | -0.273 | -0.161 | -0.029 | 0.012 | 0.211 | 0.253 | 0.298 |
| Terr. | -0.248 | 0.077 | -0.044 | 0.131 | 0.222 | -0.029 | -0.125 | -0.174 |
| Al | -0.250 | 0.133 | -0.003 | 0.069 | -0.033 | -0.044 | 0.066 | -0.027 |
| K | -0.249 | 0.125 | 0.028 | 0.103 | -0.008 | -0.048 | 0.098 | 0.022 |
| Tl | -0.251 | 0.118 | -0.013 | -0.050 | -0.019 | 0.037 | -0.032 | -0.178 |
| I | 0.040 | 0.050 | -0.352 | -0.388 | 0.179 | -0.522 | 0.127 | 0.128 |
| Br | 0.114 | 0.141 | -0.360 | -0.128 | 0.369 | -0.278 | -0.069 | 0.173 |
| Mo | 0.186 | 0.145 | -0.031 | 0.366 | 0.076 | -0.015 | 0.026 | 0.176 |
| U | -0.025 | -0.126 | -0.431 | 0.061 | -0.112 | 0.425 | 0.148 | 0.414 |
| Ni | 0.157 | 0.167 | -0.347 | -0.057 | -0.028 | 0.178 | -0.048 | -0.163 |
| Cr | 0.066 | 0.277 | -0.282 | 0.072 | -0.219 | 0.043 | 0.012 | -0.221 |
| V | 0.147 | 0.189 | -0.135 | 0.395 | -0.160 | -0.074 | -0.057 | 0.094 |
| Cu | 0.073 | 0.281 | -0.124 | -0.183 | -0.067 | 0.372 | -0.014 | -0.241 |
| Sr | 0.028 | -0.301 | -0.154 | 0.057 | -0.425 | -0.197 | 0.162 | 0.005 |
| Ba | -0.136 | 0.004 | -0.217 | 0.481 | 0.038 | -0.147 | -0.302 | -0.081 |
| Zn | -0.104 | 0.293 | 0.028 | -0.238 | -0.231 | 0.028 | 0.157 | 0.082 |
| Rb | -0.214 | 0.207 | 0.057 | 0.005 | -0.105 | -0.053 | 0.144 | 0.102 |
| Zr | -0.229 | -0.164 | -0.124 | 0.032 | 0.108 | 0.016 | -0.058 | -0.097 |
| Zr/Rb | -0.149 | -0.278 | -0.153 | 0.043 | 0.127 | 0.039 | -0.058 | -0.121 |
| Nb | -0.242 | 0.069 | -0.061 | -0.101 | -0.032 | 0.020 | 0.287 | -0.184 |
| Pb | -0.137 | 0.242 | 0.175 | 0.187 | -0.086 | -0.156 | 0.199 | 0.398 |
| Th | -0.186 | 0.231 | -0.001 | -0.119 | 0.061 | 0.020 | 0.003 | -0.033 |
| La | -0.182 | 0.038 | -0.006 | -0.276 | -0.308 | 0.020 | -0.746 | 0.350 |
| Ce | -0.265 | 0.023 | -0.027 | 0.017 | -0.063 | -0.067 | 0.028 | 0.026 |
| Nd | -0.262 | -0.024 | -0.053 | 0.008 | -0.099 | -0.140 | -0.004 | 0.060 |
| Y | -0.224 | -0.153 | -0.177 | -0.074 | -0.082 | 0.093 | -0.036 | -0.080 |
| Sc | -0.130 | 0.270 | 0.001 | 0.071 | 0.003 | 0.053 | 0.050 | 0.081 |

| APPENDIX C.17. PRINCIPAL COMPONENT ANALYSIS RESULTS | | | | | | | | |
|---|---|---|---|---|---|---|---|---|
| CD38-02 | 2525m | | | | | | | |
| Eigenvalue | 14.675 | 4.516 | 2.412 | 1.408 | 1.215 | 0.976 | 0.732 | 0.697 |
| Proportion | 0.489 | 0.151 | 0.08 | 0.047 | 0.041 | 0.033 | 0.024 | 0.023 |
| Cumulative | 0.489 | 0.64 | 0.72 | 0.767 | 0.808 | 0.84 | 0.865 | 0.888 |
| Variable | PCF 1 | PCF 2 | PCF 3 | PCF 4 | PCF 5 | PCF 6 | PCF 7 | PCF 8 |
| Corg | -0.038 | 0.431 | -0.145 | -0.031 | 0.073 | -0.065 | -0.059 | 0.07 |
| Bio.Silica | -0.109 | 0.224 | 0.316 | 0.097 | -0.195 | -0.027 | 0.374 | -0.156 |
| CaCO3 | 0.253 | -0.033 | 0.002 | -0.113 | 0.091 | -0.022 | -0.092 | -0.022 |
| Phos. | -0.059 | -0.166 | 0.494 | -0.033 | -0.18 | 0.037 | -0.085 | -0.224 |
| Terr. | -0.254 | -0.02 | -0.06 | 0.107 | -0.065 | 0.031 | 0.036 | 0.052 |
| Al | -0.248 | -0.063 | -0.12 | 0.103 | -0.049 | 0.034 | 0.003 | 0.063 |
| K | -0.227 | -0.106 | -0.148 | 0.149 | -0.148 | 0.046 | 0.064 | 0.031 |
| Tl | -0.251 | 0.019 | -0.064 | 0.075 | 0.031 | -0.078 | -0.118 | -0.068 |
| I | 0.028 | 0.432 | -0.07 | 0.084 | -0.021 | 0.057 | 0.049 | 0.189 |
| Br | -0.011 | 0.414 | 0.072 | -0.013 | -0.013 | 0.166 | 0.032 | 0.179 |
| Mo | -0.048 | 0.285 | -0.247 | -0.115 | 0.058 | -0.138 | -0.204 | -0.612 |
| U | 0.014 | 0.05 | 0.285 | -0.056 | 0.498 | -0.651 | -0.064 | 0.124 |
| Ni | -0.116 | 0.379 | -0.021 | -0.207 | 0.071 | 0.066 | 0 | 0.011 |
| Cr | -0.195 | 0.13 | 0.193 | -0.041 | 0.013 | 0.167 | -0.028 | 0.367 |
| V | -0.233 | -0.102 | 0.082 | 0.024 | 0.152 | 0.02 | -0.148 | 0.033 |
| Cu | -0.227 | 0.11 | 0.142 | -0.12 | 0.042 | -0.039 | -0.234 | -0.037 |
| Sr | 0.25 | -0.069 | 0.063 | -0.106 | 0.064 | -0.003 | -0.089 | 0.048 |
| Ba | -0.17 | -0.011 | 0.421 | -0.131 | -0.123 | 0.072 | -0.065 | 0.037 |
| Zn | -0.232 | 0.102 | 0.183 | 0.006 | 0.022 | 0.054 | -0.022 | -0.026 |
| Rb | -0.251 | -0.038 | -0.14 | 0.049 | 0.03 | 0.024 | 0.01 | 0.006 |
| Zr | -0.243 | -0.006 | -0.138 | 0.166 | -0.096 | -0.144 | 0 | 0.037 |
| Zr/Rb | 0.073 | 0.119 | 0.048 | 0.384 | -0.458 | -0.584 | -0.032 | 0.09 |
| Nb | -0.206 | -0.05 | -0.083 | 0.163 | -0.045 | -0.046 | 0.04 | -0.277 |
| Pb | -0.156 | -0.184 | -0.176 | 0.042 | 0.092 | -0.065 | -0.177 | 0.397 |
| Th | -0.202 | -0.049 | -0.082 | -0.103 | 0.117 | -0.126 | 0.035 | 0.105 |
| La | -0.181 | -0.052 | -0.079 | -0.015 | 0.155 | 0.042 | -0.284 | -0.124 |
| Ce | -0.129 | -0.134 | -0.175 | -0.44 | -0.166 | -0.225 | 0.298 | 0.084 |
| Nd | -0.127 | -0.025 | -0.085 | -0.591 | -0.224 | -0.171 | 0.232 | 0.007 |
| Y | -0.234 | -0.038 | 0.165 | -0.101 | -0.009 | -0.009 | -0.193 | -0.099 |
| Sc | -0.131 | -0.048 | 0.058 | 0.21 | 0.49 | 0.021 | 0.622 | -0.145 |
| CD38-11 | 3835m | | | | | | | |
| Eigenvalue | 12.217 | 5.051 | 4.289 | 2.218 | 1.127 | 0.985 | 0.865 | 0.590 |
| Proportion | 0.407 | 0.168 | 0.143 | 0.074 | 0.038 | 0.033 | 0.029 | 0.020 |
| Cumulative | 0.407 | 0.576 | 0.719 | 0.793 | 0.830 | 0.863 | 0.892 | 0.911 |
| Variable | PCF 1 | PCF 2 | PCF 3 | PCF 4 | PCF 5 | PCF 6 | PCF 7 | PCF 8 |
| Corg | 0.085 | 0.205 | -0.374 | 0.049 | -0.025 | 0.139 | 0.178 | -0.083 |
| Bio.Silica | -0.137 | 0.283 | 0.233 | -0.020 | 0.112 | 0.131 | 0.126 | 0.038 |
| CaCO3 | 0.265 | 0.035 | -0.043 | -0.122 | -0.213 | -0.047 | -0.070 | -0.065 |
| Phos. | 0.140 | -0.205 | 0.143 | 0.412 | 0.024 | -0.077 | 0.036 | -0.055 |
| Terr. | -0.207 | -0.259 | -0.113 | 0.065 | 0.134 | -0.062 | -0.060 | 0.060 |
| Al | -0.236 | -0.159 | -0.092 | -0.098 | 0.009 | -0.084 | -0.202 | -0.126 |
| K | -0.257 | -0.128 | -0.029 | -0.134 | -0.054 | -0.049 | -0.128 | -0.051 |
| Tl | -0.213 | -0.238 | -0.112 | 0.110 | 0.106 | 0.044 | -0.007 | -0.080 |
| I | -0.037 | 0.206 | -0.354 | -0.065 | 0.142 | -0.310 | -0.052 | 0.064 |
| Br | 0.064 | 0.160 | -0.356 | 0.058 | 0.395 | 0.027 | 0.191 | 0.061 |
| Mo | 0.156 | 0.023 | -0.204 | 0.135 | -0.330 | 0.546 | -0.020 | -0.122 |
| U | 0.078 | 0.055 | -0.160 | 0.332 | -0.247 | -0.547 | -0.340 | -0.031 |
| Ni | 0.019 | 0.255 | -0.287 | 0.249 | -0.188 | 0.072 | 0.178 | -0.011 |
| Cr | -0.194 | 0.129 | -0.203 | 0.288 | 0.053 | -0.067 | 0.057 | 0.044 |
| V | -0.266 | -0.001 | 0.036 | 0.056 | -0.106 | 0.029 | -0.063 | -0.090 |
| Cu | -0.221 | 0.208 | 0.099 | 0.190 | -0.099 | 0.054 | -0.074 | 0.005 |
| Sr | 0.263 | -0.008 | 0.038 | -0.029 | -0.224 | -0.110 | -0.122 | -0.033 |
| Ba | -0.197 | 0.196 | 0.229 | 0.169 | -0.054 | -0.031 | -0.051 | -0.001 |
| Zn | -0.212 | 0.224 | -0.101 | 0.193 | 0.018 | 0.017 | -0.111 | 0.020 |
| Rb | -0.251 | -0.007 | -0.181 | -0.153 | -0.059 | 0.024 | -0.074 | -0.009 |
| Zr | 0.070 | -0.346 | -0.039 | 0.348 | 0.111 | 0.009 | 0.100 | 0.041 |
| Zr/Rb | 0.178 | -0.239 | 0.062 | 0.339 | 0.083 | 0.030 | 0.129 | 0.004 |
| Nb | -0.178 | -0.226 | -0.168 | 0.041 | 0.126 | 0.158 | -0.050 | -0.013 |
| Pb | 0.014 | -0.289 | -0.267 | -0.059 | 0.021 | 0.224 | -0.223 | -0.151 |
| Th | -0.158 | -0.108 | -0.099 | -0.014 | -0.321 | 0.158 | -0.160 | 0.771 |
| La | -0.183 | -0.054 | -0.100 | -0.108 | -0.342 | -0.031 | 0.083 | -0.501 |
| Ce | -0.084 | -0.215 | -0.108 | -0.106 | -0.316 | -0.303 | 0.557 | 0.069 |
| Nd | -0.205 | -0.079 | 0.064 | -0.030 | -0.133 | -0.060 | 0.477 | 0.093 |
| Y | -0.188 | 0.063 | 0.212 | 0.301 | -0.195 | 0.145 | -0.002 | -0.095 |
| Sc | -0.232 | 0.046 | 0.111 | 0.051 | 0.188 | -0.012 | 0.047 | -0.168 |

APPENDIX C.18. MULTI-COMPONENT ANALYSIS RESULTS

| CD38-09 Depth (cm) | (148m) TERR (%) | BIOG (%) | AUTH (%) | RESID (%) | HYDRO (%) | CD38-10 Depth (cm) | (257m) TERR (%) | BIOG (%) | AUTH (%) | RESID (%) | HYDRO (%) |
|---|---|---|---|---|---|---|---|---|---|---|---|
| 4.0 | 71.75 | 26.35 | 1.89 | 0.00 | 0.00 | 6.0 | 64.89 | 30.40 | 4.71 | 0.00 | 0.00 |
| 13.0 | 68.12 | 30.84 | 1.04 | 0.00 | 0.00 | 14.0 | 72.54 | 14.19 | 13.27 | 0.00 | 0.00 |
| 23.0 | 79.94 | 18.95 | 1.11 | 0.00 | 0.00 | 24.0 | 70.94 | 4.34 | 24.72 | 0.00 | 0.00 |
| 34.0 | 78.26 | 20.53 | 1.21 | 0.00 | 0.00 | 34.0 | 74.30 | 12.53 | 13.18 | 0.00 | 0.00 |
| 43.0 | 85.54 | 12.35 | 2.10 | 0.00 | 0.00 | 44.0 | 80.49 | 14.66 | 4.85 | 0.00 | 0.00 |
| 53.0 | 74.52 | 23.32 | 2.16 | 0.00 | 0.00 | 54.0 | 79.51 | 17.73 | 2.77 | 0.00 | 0.00 |
| 62.0 | 69.36 | 29.03 | 1.62 | 0.00 | 0.00 | 64.0 | 80.46 | 14.38 | 5.15 | 0.00 | 0.00 |
| 73.0 | 78.88 | 19.79 | 1.33 | 0.00 | 0.00 | 74.0 | 83.26 | 8.29 | 8.46 | 0.00 | 0.00 |
| 84.0 | 84.76 | 14.57 | 0.68 | 0.00 | 0.00 | 84.0 | 80.70 | 3.67 | 15.63 | 0.00 | 0.00 |
| 94.0 | 80.00 | 19.21 | 0.79 | 0.00 | 0.00 | 94.0 | 77.03 | 3.25 | 19.72 | 0.00 | 0.00 |
| 104.0 | 75.42 | 23.88 | 0.70 | 0.00 | 0.00 | 104.0 | 75.55 | 12.98 | 11.47 | 0.00 | 0.00 |
| 113.0 | 85.09 | 14.26 | 0.65 | 0.00 | 0.00 | 113.0 | 79.46 | 12.95 | 7.59 | 0.00 | 0.00 |
| 124.0 | 84.02 | 14.26 | 1.72 | 0.00 | 0.00 | 126.0 | 61.75 | 32.24 | 6.01 | 0.00 | 0.00 |
| 134.0 | 75.90 | 21.61 | 2.49 | 0.00 | 0.00 | 134.0 | 61.89 | 31.63 | 6.48 | 0.00 | 0.00 |
| 144.0 | 69.62 | 28.90 | 1.48 | 0.00 | 0.00 | 146.0 | 71.78 | 23.47 | 4.74 | 0.00 | 0.00 |
| 152.0 | 70.68 | 28.42 | 0.89 | 0.00 | 0.00 | 154.0 | 63.93 | 31.43 | 4.64 | 0.00 | 0.00 |
| 165.0 | 68.57 | 29.32 | 2.10 | 0.00 | 0.00 | 167.0 | 69.82 | 26.95 | 3.24 | 0.00 | 0.00 |
| 174.0 | 83.36 | 14.23 | 2.41 | 0.00 | 0.00 | 174.0 | 72.72 | 23.60 | 3.68 | 0.00 | 0.00 |
| 185.0 | 79.96 | 15.18 | 4.86 | 0.00 | 0.00 | 185.0 | 73.45 | 23.62 | 2.94 | 0.00 | 0.00 |
| 194.0 | 81.70 | 13.70 | 4.60 | 0.00 | 0.00 | 194.0 | 62.28 | 35.09 | 2.63 | 0.00 | 0.00 |
| 205.0 | 83.86 | 15.08 | 1.06 | 0.00 | 0.00 | 203.0 | 76.27 | 19.75 | 3.98 | 0.00 | 0.00 |
| 214.0 | 74.27 | 21.48 | 4.25 | 0.00 | 0.00 | 216.0 | 60.21 | 36.18 | 3.61 | 0.00 | 0.00 |
| 224.0 | 85.33 | 8.41 | 6.26 | 0.00 | 0.00 | 224.0 | 64.72 | 32.62 | 2.66 | 0.00 | 0.00 |
| 234.0 | 74.09 | 18.47 | 7.44 | 0.00 | 0.00 | 233.0 | 69.75 | 27.46 | 2.79 | 0.00 | 0.00 |
| 243.0 | 59.88 | 36.16 | 3.96 | 0.00 | 0.00 | 244.0 | 70.40 | 25.81 | 3.79 | 0.00 | 0.00 |
| 257.0 | 71.27 | 25.42 | 3.31 | 0.00 | 0.00 | 254.0 | 69.64 | 21.87 | 8.48 | 0.00 | 0.00 |
| 267.0 | 70.57 | 15.67 | 13.76 | 0.00 | 0.00 | 263.0 | 65.77 | 27.42 | 6.81 | 0.00 | 0.00 |
| 273.0 | 26.89 | 9.86 | 60.90 | 0.00 | 2.35 | 273.0 | 70.89 | 25.94 | 3.17 | 0.00 | 0.00 |
| 284.0 | 75.73 | 21.29 | 2.98 | 0.00 | 0.00 | 284.0 | 67.53 | 28.61 | 3.86 | 0.00 | 0.00 |
| 294.0 | 67.47 | 31.20 | 1.33 | 0.00 | 0.00 | 295.0 | 52.61 | 44.20 | 3.19 | 0.00 | 0.00 |
| 304.0 | 76.23 | 22.66 | 1.11 | 0.00 | 0.00 | 305.0 | 67.56 | 29.90 | 2.53 | 0.00 | 0.00 |
| 314.0 | 76.50 | 22.78 | 0.72 | 0.00 | 0.00 | 314.0 | 71.00 | 25.86 | 3.15 | 0.00 | 0.00 |
| 324.0 | 77.34 | 20.96 | 1.70 | 0.00 | 0.00 | 324.0 | 57.63 | 39.42 | 2.95 | 0.00 | 0.00 |
| 335.0 | 71.38 | 27.55 | 1.07 | 0.00 | 0.00 | 335.0 | 70.05 | 26.95 | 3.00 | 0.00 | 0.00 |
| 344.0 | 66.59 | 32.28 | 1.12 | 0.00 | 0.00 | 344.0 | 51.95 | 44.62 | 3.43 | 0.00 | 0.00 |
| 355.0 | 61.18 | 38.27 | 0.55 | 0.00 | 0.00 | 354.0 | 52.81 | 44.55 | 2.64 | 0.00 | 0.00 |
| 364.0 | 56.73 | 42.77 | 0.50 | 0.00 | 0.00 | 364.0 | 43.90 | 53.20 | 2.90 | 0.00 | 0.00 |
| 375.0 | 73.13 | 26.46 | 0.41 | 0.00 | 0.00 | 374.0 | 47.74 | 49.92 | 2.35 | 0.00 | 0.00 |
| 384.0 | 72.03 | 26.32 | 1.65 | 0.00 | 0.00 | 383.0 | 70.23 | 27.79 | 1.98 | 0.00 | 0.00 |
| 394.0 | 65.28 | 33.62 | 1.10 | 0.00 | 0.00 | 394.0 | 62.13 | 34.98 | 2.89 | 0.00 | 0.00 |
| 404.0 | 71.49 | 27.90 | 0.62 | 0.00 | 0.00 | 404.0 | 68.16 | 29.17 | 2.67 | 0.00 | 0.00 |
| 416.0 | 62.04 | 37.02 | 0.94 | 0.00 | 0.00 | 417.0 | 59.02 | 37.46 | 3.52 | 0.00 | 0.00 |
| 424.0 | 67.12 | 32.54 | 0.33 | 0.00 | 0.00 | 424.0 | 60.73 | 36.28 | 2.99 | 0.00 | 0.00 |
| 434.0 | 74.06 | 25.43 | 0.51 | 0.00 | 0.00 | 434.0 | 31.93 | 63.40 | 4.67 | 0.00 | 0.00 |
| 444.0 | 63.45 | 35.60 | 0.95 | 0.00 | 0.00 | 445.0 | 49.95 | 47.40 | 2.65 | 0.00 | 0.00 |
| 453.0 | 74.71 | 24.15 | 1.14 | 0.00 | 0.00 | 456.0 | 48.22 | 48.86 | 2.92 | 0.00 | 0.00 |
| 465.0 | 70.48 | 28.45 | 1.07 | 0.00 | 0.00 | 467.0 | 35.10 | 62.53 | 2.36 | 0.00 | 0.00 |
| 474.0 | 68.08 | 31.04 | 0.88 | 0.00 | 0.00 | 476.0 | 59.35 | 35.33 | 5.33 | 0.00 | 0.00 |
| 483.0 | 73.52 | 25.17 | 1.31 | 0.00 | 0.00 | 484.0 | 56.44 | 38.57 | 4.99 | 0.00 | 0.00 |
| 493.0 | 72.85 | 26.15 | 1.00 | 0.00 | 0.00 | 494.0 | 55.19 | 33.96 | 10.85 | 0.00 | 0.00 |
| 504.0 | 79.72 | 18.85 | 1.43 | 0.00 | 0.00 | 504.0 | 65.16 | 5.20 | 29.64 | 0.00 | 0.00 |
| 515.0 | 80.05 | 19.06 | 0.90 | 0.00 | 0.00 | 514.0 | 76.23 | 23.11 | 0.66 | 0.00 | 0.00 |
| 525.0 | 73.99 | 25.52 | 0.49 | 0.00 | 0.00 | 524.0 | 80.45 | 19.03 | 0.52 | 0.00 | 0.00 |
| 536.0 | 68.37 | 31.07 | 0.57 | 0.00 | 0.00 | 534.0 | 61.39 | 36.36 | 2.24 | 0.00 | 0.00 |
| 544.0 | 78.69 | 20.26 | 1.05 | 0.00 | 0.00 | 545.0 | 61.97 | 36.47 | 1.56 | 0.00 | 0.00 |
| 553.0 | 75.74 | 23.85 | 0.41 | 0.00 | 0.00 | 554.0 | 56.79 | 41.72 | 1.49 | 0.00 | 0.00 |
| 564.0 | 70.55 | 28.92 | 0.53 | 0.00 | 0.00 | 564.0 | 47.80 | 48.97 | 3.22 | 0.00 | 0.00 |
| 574.0 | 73.55 | 25.67 | 0.78 | 0.00 | 0.00 | 574.0 | 54.09 | 43.46 | 2.45 | 0.00 | 0.00 |
| 585.0 | 68.44 | 28.03 | 3.53 | 0.00 | 0.00 | 584.0 | 53.61 | 44.74 | 1.65 | 0.00 | 0.00 |
| 594.0 | 71.36 | 27.64 | 1.00 | 0.00 | 0.00 | 596.0 | 53.89 | 44.32 | 1.79 | 0.00 | 0.00 |
| 605.0 | 74.84 | 23.56 | 1.60 | 0.00 | 0.00 | 604.0 | 52.50 | 45.75 | 1.75 | 0.00 | 0.00 |
| 615.0 | 68.13 | 29.67 | 2.20 | 0.00 | 0.00 | 614.0 | 58.70 | 40.35 | 0.95 | 0.00 | 0.00 |
| 625.0 | 74.61 | 23.51 | 1.88 | 0.00 | 0.00 | 624.0 | 62.19 | 36.10 | 1.70 | 0.00 | 0.00 |
| 635.0 | 74.31 | 23.92 | 1.77 | 0.00 | 0.00 | 634.0 | 60.57 | 37.57 | 1.86 | 0.00 | 0.00 |
| 646.0 | 68.54 | 30.40 | 1.06 | 0.00 | 0.00 | 645.0 | 60.95 | 38.09 | 0.96 | 0.00 | 0.00 |
| 654.0 | 66.34 | 32.93 | 0.72 | 0.00 | 0.00 | 655.0 | 59.37 | 39.84 | 0.79 | 0.00 | 0.00 |
| 664.0 | 66.56 | 32.95 | 0.49 | 0.00 | 0.00 | 667.0 | 64.36 | 34.32 | 1.32 | 0.00 | 0.00 |
| 674.0 | 62.58 | 36.91 | 0.51 | 0.00 | 0.00 | 674.0 | 70.72 | 28.02 | 1.26 | 0.00 | 0.00 |
| 684.0 | 74.05 | 25.27 | 0.68 | 0.00 | 0.00 | 683.0 | 66.36 | 32.86 | 0.78 | 0.00 | 0.00 |
| 694.0 | 75.39 | 24.01 | 0.61 | 0.00 | 0.00 | 694.0 | 78.86 | 19.69 | 1.44 | 0.00 | 0.00 |
| 703.0 | 76.11 | 23.54 | 0.36 | 0.00 | 0.00 | 704.0 | 85.94 | 12.86 | 1.20 | 0.00 | 0.00 |
| 714.0 | 70.30 | 28.79 | 0.91 | 0.00 | 0.00 | 714.0 | 77.14 | 21.34 | 1.51 | 0.00 | 0.00 |
| 724.0 | 75.84 | 22.54 | 1.62 | 0.00 | 0.00 | 724.0 | 71.51 | 27.10 | 1.39 | 0.00 | 0.00 |
| 734.0 | 75.64 | 22.73 | 1.63 | 0.00 | 0.00 | 734.0 | 82.45 | 16.02 | 1.53 | 0.00 | 0.00 |
| 744.0 | 74.02 | 24.79 | 1.20 | 0.00 | 0.00 | 745.0 | 88.61 | 10.07 | 1.33 | 0.00 | 0.00 |
| 754.0 | 72.57 | 26.89 | 0.54 | 0.00 | 0.00 | 754.0 | 77.91 | 19.93 | 2.16 | 0.00 | 0.00 |
| 764.0 | 76.40 | 22.76 | 0.84 | 0.00 | 0.00 | 764.0 | 85.15 | 9.19 | 5.66 | 0.00 | 0.00 |
| 774.0 | 78.07 | 21.04 | 0.89 | 0.00 | 0.00 | | | | | | |
| 784.0 | 76.77 | 22.38 | 0.85 | 0.00 | 0.00 | | | | | | |
| 794.0 | 76.23 | 22.68 | 1.09 | 0.00 | 0.00 | | | | | | |
| 804.0 | 76.28 | 22.05 | 1.66 | 0.00 | 0.00 | | | | | | |
| 813.0 | 74.23 | 22.68 | 3.09 | 0.00 | 0.00 | | | | | | |
| 823.0 | 76.46 | 21.67 | 1.87 | 0.00 | 0.00 | | | | | | |
| 834.0 | 77.31 | 21.41 | 1.29 | 0.00 | 0.00 | | | | | | |
| 845.0 | 75.40 | 22.98 | 1.62 | 0.00 | 0.00 | | | | | | |
| 854.0 | 81.86 | 17.77 | 0.37 | 0.00 | 0.00 | | | | | | |

APPENDIX C.18. MULTI-COMPONENT ANALYSIS RESULTS

| CD38-02 | (2525m) | | | | | CD38-11 | (3835m) | | | | |
|---|---|---|---|---|---|---|---|---|---|---|---|
| Age (ka) | TERR (%) | BIOG (%) | AUTH (%) | RESID (%) | HYDRO (%) | Age (ka) | TERR (%) | BIOG (%) | AUTH (%) | RESID (%) | HYDRO (%) |
| 2.76 | 70.38 | 28.69 | 0.73 | 0.21 | 0.00 | 1.2 | 83.44 | 13.83 | 2.74 | 0.00 | 0.00 |
| 6.21 | 63.23 | 35.87 | 0.76 | 0.15 | 0.00 | 2.0 | 73.65 | 22.59 | 3.76 | 0.00 | 0.00 |
| 9.66 | 61.64 | 37.55 | 0.68 | 0.13 | 0.00 | 2.5 | 77.56 | 18.67 | 3.76 | 0.00 | 0.00 |
| 12.77 | 66.73 | 32.85 | 0.42 | 0.00 | 0.00 | 5.2 | 85.60 | 13.02 | 1.38 | 0.00 | 0.00 |
| 15.18 | 64.37 | 35.20 | 0.42 | 0.00 | 0.00 | 9.2 | 83.64 | 15.33 | 1.03 | 0.00 | 0.00 |
| 17.47 | 64.02 | 35.55 | 0.43 | 0.00 | 0.00 | 12.3 | 82.87 | 16.51 | 0.62 | 0.00 | 0.00 |
| 20.48 | 66.24 | 33.31 | 0.45 | 0.00 | 0.00 | 13.1 | 82.87 | 16.59 | 0.53 | 0.00 | 0.00 |
| 22.65 | 66.49 | 33.06 | 0.45 | 0.00 | 0.00 | 14.0 | 82.68 | 16.62 | 0.70 | 0.00 | 0.00 |
| 25.22 | 61.86 | 37.63 | 0.50 | 0.00 | 0.00 | 15.0 | 82.30 | 15.36 | 2.34 | 0.00 | 0.00 |
| 28.29 | 57.73 | 41.75 | 0.52 | 0.00 | 0.00 | 15.8 | 78.69 | 20.57 | 0.74 | 0.00 | 0.00 |
| 31.07 | 56.30 | 43.15 | 0.55 | 0.00 | 0.00 | 16.6 | 76.82 | 22.46 | 0.72 | 0.00 | 0.00 |
| 33.86 | 52.48 | 46.98 | 0.52 | 0.02 | 0.00 | 17.5 | 78.41 | 20.83 | 0.76 | 0.00 | 0.00 |
| 36.64 | 57.24 | 42.26 | 0.49 | 0.01 | 0.00 | 18.3 | 79.14 | 20.21 | 0.65 | 0.00 | 0.00 |
| 39.15 | 65.48 | 34.04 | 0.48 | 0.00 | 0.00 | 19.1 | 79.12 | 19.98 | 0.90 | 0.00 | 0.00 |
| 42.22 | 65.92 | 33.64 | 0.44 | 0.00 | 0.00 | 20.0 | 80.52 | 18.69 | 0.80 | 0.00 | 0.00 |
| 45.00 | 71.95 | 27.56 | 0.49 | 0.00 | 0.00 | 20.8 | 77.24 | 21.67 | 1.09 | 0.00 | 0.00 |
| 48.07 | 73.68 | 25.86 | 0.46 | 0.00 | 0.00 | 21.6 | 80.26 | 18.96 | 0.77 | 0.00 | 0.00 |
| 50.85 | 72.70 | 26.76 | 0.54 | 0.00 | 0.00 | 22.4 | 78.28 | 19.94 | 1.78 | 0.00 | 0.00 |
| 53.64 | 71.12 | 28.30 | 0.53 | 0.05 | 0.00 | 23.4 | 79.41 | 19.77 | 0.82 | 0.00 | 0.00 |
| 56.42 | 75.15 | 24.38 | 0.48 | 0.00 | 0.00 | 25.3 | 80.02 | 19.26 | 0.72 | 0.00 | 0.00 |
| 59.29 | 74.44 | 25.12 | 0.45 | 0.00 | 0.00 | 29.3 | 81.29 | 18.08 | 0.63 | 0.00 | 0.00 |
| 62.61 | 73.83 | 25.70 | 0.48 | 0.00 | 0.00 | 35.7 | 74.62 | 24.08 | 1.30 | 0.00 | 0.00 |
| 65.94 | 77.05 | 22.46 | 0.49 | 0.00 | 0.00 | 41.6 | 75.17 | 24.00 | 0.83 | 0.00 | 0.00 |
| 69.26 | 86.40 | 13.13 | 0.47 | 0.00 | 0.00 | 47.4 | 76.05 | 23.15 | 0.79 | 0.00 | 0.00 |
| 72.58 | 80.06 | 19.32 | 0.61 | 0.00 | 0.00 | 53.2 | 75.55 | 23.61 | 0.84 | 0.00 | 0.00 |
| 76.96 | 72.27 | 26.86 | 0.74 | 0.12 | 0.00 | 59.0 | 68.33 | 30.77 | 0.90 | 0.00 | 0.00 |
| 82.03 | 83.03 | 16.41 | 0.54 | 0.02 | 0.00 | 60.7 | 69.46 | 29.63 | 0.91 | 0.00 | 0.00 |
| 87.11 | 84.10 | 15.37 | 0.53 | 0.00 | 0.00 | 62.5 | 72.89 | 26.16 | 0.94 | 0.00 | 0.00 |
| 92.18 | 89.45 | 10.09 | 0.45 | 0.00 | 0.00 | 64.2 | 85.42 | 13.80 | 0.78 | 0.00 | 0.00 |
| 97.26 | 86.95 | 12.28 | 0.73 | 0.05 | 0.00 | 66.3 | 84.21 | 14.89 | 0.90 | 0.00 | 0.00 |
| 102.84 | 78.31 | 20.83 | 0.78 | 0.07 | 0.00 | 67.7 | 87.29 | 11.87 | 0.84 | 0.00 | 0.00 |
| 107.92 | 79.64 | 19.55 | 0.71 | 0.10 | 0.00 | 69.5 | 88.27 | 10.45 | 1.28 | 0.00 | 0.00 |
| 113.00 | 79.39 | 20.00 | 0.54 | 0.07 | 0.00 | 71.3 | 66.67 | 28.62 | 4.70 | 0.00 | 0.00 |
| 118.07 | 79.35 | 19.78 | 0.63 | 0.23 | 0.00 | 73.0 | 80.61 | 18.49 | 0.90 | 0.00 | 0.00 |
| 123.15 | 68.42 | 30.88 | 0.55 | 0.15 | 0.00 | 75.0 | 78.86 | 20.27 | 0.87 | 0.00 | 0.00 |
| 128.22 | 64.73 | 34.86 | 0.40 | 0.00 | 0.00 | 77.0 | 76.22 | 22.82 | 0.96 | 0.00 | 0.00 |
| 132.23 | 65.03 | 34.63 | 0.34 | 0.00 | 0.00 | 79.1 | 79.03 | 20.05 | 0.93 | 0.00 | 0.00 |
| 135.30 | 63.35 | 36.29 | 0.37 | 0.00 | 0.00 | 81.2 | 80.13 | 19.20 | 0.67 | 0.00 | 0.00 |
| 138.71 | 61.38 | 38.23 | 0.39 | 0.00 | 0.00 | 83.3 | 83.77 | 15.46 | 0.77 | 0.00 | 0.00 |
| 141.79 | 58.83 | 40.72 | 0.45 | 0.00 | 0.00 | 85.4 | 84.02 | 15.16 | 0.82 | 0.00 | 0.00 |
| 145.20 | 60.08 | 39.50 | 0.42 | 0.00 | 0.00 | 87.5 | 83.34 | 15.85 | 0.81 | 0.00 | 0.00 |
| 148.61 | 60.43 | 39.16 | 0.40 | 0.00 | 0.00 | 89.5 | 86.91 | 12.25 | 0.83 | 0.00 | 0.00 |
| 152.02 | 59.48 | 40.11 | 0.40 | 0.00 | 0.00 | 91.6 | 81.86 | 17.10 | 0.96 | 0.08 | 0.00 |
| 155.44 | 61.84 | 37.72 | 0.44 | 0.00 | 0.00 | 93.7 | 76.10 | 22.28 | 1.40 | 0.22 | 0.00 |
| 158.85 | 68.27 | 31.34 | 0.39 | 0.00 | 0.00 | 95.8 | 76.66 | 21.90 | 1.28 | 0.16 | 0.00 |
| 162.26 | 71.78 | 27.83 | 0.39 | 0.00 | 0.00 | 97.9 | 86.01 | 12.88 | 1.11 | 0.00 | 0.00 |
| 165.68 | 60.73 | 38.81 | 0.46 | 0.00 | 0.00 | 100.0 | 87.28 | 11.83 | 0.89 | 0.00 | 0.00 |
| 169.43 | 58.26 | 41.26 | 0.48 | 0.00 | 0.00 | 102.0 | 82.49 | 16.49 | 1.02 | 0.00 | 0.00 |
| 172.84 | 58.99 | 40.55 | 0.46 | 0.00 | 0.00 | 104.1 | 85.16 | 13.99 | 0.85 | 0.00 | 0.00 |
| 176.26 | 61.93 | 37.56 | 0.51 | 0.00 | 0.00 | 106.2 | 82.71 | 16.21 | 1.09 | 0.00 | 0.00 |
| 179.67 | 65.24 | 34.29 | 0.46 | 0.00 | 0.00 | 108.3 | 82.89 | 16.20 | 0.91 | 0.00 | 0.00 |
| 183.08 | 72.64 | 26.92 | 0.44 | 0.00 | 0.00 | 110.4 | 82.90 | 16.04 | 1.06 | 0.00 | 0.00 |
| 186.50 | 79.55 | 20.15 | 0.29 | 0.00 | 0.00 | 112.5 | 81.55 | 17.58 | 0.85 | 0.02 | 0.00 |
| 189.57 | 83.51 | 15.97 | 0.52 | 0.00 | 0.00 | 114.5 | 81.21 | 17.49 | 1.22 | 0.09 | 0.00 |
| 193.52 | 83.64 | 15.81 | 0.55 | 0.00 | 0.00 | 116.6 | 78.91 | 19.89 | 1.14 | 0.06 | 0.00 |
| 197.42 | 82.86 | 16.42 | 0.59 | 0.13 | 0.00 | 118.7 | 79.12 | 19.49 | 1.25 | 0.14 | 0.00 |
| 202.11 | 76.08 | 23.17 | 0.62 | 0.14 | 0.00 | 120.8 | 78.47 | 20.03 | 1.38 | 0.12 | 0.00 |
| 206.02 | 77.54 | 21.91 | 0.48 | 0.08 | 0.00 | | | | | | |
| 209.53 | 77.54 | 21.99 | 0.44 | 0.03 | 0.00 | | | | | | |
| 213.44 | 58.42 | 40.80 | 0.56 | 0.21 | 0.00 | | | | | | |
| 217.34 | 56.94 | 42.36 | 0.57 | 0.13 | 0.00 | | | | | | |
| 221.25 | 63.01 | 36.44 | 0.51 | 0.03 | 0.00 | | | | | | |
| 225.16 | 66.13 | 33.41 | 0.47 | 0.00 | 0.00 | | | | | | |
| 229.06 | 71.68 | 27.85 | 0.47 | 0.00 | 0.00 | | | | | | |
| 232.97 | 78.84 | 20.70 | 0.45 | 0.00 | 0.00 | | | | | | |
| 237.27 | 74.20 | 24.90 | 0.65 | 0.26 | 0.00 | | | | | | |
| 240.78 | 57.95 | 41.24 | 0.57 | 0.24 | 0.00 | | | | | | |
| 244.50 | 64.26 | 35.35 | 0.39 | 0.00 | 0.00 | | | | | | |
| 247.71 | 69.72 | 30.04 | 0.24 | 0.00 | 0.00 | | | | | | |
| 250.91 | 66.77 | 32.98 | 0.25 | 0.00 | 0.00 | | | | | | |
| 254.12 | 67.15 | 32.56 | 0.29 | 0.00 | 0.00 | | | | | | |
| 257.32 | 66.25 | 33.43 | 0.32 | 0.00 | 0.00 | | | | | | |
| 260.53 | 66.16 | 33.50 | 0.34 | 0.00 | 0.00 | | | | | | |
| 263.73 | 67.05 | 32.58 | 0.37 | 0.00 | 0.00 | | | | | | |

| APPENDIX C.19. MASS ACCUMULATION RATE FLUXES | | | | | | |
|---|---|---|---|---|---|---|
| | | All MARs in (mg/cm2/kyr) | | | | |
| CD38-02 | 2525m | | | | | |
| Age | Al MAR | Siterr MAR | CorgMAR | BioSilMAR | CaCO3 MAR | Palaeoprod. (g/m2/yr) |
| 2.76 | 96.23 | 311.35 | 25.03 | 159.83 | 282.07 | 44.1 |
| 6.21 | 90.30 | 298.86 | 23.42 | 148.28 | 438.15 | 43.3 |
| 9.66 | 82.12 | 275.47 | 21.49 | 120.11 | 453.87 | 37.1 |
| 12.77 | 120.88 | 369.85 | 59.01 | 157.53 | 491.95 | 60.1 |
| 15.18 | 135.49 | 417.49 | 46.89 | 150.55 | 684.64 | 54.6 |
| 17.47 | 131.69 | 412.13 | 49.11 | 160.16 | 661.20 | 57.0 |
| 20.48 | 141.25 | 437.56 | 48.15 | 138.82 | 658.66 | 55.7 |
| 22.65 | 134.84 | 421.28 | 45.58 | 129.95 | 622.64 | 51.5 |
| 25.22 | 112.22 | 347.67 | 44.88 | 117.35 | 650.45 | 63.4 |
| 28.29 | 105.22 | 321.85 | 45.86 | 133.80 | 726.29 | 65.2 |
| 31.07 | 104.26 | 318.71 | 35.96 | 162.82 | 752.49 | 51.9 |
| 33.86 | 93.53 | 285.06 | 41.09 | 174.61 | 781.06 | 57.5 |
| 36.64 | 103.70 | 318.22 | 42.58 | 144.86 | 724.04 | 60.1 |
| 39.15 | 116.87 | 356.11 | 38.26 | 125.13 | 559.83 | 52.7 |
| 42.22 | 119.01 | 349.83 | 49.19 | 150.91 | 522.89 | 67.0 |
| 45.00 | 142.19 | 437.69 | 36.91 | 102.39 | 509.06 | 55.2 |
| 48.07 | 142.81 | 435.64 | 41.56 | 132.75 | 422.29 | 61.5 |
| 50.85 | 122.28 | 399.28 | 33.65 | 177.75 | 324.39 | 44.9 |
| 53.64 | 125.03 | 402.07 | 39.14 | 178.57 | 374.49 | 54.3 |
| 56.42 | 127.80 | 410.05 | 42.34 | 157.41 | 293.80 | 56.5 |
| 59.29 | 114.83 | 351.28 | 39.26 | 118.89 | 303.11 | 69.5 |
| 62.61 | 117.32 | 365.87 | 33.76 | 112.30 | 340.09 | 61.8 |
| 65.94 | 126.48 | 389.09 | 29.07 | 115.34 | 294.56 | 54.6 |
| 69.26 | 136.03 | 428.14 | 30.72 | 129.65 | 85.69 | 55.7 |
| 72.58 | 123.77 | 395.76 | 36.92 | 143.57 | 175.14 | 67.2 |
| 76.96 | 71.13 | 230.88 | 18.74 | 95.57 | 200.43 | 64.7 |
| 82.03 | 80.89 | 255.95 | 25.40 | 100.87 | 64.00 | 84.8 |
| 87.11 | 83.09 | 267.24 | 20.29 | 79.70 | 80.79 | 69.3 |
| 92.18 | 88.18 | 273.02 | 19.98 | 91.50 | 6.98 | 66.6 |
| 97.26 | 84.53 | 267.35 | 14.96 | 92.50 | 34.65 | 49.4 |
| 102.84 | 74.61 | 244.30 | 18.29 | 105.78 | 112.13 | 59.8 |
| 107.92 | 77.88 | 246.91 | 17.13 | 101.51 | 108.94 | 57.4 |
| 113.00 | 78.95 | 246.54 | 16.25 | 110.60 | 109.94 | 55.3 |
| 118.07 | 74.36 | 239.36 | 11.83 | 100.30 | 108.58 | 38.4 |
| 123.15 | 65.09 | 208.50 | 14.87 | 113.34 | 221.54 | 48.9 |
| 128.22 | 101.39 | 301.83 | 25.95 | 152.55 | 471.52 | 49.3 |
| 132.23 | 107.14 | 326.07 | 24.38 | 103.91 | 550.93 | 48.8 |
| 135.30 | 109.48 | 340.58 | 21.54 | 101.45 | 623.57 | 45.9 |
| 138.71 | 106.92 | 324.88 | 24.00 | 133.70 | 635.07 | 51.3 |
| 141.79 | 101.66 | 312.49 | 24.56 | 127.96 | 685.28 | 51.9 |
| 145.20 | 105.03 | 320.02 | 24.10 | 124.38 | 673.51 | 51.3 |
| 148.61 | 103.51 | 319.46 | 21.04 | 142.12 | 635.34 | 44.2 |
| 152.02 | 105.74 | 319.11 | 23.56 | 117.95 | 707.34 | 51.4 |
| 155.44 | 110.99 | 344.42 | 23.37 | 119.27 | 663.31 | 51.6 |
| 158.85 | 113.32 | 354.96 | 23.25 | 97.84 | 498.12 | 47.6 |
| 162.26 | 121.43 | 369.80 | 25.72 | 101.43 | 433.41 | 53.1 |
| 165.68 | 108.93 | 332.76 | 30.68 | 87.61 | 710.43 | 66.6 |
| 169.43 | 102.53 | 317.27 | 29.69 | 96.33 | 738.40 | 64.2 |
| 172.84 | 102.82 | 322.36 | 33.34 | 97.69 | 710.38 | 70.9 |
| 176.26 | 106.56 | 335.90 | 34.11 | 95.45 | 639.88 | 70.9 |
| 179.67 | 115.01 | 363.21 | 29.61 | 116.15 | 573.94 | 63.8 |
| 183.08 | 124.51 | 403.17 | 27.34 | 95.59 | 426.43 | 57.7 |
| 186.50 | 157.49 | 551.69 | 19.06 | 110.24 | 345.64 | 45.8 |
| 189.57 | 126.37 | 389.73 | 24.91 | 97.55 | 165.24 | 57.0 |
| 193.52 | 121.86 | 374.17 | 26.04 | 106.62 | 141.52 | 57.8 |
| 197.42 | 109.58 | 332.58 | 29.28 | 140.79 | 88.38 | 61.3 |
| 202.11 | 148.82 | 468.47 | 30.25 | 179.84 | 329.46 | 93.3 |
| 206.02 | 152.67 | 469.99 | 33.28 | 132.78 | 347.43 | 101.3 |
| 209.53 | 129.45 | 392.48 | 22.66 | 90.94 | 323.52 | 57.3 |
| 213.44 | 101.84 | 313.12 | 22.92 | 85.65 | 738.20 | 61.0 |
| 217.34 | 98.88 | 312.74 | 19.83 | 82.52 | 773.44 | 52.5 |
| 221.25 | 107.93 | 336.88 | 21.48 | 90.23 | 631.35 | 56.2 |
| 225.16 | 119.02 | 369.95 | 24.42 | 75.02 | 616.40 | 66.9 |
| 229.06 | 127.54 | 391.52 | 23.63 | 91.58 | 474.75 | 61.9 |
| 232.97 | 125.63 | 389.62 | 21.59 | 97.62 | 273.55 | 52.4 |
| 237.27 | 110.93 | 356.97 | 21.37 | 124.63 | 297.15 | 49.8 |
| 240.78 | 86.23 | 281.29 | 23.08 | 115.13 | 592.26 | 54.3 |
| 244.50 | 120.65 | 378.70 | 26.26 | 94.44 | 669.55 | 52.8 |
| 247.71 | 129.71 | 396.14 | 27.91 | 83.14 | 554.23 | 54.6 |
| 250.91 | 128.17 | 388.12 | 28.97 | 108.71 | 616.09 | 58.5 |
| 254.12 | 124.98 | 400.65 | 17.98 | 94.68 | 608.71 | 35.0 |
| 257.32 | 119.83 | 381.43 | 26.84 | 125.13 | 567.93 | 52.2 |
| 260.53 | 124.13 | 381.09 | 27.63 | 140.05 | 580.54 | 54.9 |
| 263.73 | 122.55 | 375.88 | 33.95 | 140.95 | 534.07 | 66.2 |

| APPENDIX C.19. MASS ACCUMULATION RATE FLUXES | | | | | | |
|---|---|---|---|---|---|---|
| | | All MARs in (mg/cm2/kyr) | | | | |
| CD38-11 | | | | | | |
| Age | Al MAR | Siterr MAR | CorgMAR | BioSilMAR | CaCO3 MAR | Palaeoprod. (g/m2/yr) |
| 0.80 | 153.17 | 504.35 | 83.31 | 171.84 | 46.99 | 105.52 |
| 2.00 | 139.94 | 516.40 | 99.49 | 112.95 | 298.49 | 136.55 |
| 2.20 | 165.84 | 684.29 | 89.82 | 94.29 | 291.17 | 144.31 |
| 3.49 | 151.11 | 488.42 | 60.76 | 191.09 | 21.73 | 73.22 |
| 6.17 | 144.16 | 456.23 | 65.08 | 184.85 | 64.61 | 75.96 |
| 8.85 | 143.83 | 444.00 | 72.73 | 171.62 | 96.80 | 86.63 |
| 11.53 | 149.80 | 457.30 | 74.82 | 176.49 | 105.78 | 90.74 |
| 13.80 | 189.73 | 589.25 | 87.71 | 193.75 | 172.50 | 86.42 |
| 16.44 | 311.97 | 1168.69 | 70.75 | 161.31 | 461.00 | 115.35 |
| 18.63 | 183.47 | 582.31 | 90.57 | 229.24 | 251.23 | 91.43 |
| 20.82 | 173.48 | 551.05 | 90.57 | 232.27 | 280.92 | 89.90 |
| 23.23 | 179.63 | 573.17 | 96.34 | 257.46 | 214.34 | 96.70 |
| 25.11 | 200.80 | 623.59 | 101.08 | 270.55 | 238.89 | 88.40 |
| 27.10 | 207.45 | 662.31 | 99.64 | 236.92 | 286.98 | 90.57 |
| 29.09 | 209.41 | 658.49 | 98.58 | 251.38 | 228.56 | 85.02 |
| 31.08 | 208.62 | 676.01 | 94.68 | 242.32 | 359.77 | 89.82 |
| 33.07 | 206.81 | 645.66 | 88.42 | 239.60 | 253.67 | 73.69 |
| 35.07 | 249.24 | 847.42 | 94.69 | 242.74 | 418.20 | 104.79 |
| 37.26 | 201.95 | 611.50 | 110.49 | 296.98 | 191.13 | 96.45 |
| 39.45 | 200.25 | 586.30 | 114.70 | 298.27 | 160.77 | 96.92 |
| 40.84 | 200.26 | 580.95 | 112.89 | 315.16 | 102.21 | 94.02 |
| 43.03 | 182.24 | 570.59 | 105.71 | 247.88 | 346.50 | 89.87 |
| 45.03 | 176.65 | 527.65 | 113.69 | 276.94 | 280.72 | 91.02 |
| 47.02 | 186.96 | 539.39 | 127.16 | 294.22 | 256.24 | 105.72 |
| 49.01 | 190.91 | 555.19 | 123.50 | 303.13 | 283.67 | 104.47 |
| 51.00 | 169.01 | 504.06 | 112.28 | 375.83 | 417.77 | 96.24 |
| 52.99 | 168.80 | 519.29 | 112.07 | 390.64 | 354.54 | 94.76 |
| 54.99 | 176.99 | 543.82 | 101.70 | 374.71 | 279.85 | 85.54 |
| 56.98 | 221.93 | 668.15 | 110.84 | 253.72 | 62.16 | 97.09 |
| 59.62 | 153.45 | 465.03 | 67.22 | 175.01 | 80.82 | 134.84 |
| 62.28 | 153.27 | 469.41 | 57.28 | 169.03 | 21.90 | 110.42 |
| 65.60 | 162.11 | 503.03 | 61.83 | 142.02 | 24.64 | 121.34 |
| 68.93 | 150.99 | 613.17 | 88.55 | 97.13 | 585.99 | 240.60 |
| 72.25 | 121.97 | 393.75 | 64.93 | 229.75 | 38.37 | 113.65 |
| 74.95 | 190.76 | 593.26 | 108.04 | 396.54 | 79.27 | 101.49 |
| 77.04 | 178.26 | 570.80 | 97.96 | 467.15 | 70.18 | 90.05 |
| 79.12 | 190.66 | 599.26 | 117.04 | 394.69 | 64.00 | 110.58 |
| 81.20 | 198.10 | 591.99 | 123.11 | 348.24 | 93.72 | 117.61 |
| 83.29 | 225.82 | 665.95 | 120.27 | 276.58 | 99.15 | 121.05 |
| 85.37 | 238.52 | 703.49 | 107.54 | 278.53 | 126.19 | 111.82 |
| 87.45 | 223.69 | 646.52 | 112.63 | 269.29 | 124.50 | 114.42 |
| 89.54 | 250.21 | 759.95 | 92.56 | 322.21 | 5.22 | 95.69 |
| 91.62 | 202.37 | 597.19 | 90.58 | 358.56 | 54.05 | 88.79 |
| 93.70 | 198.52 | 638.52 | 89.97 | 407.12 | 194.93 | 87.22 |
| 95.79 | 186.35 | 586.65 | 89.34 | 423.66 | 120.91 | 83.18 |
| 97.87 | 229.61 | 702.16 | 97.51 | 302.39 | 9.32 | 97.33 |
| 99.95 | 232.64 | 678.79 | 93.43 | 280.44 | 1.67 | 91.63 |
| 102.04 | 229.49 | 683.75 | 95.52 | 361.09 | 89.46 | 94.92 |
| 104.12 | 225.75 | 661.59 | 78.97 | 355.48 | 6.92 | 76.97 |
| 106.20 | 210.98 | 615.33 | 65.37 | 420.42 | 6.40 | 61.84 |
| 108.29 | 212.88 | 642.12 | 76.09 | 416.79 | 2.37 | 71.86 |
| 110.37 | 213.40 | 651.57 | 73.71 | 412.58 | 5.42 | 71.53 |
| 112.45 | 208.28 | 639.08 | 65.37 | 468.98 | 0.00 | 61.54 |
| 114.54 | 201.94 | 634.75 | 71.30 | 433.74 | 12.61 | 70.91 |
| 116.62 | 202.36 | 612.94 | 67.19 | 513.93 | 26.08 | 63.89 |
| 118.70 | 205.17 | 633.85 | 60.90 | 530.61 | 10.30 | 58.93 |
| 120.79 | 200.62 | 619.25 | 69.50 | 513.38 | 26.82 | 68.88 |

# APPENDIX D

Reprint of McNeill, G.W. and Shimmield, G.B. (1991) Diagenetic controls on uranium, molybdenum and vanadium enrichment in orgnic-rich marine shelf sediments. *Proceedings of the 8th International Conference on Heavy Metals in the Environment*, (Ed. J.G.Farmer), pp.436-439.CEP Consultants, Edinburgh.

# DIAGENETIC CONTROLS ON URANIUM, MOLYBDENUM AND VANADIUM ENRICHMENT IN ORGANIC-RICH MARINE SHELF SEDIMENTS

G.W.McNeill* and G.B.Shimmield*.

## ABSTRACT

Organic-rich marine sediments are known to preferentially incorporate heavy metals *via* a variety of redox/organo-complex reactions. The elevated concentrations of redox-sensitive metals, such as U and Mo, are used increasingly as indicators of palaeoenvironmental $O_2$ conditions at the benthic boundary layer. This study presents a detailed investigation of U, Mo and V enrichment in reducing sediments in the absence of anthropogenic influence. This allows us to define the natural behaviour of these important redox-sensitive metals for investigation of both palaeoceanographic and pollution applications.

Sediment cores from the Peruvian upwelling margin record the variation in U, Mo and V with organic carbon and display a variety of redox and diagenetic controls on these metals. A model for U partitioning based on phosphorite diagenesis and organic matter complexation is presented. In contrast, Mo and V appear to be predominantly controlled by water column scavenging by the high organic matter flux followed by post-depositional redox processes.

## INTRODUCTION

Study of heavy metal deposition in the coastal marine environment is very important for the understanding of the complex pathways in which metals are incorporated into the sediment. Before any polluted environment can be examined, the natural, steady-state baseline for heavy metal enrichment associated with organic matter and/or diagenetic processes needs to be quantified.

The various mechanisms for uranium enrichment in organic-rich, anoxic marine sediments have been reviewed by Anderson *et al* (1989, ref 1) and for molybdenum and vanadium by Francois (1988, ref 2). Bertine and Turekian (1973, ref 3) used the Mo/U ratio as a palaeoenvironmental indicator of bottom-water oxygen conditions.

One site in which such marine sediments have a high organic matter content and accumulate these redox-sensitive metals to elevated concentrations, is under the upwelling zone in the coastal basins off Peru. This study measures the concentrations of organic carbon ($C_{org}$), U, Mo and V in sediments taken from this area and examines the organo-metallic relationships of Mo and V and the partitioning of U into phases according to organic and mineral diagenetic associations in a natural, unpolluted environment.

## METHODS

The samples analysed in this study were taken from piston cores collected during the R.R.S. *Charles Darwin* Leg 38 cruise (April-May 1989) off Peru, from the locations and water depths shown in Table 1. $C_{org}$ was determined by an initial acid digestion of carbonate material, followed by combustion of the sample and measurement of the $CO_2$ evolved using a LECO 572-100 carbon analyser (% std. deviation = 4.66%, n=48). Trace elements (U, Mo and V) were analysed by X-ray fluorescence of pressed pellet samples, using a Philips PW1480 X-ray spectrophotometer (XRF estimated reproducibility, U and Mo = ±1ppm, V = ±5ppm). All concentrations were corrected for their salt content, which was calculated by measuring the % weight loss upon drying each sample and assuming constant salinity of 35‰.

## RESULTS

The offshore basins on the continental shelf off Peru form sites for the accumulation of

*Depatment of Geology and Geophysics, Grant Institute, University of Edinburgh, West Mains Road, Edinburgh, EH9 3JW.

organic-rich marine sediments. Coastal upwelling of cold, nutrient-rich water, caused by offshore Ekman transport of surface nutrient-depleted water, supports intense biological productivity.

Organic material falling down through the water column is decomposed by marine organisms and only a small proportion survives down to the benthic boundary layer for incorporation into the sediment. However, off Peru, there is a large organic matter flux resulting in an oxygen minimum zone (OMZ) at 100-400m water depth (ref 4, 5).

The reducing sediments from cores CD38-09 and CD38-10 are extremely rich in organic matter with mean values of 4.4 & 5.4 wt.% $C_{org}$ respectively, with a maximum of 11.9 wt.% in CD38-10 (Table 2).

| Station | CD38-09 | CD38-10 |
|---|---|---|
| Latitude | 10°58'S | 11°04'S |
| Longitude | 77°57'W | 78°04'W |
| Water depth | 148m | 257m |
| Core length | 895cm | 822cm |

Table 1. Core stations

| | CD38-09 | CD38-10 |
|---|---|---|
| $U_{org}$ (ppm) | 0-89.7(5.0) | 0.7-20.9(7.9) |
| $U_{org}/C_{org}$($\times10^{-4}$) | 0-55.4(1.50) | 0.7-6.2(1.47) |
| $Mo/U_{org}$ | 0-34.1(19.3) | 3.1-24.1(8.5) |

Table 3. Concentration and ratios of $U_{org}$

| | CD38-09 | CD38-10 |
|---|---|---|
| $C_{org}$(wt.%) | 1.6-8.3(4.38) | 0.8-11.9(5.37) |
| U (ppm) | 4.0-167.4(9.3) | 5.9-27.2(13.1) |
| Mo (ppm) | 13-99(52.1) | 11-129(56.9) |
| V (ppm) | 63-156(118.6) | 46-363(147.1) |
| $U/C_{org}$($\times10^{-4}$) | 0.9-103.3(3.01) | 1.0-31.3(3.47) |
| $Mo/C_{org}$($\times10^{-4}$) | 7.4-32.6(12.2) | 4.9-47.6(11.4) |
| $V/C_{org}$($\times10^{-4}$) | 14.3-53.2(29.8) | 14.9-69.3(29.4) |
| Mo/U | 0.3-17.3(7.37) | 0.6-13.1(4.81) |

Table 2. Range and (mean) values for salt-corrected element concentrations and ratios

Heavy metals which are known to have an affinity with organic matter (ref 2, 3, 6, 7) are also enriched in these sediments. The range and mean concentrations of U, Mo and V are shown in Table 2, along with their ratios to $C_{org}$ and the Mo/U ratios. Depth profiles of $C_{org}$, Mo, U and V for CD38-10 are displayed in Fig. 1. The profile of $C_{org}$ does not show a simple exponential decrease with depth, but has peaks and troughs which implies a time-varying input, due to changes in either primary productivity or dilution by other components. The Mo and V depth profiles are very similar to that of $C_{org}$ (especially over the 150-550cm depth range) and illustrate a large dynamic range in concentration associated with natural fluctuations. Regression analyses on the data from CD38-10 (Fig. 2a,b) indicate an organo-metallic relationship between $C_{org}$ and V ($r^2$ = 0.61) and Mo ($r^2$ = 0.53).

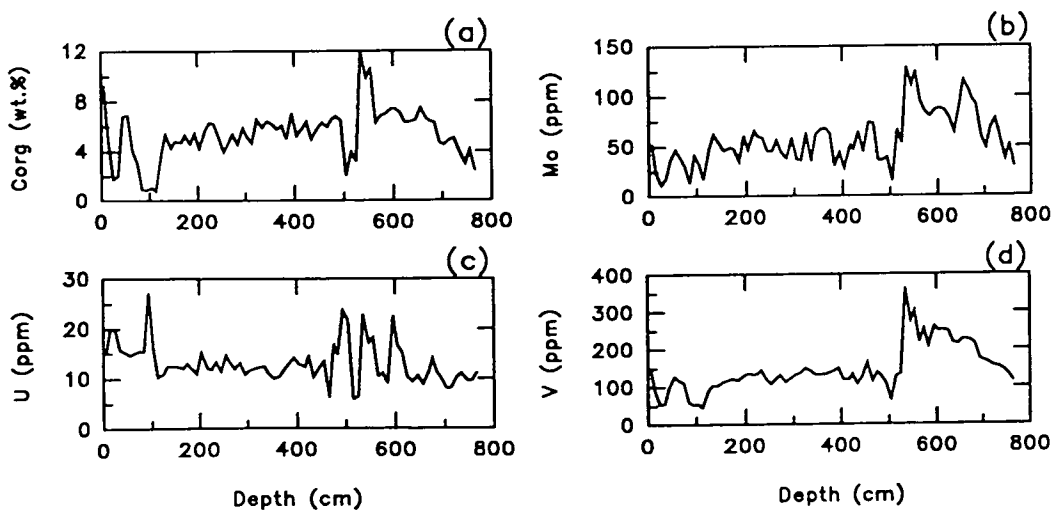


Figure 1. CD38-10(257m) : a) $C_{org}$ b) Mo c) U d) V versus depth

The depth profile of U does not display such a good correspondence to $C_{org}$ (the plot of U

against $C_{org}$ in Fig. 2c gives $r^2 = 0.005$). Therefore, we have to consider other possible sources for the uranium enrichment in these sediments. As well as organic matter content, the mineralogy of the sediment is important because U can be incorporated into both detrital and diagenetic minerals.

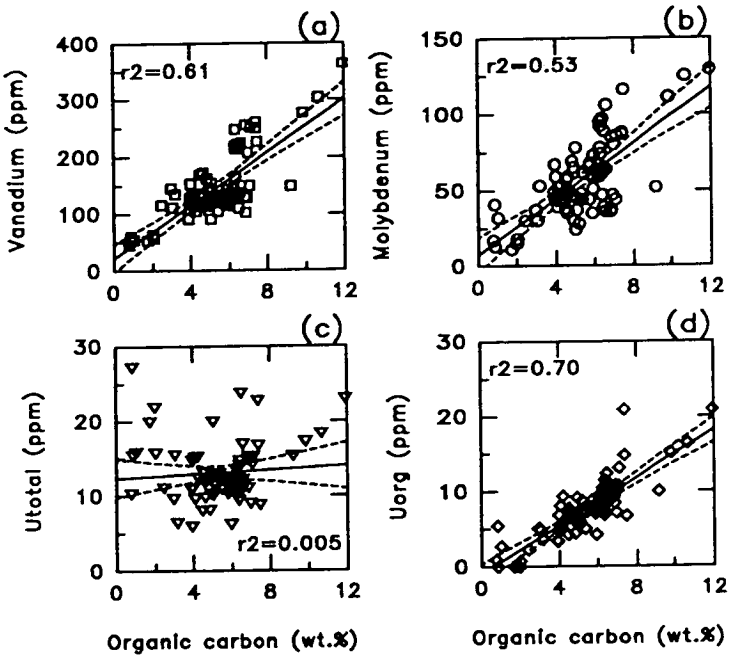


Figure 2. CD38-10(257m) : a) V b) Mo c) $U_{total}$ d) $U_{org}$ versus $C_{org}$

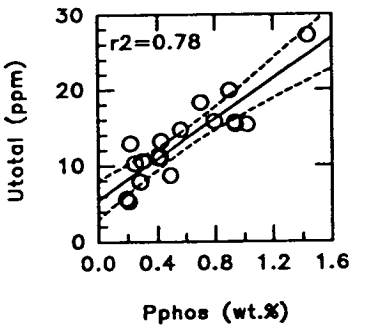


Figure 3. $U_{total}$ versus $P_{phos}$ (data from CD38-09 and CD38-10). Regression : $U=13.3xP_{phos} + 5.5$

The diagenetic formation of phosphorite is known to preferentially take up U from bottom waters (ref 8, 9) and this process has occurred to various degrees in this coastal environment throughout the Late Quaternary (ref 4, 10). In order to estimate the contribution of these various sources to the total uranium content, the following partitioning equations are used. Zones where phosphorite formation has been significant have anomalously high P/Al ratios. The total phosphorus in the sediment can be partitioned into detrital, organic and phosphorite phases. Hence,

$$P_{phos} = P_{total} - (P_{det} + P_{org}) \quad (1)$$

where, $P_{det}$ = Al x 0.00875 (ave. shale, ref 11) and $P_{org} = C_{org} / 41.0$ (ref 12). A regression analysis between the $U_{total}$ and $P_{phos}$ contents of sediments in these phosphorite zones for cores CD38-09 and CD38-10, as shown in Fig. 3, gives a regression line of :

$$U_{total}\,(ppm) = 13.33\ P_{phos} + 5.5 \quad (r^2 = 0.78) \quad (2)$$

This accounts for uranium enrichment in these zones and allows for the quantitative partitioning of U into its detrital, organic and phosphorite phases for all the other organic-rich sediments. Hence,

$$U_{org} = U_{total} - (U_{det} + U_{phos}) \quad (3)$$

where, $U_{det}$ = Al x 0.4625 (ave. shale, ref 11) and $U_{phos} = 13.33 \times P_{phos}$ (eqn. 2). The fraction of uranium associated with organic matter can now be calculated and the concentrations are shown in Table 3 and Fig. 4a. Regression analysis between $C_{org}$ and $U_{org}$ for CD38-10 gives an organo-metallic relationship with $r^2 = 0.70$ (Fig. 2d).

## DISCUSSION/CONCLUSIONS

The concentration of $C_{org}$ and associated heavy metals, Mo and V, in the coastal basins off Peru (Table 2 and Figs. 1 and 2) illustrate the high level and range of these elements possible in a natural marine environment. The enrichment of these two metals is predominantly controlled by water column scavenging by the high organic matter flux (ref 2, 13), resulting in close organo-metallic relationships. There may also be some post-depositional redox processes operating on the Mo and V concentrations, as organic matter undergoes bacterial decomposition upon burial (ref 6).

Mineral diagenesis may also affect the concentration of heavy metals in the marine environment. The formation of phosphorite can considerably enrich the U concentration of the sediment. By partitioning the total U content into $U_{det}$, $U_{phos}$ (eqn. 2) and $U_{org}$ (eqn. 3), the relative influences of phosphorite or organic matter can be seen (Fig. 4a).

The organo-metallic relationships in the Peru sediments can be quantified (given by the mean values of $V/C_{org}$ and $Mo/C_{org}$ in Table 2 and $U_{org}/C_{org}$ in Table 3) and may be used in any future studies in a polluted coastal marine environment as the natural, baseline flux for comparison with any anthropogenic input (ref 13).

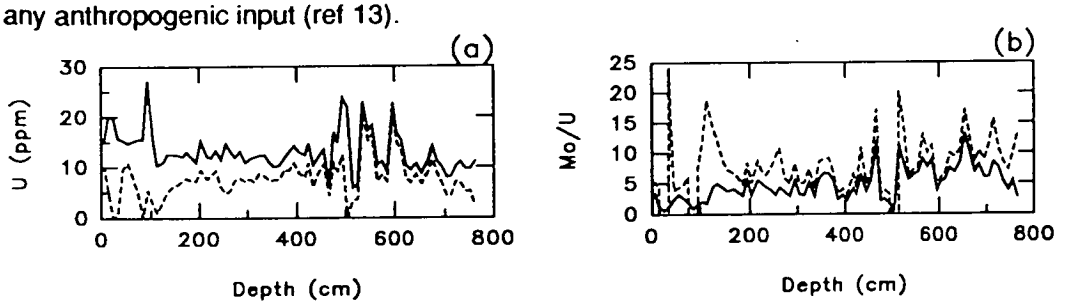


Figure 4. CD38-10(257m) : a) U b) U/Mo versus depth. Full line = $U_{total}$, dotted line = $U_{org}$

The Mo/U ratios are of interest because these two heavy metals have previously been used as palaeoenvironmental indicators of oxygen conditions at the benthic boundary layer, producing a Mo/U ratio of close to unity for anoxic sediments (ref 3) and higher values (3-4) for oxic, deep-sea sediments. Figure 4b displays the high Mo/U measured for the sediments in this study (4.8 and 7.4, Table 2) and even higher $Mo/U_{org}$ calculated (19.3 and 8.5, Table 3) in zones where phosphorite formation is minimal. From this study, we suggest that the natural processes contributing to U and Mo enrichment in anoxic marine sediments result in variable Mo/U ratios. Consequently the statement of Bertine and Turekian (1973, ref 3) that anoxic sediments have a ratio of unity is invalid.

## ACKNOWLEDGEMENTS

The authors gratefully acknowledge the funding of N.E.R.C. (Grant No. GT4/89/GS/040).

## REFERENCES

1. R F Anderson *et al*, Geochim Cosmochim Acta 53, 2215-2224 (1989)
2. R Francois, Mar Geol 83, 285-308 (1988)
3. K K Bertine and K K Turekian, Geochim Cosmochim Acta 37, 1415-1434 (1973)
4. H H Veeh *et al*, Science 181, 844-845 (1973)
5. C E Reimers and E Suess, Coastal Upwelling IV:10b (Plenum Press, NY, 1983) p311-337
6. S E Calvert *et al*, Oceanologica Acta 8, 167-173 (1985)
7. G N Baturin, Geochem Int 10, 1031-1041 (1973)
8. H H Veeh *et al*, Mar Chem 2, 189-202 (1974)
9. G N Baturin *et al*, Geochem Int 8, 281-286 (1971)
10. F Manheim *et al*, Jour Sed Pet 45, 243-251 (1975)
11. K K Turekian and K H Wedepohl, Bull Geol Soc Amer 72, 175-192 (1961)
12. A C Redfield *et al*, The Sea 2 (Wiley, NY, 1963) p26-77
13. K W Bruland *et al*, Environ Sci Tech 8, 425-432 (1974)